

Asymmetric Photocatalysis by Hydrogen Atom Transfer with Chiral-at-Rhodium Complexes

A DISSERTATION

In

Chemistry

Presented to the Faculties of Philipps-Universität Marburg in Partial Fulfillment
of the Requirements for the Degree of Doctor of Science
(Dr. rer. nat.)

Chenhao Zhang

Henan, P. R. China

Marburg/Lahn 2021

Die vorliegende Dissertation entstand in der Zeit von Dezember 2017 bis August 2021 am Fachbereich Chemie der Philipps-Universität Marburg unter der Betreuung von Herrn Prof. Dr. Eric Meggers.

Vom Fachbereich Chemie der Philipps-Universität Marburg (Hochschulkennziffer: 1180) als Dissertation am _____ angenommen.

Erstgutachter:	Prof. Dr. Eric Meggers
Zweitgutachter:	Prof. Dr. Armin Geyer
weitere Mitglieder Prüfungskommission:	Prof. Dr. Jörg Sundermeyer Prof. Dr. Bernhard Roling

Tag der mündlichen Prüfung: _____

Acknowledgements

Coming to Germany to study for my Ph.D. gave me an unforgettable experience in my life.

My sincere appreciation goes first and foremost to my advisor, Prof. Eric Meggers, who has given me invaluable supervision and suggestions over the past years. His love and dedication to scientific research deeply impressed me, and his attitude toward academic research has been invaluable and admirable. I am deeply grateful for the opportunity he gives me to study in his research group. I wish him all the best in his future endeavors. Next, I am grateful to my master supervisor, Prof. Zhiyong Jiang, for introducing me to the academic research and for his constant support and encouragement.

I am grateful to Prof. Armin Geyer, Prof. Jörg Sundermeyer and Prof. Bernhard Røling for referring my thesis and participating in the defense committee.

I would like to thank all the members of the Meggers group. First of all, I would like to express my gratitude to Dr. Lili Zhang for her encouragement and kind help. Thanks a lot to Dr. Sabrina Höbenreich and Ina Pinnschmidt for their kind help. Special thanks to Chenxi Ye and Xin Nie for their cooperation and help on my research and publications. Thanks a lot to Philipp Steinlandt for translating the abstract into the German version. Thanks a lot to all of the former and current group members, Dr. Yu Zheng, Dr. Jie Qin, Dr. Shipeng Luo, Dr. Qi Zhang, Dr. Naifu Hu, Dr. Guanghui Wang, Dr. Lucie Jarrige, Dr. Long Li, Dr. Xiaoqiang Huang, Dr. Jiajia Ma, Dr. Yuqi Tan, Dr. Zijun Zhou, Dr. Yubiao Hong, Dr. Peng Xiong, Yvonne Grell, Erik Winterling, Xiang Shen, Tianjiao Cui, Feng Han, Marcel Hemming, Lifang Zhao, Jiahui Lin, Xingwen Zheng and Wenjian Zhou. I really appreciate their kind help and cooperation.

Furthermore, I would like to thank all the collaborators from the chemistry department and other institutes. Thanks a lot to Dr. Xiulan Xie for assistant in NMR issues. Thanks a lot to Dr. Klaus Harms and Sergei Ivlev for the measurement and analysis of all the single crystals. Thanks a lot to Dr. Shuming Chen and Prof. K. N. Houk for the computational support for my publications.

I am very grateful to the Chinese Scholarship Council for providing me with the support to live and study in Germany.

Last but not the least, there aren't enough words to describe my gratitude to my dear wife and my son for their unconditional love and support. To my dear parents and sisters, thank them for their constant interest in my life and support for my career. I want to say that there is nothing I would ever rather do than spend time with any one of them, thank them for believing in me and I will do my best for my whole life.

Publications

Part of this work has already been published or submitted for publication:

1. **Chenhao Zhang**, Shuming Chen, Chen-Xi Ye, Klaus Harms, Lili Zhang, K. N. Houk, Eric Meggers, Asymmetric Photocatalysis via Intramolecular Hydrogen Atom Transfer in Photoexcited Catalyst-Substrate Complex. *Angew. Chem. Int. Ed.* **2019**, 58, 14462.
2. **Chenhao Zhang**, Anthony Z. Gao, Xin Nie, Chen-Xi Ye, Sergei Ivlev, Shuming Chen, Eric Meggers, Catalytic α -Deracemization of Ketones Enabled by Photoredox Deprotonation and Enantioselective Protonation. (submitted for publication)

Abstract

Hydrogen atom transfer (HAT) provides straightforward methods to generate open-shell radical intermediates from C-H bonds and offers unique opportunities for green and sustainable synthesis. Visible-light-induced C-H functionalization enabled by HAT is an emerging strategy for substrate activation in photocatalyzed organic synthesis. In recent years, photoinduced HAT reactions have seen substantial development of their versatility, efficiency, and selectivity. However, asymmetric photocatalysis via hydrogen atom transfer has rarely been reported.

In the first section, a visible-light-induced asymmetric rearrangement of 3-(2-formylphenyl)-1-pyrazol-1-yl-propenones to benzo-[d]cyclopropa[b]pyranones with up to > 99% ee is introduced, which is catalyzed by a bis-cyclometalated chiral-at-metal rhodium complex (**RhS**). Mechanistic experiments and DFT calculations support a mechanism whereby the photoexcited catalyst/substrate complex generates triplet excited-state species through photoinduced intersystem crossing, which triggers an intramolecular hydrogen atom transfer subsequent highly stereocontrolled hetero-Diels–Alder reaction. In this reaction scheme, the rhodium catalyst fulfills multiple functions by 1) enabling visible-light $\pi \rightarrow \pi^*$ excitation of the catalyst-bound enone substrate, 2) facilitating the hydrogen atom transfer, and 3) providing the asymmetric induction for the hetero-Diels–Alder reaction.

In the second section, a visible light driven deracemization of ketones as a new type of deprotonation and asymmetric protonation is demonstrated for the first time, which leads to the formation of chiral carbonyl compounds in an efficient way with high yield (up to 97%) and high enantioselectivity (up to 97%). This new photoinduced deprotonation process is achieved by single electron transfer (SET) and subsequent hydrogen atom transfer. A bis-cyclometalated chiral-at-metal rhodium complex (**RhInd**) is used as the photocatalyst to induce the redox process and is responsible for the asymmetric induction, while the amine acts as the single electron reductant, HAT reagent and proton source. This conceptually simple light-driven strategy of coupling a photoredox deprotonation with a stereocontrolled protonation serves as a blueprint for other deracemizations of ubiquitous carbonyl compounds.

Zusammenfassung

Wasserstoffatom-Transfer-Prozesse (HAT, *hydrogen atom transfer*) bieten nützliche Methoden zur Erzeugung offenschaliger Radikalintermediate aus C-H-Bindungen und ermöglichen einzigartige Wege für eine effiziente und nachhaltige Synthese. Die durch sichtbares Licht induzierte C-H-Funktionalisierung, die durch HAT ermöglicht wird, ist eine neuartige Strategie zur Substrataktivierung in der photokatalysierten, organischen Synthese. Obwohl die Vielseitigkeit, Effizienz und Selektivität von photoinduzierten HAT-Reaktionen in den letzten Jahren maßgeblich weiterentwickelt wurde, konnte nur selten über asymmetrische Photokatalyse durch Wasserstoffatom-Transfer berichtet werden.

Im ersten Abschnitt wird eine durch sichtbares Licht induzierte, asymmetrische Umlagerung von 3-(2-Formylphenyl)-1-pyrazol-1-yl-propenonen zu Benzo-[d]cyclopropa[b]pyranonen mit bis zu > 99% ee eingeführt, die durch einen bis-cyclometallierten, *chiral-at-metal* Rhodiumkomplex (**RhS**) katalysiert wird. Mechanistische Experimente und DFT-Rechnungen unterstützen einen Mechanismus, bei dem der angeregte Katalysator-/Substrat-Komplex durch photoinduziertes *intersystem crossing* eine Spezies im angeregten Triplett-Zustand erzeugt, die einen intramolekularen Wasserstoffatomtransfer und eine anschließende stereokontrollierte Hetero-Diels-Alder Reaktion auslöst. In dieser Reaktion erfüllt der Rhodium-Katalysator mehrere Funktionen: 1) Er ermöglicht die π - π^* -Anregung des Katalysator-gebundenen Enon-Substrates durch sichtbares Licht; 2) er erleichtert den Wasserstoffatom-Transfer und 3) er sorgt für die asymmetrische Induktion der Hetero-Diels-Alder Reaktion.

Im zweiten Abschnitt wird erstmals eine durch sichtbares Licht induzierte Deracemisierung von Ketonen über eine neue Art von Deprotonierung und anschließender asymmetrischer Reprotonierung gezeigt, die eine effiziente Synthese von chiralen Carbonyl-Verbindungen mit hoher Ausbeute (bis zu 97%) und hoher Enantioselektivität (bis zu 97%) ermöglicht. Dieser neuartige, photoinduzierte Deprotonierungs-Prozess wird durch eine Ein-Elektron-Übertragung (SET, *single electron transfer*) und anschließenden Wasserstoffatom-Transfer erreicht. Ein bis-cyclometallierter *chiral-at-metal* Rhodiumkomplex (**RhInd**) dient als Photokatalysator zur Induktion des Redoxprozesses und ist für die asymmetrische Induktion verantwortlich, während das Amin als Ein-Elektron-Reduktionsmittel, HAT-Reagenz und Protonenquelle fungiert. Dieses simple licht-induzierte Konzept der Kombination einer Photoredox-Deprotonierung mit einer stereokontrollierten Protonierung dient als Blaupause für andere Deracemisierungen von allgegenwärtigen Carbonyl-Verbindungen.

Table of Contents

Acknowledgements.....	I
Publications.....	III
Abstract.....	V
Zusammenfassung.....	VII
Table of Contents.....	IX
Chapter 1: Theoretical Part	1
1.1 Introduction.....	1
1.2 Photoinduced Intermolecular HAT Reactions	2
1.2.1 Direct Photoinduced HAT Catalysis	3
1.2.2 Indirect Photoinduced HAT Catalysis.....	9
1.2.2.1 N-Centered Abstractors	9
1.2.2.2 O-Centered Abstractors	14
1.2.2.3 S-Centered Abstractors.....	19
1.2.2.4 Halogen-Centered Abstractors.....	21
1.2.2.5 C-Centered Abstractors	25
1.3 Photoinduced Intramolecular HAT Reactions	26
Chapter 2: Results and Discussion.....	33
2.1 Asymmetric Photocatalysis by Intramolecular Hydrogen Atom Transfer in Photoexcited Catalyst/Substrate Complex	33
2.1.1 Research Background and Reaction Design	33
2.1.2 Initial Experiments and Reaction Development.....	34
2.1.3 Substrate Scope	35
2.1.4 Mechanistic Study.....	37
2.1.6 Conclusions	41
2.2 Catalytic α-Deracemization of Ketones Enabled by Photoredox Deprotonation and Enantioselective Protonation	43
2.2.2 Initial Experiments and Reaction Development.....	46
2.2.3 Substrate Scope	48
2.2.4 Mechanistic Study.....	51
2.2.5 Follow-up chemistry	56
2.2.6 Conclusions	57
Chapter 3: Summary and Outlook	59
3.1 Summary	59
3.2 Outlook	61
Chapter 4: Experimental Part.....	62
4.1 Materials and Methods.....	62
4.2 Asymmetric Photocatalysis by Intramolecular Hydrogen Atom Transfer in Photoexcited Catalyst-Substrate Complex	65
4.2.1 Synthesis of the Substrates.....	65
4.2.2 General Procedure.....	75
4.2.3 Experimental and Characterization Data of New Products.....	75
4.2.4 Mechanistic Experiments	88
4.2.5 Gram-Scale Reaction and Catalyst Recovery	90

4.2.6 Follow-Up Conversion.....	92
4.2.7 Single-Crystal X-Ray Diffraction Studies.....	92
4.3 Catalytic α-Deracemization of Ketones Enabled by Photoredox Deprotonation and Enantioselective Protonation	97
4.3.1 Synthesis of Substrates.....	97
4.3.2 General Procedure.....	119
4.3.3 Experimental and Characterization Data of the Products	122
4.3.4 Mechanistic Experiments.....	134
4.3.5 Follow-Up Chemistry.....	139
4.3.6 Single Crystal X-Ray Analysis of Compound (<i>R</i>)- 3I	144
Chapter 5: Appendices.....	147
5.1 List of Abbreviations	147
5.2 List of Figures.....	149
5.3 List of Tables	150
5.4 List of Organometallic Complexes.....	151
5.5 List of Organic Compounds.....	151
5.6 Enantiomeric Excess for Catalytic Reactions.....	155
5.7 List of NMR Spectra of New Complexes	220
Statement.....	321
Curriculum Vitae.....	322

Chapter 1: Theoretical Part

1.1 Introduction

In the past few years, there has been a resurgence of interest in visible-light photocatalysis, owing to its great potential for engineering chemical reactions under mild conditions. The visible-light-absorbing species (photocatalysts) can selectively be excited by visible light irradiation undergo single electron transfer or transfer their excited state energy to the substrate or reagent (**Figure 1**, right). The commonly employed photocatalysts are metal complexes or organic dyes that allow visible light as the irradiation source, making this type of catalysis more advantageous than using a harmful high-intensity light source to trigger the photoreaction reactants directly. After the photocatalyst is excited by visible light, the lowest singlet excited state can undergo an intersystem crossing to the long-lived triplet state, depending on the nature of the photocatalyst. These ground state compounds are poor oxidants and poor reductants, but upon excitation, the photocatalysts become strong oxidants and strong reductants in their excited state (**Figure 1**, left). As a result, this excited triplet-state photocatalyst can achieve single electron transfer (SET) through reductive quenching or oxidative quenching pathways, resulting in various radical ions or radicals. On the other hand, the excited triplet photocatalyst can also be quenched through energy transfer events (ET), generating relatively unstable triplet state substrates. The quenching pathway may vary for the same catalyst depending on the valence energies of the catalysts and the reactants (**Figure 1**, right).¹

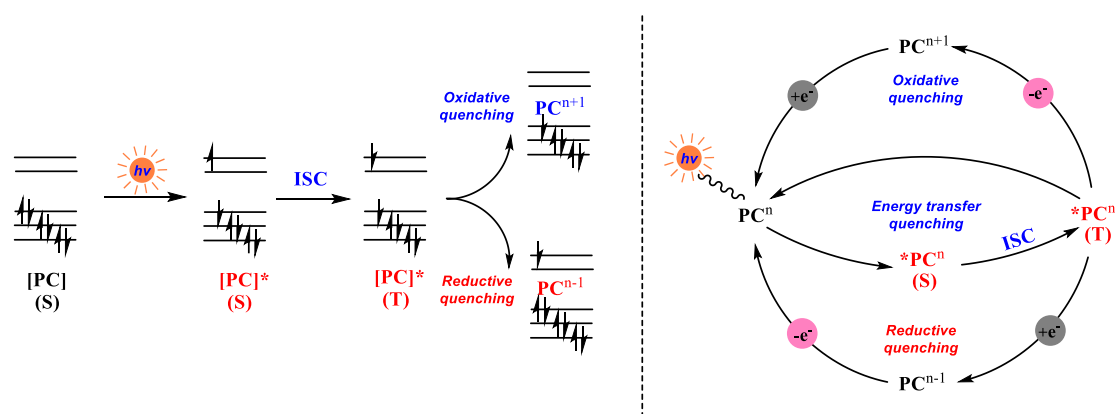


Figure 1. Photocatalysts possible quenching pathways. ISC = intersystem crossing.

It is well known that selective functionalization of the unactivated C–H bond is a continuous pursuit of synthetic organic chemists. Visible-light-mediated C–H activation has recently emerged as a powerful tool for the functionalization of C–H bonds. Hydrogen atom transfer (HAT) is a chemical transformation consisting of the concerted transfer of a proton and an electron from one to another in a single kinetic step.² Significantly, hydrogen atom transfer provides a versatile strategy for the activation of the substrate in photocatalyzed organic synthesis. Visible-light-induced catalysis combined with hydrogen atom transfer can serve as a unique tool for achieving new bond formation.³ Several methods operating via photoinduced intermolecular HAT^{3a,3c} or intramolecular HAT^{3b,3d} have been extensively reported

over the past few years. In these reactions, an excited photocatalyst is responsible for activating the reaction partners (leading to the formation of reactive intermediates) and then reverting to its original form, ready to start a new cycle.

1.2 Photoinduced Intermolecular HAT Reactions

Upon absorption of light, the activation of C–H bonds through photoinduced intermolecular HAT can occur according to four different kinds of reactivity. The first family of reactions is direct HAT catalysis, in which the excited state of the photocatalyst (PC*) directly abstracts a hydrogen atom from the R–H substrate. The second family of reactions involves indirect HAT catalysis, where PC* can be utilized to generate thermal hydrogen atom abstractor by interaction with a purposely added co-catalyst Y–W(H), by three different mechanisms. The first pathway is to take advantage of the intrinsic capability of excited states to act as oxidants or reductants. Accordingly, PC* can promote a single-electron-transfer step (SET), thus converting Y–W into the corresponding radical ion. On the one hand, the radical cation Y–W^{•+} is formed in the case of reductive quenching of the photocatalyst. On the other hand, PC* can undergo an oxidative quenching to produce the radical anion Y–W^{•-}. This intermediate might directly abstract a hydrogen atom from the substrate R–H or might undergo the loss of a charged moiety (W⁺ or W⁻) to give a hydrogen abstractor species Y[•]. An alternative option involves an energy-transfer step (ET) between PC* and Y–W. The resulting excited species Y–W* then undergoes the homolytic cleavage of a labile bond, again generating a thermal hydrogen abstractor (Y[•]) prone to activate R–H through HAT. Finally, PC* can promote a PCET with an additive Y–H, also involving a suitable base (B⁻). As a result, radical Y[•] is formed, and is in turn able to promote the desired HAT step (**Figure 2**).^{3a}

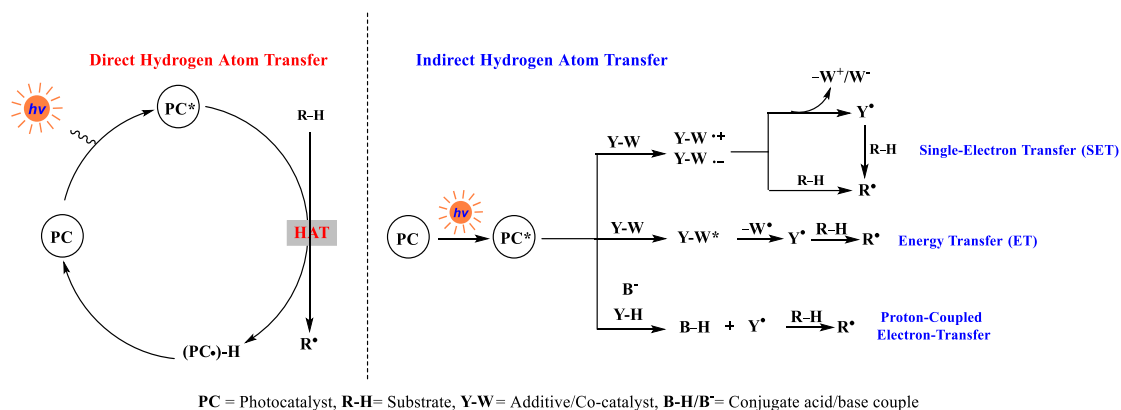


Figure 2. Substrate activation through photoinduced intermolecular HAT promoted through a direct or indirect photocatalytic approach.

The following section will highlight representative examples on the activation of R–H bonds through photoinduced intermolecular HAT. Some common HAT reagents were applied in these photocatalytic HAT reactions. **Figure 3** (left) shows some of the direct HAT photocatalysts used in direct HAT catalysis, and **Figure 3** (right) shows some of the indirect HAT reagents used in indirect HAT catalysis.

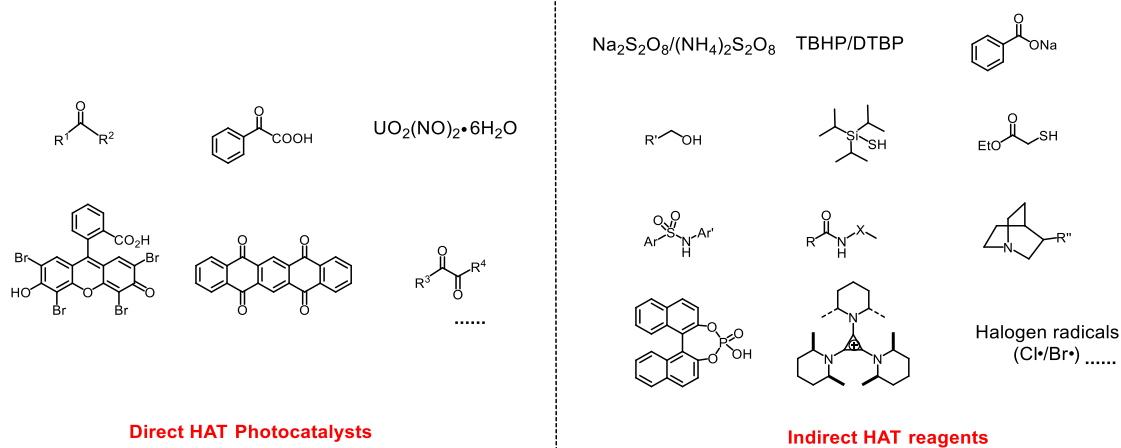


Figure 3. Representative direct HAT photocatalysts and representative indirect HAT reagents.

1.2.1 Direct Photoinduced HAT Catalysis

Upon excitation with light, carbonyl compounds can undergo rapid and efficient intersystem crossing. As a result, carbonyl compounds are often used as photocatalysts for photoinduced direct HAT chemistry. The capability of triplet aromatic ketones to abstract a hydrogen atom has been known since the birth of photochemistry. In 2015, Inoue group reported an interesting enantioselective radical alkylation reaction carried out in the presence of benzophenone and chiral ethynyl sulfoximine under irradiation with a medium-pressure lamp. In this reaction, the C(sp³)-H bond in a protected amine was alkylated with good enantiomeric excess. The chirality in the sulfoximine was efficiently transmitted to the alkyne products, while the chiral sulfonylimine acted as a traceless chiral auxiliary group. The stereochemical output was interpreted based on the preferential formation of the transition state, in which the hydrogen bonding between HN=S and HNBoc was stronger than that between O=S and HNBoc, resulting in a favored transition state and gave the S configuration as the primary product **Figure 4**.⁴

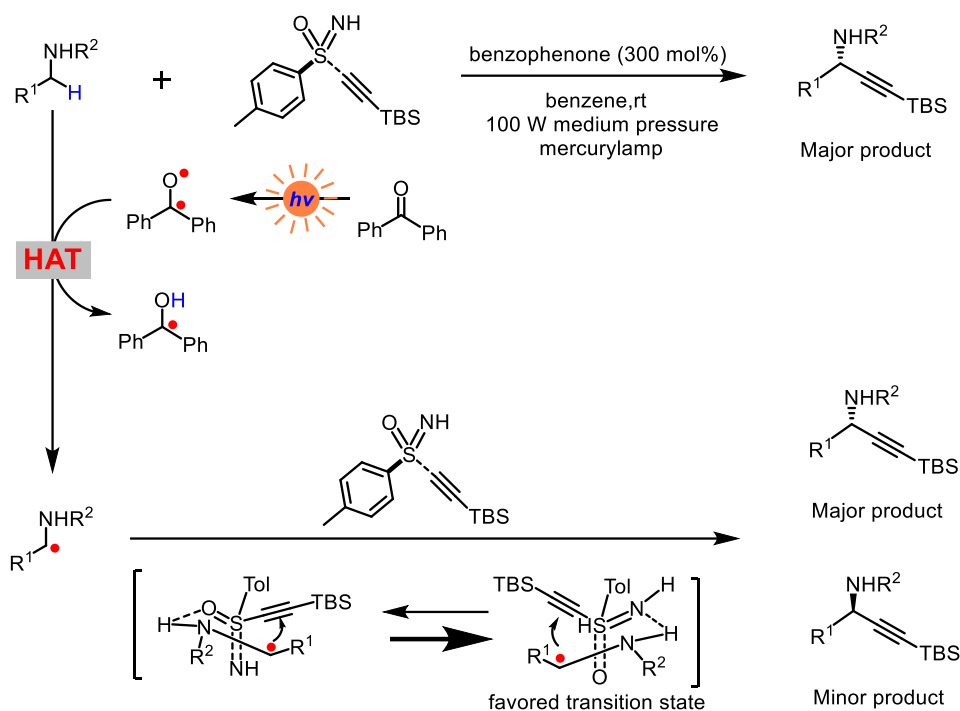


Figure 4. Photoinduced enantioselective alkynylation of $C(sp^3)$ -H bonds, TBS = *tert*-butyldimethylsilyl.

In 2018, Martin and coworkers designed a catalytic platform that employs a synergistic combination of nickel and diaryl ketone for the cross-coupling of unactivated $C(sp^3)$ -H bonds with aryl or alkyl bromides under visible light irradiation, in which the triplet diaryl excited ketones act as both direct HAT and SET catalysts. Mechanistically, the carbon radical would be generated upon HAT from the triplet excited species along with the formation of a ketyl radical. Concurrently, oxidative addition of low-valent Ni(0) into the aryl or alkyl halides would produce an electrophilic nickel(II) complex. The Ni(II) complex captures the alkyl radical rapidly and might afford a discrete Ni(III) species, which would deliver the targeted C-H functionalization product and the Ni(I) intermediate through reductive elimination. Finally, the two catalytic cycles could be interfaced under basic conditions by a final SET from the ketyl radical to the Ni(I) intermediate, thus recovering both the diaryl ketone and the Ni(0) catalysts (Figure 5).⁵

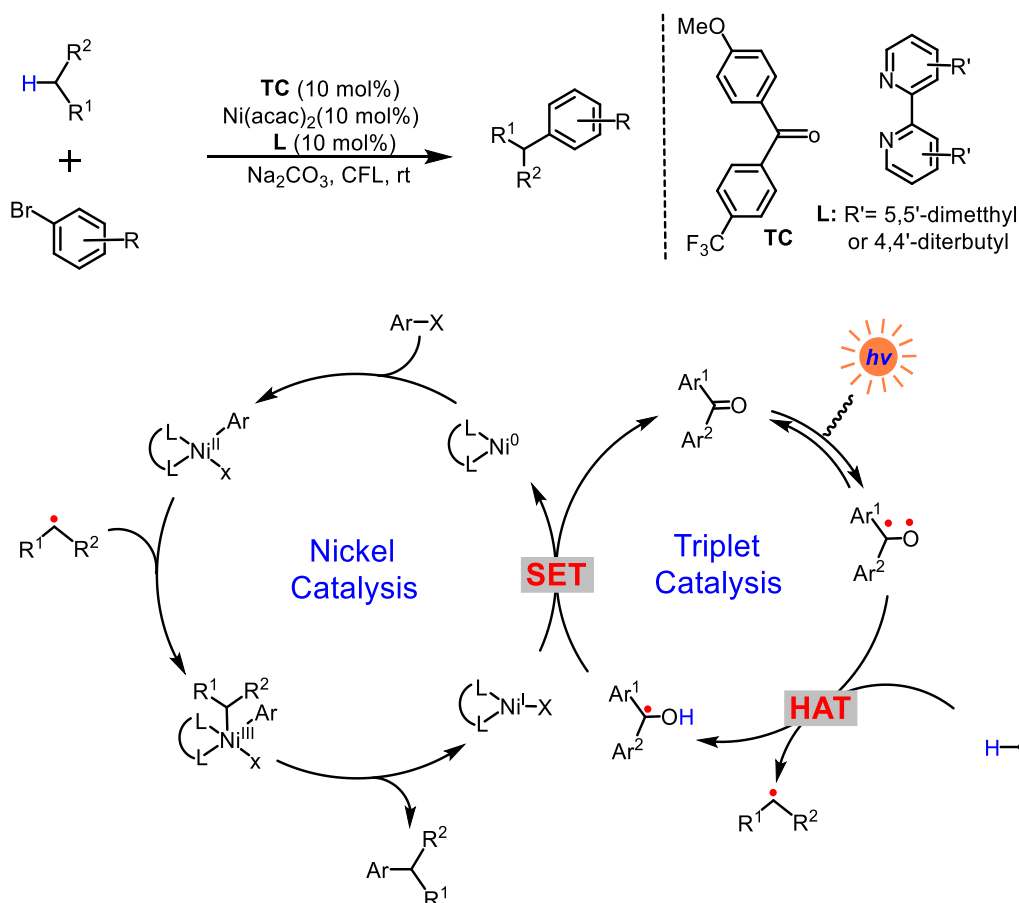


Figure 5. sp³ C–H arylation and alkylation enabled by the synergy of triplet excited ketones and nickel catalysts.

In 2019, Gong and coworkers demonstrated a photoinduced asymmetric C(sp³)-H functionalization of benzylic, allylic hydrocarbons and unactivated alkanes by using the dual a direct HAT photocatalyst (5,7,12,14-pentacenetrone) with a tunable chiral catalyst of metal (BOX-M where M = Cu or Co and BOX = chiral bisoxazoline) under blue-light irradiation (**Figure 6**).⁶ The authors proposed that the excited 5,7,12,14-pentacenetrone abstracts a hydrogen atom from the unactivated C(sp³)-H bond, generating the carbon radical and semiquinone-type radical. At the same time, the imine substrate coordinates with the chiral metal catalyst to give the intermediate, followed by a SET with the semiquinone-type radical to close the photocatalytic cycle and give the metal-stabilized carbon radical. Subsequently, the intermediate complex was obtained by cross-coupling. Finally, protonation and ligand substitution give the product with regeneration of the coordinated imine.

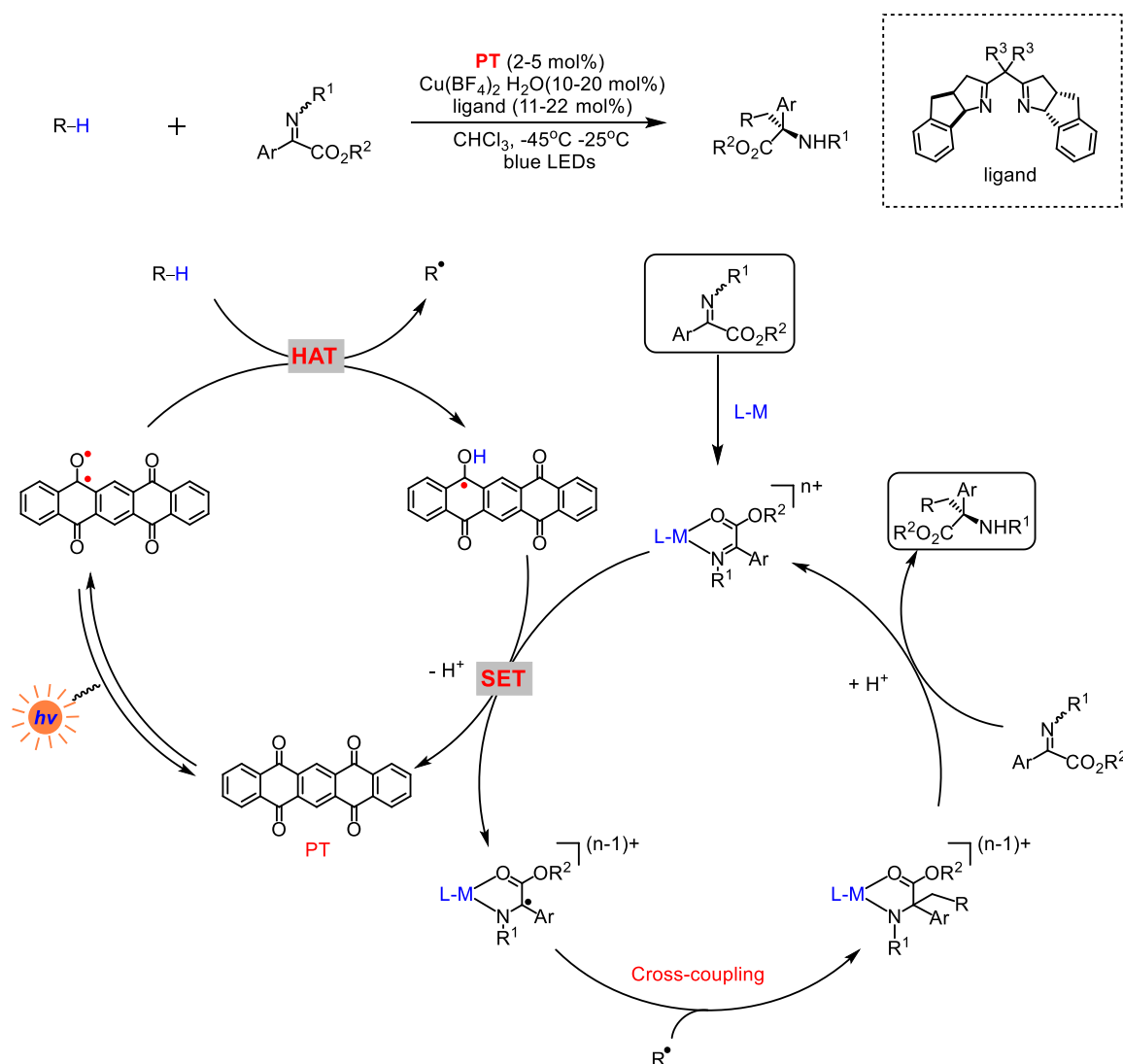


Figure 6. Proposed mechanism for selective $C(sp^3)$ -H functionalization.

Eosin Y is a metal-free and readily available organic dye, which is a well-known organic photocatalyst for visible-light-driven SET-based transformations. However, inspired by the structural features of eosin Y, the groups of Wang⁷ and Wu⁸ have recently made a breakthrough in discovering new activation modes of photoexcited eosin Y in 2018. They found that excited neutral eosin Y can serve as a direct hydrogen atom transfer (HAT) catalyst. After the excited neutral eosin Y abstracts a hydrogen atom, the photocatalytic cycle subsequently proceeds through a reverse hydrogen atom transfer (RHAT) to one of the intermediates generated in the reaction. In 2020, Wu and co-workers expanded their C-H functionalization protocol using neutral eosin Y as a direct HAT photocatalyst on radical Smiles rearrangement. The final product was obtained by visible light direct HAT photocatalysis, 1,4-addition, Smiles rearrangement, 5-endo-trig cyclization and reverse hydrogen atom transfer processes. (**Figure 7**).

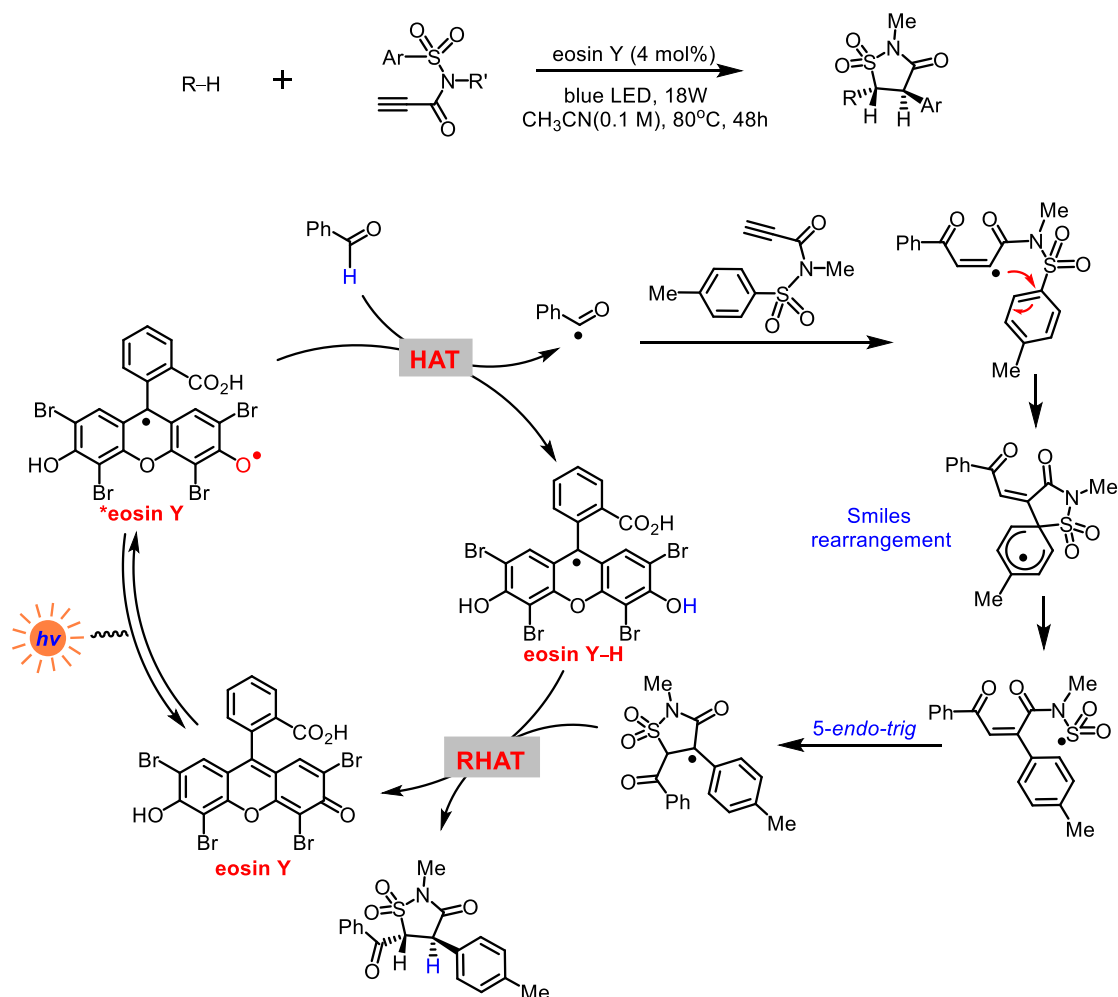


Figure 7. A radical Smiles rearrangement promoted by neutral eosin Y.

Organofluorine compounds are an important class of molecules that are widely used in various fields. However, the formation of C–F bonds is commonly associated with large kinetic barriers. In 2016, Sorensen and coworkers reported a novel photocatalytic system for C–H fluorination of the unactivated alkanes, which employed $\text{UO}_2(\text{NO}_3)_2 \cdot 6\text{H}_2\text{O}$ as a direct HAT photocatalyst to promote $\text{C}(\text{sp}^3)\text{--H}$ bond fluorination reaction under visible light irradiation.⁹ Upon absorption of light, $[\text{UO}_2]^{2+*}$ abstracted a hydrogen atom to generate an alkyl radical, which then interaction with electrophilic fluorinating reagent *N*-fluorobenzenesulfonimide (NFSI) to form the desired C–F bond. The radical of NFSI returns the photoreduced HAT catalyst to regenerate the catalyst to undergo further reaction (**Figure 8**).

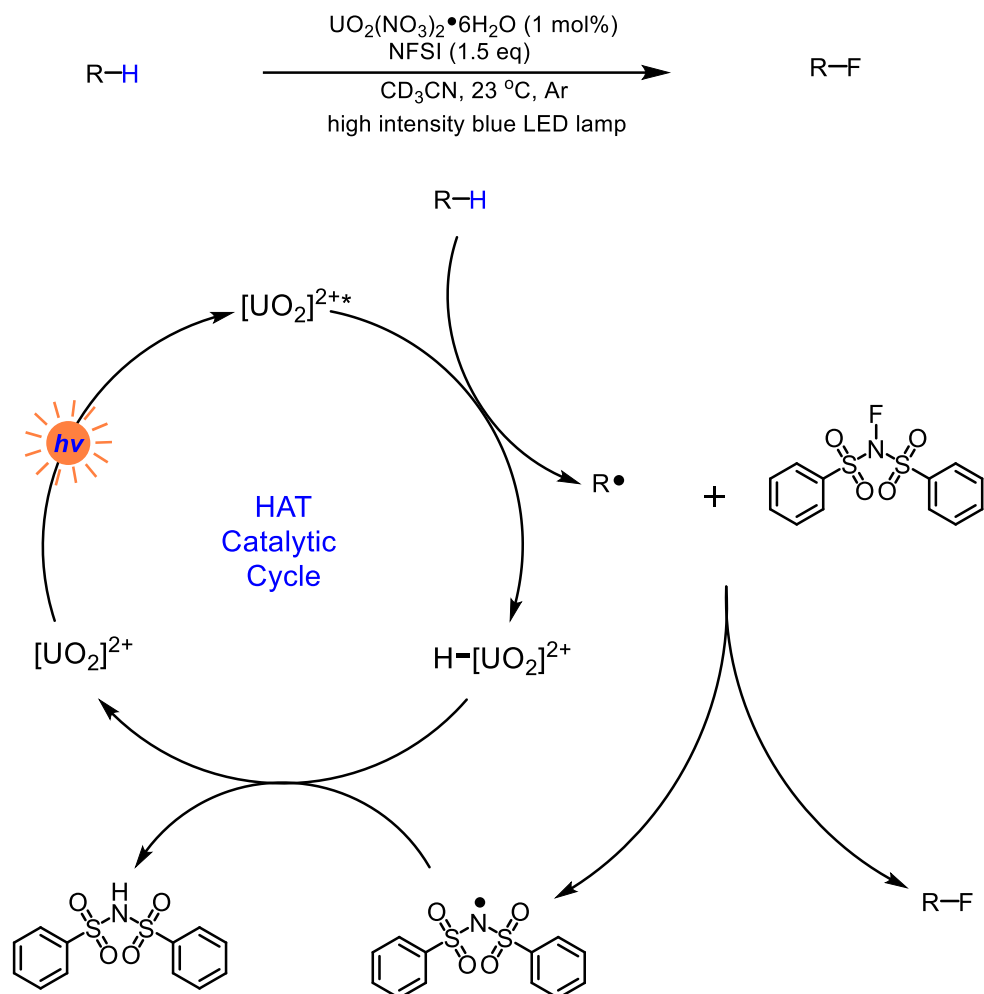


Figure 8. The fluorination of unactivated C(sp³)-H by UO₂²⁺ and NFSI.

In 2019, Li and co-workers reported an interesting metal-free photoinduced HAT Minisci reaction, which is carried out simply by visible light irradiation of diacetyl in the presence of TFA (**Figure 9**).¹⁰ Diacetyl is a cheap, visible-light-sensitive ketone that absorbs in the 380–460 nm region. The authors propose that diacetyl acts as a direct HAT photosensitizer, which is competent at performing HAT on certain ethers possessing easily cleavable α-C-H bonds. A plausible mechanism was proposed in which excited diacetyl abstracts a hydrogen atom from the ether to generate the alkyl radical, which successfully coupled with the electron-deficient heteroarenes to give a neutral radical intermediate. Then the neutral radical intermediate is oxidized by ketyl radical with an accompanied proton transfer, giving the Minisci product together with acetoin as the byproduct.

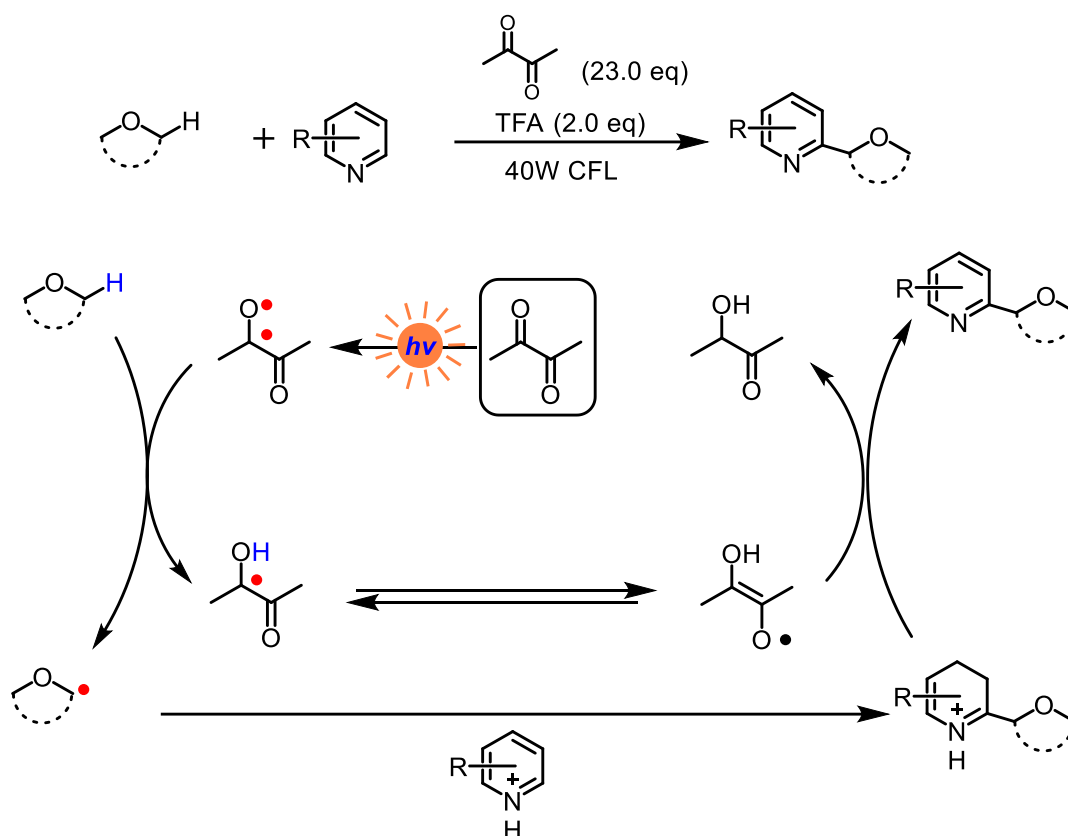


Figure 9. Diacetyl as a direct HAT photosensitizer in Minisci alkylation.

1.2.2 Indirect Photoinduced HAT Catalysis

1.2.2.1 N-Centered Abstractors

In recent years, a series of pioneering and groundbreaking discovery in photoredox C(sp³)–H HAT-type functionalization were reported by MacMillan group. In 2015, Macmillan and co-workers were successfully developed a strategy for the selective alkylation of α -hydroxy C–H bonds with Michael acceptors (**Figure 10**).¹¹ In this reaction, both a quinuclidine HAT catalyst and a phosphate hydrogen bonding catalyst are required to achieve selective functionalization of α -hydroxy C–H bonds. Interestingly, tetra-n-butylammonium phosphate act as a key additive to make the alcohol α -C–H more hydridic, via formation of a hydrogen bond between the phosphate acceptor and the hydroxyl group of the alcohol. As a result, the highly electrophilic nitrogen radical cation formed via single electron oxidation of quinuclidine can readily abstract the activated α - alcohol C–H bond to form a carbon radical. The resultant carbon radical is highly nucleophilic and is readily trapped by electron-deficient alkenes, Subsequent single electron reduction and cyclization affords the lactone product.

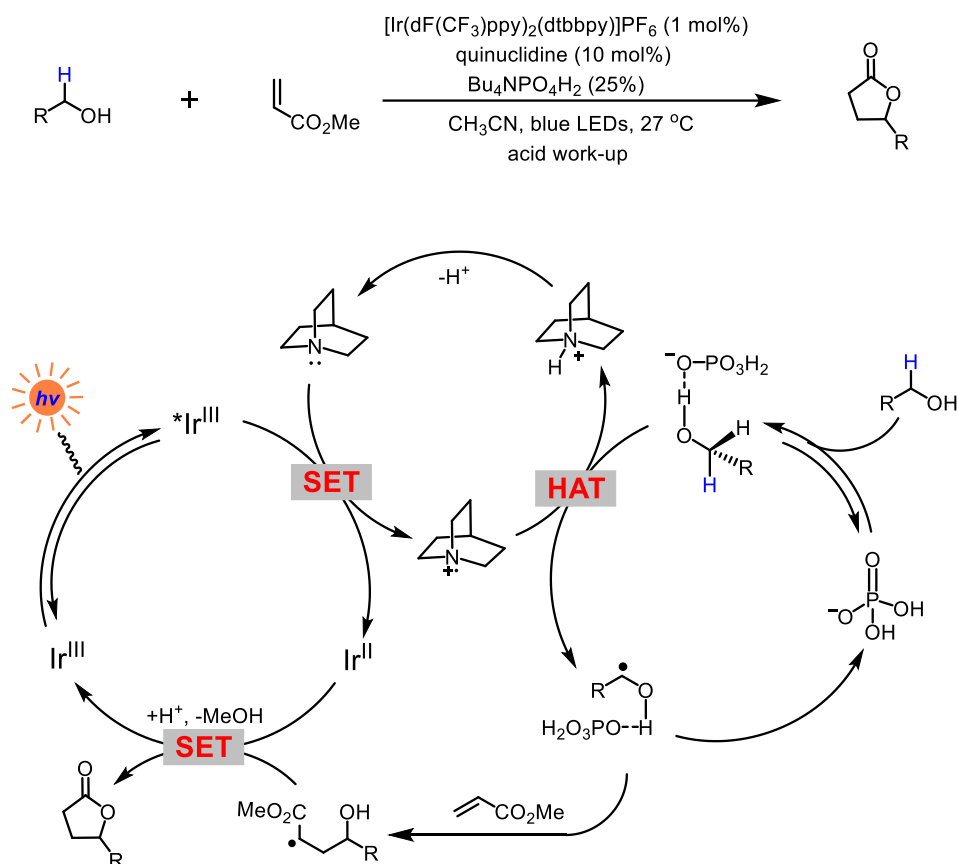


Figure 10. Photoinduced C–H alkylation of alcohols.

The photoinduced indirect HAT process could also be merged with transition metal-catalyzed cross-coupling reactions. In 2016, Macmillan and co-workers developed a unique coupling of α -amino, α -ether, and benzylic C–H bonds with aryl halides using a combination of an Ir photocatalyst, 3-acetoxyquinuclidine, and a Ni complex (**Figure 11**).¹² In this catalytic system, a stoichiometric amount of 3-acetoxyquinuclidine was utilized as the HAT catalyst to generate the carbon radicals. The photoexcited *Ir(III) catalyst were quenched by 3-acetoxyquinuclidine to generate an amino radical cation, which to accomplish hydrogen atom abstraction from a diverse range of substrates. Given the reactive carbon-centered radicals, subsequently entered the nickel catalytic cycle and reacted with the Ni(II) complexes, which were generated from oxidative addition of Ni(0) to the aryl bromide. After reductive elimination provide the cross-coupled product. A final SET between Ni(I) and reduced photocatalyst closes these two catalytic cycles.

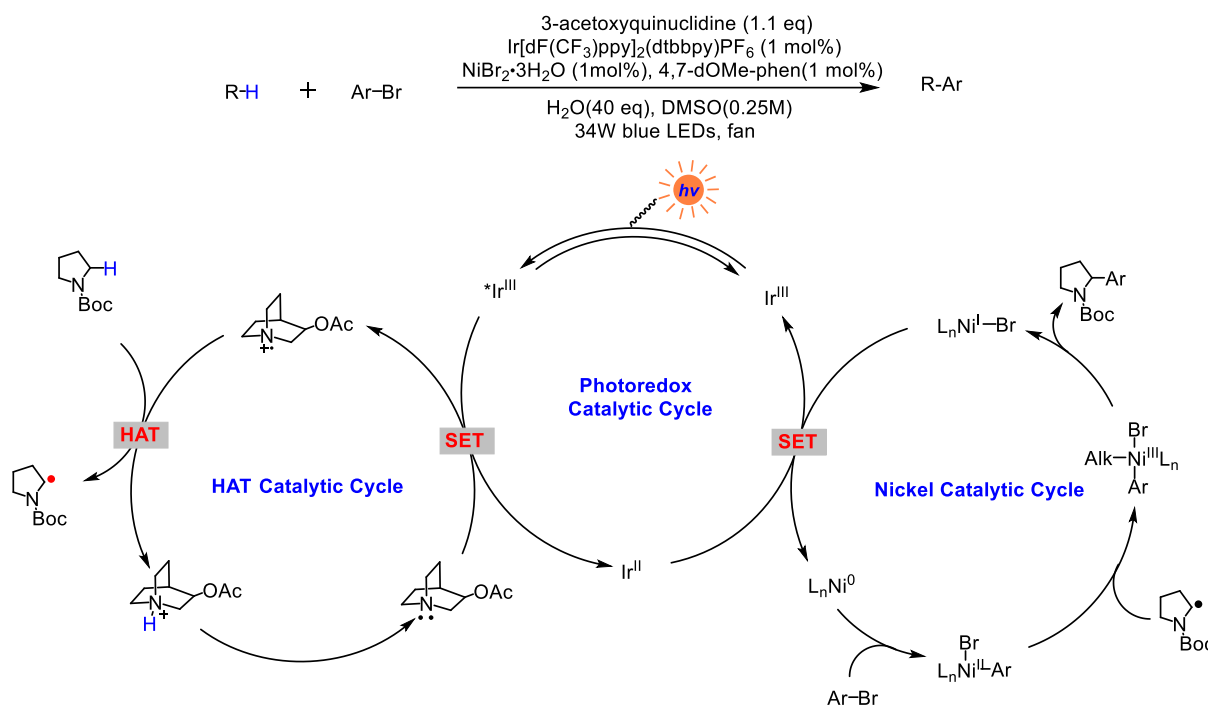


Figure 11. Photoinduced C–H arylation through photoredox, quinuclidine, and nickel catalysis.

Amides and sulfonamides can serve as source of N-centred radicals for hydrogen atom transfer. Typically, these compounds are conveniently deprotonated by weak bases and the resulting anions can be oxidized by the excited photocatalysts. In 2016, the Knowles group¹³ demonstrated that the N–H bond in amides can be activated through proton-coupled electron transfer mechanism involving an excited photocatalyst and a base (tetrabutylammonium dibutyl phosphate) to give the corresponding nitrogen-centered radical. The nitrogen-centered radical can act as a hydrogen abstractor to generate the carbon-centered radicals in alkanes, ethers, and protected amines. and ensuing addition onto electron-poor olefin. The authors propose a catalytic cycle wherein the phosphate base associate to the N–H bond of N-ethyl-4-methoxybenz-amide via hydrogen bonding. Upon excitation with light, oxidation of this hydrogen-bond complex by the excited photocatalyst would result in formal homolysis of the strong N–H bond via concerted PCET to give a neutral amidyl radical. Amidyl radical was in turn able to abstract a hydrogen atom from the substrates to give carbon-centered radicals and then trapping by an electron-deficient olefin partner to furnish a new C–C bond and an α -carbonyl radical. The electron transfer from the reduced Ir(II) to this electrophilic radical will generate an enolate anion, which is subsequently protonation by phosphoric acid to give the final product and return both catalysts to their active forms (**Figure 12**).

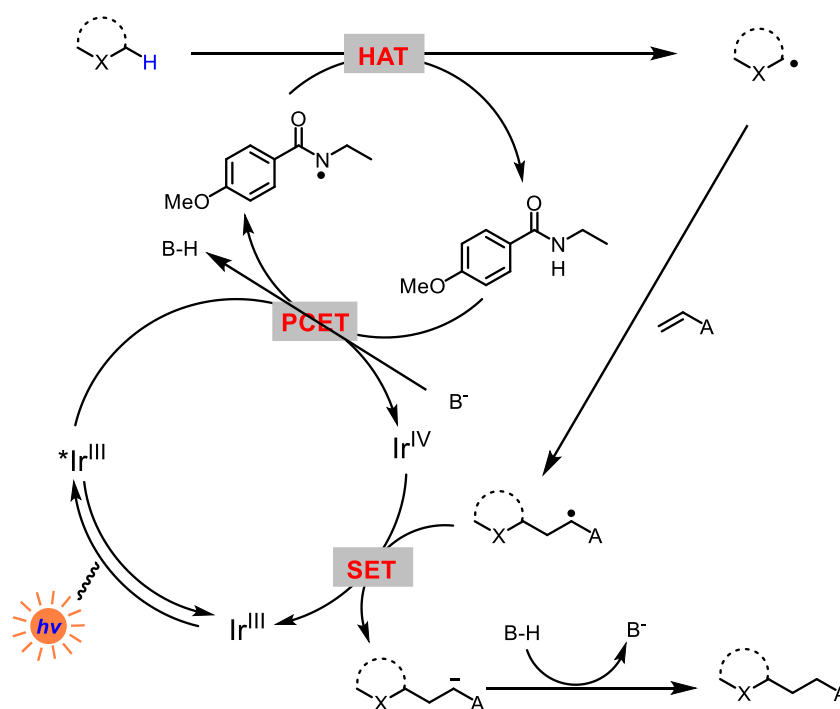
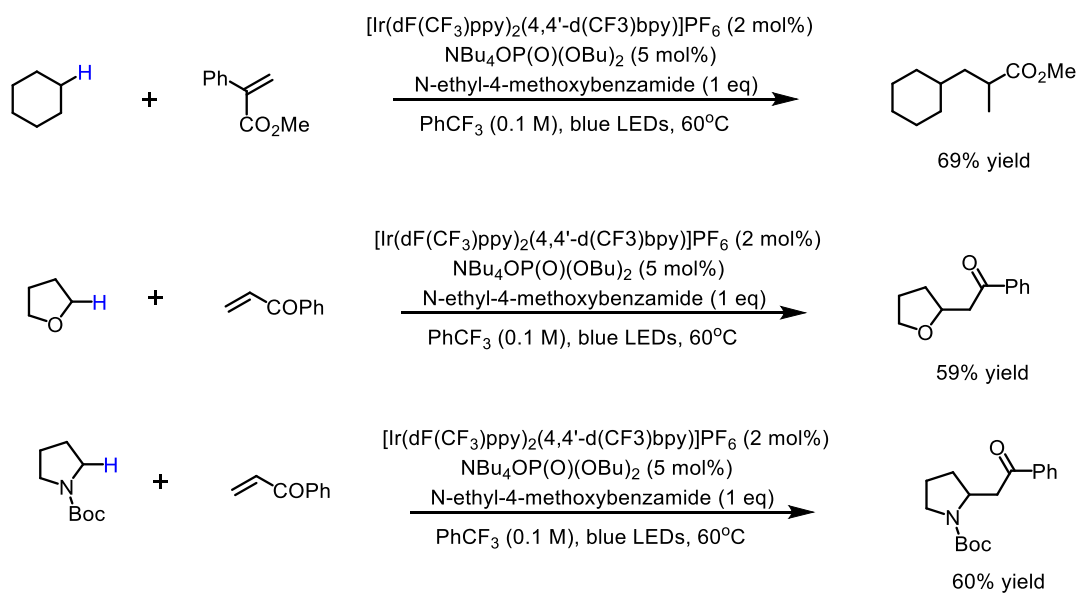


Figure 12. C–H activation in alkanes through the action of photogenerated amidyl radical.

In 2018, Kanai and co-workers demonstrated that sulfonamides can function as novel HAT catalysts applicable to allylic or benzylic C–H arylations (**Figure 13**).¹⁴ The authors propose that the deprotonated sulfonamide could be readily oxidized by the excited photocatalyst to afford the sulfonamidyl radical behaving as a hydrogen atom transfer (HAT) agent. The alkyl radical intermediate is then generated by the HAT process, which reacted with the reduced radical anion of the starting 1,4-dicyanobenzene to afford the desired C–H arylation product after the elimination of a cyanide ion.

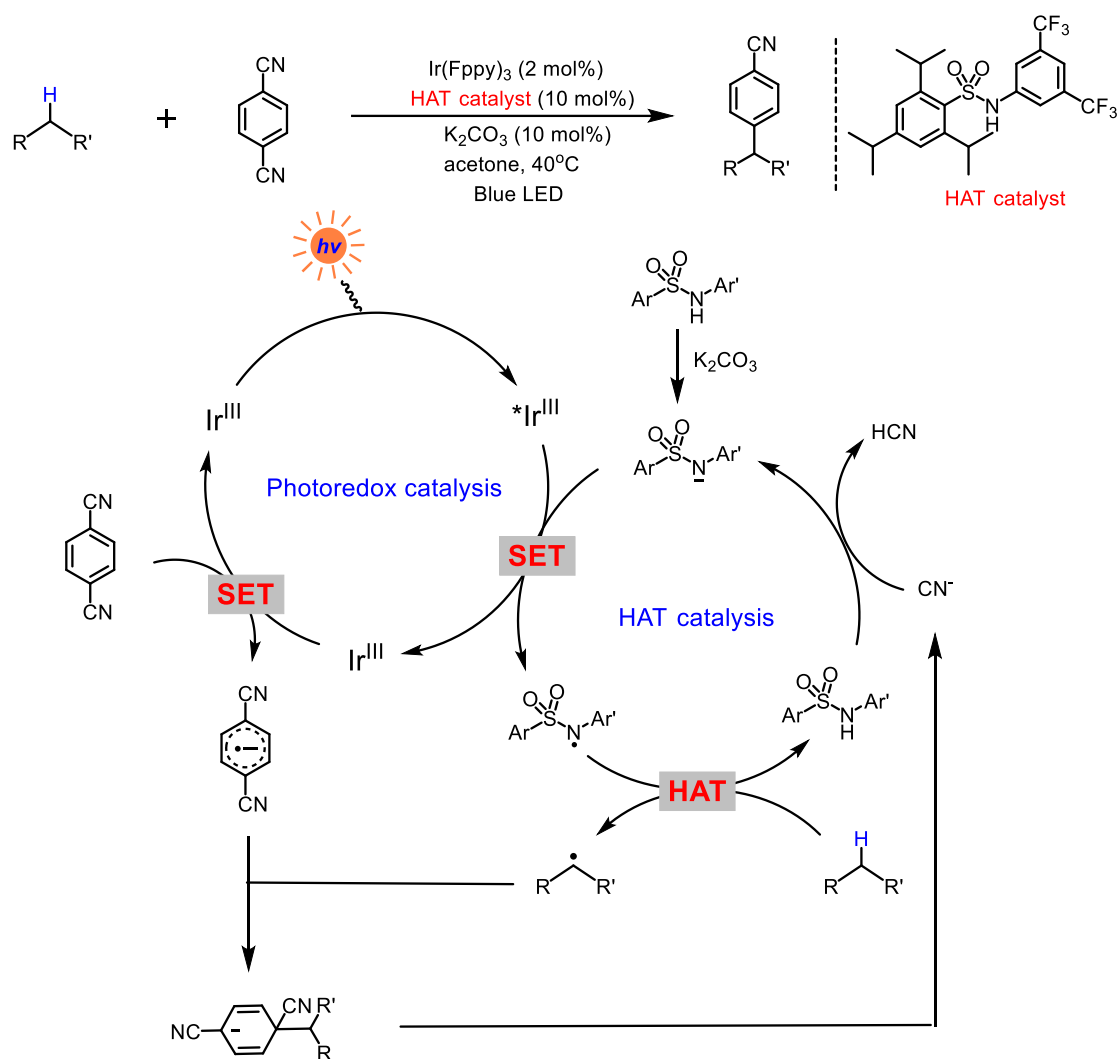


Figure 13. Arylation of $\text{C}(\text{sp}^3)\text{-H}$ bonds through the action of photogenerated sulfonamidyl radical.

In 2020, Lambert and coworkers reported a trisaminocyclopropenium cation (TAC) as an electrophotocatalyst for oxidant-free coupling of ethers with isoquinolines, alkenes, alkynes, pyrazoles, and purines selectively at the less-hindered α position (**Figure 14**).¹⁵ In this catalytic system, the colorless TAC was converted by anodic oxidation at mild potential to generate a radical dication, which upon excitation with visible light, affords an extremely oxidizing excited state. Photoexcitation then leads to an intermediate bearing aminyl radical cation character. Hydrogen atom transfer from the ether substrate generates the corresponding carbon radical along with the protonated TAC. The carbon radical readily reacts with isoquinoline to produce an intermediate radical, and this was followed by a second single electron oxidation and deprotonation to furnish the product. Meanwhile, deprotonation of the dication regenerates the catalyst.

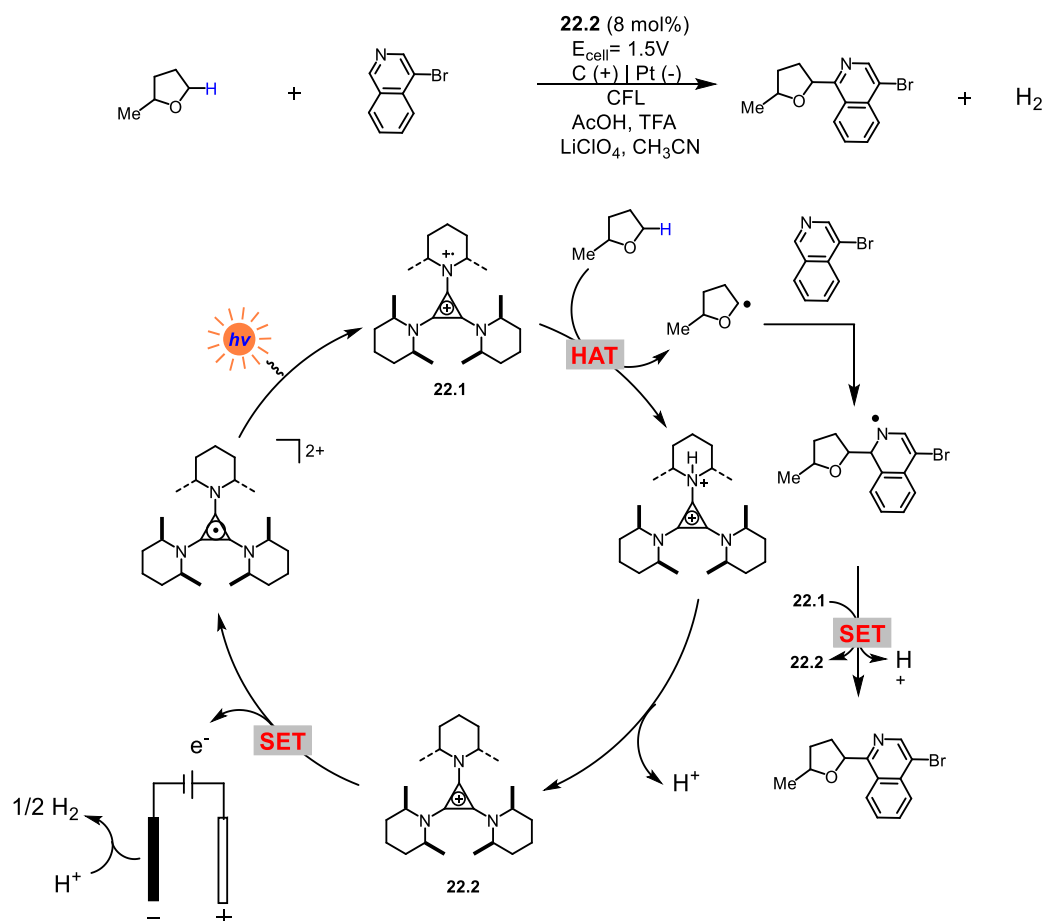


Figure 14. Electrophotocatalytic arylation of ether.

1.2.2.2 O-Centered Abstractors

It is well established that the direct oxidation of ethers is challenging due to their high oxidation potentials and can be difficult to achieve using most photocatalysts. In 2014, MacMillan and coworkers developed a new approach to the direct α -arylation of cyclic and acyclic ethers with heteroarenes via a photoredox-mediated C–H functionalization pathway (Figure 15).¹⁶ The authors proposed that $\text{S}_2\text{O}_8^{2-}$ was used as an oxidant via single electron reduction to generate a sulfate radical anion ($\text{SO}_4^{\cdot-}$), which can abstract a hydrogen atom from the ether to afford the α -oxyalkyl radical. The high reactivity of sulfate radical anion allowed for a range of cyclic and acyclic ethers to be used as radical precursors. This α -oxyalkyl radical reacted with the protonated heteroarene and formed the amine radical cation, which transformed into the α -amino radical via deprotonation. The radical intermediate on single electron transfer to the PC (IV) regenerated the PC (III) and the product. In addition to the functionalization of ethers, photogenerated sulfate radical anions have also been used to activate α -amides and formyl and methylene C–H bonds.

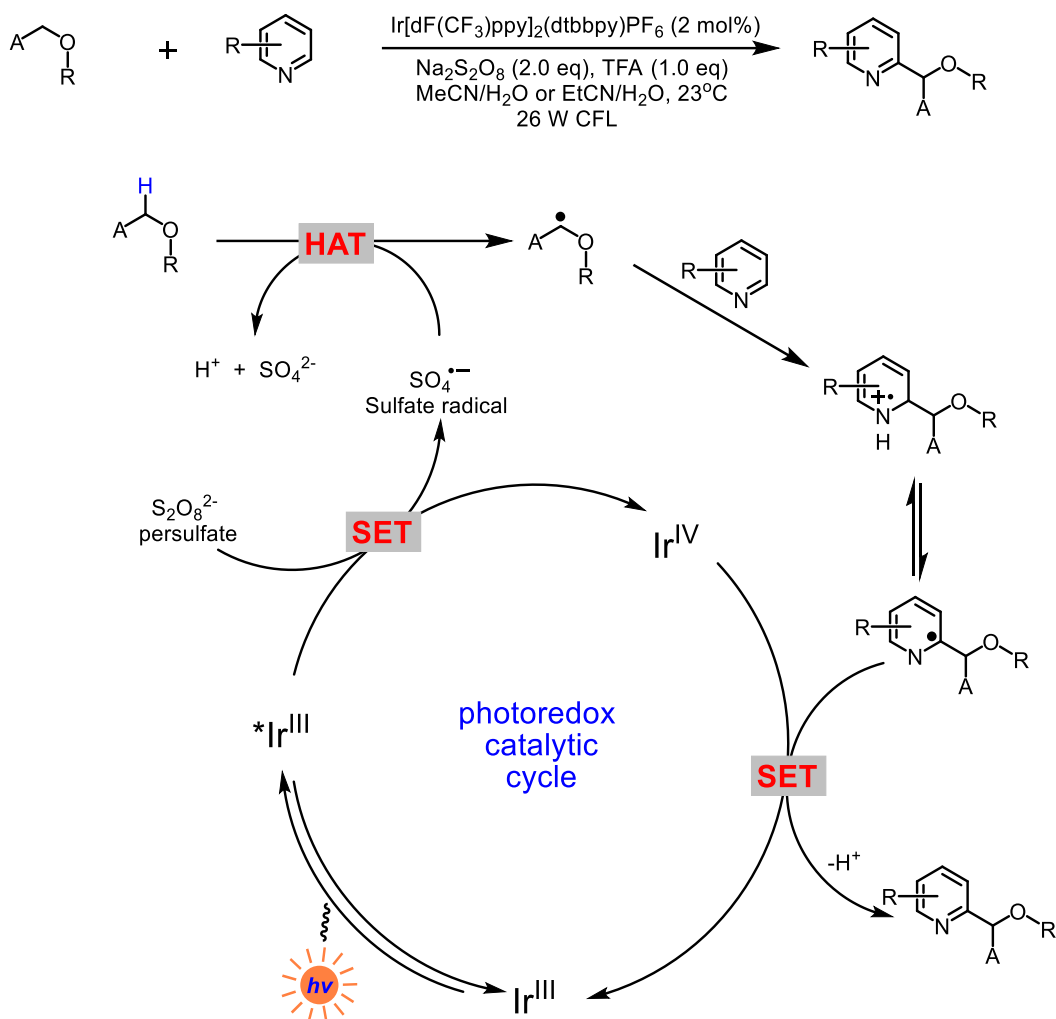


Figure 15. Photoinduced arylation of ethers using persulfate as an indirect HAT reagent.

In 2015, König and coworkers demonstrated that nitrate radicals could be easily accessed from nitrate anion by visible light photoredox catalysis using a purely organic dye as the catalyst and oxygen as the terminal oxidant (**Figure 16**).¹⁷ Nitrate radical can oxidize substrates by hydrogen atom abstraction, which was applied to the aerobic oxidation of alcohols.

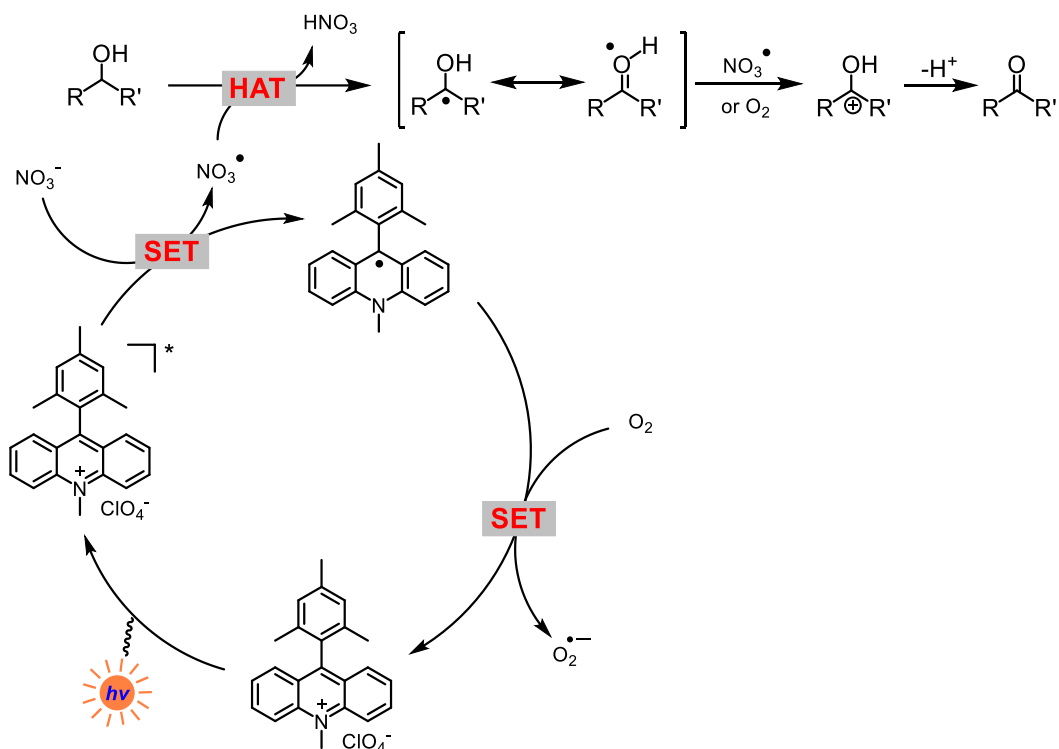


Figure 16. The nitrate radical induced oxidation of alkenes and alcohols.

In 2015, Wang and coworkers studied the combined effect of $Ru(bpy)_3Cl_2$ as photocatalyst, tert-butyl hydroperoxide (TBHP) as oxidant, a HAT precursor and an oxygen source for single step oxidative coupling of aldehydes and styrenes to yield α,β -epoxy ketones (**Figure 17**).¹⁸ The reaction mechanism is depicted in Scheme and involved the activation of TBHP by the excited $Ru(II)$ transferring electron to TBHP, forming tert-butoxyl radical, which in turn abstract the hydrogen atom from aldehyde to form *t*-BuOH and benzoyl radical. The benzoyl radical gets trapped by alkenes to give radical intermediate, which undergoes radical-radical cross coupling with tert-butyl peroxide radical to yield the target product.

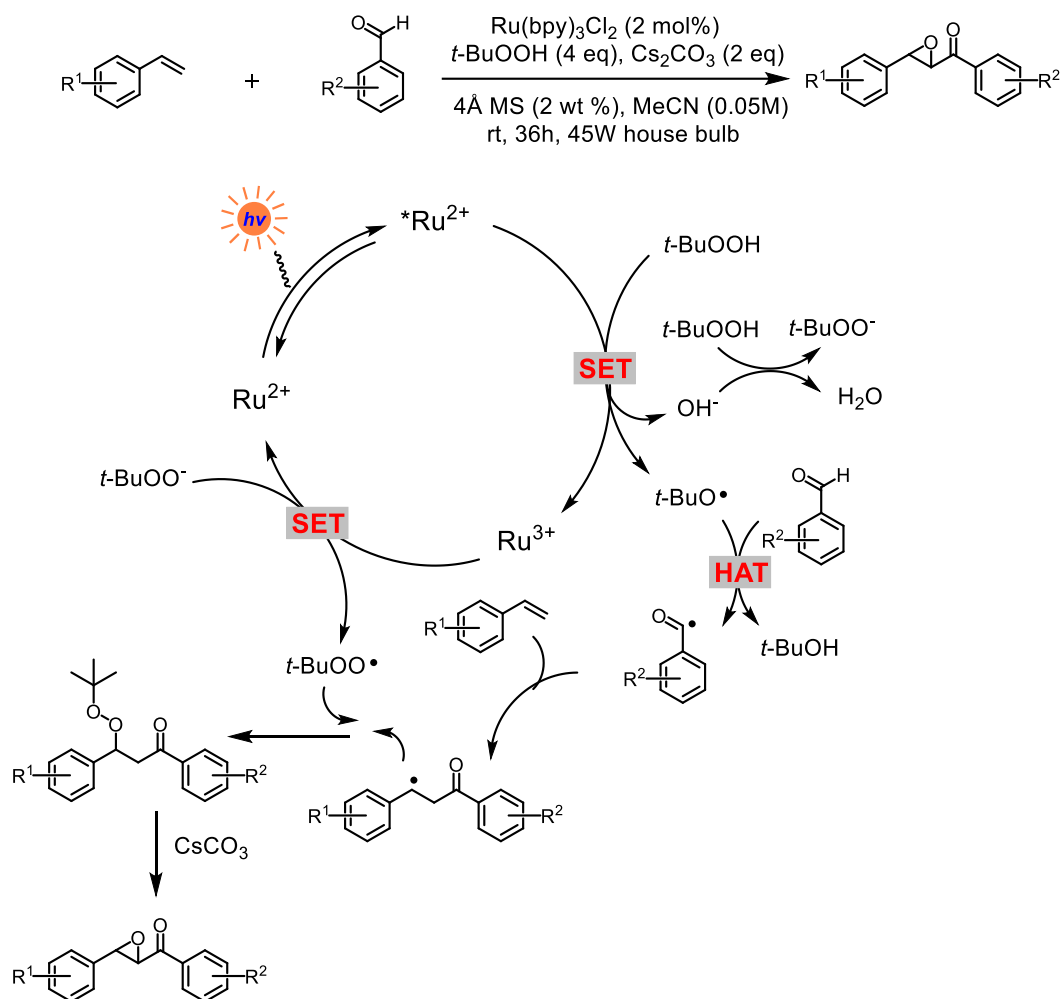


Figure 17. The difunctionalization of simple alkenes for the synthesis of α,β -epoxy ketones

In 2016, Glorius and coworkers reported a photoredox-mediated hydrogen atom transfer catalysis for the selective activation of unactivated $\text{C}(\text{sp}^3)\text{-H}$ bonds, followed by their selective trifluoromethylthiolation of several alkyl compounds, which can be accomplished with high selectivity in good yields (**Figure 18**).¹⁹ Benzoate salts used as precursor of benzoyloxy radical (PhCOO^\cdot), which acted as HAT reagent formed upon electron transfer with the excited Ir catalyst. The benzoyloxy radical that formed was highly electrophilic and could abstract a hydrogen atom from the tertiary C-H bond, while the alkyl radical reacts with the electrophilic trifluoromethylthiolating reagent Phth-SCF_3 gave the desired product R-SCF_3 along with a phthalimide radical (Phth^\cdot). Oxidation of the reduced photoredox catalyst with Phth^\cdot via single-electron transfer would regenerate the photocatalyst and Phth^- . Finally, Phth^- deprotonates benzoic acid to regenerate the benzoate salt and completes the catalytic cycle.

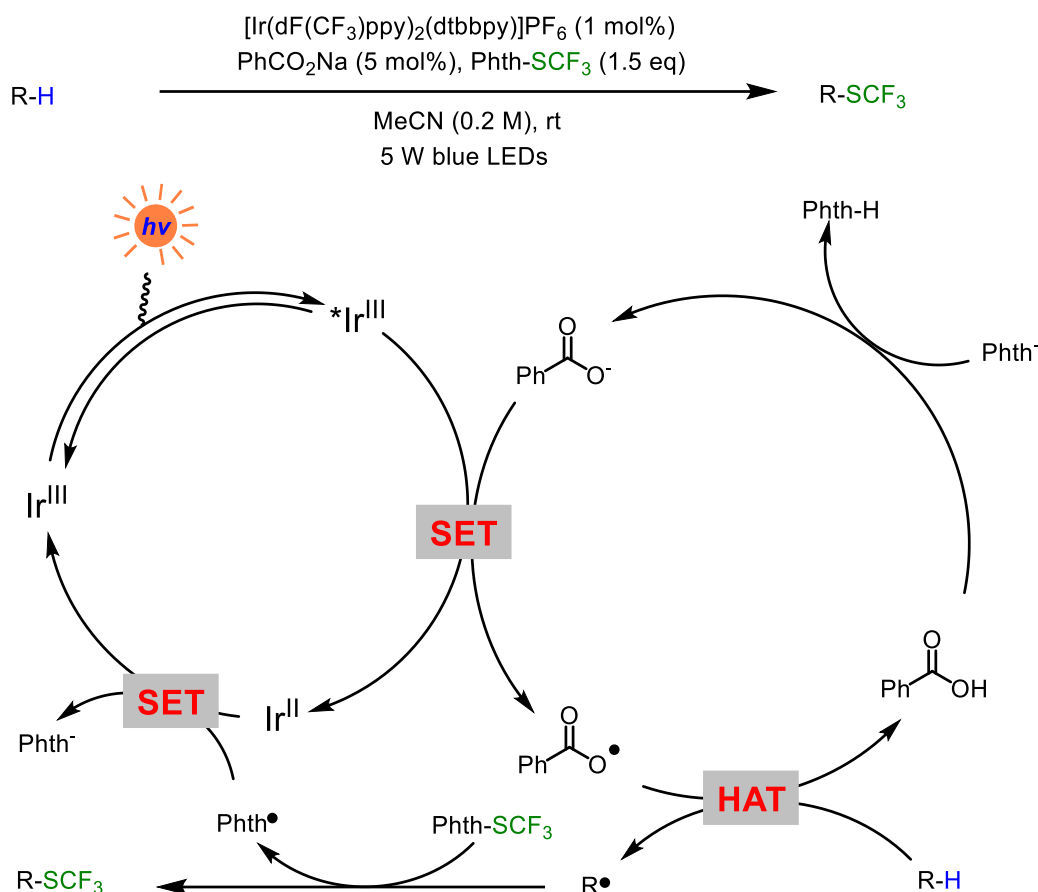


Figure 18. Photoinduced $\text{C}(\text{sp}^3)\text{-H}$ trifluoromethylthiolation using benzoate salt as an indirect HAT catalyst.

The alkoxy radical is an important reactive intermediate in organic synthesis and its highly reactive character enables unactivated C-H bond functionalization with the hydrogen atom transfer (HAT) reactivity. Abundant free alcohols are ideal precursors for alkoxy radicals, but direct generation of alkoxy radicals from alcohols is a formidable challenge due to the high oxidation potential of alkoxides and the high bond dissociation energy (BDE) of O-H bond of alcohols. In 2018, Zuo and co-workers reported the photocatalytic properties of Ce^{III} chloride complexes for C-C bond-cleavage and the functionalization of methane, ethane, and higher alkanes via ligand-to-metal charge-transfer (LMCT) generation of alkoxy radicals (**Figure 19**).²⁰ The authors proposed mechanism that a Ce^{IV} -alkoxy complex, generated in situ from alcohol and a Ce^{IV} salt, undergoes photoinduced LMCT to generate the electrophilic alkoxy radical and a reduced Ce^{III} species. The alkoxy radical then abstracts a hydrogen atom from the alkane to generate the carbon-center radical, which readily couples with the electron-deficient azo compound to give the radical species. Single electron reduction of the resulting radical intermediate by reduced Ce^{III} regenerates Ce^{IV} and furnishes the target product after protonation.

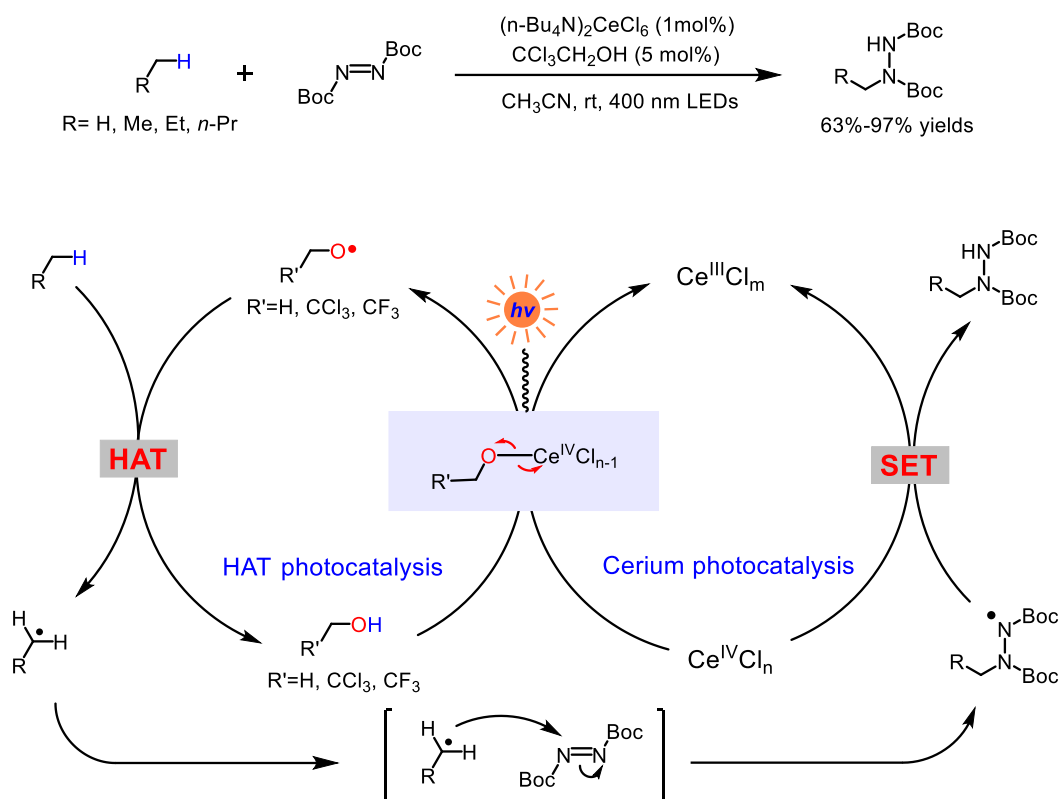


Figure 19. Photoinduced C(sp³)-H amination using alcohols as indirect HAT catalyst.

1.2.2.3 S-Centered Abstractors

Thiyl radicals are powerful HAT catalysts that can react with various C-H bonds via hydrogen atom transfer, leading to the formation of carbon-centered radicals. The hydrogen atom abstracting reactivity of thiyl radicals has been known for decades.²¹ The activation of the S-H bond by the photocatalyst actually involves the formation of a thiyl radical by transferring one electron and a proton, which may occur through a concerted proton-coupled electron transfer (PCET). A pioneering report was published by MacMillan and co-workers in 2015, in which the triisopropylsilanethiol was used as the hydrogen atom transfer catalyst (**Figure 20**).²² In the proposed reaction mechanism, the excited Ir(ppy)₃ could be quenched by the electron-deficient arene to generate a persistent arene radical anion along with the oxidized photocatalyst Ir^{IV}. The thiol catalyst is subsequently through proton-coupled electron transfer (PCET) in the presence of a base to generate the thiyl radical, which could abstract a hydrogen atom from allylic C-H bonds and give the allylic radical. Finally, an intermolecular radical-radical coupling furnishes the C-C coupled product, followed by the elimination of cyanide to obtain the desired arylated product.

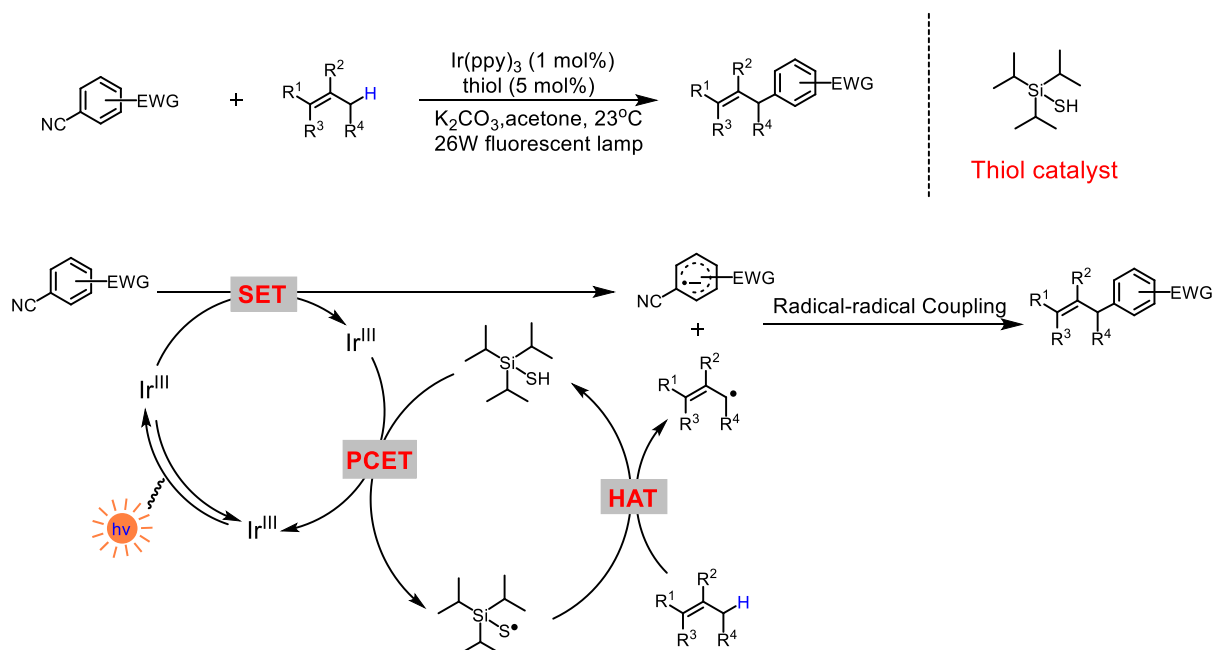


Figure 20. Photoinduced allylic arylation with triisopropylsilanethiol as an indirect HAT catalyst.

By employing a photoredox HAT strategy, MacMillan and coworkers²³ developed a protocol for the direct alkylation of heteroarenes using simple alcohols as the alkylating reagents (**Figure 21**). In this reaction, thiyl radical, generated by SET from the thiol catalyst, can abstract a hydrogen atom from alcohol to generate an α -hydroxy radical. The generated nucleophilic radical would then add to protonated heteroarenes to afford the aminyl radical cation, and subsequent deprotonation gave an α -amino radical. At this juncture, the intermediate is primed to undergo spin-center shift (SCS) to cleave the C–O bond and eliminate one molecule of H₂O and generate the benzylic radical. Finally, the benzylic radical can be reduced by the excited photocatalyst and protonated to provide the alkylated heteroarene.

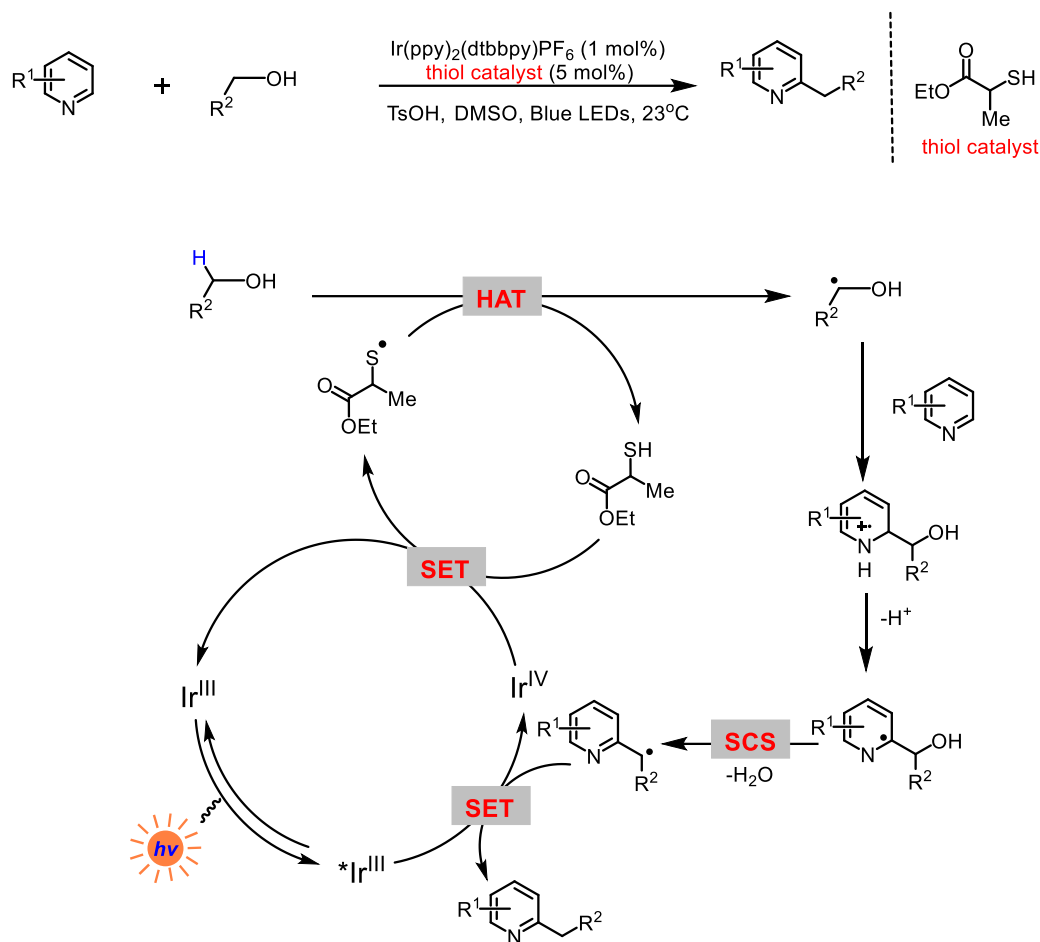


Figure 21. Photoinduced C–H alkylation of heteroarenes with alcohols as the alkylating reagents.

1.2.2.4 Halogen-Centered Abstractors

Halogen radicals can be formed by photoexcitation of high-oxidation-state transition-metal halides via dissociation from a charge-transfer excited state.²⁴ The chlorine radical (Cl•) can abstract a hydrogen atom from a wide range of activated and unactivated aliphatic C–H bonds due to its electrophilic nature and the relatively large BDE of HCl (103 kcal/mol). In 2016, Doyle and co-workers reported the pioneering C(sp³)–H cross-coupling reactions based on the catalytic generation of chlorine radicals through nickel and photoredox catalysis.²⁵ The authors proposed that the arylation of ethers could proceed via the mechanism shown in **Figure 22**. In which, oxidative addition of Ni(0) complex into an aryl chloride would produce Ni(II) aryl chloride intermediate. Concurrently, irradiation of Ir(III) photocatalyst affords triplet excited state ^{*}Ir(III) photocatalyst, which could oxidize Ni(II) aryl chloride intermediate to Ni(III) aryl chloride species. The Ni(III)-chlorine bond is then rendered sufficiently weak that a photon of visible light can homolyze the bond (BDFE = 47 kcal/mol), resulting in Ni(II) aryl species and a chlorine radical, which readily abstracts an hydrogen atom from the ether. Reaction of the ether radical would produce the Ni(III) species. Subsequent reductive elimination from the Ni(III) species would afford the desired C(sp³)–H cross-coupling product and Ni(I) intermediate. Finally, single-electron-transfer reduction of the resulting Ni(I) intermediate by reduced Ir(II) photocatalyst

regenerates both the Ni(0) and Ir(III) catalysts.

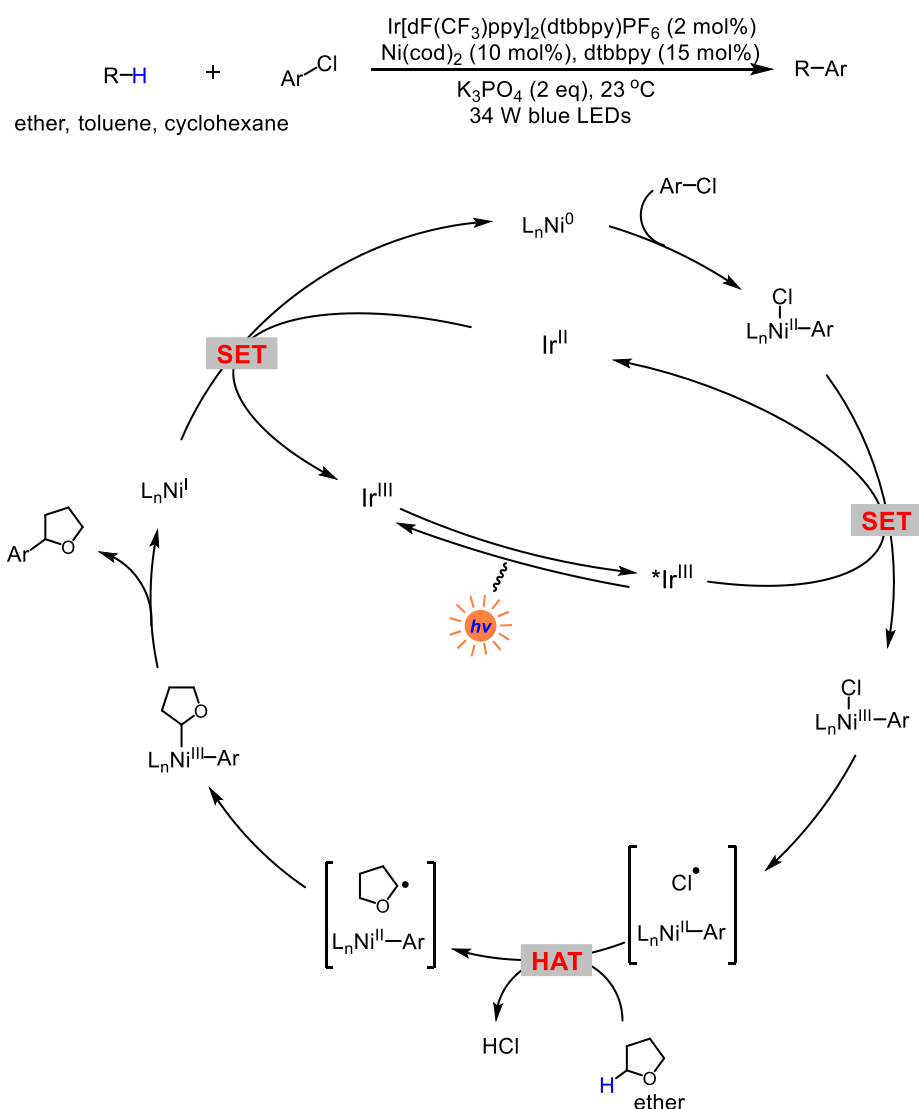


Figure 22. C(sp³)-H cross-coupling enabled by the catalytic generation of chlorine radicals by nickel and photoredox catalysis.

In 2018, Barriault and co-workers reported the photocatalytic generation of chlorine radical based photoredox catalyst oxidized the chloride anion. The authors demonstrate that the chloride anion is derived from the counterion of the Ir complex ([Ir(dF(CF₃)ppy)₂(dtbbpy)]Cl) (**Figure 23**).²⁶ Upon generation of the electrophilic chlorine radical, complexation to pyridine could attenuate the high reactivity of the chlorine radical and thus improves the selectivity of HAT. Subsequently the chlorine radical can undergo hydrogen atom transfer with a variety of substrates such as alkanes, alcohols, ethers, ester, amides, aldehydes, and silanes, giving nucleophilic radicals. Finally, through Giese-type addition to activated alkenes affords the target product.

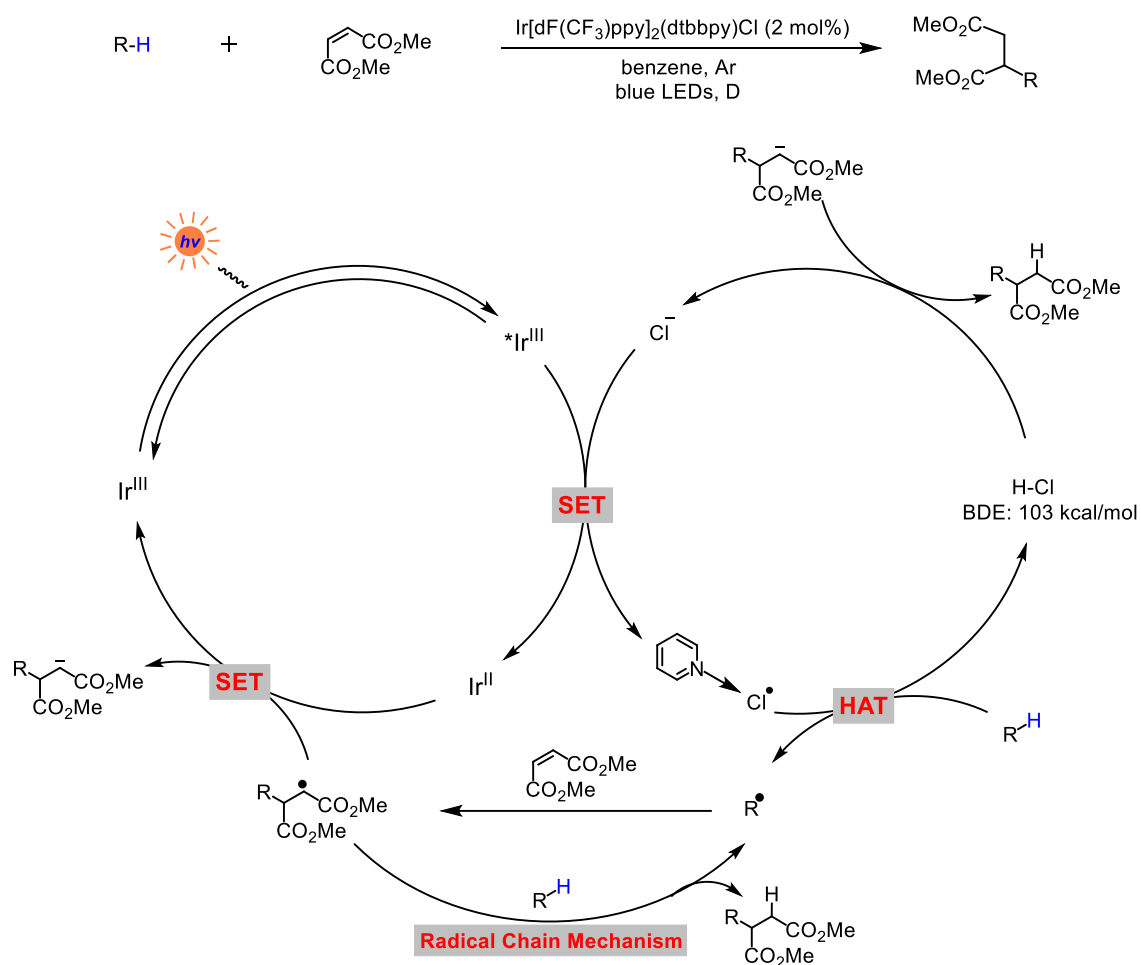


Figure 23. Hydrogen atom transfer reactions via photoredox catalyzed chlorine radical generation.

In 2016, Molander's group demonstrated that arylation of $\text{C}(\text{sp}^3)\text{-H}$ bonds with aryl bromides through nickel catalysis and photocatalysis (**Figure 24**).²⁷ Detailed mechanistic studies revealed that a triplet-triplet energy transfer from the excited state of Ir photocatalyst to the Ni^{II} aryl bromide complex. Subsequently the excited-state Ni^{II} aryl bromide complex offers the bromine radical upon Ni-Br bond homolysis, which undergoes HAT with the substrates to form the carbon-centered radicals. The carbon-centered radical recombination with the remaining Ni^{I} complex affords a Ni^{II} complex intermediate. Finally, reductive elimination subsequently delivers the target product and regenerates nickel (0) species.

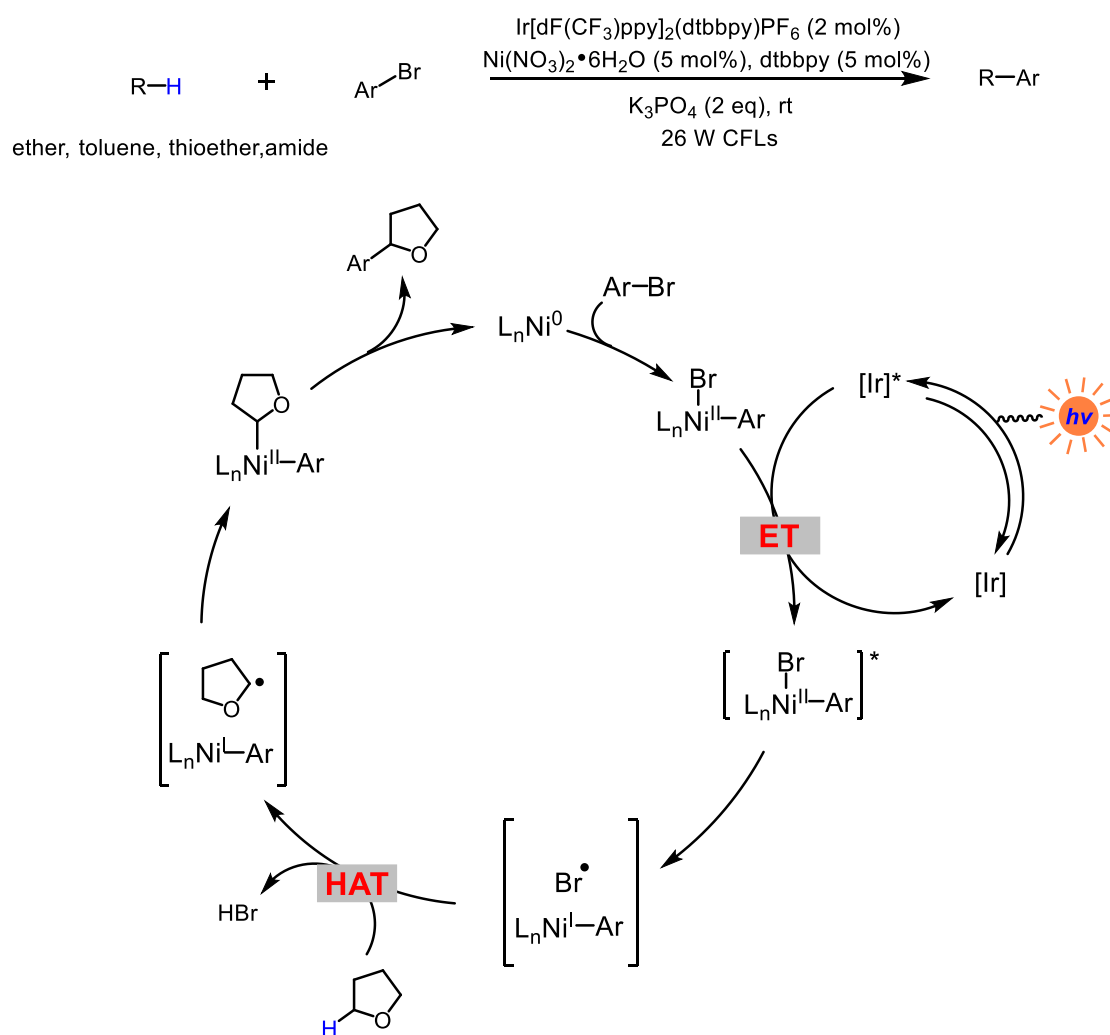


Figure 24. C(sp³)-H cross-coupling enabled by the catalytic generation of bromine radical by nickel and photoredox catalysis.

In 2020, Huo and co-workers reported a direct enantioselective acylation of α -amino C(sp³)-H bonds for the synthesis of α -amino ketones based on the catalytic generation of bromine radicals through nickel with the chiral ligands and photoredox catalysis (**Figure 25**).²⁸ The authors propose that the reaction is initiated by oxidative addition of Ni(0) intermediate to acyl electrophile formed in situ to provide Ni(II) intermediate. Concurrently, single electron transfer from the bromide anion to excited-state Ir(III) produces a bromine radical that could abstracts a hydrogen atom from the α -amino C(sp³)-H bond. At the same time, the chiral nickel catalyst could engage sequentially with the acyl electrophiles formed in situ from carboxylic acids and α -amino radicals through oxidative addition and radical trapping. The resulting diorgano nickel(III) adduct would then undergo reductive elimination to form the enantioenriched α -amino ketones.

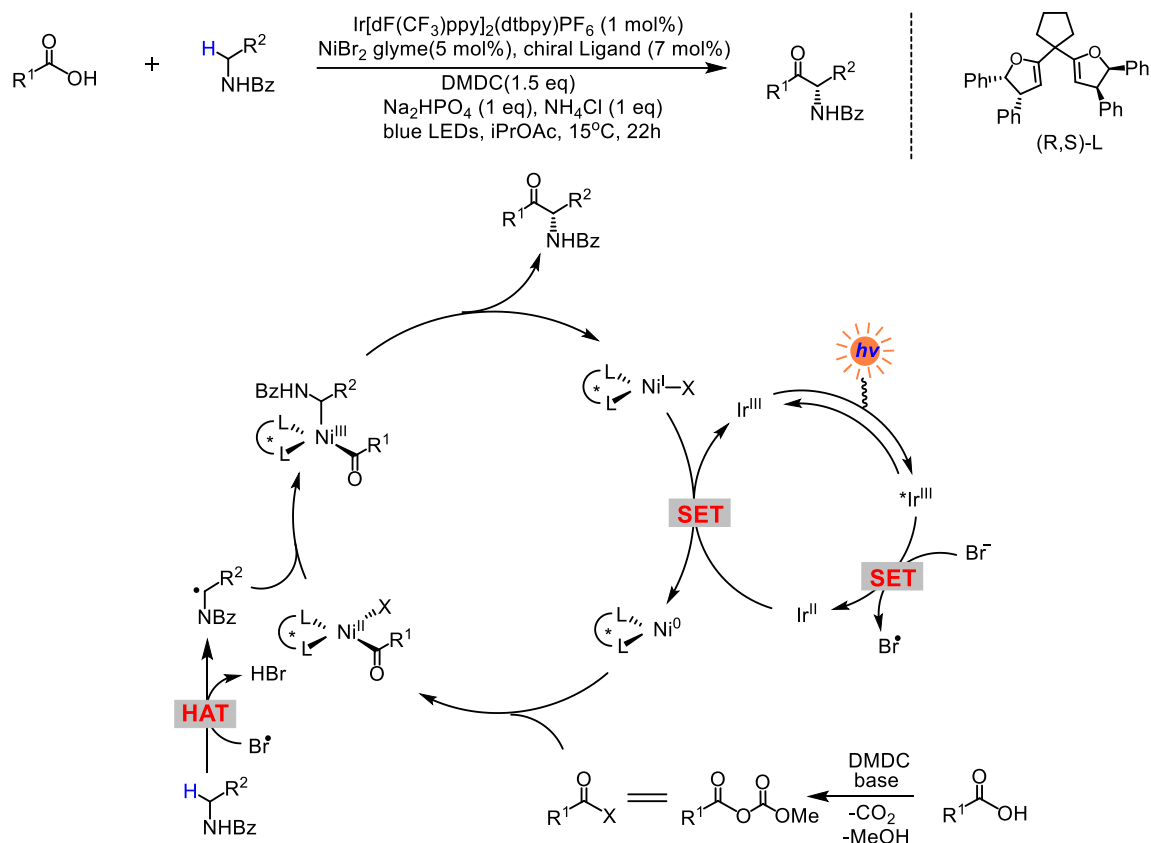


Figure 25. Enantioselective α -amino $\text{C}(\text{sp}^3)\text{-H}$ acylation enabled by the catalytic generation of bromine radical by nickel and photoredox catalysis.

1.2.2.5 C-Centered Abstractors

$\text{X}_3\text{C}^\bullet$ radicals, where $\text{X} = \text{Br}, \text{Cl}, \text{F}$, could be formed via single electron reduction of $\text{X}_3\text{C-Y}$ ($\text{Y} = \text{Br}, \text{I}$) by excited photocatalysts. In 2019, Studer and co-workers²⁹ disclosed the selective generation of carbon radicals via intermolecular HAT from alkyl boron-ate complexes to CF_3 radical, leading to the α -functionalization of boronated compounds (**Figure 26**). The authors proposed that the reactive CF_3 radical, generated by oxidative quenching of the excited photocatalyst, has the ability to abstract a hydrogen atom from the $\alpha\text{-C}(\text{sp}^3)\text{-H}$ bond of the boron-ate complexes, forming the α -radical anion. Subsequent oxidation of the resulting radical anion to afford the zwitterion species. A following 1,2-alkyl/aryl migration furnishes the targeted α -functionalized boronic ester. Moreover, it is well established that CF_3I is an excellent terminal oxidant for the oxidation of the resulting radical anion.

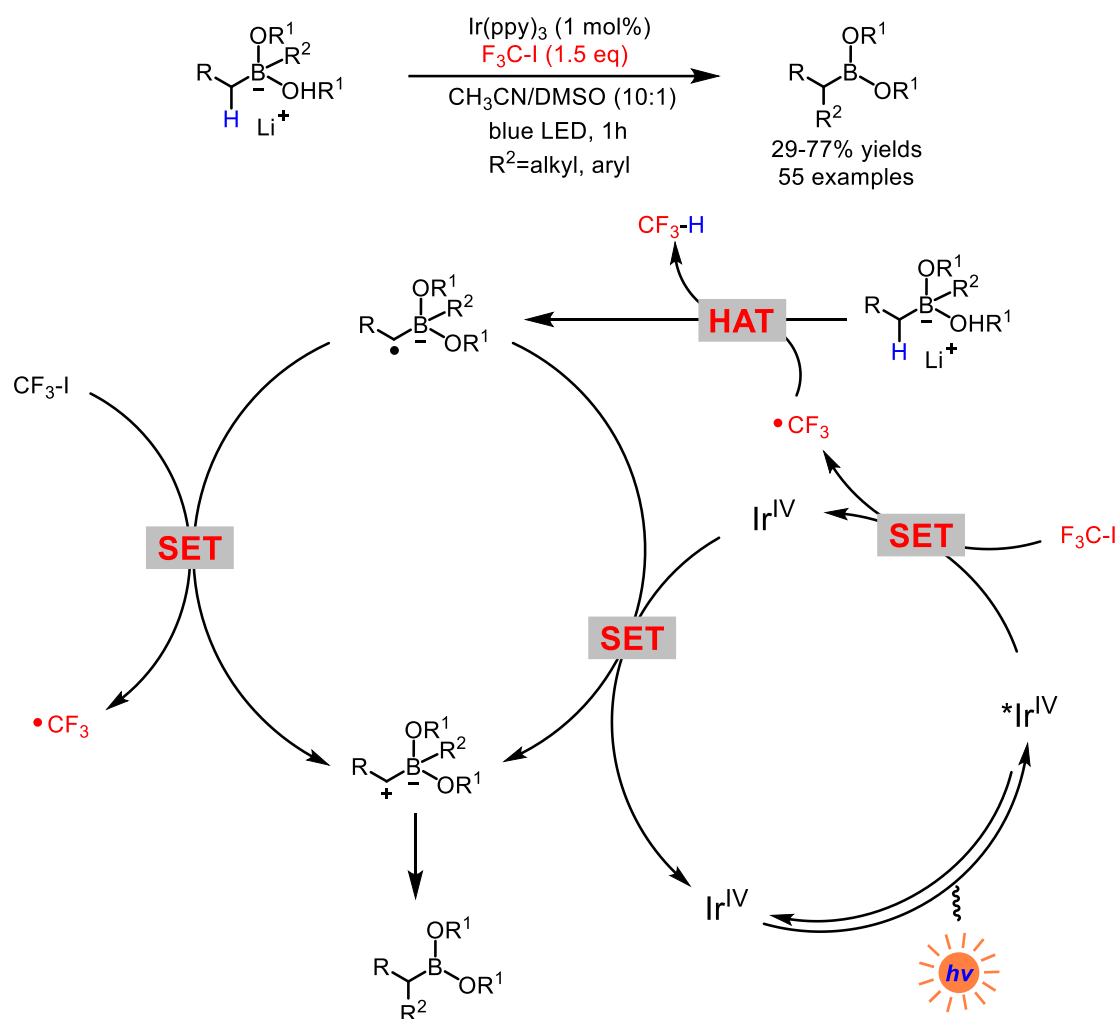
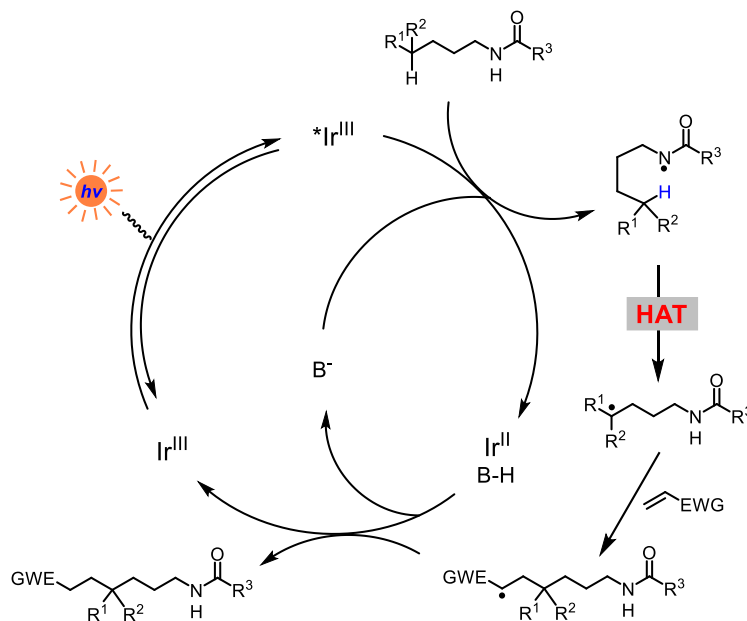
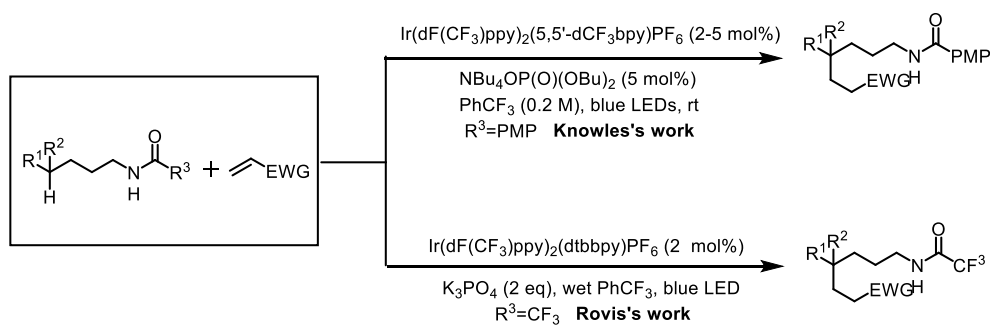


Figure 26. α -functionalization of boronate complexes via trifluoromethyl radicals.

1.3 Photoinduced Intramolecular HAT Reactions

In 2016, the groups of Knowles and Rovis independently reported photoredox-catalyzed remote $\text{C}(\text{sp}^3)\text{-H}$ alkylation with electron-deficient alkenes (**Figure 27**).^{13,30} This remote C-C bond formation is realized an amidyl radical promoted intramolecular 1,5-HAT and intermolecular radical addition. The authors propose the mechanism that the amidyl radical, generated from an N-alkyl amide by photoredox catalyzed proton-coupled electron transfer (PCET) with an excited iridium photocatalyst, undergoes an intramolecular 1,5-HAT to form the carbon radical. Subsequently, the resulting carbon radicals directed remote $\text{C}(\text{sp}^3)\text{-H}$ alkylation with electron-deficient alkenes as radical acceptors to afford a new carbon radical intermediate. Finally, reduction and then protonation of the new carbon radical intermediate give the final product and regenerates the Ir (III) photocatalyst. In 2017, Meggers group developed a visible-light-induced enantioselective alkylation of remote $\text{C}(\text{sp}^3)\text{-H}$ bonds of N-alkyl amides by the combination of photoinduced PCET, 1,5-HAT, and chiral Lewis acid catalysis (**Figure 27**).³¹



Meggers's work: Enantioselective alkylation of remote C(sp³)-H

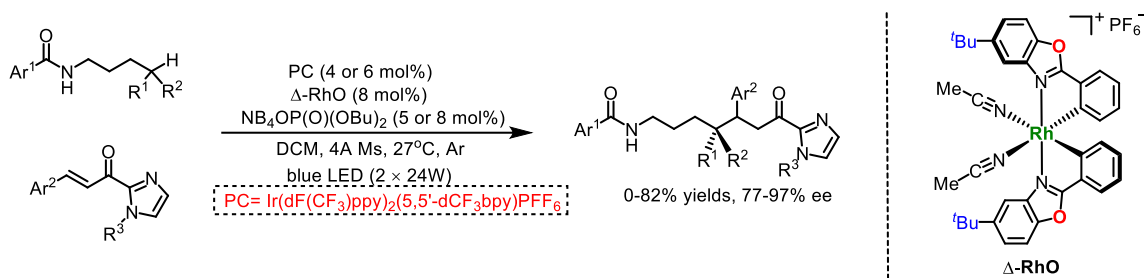


Figure 27. Photoredox-catalyzed remote C(sp³)-H alkylation via an amidyl radical.

Compared with amidyl radicals, the generation of an iminyl radical and its subsequent 1,5-HAT has been much less explored. In 2018, Studer and co-workers developed a photoredox-catalyzed iminyl radical-based γ -alkylation of α -imino-oxy acids using Michael acceptors as alkylating reagents (**Figure 28**).³² In this reaction, the readily accessible α -aminoxy propionic acid was used as an auxiliary to form the iminyl radical. The iminyl radical is generated by visible light-induced single electron transfer of the carboxyl anion and then fragmentation. Immediately following the 1,5-HAT from the distal C(sp³)-H bond with the iminyl radical generating the γ -carbon radical, which is trapped by the Michael acceptor delivering the adduct radical. Finally, reduction and then protonation of the adduct radical give the final

product and regenerates the Ir (III) photocatalyst.

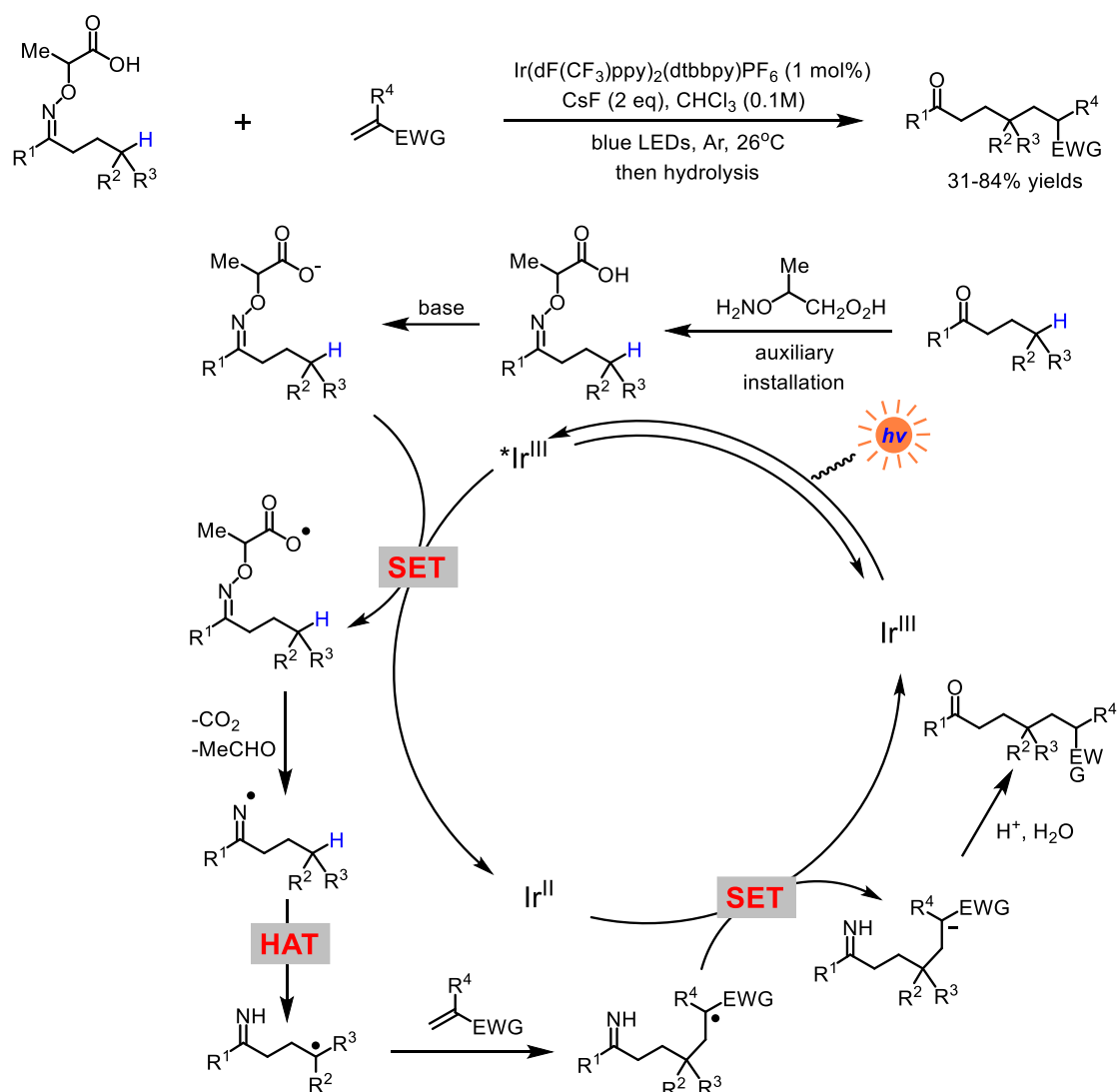
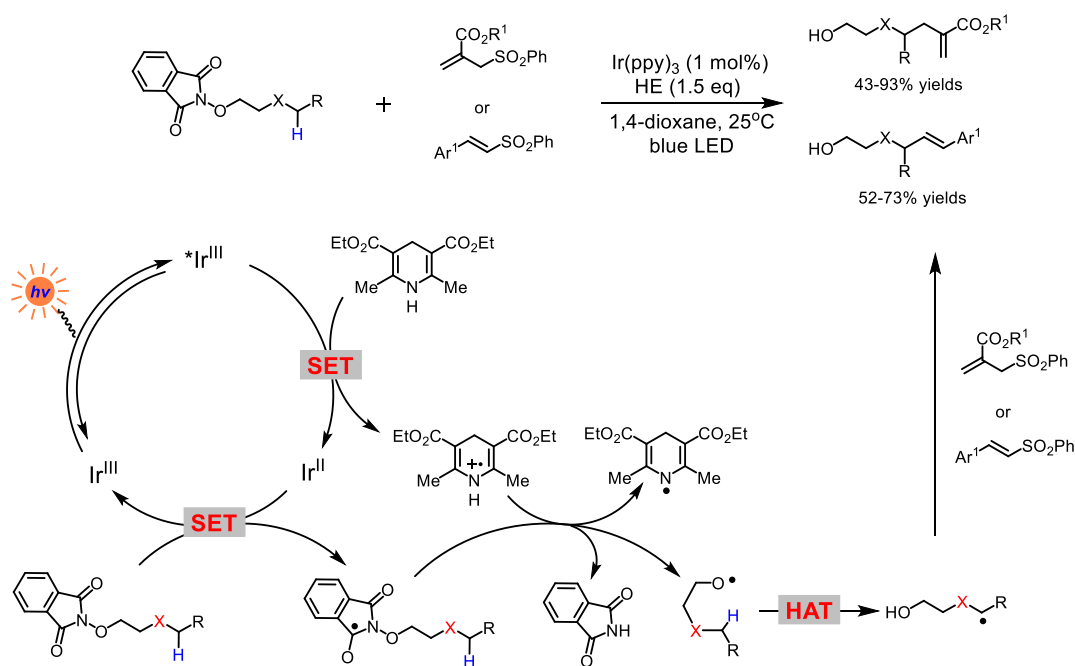


Figure 28. Photocatalytic iminyl radical-mediated γ -alkylation of α -iminoxy-acids.

The 1,5-hydrogen atom transfer of oxygen-centred radicals as exemplified by the Barton reaction has played an important role in the C(sp³)-H bond functionalisation of alcohols. In 2015, Chen and co-workers first reported the visible-light-induced allylation and alkenylation of remote C(sp³)-H bonds of alcohols from N-alkoxyphthalimides with the Hantzsch ester (HE) as the reductant (**Figure 29**).^{33a} The key step in the reaction is selective 1,5-hydrogen atom abstraction by the alkoxy radical. The authors propose that the excited photocatalyst is reduced by single-electron transfer from HE to form the reduced Ir(II) with Hantzsch ester radical cation. The resulting Ir(II) photocatalyst then reduces the N-alkoxyphthalimide by single-electron transfer to yield the N-alkoxyphthalimide radical anion, which is further protonated by the Hantzsch ester radical cation to facilitate the formation of the alkoxy radical. The alkoxy radical undergoes a 1,5-HAT reaction and subsequent reaction with allyl sulfones or vinyl sulfones to give the adduct radicals. Finally, the product is obtained by extruding the sulfone radical of the resulting remote C-C bond coupling adduct. In 2016, Meggers and co-workers applied a similar strategy to achieve asymmetric alkylation of the remote C(sp³)-H bond. In which N-

alkoxyphthalimides is used as a redox-active radical precursor and N-acylpyrazoles as Lewis acid activatable functional groups (**Figure 29**).^{33b}

Chen group:



Meggers group:

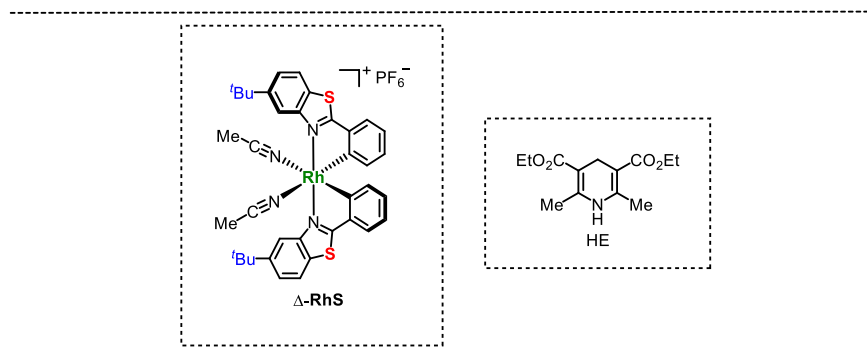
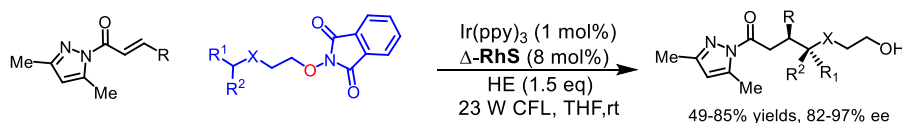


Figure 29. Visible-light-induced allylation and alkylation of remote C(sp³)-H bonds of alcohols.

The bond dissociation energy (BDE) difference between an olefinic C(sp²)-H bond (ca. 110 kcal mol⁻¹) and aliphatic C(sp³)-H bond (ca. 100 kcal mol⁻¹) promotes the hydrogen atom transfer from the aliphatic C(sp³)-H bond to the alkenyl radical. In 2017, Zhu and coworkers developed a photoredox catalyzed site-selective vinylation of remote C(sp³)-H bonds promoted by alkenyl radical mediated intramolecular HAT and functional group migration process (**Figure 30**).³⁴ Zhu's group proposed that the active alkenyl radical, generated by the addition of fluoroalkyl radical to the alkyne, undergoes intramolecular 1,5-HAT to form the alkyl radical. Subsequently, the addition of the alkyl radicals to intramolecular olefins leads to the production of a cyclopentanol intermediate through a 5-exo-trig

cyclisation. Cleavage of the cyclic C-C bond of the cyclopentanol intermediate affords an α -hydroxy radical. Finally, the resulting radical intermediate upon single atom transfer oxidation by Ir(IV) and deprotonation would provide the product.

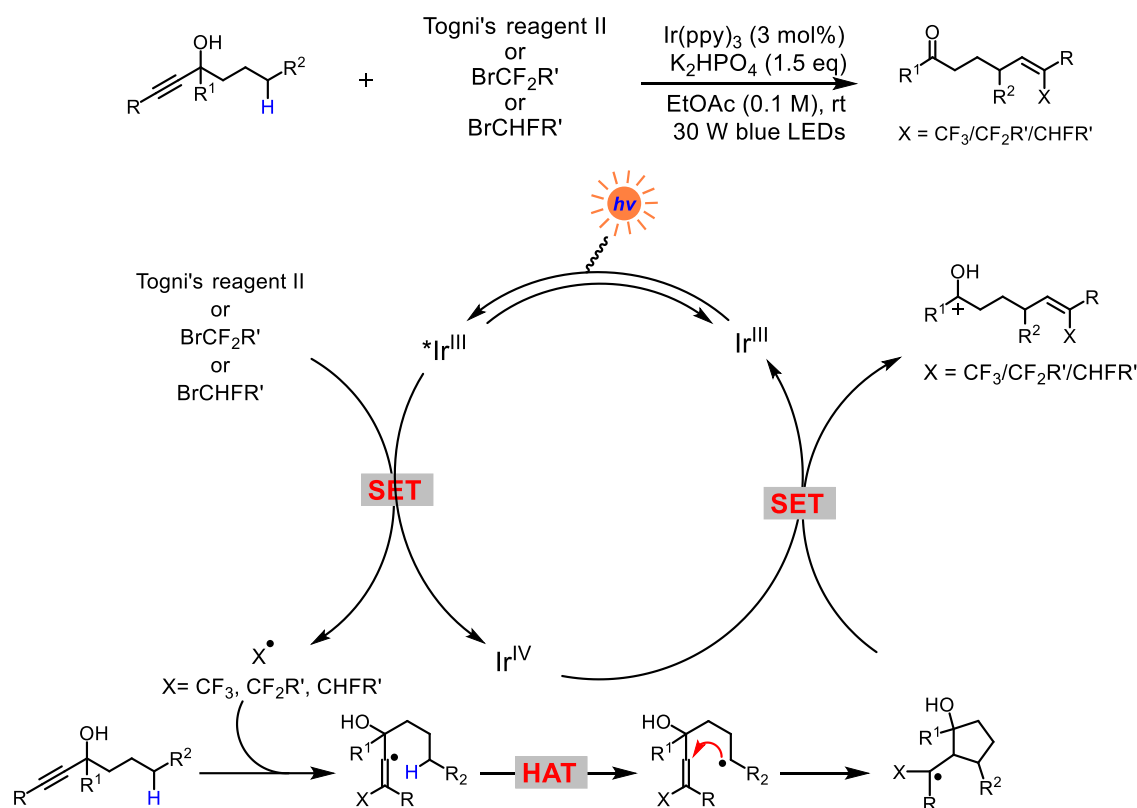


Figure 30. Photoredox catalyzed C(sp²)-radical mediated remote C(sp³)-H vinylation.

In 2018, visible-light-induced 1,6-difunctionalizations of alkenes with electron-deficient alkyl halides were developed by the Nevado group (**Figure 31**).³⁵ The authors proposed that the alkyl radicals, generated by the photoinduced reduction of the C-Br bonds, add to the double bond to form the alkyl C(sp³)-radicals. Then a intramolecular 1,5-HAT was carried out between the resulting alkyl C(sp³)-radicals and the benzyl C(sp³)-H bond to produce the benzyl radical intermediate, mainly because of the higher stability of the benzyl carbon radical. DFT calculations indicate that 1,5-HAT is an exergonic process with a lower energy barrier than the radical addition to the alkene. Once the radical center shifts to the benzylic carbon, which undergoes an oxidative SET with the Ir^{IV} to form a cationic intermediate. The resulting cationic intermediate thus subsequently quenched in the presence of either an O- or a C-based nucleophile to produce the remote dicarbo- or oxocarbofunctionalization products observed in these transformations.

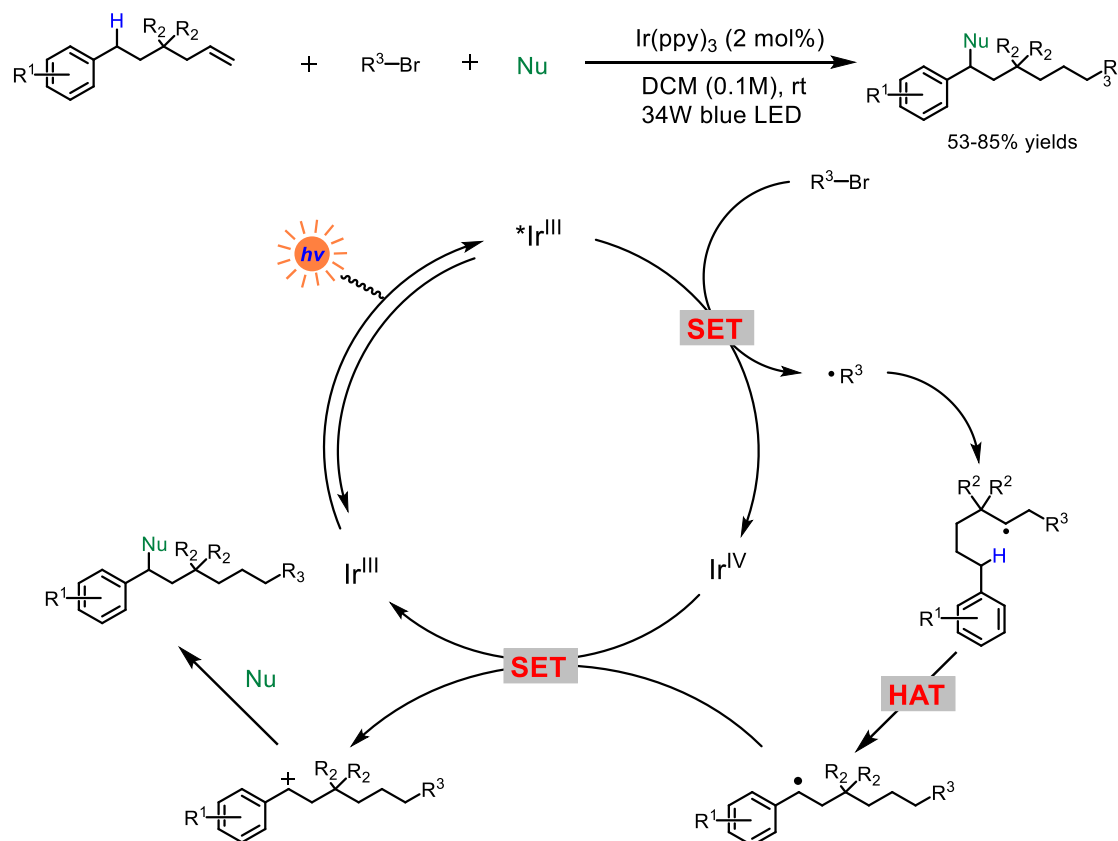


Figure 31. Photoredox catalyzed 1,6-carboalkylation of alkenes.

Reference

1. C. Prier, D. Rankic, D. W. C. MacMillan, *Chem. Rev.* **2013**, *113*, 5322; b) J. M. R. Narayanam, C. R. J. Stephenson, *Chem. Soc. Rev.* **2011**, *40*, 102; c) N. A. Romero, D. A. Nicewicz, *Chem. Rev.* **2016**, *116*, 10075; d) M. H. Shaw, J. Twilton, D. W. C. MacMillan, *J. Org. Chem.* **2016**, *81*, 6898; e) J. Twilton, C. Le, P. Zhang, M. H. Shaw, R. W. Evans, D. W. C. MacMillan, *Nat. Rev. Chem.* **2017**, *1*, 0052; Y. Abderrazak, *J. Organomet. Chem.* **2020**, *920*, 121335
2. J. W. Darcy, B. Koronkiewicz, G. A. Parada, J. M. Mayer, *Acc. Chem. Res.*, **2018**, *51*, 2391
3. a, L. Capaldo, D. Ravelli, *Eur. J. Org. Chem.* **2017**, 2056; b H. Chen and S. Yu, *Org. Biomol. Chem.*, **2020**, *18*, 4519; c, H. Cao, X. Tang, H. Tang, Y. Yuan, J. Wu, *Chem. Cata.* **2021**, In press, 10.1016/j.checat.2021.04.008. d) W. S. Guo, Q. Wang, J. P. Zhu, *Chem. Soc. Rev.* **2021**, In press, 10.1039/D0CS00774A.
4. M. Nagatomo, S. Yoshioka, M. Inoue, *Chem. Asian J.* **2015**, *10*,120.
5. Y. Shen, Y. Gu, R. Martin, *J. Am. Chem. Soc.* **2018**, *140*, 12200.
6. Y. Li, M. Lei, L. Gong, *Nat. Catal.* **2019**, *2*, 1016.
7. G. Zhao, T. Wang, *Angew. Chem. Int. Ed.* **2018**, *57*,6120.
8. X.-Z. Fan, J.-W. Rong, H.-L. Wu, Q. Zhou, H.-P. Deng, J. D. Tan, C.-W. Xue, L.-Z. Wu, H.-R. Tao, J. Wu, *Angew. Chem. Int. Ed.* **2018**, *57*, 8514.
9. J. G. West, T. A. Bedell, E. J. Sorensen, *Angew. Chem., Int. Ed.* **2016**, *55*, 8923.

10. C. Y. Huang, J. Li, W. Liu, C. J. Li, *Chem. Sci.*, **2019**, *10*, 5018.
11. J. L. Jeffrey, J. A. Terrett, D. W. C. MacMillan, *Science* **2015**, *349*, 1532.
12. M. H. Shaw, V. W. Shurtleff, J. A. Terrett, J. D. Cuthbertson, D. W. C. MacMillan, *Science* **2016**, *352*, 1304.
13. G. J. Choi, Q. Zhu, D. C. Miller, C. J. Gu, R. R. Knowles, *Nature* **2016**, *539*, 268.
14. H. Tanaka, K. Sakai, A. Kawamura, K. Oisaki, M. Kanai, *Chem. Commun.* **2018**, *54*, 3215.
15. H. Huang, Z. M. Strater, T. H. Lambert, *J. Am. Chem. Soc.* **2020**, *142*, 1698.
16. J. Jin, D. W. MacMillan, *Angew. Chem. Int. Ed.* **2015**, *54*, 1565.
17. T. Hering, T. Slanina, A. Hancock, U. Wille, B. König, *Chem. Commun.* **2015**, *51*, 6568.
18. J. Li, D. Z. Wang, *Org. Lett.* **2015**, *17*, 5260.
19. S. Mukherjee, B. Maji, A. Tlahuext-Aca, F. Glorius, *J. Am. Chem. Soc.* **2016**, *138*, 16200.
20. A. Hu, J.-J. Guo, H. Pan, Z. Zuo, *Science* **2018**, *361*, 668.
21. F. Dénès, M. Pichowicz, G. Povie, P. Renaud, *Chem. Rev.* **2014**, *114*, 2587.
22. J. D. Cuthbertson, D. W. C. MacMillan, *Nature* **2015**, *519*, 74.
23. J. Jin, D. W. C. MacMillan, *Nature* **2015**, *525*, 87.
24. A. J. Esswein, D. G. Nocera, *Chem. Rev.* **2007**, *107*, 4022.
25. B. J. Shields, A. G. Doyle, *J. Am. Chem. Soc.* **2016**, *138*, 12719.
26. S. Rohe, A. O. Morris, T. McCallum, L. Barriault, *Angew. Chem. Int. Ed.* **2018**, *57*, 15664.
27. D. R. Heitz, J. C. Tellis, G. A. Molander, *J. Am. Chem. Soc.* **2016**, *138*, 12715.
28. X. Shu, L. Huan, Q. Huang, H. Huo, *J. Am. Chem. Soc.* **2020**, *142*, 19058.
29. D. Wang, C. Mück-Lichtenfeld, A. Studer, *J. Am. Chem. Soc.* **2019**, *141*, 14126.
30. J. C. K. Chu, T. Rovis, *Nature* **2016**, *539*, 272-275.
31. W. Yuan, Z. Zhou, L. Gong, E. Meggers, *Chem. Commun.* **2017**, *53*, 8964
32. H. Jiang, A. Studer, *Angew. Chem. Int. Ed.* **2018**, *57*, 1692.
33. a) J. Zhang, Y. Li, F. Zhang, C. Hu, Y. Chen, *Angew. Chem. Int. Ed.* **2016**, *55*, 1872. b) C. Wang, K. Harms, E. Meggers, *Angew. Chem. Int. Ed.* **2016**, *55*, 13495.
34. S. Wu, X. Wu, D. Wang, C. Zhu, *Angew. Chem. Int. Ed.* **2019**, *58*, 1499.
35. W. Shu, E. Merino, C. Nevado, *ACS Catal.* **2018**, *8*, 6401.

Chapter 2: Results and Discussion

2.1 Asymmetric Photocatalysis by Intramolecular Hydrogen Atom Transfer in Photoexcited Catalyst/Substrate Complex

2.1.1 Research Background and Reaction Design

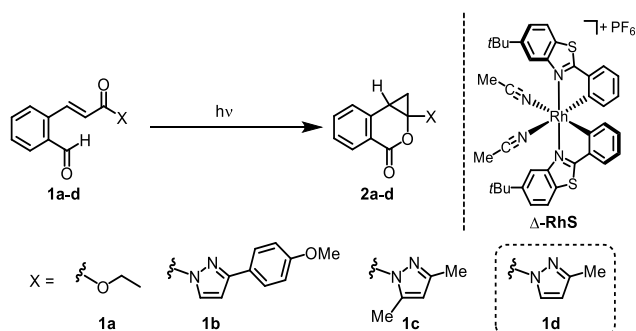
Chiral transition metal complexes play an important role as catalysts for the asymmetric synthesis of chiral nonracemic compounds. Meggers research group developed a series of chiral-at-metal compounds for asymmetric photocatalysis. The former group members in Meggers group have demonstrated that bis-cyclometalated iridium(III) and rhodium(III) complexes are exquisite catalysts for realizing visible light activated asymmetric catalysis.¹ Upon binding to a substrate and selective visible light activation of the formed catalyst/substrate complexes, such photoexcited assemblies are capable of undergoing stereo-controlled chemical transformations, either through an initial outer sphere electron transfer or by engaging in direct stereocontrolled bond forming reactions. In 2017, Meggers group proposes a highly stereoselective direct bonding of the directly visible-light-excited state.² The authors proposed that the catalytic cycle begins with the association of the *N*-acylpyrazole substrate with the chiral rhodium catalyst. The resulting reactant complex absorbs blue light to reach its singlet excited state through $\pi \rightarrow \pi^*$ transitions. After intersystem crossing (ISC) to form the triplet reactant complex, which can directly react with radical acceptors in a highly stereocontrolled manner. Using this method, a wide range of cyclobutanes were successfully constructed by [2+2] photocycloadditions with alkenes and various 1-pyrrolines by [2+3] photocycloadditions with vinyl azides.

Upon excitation with light, the triplet excited aromatic ketone, generated by intersystem crossing from the $n \rightarrow \pi^*$ singlet to the triplet state, behaves as a 1,2-biradical, creating significant spin density on the oxygen atom. The (n, π^*) triplet excited state has intriguing electrophilic and radical-type properties that make it particularly susceptible to hydrogen atom transfer (HAT).³

Inspired by the hydrogen atom abstracting ability of triplet aromatic ketones and based on the previous [2+2] and [2+3] photocycloadditions, we envisioned an unprecedented utilization of long-lived triplet excited enones, which behave as biradical. The two resulting radicals have different electronic characters, the α -radical is electrophilic and the β -radical is nucleophilic, in which the electrophilic α -radical could participate in hydrogen atom transfer (HAT) as a HAT agent. Based on the above research background we speculate that such photoexcited catalyst-bound enones may instead be capable of engaging in HAT reactions to generate catalyst-bound reactive intermediates followed by stereocontrolled transformations. By reviewing the literature, we found that Xia and coworkers employed (*E*)-ethyl 3-(2-formylphenyl)acrylate (**1a**), which underwent an interesting rearrangement when photolysis with a 500 W high-pressure mercury lamp to form the cyclopropane **2a** (Table 1, entry 1).⁴ This reaction was proposed to proceed through an intramolecular HAT from the aldehyde to the $\pi \rightarrow \pi^*$ excited state of the enone. As major drawbacks, the reaction required intense UV light and provided the product as a racemic mixture. We hypothesized that by replacing the ester with an *N*-acyl

of merely 0.5 mol%, 46% pyranone **4d** with 95% *ee* were isolated after an elongated irradiation for 48 hours, thus demonstrating the efficiency of this asymmetric photorearrangement (entry 7). The reaction can be performed in other solvents such as acetone with similar results (entry 8) but MeCN only provided traces of the product (entry 9). Interestingly, the presence of air only slightly affects yield and enantioselectivity, indicating that free radical chemistry is not operational in this photoreaction (entry 10). Finally, CFL as light source provided similar results (entry 11). Control experiments furthermore confirmed that the reaction requires the rhodium catalyst and light for product formation (entries 12 and 13).

Table 1. Initial experiments and optimization of reaction conditions^[a]



Entry	Substrate	Cat (mol%)	light ^[b]	solvent	t (h)	yield (%) ^[c]	ee (%) ^[d]
1 ^[e]	1a	none	UV light	benzene	5	89	–
2	1b	4	blue LEDs	CH ₂ Cl ₂	16	60	38
3	1c	4	blue LEDs	CH ₂ Cl ₂	16	74	97
4	1d	4	blue LEDs	CH ₂ Cl ₂	16	83	98
5	1d	2	blue LEDs	CH ₂ Cl ₂	24	71	95
6	1d	1	blue LEDs	CH ₂ Cl ₂	24	70	95
7	1d	0.5	blue LEDs	CH ₂ Cl ₂	48	46 ^[f]	95
8	1d	4	blue LEDs	acetone	16	72	97
9	1d	4	blue LEDs	MeCN	16	trace	–
10 ^[g]	1d	4	blue LEDs	CH ₂ Cl ₂	20	75	96
11	1d	4	CFL	CH ₂ Cl ₂	36	86	96
12	1d	none	blue LEDs	CH ₂ Cl ₂	48	0	–
13	1d	4	dark	CH ₂ Cl ₂	48	0	–

[a] Standard conditions for entries 2-8: Substrates **1b-d** (0.1 mmol) in the indicated solvent (2.0 mL) with Δ -**RhS** (0.5–4 mol%) photolyzed for the indicated time under an atmosphere of N₂. [b] 24 W blue LEDs with emission maximum at 450 nm or 23 W CFL. [c] Isolated yields. [d] Enantioselectivities determined by HPLC on chiral stationary phase. [e] Taken from ref. 8. Irradiation with a 500 W medium pressure mercury lamp in combination with a Pyrex filter. [f] The conversion was 67%. [g] Under an atmosphere of air.

2.1.3 Substrate Scope

With optimized conditions in hand, we screened substrates for this reaction. **Figure 33** reveals that this asymmetric visible light activated photorearrangement tolerates methyl substituents at any position

of the phenyl moiety (see cyclopropanes **2e-h**), bulky substituents (**2i**, **2j**), electron withdrawing substituents (**2k-q**), electron donating substituents (**2r-u**), and a thioether (**2v**). For all these reactions, yields of 50-93% and enantioselectivities of 87-99% *ee* were observed. Lower yields and lower enantioselectivity were obtained with a benzothiophene derivative (cyclopropane **2w**) but a methyl group in the β -position of the α,β -unsaturated *N*-acyl pyrazole provided the corresponding rearrangement product **2x** containing an all-carbon quaternary center in 67% yield and excellent 99% *ee*. For practical reasons, it is worth noting that this new asymmetric photoreaction can be upscaled. On a scale of 4.5 mmol (1.08 g), the reaction **1d**→**2d** afforded an improved yield of 90% with a slightly increased enantiomeric excess of 99% and the rhodium catalyst was reisolated in 86% yield by capturing with an auxiliary ligand in a procedure reported recently.⁵

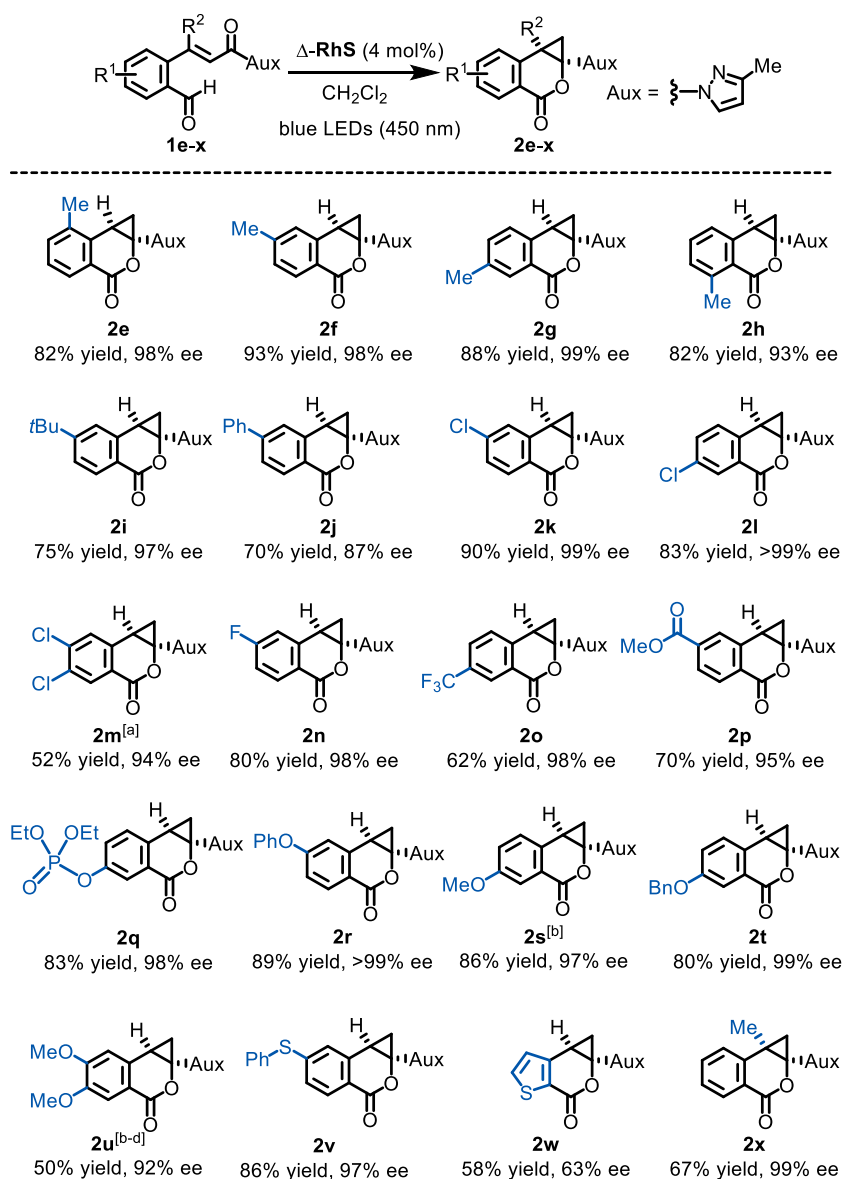


Figure 33. Substrate scope. Standard conditions (entry 4 of Table 1) were applied if not indicated otherwise. Modified reaction conditions were used for obtaining products **2m**, **2s**, and **2u**. ^[a]Catalyst loading of 8 mol% was used to increase the ee. ^[b]Reduced substrate concentration of 0.005 M was used to improve the yield. ^[c]Photolysis with weaker blue LEDs (3 W, 420 nm) for 10 h afforded an improved yield. ^[d]1,2-Dichloroethane was used as the solvent which provided a higher ee.

2.1.4 Mechanistic Study

The proposed mechanism is displayed in **Figure 34**. The catalytic cycle starts with the rhodium catalyst binding to the *N*-acyl pyrazole substrate in a bidentate fashion (int. **I**). This catalyst/substrate complex constitutes the photoactive species. Upon absorption of visible light, a photoexcited catalyst/substrate complex **II** is formed. In previous work we demonstrated that such rhodium-bound α,β -unsaturated *N*-acyl pyrazoles populate a ligand-centered $\pi \rightarrow \pi^*$ photoexcited state with the spin density localized mainly at the olefinic double bond. The close vicinity of the aldehyde moiety now permits a hydrogen atom transfer to the α -position to generate the diradical intermediate **III**.^{6,7} An intersystem crossing to the singlet-state ketene **IV** sets the stage for an intramolecular asymmetric hetero-Diels-Alder reaction⁸ to form the rhodium bound cyclopropane product **VI**. Product release and recoordination of new substrate then initiates a new catalytic cycle.

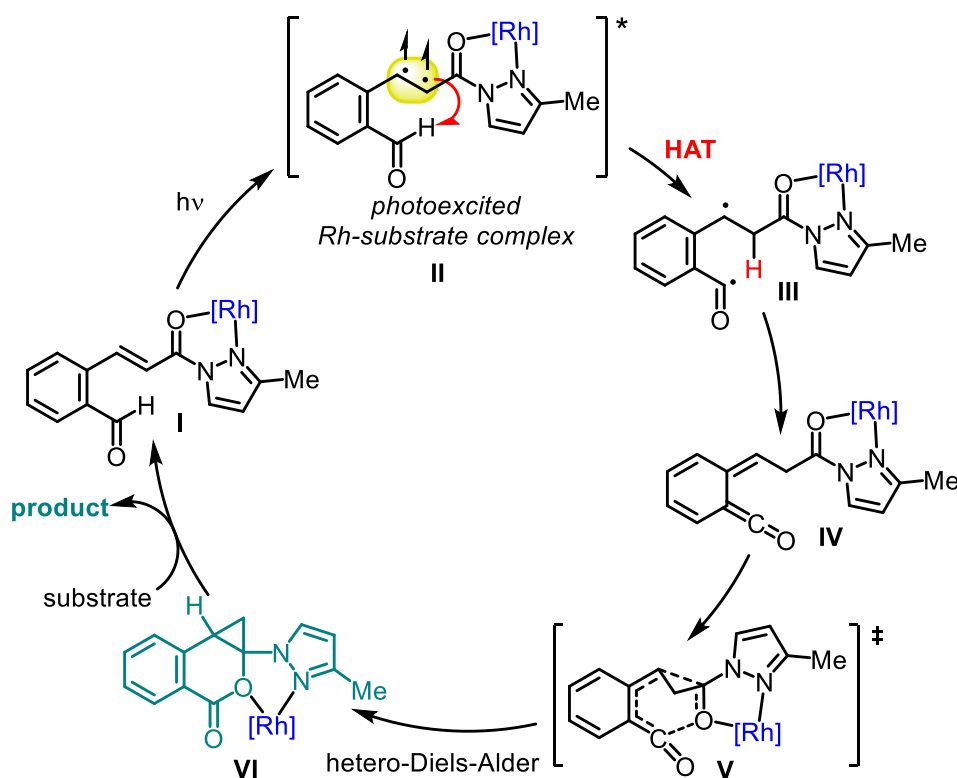
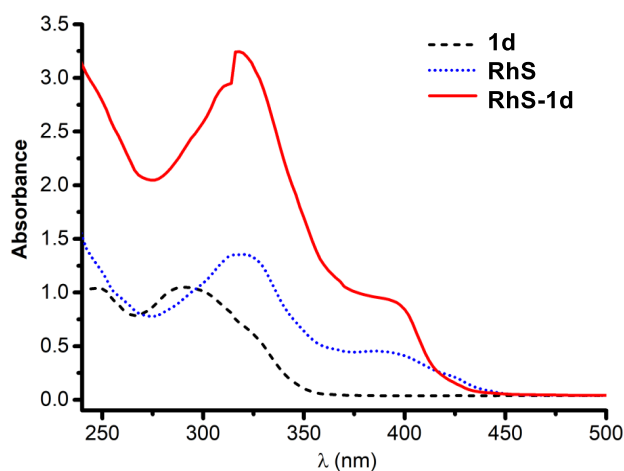


Figure 34. Proposed mechanism.

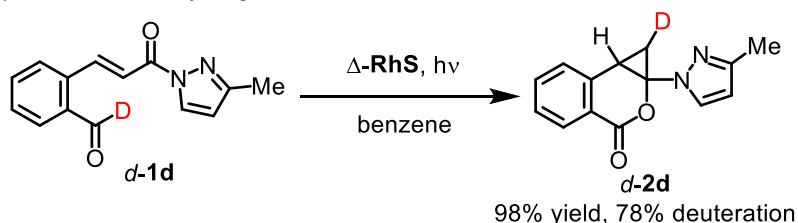
Several control experiments back up this mechanism. Absorption spectra shown in **Figure 35a** reveal that the catalyst/substrate complex absorbs visible light significantly more efficiently compared to the catalyst (**RhS**), whereas the free substrate does not absorb significantly in the visible light region. Thus, under the reaction conditions, the catalyst/substrate complex is the main light absorbing species. The HAT reaction from the photoexcited catalyst/substrate complex **II** was verified by a deuterium isotope-labeling experiment. The reaction of substrate *d*-**1d** with a deuterated aldehydic position yielded *d*-**2d**, in which the deuterium ended up in the expected position of the cyclopropane moiety (78% deuteration) (**Figure 35b**). We propose that the reduced deuteration level is due to a keto-enol tautomerism

or reversible deprotonation of intermediate **IV** of the catalytic cycle (**Figure 34**).

a) UV/Vis-absorption



b) Verification of hydrogen atom transfer



c) Background sensitization

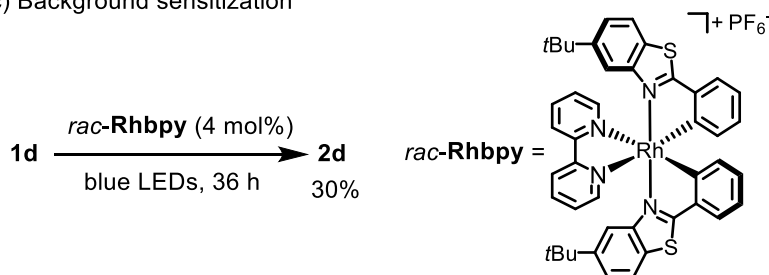


Figure 35. Mechanistic experiments. UV/Vis-absorption spectra measured in CH_2Cl_2 (0.05 mm).

The Houk group cooperated with our research group on this project and performed a detailed computational study, which was done by Dr. Shuming Chen. Density functional theory (DFT) calculations were performed to evaluate the energetic feasibility of the proposed mechanistic pathway (**Figure 36a**). The intramolecular HAT reaction of the Rh-bound substrate was found to have a free energy barrier of 8.0 kcal/mol, compared to 9.7 kcal/mol for the free substrate. After intersystem crossing back to the singlet state to furnish ketene **IV**, the intramolecular hetero-Diels-Alder reaction leading to the major enantiomer proceeds through **hDA-TS-1** with a barrier of 5.4 kcal/mol. In contrast, **hDA-TS-2**, the hetero-Diels-Alder TS leading to the minor enantiomer, has a much higher barrier of 16.6 kcal/mol (**Figure 36b**). The 11.2 kcal/mol difference in free energy between **hDA-TS-1** and **hDA-TS-2** can be attributed to (1) stabilization from a π - π stacking interaction between the aryl group on the substrate and the ligand framework in **hDA-TS-1**, and (2) severe steric clashes between the substrate and the *tert*-butyl group on the ligand in **hDA-TS-2**.

Even though the direction of enantioselectivity predicted by our calculations is in good agreement with the experimentally observed asymmetric induction, the calculated $\Delta\Delta G^\ddagger$ value of 11.2 kcal/mol far exceeds the experimental value of 2.2–2.4 kcal/mol (corresponding to 98% *ee*). Further calculations revealed that two possible triplet excited state structures exist for Rh-bound substrate complex **II**, one with the substrate alkene carbons possessing most of the spin density (**II-1** in **Figure 36c**) and the other with the majority of its spin density localized on Rh (**II-2** in **Figure 36c**). Though the two triplet excited species lie close in energy, **II-2** is incapable of undergoing the intramolecular HAT reaction, and instead serves as a triplet sensitizer⁹ transferring its energy to free substrate **1d**. The resultant background reaction might account for the lower than computationally predicted experimental *ee* value. To experimentally confirm that background sensitization is eroding enantioselectivity, *rac*-**Rhbpy**, a Rh complex incapable of coordinating to the substrate was synthesized and subjected to standard experimental conditions with **1d** (**Figure 35c**). And indeed, as a result **2d** was obtained in 30% yield after photolysis for 36 hours. Despite this undesirable background sensitization, high enantioselectivities are obtained because of extremely high levels of asymmetric induction in the Rh-mediated hetero-Diels–Alder reaction.

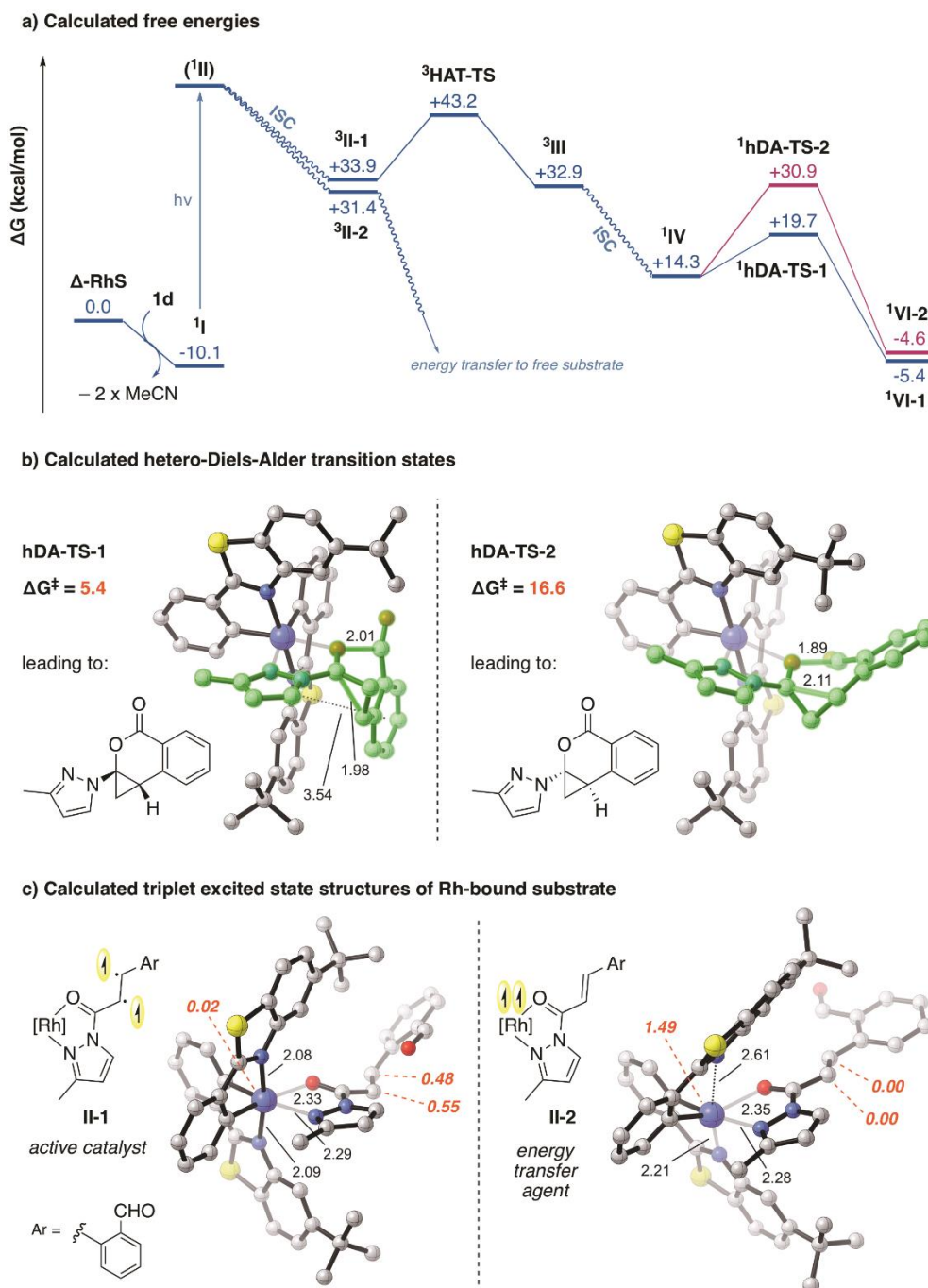


Figure 36. Computational study. a) Computed free energy diagram of the photoinduced HAT/hetero-Diels-Alder cascade reaction catalyzed by Δ -RhS. b) Calculated transition states for the intramolecular hetero-Diels-Alder reaction leading to major and minor product enantiomers. Energies are in kcal/mol, and interatomic distances are in ångströms. Hydrogen atoms are omitted for clarity. c) Two different calculated triplet excited states, **II-1** and **II-2**, for the Rh-bound substrate. Interatomic distances denoted in ångströms. Hydrogens are omitted for clarity. Spin densities on atoms are shown with red italic numbers.

2.1.5 Follow-up Chemistry

The pyrazole moiety in this case is both a directing group and a masked amination reagent. Mr. Chen-Xi Ye, a current Ph.D. student in the Meggers group, successfully subjected the compound **2d** to reductive ozonolysis following the method of Daugulis and co-workers,¹⁰ resulting in the conversion of

the pyrazole group into a formamide in 58% yield, without affecting the enantiomeric excess (**Figure 37**).

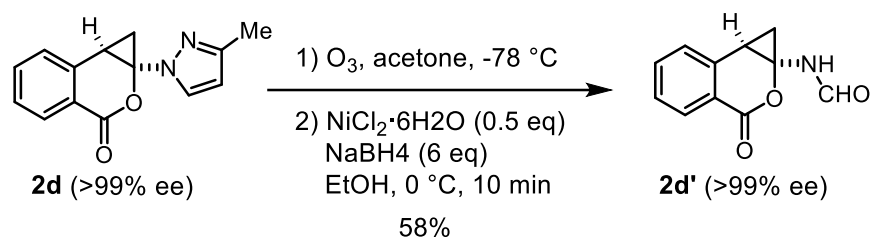


Figure 37. Subjected the compound **2d** to reductive ozonolysis.

2.1.6 Conclusions

We here reported a unique example of a catalytic asymmetric photoreaction which closely intertwines a hydrogen atom transfer from a photoexcited catalyst/substrate complex followed by a highly stereocontrolled intramolecular oxo-Diels-Alder reaction. Rhodium catalyst binding to the substrate does not only facilitate a visible-light-induced substrate-centered $\pi \rightarrow \pi^*$ excitation which permits the intramolecular hydrogen atom transfer, but also enables a highly stereocontrolled intramolecular oxo-Diels-Alder reaction through a very congested transition state. Further catalytic schemes which exploit the unique reactivities of photoexcited catalyst/substrate complexes in the context of asymmetric catalysis are ongoing in our laboratory.

References

1. a) L. Zhang, E. Meggers, *Acc. Chem. Res.* **2017**, *50*, 320-330. b) X. Huang, E. Meggers, *Acc. Chem. Res.* **2019**, *52*, 833.
2. a) X. Huang, T. R. Quinn, K. Harms, R. D. Webster, L. Zhang, O. Wiest, E. Meggers, *J. Am. Chem. Soc.* **2017**, *139*, 9120. b) X. Huang, X. Li, X. Xie, K. Harms, R. Riedel, E. Meggers, *Nat. Commun.* **2017**, *8*, 2245. N. Hu, H. Jung, Y. Zheng, J. Lee, L. Zhang, Z. Ullah, X. Xie, K. Harms, M.-H. Baik, E. Meggers, *Angew. Chem. Int. Ed.* **2018**, *57*, 6242.
3. J. Pérez-Prietoa, R.E. Galiana, M.A. Mirandab, *Mini-Rev. Org. Chem.* **2006**, *3*, 117.
4. W. Xia, Y. Shao, W. Gui, C. Yang, *Chem. Commun.* **2011**, *47*, 11098.
5. J. Ma, X. Xie, E. Meggers, *Chem. Eur. J.* **2018**, *24*, 259.
6. For early reports on HAT reactions to the triplet state of alkenes, see: a) E. F. Ullman, R. Weinkam, *J. Am. Chem. Soc.* **1970**, *92*, 5256. b) S. Ayral-Kaloustian, S. Wolff, W. C. Agosta, *J. Am. Chem. Soc.* **1977**, *99*, 5984.
7. For a recent photocyclization that is proposed to involve a similar intramolecular 1,6-HAT from an aldehyde to the triplet state of an alkene, see: W. Ding, C. C. Ho, N. Yoshikai, *Org. Lett.* **2019**, *21*, 1202.
8. a) H. Waldmann, *Synthesis* **1994**, 535. b) H. Pellissier, *Tetrahedron* **2009**, *65*, 2839; c) V.

- Eschenbrenner-Lux, K. Kumar, H. Waldmann, *Angew. Chem. Int. Ed.* **2014**, *53*, 11146.
9. For recent reviews on catalysis mediated by visible light energy transfer, see: a) F. Strieth-Kalthoff, M. J. James, M. Teders, L. Pitzer, F. Glorius, *Chem. Soc. Rev.* **2018**, *47*, 7190. b) Q.-Q. Zhou, Y.-Q. Zou, L.-Q. Lu, W.-J. Xiao, *Angew. Chem. Int. Ed.* **2019**, *58*, 1586.
10. S. H. Kwak, N. Gulia, O. Daugulis, *J. Org. Chem.* **2018**, *83*, 5844.

2.2 Catalytic α -Deracemization of Ketones Enabled by Photoredox Deprotonation and Enantioselective Protonation

2.2.1 Research Background and Reaction Design

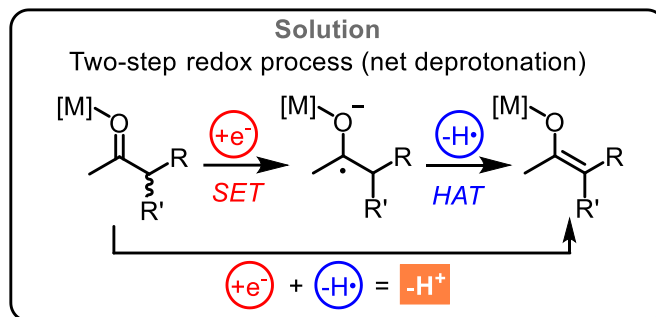
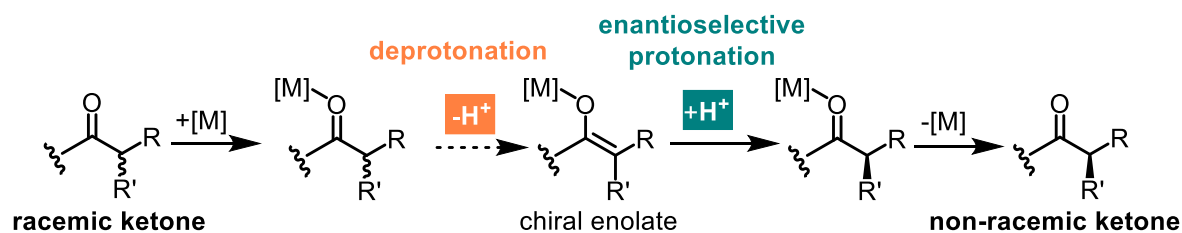
Chiral resolution of racemic mixtures is one of the most important methodology to obtain chiral products in an efficient way with practical value.¹ However, the biggest challenge is during the separation process, the theoretical yield of the expected enantiomerically pure product couldn't exceed a limit of 50%, which leads to a serious waste of chiral resources. Although dynamic kinetic resolution can achieve complete conversion to a single enantiomer, the product is structurally modified. Deracemization is an ideal method for asymmetric synthesis but challenging strategy for the conversion of a racemic mixture to its single enantiomer, without any further structural modification.² The deracemization strategy may provide an effective way to solve the shackles of the inefficiency of the splitting process. Despite the conceptual simplicity and potential practicality, deracemization is a thermodynamically disfavored process, which has limited its development, thus, to accomplish a deracemization reaction is very challenging. Despite, significant progress has been made in enzymatic deracemization.³ So far, there are only limited examples existing based on nonenzymatic deracemization, especially deracemization enabled by visible light photocatalysis still remains underdeveloped. Only few examples with insufficient enantioselectivities have been described by Bach and Knowles (**Figure 38a**). The Bach group reported several groundbreaking examples of visible light driven deracemizations of allenes and cyclopropyl quinolones using a chiral photosensitizer that exhibits different energy-transfer efficiencies for the two substrate enantiomers, resulting in get enantioenriched compounds.⁴ Instead of energy transfer, the Knowles group developed a conceptually novel approach for the deracemization of ureas through PCET hydroamination process, using an iridium photocatalyst, together with chiral base and chiral thiol catalyst.⁵

Carbonyl groups are one of the most important and abundant functional groups in organic chemistry. Carbonyl compounds are often key intermediates for the synthesis of more complex molecules. A prominent example is the C–H functionalization of carbonyl compounds at the α -position, which takes advantage of the intrinsic acidity of the α -C–H bond. This transformation not only offers a straightforward handle to introduce further functionality but often also generates a stereocenter (**Figure 38b**). The α -deracemization of carbonyl compounds is therefore an attractive strategy for generating enantiomerically pure carbonyl compounds. Surprisingly, α -deracemizations of carbonyl compounds are rare. Tsunoda^{6,7} and Matsumoto⁸ reported the α -deracemization of 2-alkylketones and 2-hydroxyketones, respectively, utilizing host-guest chemistry with a chiral host, while Wu⁹ developed an α -deracemization via crystallization-induced dynamic resolution of corresponding chiral imines. In these cases, equimolar amounts of a chiral reagent were needed.

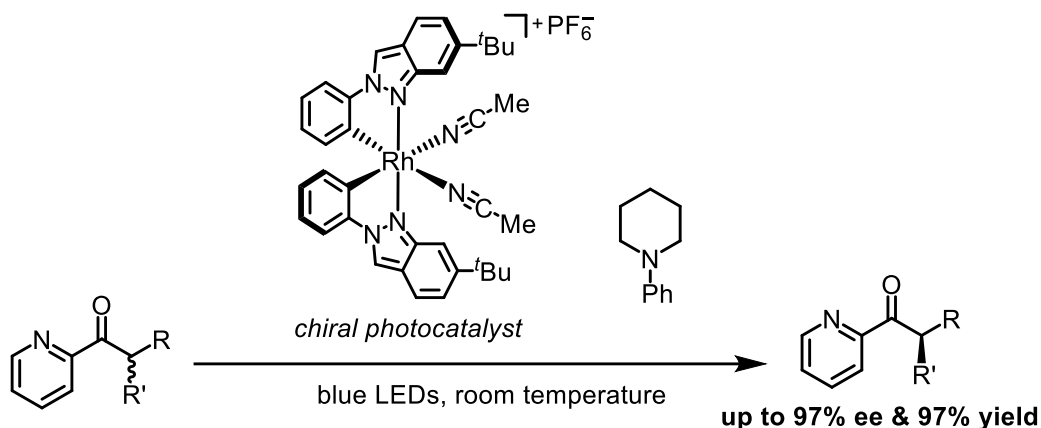
Enantioselective protonation is a fundamental method for synthesizing enantioenriched α -tertiary carbonyl compounds. In the past few decades, a number of enantioselective protonation reactions have

such as silyl enol ether is well established, including catalytic methods.¹¹⁻¹⁷ However, the principle of microscopic reversibility prohibits a one-pot reaction sequence of base-induced α -deprotonation of a carbonyl compound to its enolate followed by enantioselective protonation, as the equilibrium would always result in the formation of the entropically favored racemate. To circumvent the restriction of microscopic reversibility but still exploit well-established enolate chemistry, we envisioned that the enolate formation could be split into two elementary steps, a photoinduced electron transfer¹⁸ (+electron) to generate a ketyl intermediate, followed by a hydrogen atom transfer (-hydrogen), thus resulting in a net deprotonation (**Figure 39a**). In this scenario, deprotonation and protonation would follow distinct pathways, and the enrichment of one enantiomer would not violate the principle of microscopic reversibility. Using photons as a driving force,^{19,20} the conversion of a racemic carbonyl compounds into its single enantiomer may then be feasible. Herein, we demonstrate how deracemization of ketones can be accomplished by combining photoredox deprotonation with enantioselective protonation in a single reaction (**Figure 39b**), in which the photocatalyst harvests the visible light, induces the redox process, and is responsible for the asymmetric induction, while the amine serves as the single electron donor, HAT reagent and proton source. This conceptually simple light-driven strategy of coupling a photoredox deprotonation with a stereocontrolled protonation, in conjunction with an enrichment process, serves as a blueprint for other deracemizations of ubiquitous carbonyl compounds.

a Mechanistic plan: catalytic deracemization of ketones via metal enolate formation



b Realization (this work): light-driven deracemization of pyridylketones



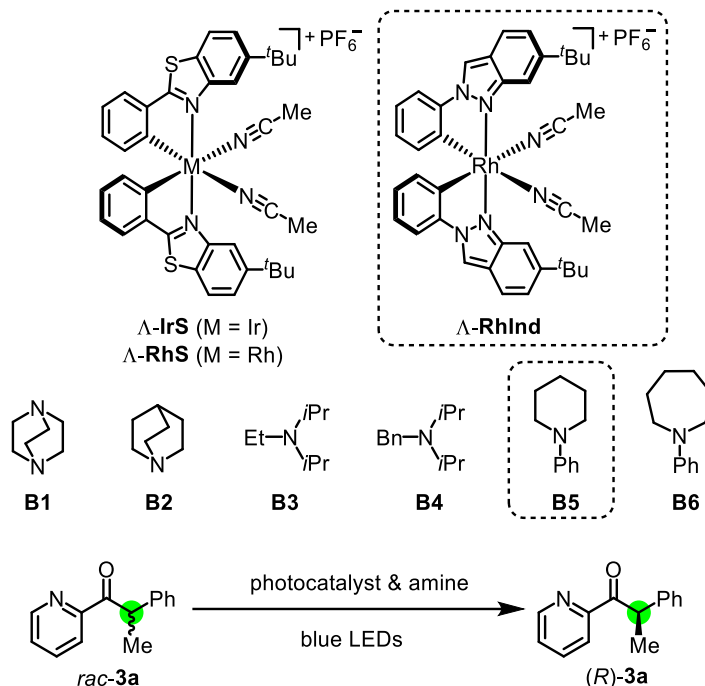
- Single catalyst for photochemistry & asymmetric induction
- Novel mechanistic concept for catalytic deracemization
- First example of catalytic deracemization via intermediate enolate

Figure 39. Catalytic deracemization of carbonyl compounds in α -position: motivation, mechanistic plan and realization.

2.2.2 Initial Experiments and Reaction Development

We commenced our study with the racemic ketone **3a**, which contains a tertiary stereogenic α -carbon. A pyridyl moiety is connected to the carbonyl group to generate a chelator for binding to photoactive bis-cyclometalated iridium or rhodium complexes for which we have demonstrated versatile asymmetric photocatalysis over the years.^{21,22} We envisioned that transition metal coordination, in combination with the withdrawing nature of the pyridine moiety, would stabilize the ketyl intermediate in the proposed SET/HAT sequence. Photolysis of *rac*-**3a** in the presence of the established chiral

iridium photocatalyst Λ -**IrS**²³ (4 mol%) in acetone together with DABCO (**B1**) or quinuclidine (**B2**) (each 3.0 equivalents) as electron donors and HAT reagents^{24,25} provided *rac*-**3a** unchanged as a complete racemate after 24 hours at room temperature (Table 2, entries 1 and 2). Replacing DABCO or quinuclidine with Hünig's base (**B3**) did not alter the outcome (entry 3). However, when we replaced the iridium photocatalyst Λ -**IrS** with the analogous bis-cyclometalated phenyl benzothiazole rhodium catalyst Λ -**RhS**,²⁶ ketone **3a** showed an enantiomeric excess (ee) of 26% (entry 4). Although this relates to a ratio of *R* and *S* enantiomers of just 63:37, this result encouraged us to further optimize the reaction conditions. Substituting Hünig's base with diisopropylbenzylamine (**B4**) saw the ee improve to 42% (entry 5). More notable results were obtained with *N*-phenylpiperidine (**B5**, 81% ee) and *N*-phenylazepane (**B6**, 84% ee) (entries 6 and 7). These results demonstrate that the efficiency of this light-driven deracemization^{4,5} is strongly affected by the structure of the amine. Nonetheless, despite significant screening efforts, we were not able not further improve the deracemization by modifying the amine. Fortuitously, we found that the related rhodium catalyst Λ -**RhInd**,²⁷ comprising of two cyclometalated 6-*tert*-butyl-2-phenyl-2*H*-indazole ligands, in combination with the base **B6**, provided an improved ee of 87% (entry 8). Combining Λ -**RhInd** with *N*-phenylpiperidine (**B5**) afforded (*R*)-**1** with 92% ee (entry 9). Having identified the optimal photocatalyst/base pair, we proceeded to finetune the reaction conditions. Other solvents or a reduced catalyst loading provided less satisfactory results (entries 10-12). However, when we decreased the amount of *N*-phenylpiperidine from 3.0 to 2.0 equivalents, the ee rose to 94%. Finally, optimal results were obtained upon addition of CaSO₄ as a drying agent. Blue light irradiation of *rac*-**3a** in the presence of Λ -**RhInd** (4.0 mol%), *N*-phenylpiperidine (2.0 equivalents) and CaSO₄ (5% m/v) in acetone for 24 hours provided the deracemized ketone (*R*)-**3a** with 96% ee and 97% isolated yield. A ¹H-NMR yield of 99% also demonstrated that under these reaction conditions no photochemical side reaction occurs. Control experiments verified that both the amine and light are required for the reaction, while air must be excluded (entries 15-17). However, catalytic amounts of amine are sufficient, although the obtained ee of (*R*)-**1** decreased somewhat (entry 18).

Table 2. Initial experiments and optimization.^a

entry	catalyst	amine	solvent	conditions	yield (%) ^b	ee (%) ^c
1	Δ -IrS (4.0)	B1 (3.0)	acetone	photolysis	quant.	0
2	Δ -IrS (4.0)	B2 (3.0)	acetone	photolysis	quant.	0
3	Δ -IrS (4.0)	B3 (3.0)	acetone	photolysis	quant.	0
4	Δ -RhS (4.0)	B3 (3.0)	acetone	photolysis	95	26
5	Δ -RhS (4.0)	B4 (3.0)	acetone	photolysis	85	42
6	Δ -RhS (4.0)	B5 (3.0)	acetone	photolysis	96	81
7	Δ -RhS (4.0)	B6 (3.0)	acetone	photolysis	94	84
8	Δ -RhInd (4.0)	B6 (3.0)	acetone	photolysis	87	87
9	Δ -RhInd (4.0)	B5 (3.0)	acetone	photolysis	94	92
10	Δ -RhInd (4.0)	B5 (3.0)	MeCN	photolysis	81	82
11	Δ -RhInd (4.0)	B5 (3.0)	THF	photolysis	85	82
12	Δ -RhInd (2.0)	B5 (3.0)	acetone	photolysis	90	89
13	Δ -RhInd (4.0)	B5 (2.0)	acetone	photolysis	91	94
14	Δ -RhInd (4.0)	B5 (2.0)	acetone	photolysis, CaSO ₄ ^d	99 (97) ^e	96
15	Δ -RhInd (4.0)	none	acetone	photolysis	quant.	0
16	Δ -RhInd (4.0)	B5 (3.0)	acetone	dark	quant.	0
17	Δ -RhInd (4.0)	B5 (3.0)	acetone	photolysis, air	quant.	0
18	Δ -RhInd (4.0)	B5 (0.1)	acetone	photolysis, CaSO ₄ ^d	99	90

^aConditions: **3a** (0.05 mmol) and amine (0.1-3.0 equiv) in acetone (0.5 mL) with Rh catalyst (2.0-4.0 mol%) irradiated with blue LEDs (24 W) for 24 hours at room temperature under an atmosphere of N₂, unless stated otherwise. ^bDetermined by ¹H NMR of the crude products using 1,1,2,2-tetrachloroethane as internal standard. ^cEnantioselectivities determined by HPLC on chiral stationary phase. ^dCaSO₄ (vacuum dried with heat gun) with 5% m/v. ^eIsolated yields.

2.2.3 Substrate Scope

To explore the scope of this new method, we applied the optimal reaction conditions in hand (Table 2, entry 14), we evaluated the substrate scope of this ketone deracemization. First, we modified the

phenyl moiety of pyridylketone **3a** (Figure 40). A methyl group in the *para*-, *meta*-, or *ortho*-position (**3b-3d**), as well as bulky *tert*-butyl (**3e**) or isobutyl (**3f**) groups in the *para*-position were well-tolerated and provided the deracemized ketones with 92-96% ee (90-98% yield). The light-driven deracemization permits electron-donating substituents in the phenyl moiety such as *para*-methoxy (**3g**) and 1,3-dioxole (**3h**), as well as electron-withdrawing substituents such as *para*-bromo (**3i**), *para*- or *ortho*-chloro (**3j**, **3k**), 3-fluoro-4-phenyl (**3l**), and 2,4-difluoro (**3m**) with 91-97% ee (87-95% yield). Only a *para*-CF₃ group provided a somewhat lower yield of 69% but with satisfactory 96% ee. An electron-rich and metal-coordinating thioether was also compatible and afforded the deracemized ketone **3o** with 97% ee (95% yield). Likewise, the double bond of an isobutenyl group was tolerated and provided the deracemized ketone **3p** with 91% ee (94% yield). The phenyl moiety can also be benzannulated to naphthalenes to efficiently provide deracemized ketones **3q** (95% ee, 88% yield) and **3r** (96% ee, 94% yield). The thiophene **3s** providing the deracemized ketone with a more moderate 86% ee (93% yield), while the dibenzofuran **3t** afforded the deracemized ketone **3t** with 95% ee (93% yield).

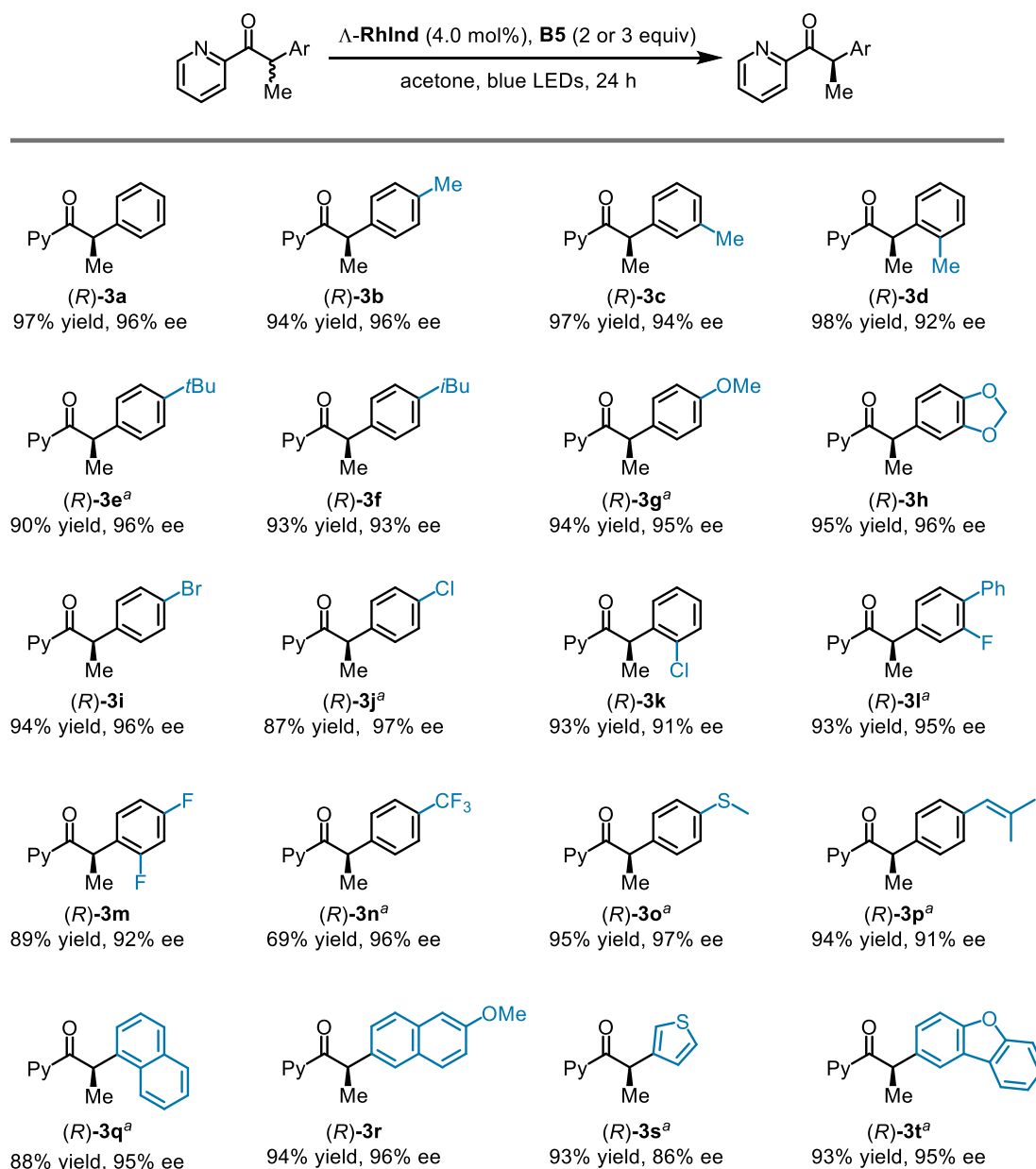


Figure 40. Substrate scope with pyridylketones bearing an aryl group at the stereocenter. Py = 2-pyridyl. Standard reaction conditions according to Table 2, entry 14. ^aDeviation from standard reaction conditions: 3.0 equivalents of *N*-phenylpiperidine (**B5**) instead. The absolute configuration of compound (*R*)-**3l** was determined by X-ray crystallography (CCDC 2081804).

Figure 41 reveals that other parts of the structural scaffold are also tolerant of modifications. Replacing the α -methyl group with an ethyl (**3u**) or isopropyl group (**3v**) or having an indane (**3w**) functionality provided the deracemized ketones with 86-89% ee (78-83% yield). An ether functionality in α -position afforded the deracemized ketone **3x** in 75% yield and with only moderate 64% ee. However, α -amino groups are compatible with the deracemization and afforded the α -aminoketones **3y-3aa** with 85-92% ee (82-95% yield). Interestingly, even a fluorine can be incorporated at the stereogenic carbon. The deracemized ketone **3ab** was isolated with 72% ee (93% yield), while the related aliphatic ketone **3ac** was isolated with only 40% ee (85% yield). Furthermore, examples **3ad-3ae** demonstrate that the pyridine moiety can be functionalized. A methyl (**3af**) or bromine (**3ag**) substituent in *ortho*-

position of the pyridine provide satisfactory enantioselectivities of 90% and 94% ee, respectively, but required an increased catalyst loading of 8.0 mol%, most likely due to a less efficient catalyst coordination to the modified pyridine moieties. The pyridine can also be replaced with a quinoline moiety to afford the deracemized ketone **3ai** with 87% ee (92% yield). Finally, ketone **3aj** reveals that a stereocenter that is connected to two aliphatic side chains provides only an inefficient deracemization.

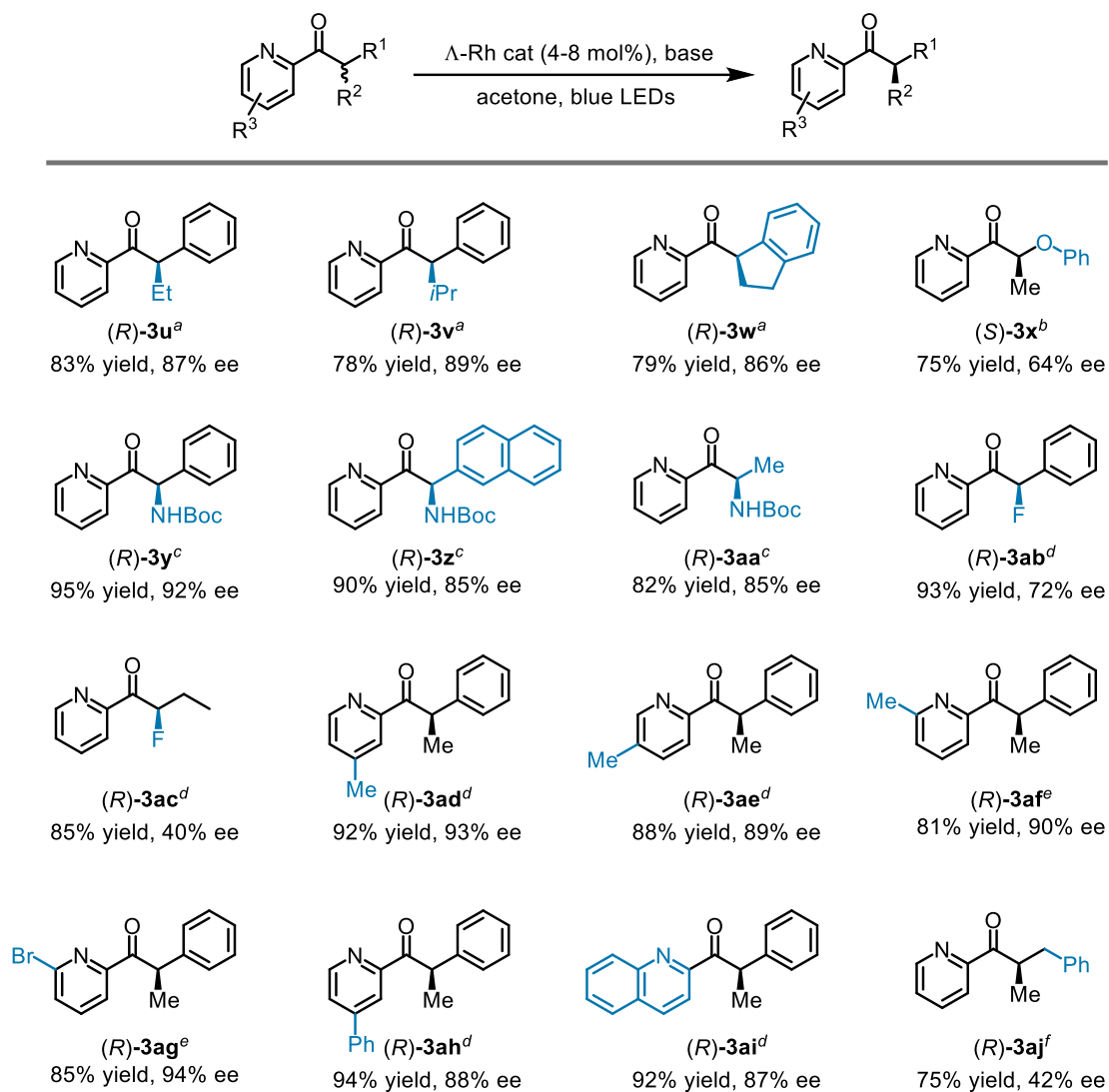


Figure 41. Expanded substrate scope. The combination of catalyst and base varied for optimal results. ^a $\Delta\text{-RhS}$ (8.0 mol%) as catalyst and 3,5-*(t*Bu)₂PhCH₂N(*i*Pr)₂ (3.0 equiv) as base. ^b $\Delta\text{-RhS}$ (4.0 mol%) as catalyst and *N*-phenylpiperidine as base (3.0 equiv). ^c $\Delta\text{-RhInd}$ (4.0 mol%) as catalyst and *N*-phenylazepane as base (3.0 equiv). ^d $\Delta\text{-RhInd}$ (4.0 mol%) as catalyst and *N*-phenylpiperidine (3.0 equiv) as base. ^e $\Delta\text{-RhInd}$ (8.0 mol%) as catalyst and *N*-phenylpiperidine (3.0 equiv) as base. ^f $\Delta\text{-RhInd}$ (4.0 mol%) as catalyst and *N,N*-diisopropylethylamine (3.0 equiv) as base.

2.2.4 Mechanistic Study

The proposed mechanism for the observed visible-light-driven deracemization of stereocenters in α -position of carbonyl groups within pyridylketones is shown in **Figure 42**. The catalytic cycle begins with the bidentate coordination of the racemic pyridylketone to the enantiomerically pure rhodium

catalyst to form complex **1I** as a mixture of two diastereomers, (*R*)-**1I** and (*S*)-**1I**. Photoexcitation to the triplet state **3I**, followed by SET from the tertiary amine, furnishes the rhodium ketyl radical complex **2II**.^{17,18} Subsequent hydrogen atom transfer (HAT) from the α -position of the ketyl to the amine radical cation generates rhodium enolate **1III** and a protonated amine, which are primed to undergo a diastereoselective proton transfer to provide the rhodium coordinated ketone **1I** as a single stereoisomer. Dissociation of the ketone then leads to a new catalytic cycle.

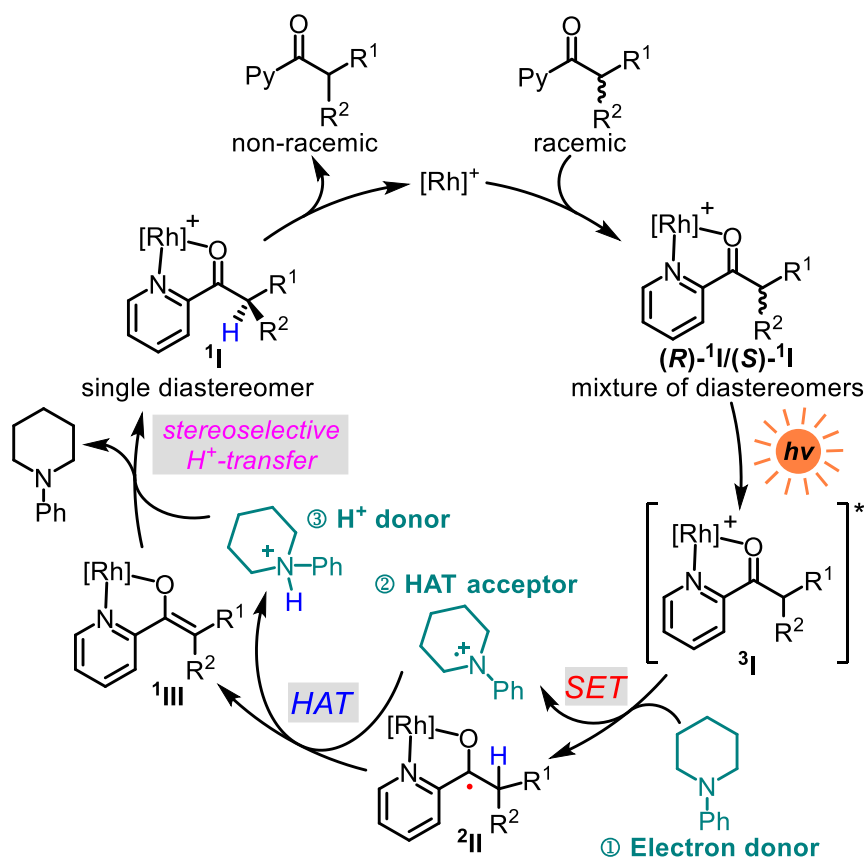


Figure 42. Proposed mechanism for the developed photoderacemization.

The independently synthesized and isolated catalyst/substrate complex **1I** displays a significantly increased absorbance in the visible region compared to the initial acetonitrile coordinated complex. It must therefore constitute the *in situ* generated main light absorbing species in this photocatalysis. Cyclic voltammetry of catalyst/substrate complex **1I** was used to determine a reduction potential $E_{pc}(^1I/^1I^-) = -0.90$ V vs. Ag/AgCl. Together with an estimated triplet energy of 2.5 eV²⁸ this leads to $E_{1/2}(^3I/^1I^-) =$ ca. 1.6 V and demonstrates that the photoexcited complex **3I** is capable of oxidizing aromatic amines (ca. 0.7-1.0 V vs. SCE),²⁹ thereby generating an amine radical cation and the Rh ketyl radical **2II**.

The following experiments provide strong support for the proposed reaction sequence. When the photoderacemization was performed with racemic ketone *rac*-**4d** in which the chiral center bears a deuterium atom (97% deuteration), the deuterated product (*R*)-**4d** was obtained in 96% yield with 95% ee and a remaining deuteration level of 40% (**Figure 43a**). The observed deuterium retention is a key experiment which verifies that the α -hydrogen of the racemic substrate is identical to the α -hydrogen of the deracemized product. This is consistent with our proposal that the amine radical cation serves

both as the HAT agent³⁰ and subsequently as the protonating agent ($^2\text{II} \rightarrow ^1\text{III} \rightarrow ^1\text{I}$). The somewhat reduced deuteration level can be attributed to the interference of residual water in the reaction mixture through direct protonation of the enolate. When the deracemization of *rac*-**3a** was performed in the presence of just one equivalent of D₂O under otherwise standard conditions, deracemized (*R*)-**4d** was isolated in 85% yield with 82% ee and a deuteration level of 30% (**Figure 43b**). This experiment demonstrates that even trace water interferes with the mechanism and provides support for an enolate protonation mechanism ($^1\text{III} \rightarrow ^1\text{I}$). A control experiment in which the photoderacemization was conducted with α -deuterated tertiary amine and deuterated acetone did not lead to any deuterium incorporation into the deracemized ketone, which excludes the alternative reaction pathway via α -deprotonation of the intermediate amine radical cation as well as scenarios in which the solvent serves as the hydrogen atom source (**Figure 43c**). The involvement of an α -deprotonation of the intermediate amine radical cation, otherwise a preferred reaction pathway for amine radical cations,³¹ can be excluded based on another experiment in which *N*-phenylpiperidine is replaced with triphenylamine, which does not possess any aliphatic α -C–H bonds (**Figure 43d**). Triphenylamine can indeed serve as an alternative base providing the deracemized ketone with 85% ee (93% yield).

Additional experiments shine further light on the role of the amine. Replacing the amine with a Hantzsch ester resulted in efficient formation of the alcohol **5** (**Figure 43e**). This result can be rationalized by reduction of the photoexcited catalyst/substrate complex ^3I with the Hantzsch ester to generate the ketyl intermediate ^2II ,³² followed by protonation and hydrogen donation from the Hantzsch ester radical cation to generate the alcohol **5**. Enolate ^1III cannot be formed in this case because although the Hantzsch ester can serve as an electron donor, it lacks the ability to act as a hydrogen atom acceptor after its initial oxidation. Finally, we probed the stereocontrolled protonation step $^1\text{III} \rightarrow ^1\text{I}$. The following experiment was performed by Mr. Xin Nie, a Ph.D. student in the Meggers group. Starting from the synthesized catalyst/substrate complex **6** from Δ -**RhInd** (intermediate ^1I in **Figure 42**), the strong base DBU (1.1 equiv) was used to generate the enolate complex **7** (intermediate ^1III in **Figure 42**) (**Figure 43f**). Without any purification, the enolate **7** was protonated with the hydrochloride salt of *N*-phenylpiperidine (5 equiv), followed by release of the coordinated compound **3a** from the rhodium center using 2,2'-bipyridine (10 equiv) as a competing ligand, to afford (*S*)-**3a** in 96% yield and with 50% ee. This result verifies the ability of enolate ^1III to undergo a stereocontrolled protonation ($^1\text{III} \rightarrow ^1\text{I}$ in **Figure 42**). These experiments further support the triple function of the amine as a single electron donor, hydrogen atom acceptor and proton source in sequential fashion within the same catalytic cycle. It is noteworthy that although stoichiometric and stepwise deprotonation/protonation allows for a partial deracemization in this experiment, the rhodium catalyzed reaction in the presence of catalytic or stoichiometric amounts of DBU only leads to racemization of (*R*)-**3a**, thus revealing that a base-catalyzed deracemization in the absence of light is not feasible (**Figure 43g**, left reaction). However, (*R*)-**3a**, which was synthesized from *rac*-**3a** using Δ -**RhInd**, can be readily converted by

photoderacemization to (*S*)-**3a** by just using the mirror-imaged catalyst Δ -**RhInd** (Figure 43g, right reaction).

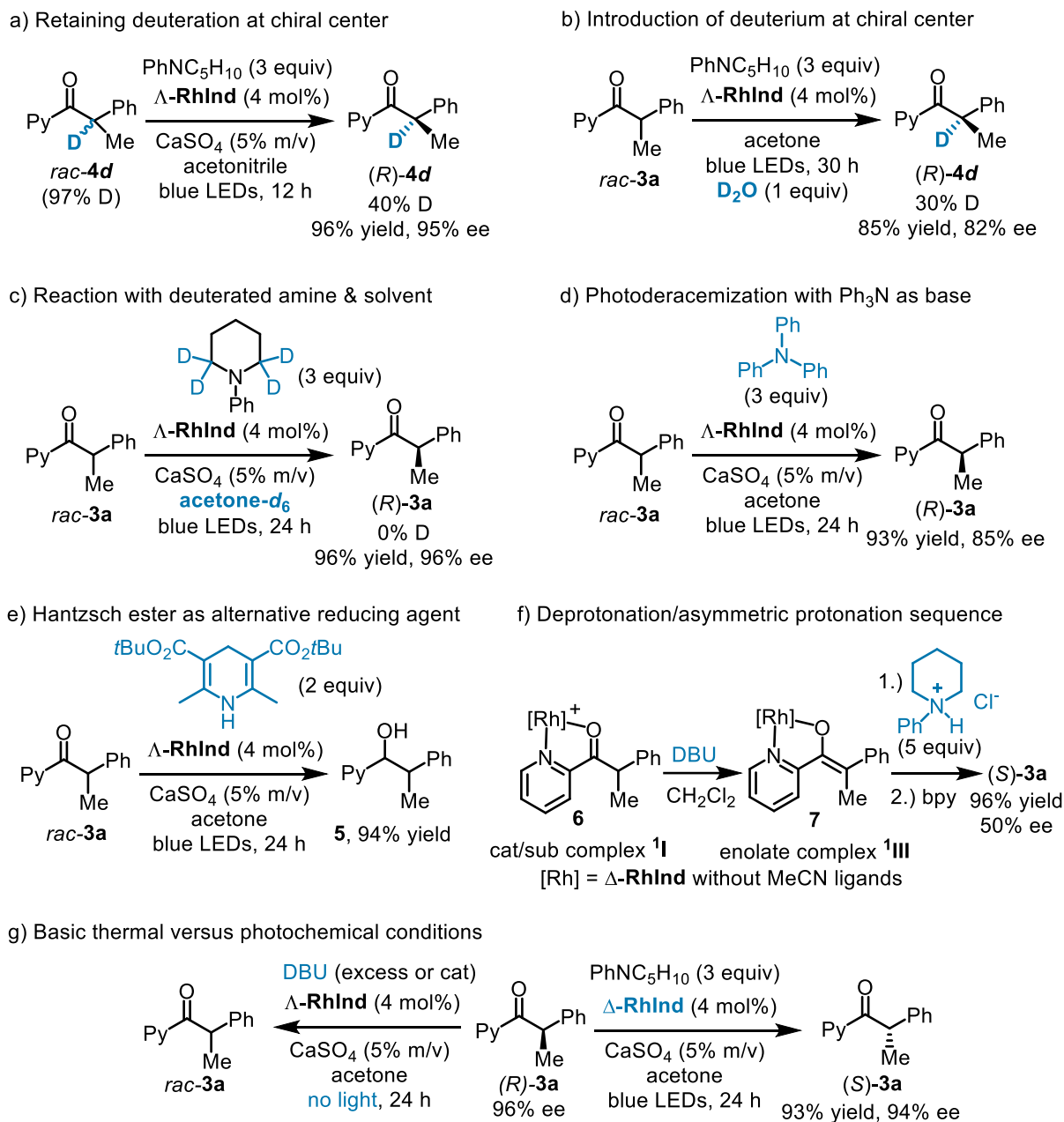


Figure 43. Supporting mechanistic experiments. bpy = 2,2'-bipyridine.

To provide further support to our proposed mechanism, Dr. Shuming Chen's research group cooperated with us and performed density functional theory (DFT) calculations (Figure 44). The bidentate coordination of pyridylketone (*S*)-**3a** to Δ -**RhInd**, with the displacement of two acetonitrile ligands, leads to photoactive complex (*S*)-**1**. Under visible light, (*S*)-**1** is excited to the triplet state (*S*)-**3** with a 52.5 kcal/mol increase in free energy. The SET between (*S*)-**3** and *N*-phenylpiperidine is exergonic by 13.5 kcal/mol. The resulting Rh ketyl complex (*S*)-**2** undergoes HAT with the amine radical cation with an activation free energy of 20.3 kcal/mol. Subsequent intersystem crossing (ISC) generates closed-shell Rh enolate **1III**. Protonation of Δ -**1III** by the ammonium species at the pro-*R* face

gives rise to (*R*)-**1I**, the diastereomeric counterpart of (*S*)-**1I** which is 2.9 kcal/mol higher in free energy. As (*R*)-**1I** is less stable, ligand exchange readily occurs to replace (*R*)-**1** with another molecule of (*S*)-**1** at its coordination sites, commencing another iteration of the photoinduced SET/HAT/protonation sequence. Over time, this leads to the enrichment of (*R*)-**3a** in the reaction mixture.

In conjunction with the control experiments (Figure 43), our computational results show that two enantioselectivity filters work in tandem in this reaction to achieve high ee. Firstly, the stereoselectivity of the enolate protonation step leads to the preferential formation of (*R*)-**1I**. Secondly, the favorability of (*S*)-**1I** over (*R*)-**1I** ensures that product inhibition does not occur and the enrichment process of (*R*)-**3a** does not arrest itself. The calculated structure of Rh enolate **1III** provides insight on why the enolate protonation is stereoselective. The π - π stacking between the enolate phenyl substituent and the indazole ligand is particularly strong in **1III**, with an Ar-Ar centroid distance of only 3.66 Å. This π - π stacking causes the pro-*R* face of the enolate to be much more exposed and accessible for protonation than the pro-*S* face. Calculated geometries of (*S*)-**1I** and (*R*)-**1I** also reveal the structural features underpinning the favorability of (*S*)-**1I** (Figure 44b). In (*S*)-**1I**, stronger π - π stacking is observed between the α -phenyl substituent of (*S*)-**1** and the indazole ligand. The role of π - π stacking in energetically differentiating the diastereomeric (*S*)-**1I** and (*R*)-**1I** also explains the lower ee values when ketones with aliphatic α -substituents are used. In addition, (*R*)-**1I** suffers from a steric clash (H...H distance 2.14 Å) between the α -methyl substituent of (*R*)-**1** and the *tert*-butyl group on the ligand. Both of these features explain why (*S*)-**1I** is 2.9 kcal/mol more stable than (*R*)-**1I**.

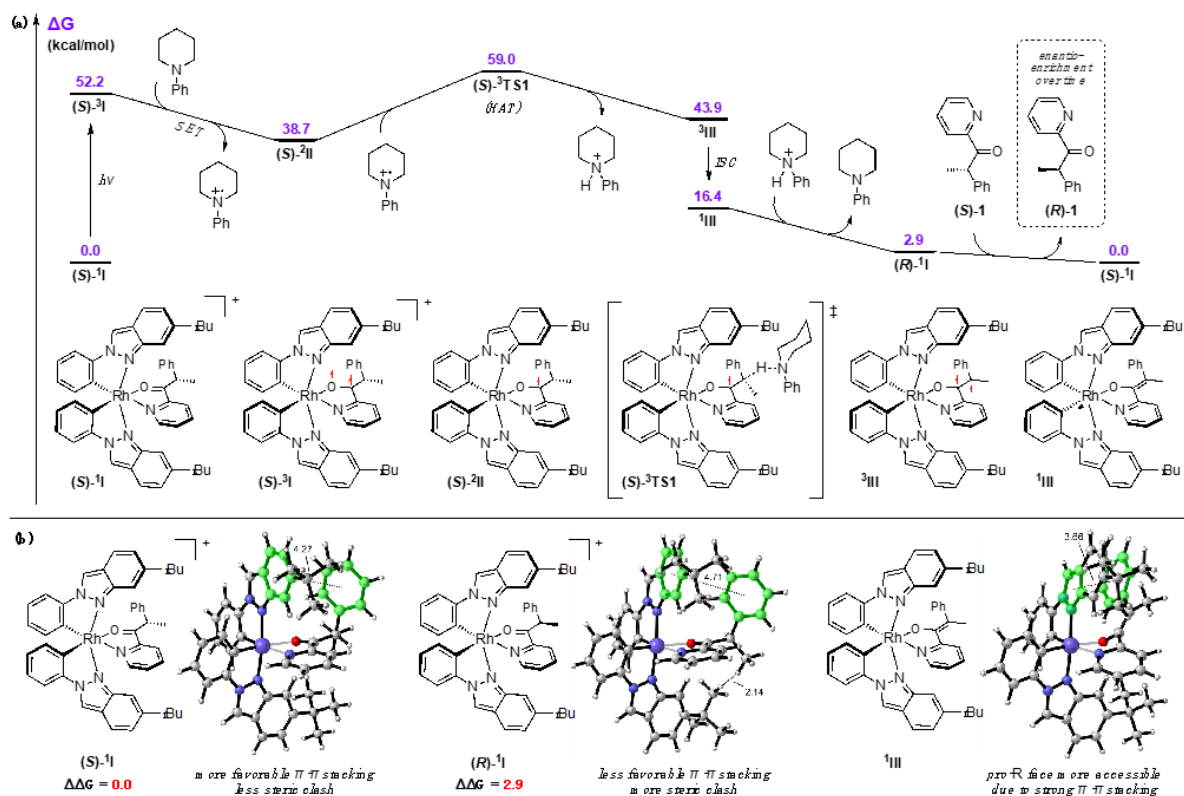


Figure 44. Computational study. (a) Calculated free energy diagram of the Λ -RhInd-catalyzed conversion of (*S*)-**3a** into (*R*)-**3a** at the ω B97X-D/def2-TZVPP-SDD(Rh), SMD (acetone)//B3LYP-D3BJ/def2-SVP-LANL2DZ(Rh) level of theory. (b) Calculated geometries and relative free energies

(kcal/mol) of intermediates. Interatomic distances are shown in ångströms (Å).

2.2.5 Follow-up chemistry

The transformations of the product (*S*)-**3a** are shown in **Figure 45**. By treating with sodium borohydride, the carbonyl group of (*S*)-**3a** was hydrogenated to give chiral alcohol **8** with high diastereoselectivity (dr = 32:1). Reductive deoxygenation of **8** gave chiral pyridine derivative **9** without affecting the enantiomeric excess. By Wittig reaction, **8** was successfully converted to the corresponding olefin **10** with full retention of the chiral center. On the other hand, my colleague Chen-Xi Ye also explored some follow-up chemistry of (*S*)-**3a**. Chen-Xi Ye tried to use (*S*)-**3a** and Grignard reagent for the reaction and finally obtained a chiral tertiary alcohol **11** with high ee and high dr. On the other hand, Chen-Xi Ye used (*S*)-**3a** as the starting substrate to obtain the chiral 1-Phenylethanol **12** after the Baeyer-Villiger-Oxidation and subsequent removal of the carbonyl pyridine group. Finally, Chen-Xi Ye successfully obtained chiral triazole compound **13** by dearomatization of pyridine. Moreover, the modification of pyridine group was demonstrated by nucleophilic addition of cyano group to the pyridine nitrogen oxides in a two-step procedure to afford compound **14** with nearly full retention of the enantiomeric excess.

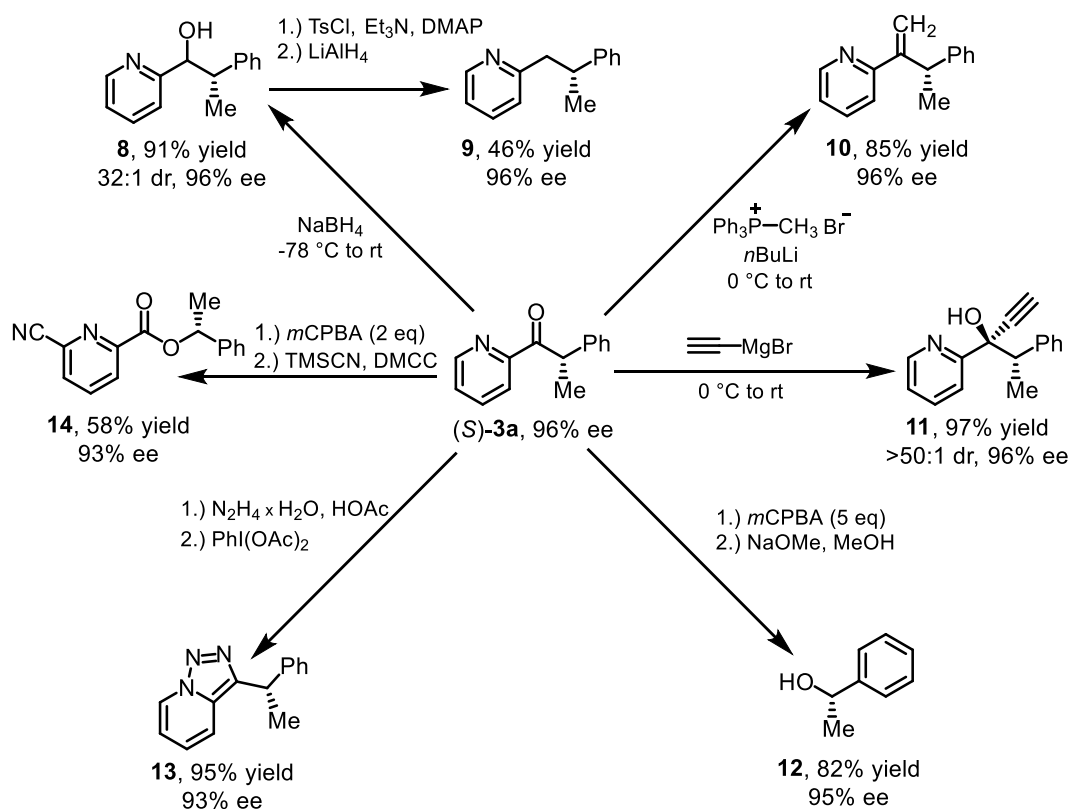


Figure 45. Follow-up chemistry. Conversions starting from compound (*S*)-**3a**.

2.2.6 Conclusions

Deracemization is an ideal but challenging strategy for the conversion of racemic mixtures to a single enantiomer. We here reported the first example of a photoderacemization of carbonyl compounds bearing an α -stereogenic center. The visible light photolysis of racemic pyridylketones in the presence of a single photocatalyst and a simple tertiary amine provides non-racemic carbonyl compounds with up to 97% enantiomeric excess. Mechanistic experiments and DFT calculations support a novel mechanism through a photoredox deprotonation to an intermediate enolate, followed by a stereocontrolled protonation step. A combination of stereoselective protonation and an enrichment process due to the different Rh-coordination preference of the two enantiomers results in an efficient overall deracemization. While catalytic one-step deracemization through a simple deprotonation/reprotonation sequence is prohibited by the principle of microscopic reversibility, we demonstrate that this can be overcome by splitting the deprotonation step into a photoinduced SET/HAT sequence. A chiral rhodium catalyst serves a dual function as the photoredox catalyst and chiral Lewis acid catalyst, while a tertiary amine co-catalyst plays a triple role sequentially as the single electron donor, hydrogen atom acceptor and proton source within one catalytic cycle. Innumerable methods exist for introducing substituents into the α -position of carbonyl compounds. This photochemical deracemization will serve as a blueprint for other deracemizations of ubiquitous carbonyl compounds and thus expand the synthetic toolbox for the synthesis of functionalized non-racemic carbonyl compounds.

References

1. Forselected reviews, see: a) E. Vedejs, M. Jure, *Angew. Chem. Int. Ed.* **2005**, *44*, 3974. b) M. Rachwalski, N. Vermue, F. P. J. T. Rutjes, *Chem. Soc. Rev.* **2013**, *42*, 9268. c) O. Verho, J.-E. Bäckvall, *J. Am. Chem. Soc.* **2015**, *137*, 3996.
2. Forselected reviews, see: a) C. C. Gruber, I. Lavandera, K. Faber, W. Kroutil, *Adv. Synth. Catal.* **2006**, *348*, 1789. b.) A. R. A. Palmans, *Mol. Syst. Des. Eng.* **2017**, *2*, 34.
3. M. Hall, A. S. Bommarius, *Chem. Rev.* **2011**, *111*, 4088.
4. A. Hölzl-Hobmeier, A. Bauer, A. V. Silva, S. M. Huber, C. Bannwarth, T. Bach, *Nature* **2018**, *564*, 240.
5. N. Y. Shin, J. M. Ryss, X. Zhang, S. J. Miller, R. R. Knowles, *Science* **2019**, *366*, 364.
6. T. Tsunoda, H. Kaku, M. Nagaku, E. Okuyama, *Tetrahedron Lett.* **1977**, *38*, 7759.
7. H. Kaku, T. Imai, R. Kondo, S. Mamba, Y. Watanabe, M. Inai, T. Nishii, M. Horikawa, T. Tsunoda, *Eur. J. Org. Chem.* **2013**, 8208.
8. K. Matsumoto, K. Otsuka, T. Okamoto, H. Mogi, *Synlett.* **2007**, 729.
9. J. Košmrlj, L. O. Weigel, D. A. Evans, C. W. Downey, J. Wu, *J. Am. Chem. Soc.* **2003**, *125*, 3208.
10. a) J. T. Mohr, A. Y. Hong, B. M. Stoltz, *Nat. Chem.* **2009**, *1*, 359. b) T. K. Hyster, *Synlett* **2020**, *31*,

248. c) M. Hou, L. Lin, X. Chai, X. Zhao, B. Qiao, Z. Jiang, *Chem. Sci.* **2019**, *10*, 6629
11. C. Fehr and J. Galindo, *Angew. Chem., Int. Ed. Engl.* **1994**, *33*, 1888.
12. E. Vedejs, N. Lee, S. T. Sakata, *J. Am. Chem. Soc.* **1994**, *116*, 2175.
13. K. Ishihara, S. Nakamura, M. Kaneeda, H. Yamamoto, *J. Am. Chem. Soc.* **1996**, *118*, 12854.
14. S. Nakamura, M. Kaneeda, K. Ishihara, H. Yamamoto, *J. Am. Chem. Soc.* **2000**, *122*, 8120.
15. D. Uraguchi, N. Kinoshita, T. Ooi, *J. Am. Chem. Soc.* **2010**, *132*, 12240.
16. C. H. Cheon, O. Kanno, F. D. Toste, *J. Am. Chem. Soc.* **2011**, *133*, 13248.
17. F. Mandrelli, A. Blond, T. James, H. Kim, B. List, *Angew. Chem. Int. Ed.* **2019**, *58*, 11479.
18. G. Pandey, *Top. Curr. Chem.* **1993**, *168*, 175.
19. R. C. McAtee, E. J. McClain, C. R. J. Stephenson, *Trends Chem.* **2019**, *1*, 111.
20. C. Prentice, J. Morrisson, A. D. Smith, E. Zysman-Colman, *Beilstein J. Org. Chem.* **2020**, *16*, 2363.
21. L. Zhang, E. Meggers, *Acc. Chem. Res.* **2017**, *50*, 320.
22. X. Huang, E. Meggers, *Acc. Chem. Res.* **2019**, *52*, 833.
23. H. Huo, X. Shen, C. Wang, L. Zhang, P. Rose, L.-A. Chen, K. Harms, M. Marsch, G. Hilt, E. Meggers, *Nature* **2014**, *515*, 100.
24. J. Jeffrey, F. R. Petronijevic, D. W. C. MacMillan, *J. Am. Chem. Soc.* **2015**, *137*, 8404.
25. J. L. Jeffrey, J. A. Terrett, D. W. C. MacMillan, *Science* **2015**, *349*, 1532.
26. J. Ma, X. Shen, K. Harms, E. Meggers, *Dalton Trans.* **2016**, *45*, 8320.
27. P. S. Steinlandt, W. Zuo, K. Harms, E. Meggers, *Chem. Eur. J.* **2019**, *25*, 15333.
28. X. Huang, J. Lin, T. Shen, K. Harms, M. Marchini, P. Ceroni, E. Meggers, *Angew. Chem. Int. Ed.* **2018**, *57*, 5454.
29. H. G. Roth, N. A. Romero, D. A. Nicewicz, *Synlett* **2016**, *27*, 714.
30. L. Capaldo, D. Ravelli, *Eur. J. Org. Chem.* **2017**, 2056.
31. J. Hu, J. Wang, T. H. Nguyen, N. Zheng, *Beilstein J. Org. Chem.* **2013**, *9*, 1977.
32. P.-Z. Wang, J.-R. Chen, W.-J. Xiao, *Org. Biomol. Chem.* **2019**, *17*, 6936.

Chapter 3: Summary and Outlook

3.1 Summary

1) Asymmetric photorearrangement to benzo-[d]cyclopropa[b]pyranones involving intramolecular hydrogen atom transfer

We demonstrated that a **RhS** catalyst/substrate complex irradiated by visible light behaved like a diradical upon photoexcitation. Intramolecular HAT from the nearby aldehyde to the α -position radical produces an acyl radical, followed by a highly stereocontrolled hetero-Diels-Alder reaction to give the cyclopropane products. This work expands the reaction modes of photoexcited catalyst/substrate complexes for applications in asymmetric catalysis.

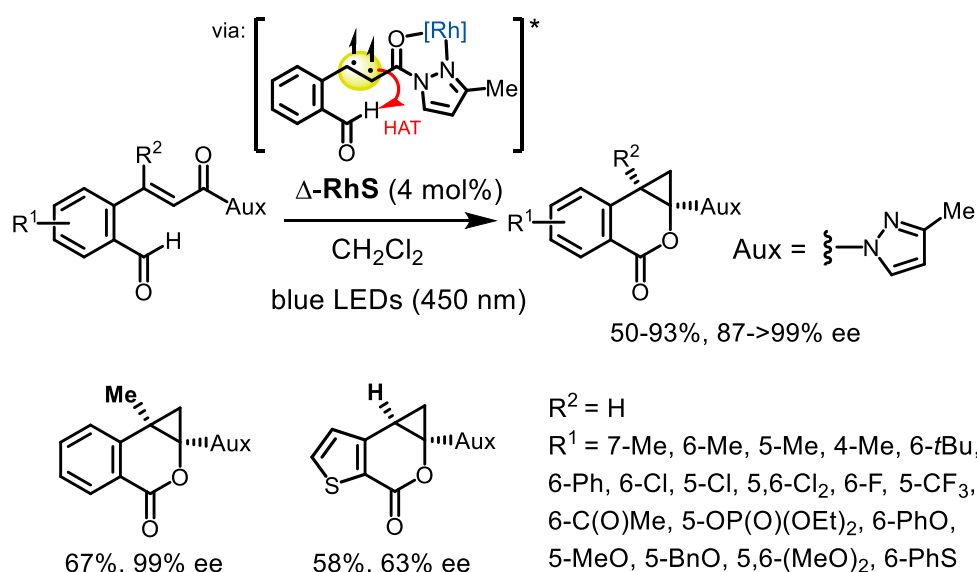
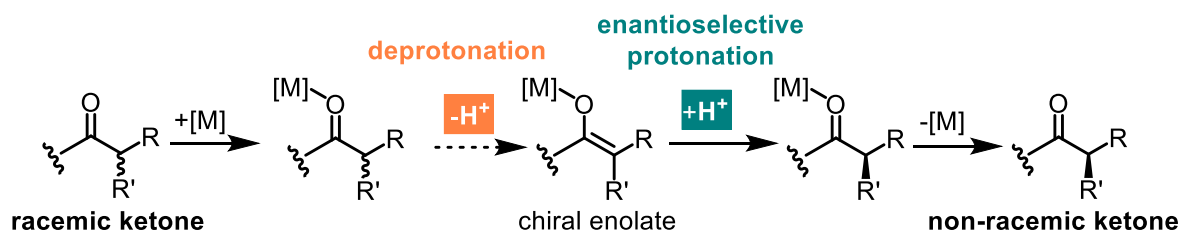


Figure 46. Asymmetric photorearrangement to benzo-[d]cyclopropa[b]pyranones involving intramolecular hydrogen atom transfer.

2) Photoinduced deracemization of carbonyl compounds *via* photoredox deprotonation and enantioselective protonation

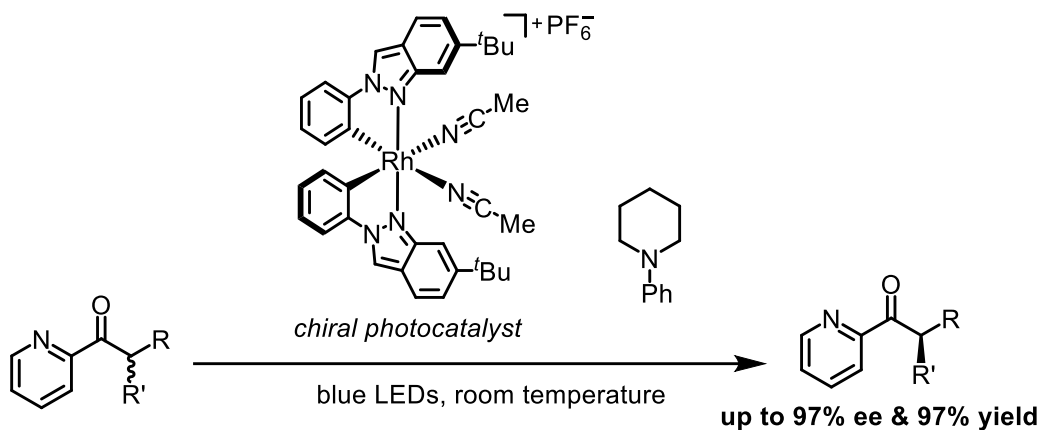
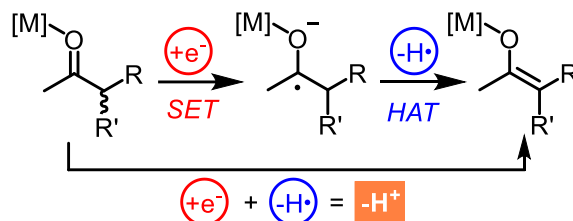
The first example of a single-operation catalytic deracemization of ketones has been developed, which lead to the formation of chiral carbonyl compounds in an efficient way with high yield (up to 97%) and high enantioselectivity (up to 97%). We achieved this with a novel mechanism by coupling a deprotonation with an enantioselective protonation. In which, we proposed a strategy for photoredox deprotonation through single electron transfer (SET) and subsequent intermolecular hydrogen atom transfer (HAT). This unprecedented light-driven deracemization strategy will serve as a blueprint for other deracemizations of ubiquitous carbonyl compounds.

**Challenge**

Microscopic reversibility prohibits base-induced deprotonation for deracemization!

Solution

Two-step redox process (net deprotonation)



- Single catalyst for photochemistry & asymmetric induction
- Novel mechanistic concept for catalytic deracemization
- First example of catalytic deracemization via intermediate enolate

Figure 47. Photoinduced deracemization of carbonyl compounds via photoredox deprotonation and enantioselective protonation.

3.2 Outlook

Recent work by the Meggers group clearly demonstrates the versatility and powerful reactivity of bis-cyclometalated chiral-at-metal rhodium(III) complexes as bifunctional photoredox catalysts in photocatalysis. Therefore, it should be of high interest for further broad synthetic applications.

1) Expanding new substrate activation modes in enantioselective photoredox catalysis

These chiral-at-metal catalysis have the limitation of requiring substrates with bidentate N,O-based metal-binding sites, such as 2-acyl imidazoles, 2-acyl pyridines, and N-acyl pyrazoles. The limitations of the substrates seriously affect the generality and application of the product. Considering the bis-cyclometalated chiral-at-metal rhodium(III) complexes as excellent Lewis acids, perhaps just using the chiral-at-metal rhodium as Lewis acid and adding additional photocatalysts would extend the application of the substrate.

2) Combining chiral-at-metal complexes with enzyme catalysis

Compared with traditional chemical synthesis, enzyme-catalyzed biosynthesis has been an important area of research because of its advantages of mild reaction conditions, high selectivity and green sustainability. However, the types of enzyme-catalyzed reactions are often limited to those exclusively catalyzed by the enzyme itself, which greatly limits the variety of chemicals that can be synthesized by biosynthetic methods. Photoenzymatic catalysis involves combining photocatalysis and enzymatic catalysis in a single system to synthesize compounds that are difficult to obtain in one catalytic domain alone. This novel organocatalytic approach shows great potential for economically and ecologically more efficient synthesis. Combining chiral-at-metal complexes with enzymes (such as oxidases, reductases, etc.) for photoenzymatic catalysis or synthesizing new biological enzymes by modifying chiral-at-metal complexes into biological enzymes through click chemistry will expand the scope of utilization of chiral metal complexes.

Chapter 4: Experimental Part

4.1 Materials and Methods

All reactions were carried out under an atmosphere of nitrogen with magnetic stirring unless indicated otherwise. The catalytic reactions were performed in Schlenk tube.

Solvents and Reagents

The oxygen free and water free solvents were distilled under nitrogen from calcium hydride (CH_2Cl_2 and CH_3CN) or sodium/benzophenone (Et_2O and THF). Super-dry solvents, such as Acetone (max. 0.01% water, purchased from AppliChem GmbH) were purchased from commercial available source and used directly without further drying. All reagents were purchased from Acros, Alfa aesar, Sigma Aldrich, TCI, ChemPur, Merck and Fluorochem were used without any further purification.

Chromatographic Methods

The course of the reactions and the column chromatographic elution were monitored by thin layer chromatography (TLC) [Macherey-Nagel (ALUGRAM®Xtra Sil G/UV254)]. Flash column chromatography was performed with silica gel from (particle size 0.040-0.063 mm)

Nuclear Magnetic Resonance Spectroscopy (NMR)

^1H NMR, proton decoupled ^{13}C NMR, and proton coupled ^{19}F NMR spectra were recorded on Bruker Avance 300 system (^1H NMR: 300 MHz, ^{13}C NMR: 75 MHz, ^{19}F NMR: 282 MHz) spectrometers and Bruker Avance 250 system (^1H NMR: 250 MHz, ^{19}F NMR: 235 MHz) spectrometers at ambient temperature. Chemical shifts are given in ppm on the δ scale, and were determined after calibration to the residual signals of the solvents, which were used as an internal standard. NMR standards were used are as follows: ^1H NMR spectroscopy: $\delta = 7.26$ ppm (CDCl_3), $\delta = 5.32$ ppm (CD_2Cl_2), $\delta = 1.94$ ppm (CD_3CN), $\delta = 4.78, 3.31$ ppm (CD_3OD), $\delta = 2.50$ ppm ($(\text{CD}_3)_2\text{SO}$); ^{13}C NMR spectroscopy: $\delta = 77.16$ ppm (CDCl_3), $\delta = 54.0$ ppm (CD_2Cl_2), $\delta = 118.26, 1.32$ ppm (CD_3CN), $\delta = 49.0$ ppm (CD_3OD), $\delta = 39.52$ ppm ($(\text{CD}_3)_2\text{SO}$). ^{19}F NMR spectroscopy: $\delta = 0$ ppm (CFCl_3). The characteristic signals were specified from the low field to high field with the chemical shifts (δ in ppm). ^1H NMR spectra peak multiplicities indicated as singlet (s), doublet (d), doublet of doublet (dd), doublet of doublet of doublet (ddd), doublet of doublet of doublet of doublet (dddd), triplet (t), doublet of triplet (dt), triplet of triplet (tt), quartet (q), multiplet (m). The coupling constant J indicated in hertz (Hz).

NMR yields were determined using 1,1,2,2-tetrachloroethane as internal standard.

High-Performance Liquid Chromatography (HPLC)

Chiral HPLC was performed with an Agilent 1200 Series or Agilent 1260 Series HPLC System. All the HPLC conditions were detailed in the individual procedures. The type of the columns, mobile phase and the flow rate were specified in the individual procedures.

Infrared Spectroscopy (IR)

IR measurements were recorded on a Bruker Alpha-P FT-IR spectrometer. The absorption bands were indicated a wave numbers ν (cm^{-1}). All substances were measured as films or solids.

Mass Spectrometry (MS)

High-resolution mass spectra were recorded on a Bruker En Apex Ultra 7.0 TFT-MS instrument using ESI or APCI or FD technique. Ionic masses are given in units of m/z for the isotopes with the highest natural abundance.

UV/Vis Analysis Spectroscopy and Stern-Volmer Quenching Experiments

UV/Vis measurements and quenching experiments were taken on a Spectra Max M5 microplate reader in a 10.0 mm quartz cuvette.

Crystal Structure Analysis

Crystal X-ray measurements and the crystal structure analysis were carried out by Dr. Klaus Harms and Dr. Sergei Ivlev (Chemistry Department, Philipps University of Marburg). X-ray data were collected with an STOE STADIVARI diffractometer equipped with with CuK radiation, a graded multilayer mirror monochromator ($\lambda = 1.54178 \text{ \AA}$) and a DECTRIS PILATUS 300K detector using an oil-coated shock-cooled crystal at 100(2) K. Scaling and absorption correction was performed by using the SADABS software package of Bruker. The structure was solved by direct methods by using the program XT V2014/1 (Bruker AXS Inc., 2014) and refined by full matrix least squares procedures on F^2 using SHELXL-2018/1 (Sheldrick, 2018). The Flack parameter is a factor used to estimate the absolute configuration of the compounds.

Optical Rotation Polarimeter

Optical rotations were measured on a Krüss P8000-T or Perkin-Elmer 241 polarimeter with $[\alpha]_D^{25}$ values reported in degrees with concentrations reported in g/100 mL.

Light Source

A 24 W Blue LEDs (Hongchangzhaoming from Chinese Taobao, <https://hongchang-led.taobao.com>) served as light sources. See **Figure 48** for the emission spectrum.

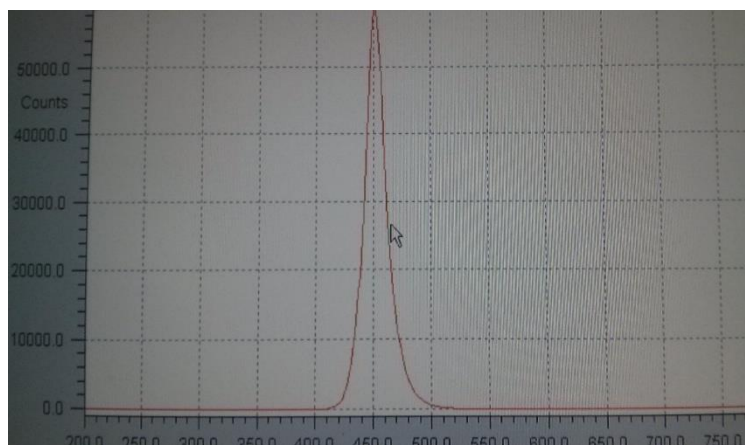
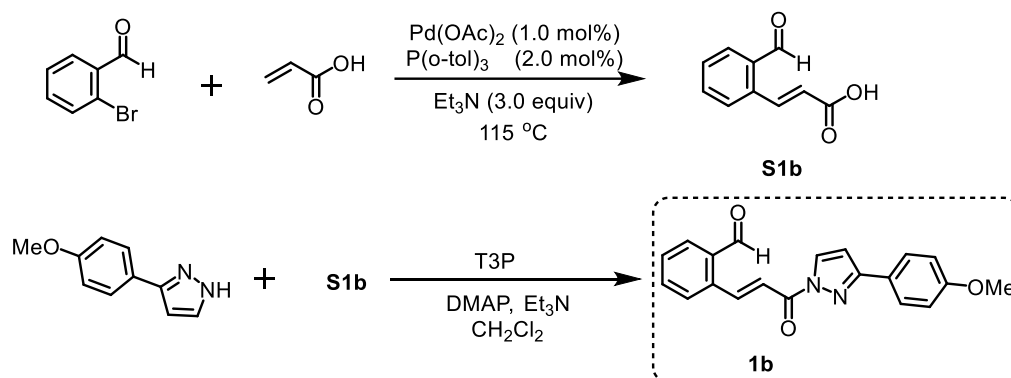


Figure 48. Emission spectrum of the 24 W blue LEDs lamp use in this study. Picture from Christian P. Haas.

4.2 Asymmetric Photocatalysis by Intramolecular Hydrogen Atom Transfer in Photoexcited Catalyst-Substrate Complex

4.2.1 Synthesis of the Substrates



First step: 2-Formylcinnamic acid S1b was synthesized by a Heck reaction.¹ The 2-bromobenzaldehyde (1.0 equiv) was dissolved in dimethylformamide (2.0 mL/mmol aldehyde). Then $\text{Pd}(\text{OAc})_2$ (0.01 equiv), $\text{P}(\text{o-tol})_3$ (0.02 equiv), the acrylic acid (2.0 equiv) and Et_3N (3.0 equiv) were added. The mixture was degassed under nitrogen purge for 15 min and then the resulting mixture was heated in an oil bath at $115\text{ }^\circ\text{C}$ and magnetically stirred under nitrogen overnight. After the reaction was completed, the mixture was cooled to room temperature. Then the mixture was acidified with 2 N HCl at $0\text{ }^\circ\text{C}$. The white precipitate appeared and was collected by filtration and washed to neutrality with water. The obtained solid was dried in vacuum to give the crude product which was directly used for the next step without further purification.

Second step: α,β -Unsaturated N-acylpyrazole 1b was synthesized according to our recent published procedure.² To a solution of pyrazole (1.0 equiv) and α,β -unsaturated carboxyl acid (1.5 equiv) in CH_2Cl_2 (0.2 M) at room temperature, 1-propanephosphonic acid cyclic anhydride (T3P, 50% solution in EtOAc; 1.5 equiv) was added dropwise. After stirring for 1 hour at room temperature, the mixture was cooled to $0\text{ }^\circ\text{C}$ and then DMAP (0.2 equiv) and Et_3N (3.0 equiv) were added dropwise. The reaction mixture was then allowed to warm to room temperature with stirring. After complete conversion of pyrazole was detected by TLC, the mixture was poured into hydrochloric acid solution (1 M) and extracted with EtOAc for three times. The combined organic layers were washed with NaOH solution (2 M), saturated NaHCO_3 solution and brine. After dried with anhydrous Na_2SO_4 , filtration and concentration under reduced pressure, the crude residue was purified by flash chromatography on silica gel (*n*-hexane/EtOAc = 30:1 to 3:1) to afford the substrate **1b** as a white solid. Yield: 80%.

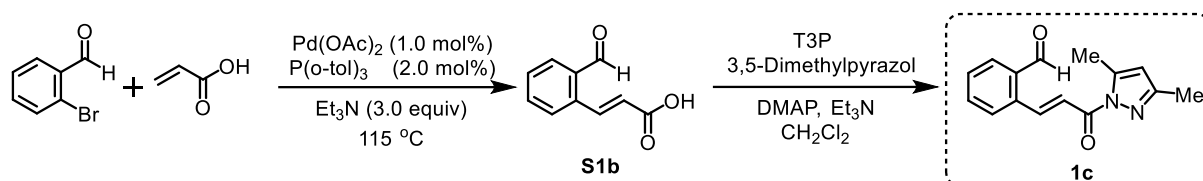
(*E*)-2-(3-(3-(4-Methoxyphenyl)-1H-pyrazol-1-yl)-3-oxoprop-1-en-1-yl)benzaldehyde (**1b**)

$^1\text{H NMR}$ (300 MHz, CDCl_3) δ 10.37 (s, 1H), 8.86 (d, $J = 15.9$ Hz, 1H), 8.40 (d, $J = 2.9$ Hz, 1H), 8.00–7.81 (m, 5H), 7.64 (dtd, $J = 22.0, 7.4, 1.2$ Hz, 2H), 7.02–6.93 (m, 2H), 6.77 (d, $J = 2.9$ Hz, 1H), 3.85 (s, 3H).

$^{13}\text{C NMR}$ (75 MHz, CDCl_3) δ 191.6, 162.8, 160.5, 155.3, 143.5, 136.6, 134.2, 133.9, 132.2, 130.3,

130.0, 128.4, 127.7, 124.4, 121.0, 114.2, 107.7, 55.3.

HRMS (ESI, m/z) calcd for $C_{20}H_{16}N_2O_3Na$ $[M+Na]^+$: 355.1059, found: 355.1055.



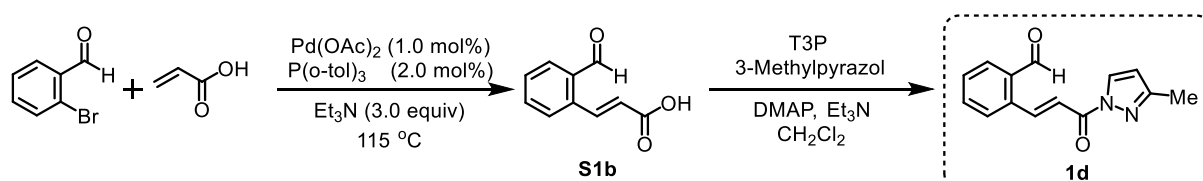
According to the same procedure used as for the preparation of **1b**, 2-bromobenzaldehyde as the starting material provided **1c** as a white solid. Yield: 80%.

(E)-2-(3-(3,5-Dimethyl-1H-pyrazol-1-yl)-3-oxoprop-1-en-1-yl)benzaldehyde (1c)

1H NMR (300 MHz, $CDCl_3$) δ 10.36 (s, 1H), 8.73 (d, $J = 15.9$ Hz, 1H), 7.92-7.81 (m, 3H), 7.60 (dtd, $J = 21.1, 7.5, 1.3$ Hz, 2H), 6.02 (s, 1H), 2.63 (s, 3H), 2.27 (s, 3H).

^{13}C NMR (75 MHz, $CDCl_3$) δ 191.5, 164.6, 152.1, 144.5, 141.9, 136.9, 134.1, 133.8, 131.9, 130.0, 128.4, 122.9, 111.6, 14.6, 13.8.

HRMS (ESI, m/z) calcd for $C_{15}H_{14}N_2O_2Na$ $[M+Na]^+$: 277.0953, found: 277.0949.



According to the same procedure used as for the preparation of **1b**, 2-bromobenzaldehyde as the starting material provided **1d** as pale yellow solid. Yield: 85%.

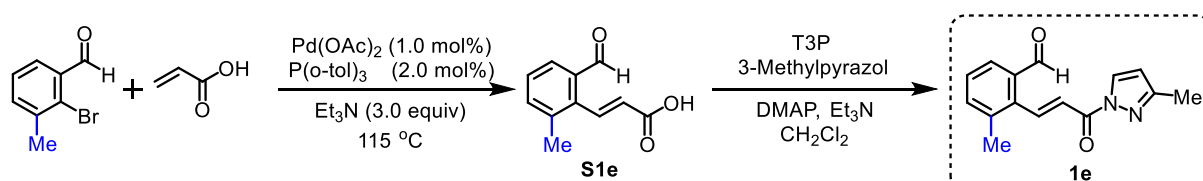
(E)-2-(3-(3-Methyl-1H-pyrazol-1-yl)-3-oxoprop-1-en-1-yl)benzaldehyde (1d)

A pale yellow solid. Yield: 85%.

1H NMR (300 MHz, $CDCl_3$) δ 7.48-7.41 (m, 3H), 7.30-7.28 (m, 1H), 7.28-7.22 (m, 2H), 7.17-7.14 (m, 1H), 3.16 (dd, $J_1 = 7.8$ Hz, $J_2 = 5.7$ Hz, 1H), 1.73-1.38 (m, 9H), 1.33 (dd, $J_1 = 5.7$ Hz, $J_2 = 3.9$ Hz, 1H), 1.28-1.12 (m, 1H), 0.96 (dd, $J_1 = 7.5$ Hz, $J_2 = 3.9$ Hz, 1H).

^{13}C NMR (75 MHz, $CDCl_3$) δ 188.6, 144.4, 138.9, 129.4, 128.9, 128.6, 126.4, 125.9, 37.8, 36.5, 31.7, 28.0, 26.2, 26.1, 25.9, 22.6.

HRMS (ESI, m/z) calcd for $C_{14}H_{12}N_2O_2Na$ $[M+Na]^+$: 263.0796, found: 263.0791.



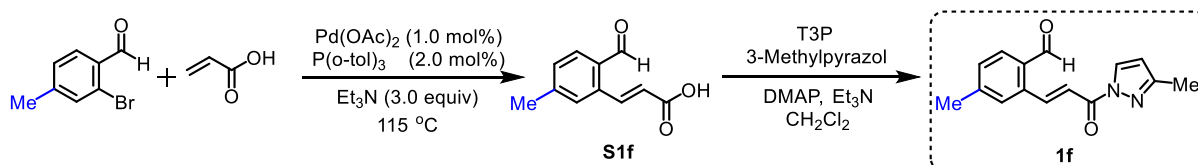
According to the same procedure used as for the preparation of **1b**, 2-bromo-3-methylbenzaldehyde³ as the starting material provided **1e** as a pale yellow solid. Yield: 85%.

(E)-3-Methyl-2-(3-(3-methyl-1H-pyrazol-1-yl)-3-oxoprop-1-en-1-yl)benzaldehyde (1e)

$^1\text{H NMR}$ (300 MHz, CDCl_3) δ 10.65 (s, 1H), 8.58 (d, $J = 15.8$ Hz, 1H), 8.27 (d, $J = 2.8$ Hz, 1H), 7.70 (d, $J = 15.8$ Hz, 1H), 7.59 (d, $J = 7.7$ Hz, 1H), 7.48 (t, $J = 7.7$ Hz, 1H), 7.31 (d, $J = 7.5$ Hz, 1H), 6.29 (d, $J = 2.8$ Hz, 1H), 2.65 (s, 3H), 2.34 (s, 3H).

$^{13}\text{C NMR}$ (75 MHz, CDCl_3) δ 192.4, 162.6, 153.9, 145.3, 141.1, 137.5, 133.5, 133.0, 132.9, 129.4, 126.8, 120.5, 110.7, 20.0, 13.9.

HRMS (ESI, m/z) calcd for $\text{C}_{15}\text{H}_{15}\text{N}_2\text{O}_2$ $[\text{M}+\text{H}]^+$: 255.1134, found: 255.1129.



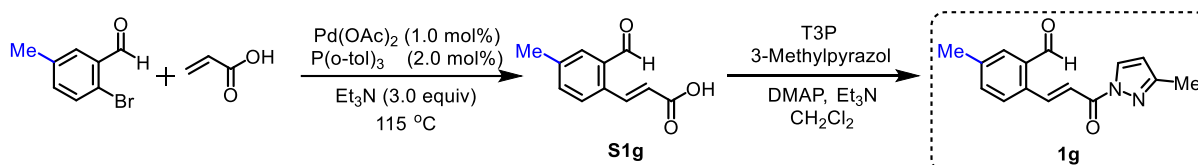
According to the same procedure used as for the preparation of **1b**, 2-bromo-4-methylbenzaldehyde⁴ as the starting material provided **1f** as a pale yellow solid. Yield: 79%.

(E)-4-Methyl-2-(3-(3-methyl-1H-pyrazol-1-yl)-3-oxoprop-1-en-1-yl)benzaldehyde (1f)

$^1\text{H NMR}$ (300 MHz, CDCl_3) δ 10.29 (s, 1H), 8.82 (d, $J = 15.9$ Hz, 1H), 8.29 (d, $J = 2.8$ Hz, 1H), 7.81 (d, $J = 2.2$ Hz, 1H), 7.77 (d, $J = 5.8$ Hz, 1H), 7.63 (s, 1H), 7.39 (d, $J = 7.8$ Hz, 1H), 6.31 (d, $J = 2.8$ Hz, 1H), 2.48 (s, 3H), 2.37 (s, 3H).

$^{13}\text{C NMR}$ (75 MHz, CDCl_3) δ 191.2, 162.6, 154.0, 144.9, 143.6, 136.5, 132.4, 132.0, 131.1, 129.5, 128.9, 120.6, 110.8, 21.7, 14.0.

HRMS (ESI, m/z) calcd for $\text{C}_{15}\text{H}_{14}\text{N}_2\text{O}_2\text{Na}$ $[\text{M}+\text{Na}]^+$: 277.0953, found: 277.0948.



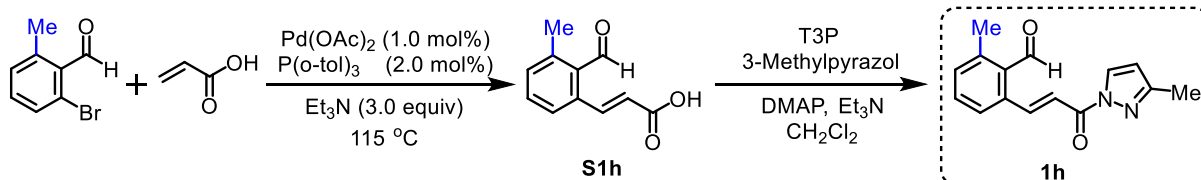
According to the same procedure used as for the preparation of **1b**, 2-bromo-5-methylbenzaldehyde⁵ as the starting material provided **1g** as a white solid. Yield: 87%.

(E)-5-Methyl-2-(3-(3-methyl-1H-pyrazol-1-yl)-3-oxoprop-1-en-1-yl)benzaldehyde (1g)

$^1\text{H NMR}$ (300 MHz, CDCl_3) δ 10.33 (s, 1H), 8.79 (d, $J = 15.9$ Hz, 1H), 8.27 (d, $J = 2.7$ Hz, 1H), 7.81-7.774 (m, 2H), 7.69 (s, 1H), 7.44 (d, $J = 7.9$ Hz, 1H), 6.29 (d, $J = 2.8$ Hz, 1H), 2.45 (s, 3H), 2.35 (s, 3H).

$^{13}\text{C NMR}$ (75 MHz, CDCl_3) δ 191.6, 162.7, 153.9, 143.0, 141.0, 134.6, 134.0, 133.8, 132.5, 129.4, 128.3, 120.0, 110.7, 21.2, 13.9.

HRMS (ESI, m/z) calcd for $\text{C}_{15}\text{H}_{14}\text{N}_2\text{O}_2\text{Na}$ $[\text{M}+\text{Na}]^+$: 277.0953, found: 277.0949.



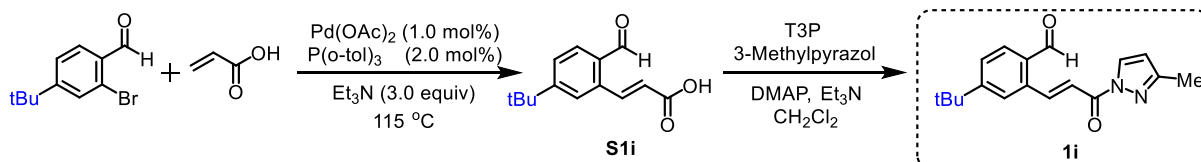
According to the same procedure used as for the preparation of **1b**, 2-bromo-5-methylbenzaldehyde^{4,6} as the starting material provided **1h** as a yellow solid. Yield: 85%.

(E)-2-Methyl-6-(3-(3-methyl-1H-pyrazol-1-yl)-3-oxoprop-1-en-1-yl)benzaldehyde (1h)

¹H NMR (300 MHz, CDCl₃) δ 10.21 (s, 1H), 8.33-8.27 (m, 2H), 7.82 (dd, *J* = 7.5, 0.9 Hz, 1H), 7.50-7.36 (m, 3H), 6.30 (d, *J* = 2.8 Hz, 1H), 2.43 (s, 3H), 2.30 (s, 3H).

¹³C NMR (75 MHz, CDCl₃) δ 191.6, 161.9, 154.2, 142.4, 138.0, 137.9, 135.5, 135.0, 129.4, 128.9, 127.1, 125.9, 111.1, 77.4, 77.0, 76.6, 20.0, 13.9.

HRMS (ESI, *m/z*) calcd for C₁₅H₁₄N₂O₂Na [M+Na]⁺: 277.0953, found: 277.0948.



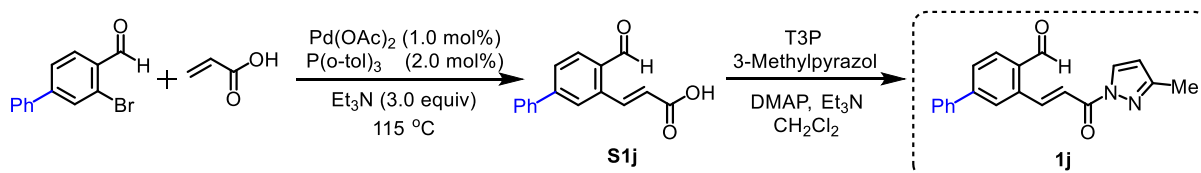
According to the same procedure used as for the preparation of **1b**, 2-bromo-4-*tert*-butylbenzaldehyde^{7,8,9} as the starting material provided **1i** as a yellow oli. Yield: 78%.

(E)-4-(tert-Butyl)-2-(3-(3-methyl-1H-pyrazol-1-yl)-3-oxoprop-1-en-1-yl)benzaldehyde (1i)

¹H NMR (300 MHz, CDCl₃) δ 10.30 (s, 1H), 8.82 (d, *J* = 15.9 Hz, 1H), 8.29 (d, *J* = 2.9 Hz, 1H), 7.85-7.73(m, 3H), 7.63-7.59(m, 1H), 6.31 (d, *J* = 2.8 Hz, 1H), 2.37 (s, 3H), 1.39 (s, 9H).

¹³C NMR (75 MHz, CDCl₃) δ 191.2, 162.7, 157.8, 154.0, 144.3, 136.5, 132.2, 131.9, 129.5, 127.5, 125.3, 120.6, 110.8, 35.4, 30.99, 13.96.

HRMS (ESI, *m/z*) calcd for C₁₈H₂₀N₂O₂Na [M+Na]⁺: 319.1422, found: 319.1428.



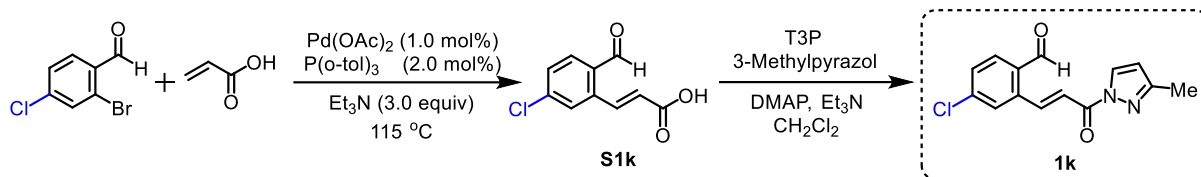
According to the same procedure used as for the preparation of **1b**, 3-bromo-[1,1'-biphenyl]-4-carbaldehyde¹⁰ as the starting material provided **1j** as a white solid. Yield: 80%.

(E)-3-(3-(3-Methyl-1H-pyrazol-1-yl)-3-oxoprop-1-en-1-yl)-[1,1'-biphenyl]-4-carbaldehyde (1j)

¹H NMR (300 MHz, CDCl₃) δ 10.45 (s, 1H), 8.86 (d, *J* = 15.9 Hz, 1H), 8.30 (d, *J* = 2.8 Hz, 1H), 8.13 (d, *J* = 1.9 Hz, 1H), 7.99-7.84 (m, 3H), 7.67 (dd, *J* = 5.2, 3.3 Hz, 2H), 7.54-7.39 (m, 3H), 6.32 (d, *J* = 2.8 Hz, 1H), 2.37 (s, 3H).

¹³C NMR (75 MHz, CDCl₃) δ 191.4, 162.6, 154.0, 143.3, 142.5, 138.8, 135.2, 134.5, 132.0, 130.4, 129.5, 129.1, 128.9, 128.5, 127.0, 120.7, 110.9, 14.0.

HRMS (ESI, m/z) calcd for $C_{20}H_{16}N_2O_2Na$ $[M+Na]^+$: 339.1109, found: 339.1107.



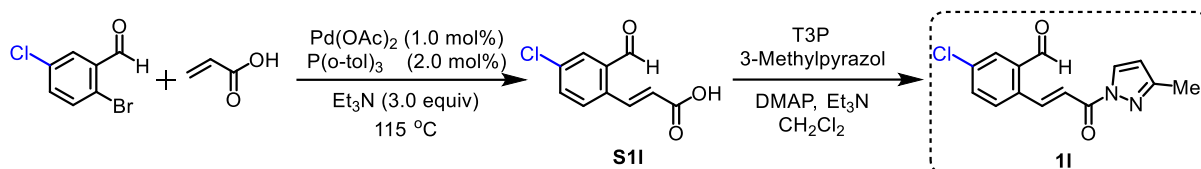
According to the same procedure used as for the preparation of **1b**, 2-bromo-4-chlorobenzaldehyde as the starting material provided **1k** as a white solid. Yield: 88%.

(E)-4-Chloro-2-(3-(3-methyl-1H-pyrazol-1-yl)-3-oxoprop-1-en-1-yl)benzaldehyde (1k)

$^1\text{H NMR}$ (300 MHz, $CDCl_3$) δ 10.30 (s, 1H), 8.73 (d, $J = 15.9$ Hz, 1H), 8.27 (d, $J = 2.6$ Hz, 1H), 7.86-7.78 (m, 3H), 7.54 (dd, $J = 8.3, 1.6$ Hz, 1H), 6.31 (d, $J = 2.7$ Hz, 1H), 2.36 (s, 3H).

$^{13}\text{C NMR}$ (75 MHz, $CDCl_3$) δ 190.1, 162.2, 154.2, 141.5, 140.5, 138.2, 133.2, 132.4, 130.3, 129.5, 128.3, 122.2, 111.1, 13.9.

HRMS (ESI, m/z) calcd for $C_{14}H_{11}ClN_2O_2Na$ $[M+Na]^+$: 297.0407, found: 297.0404.



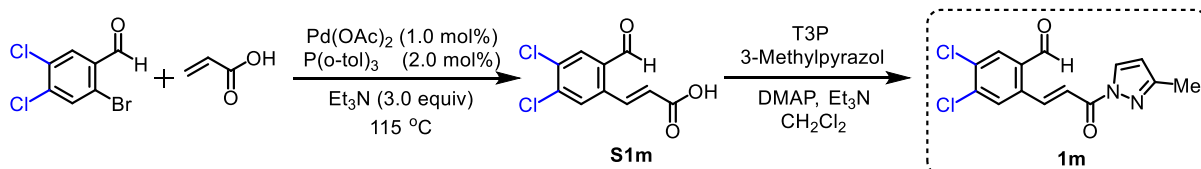
According to the same procedure used as for the preparation of **1b**, 2-bromo-5-chlorobenzaldehyde as the starting material provided **1l** as a white solid. Yield: 86%.

(E)-5-Chloro-2-(3-(3-methyl-1H-pyrazol-1-yl)-3-oxoprop-1-en-1-yl)benzaldehyde (1l)

$^1\text{H NMR}$ (300 MHz, $CDCl_3$) δ 10.33 (s, 1H), 8.71 (d, $J = 15.9$ Hz, 1H), 8.27 (d, $J = 2.8$ Hz, 1H), 7.91-7.75 (m, 3H), 7.63-7.59 (m, 1H), 6.31 (d, $J = 2.8$ Hz, 1H), 2.35 (s, 3H).

$^{13}\text{C NMR}$ (75 MHz, $CDCl_3$) δ 189.9, 162.3, 154.2, 141.4, 136.8, 135.2, 134.9, 133.8, 131.3, 129.8, 129.5, 121.6, 111.0, 13.9.

HRMS (ESI, m/z) calcd for $C_{14}H_{11}ClN_2O_2Na$ $[M+Na]^+$: 297.0407, found: 297.0403.



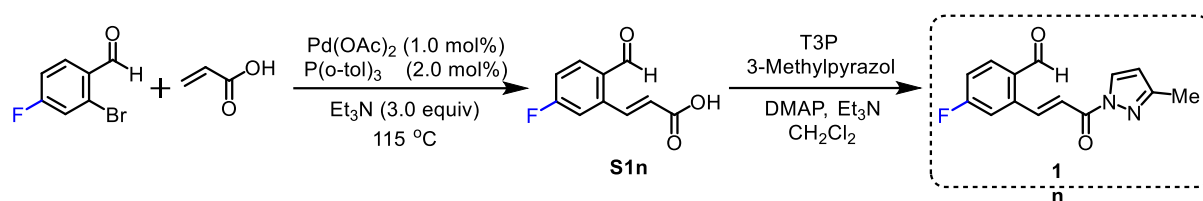
According to the same procedure used as for the preparation of **1b**, 2-bromo-4,5-dichlorobenzaldehyde¹¹ as the starting material provided **1m** as a yellow solid. Yield: 82%.

(E)-4,5-Dichloro-2-(3-(3-methyl-1H-pyrazol-1-yl)-3-oxoprop-1-en-1-yl)benzaldehyde (1m)

$^1\text{H NMR}$ (300 MHz, $CDCl_3$) δ 10.27 (s, 1H), 8.64 (d, $J = 15.9$ Hz, 1H), 8.26 (d, $J = 2.8$ Hz, 1H), 7.96 (s, 1H), 7.91 (s, 1H), 7.80 (d, $J = 15.9$ Hz, 1H), 6.32 (d, $J = 2.8$ Hz, 1H), 2.36 (s, 3H).

$^{13}\text{C NMR}$ (75 MHz, $CDCl_3$) δ 188.9, 162.0, 154.3, 140.1, 138.7, 135.9, 135.0, 133.2, 130.0, 129.5,

122.4, 111.2, 13.9.

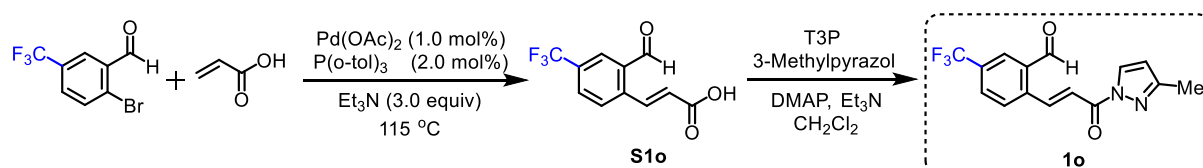
HRMS (ESI, *m/z*) calcd for C₁₄H₁₀Cl₂N₂O₂Na [M+Na]⁺: 331.0017, found: 331.0014.

According to the same procedure used as for the preparation of **1b**, 2-bromo-4-fluorobenzaldehyde⁴ as the starting material provided **1n** as a pale yellow solid. Yield: 84%.

(*E*)-4-Fluoro-2-(3-(3-methyl-1H-pyrazol-1-yl)-3-oxoprop-1-en-1-yl)benzaldehyde (1n)

¹H NMR (300 MHz, CDCl₃) δ 10.28 (s, 1H), 8.76 (d, *J* = 15.9 Hz, 1H), 8.26 (d, *J* = 2.8 Hz, 1H), 7.93 (dd, *J* = 8.6, 5.8 Hz, 1H), 7.80 (d, *J* = 15.9 Hz, 1H), 7.49 (dd, *J* = 9.5, 2.5 Hz, 1H), 7.30-7.19 (m, 1H), 6.31 (d, *J* = 2.8 Hz, 1H), 2.34 (s, 3H).

¹³C NMR (75 MHz, CDCl₃) δ 189.8, 167.3, 163.9, 162.2, 154.2, 141.6 (d, *J*_{CF} = 2.1 Hz), 139.6 (d, *J*_{CF} = 9.1 Hz), 134.8 (d, *J*_{CF} = 9.9 Hz), 130.7 (d, *J*_{CF} = 2.9 Hz), 129.4, 122.2, 117.4 (d, *J*_{CF} = 22.1 Hz), 115.2 (d, *J*_{CF} = 23.0 Hz), 111.1, 13.9.

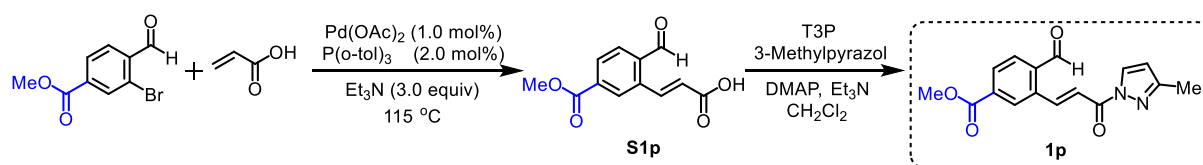
HRMS (ESI, *m/z*) calcd for C₁₄H₁₁FN₂O₂Na [M+Na]⁺: 281.0702, found: 281.0696.

According to the same procedure used as for the preparation of **1d**, 2-bromo-5-(trifluoromethyl)benzaldehyde¹² as the starting material provided **1o** as a white solid. Yield: 77%.

(*E*)-2-(3-(3-Methyl-1H-pyrazol-1-yl)-3-oxoprop-1-en-1-yl)-5-(trifluoromethyl)benzaldehyde (1o)

¹H NMR (300 MHz, CDCl₃) δ 10.39 (s, 1H), 8.75 (d, *J* = 15.9 Hz, 1H), 8.27 (d, *J* = 2.8 Hz, 1H), 8.17 (s, 1H), 8.01-7.84 (m, 3H), 6.32 (d, *J* = 2.8 Hz, 1H), 2.35 (s, 3H).

¹³C NMR (75 MHz, CDCl₃) δ 189.9, 162.1, 154.3, 141.2, 139.9, 134.3, 132.3 (q, *J* = 33.7 Hz), 130.1 (q, *J* = 3.5 Hz), 129.5, 129.2, 128.5 (q, *J* = 3.8 Hz), 125.0, 123.3, 121.4, 111.2, 13.9.

HRMS (ESI, *m/z*) calcd for C₁₅H₁₁F₃N₂O₂Na [M+Na]⁺: 331.0670, found: 331.0667.

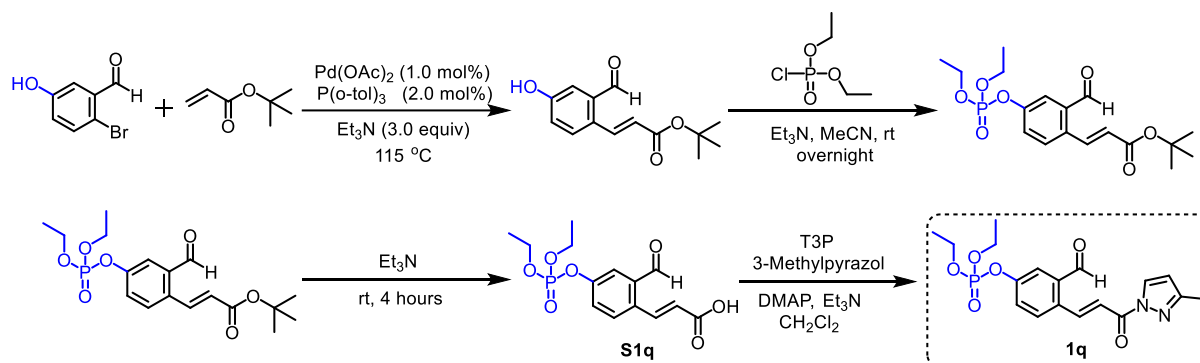
According to the same procedure used as for the preparation of **1d**, methyl 3-bromo-4-formylbenzoate¹¹ as the starting material provided **1p** as a white solid. Yield: 78%.

Methyl (*E*)-4-formyl-3-(3-(3-methyl-1H-pyrazol-1-yl)-3-oxoprop-1-en-1-yl)benzoate (1p)

¹H NMR (300 MHz, CDCl₃) δ 10.43 (s, 1H), 8.78 (d, *J* = 15.9 Hz, 1H), 8.48 (d, *J* = 1.2 Hz, 1H), 8.29 (d, *J* = 2.7 Hz, 1H), 8.22 (dd, *J* = 8.0, 1.5 Hz, 1H), 7.99 (d, *J* = 8.0 Hz, 1H), 7.90 (d, *J* = 15.9 Hz, 1H), 6.33 (d, *J* = 2.8 Hz, 1H), 4.00 (s, 3H), 2.38 (s, 3H).

¹³C NMR (75 MHz, CDCl₃) δ 190.9, 165.6, 162.4, 154.2, 142.0, 136.8, 136.7, 134.7, 131.8, 130.9, 129.6, 129.5, 122.2, 111.1, 52.8, 14.0.

HRMS (ESI, *m/z*) calcd for C₁₆H₁₄N₂O₄Na [M+Na]⁺: 321.0851, found: 321.0846.



The 2-bromo-5-hydroxybenzaldehyde (1.0 equiv) was dissolved in dimethylformamide (2.0 mL/mmol aldehyde). Then Pd(OAc)₂ (0.01 equiv), P(*o*-tol)₃ (0.02 equiv), *tert*-butyl acrylate (2.0 equiv) and Et₃N (3.0 equiv) were added, The mixture was degassed under nitrogen purge for 15 min and then the resulting mixture was heated in an oil bath at 115 °C and magnetically stirred under nitrogen. The reaction was monitored by TLC. After the reaction was completed, the reaction was then cooled to room temperature, diluted with H₂O and extracted with CH₂Cl₂. After dried with anhydrous Na₂SO₄, filtration and concentration under reduced pressure, the crude residue was purified by flash chromatography on silica gel (*n*-hexane/EtOAc = 30:1 to 3:1) to afford the product.¹³

The above compound was dissolved in acetonitrile. Then the Et₃N (1.1 equiv) and diethyl chlorophosphite (1.1 equiv) were added. The mixture was stirred at room temperature for 12 hours. After that, acetonitrile was removed by rotary evaporator and the crude mixture was purified by flash column chromatography on a silica gel column (*n*-hexane/EtOAc = 20:1 to 3:1).¹⁴

To a solution of the above α,β-unsaturated *tert*-butyl ester in trifluoroacetic acid and dichloromethane (volume ratio: 1:1) was stirred at room temperature for 4 hours and the solvents were removed under reduced pressure. The crude solid was triturated in hexane, filtered, and dried under vacuum to give the **S1q**.

Last step: According to the same procedure used as for the preparation of **1d**, the compound **1q** was obtained as a yellow oil. Yield: 70%.

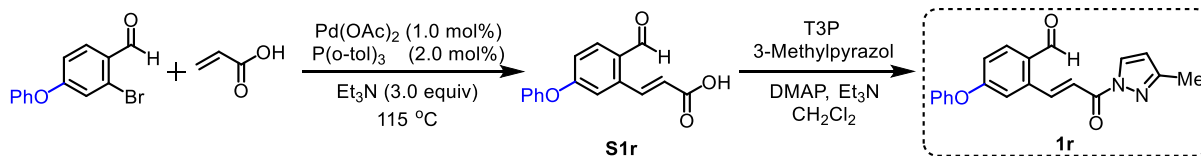
Diethyl (3-formyl-4-(3-(3-methyl-1H-pyrazol-1-yl)-3-oxoprop-1-en-1-yl)phenyl) phosphate (1q) (*Z/E* ≈ 1:4)

¹H NMR (300 MHz, CDCl₃) δ 10.30 (s, 1H), 8.69 (d, *J* = 15.9 Hz, 1H), 8.22 (d, *J* = 2.6 Hz, 1H), 7.82 (d, *J* = 8.6 Hz, 1H), 7.75 (d, *J* = 15.8 Hz, 1H), 7.70 (dd, *J* = 2.5, 0.8 Hz, 1H), 7.49 (dd, *J* = 8.6, 2.5 Hz, 1H), 6.27 (d, *J* = 2.7 Hz, 1H), 4.30-4.13 (m, 4H), 2.30 (s, 3H), 1.41-1.25 (m, 6H).

¹³C NMR (75 MHz, CDCl₃) δ 190.1, 162.3, 154.0, 152.3 (d, *J* = 6.6 Hz), 141.6, 135.4, 133.1, 130.1,

129.3, 125.4 (d, $J = 4.9$ Hz), 122.5 (d, $J = 5.4$ Hz), 120.9 (s), 110.9 (s), 65.0 (t, $J = 5.9$ Hz), 16.0 (d, $J = 6.5$ Hz), 13.8 (s).

HRMS (ESI, m/z) calcd for $C_{18}H_{21}N_2O_6PNa$ $[M+Na]^+$: 415.1035, found: 415.1030.



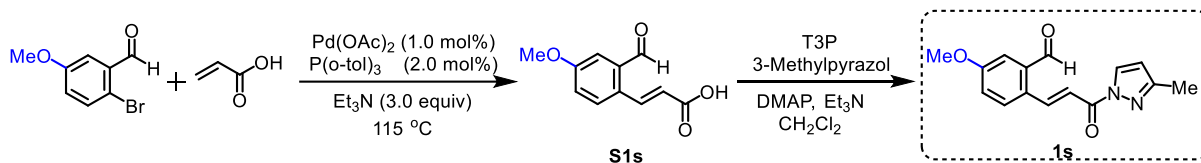
According to the same procedure used as for the preparation of **1d**, methyl 3-bromo-4-formylbenzoate^{4,15} as the starting material provided **1r** as a white solid. Yield: 80%.

(E)-2-(3-(3-Methyl-1H-pyrazol-1-yl)-3-oxoprop-1-en-1-yl)-4-phenoxybenzaldehyde (1r)

¹H NMR (300 MHz, CDCl₃) δ 10.24 (s, 1H), 8.78 (d, $J = 15.9$ Hz, 1H), 8.27 (d, $J = 2.8$ Hz, 1H), 7.85 (d, $J = 8.6$ Hz, 1H), 7.73 (d, $J = 15.9$ Hz, 1H), 7.47-7.37 (m, 3H), 7.24 (ddd, $J = 7.0, 2.1, 1.1$ Hz, 1H), 7.14-7.08 (m, 2H), 7.04 (dd, $J = 8.6, 2.4$ Hz, 1H), 6.30 (d, $J = 2.8$ Hz, 1H), 2.34 (s, 3H).

¹³C NMR (75 MHz, CDCl₃) δ 190.0, 162.4, 162.3, 154.9, 154.0, 142.8, 139.2, 134.5, 130.2, 129.4, 129.1, 125.1, 121.6, 120.2, 118.3, 117.1, 110.9, 13.9.

HRMS (ESI, m/z) calcd for $C_{20}H_{16}N_2O_3Na$ $[M+Na]^+$: 355.1059, found: 355.1056.



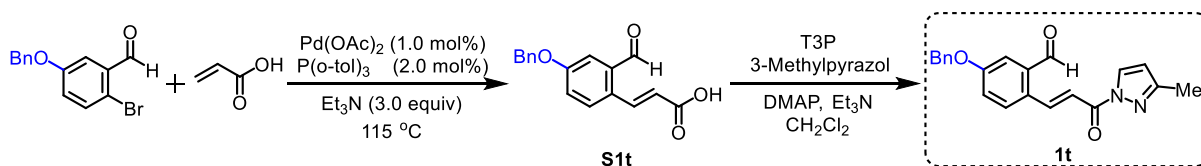
According to the same procedure used as for the preparation of **1d**, 2-bromo-5-methoxybenzaldehyde as the starting material provided **1s** as a white solid. Yield: 75%.

(E)-5-Methoxy-2-(3-(3-methyl-1H-pyrazol-1-yl)-3-oxoprop-1-en-1-yl)benzaldehyde (1s)

¹H NMR (300 MHz, CDCl₃) δ 10.41 (s, 1H), 8.74 (d, $J = 15.8$ Hz, 1H), 8.26 (d, $J = 2.8$ Hz, 1H), 7.83 (d, $J = 8.7$ Hz, 1H), 7.75 (d, $J = 15.8$ Hz, 1H), 7.38 (d, $J = 2.8$ Hz, 1H), 7.16 (dd, $J = 8.7, 2.8$ Hz, 1H), 6.29 (d, $J = 2.8$ Hz, 1H), 3.90 (s, 3H), 2.35 (s, 3H).

¹³C NMR (75 MHz, CDCl₃) δ 190.7, 162.8, 161.4, 153.8, 141.9, 135.5, 129.9, 129.4, 129.3, 120.7, 118.8, 114.4, 110.7, 55.7, 13.9.

HRMS (ESI, m/z) calcd for $C_{15}H_{14}N_2O_3Na$ $[M+Na]^+$: 293.0902, found: 293.0898.



According to the same procedure used as for the preparation of **1d**, 2-bromo-5-phenylmethoxybenzaldehyde¹⁶ as the starting material provided **1t** as a white solid. Yield: 75%.

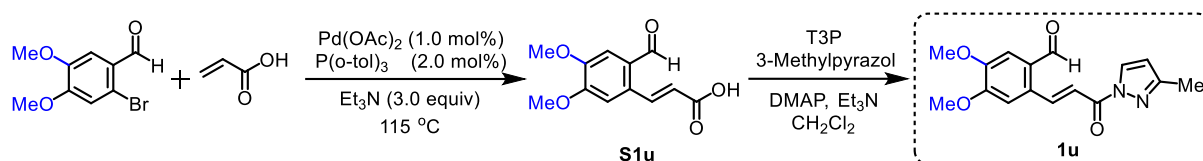
5-(Benzyloxy)-2-(3-(3-methyl-1H-pyrazol-1-yl)-3-oxoprop-1-en-1-yl)benzaldehyde (1t)

(*Z/E* ≈ 1:3)

¹H NMR (300 MHz, CDCl₃, *Z/E* mixture) δ 10.41 (s, 1H), 8.76 (d, *J* = 15.8 Hz, 1H), 8.28 (d, *J* = 2.8 Hz, 1H), 7.84 (d, *J* = 8.7 Hz, 1H), 7.77 (d, *J* = 15.8 Hz, 1H), 7.49 (d, *J* = 2.8 Hz, 1H), 7.47-7.32 (m, 5H), 7.24 (dd, *J* = 8.8, 2.9 Hz, 1H), 6.30 (d, *J* = 2.7 Hz, 1H), 5.17 (s, 2H), 2.36 (s, 3H).

¹³C NMR (75 MHz, CDCl₃, *Z/E* mixture) δ 190.7, 190.0, 162.8, 162.8, 162.5, 160.5, 153.9, 153.8, 143.3, 141.8, 138.9, 135.8, 135.6, 135.5, 134.7, 129.9, 129.5, 129.4, 128.8, 128.7, 128.4, 128.3, 128.0, 127.6, 127.5, 121.3, 121.1, 118.9, 115.9, 115.5, 114.5, 110.9, 110.7, 70.5, 70.4, 13.9.

HRMS (ESI, *m/z*) calcd for C₂₁H₁₈N₂O₃Na [M+Na]⁺: 369.1215, found: 369.1211.



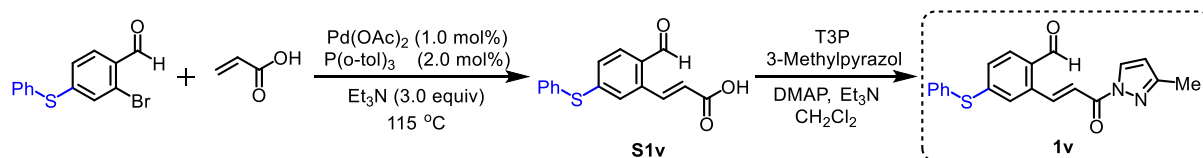
According to the same procedure used as for the preparation of **1d**, 2-bromo-4,5-dimethoxybenzaldehyde as the starting material provided **1u** as a white solid. Yield: 80%.

(*E*)-4,5-Dimethoxy-2-(3-(3-methyl-1H-pyrazol-1-yl)-3-oxoprop-1-en-1-yl)benzaldehyde (1u)

¹H NMR (300 MHz, CDCl₃) δ 10.42 (s, 1H), 8.78 (d, *J* = 15.7 Hz, 1H), 8.30 (d, *J* = 2.8 Hz, 1H), 7.76 (d, *J* = 15.7 Hz, 1H), 7.44 (s, 1H), 7.24 (s, 1H), 6.32 (d, *J* = 2.8 Hz, 1H), 4.06 (s, 3H), 3.99 (s, 3H), 2.38 (s, 3H).

¹³C NMR (75 MHz, CDCl₃) δ 188.9, 162.6, 154.0, 153.6, 151.1, 141.7, 131.5, 129.5, 128.3, 119.3, 111.0, 110.9, 109.3, 56.4, 56.2, 13.9.

HRMS (ESI, *m/z*) calcd for C₁₆H₁₆N₂O₄Na [M+Na]⁺: 323.1008, found: 323.1004.



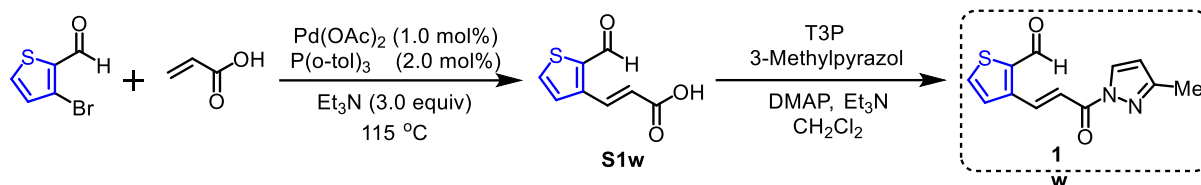
According to the same procedure used as for the preparation of **1d**, 2-bromo-4-phenylthiobenzaldehyde¹⁵ as the starting material provided **1v** as a yellow solid. Yield: 85%.

(*E*)-2-(3-(3-Methyl-1H-pyrazol-1-yl)-3-oxoprop-1-en-1-yl)-4-(phenylthio)benzaldehyde (1v)

¹H NMR (300 MHz, CDCl₃) δ 10.22 (s, 1H), 8.71 (d, *J* = 15.9 Hz, 1H), 8.25 (d, *J* = 2.8 Hz, 1H), 7.73-7.66 (m, 2H), 7.59-7.38 (m, 6H), 7.18 (dd, *J* = 8.2, 1.8 Hz, 1H), 6.30 (d, *J* = 2.8 Hz, 1H), 2.36 (s, 3H).

¹³C NMR (75 MHz, CDCl₃) δ 190.4, 162.3, 153.9, 146.9, 142.7, 137.1, 134.4, 132.5, 131.3, 130.8, 129.9, 129.4, 129.3, 128.0, 126.2, 121.5, 110.9, 13.9.

HRMS (ESI, *m/z*) calcd for C₂₀H₁₆N₂O₂SNa [M+Na]⁺: 371.0830, found: 371.0826.



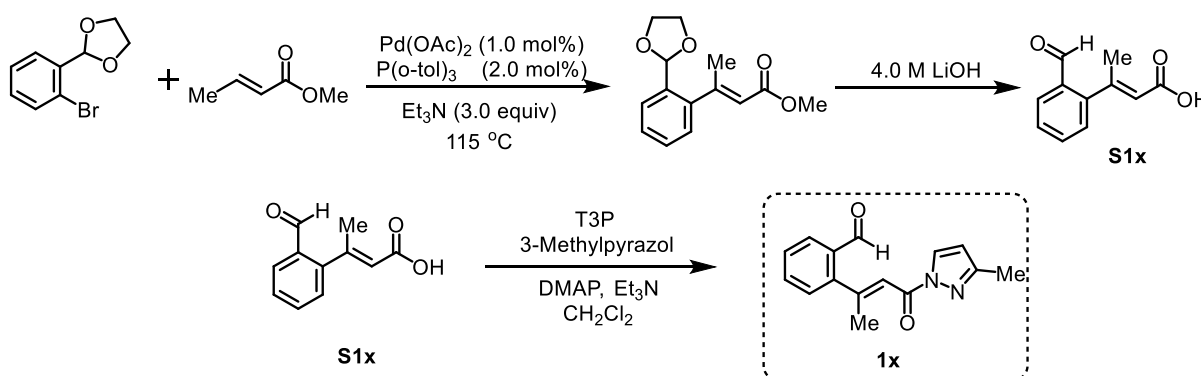
According to the same procedure used as for the preparation of **1d**, 3-bromothiophene-2-carbaldehyde¹⁷ as the starting material provided **1w** as a yellow solid. Yield: 80%.

(E)-3-(3-(3-Methyl-1H-pyrazol-1-yl)-3-oxoprop-1-en-1-yl)thiophene-2-carbaldehyde (1w)

¹H NMR (300 MHz, CDCl₃) δ 10.30 (s, 1H), 8.44 (d, *J* = 15.8 Hz, 1H), 8.27 (d, *J* = 2.4 Hz, 1H), 7.87 (d, *J* = 15.8 Hz, 1H), 7.73 (d, *J* = 5.0 Hz, 1H), 7.60 (d, *J* = 5.1 Hz, 1H), 6.32 (d, *J* = 2.5 Hz, 1H), 2.37 (s, 3H)

¹³C NMR (75 MHz, CDCl₃) δ 181.6, 162.7, 154.2, 143.0, 142.3, 135.7, 134.4, 129.5, 127.6, 121.1, 111.1, 14.0.

HRMS (ESI, *m/z*) calcd for C₁₂H₁₀N₂O₂Na [M+Na]⁺: 269.0361, found: 269.0356.



2-(2-Bromophenyl)-1,3-dioxolane (1.0 equiv) was dissolved in dimethylformamide (2.0 mL/mmol aldehyde). Pd(OAc)₂ (0.01 equiv), then P(o-tol)₃ (0.02 equiv), (*E*)-2-butenoic acid ethyl ester (2.0 equiv) and Et₃N (3.0 equiv) were added, The mixture was degassed under nitrogen purge for 15 min and then the vial content was heated in an oil bath at 115 °C and magnetically stirred under nitrogen over night. After the reaction was completed, it was then cooled to room temperature, diluted with H₂O and extracted with EtOAc. After dried with anhydrous Na₂SO₄, filtration and concentration under reduced pressure, the crude residue was purified by flash chromatography on silica gel (*n*-hexane/EtOAc = 30:1 to 3:1) to afford the substrate.¹⁸

To a solution of the above a, β-unsaturated methyl ester in dioxane/H₂O (volume ratio: 4:1) was treated with 4 M LiOH for 6 hours at room temperature, then quenched with the addition of 1 M HCl, after being stirred for 10 min, the product was extracted with EtOAc. After dried with anhydrous Na₂SO₄, filtration and concentration under reduced pressure, the crude residue was purified by flash chromatography on silica gel (*n*-hexane/EtOAc = 20:1 to 3:1) to afford the substrate.

Last step: According to the same procedure used as for the preparation of **1d**, compound **1x** was obtained as a pale yellow solid. Yield: 79%.

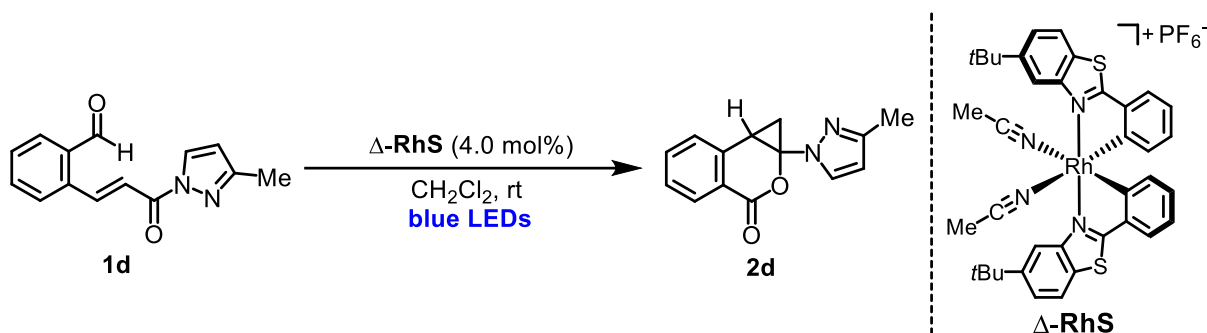
(E)-2-(4-(3-Methyl-1H-pyrazol-1-yl)-4-oxobut-2-en-2-yl)benzaldehyde (1x)

$^1\text{H NMR}$ (300 MHz, CDCl_3) δ 10.16 (s, 1H), 8.25 (d, $J = 2.8$ Hz, 1H), 7.97 (dd, $J = 7.7, 1.3$ Hz, 1H), 7.62 (td, $J = 7.5, 1.4$ Hz, 1H), 7.51 (t, $J = 7.3$ Hz, 1H), 7.37 (dd, $J = 7.6, 0.9$ Hz, 1H), 7.20 (d, $J = 1.4$ Hz, 1H), 6.26 (d, $J = 2.8$ Hz, 1H), 2.68 (d, $J = 1.4$ Hz, 3H), 2.28 (s, 3H).

$^{13}\text{C NMR}$ (75 MHz, CDCl_3) δ 191.0, 162.1, 158.5, 153.6, 147.1, 133.8, 133.1, 129.3, 129.2, 128.6, 128.4, 119.6, 110.5, 22.7, 13.9.

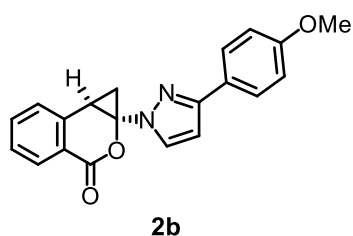
HRMS (ESI, m/z) calcd for $\text{C}_{15}\text{H}_{14}\text{N}_2\text{O}_2\text{Na}$ $[\text{M}+\text{Na}]^+$: 277.0953, found: 277.0947.

4.2.2 General Procedure



An oven-dried 10 mL Schlenk tube was charged with compound **1d** (24.0 mg, 0.10 mmol) and $\Delta\text{-RhS}$ (3.5 mg, 4.0 mol%). Then, CH_2Cl_2 (2.0 mL, 0.05 M) was added via syringe. The reaction mixture was degassed via freeze-pump-thaw for three cycles. Subsequent, the vial was sealed and placed approximately 10 cm away from the 24 W blue LEDs. After stirring for the indicated time (monitored by TLC) under nitrogen atmosphere, the mixture was diluted with CH_2Cl_2 . The combined organic solutions were concentrated, reduced pressure and purified by flash chromatography on silica gel (*n*-hexane/EtOAc) to afford the pure non-racemic product **2d**. The enantiomeric excess was determined by HPLC analysis on a chiral stationary phase. Racemic samples were obtained by carrying out the reactions with *rac*- RhS .

4.2.3 Experimental and Characterization Data of New Products



According to the general procedure, the reaction of **1b** (24.0 mg, 0.10 mmol) and $\Delta\text{-RhS}$ (3.5 mg, 4.0 mol%) in CH_2Cl_2 (2.0 mL, 0.05 M) was stirred under nitrogen atmosphere for 16 hours with 24 W blue LEDs at room temperature, affording 20.0 mg (60% yield, pale yellow solid) of **2b** as a single diastereomer. Enantiomeric excess was established by HPLC analysis using a Chiralpak IG column, ee = 38% (HPLC: 254 nm, *n*-hexane/isopropanol = 70:30, flow rate 1 mL/min, 30 °C, t_r (major) = 27.5

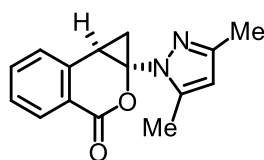
min, t_r (minor) = 23.2 min). $[\alpha]_D^{22} = -7.8^\circ$ (c 1.0, CH_2Cl_2).

^1H NMR (300 MHz, CDCl_3) δ 8.22 (d, $J = 7.7$ Hz, 1H), 7.78 (d, $J = 2.5$ Hz, 1H), 7.73 (d, $J = 8.8$ Hz, 2H), 7.64 (td, $J = 7.6, 1.1$ Hz, 1H), 7.53 (d, $J = 7.3$ Hz, 1H), 7.44 (t, $J = 7.6$ Hz, 1H), 6.92 (d, $J = 8.8$ Hz, 2H), 6.59 (d, $J = 2.5$ Hz, 1H), 3.83 (s, 3H), 3.12 (dd, $J = 10.6, 6.6$ Hz, 1H), 2.30 (dd, $J = 10.6, 6.5$ Hz, 1H), 1.30 (t, $J = 6.6$ Hz, 1H).

^{13}C NMR (75 MHz, CDCl_3) δ 160.6, 159.8, 153.2, 139.5, 134.5, 131.8, 131.4, 128.3, 127.8, 127.3, 125.6, 120.1, 114.0, 104.6, 75.4, 55.3, 22.8, 21.5.

IR (film): ν (cm^{-1}) 3107, 3011, 2961, 2925, 2842, 2039, 1991, 1712, 1607, 1507, 14817, 1447, 1415, 1364, 1284, 1247, 1214, 1176, 1119, 1084, 1056, 1028, 968, 937, 873, 841, 768, 736.7674, 688, 640, 610, 583, 528, 497, 447, 398

HRMS (ESI, m/z) calcd for $\text{C}_{20}\text{H}_{16}\text{N}_2\text{O}_3\text{Na}$ $[\text{M}+\text{Na}]^+$: 355.1059, found: 355.1053.



2c

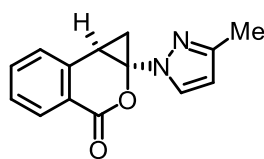
According to the general procedure, the reaction of **1c** (25.4 mg, 0.10 mmol) and Δ -**RhS** (3.5 mg, 4.0 mol%) in CH_2Cl_2 (2.0 mL, 0.05 M) was stirred under nitrogen atmosphere for 16 hours with 24 W blue LEDs at room temperature, affording 18.8 mg (74% yield, pale yellow solid) of **2c** as a single diastereomer. Enantiomeric excess was established by HPLC analysis using a Chiralpak IG column, ee = 97% (HPLC: 254 nm, n -hexane/isopropanol = 90:10, flow rate 1 mL/min, 30 $^\circ\text{C}$, t_r (major) = 22.2 min, t_r (minor) = 28.6 min). $[\alpha]_D^{22} = -37.6^\circ$ (c 1.0, CH_2Cl_2).

^1H NMR (300 MHz, CDCl_3) δ 8.19 (d, $J = 7.8$ Hz, 1H), 7.62 (t, $J = 7.5$ Hz, 1H), 7.53 (d, $J = 7.2$ Hz, 1H), 7.42 (t, $J = 7.5$ Hz, 1H), 5.90 (s, 1H), 3.02 (dd, $J = 10.6, 6.7$ Hz, 1H), 2.37 (s, 3H), 2.25-2.08 (m, 4H), 1.29 (t, $J = 6.5$ Hz, 1H).

^{13}C NMR (75 MHz, CDCl_3) δ 160.8, 149.9, 142.1, 139.5, 134.3, 131.3, 128.4, 127.8, 120.0, 107.6, 73.2, 23.1, 21.1, 13.5, 11.1.

IR (film): ν (cm^{-1}) 3118, 3024, 2961, 2923, 2033, 1980, 1720, 1604, 1570, 1482, 1404, 1354, 1312, 1283, 1220.1394, 1159, 1108, 1080, 1030, 963, 930, 883, 805, 759, 716, 684, 645, 611, 579, 552, 525, 498, 454, 418.

HRMS (ESI, m/z) calcd for $\text{C}_{15}\text{H}_{14}\text{N}_2\text{O}_2\text{Na}$ $[\text{M}+\text{Na}]^+$: 277.0953, found: 277.0948.



2d

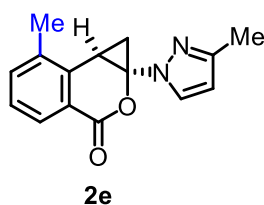
According to the general procedure, the reaction of **1d** (24.0 mg, 0.10 mmol) and Δ -**RhS** (3.5 mg, 4.0 mol%) in CH_2Cl_2 (2.0 mL, 0.05 M) was stirred under nitrogen atmosphere for 16 hours with 24 W blue LEDs at room temperature, affording 19.8 mg (83% yield, pale yellow solid) of **2d** as a single diastereomer. Enantiomeric excess was established by HPLC analysis using a Chiralpak IA column, ee = 98% (HPLC: 254 nm, *n*-hexane/isopropanol = 90:10, flow rate 1 mL/min, 30 °C, t_r (major) = 11.1 min, t_r (minor) = 13.7 min). $[\alpha]_D^{22} = -20^\circ$ (*c* 1.0, CH_2Cl_2).

^1H NMR (300 MHz, CDCl_3) δ 8.19 (d, $J = 7.9$ Hz, 1H), 7.69-7.56 (m, 2H), 7.51 (d, $J = 7.4$ Hz, 1H), 7.42 (t, $J = 7.6$ Hz, 1H), 6.15 (d, $J = 2.3$ Hz, 1H), 3.04 (dd, $J = 10.6, 6.6$ Hz, 1H), 2.29 (s, 3H), 2.22 (dd, $J = 10.6, 6.5$ Hz, 1H), 1.26 (t, $J = 6.5$ Hz, 1H).

^{13}C NMR (75 MHz, CDCl_3) δ 160.6, 151.0, 139.4, 134.4, 131.4, 131.3, 128.3, 127.8, 120.0, 107.5, 74.9, 22.7, 21.5, 13.6.

IR (film): ν (cm^{-1}) 3100, 3027, 2292, 2113, 1988, 1718, 1606, 1533, 1481, 1446, 1415, 1363, 1320, 1283, 1210, 1114, 1082, 1027, 997, 967, 927, 884, 787, 766, 731, 682, 6356, 605.6925, 574, 549, 526, 496, 442, 399.

HRMS (ESI, m/z) calcd for $\text{C}_{14}\text{H}_{13}\text{N}_2\text{O}_2$ $[\text{M}+\text{H}]^+$: 241.0977, found: 241.0972.



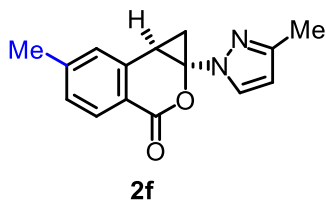
According to the general procedure, the reaction of **1e** (24.0 mg, 0.10 mmol) and Δ -**RhS** (3.5 mg, 4.0 mol%) in CH_2Cl_2 (2.0 mL, 0.05 M) was stirred under nitrogen atmosphere for 20 hours with 24 W blue LEDs at room temperature, affording 20.8 mg (82% yield, pale yellow solid) of **2e** as a single diastereomer. Enantiomeric excess was established by HPLC analysis using a Chiralpak IG column, ee = 98% (HPLC: 254 nm, *n*-hexane/isopropanol = 70:30, flow rate 1 mL/min, 30 °C, t_r (major) = 8.3 min, t_r (minor) = 9.4 min). $[\alpha]_D^{22} = -10.8^\circ$ (*c* 1.0, CH_2Cl_2).

^1H NMR (300 MHz, CDCl_3) δ 8.05 (d, $J = 7.8$ Hz, 1H), 7.67 (d, $J = 2.3$ Hz, 1H), 7.46 (d, $J = 7.5$ Hz, 1H), 7.31 (t, $J = 7.7$ Hz, 1H), 6.15 (d, $J = 2.3$ Hz, 1H), 2.97 (dd, $J = 10.5, 6.8$ Hz, 1H), 2.47 (s, 3H), 2.38-2.18 (m, 4H), 1.25 (t, $J = 6.5$ Hz, 1H).

^{13}C NMR (75 MHz, CDCl_3) δ 161.1, 150.9, 137.9, 136.4, 135.5, 131.3, 128.9, 127.3, 120.2, 107.5, 74.8, 21.5, 19.2, 18.8, 13.6.

IR (film): ν (cm^{-1}) 3104, 2960, 2922, 1953, 1747, 1714, 1596, 1531, 1480, 1450, 1411, 1361, 1288, 1260, 1206, 1117, 1083, 1024, 973, 926, 897, 855, 784, 735, 699, 669, 631, 585, 553, 498, 462, 399.

HRMS (ESI, m/z) calcd for $\text{C}_{15}\text{H}_{14}\text{N}_2\text{O}_2\text{Na}$ $[\text{M}+\text{Na}]^+$: 277.0953, found: 277.0946.



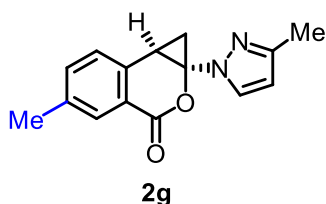
According to the general procedure, the reaction of **1f** (25.4 mg, 0.10 mmol) and Δ -**RhS** (3.5 mg, 4.0 mol%) in CH_2Cl_2 (2.0 mL, 0.05 M) was stirred under nitrogen atmosphere for 20 hours with 24 W blue LEDs at room temperature, affording 23.6 mg (93% yield, pale yellow solid) of **2f** as a single diastereomer. Enantiomeric excess was established by HPLC analysis using a Chiralpak IG column, ee = 98% (HPLC: 254 nm, *n*-hexane/isopropanol = 70:30, flow rate 1 mL/min, 30 °C, t_r (major) = 12.4 min, t_r (minor) = 15.1 min). $[\alpha]_D^{22} = -36.8^\circ$ (*c* 1.0, CH_2Cl_2).

^1H NMR (300 MHz, CDCl_3) δ 8.06 (d, $J = 8.0$ Hz, 1H), 7.64 (d, $J = 2.2$ Hz, 1H), 7.30 (s, 1H), 7.21 (d, $J = 8.0$ Hz, 1H), 6.14 (d, $J = 2.2$ Hz, 1H), 2.97 (dd, $J = 10.6, 6.6$ Hz, 1H), 2.43 (s, 3H), 2.28 (s, 3H), 2.19 (dd, $J = 10.7, 6.6$ Hz, 1H), 1.23 (t, $J = 6.6$ Hz, 1H).

^{13}C NMR (75 MHz, CDCl_3) δ 160.8, 150.9, 145.6, 139.4, 131.4, 131.3, 128.8, 128.7, 117.4, 107.5, 74.8, 22.5, 21.7, 21.5, 13.6.

IR (film): ν (cm^{-1}) 3132, 2962, 2186, 2118, 1961, 1721, 1611, 1533, 1472, 1420, 1359, 1289, 1262, 1214, 1165, 1118, 1064, 1034, 970, 878, 788, 686, 623, 572, 525, 500, 433

HRMS (ESI, m/z) calcd for $\text{C}_{15}\text{H}_{14}\text{N}_2\text{O}_2\text{Na}$ $[\text{M}+\text{Na}]^+$: 277.0953, found: 277.0946.



According to the general procedure, the reaction of **1g** (25.4 mg, 0.10 mmol) and Δ -**RhS** (3.5 mg, 4.0 mol%) in CH_2Cl_2 (2.0 mL, 0.05 M) was stirred under nitrogen atmosphere for 20 hours with 24 W blue LEDs at room temperature, affording 22.3 mg (88% yield, pale yellow solid) of **2g** as a single diastereomer. Enantiomeric excess was established by HPLC analysis using a Chiralpak IG column, ee = 99% (HPLC: 254 nm, *n*-hexane/isopropanol = 70:30, flow rate 1 mL/min, 30 °C, t_r (major) = 9.3 min, t_r (minor) = 11.3 min). $[\alpha]_D^{22} = -15.8^\circ$ (*c* 1.0, CH_2Cl_2).

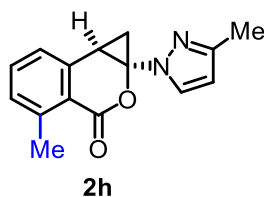
^1H NMR (300 MHz, CDCl_3) δ 7.99 (s, 1H), 7.64 (d, $J = 2.4$ Hz, 1H), 7.44-7.36 (m, 2H), 6.14 (d, $J = 2.4$ Hz, 1H), 3.00 (dd, $J = 10.6, 6.6$ Hz, 1H), 2.39 (s, 3H), 2.28 (s, 3H), 2.17 (dd, $J = 10.6, 6.5$ Hz, 1H), 1.20 (t, $J = 6.5$ Hz, 1H).

^{13}C NMR (75 MHz, CDCl_3) δ 160.9, 150.9, 137.8, 136.4, 135.3, 131.4, 131.4, 128.1, 119.7, 107.5, 74.9, 22.5, 21.2, 21.0, 13.6.

IR (film): ν (cm^{-1}) 3134, 3042, 2925, 2856, 2136, 2073, 2016, 1721, 1612, 1575, 1532, 1504, 1464, 1415, 1359, 1285, 1228, 1173, 1132, 1080, 1064, 1038, 971, 939, 908, 832, 787, 764, 697, 678, 630,

591, 553, 528, 498, 432.

HRMS (ESI, m/z) calcd for C₁₅H₁₄N₂O₂Na [M+Na]⁺: 277.0953, found: 277.0948.



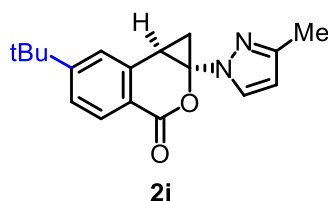
According to the general procedure, the reaction of **1h** (25.4 mg, 0.10 mmol) and Δ -**RhS** (3.5 mg, 4.0 mol%) in CH₂Cl₂ (2.0 mL, 0.05 M) was stirred under nitrogen atmosphere for 20 hours with 24 W blue LEDs at room temperature, affording 21.0 mg (82% yield, white solid) of **2h** as a single diastereomer. Enantiomeric excess was established by HPLC analysis using a Chiralpak IG column, ee = 93% (HPLC: 254 nm, *n*-hexane/isopropanol = 90:10, flow rate 1 mL/min, 30 °C, t_r (major) = 18.1 min, t_r (minor) = 20.7 min). [α]_D²² = -2.4° (*c* 1.0, CH₂Cl₂).

¹H NMR (300 MHz, CDCl₃) δ 7.65 (d, *J* = 2.4 Hz, 1H), 7.45 (t, *J* = 7.6 Hz, 1H), 7.34 (d, *J* = 7.4 Hz, 1H), 7.22 (d, *J* = 7.5 Hz, 1H), 6.14 (d, *J* = 2.4 Hz, 1H), 3.01 (dd, *J* = 10.7, 6.5 Hz, 1H), 2.70 (s, 3H), 2.29 (s, 3H), 2.16 (dd, *J* = 10.7, 6.3 Hz, 1H), 1.24 (t, *J* = 6.4 Hz, 1H).

¹³C NMR (75 MHz, CDCl₃) δ 160.1, 150.9, 144.9, 140.6, 133.5, 131.5, 131.4, 126.6, 118.3, 107.3, 74.2, 23.8, 22.5, 22.0, 13.6.

IR (film): ν (cm⁻¹) 3099, 2969, 2924, 2852, 2021, 1963, 1713, 1591, 1532, 1479, 1447, 1411, 1364, 1296, 1261, 1207, 1108, 1053, 1022, 970, 941, 916, 886, 852, 774, 738, 685, 627, 576, 532, 494, 462, 430.

HRMS (ESI, m/z) calcd for C₁₅H₁₄N₂O₂Na [M+Na]⁺: 277.0953, found: 277.0946.



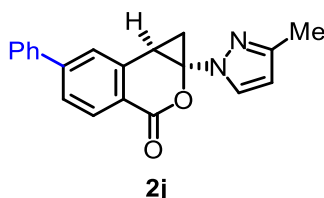
According to the general procedure, the reaction of **1i** (29.6 mg, 0.10 mmol) and Δ -**RhS** (3.5 mg, 4.0 mol%) in CH₂Cl₂ (2.0 mL, 0.05 M) was stirred under nitrogen atmosphere for 16 hours with 24 W blue LEDs at room temperature, affording 22.3 mg (70% yield, pale yellow solid) of **2i** as a single diastereomer. Enantiomeric excess was established by HPLC analysis using a Chiralpak IG column, ee = 97% (HPLC: 254 nm, *n*-hexane/isopropanol = 70:30, flow rate 1 mL/min, 30 °C, t_r (major) = 7.7 min, t_r (minor) = 8.8 min). [α]_D²² = -46.0° (*c* 1.0, CH₂Cl₂).

¹H NMR (300 MHz, CDCl₃) δ 8.10 (d, *J* = 8.3 Hz, 1H), 7.65 (d, *J* = 2.4 Hz, 1H), 7.52-7.38 (m, 2H), 6.15 (d, *J* = 2.3 Hz, 1H), 3.02 (dd, *J* = 10.6, 6.6 Hz, 1H), 2.29 (s, 3H), 2.20 (dd, *J* = 10.7, 6.5 Hz, 1H), 1.36 (s, 9H), 1.26 (t, *J* = 6.5 Hz, 1H).

^{13}C NMR (75 MHz, CDCl_3) δ 160.8, 158.548, 150.9, 139.1, 131.4, 131.2, 125.2, 125.2, 117.3, 107.5, 74.9, 35.3, 31.0, 22.6, 21.8, 13.6.

IR (film): ν (cm^{-1}) 3114, 3052, 2957, 2867, 2249, 2137, 2006, 1943, 1721, 1607, 1534, 1419, 1366, 1290, 1263, 1212, 1139, 1121, 1057, 972, 911, 878, 845, 790, 764, 728, 694, 645, 620, 581, 532, 510, 475.

HRMS (ESI, m/z) calcd for $\text{C}_{18}\text{H}_{20}\text{N}_2\text{O}_2\text{Na}$ $[\text{M}+\text{Na}]^+$: 319.1422, found: 319.1415.



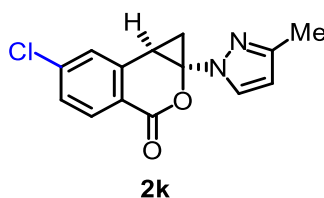
According to the general procedure, the reaction of **1j** (31.6 mg, 0.10 mmol) and Δ -RhS (3.5 mg, 4.0 mol%) in CH_2Cl_2 (2.0 mL, 0.05 M) was stirred under nitrogen atmosphere for 16 hours with 24 W blue LEDs at room temperature, affording 22.2 mg (70% yield, pale yellow solid) of **2i** as a single diastereomer. Enantiomeric excess was established by HPLC analysis using a Chiralpak IG column, ee = 87% (HPLC: 254 nm, *n*-hexane/isopropanol = 70:30, flow rate 1 mL/min, 30 °C, t_r (major) = 13.3 min, t_r (minor) = 15.8 min). $[\alpha]_D^{22} = +37.2^\circ$ (c 1.0, CH_2Cl_2).

^1H NMR (300 MHz, CDCl_3) δ 8.44 (d, $J = 1.7$ Hz, 1H), 7.85 (dd, $J = 8.0, 1.9$ Hz, 1H), 7.73-7.56 (m, 4H), 7.49-7.36 (m, 3H), 6.16 (d, $J = 2.3$ Hz, 1H), 3.09 (dd, $J = 10.5, 6.6$ Hz, 1H), 2.39-2.19 (m, 4H), 1.31 (t, $J = 6.5$ Hz, 1H).

^{13}C NMR (75 MHz, CDCl_3) δ 160.7, 151.0, 141.0, 139.2, 138.1, 132.9, 131.4, 129.6, 129.0, 128.8, 128.0, 127.0, 120.4, 107.6, 75.0, 22.8, 21.3, 13.6.

IR (film): ν (cm^{-1}) 3105, 3032, 2960, 2922, 2852, 2061, 2011, 1720, 1611, 1535, 1480, 1454, 1412, 1363, 1298, 1256, 1200, 1142, 1088, 1031, 967, 925, 895, 837, 752, 688, 637, 610, 577.9320, 528, 488, 453, 401.

HRMS (ESI, m/z) calcd for $\text{C}_{20}\text{H}_{16}\text{N}_2\text{O}_2\text{Na}$ $[\text{M}+\text{Na}]^+$: 339.1109, found: 339.1102.



According to the general procedure, the reaction of **1k** (27.5 mg, 0.10 mmol) and Δ -RhS (3.5 mg, 4.0 mol%) in CH_2Cl_2 (2.0 mL, 0.05 M) was stirred under nitrogen atmosphere for 20 hours with 24 W blue LEDs at room temperature, affording 24.8 mg (90% yield, pale yellow solid) of **2k** as a single diastereomer. Enantiomeric excess was established by HPLC analysis using a Chiralpak IG column, ee = 99% (HPLC: 254 nm, *n*-hexane/isopropanol = 70:30, flow rate 1 mL/min, 30 °C, t_r (major) = 9.8 min,

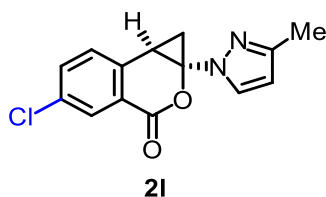
t_r (minor) = 11.5 min). $[\alpha]_D^{22} = -43.6^\circ$ (c 1.0, CH_2Cl_2).

$^1\text{H NMR}$ (300 MHz, CDCl_3) δ 8.12 (d, $J = 8.4$ Hz, 1H), 7.64 (d, $J = 1.9$ Hz, 1H), 7.51 (s, 1H), 7.39 (d, $J = 8.4$ Hz, 1H), 6.15 (d, $J = 1.9$ Hz, 1H), 3.00 (dd, $J = 10.6, 6.6$ Hz, 1H), 2.38-2.14 (m, 4H), 1.29 (t, $J = 6.6$ Hz, 1H).

$^{13}\text{C NMR}$ (75 MHz, CDCl_3) δ 159.8, 151.2, 141.0, 132.9, 131.4, 128.4, 128.3, 118.5, 107.7, 75.0, 22.9, 21.3, 13.6.

IR (film): ν (cm^{-1}) 3141, 3102, 3073, 2924, 2217, 2157, 2003, 1712, 1598, 1537, 1461, 1417, 1369, 1284, 1211, 1126, 1093, 1060, 1032, 970, 935, 900, 838, 806, 763, 685, 640, 611, 560, 532, 487, 448.

HRMS (ESI, m/z) calcd for $\text{C}_{14}\text{H}_{11}\text{ClN}_2\text{O}_2\text{Na}$ $[\text{M}+\text{Na}]^+$: 297.0407, found: 297.0400.



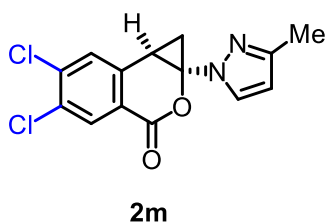
According to the general procedure, the reaction of **1l** (27.5 mg, 0.10 mmol) and Δ -**RhS** (3.5 mg, 4.0 mol%) in CH_2Cl_2 (2.0 mL, 0.05 M) was stirred under nitrogen atmosphere for 24 hours with 24 W blue LEDs at room temperature, affording 22.7 mg (83% yield, pale yellow solid) of **2l** as a single diastereomer. Enantiomeric excess was established by HPLC analysis using a Chiralpak IG column, ee = 99% (HPLC: 254 nm, *n*-hexane/isopropanol = 70:30, flow rate 1 mL/min, 30 °C, t_r (major) = 9.0 min, t_r (minor) = 9.7 min). $[\alpha]_D^{22} = +14.4^\circ$ (c 1.0, CH_2Cl_2).

$^1\text{H NMR}$ (300 MHz, CDCl_3) δ 8.16 (d, $J = 2.2$ Hz, 1H), 7.65 (d, $J = 2.3$ Hz, 1H), 7.58 (dd, $J = 8.2, 2.2$ Hz, 1H), 7.46 (d, $J = 8.2$ Hz, 1H), 6.15 (d, $J = 2.3$ Hz, 1H), 3.02 (dd, $J = 10.6, 6.6$ Hz, 1H), 2.28 (s, 3H), 2.23 (dd, $J = 10.6, 6.6$ Hz, 1H), 1.25 (t, $J = 6.6$ Hz, 1H).

$^{13}\text{C NMR}$ (75 MHz, CDCl_3) δ 159.5, 151.2, 137.7, 134.5, 133.9, 131.5, 131.0, 129.8, 121.5, 107.7, 75.0, 22.8, 21.0, 13.6.

IR (film): ν (cm^{-1}) 3132, 3080, 2960, 2921, 2851, 2221, 2123, 1942, 1728, 1597, 1535, 1478, 1411, 1361, 1290, 1260, 1202, 1126, 1099, 1069, 1036, 968, 937, 887, 832, 789, 755, 690, 628, 587, 545, 467, 411

HRMS (ESI, m/z) calcd for $\text{C}_{14}\text{H}_{11}\text{ClN}_2\text{O}_2\text{Na}$ $[\text{M}+\text{Na}]^+$: 297.0407, found: 297.0400.



According to the general procedure, the reaction of **1m** (30.9 mg, 0.10 mmol) and Δ -**RhS** (6.9 mg, 8mol%) in CH_2Cl_2 (20.0 mL, 0.005 M) was stirred under nitrogen atmosphere for 48 hours with 24 W

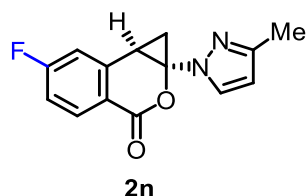
blue LEDs at room temperature, affording 16.0 mg (52% yield, pale yellow solid) of **2m** as a single diastereomer. Enantiomeric excess was established by HPLC analysis using a Chiralpak IA column, ee = 94% (HPLC: 254 nm, *n*-hexane/isopropanol = 90:10, flow rate 1 mL/min, 30 °C, t_r (major) = 11.9 min, t_r (minor) = 15.4 min). $[\alpha]_D^{22} = -9^\circ$ (*c* 1.0, CH₂Cl₂).

¹H NMR (300 MHz, CDCl₃) δ 8.26 (s, 1H), 7.64 (d, *J* = 2.7 Hz, 2H), 6.16 (d, *J* = 2.4 Hz, 1H), 3.00 (dd, *J* = 10.6, 6.6 Hz, 1H), 2.31-2.22 (m, 4H), 1.29 (t, *J* = 6.7 Hz, 1H).

¹³C NMR (75 MHz, CDCl₃) δ 158.9, 151.3, 139.3, 138.8, 133.0, 132.6, 131.4, 130.2, 119.8, 107.9, 75.1, 23.0, 20.8, 13.6.

IR (film): ν (cm⁻¹) 3150, 2961, 2927, 2224, 2037, 1985, 1721, 1594, 1539, 1454, 1407, 1344, 1291, 1252, 1202, 1122, 1095, 1032, 971, 931, 881, 848, 795, 763, 697, 663, 627, 596, 569, 515, 469, 445, 410.

HRMS (ESI, *m/z*) calcd for C₁₄H₁₁Cl₂N₂O₂ [M+H]⁺: 309.0198, found: 309.0193.



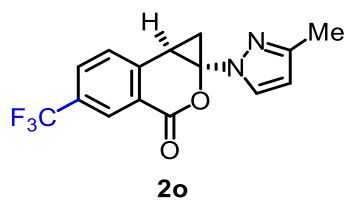
According to the general procedure, the reaction of **1n** (25.8 mg, 0.10 mmol) and Δ -**RhS** (3.5 mg, 4.0 mol%) in CH₂Cl₂ (2.0 mL, 0.05 M) was stirred under nitrogen atmosphere for 20 hours with 24 W blue LEDs at room temperature, affording 20.6 mg (80% yield, pale yellow solid) of **2n** as a single diastereomer. Enantiomeric excess was established by HPLC analysis using a Chiralpak IG column, ee = 98% (HPLC: 254 nm, *n*-hexane/isopropanol = 70:30, flow rate 1 mL/min, 30 °C, t_r (major) = 7.8 min, t_r (minor) = 9.3 min). $[\alpha]_D^{22} = -11.8^\circ$ (*c* 1.0, CH₂Cl₂).

¹H NMR (300 MHz, CDCl₃) δ 8.21 (dd, *J* = 8.7, 5.7 Hz, 1H), 7.65 (d, *J* = 2.3 Hz, 1H), 7.20 (dd, *J* = 8.5, 2.4 Hz, 1H), 7.10 (td, *J* = 8.5, 2.5 Hz, 1H), 6.15 (d, *J* = 2.3 Hz, 1H), 3.01 (dd, *J* = 10.6, 6.6 Hz, 1H), 2.42-2.13 (m, 4H), 1.30 (t, *J* = 6.6 Hz, 1H).

¹³C NMR (75 MHz, CDCl₃) δ 168.0, 164.5, 159.7, 151.1, 142.43 (d, J_{CF} = 10.1 Hz), 134.53 (d, J_{CF} = 10.2 Hz), 131.4, 116.4 (d, J_{CF} = 2.7 Hz), 115.7 (d, J_{CF} = 22.3 Hz), 115.0 (d, J_{CF} = 22.8 Hz), 107.7, 75.0, 22.9, 21.54 (d, J_{CF} = 2.1 Hz), 13.6.

IR (film): ν (cm⁻¹) 3104, 2924, 2008, 1954, 1716, 1615, 1591, 1535, 1483, 1364, 1293, 1245, 1211, 1151, 1112, 1085, 1060, 1030, 1001, 971, 944, 916, 869, 836, 783, 760, 682, 634, 597, 567, 531, 502, 446, 397

HRMS (ESI, *m/z*) calcd for C₁₄H₁₁FN₂O₂Na [M+Na]⁺: 281.0702, found: 281.0696.



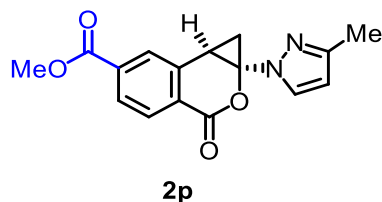
According to the general procedure, the reaction of **1o** (30.8 mg, 0.10 mmol) and Δ -**RhS** (3.5 mg, 4.0 mol%) in CH_2Cl_2 (2.0 mL, 0.05 M) was stirred under nitrogen atmosphere for 48 hours with 24 W blue LEDs at room temperature, affording 19.1 mg (62% yield, pale yellow solid) of **2o** as a single diastereomer. Enantiomeric excess was established by HPLC analysis using a Chiralpak IG column, ee = 98% (HPLC: 254 nm, *n*-hexane/isopropanol = 80:20, flow rate 1 mL/min, 30 °C, t_r (major) = 7.9 min, t_r (minor) = 8.8 min). $[\alpha]_{\text{D}}^{22} = -5.4^\circ$ (*c* 1.0, CH_2Cl_2).

^1H NMR (300 MHz, CDCl_3) δ 8.47 (s, 1H), 7.85 (dd, $J = 8.1, 1.3$ Hz, 1H), 7.75-7.60 (m, 2H), 6.17 (d, $J = 2.4$ Hz, 1H), 3.11 (dd, $J = 10.7, 6.6$ Hz, 1H), 2.38-2.21 (m, 4H), 1.33 (t, $J = 6.6$ Hz, 1H).

^{13}C NMR (75 MHz, CDCl_3) δ 159.4, 151.3, 143.1, 131.5, 130.7 (q), 129.2, 128.5(q), 125.0, 121.5, 120.8, 107.9, 75.1, 23.3, 21.4, 13.6.

IR (film): ν (cm^{-1}) 3106, 2961, 2924, 1728, 1623, 1536, 1460, 1419, 1364, 1333, 1261, 1205, 1170, 1128, 1065, 1031, 970, 924, 893, 842, 811, 775, 719, 707, 620, 585, 544, 518, 459, 412.

HRMS (ESI, *m/z*) calcd for $\text{C}_{15}\text{H}_{11}\text{F}_3\text{N}_2\text{O}_2\text{Na}$ $[\text{M}+\text{Na}]^+$: 331.0670, found: 331.0665.



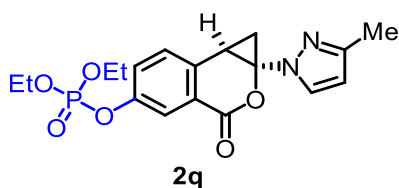
According to the general procedure, the reaction of **1p** (30.8 mg, 0.10 mmol) and Δ -**RhS** (3.5 mg, 4.0 mol%) in CH_2Cl_2 (2.0 mL, 0.05 M) was stirred under nitrogen atmosphere for 24 hours with 24 W blue LEDs at room temperature, affording 19.1 mg (62% yield, pale yellow solid) of **2p** as a single diastereomer. Enantiomeric excess was established by HPLC analysis using a Chiralpak IG column, ee = 95% (HPLC: 254 nm, *n*-hexane/isopropanol = 70:30, flow rate 1 mL/min, 30 °C, t_r (major) = 12.9 min, t_r (minor) = 15.5 min). $[\alpha]_{\text{D}}^{22} = -27.0^\circ$ (*c* 1.0, CH_2Cl_2).

^1H NMR (300 MHz, CDCl_3) δ 8.26 (d, $J = 8.0$ Hz, 1H), 8.18 (s, 1H), 8.04 (d, $J = 7.9$ Hz, 1H), 7.65 (s, 1H), 6.16 (s, 1H), 3.97 (s, 3H), 3.10 (dd, $J = 9.9, 6.9$ Hz, 1H), 2.43-2.14 (m, 4H), 1.29 (t, $J = 6.3$ Hz, 1H).

^{13}C NMR (75 MHz, CDCl_3) δ 165.6, 159.8, 151.2, 139.5, 135.2, 131.5, 131.5, 129.6, 128.5, 123.5, 107.7, 75.0, 52.7, 22.9, 21.4, 13.6.

IR (film): ν (cm^{-1}) 3104, 2953, 2923, 2270, 2204, 2166, 2058, 1955, 1717, 1615, 1583, 1536, 1434, 1356, 1267, 1206, 1110, 1076, 1033, 1002, 970, 936, 862, 830, 774, 742, 678, 641, 616, 567, 486, 398.

HRMS (ESI, *m/z*) calcd for $\text{C}_{16}\text{H}_{14}\text{N}_2\text{O}_4\text{Na}$ $[\text{M}+\text{Na}]^+$: 321.0851, found: 321.0846.



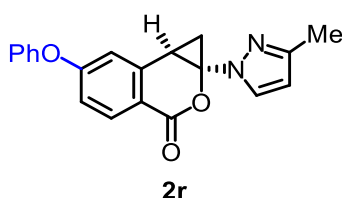
According to the general procedure, the reaction of **1q** (39.2 mg, 0.10 mmol) and Δ -**RhS** (3.5 mg, 4.0 mol%) in CH_2Cl_2 (2.0 mL, 0.05 M) was stirred under nitrogen atmosphere for 20 hours with 24 W blue LEDs at room temperature, affording 32.5 mg (83% yield, pale yellow solid) of **2q** as a single diastereomer. Enantiomeric excess was established by HPLC analysis using a Chiralpak IG column, ee = 98% (HPLC: 254 nm, *n*-hexane/isopropanol = 70:30, flow rate 1 mL/min, 30 °C, t_r (major) = 17.8 min, t_r (minor) = 21.4 min). $[\alpha]_{\text{D}}^{22} = -8.4^\circ$ (*c* 1.0, CH_2Cl_2).

^1H NMR (300 MHz, CDCl_3) δ 7.95 (s, 1H), 7.63 (d, $J = 2.2$ Hz, 1H), 7.51 (d, $J = 1.7$ Hz, 1H), 7.49 (s, 1H), 6.14 (d, $J = 2.3$ Hz, 1H), 4.42-4.09 (m, 4H), 3.01 (dd, $J = 10.6, 6.6$ Hz, 1H), 2.27 (s, 3H), 2.20 (dd, $J = 10.6, 6.6$ Hz, 1H), 1.52-1.29 (m, 6H), 1.23 (t, $J = 6.6$ Hz, 1H).

^{13}C NMR (75 MHz, CDCl_3) δ 159.8, 151.1, 150.2 (d, $J = 6.8$ Hz), 135.9, 131.4, 129.8, 126.64 (d, $J = 4.3$ Hz), 122.26 (d, $J = 5.4$ Hz), 121.4, 107.6, 74.9, 64.87 (d, $J = 6.1$ Hz), 22.6, 20.9, 16.0 (d, $J = 6.5$ Hz), 13.6.

IR (film): ν (cm^{-1}) 3104, 2985, 2922, 2854, 1728, 1610, 1537, 1497, 1368, 1272, 1218, 1163, 1126, 1024, 950, 886, 808, 759, 684, 631, 598, 541, 505

HRMS (ESI, *m/z*) calcd for $\text{C}_{18}\text{H}_{21}\text{N}_2\text{O}_6\text{PNa}$ $[\text{M}+\text{Na}]^+$: 415.1035, found: 415.1030.



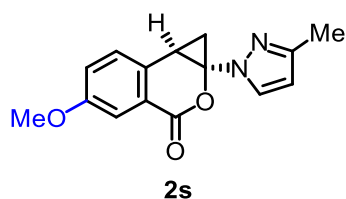
According to the general procedure, the reaction of **1r** (33.2 mg, 0.10 mmol) and Δ -**RhS** (3.5 mg, 4.0 mol%) in CH_2Cl_2 (2.0 mL, 0.05 M) was stirred under nitrogen atmosphere for 16 hours with 24 W blue LEDs at room temperature, affording 29.5 mg (89% yield, pale yellow solid) of **2r** as a single diastereomer. Enantiomeric excess was established by HPLC analysis using a Chiralpak IG column, ee >99% (HPLC: 254 nm, *n*-hexane/isopropanol = 80:20, flow rate 1 mL/min, 30 °C, t_r (major) = 17.3 min, t_r (minor) = 19.0 min). $[\alpha]_{\text{D}}^{22} = -58.6^\circ$ (*c* 1.0, CH_2Cl_2).

^1H NMR (300 MHz, CDCl_3) δ 8.13 (d, $J = 9.5$ Hz, 1H), 7.63 (d, $J = 2.4$ Hz, 1H), 7.48-7.38 (m, 2H), 7.27-7.21 (m, 1H), 7.14-7.06 (m, 2H), 7.01-6.92 (m, 2H), 6.13 (d, $J = 2.4$ Hz, 1H), 2.92 (dd, $J = 10.7, 6.6$ Hz, 1H), 2.28 (s, 3H), 2.18 (dd, $J = 10.7, 6.5$ Hz, 1H), 1.27 (t, $J = 6.5$ Hz, 1H).

^{13}C NMR (75 MHz, CDCl_3) δ 163.1, 160.3, 154.8, 150.9, 141.8, 133.8, 131.4, 130.2, 125.2, 120.6, 117.0, 115.7, 114.0, 107.5, 74.9, 22.6, 21.7, 13.6.

IR (film): ν (cm^{-1}) 3099, 3062, 2957, 2921, 2063, 1713, 1615, 1583, 1534, 1484, 1449, 1371, 1288,

1247, 1207, 1160, 1117, 1064, 1028, 1000, 971, 916, 857, 831, 765, 686, 633, 567, 512, 486, 451, 398.
HRMS (ESI, m/z) calcd for C₂₀H₁₆N₂O₃Na [M+Na]⁺: 355.1059, found: 355.1051.



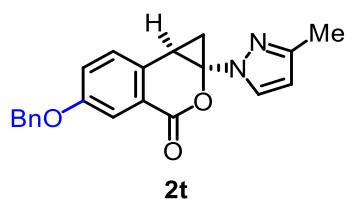
According to the general procedure, the reaction of **1s** (27.0 mg, 0.10 mmol) and Δ -**RhS** (3.5 mg, 4.0 mol%) in CH₂Cl₂ (20.0 mL, 0.005 M) was stirred under nitrogen atmosphere for 16 hours with 24 W blue LEDs at room temperature, affording 23.2 mg (89% yield, pale yellow solid) of **2s** as a single diastereomer. Enantiomeric excess was established by HPLC analysis using a Chiralpak IG column, ee = 97% (HPLC: 254 nm, *n*-hexane/isopropanol = 70:30, flow rate 1 mL/min, 30 °C, t_r (major) = 10.1 min, t_r (minor) = 12.1 min). [α]_D²² = -1.0° (*c* 1.0, CH₂Cl₂).

¹H NMR (300 MHz, CDCl₃) δ 7.65 (t, *J* = 2.9 Hz, 2H), 7.40 (d, *J* = 8.5 Hz, 1H), 7.18 (dd, *J* = 8.5, 2.8 Hz, 1H), 6.14 (d, *J* = 2.3 Hz, 1H), 3.84 (s, 3H), 2.98 (dd, *J* = 10.4, 6.6 Hz, 1H), 2.28 (s, 3H), 2.15 (dd, *J* = 10.4, 6.4 Hz, 1H), 1.18 (t, *J* = 6.5 Hz, 1H).

¹³C NMR (75 MHz, CDCl₃) δ 160.8, 159.1, 150.9, 131.7, 131.4, 129.4, 122.7, 120.9, 113.5, 107.5, 74.9, 55.7, 22.3, 20.9, 13.6.

IR (film): ν (cm⁻¹) 3127, 2960, 2925, 2844, 1724, 1615, 1577, 1535, 1503, 1462, 1423, 1364, 1333, 1283, 1233, 1202, 1130, 1071, 1028, 972, 908, 880, 827, 759, 700, 632, 597, 566, 521.9426, 410.

HRMS (ESI, m/z) calcd for C₁₅H₁₄N₂O₃Na [M+Na]⁺: 293.0902, found: 293.0895.



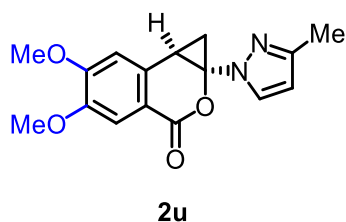
According to the general procedure, the reaction of **1t** (34.6 mg, 0.10 mmol) and Δ -**RhS** (3.5 mg, 4.0 mol%) in CH₂Cl₂ (2.0 mL, 0.05 M) was stirred under nitrogen atmosphere for 20 hours with 24 W blue LEDs at room temperature, affording 30.0 mg (87% yield, pale yellow solid) of **2t** as a single diastereomer. Enantiomeric excess was established by HPLC analysis using a Chiralpak IG column, ee = 99% (HPLC: 254 nm, *n*-hexane/isopropanol = 80:20, flow rate 1 mL/min, 30 °C, t_r (major) = 19.5 min, t_r (minor) = 22.3 min). [α]_D²² = -58.6° (*c* 1.0, CH₂Cl₂).

¹H NMR (300 MHz, CDCl₃) δ 7.68 (s, 1H), 7.57 (s, 1H), 7.50-6.83 (m, 7H), 6.07 (s, 1H), 5.03 (s, 2H), 2.94-2.86 (m, 1H), 2.21 (s, 3H), 2.14-2.00 (m, 1H), 1.21-1.09 (m, 1H).

¹³C NMR (75 MHz, CDCl₃) δ 163.5, 160.7, 158.2, 150.9, 136.1, 131.9, 131.4, 128.6, 128.2, 127.5, 123.3, 120.9, 114.7, 107.5, 74.9, 70.3, 22.3, 20.9, 13.6.

IR (film): ν (cm⁻¹) 3104, 3036, 2961, 2924, 2863, 2147, 2085, 2021, 1719, 1608, 1535, 1501, 1461, 1372, 1330, 1280, 1230, 1125, 1074, 1021, 972, 922, 826, 759, 739, 694, 598, 565, 537, 457.

HRMS (ESI, m/z) calcd for C₂₁H₁₉N₂O₃ [M+H]⁺: 347.1396, found: 347.1392.



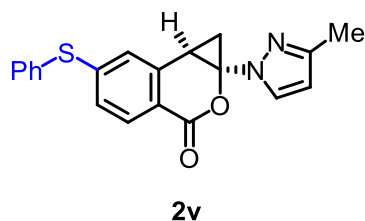
According to the general procedure, the reaction of **1u** (30.0 mg, 0.10 mmol) and Δ -**RhS** (3.5 mg, 4.0 mol%) in CH₂Cl₂ (20.0 mL, 0.005 M) was stirred under nitrogen atmosphere for 10 hours with 3W blue LEDs at room temperature, affording 15.0 mg (50% yield, pale yellow solid) of **2u** as a single diastereomer. Enantiomeric excess was established by HPLC analysis using a Chiralpak IG column, ee = 93% (HPLC: 254 nm, *n*-hexane/isopropanol = 70:30, flow rate 1 mL/min, 30 °C, *t_r* (major) = 18.2 min, *t_r* (minor) = 16.5 min). [α]_D²² = -34.4° (*c* 1.0, CH₂Cl₂).

¹H NMR (300 MHz, CDCl₃) δ 7.65 (d, *J* = 2.3 Hz, 1H), 7.60 (s, 1H), 6.91 (s, 1H), 6.15 (d, *J* = 2.3 Hz, 1H), 3.98 (s, 3H), 3.92 (s, 3H), 2.95 (dd, *J* = 10.4, 6.5 Hz, 1H), 2.29 (s, 3H), 2.16 (dd, *J* = 10.4, 6.4 Hz, 1H), 1.21 (t, *J* = 6.5 Hz, 1H).

¹³C NMR (75 MHz, CDCl₃) δ 160.7, 154.5, 150.9, 148.8, 134.0, 131.4, 112.3, 109.8, 107.5, 74.83, 56.3, 56.2, 22.2, 21.3, 13.6.

IR (film): ν (cm⁻¹) 3359, 3268, 3115, 2923, 2849, 1713, 1604, 1514, 1477, 1455, 1420, 1368, 1297, 1271, 1229, 1203, 1161, 1122, 1067, 1030, 969, 933, 877, 793, 761, 732, 693, 657, 618, 580, 544, 516, 491, 431.

HRMS (ESI, m/z) calcd for C₁₆H₁₆N₂O₄Na [M+Na]⁺: 323.1008, found: 323.1004.



According to the general procedure, the reaction of **1v** (34.8 mg, 0.10 mmol) and Δ -**RhS** (3.5 mg, 4mol%) in CH₂Cl₂ (2.0 mL, 0.05 M) was stirred under nitrogen atmosphere for 20 hours with 24 W blue LEDs at room temperature, affording 30.0 mg (86% yield, pale yellow solid) of **2v** as a single diastereomer. Enantiomeric excess was established by HPLC analysis using a Chiralpak IG column, ee = 97% (HPLC: 254 nm, *n*-hexane/isopropanol = 70:30, flow rate 1 mL/min, 30 °C, *t_r* (major) = 11.6 min, *t_r* (minor) = 13.5 min). [α]_D²² = -87.0° (*c* 1.0, CH₂Cl₂).

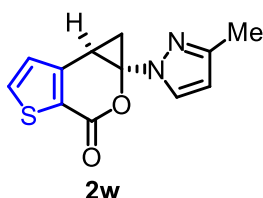
¹H NMR (300 MHz, CDCl₃) δ 8.00 (d, *J* = 8.2 Hz, 1H), 7.62 (d, *J* = 2.3 Hz, 1H), 7.56-7.43 (m, 5H), 7.20-7.05 (m, 2H), 6.12 (d, *J* = 2.3 Hz, 1H), 2.88 (dd, *J* = 10.6, 6.6 Hz, 1H), 2.27 (s, 3H), 2.15 (dd, *J* =

10.6, 6.5 Hz, 1H), 1.24 (t, $J = 6.5$ Hz, 1H).

^{13}C NMR (75 MHz, CDCl_3) δ 160.3, 150.9, 147.7, 139.9, 134.7, 131.6, 131.4, 130.7, 129.9, 129.4, 126.0, 125.6, 116.8, 107.5, 74.8, 22.6, 21.4, 13.6.

IR (film): ν (cm^{-1}) 3100, 3056, 2922, 1714, 1590, 1533, 1465, 1449, 1415, 1357, 1280, 1208, 1092, 1057, 1027, 997, 967, 930, 894, 827, 748, 681, 615, 565, 542, 507, 434, 412

HRMS (ESI, m/z) calcd for $\text{C}_{20}\text{H}_{16}\text{N}_2\text{O}_2\text{SNa}$ $[\text{M}+\text{Na}]^+$: 371.0830, found: 371.0826.



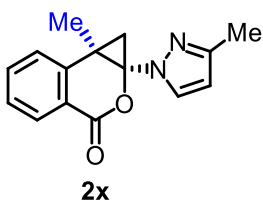
According to the general procedure, the reaction of **1w** (24.6 mg, 0.10 mmol) and Δ -**RhS** (3.5 mg, 4mol%) in CH_2Cl_2 (20.0 mL, 0.005 M) was stirred under nitrogen atmosphere for 36 hours with 24 W blue LEDs at room temperature, affording 14.3 mg (58% yield, pale yellow solid) of **2w** as a single diastereomer. Enantiomeric excess was established by HPLC analysis using a Chiralpak IG column, ee = 63% (HPLC: 254 nm, *n*-hexane/isopropanol = 90:10, flow rate 1 mL/min, 30 °C, t_r (major) = 29.3 min, t_r (minor) = 37.6 min). $[\alpha]_D^{22} = -4.4^\circ$ (c 1.0, CH_2Cl_2).

^1H NMR (300 MHz, CDCl_3) δ 7.74 (d, $J = 5.0$ Hz, 1H), 7.65 (d, $J = 2.4$ Hz, 1H), 7.21 (d, $J = 5.0$ Hz, 1H), 6.15 (d, $J = 2.4$ Hz, 1H), 3.06 (dd, $J = 10.3, 6.5$ Hz, 1H), 2.28 (s, 3H), 2.23 (dd, $J = 10.3, 6.6$ Hz, 1H), 1.28 (t, $J = 6.5$ Hz, 1H).

^{13}C NMR (75 MHz, CDCl_3) δ 156.5, 151.0, 147.8, 135.9, 131.5, 127.2, 122.4, 107.6, 21.7, 20.3, 13.6.

IR (film): ν (cm^{-1}) 3104, 2926, 1708, 1661, 1537, 1462., 1427, 1405, 1364, 1291, 1204, 1118, 1043, 959, 920, 851, 814, 753, 682, 638, 583, 530, 446.

HRMS (ESI, m/z) calcd for $\text{C}_{12}\text{H}_{10}\text{N}_2\text{O}_2\text{SNa}$ $[\text{M}+\text{Na}]^+$: 269.0361, found: 269.0356.



According to the general procedure, the reaction of **1x** (25.4 mg, 0.10 mmol) and Δ -**RhS** (3.5 mg, 4mol%) in CH_2Cl_2 (2.0 mL, 0.05 M) was stirred under nitrogen atmosphere for 24 hours with 24 W blue LEDs at room temperature, affording 17.0 mg (67% yield, pale yellow solid) of **2x** as a single diastereomer. Enantiomeric excess was established by HPLC analysis using a Chiralpak IG column, ee = 99% (HPLC: 254 nm, *n*-hexane/isopropanol = 70:30, flow rate 1 mL/min, 30 °C, t_r (major) = 8.4 min, t_r (minor) = 9.1 min). $[\alpha]_D^{22} = -25.2^\circ$ (c 1.0, CH_2Cl_2).

^1H NMR (300 MHz, CDCl_3) δ 8.23 (d, $J = 7.8$ Hz, 1H), 7.71-7.54 (m, 3H), 7.47-7.37 (m, 1H), 6.16 (d, $J = 2.2$ Hz, 1H), 2.30 (s, 3H), 2.10 (d, $J = 6.7$ Hz, 1H), 1.43 (s, 3H), 1.32 (d, $J = 6.7$ Hz, 1H).

^{13}C NMR (75 MHz, CDCl_3) δ 160.6, 151.0, 143.2, 134.4, 131.9, 131.2, 127.3, 125.8, 120.2, 107.3, 78.9, 27.4, 25.2, 17.73, 13.7.

IR (film): ν (cm^{-1}) 3130, 2971, 2929, 1718, 1604, 1532, 1467, 1443, 1413, 1357, 1296, 1250, 1220, 1113, 1030, 956, 882, 766, 732, 688, 614, 585, 549, 490, 458.

HRMS (ESI, m/z) calcd for $\text{C}_{15}\text{H}_{14}\text{N}_2\text{O}_2\text{Na}$ $[\text{M}+\text{Na}]^+$: 277.0953, found: 277.0948.

4.2.4 Mechanistic Experiments

1) Absorption Spectra

RhS-1d was prepared according to our previously developed well-documented method.¹⁹ As shown in **Figure 49**, free substrate **1d**, which has a maximum absorption at around 290 nm, can not be excited by visible light. In contrast, strong absorption of **RhS-1d** appears at near UV and visible-light region. These results support the role of **RhS** for the direct visible light excitation of catalyst bound substrate. Otherwise to reach the excited state of the substrate needs a high energy UV-light.

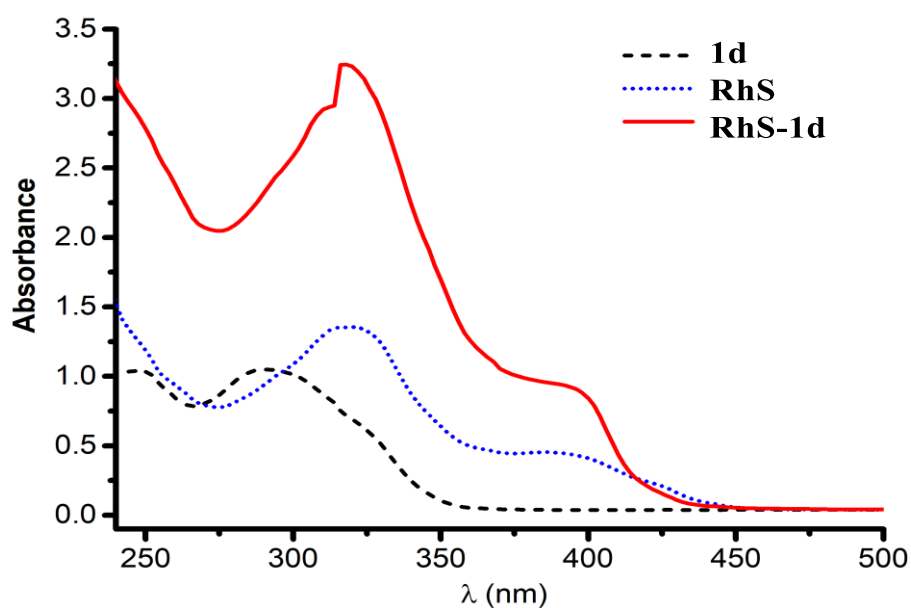
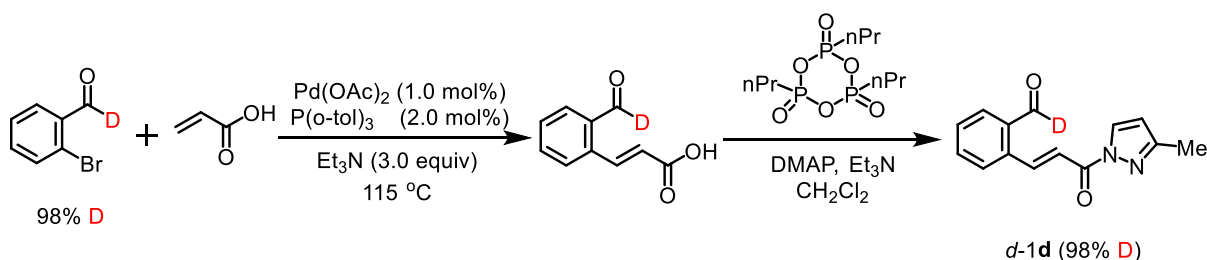
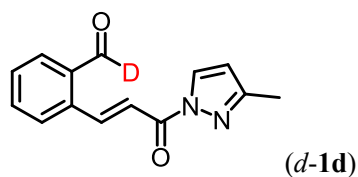


Figure 49. UV/Vis absorption spectra of **1d** (0.05 mM), **RhS** (0.05 mM) and **RhS-1d** (0.05 mM). Recorded in CH_2Cl_2 .

2) Deuteration Experiment



Substrate synthesis: According to the same procedure for the preparation of **1d**, the compound **d-1d** (98% D) was obtained as a white solid starting from 2-bromobenzaldehyde-formyl-d (98% D).



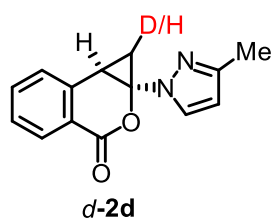
A white solid. Yield: 88%.

$^1\text{H NMR}$ (300 MHz, CDCl_3) δ 8.81 (d, $J = 15.9$ Hz, 1H), 8.28 (d, $J = 2.6$ Hz, 1H), 7.98-7.75 (m, 3H), 7.71-7.52 (m, 2H), 6.30 (d, $J = 2.7$ Hz, 1H), 2.35 (s, 3H).

$^{13}\text{C NMR}$ (75 MHz, CDCl_3) δ 162.5, 154.0, 143.1, 136.6, 133.8, 132.0, 130.3, 129.4, 128.3, 121.0, 110.9, 13.9.

HRMS (ESI, m/z) calcd for $\text{C}_{14}\text{H}_{11}\text{DN}_2\text{O}_2\text{Na}$ $[\text{M}+\text{Na}]^+$: 264.0859, found: 264.0855.

Photocyclization: An oven-dried 10 mL Schlenk tube was charged with compound *d-1d* (24.1 mg, 0.10 mmol) and *rac-RhS* (3.5 mg, 4.0 mol%). Then benzene (2.0 mL, 0.05 M) was added via syringe. The reaction mixture was degassed via freeze-pump-thaw for three cycles. Subsequent, the vial was sealed and placed approximately 10 cm away from the 24 W blue LEDs. After stirring for the indicated time (monitored by TLC) under nitrogen atmosphere, the mixture was diluted with CH_2Cl_2 . The combined organic solutions were concentrated, reduced pressure and purified by flash chromatography on silica gel (*n*-hexane/EtOAc) to afford 23.0 mg (96% yield) of *d-2d* as a pale yellow solid. Through $^1\text{H NMR}$ analysis it can be seen that the methylene group of the cyclopropane is 78% deuterated.

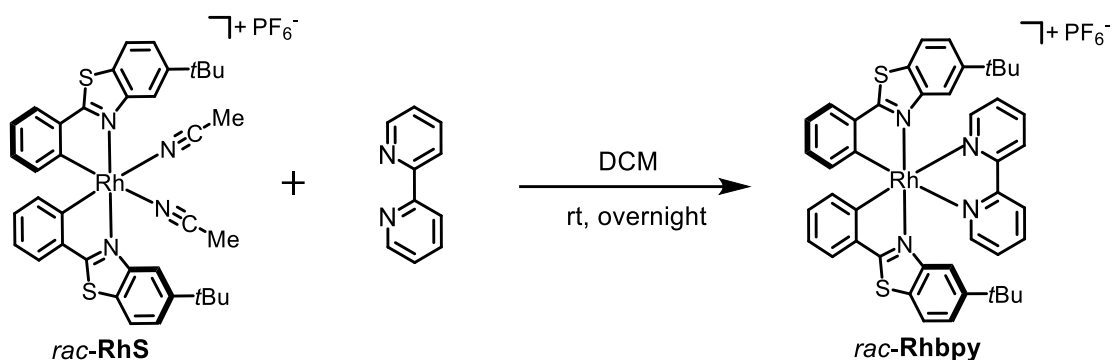


$^1\text{H NMR}$ (500 MHz, CDCl_3) δ 8.21-8.15 (m, 1H), 7.65 (d, $J = 2.5$ Hz, 1H), 7.61 (td, $J = 7.6, 1.4$ Hz, 1H), 7.51-7.48 (m, 1H), 7.41 (td, $J = 7.7, 1.2$ Hz, 1H), 6.14 (d, $J = 2.5$ Hz, 1H), 3.02 (d, $J = 6.7$ Hz, 1H), 2.28 (s, 3H), 2.20 (d, $J = 10.6$ Hz, 0.22H for 22% H and 78% D), 1.24 (d, $J = 6.6$ Hz, 1H).

$^{13}\text{C NMR}$ (75 MHz, CDCl_3) δ 160.6, 151.0, 139.4, 134.4, 131.4, 131.3, 128.3, 127.8, 120.0, 107.5, 74.8, 22.36 (m), 21.4, 13.6.

HRMS (ESI, m/z) calcd for $\text{C}_{14}\text{H}_{11}\text{DN}_2\text{O}_2\text{Na}$ $[\text{M}+\text{Na}]^+$: 264.0859, found: 264.0852.

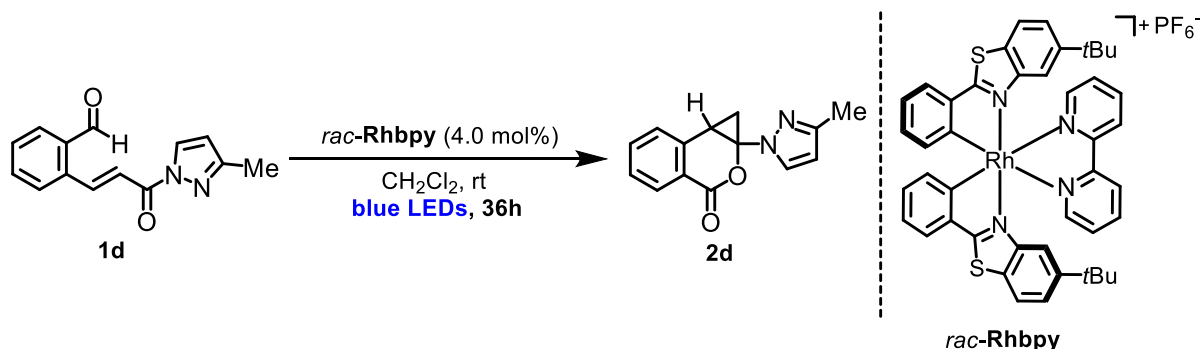
3) Photosensitization with Unreactive Rhodium Complex



The racemic catalyst *rac*-**RhS** complex (34.5 mg, 1.0 equiv) was dissolved in CH₂Cl₂ (0.1 M), and then 2,2'-bipyridine (6.9 mg, 1.1 equiv) was added. The mixture was stirred overnight at room temperature, and then the solvent was evaporated. The solid was washed three times with diethyl ether to afford pure *rac*-**Rhbpy** complex (35.8 mg, Yield: 92%).

¹H NMR (300 MHz, CD₂Cl₂) δ 8.45 (d, *J* = 8.1 Hz, 2H), 8.25 (d, *J* = 5.2 Hz, 2H), 8.14 (td, *J* = 7.9, 1.6 Hz, 2H), 7.91-7.79 (m, 4H), 7.58-7.50 (m, 2H), 7.44 (dd, *J* = 8.6, 1.8 Hz, 2H), 7.19 (td, *J* = 7.5, 0.9 Hz, 2H), 6.99 (td, *J* = 7.6, 1.4 Hz, 2H), 6.62 (d, *J* = 1.5 Hz, 2H), 6.43 (d, *J* = 7.8 Hz, 2H), 0.91 (s, 18H).

¹³C NMR (75 MHz, CD₂Cl₂) δ 177.2(2C), 166.3, 165.8, 155.7, 152.6, 150.8, 149.7, 140.7, 140.4, 134.2, 131.9, 129.1, 128.5, 126.9, 124.9, 124.7, 124.3, 123.1, 115.4, 35.0, 31.2.

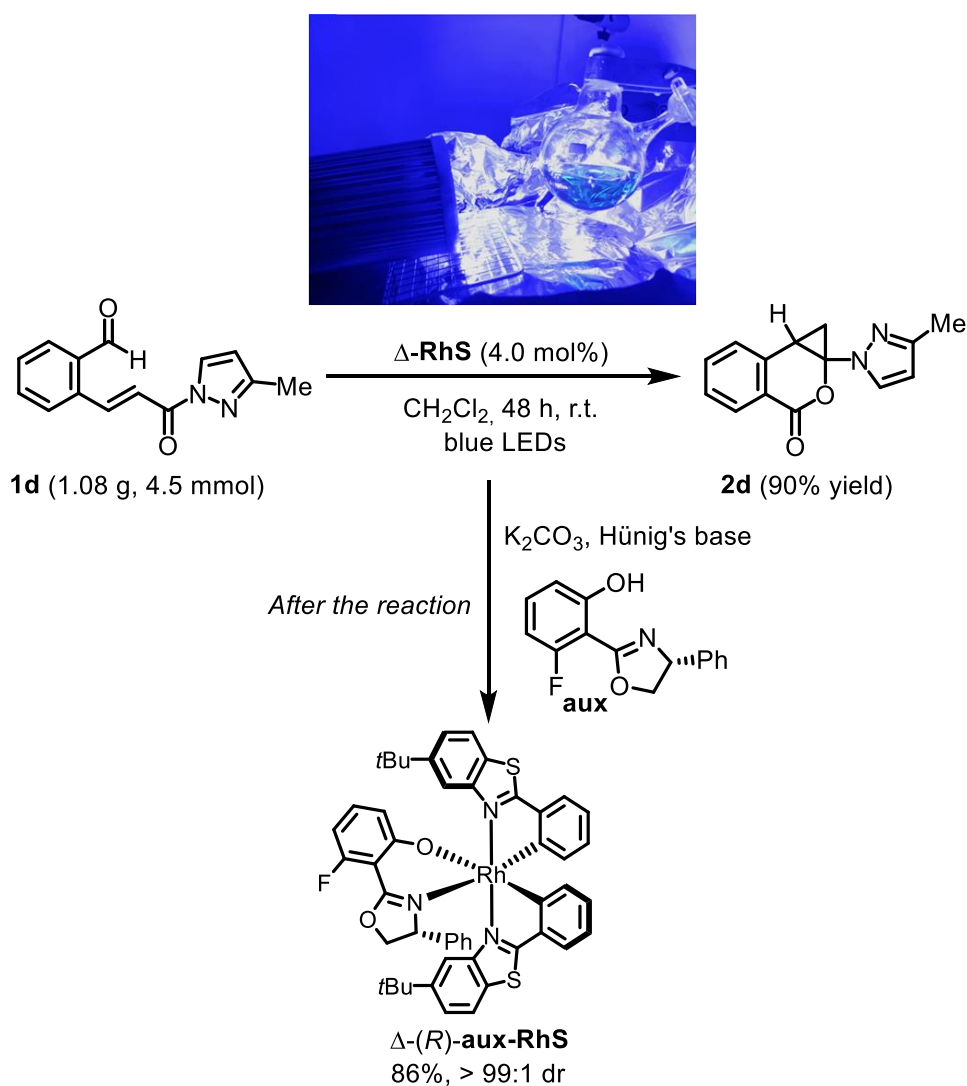


An oven-dried 10 mL Schlenk tube was charged with compound **1d** (24.0 mg, 0.10 mmol) and *rac*-**Rhbpy** (3.5 mg, 4.0 mol%). Then, CH₂Cl₂ (2.0 mL, 0.05 M) was added via syringe. The reaction mixture was degassed via freeze-pump-thaw for three cycles. Subsequent, the vial was sealed and placed approximately 10 cm away from the 24 W blue LEDs. After stirring 36 hours under nitrogen atmosphere, the mixture was directly transferred to column and purified by flash chromatography on silica gel (*n*-hexane/EtOAc = 50:1 to 3:1) to afford the analytically pure product **2d** (5.8 mg, Yield 24%).

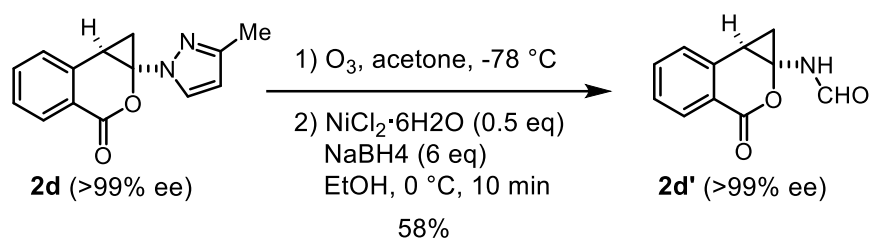
4.2.5 Gram-Scale Reaction and Catalyst Recovery

An oven-dried 250 mL Schlenk tube was charged with compound **1d** (1.08 g, 4.5 mmol) and Δ-**RhS** (155 mg, 0.18 mmol, 4.0 mol%). CH₂Cl₂ (90 mL, 0.05 M) was added via syringe and stirred under an atmosphere of nitrogen. The blue LEDs light source (24 W) was positioned approximately 10 cm away from the Schlenk tube. After photolysis for 48 h under an atmosphere of nitrogen, K₂CO₃ (6.22 g, 45.0

mmol), Hünig's base (47 μ L, 0.27 mmol, 6.0 mol%), and the chiral salicyloxazoline **aux**^{20,21} (69 mg, 0.27 mmol, 6.0 mol%) were added stepwise, and then stirred for another 2 h at room temperature.²² Afterwards, the solvent was concentrated and the residue was filtered through a thin pad of silica gel to remove the inorganic salts. The entire mixture was collected and purified by flash chromatography on silica gel (*n*-hexane/EtOAc 20:1 to 10:1) to afford Δ -(*R*)-**aux-RhS**²² (138 mg, 0.155 mmol, 86%) as a yellow solid with a dr > 99:1 as judged from ¹⁹F NMR analysis. The analytically pure product **2d** eluted last and was isolated (970 mg, 90% yield) and the enantiomeric excess determined as ee > 99% by HPLC analysis (Chiralpak IA column, 254 nm, *n*-hexane/isopropanol = 90:10, flow rate 1 mL/min, 30 °C, tr (major) = 11.1 min, tr (minor) = 13.6 min).



4.2.6 Follow-Up Conversion



Following a modified literature procedure,²³ a solution of compound **2d** (30 mg, 0.125 mmol) in acetone (12.5 mL, $c = 0.01 \text{ M}$) was cooled to -78°C . A stream of O_3/O_2 was bubbled into the reaction solution until the solution became pale blue (15 min). Then, excess ozone was replaced by bubbling O_2 for 5 min and bubbling N_2 for 5 min. Thereafter, the mixture was allowed to warm to room temperature, and was concentrated to $\sim 1 \text{ mL}$ volume. Ethanol (5 mL) was added, the solution was cooled to 0°C , and $\text{NiCl}_2 \cdot 6\text{H}_2\text{O}$ (15 mg, 0.0625 mmol, 0.5 eq) and NaBH_4 (29 mg, 0.75 mmol, 6 eq) were added. After being stirred at 0°C for 10 min, NaHCO_3 (sat.) (5 mL) was added to quench the reaction, and the mixture was extracted with EtOAc ($3 \times 10 \text{ mL}$). The combined organic layer was washed with brine, dried over Na_2SO_4 and filtered. The residue was purified by column chromatography on silica gel to afford the formamide product **2d'** as a colorless oil (eluent: $\text{EtOAc}/\text{hexane} = 3:1$, 14.7 mg, 58% yield). Enantiomeric excess was established by HPLC analysis on chiral stationary phase to be ee $>99\%$ (Chiralpak IG column, 254 nm, n -hexane/isopropanol = 80:20, flow rate 1 mL/min, 25°C , t_r (major) = 21.0 min, t_r (minor) = 24.6 min). $[\alpha]_D^{22} = -38.2^\circ$ ($c 1.0, \text{CH}_2\text{Cl}_2$).

^1H NMR (CD_3CN , as a mixture of rotamer): 0.99 (major, t, $J = 6.6 \text{ Hz}$, 0.68H), 1.06 (minor, t, $J = 6.5 \text{ Hz}$, 0.32H), 1.76 (major, dd, $J = 10.6, 6.5 \text{ Hz}$, 0.68H), 1.92-1.99 (minor, overlapped with CD_2HCN , 0.32H), 2.62 (major, dd, $J = 10.6, 6.8 \text{ Hz}$, 0.68H), 2.78 (minor, dd, $J = 10.6, 6.5 \text{ Hz}$, 0.32H), 7.38-7.48 (major and minor, m, 1H), 7.52-7.60 (major and minor, m, 1H), 7.52-7.60 (minor NH, m, 0.32H), 7.60-7.70 (major and minor, m, 1H), 7.78-8.02 (major NH, br, 0.68 H), 8.03-8.11 (major and minor, m, 1H), 8.18 (major, s, 0.68 H), 8.48 (minor, d, $J = 11.28 \text{ Hz}$, 0.32H).

^{13}C NMR (CD_3CN , as a mixture of rotamer): 22.3 (minor), 22.4 (major), 22.9 (major), 23.1 (minor), 68.8, 121.7, 128.8 (major), 129.0 (minor), 129.9, 131.86 (major), 131.93 (minor), 135.8 (major), 135.9 (minor), 142.3, 162.9 (minor), 163.3 (major), 167.1.

HRMS (ESI, m/z) calcd for $\text{C}_{11}\text{H}_9\text{NO}_3\text{Na}$ $[\text{M}+\text{Na}]^+$: 226.0480, found: 277.0475.

4.2.7 Single-Crystal X-Ray Diffraction Studies

Single crystals of **2k** suitable for X-ray diffraction were obtained by slow diffusion from of a solution of **2k** (30 mg) in CH_2Cl_2 (0.5 mL) layered with n -hexane (1.0 mL) at room temperature for several days in a NMR tube.

Data was collected with an STOE STADIVARI diffractometer equipped with with $\text{CuK}\alpha$ radiation, a graded multilayer mirror monochromator ($\lambda = 1.54186 \text{ \AA}$) and a DECTRIS PILATUS 300K detector

using an oil-coated shock-cooled crystal at 100(2) K. Absorption effects were corrected semi-empirical using multiscanned reflexions (STOE LANA, absorption correction by scaling of reflection intensities). Cell constants were refined using 20551 of observed reflections of the data collection. The structure was solved by direct methods by using the program XT V2014/1 (Bruker AXS Inc., 2014) and refined by full matrix least squares procedures on F^2 using SHELXL-2018/3 (Sheldrick, 2018). The non-hydrogen atoms have been refined anisotropically, carbon bonded hydrogen atoms were included at calculated positions and refined using the 'riding model' with isotropic temperature factors at 1.2 times (for CH_3 groups 1.5 times) that of the preceding carbon atom. CH_3 groups were allowed to rotate about the bond to their next atom to fit the electron density. Nitrogen or oxygen bonded hydrogen atoms were located and allowed to refine isotropically. The Flack parameter refined to -0.005(5). The absolute structure of this crystal has been determined.

Crystal structure, data and details of the structure determination for **2k** are presented in the **Figure 50**.

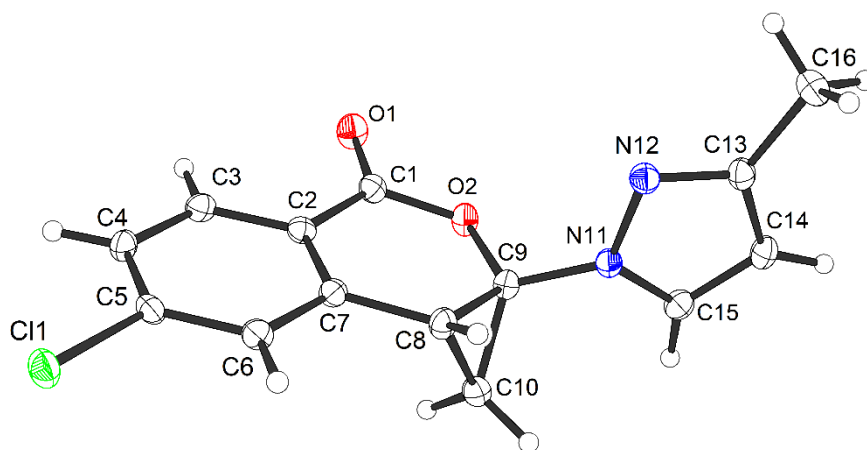


Figure 50. Crystal structure of **2k**.

Data / restraints / parameters	ShelXle (Hübschle, Sheldrick, Dittrich, 2011) ³⁹ 2188 / 1 / 173
Goodness-of-fit on F ²	1.048
R index (all data)	wR2 = 0.0568
R index conventional [I>2sigma(I)]	R1 = 0.0214

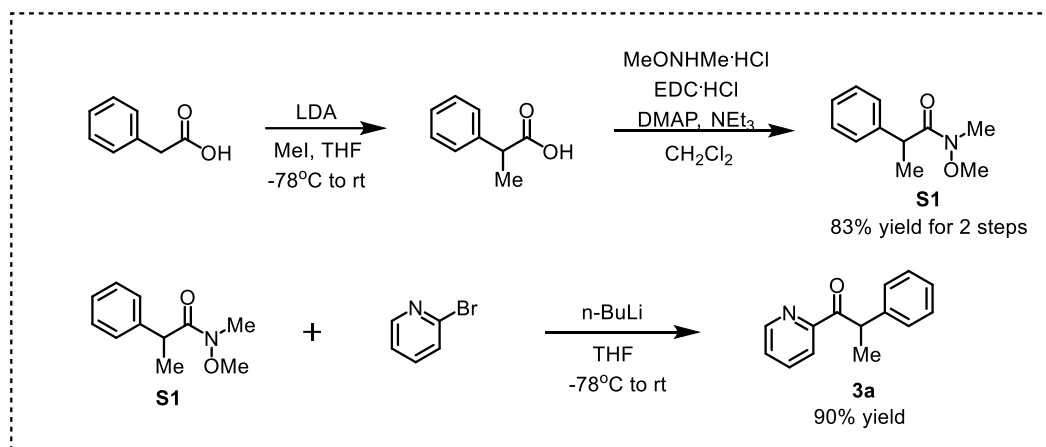
Reference

1. R. F. Heck, Palladium-Catalyzed Vinylation of Organic Halides. *Organic Reactions*. 1982, 345.
2. X. Huang, X. Li, X. Xie, K. Harms, R. Riedel, E. Meggers, *Nat. Commun.* **2017**, 8, 2245.
3. B. Schulte, R. Fröhlich, A. Studer, *Tetrahedron* **2008**, 64, 11852.
4. Y. Hu, Y. Xie, Z. Shen, H. Huang, *Angew. Chem. Int. Ed.* **2017**, 56, 2473.
5. J. M. Wurst, G. Liu, D. S. Tan, *J. Am. Chem. Soc.* **2011**, 133, 7916.
6. B. Du, X. Jiang, P. Sun, *J. Org. Chem.* **2013**, 78, 2786.
7. J. J. Dressler, S. A. Miller, B. T. Meeuwsen, A. M. S. Riel, B. J. Dahl, *Tetrahedron* **2015**, 71, 283.
8. K. Skrabania, A. Miasnikova, A. M. Bivigou-Koumba, D. Zehm, A. Laschewsky, *Polym. Chem.* **2011**, 2, 2074.
9. W. Li, J. Li, D. DeVincentis, T. S. Mansour, *Tetrahedron Lett.* **2004**, 45, 1071.
10. R. D. Grigg, R. Van Hoveln, J. M. Schomaker, *J. Am. Chem. Soc.* **2012**, 134, 16131.
11. X.-H. Liu, H. Park, J.-H. Hu, Y. Hu, Q.-L. Zhang, B.-L. Wang, B. Sun, K.-S. Yeung, F.-L. Zhang, J.-Q. Yu, *J. Am. Chem. Soc.* **2017**, 139, 888.
12. R. Van Hoveln, B. M. Hudson, H. B. Wedler, D. M. Bates, G. Le Gros, D. J. Tantillo, J. M. Schomaker, *J. Am. Chem. Soc.* **2015**, 137, 5346.
13. A. M. Warshawsky, C. A. Alt, J. T. Brozinick, A. R. Harkness, E.D. Hawkins, et al. *Bioorg. Med. Chem. Lett.* **2006**, 16, 6328.
14. Y. J. Jang, O. G. Tsay, D. P. Murale, J. A. Jeong, A. Segev; D. G. Churchill, *Chem. Commun.* **2014**, 50, 7531.
15. D. Ding, Y. Zhao, Q. Meng, D. Xie, B. Nare, D. Chen, C. J. Bacchi, N. Yarlett, Y.-K. Zhang, V. Hernandez, Y. Xia, Y. Freund, M. Abdulla, K.-H. Ang, J. Ratnam, J.-H. McKerrow, R. T. Jacobs, H. Zhou, J. J. Plattner, *ACS Med. Chem. Lett.* **2010**, 1, 165.
16. J. Lin, W. Zhang, N. Jiang, Z. Niu, Z. K. Bao, L. Zhang, D. Liu, C. Pan, X. J. Yao, *J. Nat. Prod.* **2008**, 71, 1938.
17. M. M. M. Raposo, C. Herbivo, V. Hugues, G. Clermont, M. C. R. Castro, A. Comel, M. Blanchard-Desce, M. Manuela, *Eur. J. Org. Chem.* **2016**, 2016, 5263.
18. L. R. Peacock, R. S. L. Chapman, A. C. Sedgwick, M. F. Mahon, D. Amans, S. D. Bull, *Org. Lett.* **2015**, 17, 994.
19. X. Huang, S. Luo, O. Burghaus, R. D. Webster, K. Harms, E. Meggers, *Chem. Sci.* **2017**, 8, 7126.
20. M. Enrico, S. Riccardo, B. Giacomo, T. Michele, M. Magda, B. Marco, C. Paola, *Chem. Eur. J.* **2012**, 18, 8765-8773.

21. J. Ma, X. Shen, K. Harms, E. Meggers, *Dalton Trans.* **2016**, 45, 8320-8323.
22. J. Ma, X. Xie, E. Meggers, *Chem. Eur. J.* **2018**, 24, 259-265.
23. S. H. Kwak, N. Gulia, O. Daugulis, *J. Org. Chem.* **2018**, 83, 5844-5850.

4.3 Catalytic α -Deracemization of Ketones Enabled by Photoredox Deprotonation and Enantioselective Protonation

4.3.1 Synthesis of Substrates



First step: *n*-BuLi (1.6 M in hexane, 2.2 eq) was added dropwise to a solution of diisopropylamine (2.2 eq) in THF at 0 °C. The mixture was stirred for additional 30 min at the same temperature. After cooling to -78 °C, a solution of phenylacetic acid (1.0 eq) in THF was added dropwise at -78 °C. The mixture was stirred for an additional 1 h. Iodomethane (1.5 eq) was added in one portion at -78 °C. The mixture was allowed to warm to rt overnight, quenched by adding of H₂O to obtain a clear yellow solution that was concentrated under reduced pressure. The residue was taken up in H₂O, acidified with HCl (1M) and extracted with EtOAc for three times. The combined organic layers were washed with brine. The solution was dried with anhydrous Na₂SO₄, filtrated and concentrated under reduced pressure. The obtained liquid was dried in vacuum to give the crude product which was directly used for the next step without further purification.

Second step: To a mixture of the 2-phenylpropionic acid (1.0 eq), *N,O*-dimethylhydroxylamine hydrochloride (1.3eq) and DMAP (10% mol) in CH₂Cl₂ (0.2M) at 0 °C were added NEt₃ (1.33 eq) and EDCI (1.3eq) successively. The reaction mixture was stirred at 0 °C for 1 h, then allowed to warm to room temperature and stirred overnight. The reaction was diluted with EtOAc. The organic layer was washed with 1 N HCl (3 × 10 mL), aqueous saturated NaHCO₃ (3 × 10 mL), and brine (20 mL). The combined organic layers were dried over anhydrous Na₂SO₄, filtered, and concentrated under reduced pressure. The crude mixtute was purified by flash chromatography on silica gel (*n*-hexane/EtOAc = 30:1 to 3:1) to give the pure Weinreb amide **S1**. Yield: 83% for 2 steps. The procedure was adapted and modified from a previous report.¹

Third step: To a solution of 2-bromopyridine (1.5 eq) in THF at -78 °C was added *n*-BuLi (1.5 eq) dropwise under a nitrogen atmosphere. The reaction was stirred at -78 °C for 1 h. The corresponding Weinreb amide **S1** (1.0 eq in THF) was added dropwise to the flask after the reaction was cooled back down to -78 °C. The reaction was allowed to warm to room temperature slowly and stirred overnight. The reaction was quenched with a saturated aqueous NH₄Cl solution at room temperature and extracted

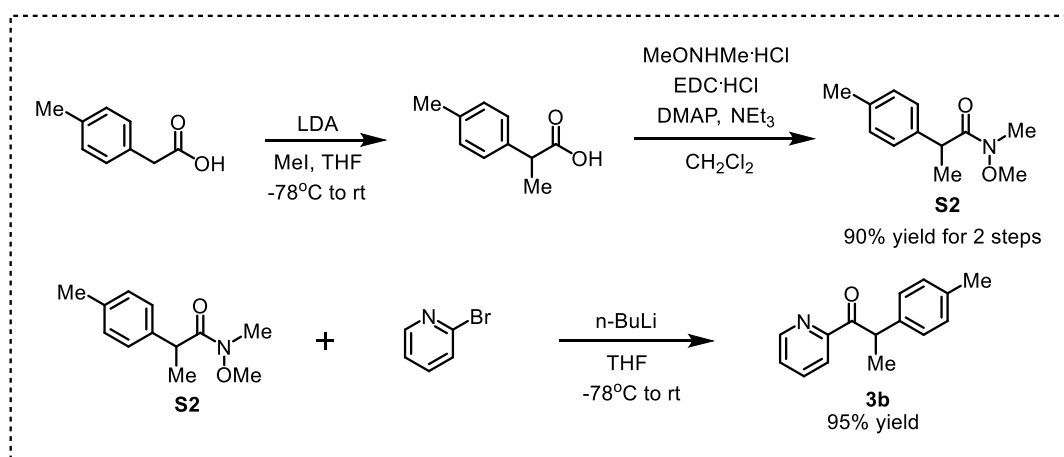
with EtOAc. The organic layer was washed with brine. After drying with anhydrous Na₂SO₄, filtration and concentration under reduced pressure, the crude residue was purified by flash chromatography on silica gel (*n*-hexane/EtOAc = 30:1 to 3:1) to afford the substrate **3a** as a white solid. Yield: 90%.

2-Phenyl-1-(pyridin-2-yl)propan-1-one (**1**)

¹H NMR (300 MHz, CDCl₃) δ 8.80 – 8.70 (m, 1H), 8.10 (d, *J* = 7.9 Hz, 1H), 7.85 (td, *J* = 7.7, 1.7 Hz, 1H), 7.54 – 7.41 (m, 3H), 7.30 (ddd, *J* = 11.0, 9.4, 6.1 Hz, 3H), 5.59 (q, *J* = 7.1 Hz, 1H), 1.66 (d, *J* = 7.1 Hz, 3H).

¹³C NMR (75 MHz, CDCl₃) δ 201.8, 153.0, 148.8, 140.9, 136.8, 128.5, 126.8, 126.6, 122.7, 44.9, 18.2.

HRMS (ESI, *m/z*) calcd for C₁₄H₁₃NNaO [M+Na]⁺: 234.0889, found: 234.0900.



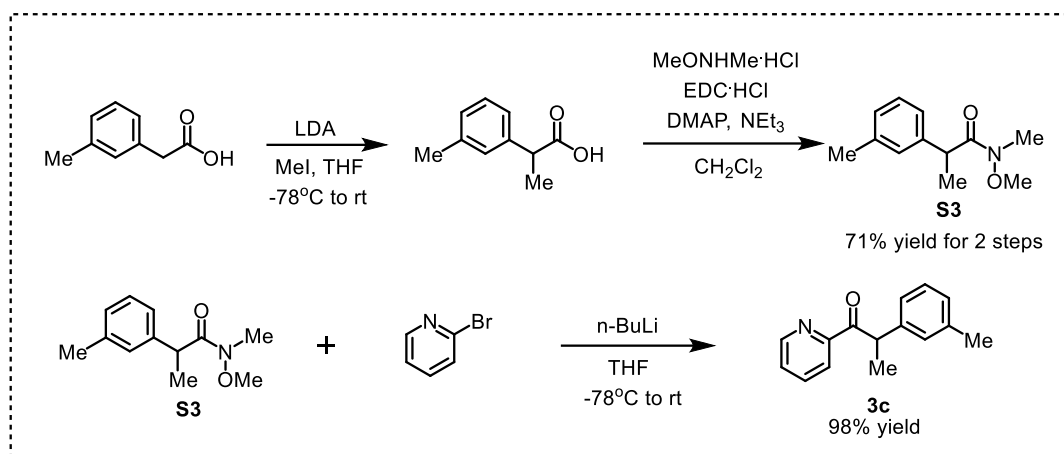
According to the same procedure used as for the preparation of **1**, 4-methylphenylacetic acid as the starting material provided **3b** as a white solid. Yield: 86% over three steps.

1-(Pyridin-2-yl)-2-(*p*-tolyl) propan-1-one (**2**)

¹H NMR (300 MHz, CDCl₃) δ 8.78 – 8.52 (m, 1H), 8.11 – 7.90 (m, 1H), 7.75 (td, *J* = 7.7, 1.4 Hz, 1H), 7.43 – 7.34 (m, 1H), 7.28 (d, *J* = 8.0 Hz, 2H), 7.08 (d, *J* = 7.9 Hz, 2H), 5.46 (q, *J* = 7.1 Hz, 1H), 2.27 (s, 3H), 1.55 (d, *J* = 7.1 Hz, 3H).

¹³C NMR (75 MHz, CDCl₃) δ 201.9, 153.0, 148.8, 137.8, 136.7, 136.2, 129.2, 128.3, 126.8, 122.7, 74.5, 21.0, 18.2.

HRMS (ESI, *m/z*) calcd for C₁₅H₁₆NO [M+H]⁺: 226.1226, found: 226.1230.



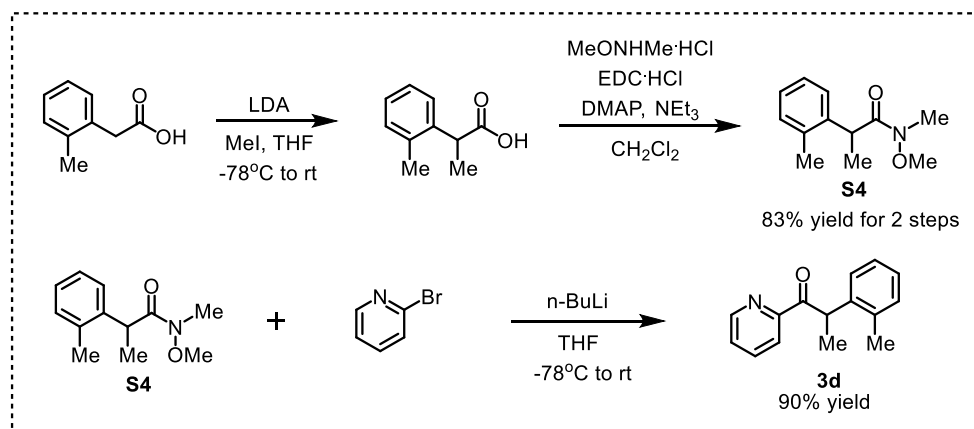
According to the same procedure used as for the preparation of **1**, 3-methylphenylacetic acid as the starting material provided **3c** as a white solid. Yield: 70% over three steps.

1-(Pyridin-2-yl)-2-(*m*-tolyl) propan-1-one

$^1\text{H NMR}$ (300 MHz, CDCl_3) δ 8.76 (dd, $J = 4.0, 0.7$ Hz, 1H), 8.11 (dd, $J = 7.9, 0.9$ Hz, 1H), 7.85 (td, $J = 7.7, 1.5$ Hz, 1H), 7.53 – 7.45 (m, 1H), 7.33 – 7.21 (m, 3H), 7.12 – 7.05 (m, 1H), 5.56 (q, $J = 7.1$ Hz, 1H), 2.40 (s, 3H), 1.65 (d, $J = 7.1$ Hz, 3H).

$^{13}\text{C NMR}$ (75 MHz, CDCl_3) δ 201.9, 153.0, 148.8, 140.8, 138.0, 136.7, 129.0, 128.3, 127.4, 126.8, 125.6, 122.7, 44.8, 21.4, 18.23.

HRMS (ESI, m/z) calcd for $\text{C}_{15}\text{H}_{16}\text{NO}$ $[\text{M}+\text{H}]^+$: 226.1226, found: 226.1231.



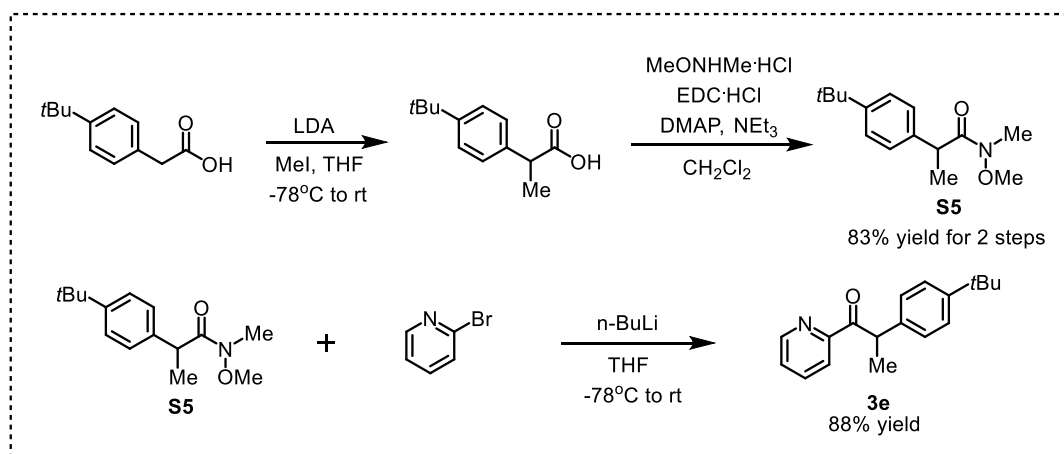
According to the same procedure used as for the preparation of **1**, 2-methylphenylacetic acid as the starting material provided **3d** as a white solid. Yield: 75% over three steps.

1-(Pyridin-2-yl)-2-(*o*-tolyl) propan-1-one

$^1\text{H NMR}$ (300 MHz, CDCl_3) δ 8.58 (d, $J = 4.6$ Hz, 1H), 8.01 (d, $J = 7.8$ Hz, 1H), 7.74 (td, $J = 7.7, 1.6$ Hz, 1H), 7.34 (ddd, $J = 7.4, 4.8, 1.0$ Hz, 1H), 7.20 – 7.03 (m, 4H), 5.57 (q, $J = 7.0$ Hz, 1H), 2.57 (s, 3H), 1.50 (d, $J = 7.0$ Hz, 3H).

$^{13}\text{C NMR}$ (75 MHz, CDCl_3) δ 202.6, 153.2, 148.8, 139.8, 136.7, 136.3, 130.5, 126.9, 126.8, 126.6, 126.1, 122.5, 41.7, 19.9, 17.7.

HRMS (ESI, m/z) calcd for $\text{C}_{15}\text{H}_{16}\text{NO}$ $[\text{M}+\text{H}]^+$: 226.1226, found: 226.1232.



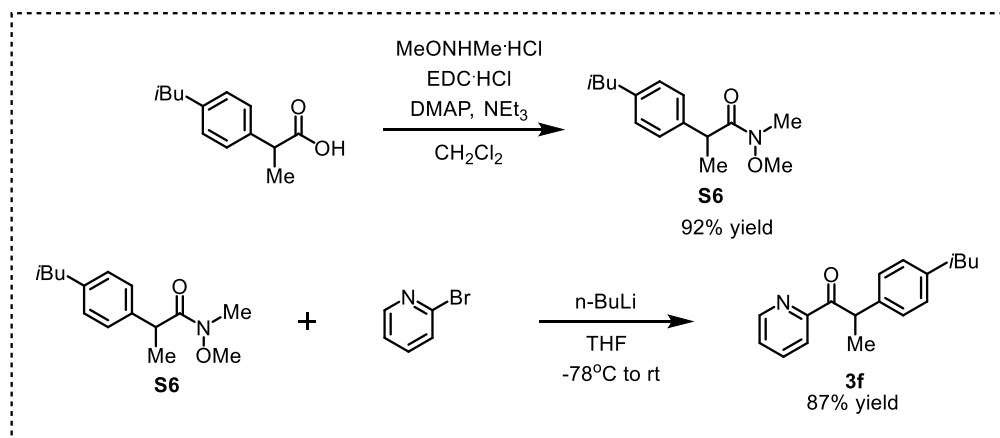
According to the same procedure used as for the preparation of **1**, 4-*tert*-butylphenylacetic acid as the starting material provided **3e** as a white solid. Yield: 73% over three steps.

2-(4-(*tert*-Butyl) phenyl)-1-(pyridin-2-yl) propan-1-one

¹H NMR (300 MHz, CDCl₃) δ 8.67 (d, *J* = 4.2 Hz, 1H), 8.01 (d, *J* = 7.9 Hz, 1H), 7.75 (td, *J* = 7.7, 1.7 Hz, 1H), 7.39 (ddd, *J* = 7.5, 4.8, 1.2 Hz, 1H), 7.30 (q, *J* = 8.5 Hz, 4H), 5.50 (q, *J* = 7.1 Hz, 1H), 1.55 (d, *J* = 7.1 Hz, 3H), 1.27 (s, 9H).

¹³C NMR (75 MHz, CDCl₃) δ 202.0, 153.1, 149.4, 148.8, 137.6, 136.7, 128.0, 126.8, 125.4, 122.8, 44.11, 34.32, 31.29, 18.17.

HRMS (ESI, *m/z*) calcd for C₁₈H₂₂NO [M+H]⁺: 268.1696, found: 268.1702.



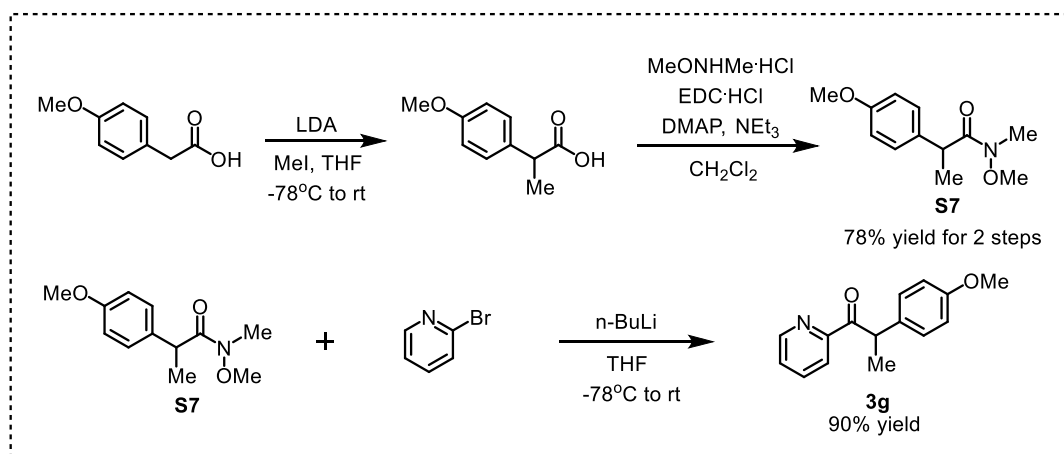
According to the similar procedure used as for the preparation of **1**, 2-(4-Isobutylphenyl)propionic Acid as the starting material provided **3f** as a white solid. Yield: 80% over three steps.

2-(4-Isobutylphenyl)-1-(pyridin-2-yl) propan-1-one

¹H NMR (300 MHz, CDCl₃) δ 8.66 (d, *J* = 4.1 Hz, 1H), 8.00 (d, *J* = 7.8 Hz, 1H), 7.74 (td, *J* = 7.7, 1.7 Hz, 1H), 7.43 – 7.32 (m, 1H), 7.29 (d, *J* = 8.1 Hz, 2H), 7.04 (d, *J* = 8.1 Hz, 2H), 5.48 (q, *J* = 7.1 Hz, 1H), 2.39 (d, *J* = 7.2 Hz, 2H), 1.91 – 1.71 (m, 1H), 1.55 (d, *J* = 7.1 Hz, 3H), 0.86 (d, *J* = 6.6 Hz, 6H).

¹³C NMR (75 MHz, CDCl₃) δ 202.0, 153.1, 148.7, 140.0, 138.0, 136.7, 129.2, 128.1, 126.8, 122.7, 45.0, 44.4, 30.1, 22.4, 18.2.

HRMS (ESI, *m/z*) calcd for C₁₈H₂₂NO [M+H]⁺: 268.1696, found: 268.1707.



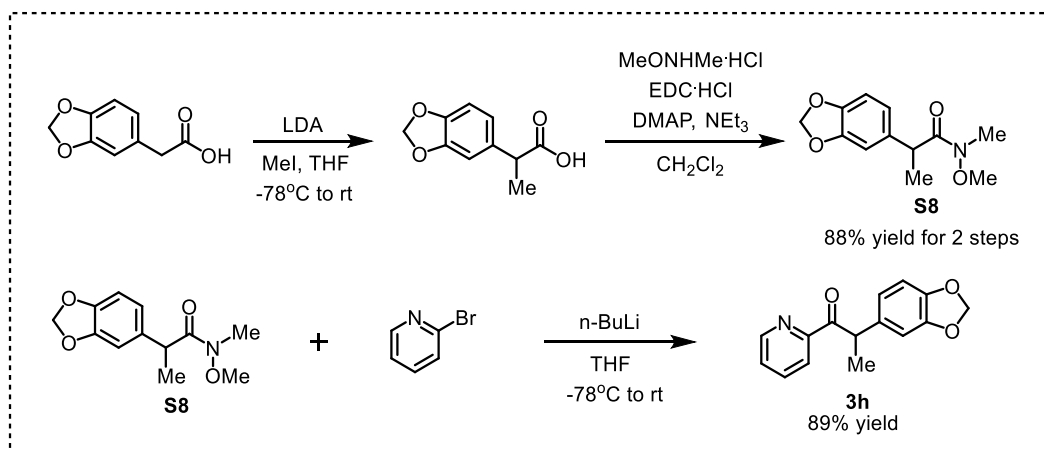
According to the same procedure used as for the preparation of **1**, 4-methoxyphenylacetic acid as the starting material provided **3g** as a colorless liquid. Yield: 70% over three steps.

2-(4-Methoxyphenyl)-1-(pyridin-2-yl) propan-1-one

$^1\text{H NMR}$ (300 MHz, CDCl_3) δ 8.70 – 8.61 (m, 1H), 7.99 (d, $J = 7.9$ Hz, 1H), 7.75 (td, $J = 7.7, 1.7$ Hz, 1H), 7.43 – 7.25 (m, 3H), 6.80 (d, $J = 8.8$ Hz, 2H), 5.43 (q, $J = 7.1$ Hz, 1H), 3.73 (s, 3H), 1.53 (d, $J = 7.1$ Hz, 3H).

$^{13}\text{C NMR}$ (75 MHz, CDCl_3) δ 201.9, 158.3, 153.0, 148.7, 136.7, 132.8, 129.4, 126.8, 122.7, 113.9, 55.1, 43.9, 18.1.

HRMS (ESI, m/z) calcd for $\text{C}_{15}\text{H}_{16}\text{NO}_2$ $[\text{M}+\text{H}]^+$: 242.1176, found: 242.1181.



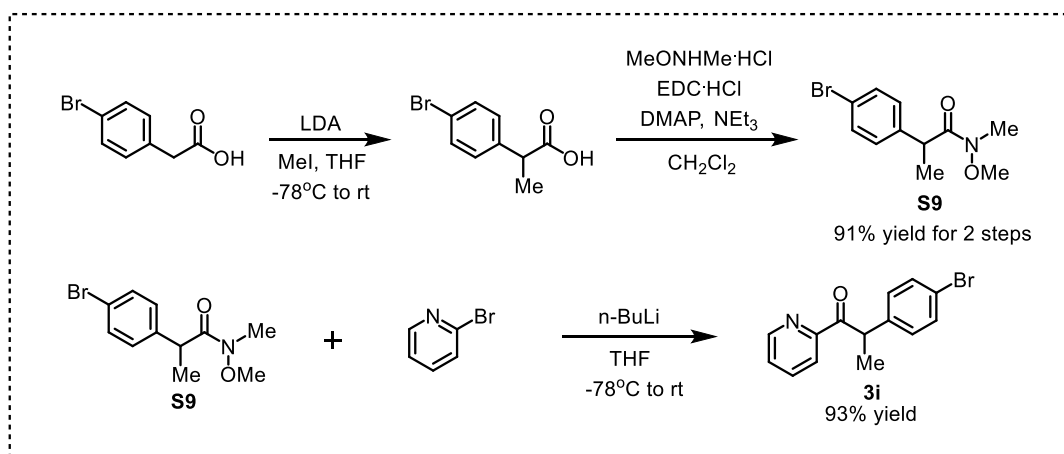
According to the same procedure used as for the preparation of **1**, 3,4-methylenedioxyphenylacetic acid as the starting material provided **3h** as a white solid. Yield: 78% over three steps.

2-(Benzo[d][1,3]dioxol-5-yl)-1-(pyridin-2-yl) propan-1-one

$^1\text{H NMR}$ (300 MHz, CDCl_3) δ 8.76 – 8.53 (m, 1H), 7.99 (d, $J = 7.9$ Hz, 1H), 7.76 (td, $J = 7.7, 1.7$ Hz, 1H), 7.39 (ddd, $J = 7.5, 4.8, 1.1$ Hz, 1H), 6.90 (d, $J = 1.6$ Hz, 1H), 6.83 (dd, $J = 8.0, 1.7$ Hz, 1H), 6.68 (d, $J = 8.0$ Hz, 1H), 5.87 (s, 2H), 5.40 (q, $J = 7.1$ Hz, 1H), 1.51 (d, $J = 7.1$ Hz, 3H).

$^{13}\text{C NMR}$ (75 MHz, CDCl_3) δ 201.6, 152.9, 148.8, 147.6, 146.3, 136.8, 134.6, 126.8, 122.7, 121.6, 108.9, 108.2, 100.8, 44.3, 18.2.

HRMS (ESI, m/z) calcd for $\text{C}_{15}\text{H}_{14}\text{NO}_3$ $[\text{M}+\text{H}]^+$: 256.0968, found: 256.0978.



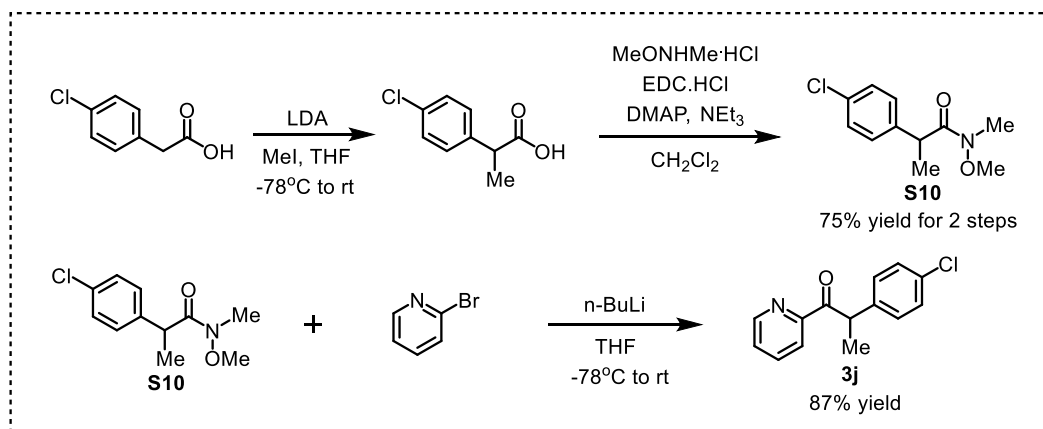
According to the same procedure used as for the preparation of **1**, 4-bromophenylacetic acid as the starting material provided **3i** as a white solid. Yield: 85% over three steps.

2-(4-Bromophenyl)-1-(pyridin-2-yl) propan-1-one

$^1\text{H NMR}$ (300 MHz, CDCl_3) δ 8.64 (ddd, $J = 4.7, 1.6, 0.8$ Hz, 1H), 8.00 (dd, $J = 7.9, 1.0$ Hz, 1H), 7.76 (td, $J = 7.7, 1.7$ Hz, 1H), 7.44 – 7.33 (m, 3H), 7.29 – 7.22 (m, 2H), 5.45 (q, $J = 7.1$ Hz, 1H), 1.53 (d, $J = 7.1$ Hz, 3H).

$^{13}\text{C NMR}$ (75 MHz, CDCl_3) δ 201.3, 152.6, 148.8, 139.9, 136.8, 131.5, 130.2, 127.0, 122.7, 120.6, 44.3, 18.0.

HRMS (ESI, m/z) calcd for $\text{C}_{14}\text{H}_{13}\text{BrNO}$ $[\text{M}+\text{H}]^+$: 290.0185, found: 290.0185.



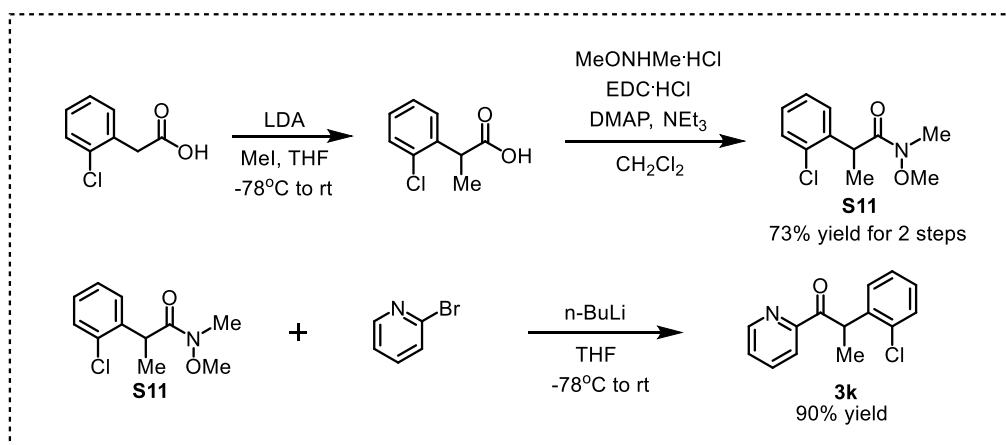
According to the same procedure used as for the preparation of **1**, 4-chlorophenylacetic acid as the starting material provided **3j** as a white solid. Yield: 65% over three steps.

2-(4-Chlorophenyl)-1-(pyridin-2-yl) propan-1-one

$^1\text{H NMR}$ (300 MHz, CDCl_3) δ 8.73 – 8.57 (m, 1H), 8.00 (d, $J = 7.9$ Hz, 1H), 7.77 (td, $J = 7.7, 1.6$ Hz, 1H), 7.45 – 7.37 (m, 1H), 7.32 (dd, $J = 8.7, 2.1$ Hz, 2H), 7.25 – 7.15 (m, 2H), 5.46 (q, $J = 7.1$ Hz, 1H), 1.53 (d, $J = 7.1$ Hz, 3H).

$^{13}\text{C NMR}$ (75 MHz, CDCl_3) δ 201.4, 152.6, 148.8, 139.4, 136.8, 132.5, 129.8, 128.6, 127.0, 122.8, 44.3, 18.1.

HRMS (ESI, m/z) calcd for $\text{C}_{14}\text{H}_{13}\text{ClNO}$ $[\text{M}+\text{H}]^+$: 246.0680, found: 246.0690.



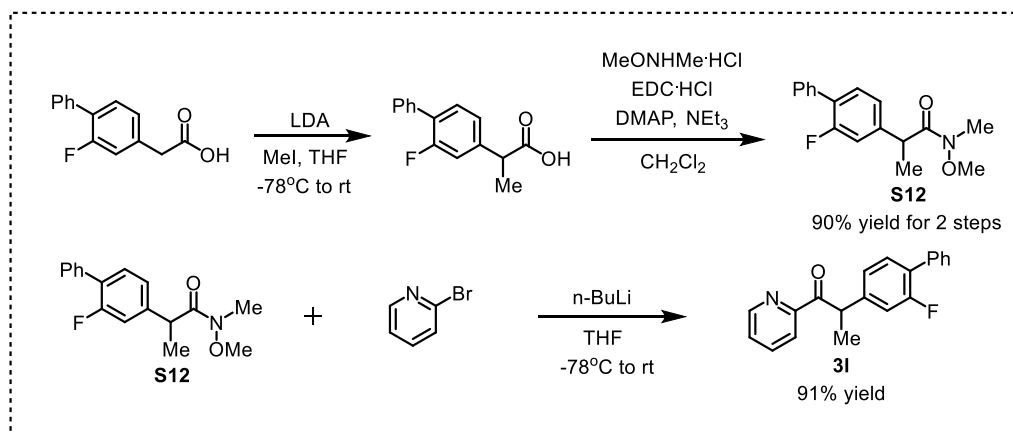
According to the same procedure used as for the preparation of **1**, 2-chlorophenylacetic acid as the starting material provided **3k** as a white solid. Yield: 65% over three steps.

2-(2-Chlorophenyl)-1-(pyridin-2-yl) propan-1-one

$^1\text{H NMR}$ (300 MHz, CDCl_3) δ 8.66 (d, $J = 4.5$ Hz, 1H), 8.06 (d, $J = 7.8$ Hz, 1H), 7.86 – 7.75 (m, 1H), 7.48 – 7.34 (m, 2H), 7.29 (dd, $J = 7.5, 2.0$ Hz, 1H), 7.25 – 7.09 (m, 2H), 5.81 (q, $J = 7.1$ Hz, 1H), 1.58 (d, $J = 7.1$ Hz, 3H).

$^{13}\text{C NMR}$ (75 MHz, CDCl_3) δ 201.9, 152.7, 149.0, 139.2, 136.7, 133.9, 129.5, 128.6, 127.8, 126.8, 122.4, 42.8, 17.0.

HRMS (ESI, m/z) calcd for $\text{C}_{14}\text{H}_{13}\text{ClNO}$ $[\text{M}+\text{H}]^+$: 246.0680, found: 246.0690.



According to the same procedure used as for the preparation of **1**, (2-fluoro-4-biphenyl) acetic acid as the starting material provided **3l** as a white solid. Yield: 82% over three steps.

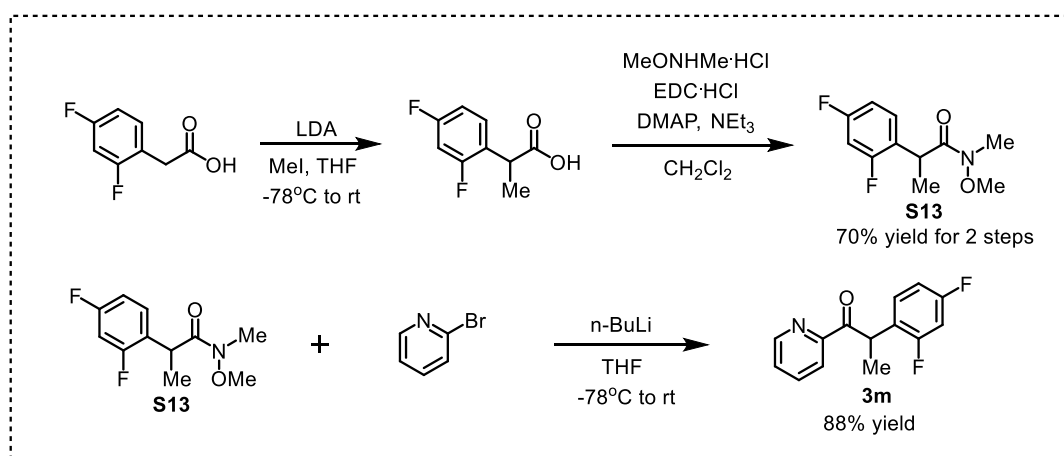
2-(2-Fluoro-[1,1'-biphenyl]-4-yl)-1-(pyridin-2-yl) propan-1-one

$^1\text{H NMR}$ (300 MHz, CDCl_3) δ 8.83 – 8.64 (m, 1H), 8.10 (d, $J = 7.9$ Hz, 1H), 7.83 (td, $J = 7.7, 1.6$ Hz, 1H), 7.59 – 7.50 (m, 2H), 7.50 – 7.33 (m, 5H), 7.27 (dd, $J = 7.7, 6.3$ Hz, 2H), 5.60 (q, $J = 7.0$ Hz, 1H), 1.64 (d, $J = 7.1$ Hz, 3H).

$^{13}\text{C NMR}$ (75 MHz, CDCl_3) δ 201.3, 161.3, 158.0, 152.6, 148.9, 142.4 (d, $J = 7.7$ Hz), 136.9, 135.6, 130.6 (d, $J = 3.9$ Hz), 128.9 (d, $J = 2.9$ Hz), 128.3, 127.5, 127.1, 124.4 (d, $J = 3.1$ Hz), 122.8, 116.3, 116.0, 44.3, 18.0.

^{19}F NMR (282 MHz, CDCl_3) δ -117.95.

HRMS (ESI, m/z) calcd for $\text{C}_{20}\text{H}_{17}\text{FNO}$ $[\text{M}+\text{H}]^+$: 306.1289, found: 306.1298.



According to the same procedure used as for the preparation of **1**, 2,4-difluorophenylacetic acid as the starting material provided **3m** as a pale yellow solid. Yield: 62% over three steps.

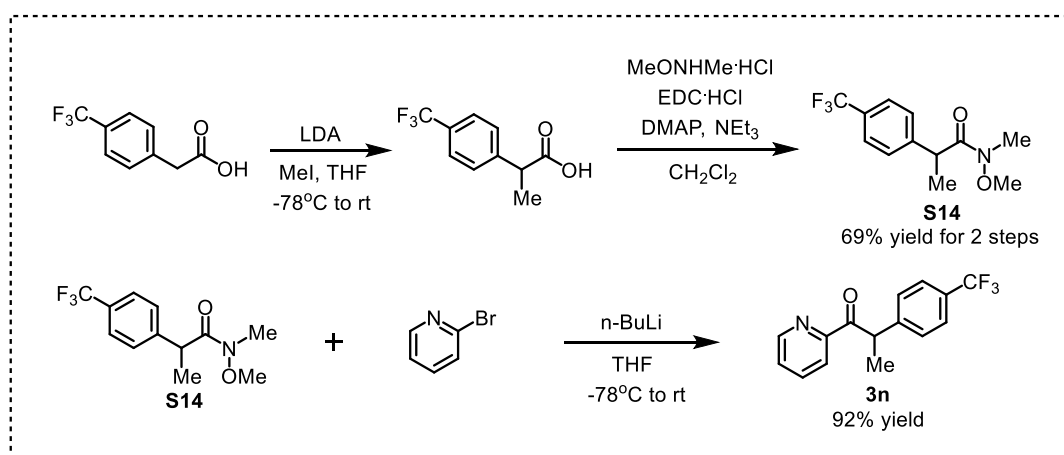
2-(2,4-Difluorophenyl)-1-(pyridin-2-yl) propan-1-one

^1H NMR (300 MHz, CDCl_3) δ 8.74 – 8.58 (m, 1H), 8.06 (d, $J = 7.9$ Hz, 1H), 7.83 (td, $J = 7.7$, 1.7 Hz, 1H), 7.44 (ddd, $J = 7.5$, 4.8, 1.1 Hz, 1H), 7.28 (td, $J = 8.2$, 4.1 Hz, 1H), 6.89 – 6.71 (m, 2H), 5.63 (q, $J = 7.1$ Hz, 1H), 1.57 (d, $J = 7.1$ Hz, 3H).

^{13}C NMR (75 MHz, CDCl_3) δ 201.2, 163.4 (d, $J = 12.3$ Hz), 162.0 (d, $J = 12.4$ Hz), 160.2 (d, $J = 12.3$ Hz), 158.7 (d, $J = 12.2$ Hz), 152.5, 149.0, 136.8, 129.9 (dd, $J = 9.6$, 5.9 Hz), 127.0, 124.8 – 123.8 (m), 122.6, 111.1 (dd, $J = 21.0$, 3.7 Hz), 104.3 – 103.0 (m), 38.2 (d, $J = 1.7$ Hz), 17.1.

^{19}F NMR (282 MHz, CDCl_3) δ -112.62 (d, $J = 7.2$ Hz), -112.95 (d, $J = 7.2$ Hz).

HRMS (ESI, m/z) calcd for $\text{C}_{14}\text{H}_{12}\text{F}_2\text{NO}$ $[\text{M}+\text{H}]^+$: 248.0881, found: 248.0889.



According to the same procedure used as for the preparation of **1**, 4-(trifluoromethyl)phenylacetic acid as the starting material provided **3n** as a white solid. Yield: 63% over three steps.

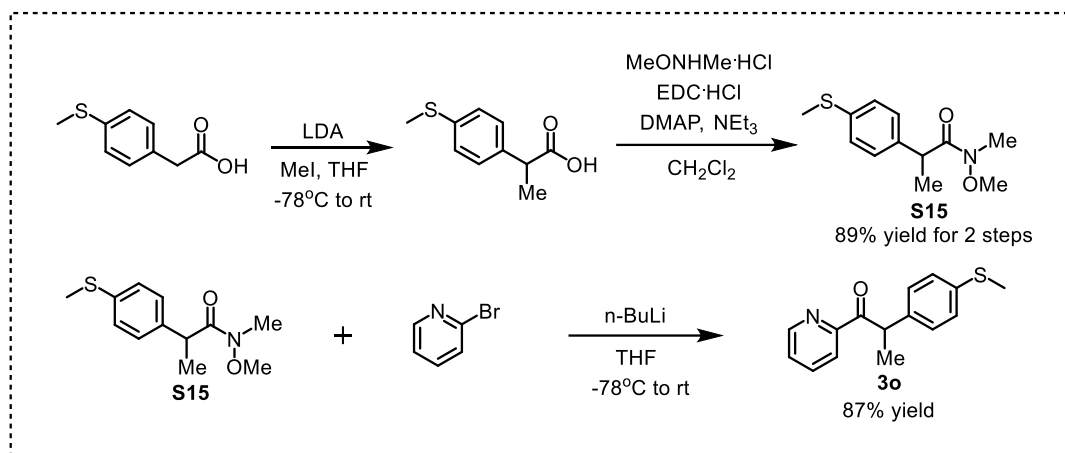
1-(Pyridin-2-yl)-2-(4-(trifluoromethyl) phenyl) propan-1-one

^1H NMR (300 MHz, CDCl_3) δ 8.71 – 8.60 (m, 1H), 8.02 (d, $J = 7.9$ Hz, 1H), 7.78 (td, $J = 7.7, 1.7$ Hz, 1H), 7.52 (s, 4H), 7.41 (ddd, $J = 7.5, 4.8, 1.1$ Hz, 1H), 5.56 (q, $J = 7.1$ Hz, 1H), 1.57 (d, $J = 7.1$ Hz, 3H).

^{13}C NMR (75 MHz, CDCl_3) δ 201.1, 152.5, 148.9, 145.1, 136.9, 128.8, 127.1, 125.4 (q, $J = 3.8$ Hz), 122.8, 44.8, 18.1.

^{19}F NMR (282 MHz, CDCl_3) δ -62.47.

HRMS (ESI, m/z) calcd for $\text{C}_{15}\text{H}_{13}\text{F}_3\text{NO}$ $[\text{M}+\text{H}]^+$: 280.0944 found: 280.0955.



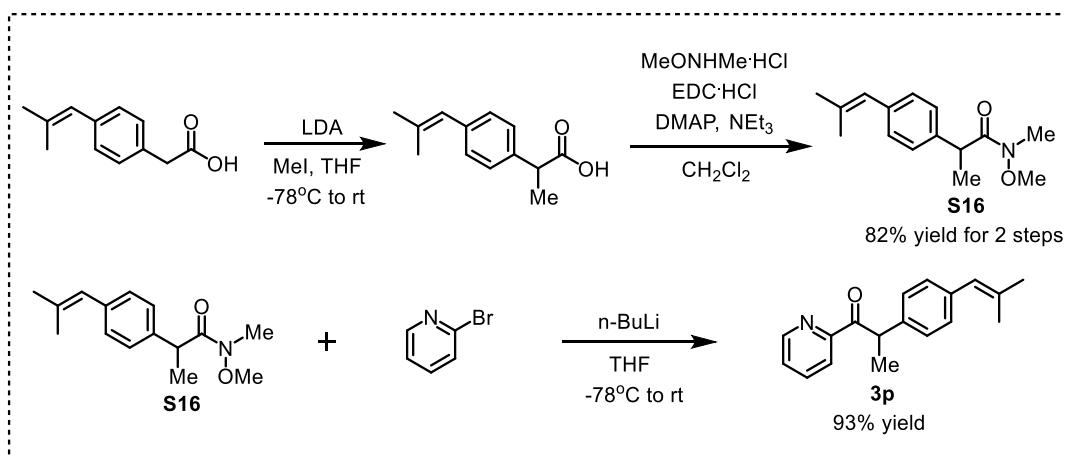
According to the same procedure used as for the preparation of **1**, 4-(methylthio)phenylacetic acid as the starting material provided **3o** as a yellow solid. Yield: 77% over three steps.

2-(4-(Methylthio)phenyl)-1-(pyridin-2-yl)propan-1-one

^1H NMR (300 MHz, CDCl_3) δ 8.65 (d, $J = 4.7$ Hz, 1H), 7.99 (d, $J = 7.9$ Hz, 1H), 7.75 (td, $J = 7.7, 1.7$ Hz, 1H), 7.43 – 7.35 (m, 1H), 7.31 (d, $J = 8.4$ Hz, 2H), 7.15 (d, $J = 8.4$ Hz, 2H), 5.44 (q, $J = 7.1$ Hz, 1H), 2.41 (s, 3H), 1.53 (d, $J = 7.1$ Hz, 3H).

^{13}C NMR (75 MHz, CDCl_3) δ 201.6, 152.9, 148.8, 137.8, 136.8, 136.5, 128.9, 126.9, 126.8, 122.7, 44.4, 18.0, 15.9.

HRMS (ESI, m/z) calcd for $\text{C}_{15}\text{H}_{15}\text{NNaOS}$ $[\text{M}+\text{Na}]^+$: 280.0767 found: 280.0777.



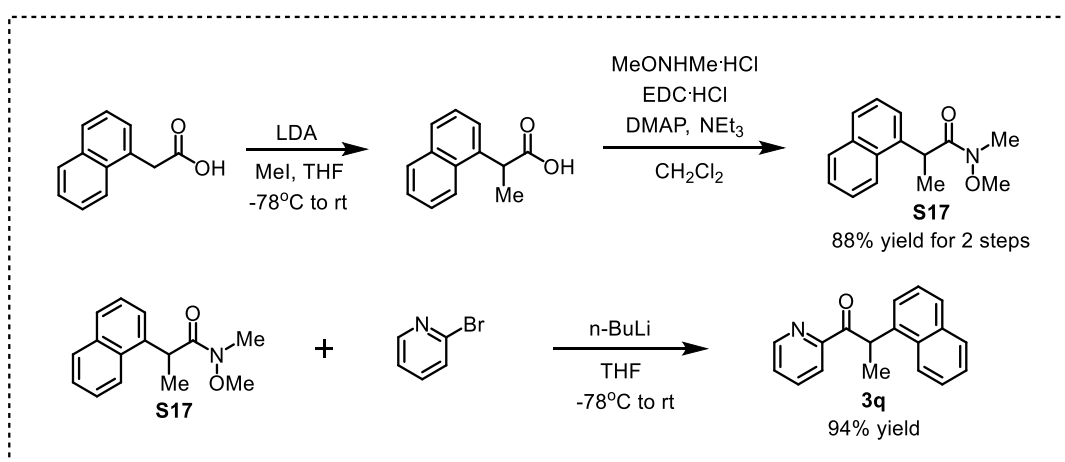
According to the same procedure used as for the preparation of **1**, 4-(2-methyl-1-propen-1-yl)phenylacetic acid as the starting material provided **3p** as a pale yellow liquid. Yield: 76% over three steps.

2-(4-(2-Methylprop-1-en-1-yl)phenyl)-1-(pyridin-2-yl)propan-1-one

$^1\text{H NMR}$ (300 MHz, CDCl_3) δ 8.66 (ddd, $J = 4.7, 1.6, 0.8$ Hz, 1H), 8.00 (d, $J = 7.8$ Hz, 1H), 7.75 (td, $J = 7.7, 1.7$ Hz, 1H), 7.38 (ddd, $J = 7.5, 4.8, 1.2$ Hz, 1H), 7.35 – 7.28 (m, 2H), 7.12 (d, $J = 8.2$ Hz, 2H), 6.18 (s, 1H), 5.47 (q, $J = 7.0$ Hz, 1H), 1.84 (dd, $J = 12.2, 1.1$ Hz, 6H), 1.56 (d, $J = 7.1$ Hz, 3H).

$^{13}\text{C NMR}$ (75 MHz, CDCl_3) δ 201.9, 153.0, 148.8, 138.2, 137.1, 136.7, 135.2, 128.8, 128.1, 126.8, 124.7, 122.8, 44.5, 26.9, 19.4, 18.1.

HRMS (ESI, m/z) calcd for $\text{C}_{18}\text{H}_{20}\text{NO}$ $[\text{M}+\text{H}]^+$: 266.1539, found: 266.1553.

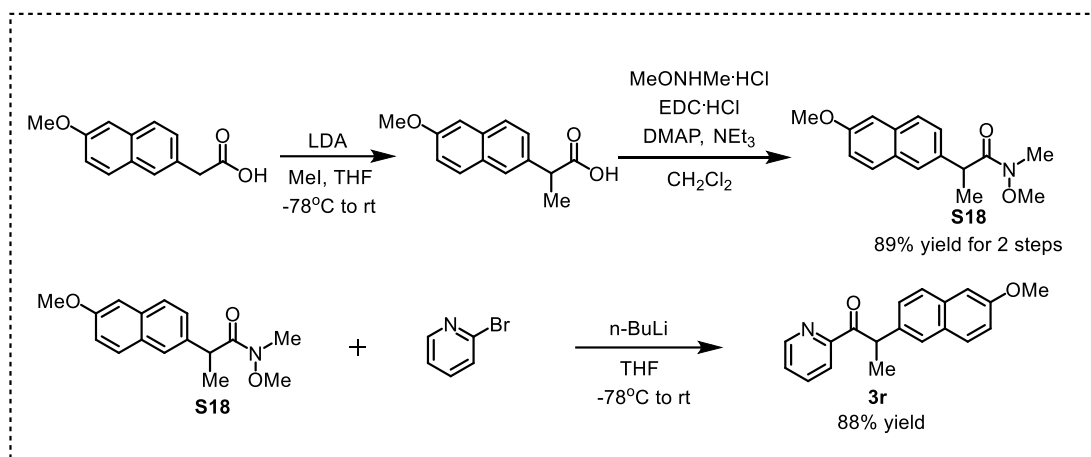


According to the same procedure used as for the preparation of **1**, 1-naphthylacetic acid as the starting material provided **3q** as a pale yellow solid. Yield: 83% over three steps.

$^1\text{H NMR}$ (300 MHz, CDCl_3) δ 8.55 (ddd, $J = 4.7, 1.6, 0.9$ Hz, 1H), 8.39 (d, $J = 8.5$ Hz, 1H), 8.11 – 7.98 (m, 1H), 7.84 (dd, $J = 7.8, 1.0$ Hz, 1H), 7.79 – 7.67 (m, 2H), 7.62 – 7.44 (m, 2H), 7.43 – 7.36 (m, 2H), 7.32 (ddd, $J = 7.6, 4.8, 1.2$ Hz, 1H), 6.26 (q, $J = 7.0$ Hz, 1H), 1.69 (d, $J = 7.0$ Hz, 3H).

$^{13}\text{C NMR}$ (75 MHz, CDCl_3) δ 202.6, 153.0, 148.9, 137.7, 136.7, 134.1, 131.4, 128.8, 127.3, 126.8, 126.0, 125.5, 124.9, 123.8, 122.5, 40.7, 17.9.

HRMS (ESI, m/z) calcd for $\text{C}_{18}\text{H}_{16}\text{NO}$ $[\text{M}+\text{H}]^+$: 262.1226, found: 262.1231.



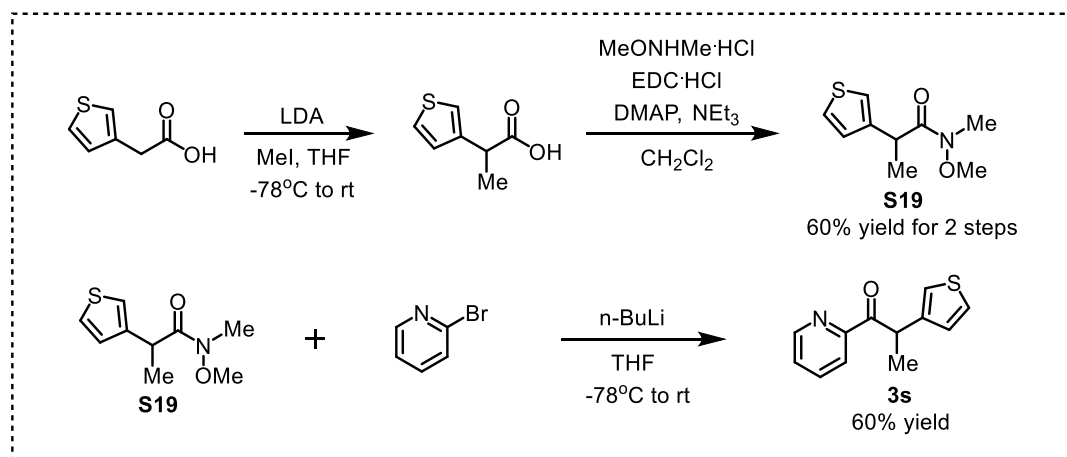
According to the same procedure used as for the preparation of **1**, 6-methoxy-2-naphthylacetic acid as the starting material provided **3r** as a white solid. Yield: 83% over three steps.

2-(6-Methoxynaphthalen-2-yl)-1-(pyridin-2-yl)propan-1-one

¹H NMR (300 MHz, CDCl₃) δ 8.65 (d, *J* = 4.3 Hz, 1H), 8.02 (d, *J* = 7.9 Hz, 1H), 7.80 – 7.60 (m, 4H), 7.53 (dd, *J* = 8.5, 1.6 Hz, 1H), 7.34 (ddd, *J* = 7.5, 4.8, 1.1 Hz, 1H), 7.17 – 6.98 (m, 2H), 5.62 (q, *J* = 7.0 Hz, 1H), 3.87 (s, 3H), 1.65 (d, *J* = 7.1 Hz, 3H).

¹³C NMR (75 MHz, CDCl₃) δ 201.8, 157.5, 153.0, 148.7, 136.7, 136.1, 133.4, 129.2, 129.0, 127.3, 126.9, 126.85, 126.8, 122.7, 118.7, 105.5, 55.2, 44.9, 18.2.

HRMS (ESI, *m/z*) calcd for C₁₉H₁₈NO₂ [M+H]⁺: 292.1332, found: 292.1337.



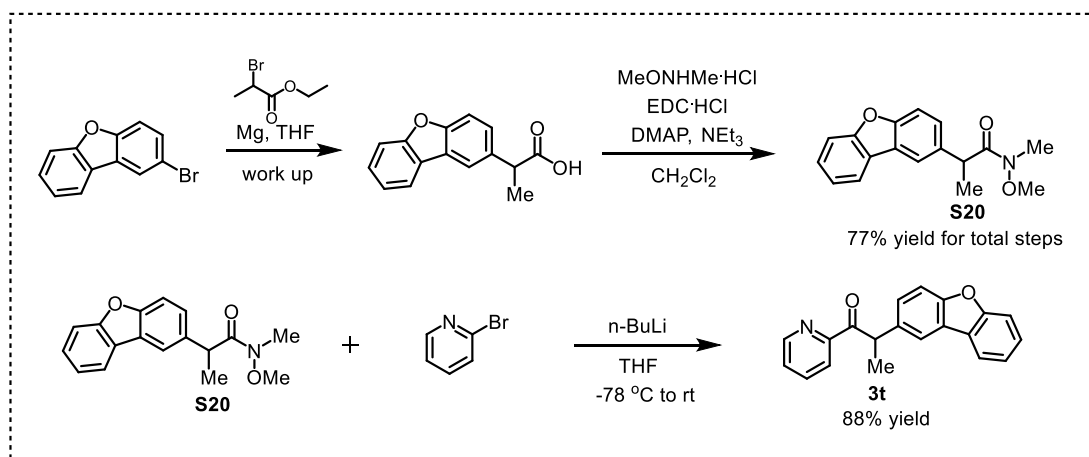
According to the same procedure used as for the preparation of **1**, 3-thiopheneacetic acid as the starting material provided **3s** as a colorless liquid. Yield: 36% over three steps.

1-(Pyridin-2-yl)-2-(thiophen-3-yl)propan-1-one

¹H NMR (300 MHz, CDCl₃) δ 8.75 – 8.59 (m, 1H), 8.02 (d, *J* = 7.8 Hz, 1H), 7.78 (td, *J* = 7.7, 1.7 Hz, 1H), 7.49 – 7.35 (m, 1H), 7.25 – 6.99 (m, 3H), 5.63 (q, *J* = 6.7 Hz, 1H), 1.56 (d, *J* = 7.1 Hz, 3H).

¹³C NMR (75 MHz, CDCl₃) δ 201.3, 152.8, 148.8, 141.0, 136.8, 127.7, 126.9, 125.2, 122.8, 121.8, 40.2, 17.8.

HRMS (ESI, *m/z*) calcd for C₁₂H₁₁NNaOS [M+Na]⁺: 240.0454, found: 240.0461.



First step: To a flask charged with THF (0.2M) and purged with argon was added magnesium turnings (1.5 eq) and iodine (a few grains). To this solution was added 2-bromodibenzofuran (1.0 eq) in THF, and the mixture was gently heated with a heat gun until the solution color changed from brown to colorless. Then, the reaction was allowed to reflux for 1 h. The reaction was then allowed to cool, and ethyl 2-bromopropionate (2.0 eq) was added. Following 5 h of reflux, the reaction was quenched with 1 M HCl, then extracted with EtOAc for three times, washed with brine, dried with Na_2SO_4 , and concentrated under reduced pressure. The crude mixture was suspended in a 3 M KOH solution in MeOH, kept at reflux for 2 h, cooled, and then quenched with water. The reaction mixture was extracted with EtOAc for three times. The aqueous layer was then acidified with 1 M HCl, extracted with EtOAc for three times. After drying with anhydrous Na_2SO_4 , the solution was filtered and concentrated under reduced pressure. The obtained product was dried under vacuum to give the crude product which was directly used for the next step without further purification. The procedure was adapted and modified from a previous report.²

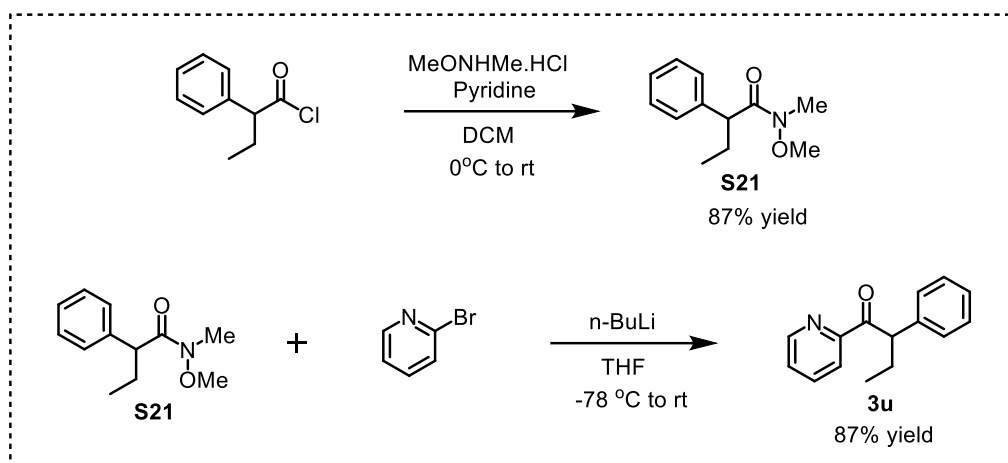
The next steps were performed according to the same procedure used as for the preparation of **1** to provide **3t** as a pale yellow solid. Yield: 68% for total steps.

2-(Dibenzo[b,d]furan-2-yl)-1-(pyridin-2-yl)propan-1-one

$^1\text{H NMR}$ (300 MHz, CDCl_3) δ 8.75 – 8.59 (m, 1H), 8.03 (d, $J = 7.9$ Hz, 1H), 7.97 (d, $J = 1.6$ Hz, 1H), 7.93 (d, $J = 7.6$ Hz, 1H), 7.75 (td, $J = 7.8, 1.5$ Hz, 1H), 7.29-7.53 (m, 6H), 5.66 (q, $J = 7.1$ Hz, 1H), 1.66 (d, $J = 7.1$ Hz, 3H).

$^{13}\text{C NMR}$ (75 MHz, CDCl_3) δ 201.9, 156.5, 155.1, 152.9, 148.8, 136.8, 135.5, 127.8, 127.0, 126.9, 124.4, 124.2, 122.8, 122.6, 120.7, 120.3, 111.6, 111.5, 44.8, 18.7.

HRMS (ESI, m/z) calcd for $\text{C}_{20}\text{H}_{15}\text{NNaO}_2$ [$\text{M}+\text{Na}$] $^+$: 324.0995, found: 324.1004.



First step: To a stirred solution of pyridine (2.0 eq) and *N,O*-dimethylhydroxylamine hydrochloride (1.3 eq) in anhydrous CH_2Cl_2 (0.5 M) at 0°C was added dropwise 2-phenylbutyryl chloride (1.0 eq) dissolved in THF (0.2 M). The reaction mixture was stirred overnight at rt. H_2O was added and the mixture was extracted with CH_2Cl_2 . The organic layer was washed with 1 N HCl (3×10 mL), aqueous saturated NaHCO_3 (3×10 mL), and brine (20 mL). The combined organic layers were dried over anhydrous Na_2SO_4 , filtered, and concentrated under reduced pressure. The crude mixture was purified by flash chromatography on silica gel (*n*-hexane/EtOAc = 30:1 to 3:1) to give the pure Weinreb amide **S21**. Yield: 87%. The procedure was adapted and modified from a previous report.³

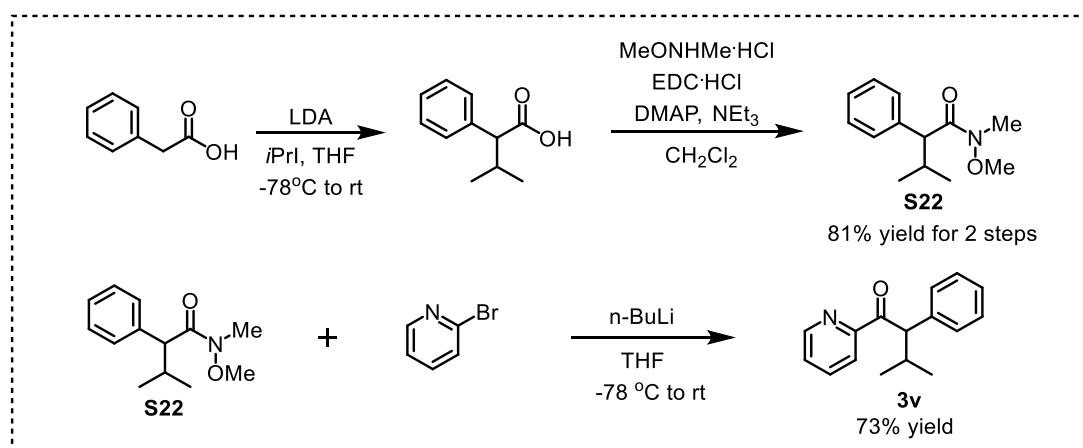
Second step: In analogy to the third step in the synthesis of compound **1** to provide **3u** as a pale yellow solid. Yield: 76% for total steps.

2-Phenyl-1-(pyridin-2-yl)butan-1-one

$^1\text{H NMR}$ (300 MHz, CDCl_3) δ 8.66 (ddd, $J = 4.7, 1.6, 0.8$ Hz, 1H), 8.08 – 7.92 (m, 1H), 7.73 (td, $J = 7.7, 1.7$ Hz, 1H), 7.48 – 7.33 (m, 3H), 7.26 (t, $J = 7.4$ Hz, 2H), 7.21 – 7.12 (m, 1H), 5.32 (t, $J = 7.6$ Hz, 1H), 2.33 – 2.11 (m, 1H), 2.04 – 1.83 (m, 1H), 0.93 (t, $J = 7.4$ Hz, 3H).

$^{13}\text{C NMR}$ (75 MHz, CDCl_3) δ 201.5, 153.2, 148.7, 139.2, 136.7, 128.9, 128.4, 126.8, 126.6, 122.6, 52.4, 26.1, 12.2.

HRMS (ESI, m/z) calcd for $\text{C}_{15}\text{H}_{16}\text{NO}$ [$\text{M}+\text{H}$] $^+$: 226.1226, found: 226.1230.



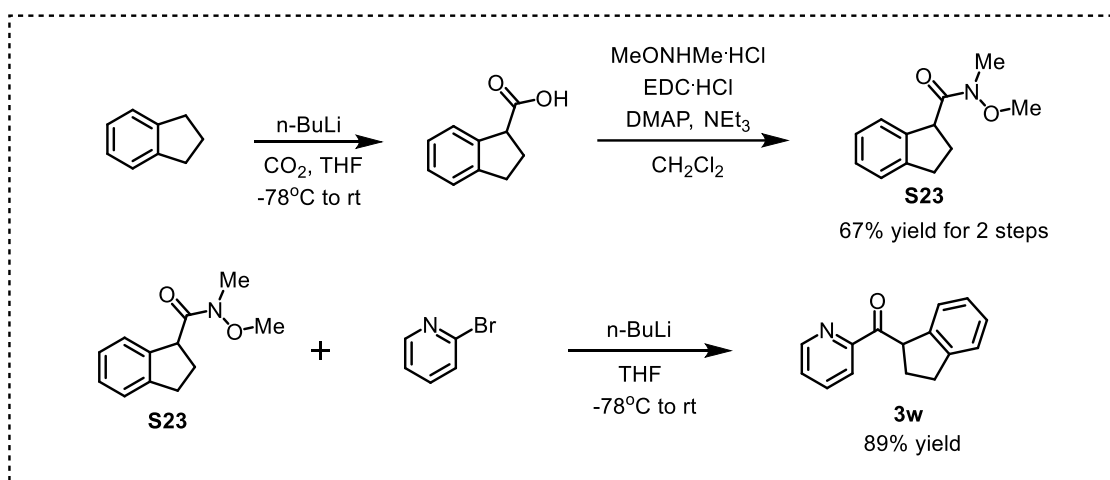
According to the similar procedure used as for the preparation of **1**, Phenylacetic acid and 2-iodopropane as the starting materials provided **3v** as a white solid. Yield: 59% over three steps.

3-Methyl-2-phenyl-1-(pyridin-2-yl)butan-1-one

¹H NMR (300 MHz, CDCl₃) δ 8.74 – 8.59 (m, 1H), 8.00 (d, *J* = 7.9 Hz, 1H), 7.72 (t, *J* = 7.7 Hz, 1H), 7.47 – 7.39 (m, 2H), 7.39 – 7.32 (m, 1H), 7.29 – 7.20 (m, 2H), 7.19 – 7.11 (m, 1H), 5.16 (d, *J* = 10.8 Hz, 1H), 2.63 (ddt, *J* = 13.2, 10.9, 6.6 Hz, 1H), 1.02 (d, *J* = 6.5 Hz, 3H), 0.80 (d, *J* = 6.7 Hz, 3H).

¹³C NMR (75 MHz, CDCl₃) δ 201.9, 153.4, 148.7, 138.6, 136.7, 129.4, 128.3, 126.8, 126.7, 122.5, 58.0, 31.3, 21.7, 20.5.

HRMS (ESI, *m/z*) calcd for C₁₆H₁₈NO [M+H]⁺: 240.1383, found: 240.1388.



First step: A flame dried Schlenk flask under nitrogen atmosphere was charged with indane via syringe, and *n*-BuLi (1.6 M in hexane, 1.1 eq) was added dropwise over 10 minutes. The solution was then placed in a dry ice/acetone bath and solid CO₂ (dry ice, small amount) was added carefully. The solution was stirred at -78 °C for 1 h. The reaction was then quenched with aqueous saturated NaHCO₃. The aqueous layer was isolated and ice cold EtOAc was added. Conc. HCl was then added until pH of 2 (pH paper). The organic layer was separated and reduced on a rotary evaporator to yield the crude product which was directly used for the next step without further purification. The procedure was adapted and modified from a previous report.⁴

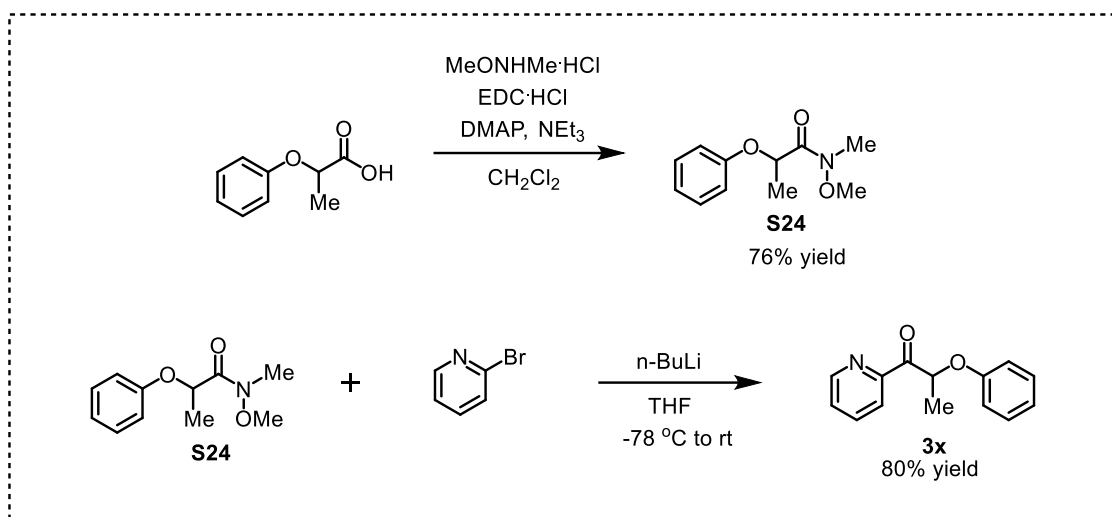
The next steps according to the same procedure used as for the preparation of **1**, to provide **3w** as a pale yellow solid. Yield: 60% for total steps.

(2,3-Dihydro-1H-inden-1-yl)(pyridin-2-yl)methanone

¹H NMR (300 MHz, CDCl₃) δ 8.92 – 8.74 (m, 1H), 8.22 – 8.05 (m, 1H), 7.88 (td, *J* = 7.7, 1.7 Hz, 1H), 7.66 – 7.46 (m, 1H), 7.31 (d, *J* = 7.3 Hz, 1H), 7.26 – 7.16 (m, 2H), 7.16 – 7.07 (m, 1H), 5.75 (dd, *J* = 7.7, 6.3 Hz, 1H), 3.25 (dt, *J* = 15.5, 7.7 Hz, 1H), 3.13 – 2.95 (m, 1H), 2.65 – 2.38 (m, 2H).

¹³C NMR (75 MHz, CDCl₃) δ 201.3, 153.4, 149.0, 144.8, 141.7, 136.9, 127.0, 126.99, 126.1, 125.4, 124.7, 122.8, 51.1, 32.1, 29.0.

HRMS (ESI, *m/z*) calcd for C₁₅H₁₄NO [M+H]⁺: 224.1070, found: 224.1078.



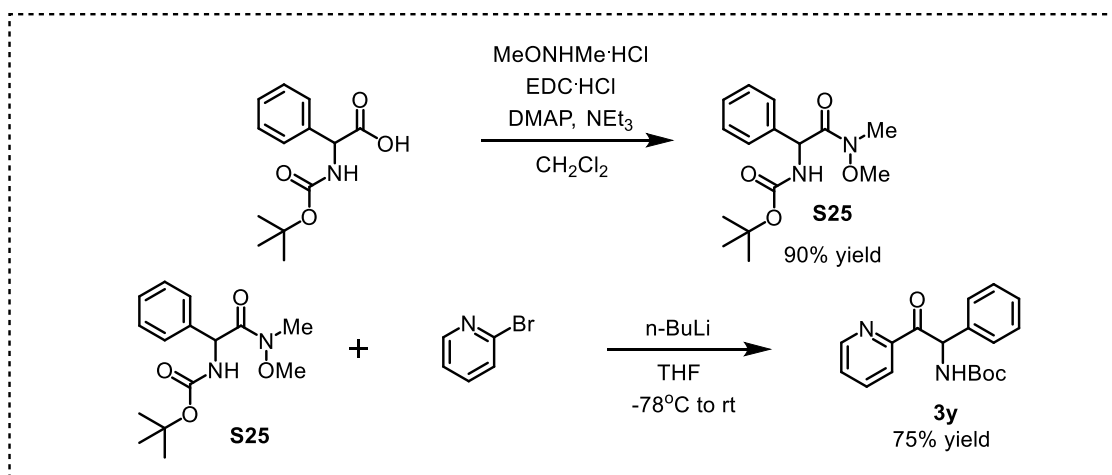
According to the similar procedure used as for the preparation of **1**, 2-phenoxypropionic acid as the starting material provided **3x** as a white solid. Yield: 61% for two steps.

2-Phenoxy-1-(pyridin-2-yl)propan-1-one

$^1\text{H NMR}$ (300 MHz, CDCl_3) δ 8.79 – 8.64 (m, 1H), 8.07 (d, $J = 7.8$ Hz, 1H), 7.87 (td, $J = 7.7, 1.7$ Hz, 1H), 7.52 (ddd, $J = 7.5, 4.8, 1.2$ Hz, 1H), 7.26 – 7.13 (m, 2H), 6.99 – 6.82 (m, 3H), 6.34 (q, $J = 6.8$ Hz, 1H), 1.68 (d, $J = 6.8$ Hz, 3H).

$^{13}\text{C NMR}$ (75 MHz, CDCl_3) δ 199.4, 157.6, 151.8, 149.1, 137.1, 129.4, 127.7, 122.7, 121.0, 115.2, 73.8, 18.3.

HRMS (ESI, m/z) calcd for $\text{C}_{14}\text{H}_{14}\text{NO}_2$ [$\text{M}+\text{H}$] $^+$: 228.1019, found: 228.1025.



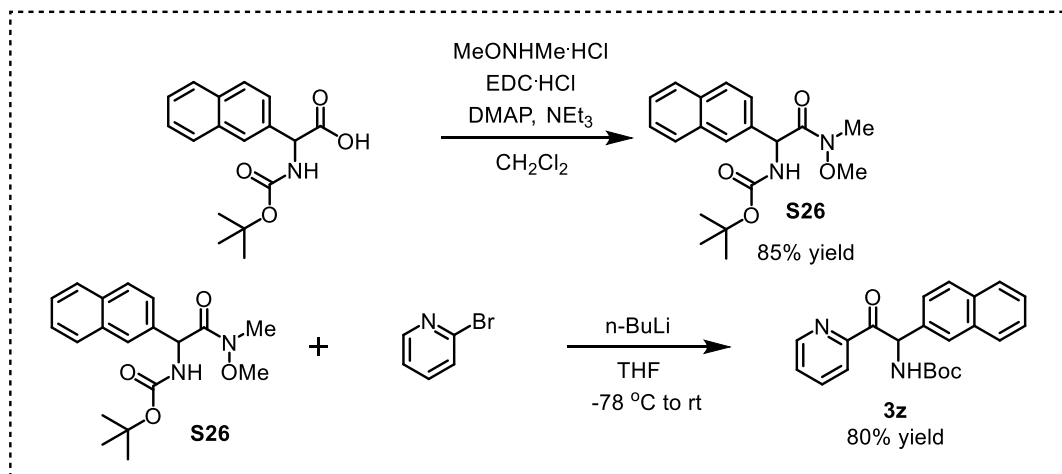
According to the similar procedure used as for the preparation of **1**, *tert*-butoxycarbonylamino-phenylacetic acid as the starting material provided **3y** as a white solid. Yield: 61% for two steps.

tert-Butyl (2-oxo-1-phenyl-2-(pyridin-2-yl)ethyl)carbamate

$^1\text{H NMR}$ (300 MHz, CDCl_3) δ 8.64 (d, $J = 4.5$ Hz, 1H), 7.99 (d, $J = 7.8$ Hz, 1H), 7.74 (t, $J = 7.7$ Hz, 1H), 7.46 (d, $J = 7.0$ Hz, 2H), 7.41 – 7.33 (m, 1H), 7.31 – 7.14 (m, 3H), 6.94 (t, $J = 16.3$ Hz, 1H), 5.97 (d, $J = 6.7$ Hz, 1H), 1.43 (s, 9H).

^{13}C NMR (75 MHz, CDCl_3) δ 197.1, 154.9, 151.4, 148.9, 137.2, 136.7, 128.6, 128.4, 127.8, 127.4, 123.1, 79.7, 58.6, 28.3.

HRMS (ESI, m/z) calcd for $\text{C}_{18}\text{H}_{21}\text{N}_2\text{O}_3$ $[\text{M}+\text{H}]^+$: 313.1547, found: 313.1558.



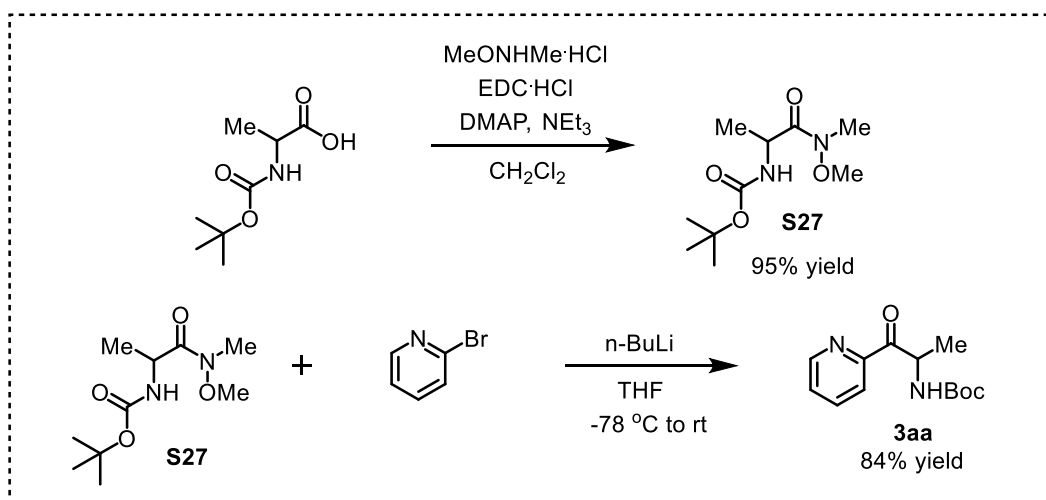
According to the similar procedure used as for the preparation of **1**, 2-((*tert*-butoxycarbonyl)amino)-2-(naphthalen-2-yl)acetic acid as the starting material provided **3z** as a pale yellow solid. Yield: 68% for two steps.

tert-Butyl (1-(naphthalen-2-yl)-2-oxo-2-(pyridin-2-yl)ethyl)carbamate

^1H NMR (300 MHz, CDCl_3) δ 8.65 (d, $J = 4.3$ Hz, 1H), 8.01 (d, $J = 7.8$ Hz, 1H), 7.90 (s, 1H), 7.82 – 7.68 (m, 4H), 7.62 (d, $J = 7.7$ Hz, 1H), 7.47 – 7.31 (m, 3H), 7.07 (d, $J = 7.5$ Hz, 1H), 6.08 (d, $J = 7.0$ Hz, 1H), 1.44 (s, 9H).

^{13}C NMR (75 MHz, CDCl_3) δ 197.0, 154.9, 151.4, 149.0, 136.8, 134.7, 133.3, 132.9, 128.4, 128.0, 127.6, 127.6, 127.4, 126.2, 126.1, 126.0, 123.1, 79.8, 58.8, 28.4.

HRMS (ESI, m/z) calcd for $\text{C}_{22}\text{H}_{23}\text{N}_2\text{O}_3$ $[\text{M}+\text{H}]^+$: 363.1703, found: 363.1716.



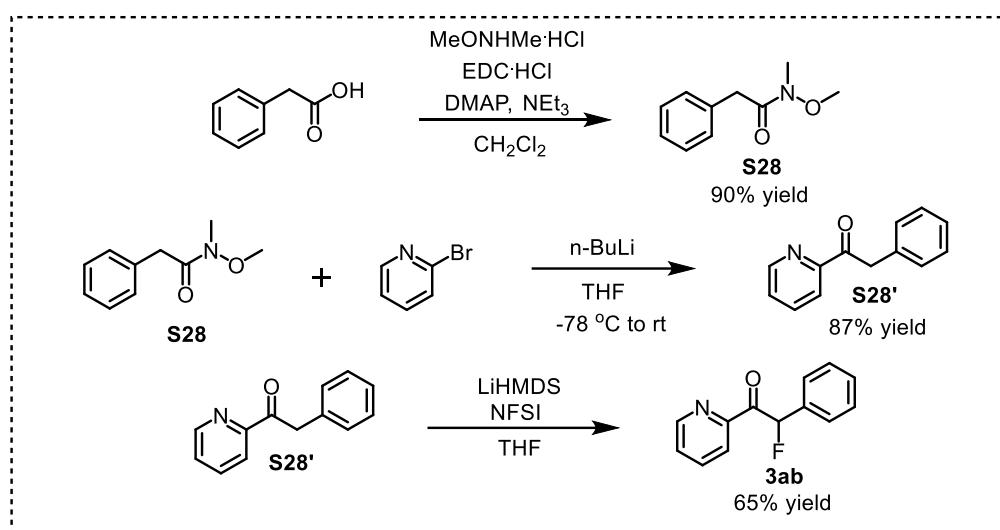
According to the similar procedure used as for the preparation of **1**, 2-(*tert*-butoxycarbonylamino)propanoic acid as the starting material provided **3aa** as a pale yellow solid. Yield: 80% for two steps.

***tert*-Butyl (1-oxo-1-(pyridin-2-yl)propan-2-yl)carbamate**

¹H NMR (300 MHz, CDCl₃) δ 8.77 – 8.61 (m, 1H), 8.05 (d, *J* = 7.8 Hz, 1H), 7.84 (td, *J* = 7.7, 1.6 Hz, 1H), 7.47 (ddd, *J* = 7.5, 4.8, 1.0 Hz, 1H), 5.70 (d, *J* = 6.5 Hz, 1H), 5.44 (s, 1H), 1.45 (m, 12H).

¹³C NMR (75 MHz, CDCl₃) δ 200.6, 155.1, 151.4, 149.1, 136.9, 127.4, 122.8, 79.5, 51.3, 28.4, 19.3.

HRMS (ESI, *m/z*) calcd for C₁₃H₁₉N₂O₃ [M+H]⁺: 251.1390, found: 251.1396.



According to the similar procedure used as for the preparation of **1**, phenyl acetic acid as the starting material provided **S28'** as a white solid. Yield: 78% for two steps.

To a solution of 2-phenyl-1-(pyridin-2-yl)ethanone (prepared similarly to substrate **1**, 1.0 eq) in anhydrous THF (0.2M) was added LiHMDS (1.5 eq, 1.0 M solution in THF) dropwise at -78 °C under nitrogen atmosphere. After stirring for 1 h, N-fluorobenzenesulfonimide (NFSI) (1.2 eq) in anhydrous THF was added dropwise under nitrogen atmosphere. The reaction mixture was stirred at -78 °C to rt overnight under nitrogen atmosphere. The reaction mixture was quenched with saturated aqueous NH₄Cl and extracted with EtOAc for three times. The organic layer thus obtained was dried over anhydrous Na₂SO₄ and filtered. The filtrate was concentrated in vacuo and purified by silica gel column chromatography to provide **3ab** as a white solid. Yield: 65%.

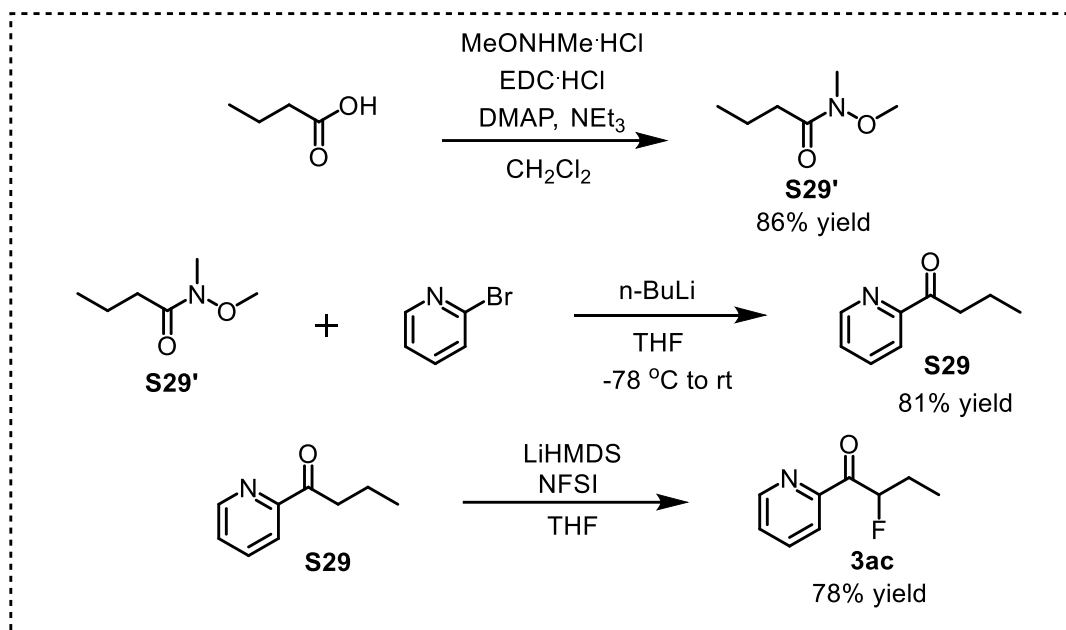
2-Fluoro-2-phenyl-1-(pyridin-2-yl)ethan-1-one

¹H NMR (300 MHz, CDCl₃) δ 8.65 (d, *J* = 4.7 Hz, 1H), 8.05 (d, *J* = 7.7 Hz, 1H), 7.80 (dd, *J* = 10.8, 4.7 Hz, 1H), 7.68 – 7.56 (m, 2H), 7.50 – 7.23 (m, 5H).

¹³C NMR (75 MHz, CDCl₃) δ 194.3 (d, *J* = 20.9 Hz), 151.1, 148.8, 137.0, 134.2 (d, *J* = 20.3 Hz), 129.2 (d, *J* = 2.5 Hz), 128.5, 128.0 (d, *J* = 5.4 Hz), 127.7, 122.9 (d, *J* = 1.8 Hz), 92.0 (d, *J* = 180.3 Hz).

¹⁹F NMR (282 MHz, CDCl₃) δ -183.48.

HRMS (ESI, *m/z*) calcd for C₁₃H₁₀FNNaO [M+Na]⁺: 251.0639, found: 251.0645.



According to the same procedure used as for the preparation of **28**, butyric acid as the starting material provided **3ac** as a colorless liquid. Yield: 54% over three steps.

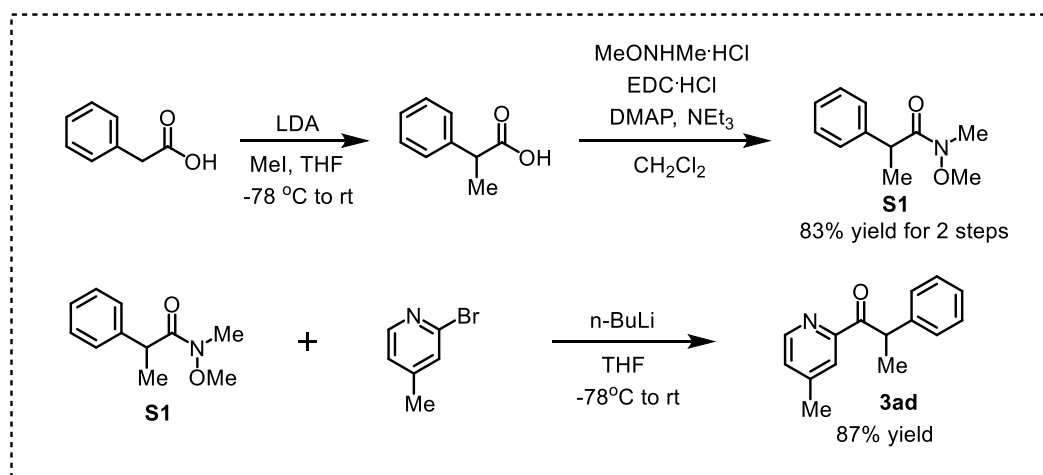
2-Fluoro-1-(pyridin-2-yl)butan-1-one

$^1\text{H NMR}$ (300 MHz, CDCl_3) δ 8.64 (d, $J = 4.5$ Hz, 1H), 8.06 (d, $J = 7.8$ Hz, 1H), 7.86 (td, $J = 7.7$, 1.6 Hz, 1H), 7.49 (ddd, $J = 7.5$, 4.8, 1.1 Hz, 1H), 6.17 (ddd, $J = 50.4$, 7.5, 3.7 Hz, 1H), 2.05-2.27 (m, 1H), 1.82-2.03 (m, 1H), 1.05 (t, $J = 7.4$ Hz, 3H).

$^{13}\text{C NMR}$ (75 MHz, CDCl_3) δ 196.8 (d, $J = 17.2$ Hz), 151.4, 149.0, 137.1, 127.7, 122.5 (d, $J = 1.9$ Hz), 93.3 (d, $J = 179.9$ Hz), 25.9 (d, $J = 21.5$ Hz), 9.0 (d, $J = 3.5$ Hz).

$^{19}\text{F NMR}$ (282 MHz, CDCl_3) δ -200.35.

HRMS (ESI, m/z) calcd for $\text{C}_9\text{H}_{10}\text{FNNaO}$ [$\text{M}+\text{Na}$] $^+$: 190.0639, found: 190.0642.



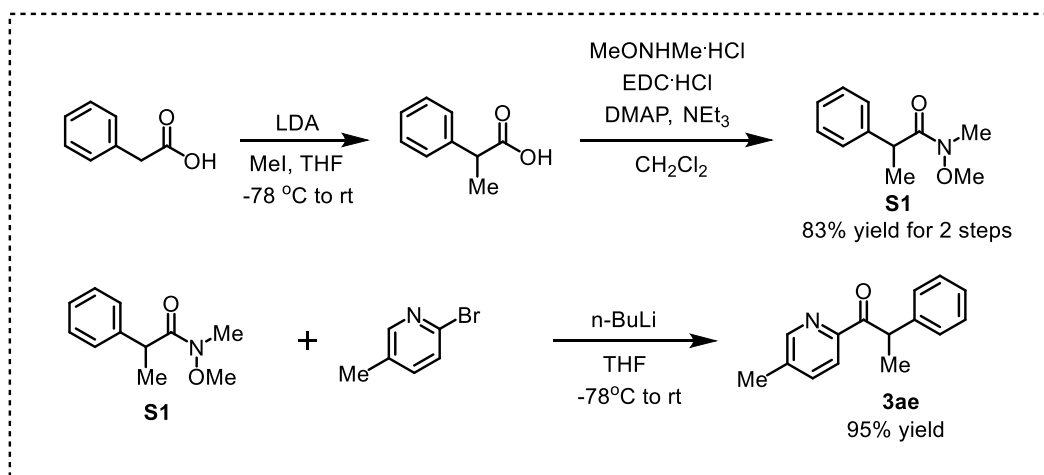
According to the similar procedure used as for the preparation of **1**, compound **3ad** was provided as a pale yellow solid. Yield: 72% for two steps.

1-(4-Methylpyridin-2-yl)-2-phenylpropan-1-one

$^1\text{H NMR}$ (300 MHz, CDCl_3) δ 8.54 (d, $J = 4.9$ Hz, 1H), 7.92 – 7.81 (m, 1H), 7.49 – 7.37 (m, 2H), 7.33 – 7.25 (m, 2H), 7.25 – 7.15 (m, 2H), 5.53 (q, $J = 7.1$ Hz, 1H), 2.39 (s, 3H), 1.59 (d, $J = 7.1$ Hz, 3H).

$^{13}\text{C NMR}$ (75 MHz, CDCl_3) δ 202.1, 152.9, 148.6, 148.0, 141.0, 128.4, 127.7, 126.6, 123.5, 44.93, 20.9, 18.1.

HRMS (ESI, m/z) calcd for $\text{C}_{15}\text{H}_{16}\text{NO}$ $[\text{M}+\text{H}]^+$: 226.1226, found: 226.1231.



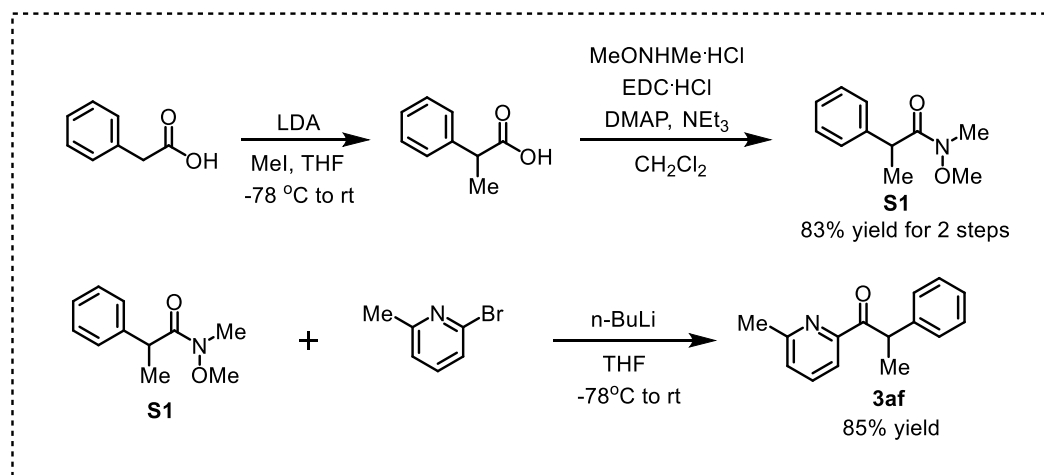
According to the similar procedure used as for the preparation of **1**, compound **3ae** was provided as a white solid. Yield: 79% for two steps.

1-(5-Methylpyridin-2-yl)-2-phenylpropan-1-one

$^1\text{H NMR}$ (300 MHz, CDCl_3) δ 8.51 (dd, $J = 1.4, 0.6$ Hz, 1H), 7.95 (d, $J = 8.0$ Hz, 1H), 7.58 (dd, $J = 8.0, 1.5$ Hz, 1H), 7.43 (dd, $J = 8.1, 0.9$ Hz, 2H), 7.35 – 7.25 (m, 2H), 7.24 – 7.13 (m, 1H), 5.51 (q, $J = 7.1$ Hz, 1H), 2.39 (s, 3H), 1.59 (d, $J = 7.1$ Hz, 3H).

$^{13}\text{C NMR}$ (75 MHz, CDCl_3) δ 201.6, 150.7, 149.3, 141.1, 137.2, 137.1, 128.4, 126.5, 122.4, 44.81, 18.6, 18.2.

HRMS (ESI, m/z) calcd for $\text{C}_{14}\text{H}_{13}\text{NO}$ $[\text{M}+\text{Na}]^+$: 277.0953, found: 277.0949.



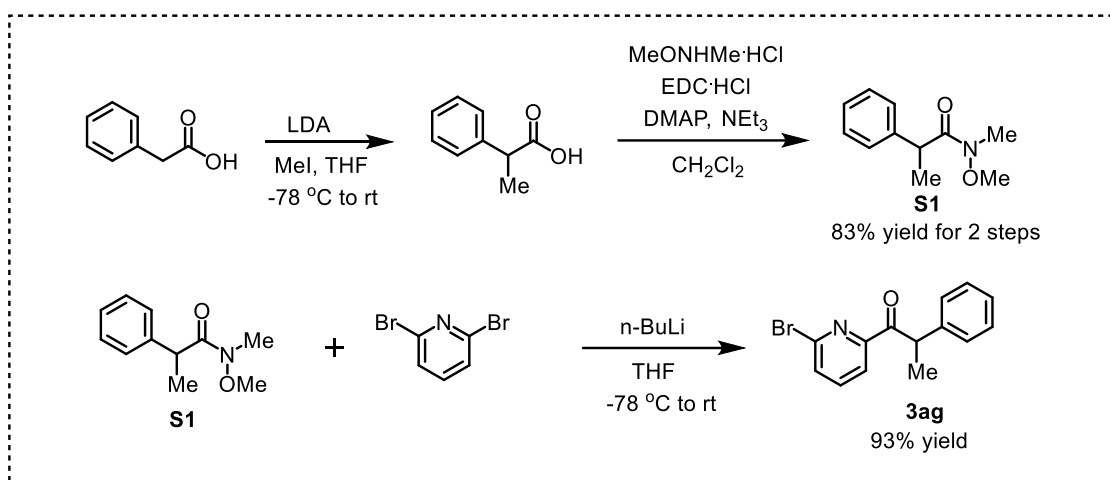
According to the similar procedure used as for the preparation of **1**, compound **3af** was provided as a pale yellow solid. Yield: 71% for two steps.

1-(6-Methylpyridin-2-yl)-2-phenylpropan-1-one

$^1\text{H NMR}$ (300 MHz, CDCl_3) δ 7.83 (d, $J = 7.7$ Hz, 1H), 7.65 (t, $J = 7.7$ Hz, 1H), 7.49 – 7.38 (m, 2H), 7.29 (td, $J = 7.1, 3.3$ Hz, 3H), 7.20 (ddd, $J = 7.3, 3.7, 1.3$ Hz, 1H), 5.56 (q, $J = 7.1$ Hz, 1H), 2.64 (s, 3H), 1.59 (d, $J = 7.1$ Hz, 3H).

$^{13}\text{C NMR}$ (75 MHz, CDCl_3) δ 202.0, 157.6, 152.3, 141.2, 136.8, 128.5, 128.4, 126.5, 126.4, 119.7, 44.8, 24.4, 18.0.

HRMS (ESI, m/z) calcd for $\text{C}_{15}\text{H}_{16}\text{NO}$ $[\text{M}+\text{H}]^+$: 226.1226, found: 226.1232.



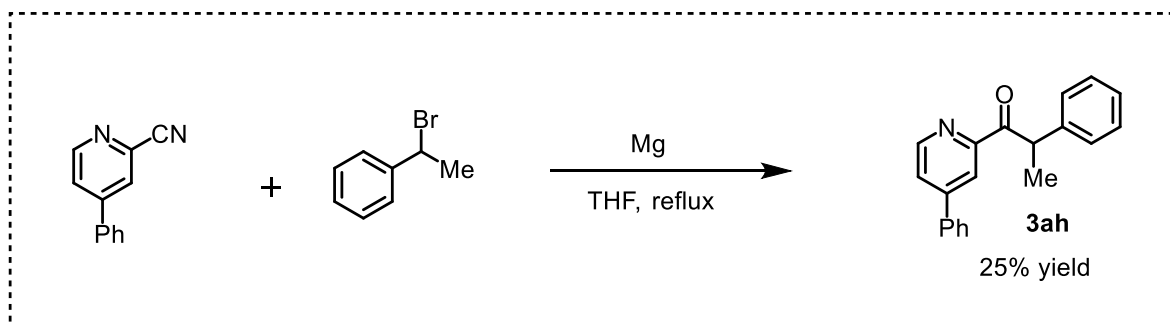
To a solution of 2,6-dibromopyridine (1.2 eq) in THF at -78 °C was added $n\text{-BuLi}$ (1.0 eq) dropwise under a nitrogen atmosphere. The reaction was stirred at -78 °C for 1 h. The corresponding Weinreb amide **S1** (1.0 eq in THF) was added dropwise to the flask after the reaction was cooled back down to -78 °C. The reaction was allowed to warm to room temperature slowly and stirred overnight. The reaction was quenched with a saturated aqueous NH_4Cl solution at room temperature and extracted with EtOAc. The organic layer was washed with brine. After dried with anhydrous Na_2SO_4 , filtration and concentration under reduced pressure, the crude residue was purified by flash chromatography on silica gel ($n\text{-hexane}/\text{EtOAc} = 100:1$ to $30:1$) to afford the substrate **3ag** as a white solid. Yield: 93%.

1-(6-Bromopyridin-2-yl)-2-phenylpropan-1-one

$^1\text{H NMR}$ (300 MHz, CDCl_3) δ 7.93 (dd, $J = 7.0, 1.5$ Hz, 1H), 7.65 – 7.51 (m, 2H), 7.43 – 7.35 (m, 2H), 7.32 – 7.24 (m, 2H), 7.22 – 7.11 (m, 1H), 5.36 (q, $J = 7.0$ Hz, 1H), 1.55 (d, $J = 7.0$ Hz, 3H).

$^{13}\text{C NMR}$ (75 MHz, CDCl_3) δ 199.9, 153.4, 141.0, 140.3, 139.1, 131.5, 128.6, 128.5, 126.8, 121.5, 45.3, 17.8.

HRMS (ESI, m/z) calcd for $\text{C}_{14}\text{H}_{12}\text{BrNNaO}$ $[\text{M}+\text{Na}]^+$: 311.9994, found: 312.0007



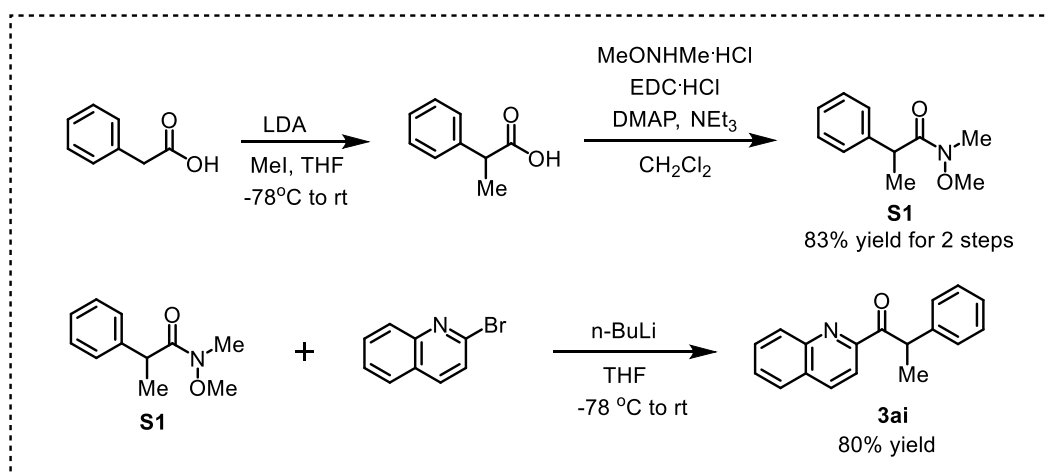
To a flask charged with THF (0.2M) and purged with argon were added magnesium turnings (4.5 eq) and iodine (a few grains). To this solution was added 1-brom-1-phenylethane (3.0 eq) in THF, and the mixture was gently heated with a heat gun until the solution color changed from brown to colorless, then the reaction was allowed to reflux. After the formation of the Grignard reagent, the solution was cooled to room temperature, and added into the solution of a solution of 2-cyano-4-phenylpyridine (1.0 eq) in THF at 0 °C dropwise. When the TLC control indicated a full conversion of the starting material, the reaction was quenched by addition of a solution of saturated NH_4Cl . The organic layer was separated and extracted twice with CH_2Cl_2 . After evaporation, the organic layer was redissolved in Et_2O (40.0 mL) and 6 M HCl (5.0 mL) was added. After 30 min, the organic layer was separated, and the aqueous layer was basified with saturated NaHCO_3 and then extracted three times with CH_2Cl_2 . The combined organic layers were dried over Na_2SO_4 and evaporated in vacuo. The residue was purified by column chromatography with *n*-hexane and ethyl acetate to afford the substrate **3ah** as a white solid. Yield: 25%. The procedure was adapted and modified from a previous report.⁵

2-Phenyl-1-(4-phenylpyridin-2-yl)propan-1-one

$^1\text{H NMR}$ (300 MHz, CDCl_3) δ 8.73 (dd, $J = 5.1, 0.4$ Hz, 1H), 8.29 (d, $J = 1.2$ Hz, 1H), 7.66 (ddd, $J = 7.2, 4.5, 1.9$ Hz, 3H), 7.56 – 7.40 (m, 5H), 7.36 – 7.27 (m, 2H), 7.25 – 7.16 (m, 1H), 5.58 (q, $J = 7.1$ Hz, 1H), 1.63 (d, $J = 7.1$ Hz, 3H).

$^{13}\text{C NMR}$ (75 MHz, CDCl_3) δ 201.9, 153.5, 149.3, 140.9, 137.5, 129.4, 129.2, 128.5, 127.0, 126.7, 124.6, 120.6, 45.1, 18.2.

HRMS (ESI, m/z) calcd for $\text{C}_{20}\text{H}_{18}\text{NO}$ $[\text{M}+\text{H}]^+$: 288.1383, found: 288.1388.



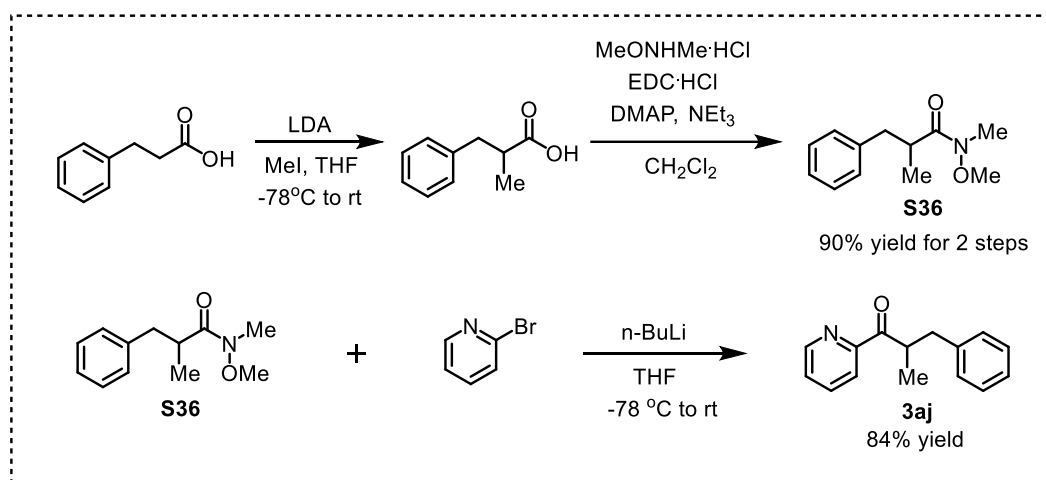
According to the similar procedure used as for the preparation of **1**, compound **3ai** was provided as a pale yellow solid. Yield: 66% for two steps.

2-Phenyl-1-(quinolin-2-yl)propan-1-one

$^1\text{H NMR}$ (300 MHz, CDCl_3) δ 8.21 (dd, $J = 13.6, 8.6$ Hz, 2H), 8.09 (d, $J = 8.5$ Hz, 1H), 7.77 (dt, $J = 8.4, 4.8$ Hz, 2H), 7.61 (t, $J = 7.5$ Hz, 1H), 7.50 (d, $J = 7.7$ Hz, 2H), 7.27 (t, $J = 7.5$ Hz, 2H), 7.21 – 7.10 (m, 1H), 5.79 (q, $J = 7.1$ Hz, 1H), 1.65 (d, $J = 7.1$ Hz, 3H).

$^{13}\text{C NMR}$ (75 MHz, CDCl_3) δ 202.0, 152.4, 147.0, 141.1, 136.8, 130.6, 129.8, 129.4, 128.5, 128.4, 127.5, 126.6, 118.9, 44.8, 18.0.

HRMS (ESI, m/z) calcd for $\text{C}_{18}\text{H}_{16}\text{NO}$ $[\text{M}+\text{H}]^+$: 262.1226, found: 262.1230.



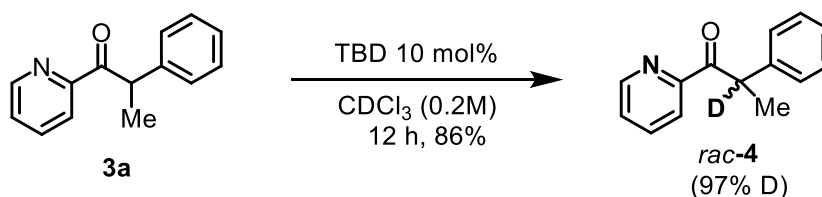
According to the similar procedure used as for the preparation of **1**, compound **3aj** was provided as a pale yellow liquid. Yield: 76% over three steps.

2-Methyl-3-phenyl-1-(pyridin-2-yl)propan-1-one

$^1\text{H NMR}$ (300 MHz, CDCl_3) δ 8.72 (ddd, $J = 4.7, 1.6, 0.9$ Hz, 1H), 8.13 – 8.02 (m, 1H), 7.84 (td, $J = 7.7, 1.7$ Hz, 1H), 7.47 (ddd, $J = 7.5, 4.8, 1.2$ Hz, 1H), 7.28 (d, $J = 4.4$ Hz, 4H), 7.24 – 7.14 (m, 1H), 4.58 – 4.37 (m, 1H), 3.23 (dd, $J = 13.6, 6.2$ Hz, 1H), 2.71 (dd, $J = 13.6, 8.2$ Hz, 1H), 1.22 (d, $J = 7.0$ Hz, 3H).

$^{13}\text{C NMR}$ (75 MHz, CDCl_3) δ 204.7, 152.9, 148.9, 140.1, 136.8, 129.2, 128.2, 126.9, 126.0, 122.4, 41.1, 38.9, 16.5.

HRMS (ESI, m/z) calcd for $\text{C}_{15}\text{H}_{15}\text{NNaO}$ $[\text{M}+\text{Na}]^+$: 248.1046, found: 248.1053.



To a solution of 10 mol % of TBD (1,5,7-Triazabicyclo[4.4.0]dec-5-en) in CDCl_3 (0.2M), was added compound **1** (1.0 eq). The reaction mixture was stirred at room temperature for 12 h, then the

mixture was diluted with CH_2Cl_2 . The combined organic solutions were concentrated under reduced pressure and purified by flash chromatography on silica gel (*n*-hexane/ EtOAc=5:1) to afford the pure *rac*-4 as a white solid. Yield: 86%. The procedure was adapted and modified from a previous report.⁶

$^1\text{H NMR}$ (300 MHz, CDCl_3) δ 8.66 (ddd, $J = 4.7, 1.6, 0.9$ Hz, 1H), 8.13 – 7.87 (m, 1H), 7.75 (td, $J = 7.7, 1.7$ Hz, 1H), 7.46 – 7.33 (m, 3H), 7.32 – 7.22 (m, 2H), 7.21 – 7.13 (m, 1H), 5.49 (q, $J = 7.1$ Hz, 0.03H), 1.56 (s, 3H).

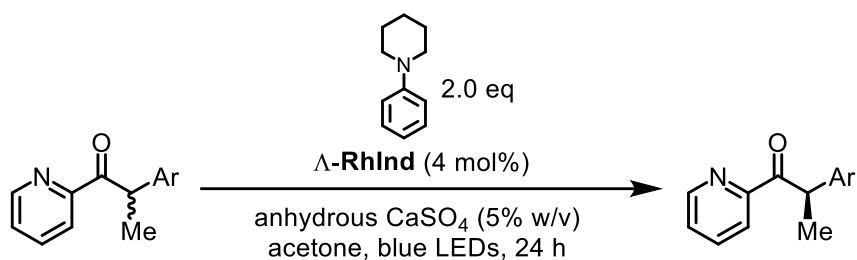
$^{13}\text{C NMR}$ (75 MHz, CDCl_3) δ 201.9, 153.0, 148.8, 140.8, 136.8, 128.5, 128.4, 126.8, 126.6, 122.72, 18.01.

HRMS (ESI, m/z) calcd for $\text{C}_{14}\text{H}_{13}\text{DNO}$ $[\text{M}+\text{H}]^+$: 213.1133, found: 213.1133.

4.3.2 General Procedure

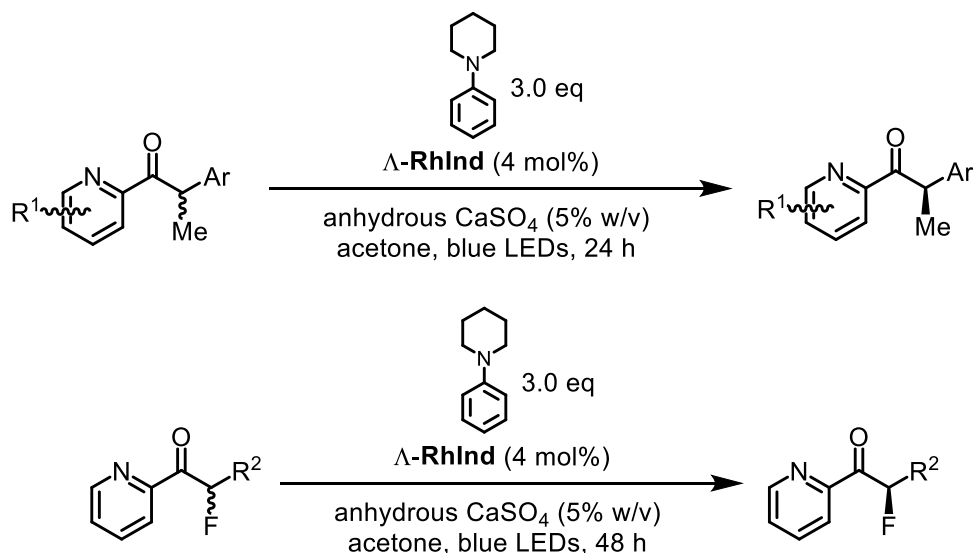
Depending on the racemic substrate, the reactions were performed with some slight modifications, especially with respect to the employed base. The methods A-G reflect these variations.

Method A:



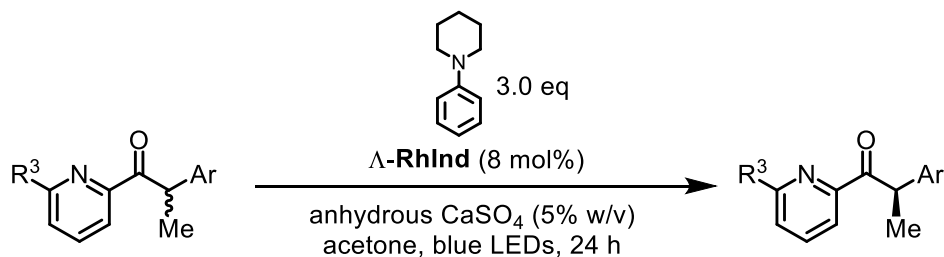
An oven-dried 10 mL Schlenk tube was charged with racemic substrate (1.0 equiv), $\Delta\text{-RhInd}$ (4.0 mol%), N-phenylpiperidine (2.0 equiv) and anhydrous CaSO_4 (5% m/v). Then, acetone (max. 0.01% water, purchased from AppliChem GmbH) (0.1 M) was added via syringe. The reaction mixture was degassed via freeze-pump-thaw for three cycles. Subsequent, the vial was sealed and placed approximately 10 cm away from the 24 W blue LEDs. After stirring for 24 hours, the mixture was diluted with CH_2Cl_2 . The combined organic solutions were concentrated, reduced pressure and purified by flash chromatography on silica gel (*n*-hexane/ EtOAc) to afford the pure non-racemic product. The enantiomeric excess was determined by HPLC analysis on a chiral stationary phase.

Method B:



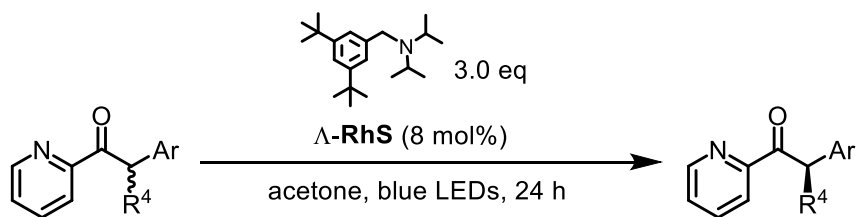
An oven-dried 10 mL Schlenk tube was charged with racemic substrate (1.0 equiv), Δ -RhInd (4.0 mol%), N-phenylpiperidine (3.0 equiv) and anhydrous CaSO₄ (5% m/v). Then, acetone (max. 0.01% water, purchased from AppliChem GmbH) (0.1 M) was added via syringe. The reaction mixture was degassed via freeze-pump-thaw for three cycles. Subsequent, the vial was sealed and placed approximately 10 cm away from the 24 W blue LEDs. After stirring for 24 hours, the mixture was diluted with CH₂Cl₂. The combined organic solutions were concentrated under reduced pressure and purified by flash chromatography on silica gel (*n*-hexane/ EtOAc) to afford the pure non-racemic product. The enantiomeric excess was determined by HPLC analysis on a chiral stationary phase.

Method C:



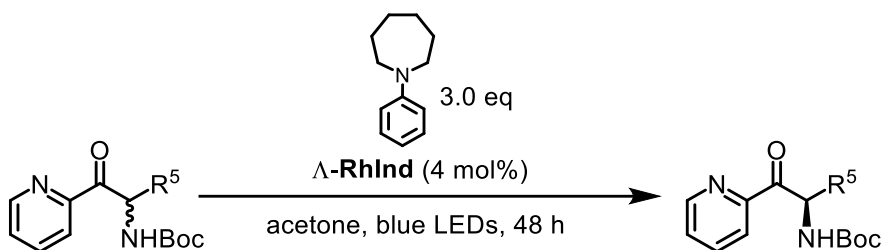
An oven-dried 10 mL Schlenk tube was charged with racemic substrate (1.0 equiv), Δ -RhInd (8.0 mol%), N-phenylpiperidine (3.0 equiv) and anhydrous CaSO₄ (5% m/v). Then, acetone (max. 0.01% water, purchased from AppliChem GmbH) (2.0 mL) was added via syringe. The reaction mixture was degassed via freeze-pump-thaw for three cycles. Subsequent, the vial was sealed and placed approximately 10 cm away from the 24 W blue LEDs. After stirring for 24 hours, CH₂Cl₂ (10 mL) and silica gel (4 g) were added to the reaction mixture. The solvent was removed in vacuo to absorb the crude reaction mixture onto the silica gel and the silica-gel-absorbed crude product was added to a silica gel column. Flash chromatography (*n*-hexane) afforded the analytically pure non-racemic product. The enantiomeric excess was determined by HPLC analysis on a chiral stationary phase.

Method D:



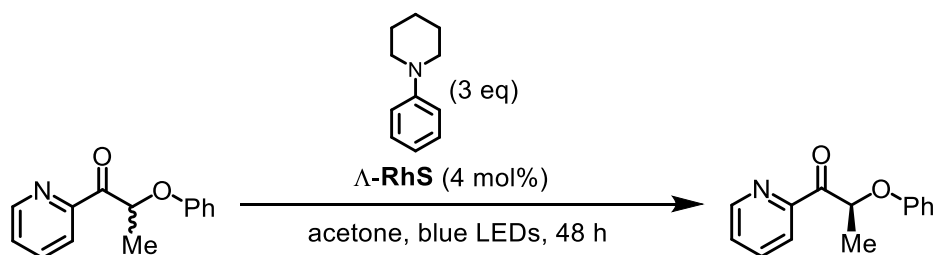
An oven-dried 10 mL Schlenk tube was charged with racemic substrate (1.0 equiv), $\Delta\text{-RhS}$ (8.0 mol%), and *N,N*-diisopropyl-3,5-di-*tert*-butylbenzenemethanamine (3.0 equiv). Then, acetone (max. 0.01% water, purchased from AppliChem GmbH) (2.0 mL, 0.1 M) was added via syringe. The reaction mixture was degassed via freeze-pump-thaw for three cycles. Subsequent, the vial was sealed and placed approximately 10 cm away from the 24 W blue LEDs. After stirring for 24 hours, the mixture was diluted with CH_2Cl_2 . The combined organic solutions were concentrated under reduced pressure and the mixture purified by flash chromatography on silica gel (*n*-hexane/EtOAc) to afford the analytically pure non-racemic product. The enantiomeric excess was determined by HPLC analysis on a chiral stationary phase.

Method E:



An oven-dried 10 mL Schlenk tube was charged with racemic substrate (1.0 equiv), $\Delta\text{-RhInd}$ (4.0 mol%), and *N*-phenylazepane (3.0 equiv). Then, acetone (max. 0.01% water, purchased from AppliChem GmbH) (2.0 mL) was added via syringe. The reaction mixture was degassed via freeze-pump-thaw for three cycles. Subsequent, the vial was sealed and placed approximately 10 cm away from the 24 W blue LEDs. After stirring for 48 hours, the mixture was diluted with CH_2Cl_2 . The combined organic solutions were concentrated under reduced pressure and the mixture was purified by flash chromatography on silica gel (*n*-hexane/EtOAc) to afford the analytically pure non-racemic product. The enantiomeric excess was determined by HPLC analysis on a chiral stationary phase.

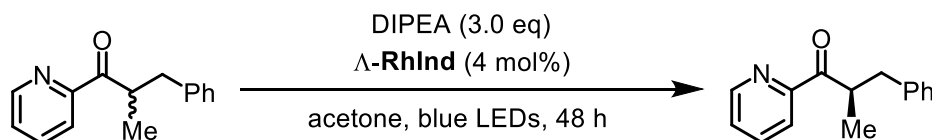
Method F:



An oven-dried 10 mL Schlenk tube was charged with racemic substrate (1.0 equiv), $\Delta\text{-RhS}$ (4.0 mol%), and *N*-phenylpiperidine (3.0 equiv). Then, acetone (max. 0.01% water, purchased from

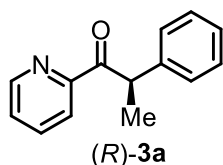
AppliChem GmbH) (2.0 mL) was added via syringe. The reaction mixture was degassed via freeze-pump-thaw for three cycles. Subsequent, the vial was sealed and placed approximately 10 cm away from the 24 W blue LEDs. After stirring for 48 hours, the mixture was diluted with CH₂Cl₂. The combined organic solutions were concentrated under reduced pressure and the mixture was purified by flash chromatography on silica gel (*n*-hexane/EtOAc) to afford the analytically pure product as a single diastereomer. The enantiomeric excess was determined by HPLC analysis on a chiral stationary phase.

Method G:

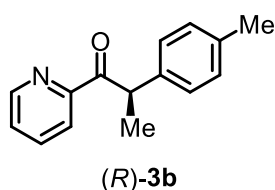


An oven-dried 10 mL Schlenk tube was charged with racemic substrate (1.0 equiv), Δ -RhInd (4.0 mol%) and DIPEA (3.0 equiv). Then, acetone (max. 0.01% water, purchased from AppliChem GmbH) (2.0 mL) was added via syringe. The reaction mixture was degassed via freeze-pump-thaw for three cycles. Subsequent, the vial was sealed and placed approximately 10 cm away from the 24 W blue LEDs. After stirring for 24 hours, the mixture was diluted with CH₂Cl₂. The combined organic solutions were concentrated under reduced pressure and the mixture was purified by flash chromatography on silica gel (*n*-hexane/EtOAc) to afford the analytically pure non-racemic product. The enantiomeric excess was determined by HPLC analysis on a chiral stationary phase.

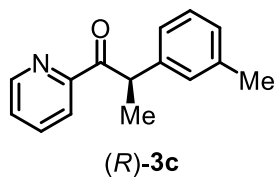
4.3.3 Experimental and Characterization Data of the Products



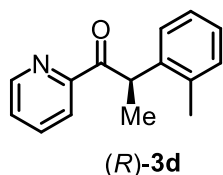
According to the **Method A**, the reaction of racemic **3a** (42.3 mg, 0.2 mmol), Δ -RhInd (6.6 mg, 4.0 mol%), *N*-phenylpiperidine (64.5 mg, 2.0 eq) and anhydrous CaSO₄ (100 mg, 5% m/v) in anhydrous acetone (2.0 mL) was stirred under nitrogen atmosphere for 24 hours with 24 W blue LEDs at room temperature, affording 41.2 mg (97% yield, white solid) of (*R*)-**3a**. Enantiomeric excess was established by HPLC analysis using a Chiralpak OD-H column, ee = 96% (HPLC: 254 nm, *n*-hexane/isopropanol = 95:5, flow rate 1 mL/min, 25 °C, *t_r* (major) = 5.9 min, *t_r* (minor) = 5.3 min). [α]_D²⁵ = -50.9° (*c* 1.0, CH₂Cl₂).



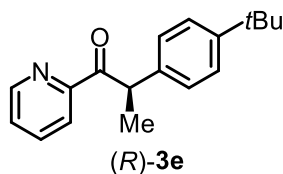
According to the **Method A**, the reaction of racemic **3b** (45.0 mg, 0.2 mmol), Λ -**RhInd** (6.6 mg, 4.0 mol%), N-phenylpiperidine (64.5 mg, 2.0 eq) and anhydrous CaSO₄ (100 mg, 5% m/v) in anhydrous acetone (2.0 mL) was stirred under nitrogen atmosphere for 24 hours with 24 W blue LEDs at room temperature, affording 42.4 mg (94% yield, white solid) of (*R*)-**3b**. Enantiomeric excess was established by HPLC analysis using a Chiralpak OD-H column, ee = 96% (HPLC: 254 nm, *n*-hexane/isopropanol = 99:1, flow rate 1 mL/min, 25 °C, t_r (major) = 6.9 min, t_r (minor) = 6.3 min). $[\alpha]_D^{25} = -54.3^\circ$ (*c* 1.0, CH₂Cl₂).



According to the **Method A**, the reaction of racemic **3c** (45.0 mg, 0.2 mmol), Λ -**RhInd** (6.6 mg, 4.0 mol%), N-phenylpiperidine (64.5 mg, 2.0 eq) and anhydrous CaSO₄ (100 mg, 5% m/v) in anhydrous acetone (2.0 mL) was stirred under nitrogen atmosphere for 24 hours with 24 W blue LEDs at room temperature, affording 43.5 mg (97% yield, white solid) of (*R*)-**3c**. Enantiomeric excess was established by HPLC analysis using a Chiralpak OD-H column, ee = 94% (HPLC: 254 nm, *n*-hexane/isopropanol = 99:1, flow rate 1 mL/min, 25 °C, t_r (major) = 6.9 min, t_r (minor) = 6.3 min). $[\alpha]_D^{25} = -48.7^\circ$ (*c* 1.0, CH₂Cl₂).

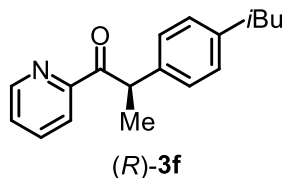


According to the **Method A**, the reaction of racemic **3d** (45.0 mg, 0.2 mmol), Λ -**RhInd** (6.6 mg, 4.0 mol%), N-phenylpiperidine (64.5 mg, 2.0 eq) and anhydrous CaSO₄ (100 mg, 5% m/v) in anhydrous acetone (2.0 mL) was stirred under nitrogen atmosphere for 24 hours with 24 W blue LEDs at room temperature, affording 44.3 mg (98% yield, white solid) of (*R*)-**3d**. Enantiomeric excess was established by HPLC analysis using a Chiralpak OD-H column, ee = 92% (HPLC: 254 nm, *n*-hexane/isopropanol = 98:2, flow rate 1 mL/min, 25 °C, t_r (major) = 7.0 min, t_r (minor) = 6.0 min). $[\alpha]_D^{25} = -176.4^\circ$ (*c* 1.0, CH₂Cl₂).

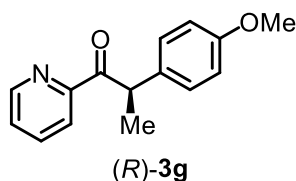


According to the **Method B**, the reaction of racemic **3e** (53.5 mg, 0.2 mmol), Λ -**RhInd** (6.6 mg, 4.0 mol%), N-phenylpiperidine (96.8 mg, 3.0 eq) and anhydrous CaSO₄ (100 mg, 5% m/v) in anhydrous

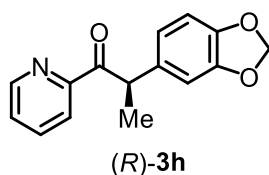
acetone (2.0 mL) was stirred under nitrogen atmosphere for 24 hours with 24 W blue LEDs at room temperature, affording 48.2 mg (90% yield, white solid) of (*R*)-**3e**. Enantiomeric excess was established by HPLC analysis using a Chiralpak IG column, ee = 92% (HPLC: 254 nm, *n*-hexane/isopropanol = 99.5:0.5, flow rate 1 mL/min, 25 °C, t_r (major) = 7.6 min, t_r (minor) = 7.2 min). $[\alpha]_D^{25} = -8.4^\circ$ (*c* 1.0, CH₂Cl₂).



According to the **Method A**, the reaction of racemic **3f** (53.5 mg, 0.2 mmol), Λ -**RhInd** (6.6 mg, 4.0 mol%), *N*-phenylpiperidine (64.5 mg, 2.0 eq) and anhydrous CaSO₄ (100 mg, 5% m/v) in anhydrous acetone (2.0 mL) was stirred under nitrogen atmosphere for 24 hours with 24 W blue LEDs at room temperature, affording 49.7 mg (93% yield, white solid) of (*R*)-**3f**. Enantiomeric excess was established by HPLC analysis using a Chiralpak OD-H column, ee = 93% (HPLC: 254 nm, *n*-hexane/isopropanol = 99:1, flow rate 1 mL/min, 25 °C, t_r (major) = 5.7 min, t_r (minor) = 5.3 min). $[\alpha]_D^{25} = -28.0^\circ$ (*c* 1.0, CH₂Cl₂).

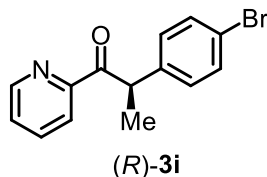


According to the **Method B**, the reaction of racemic **3g** (48.3 mg, 0.2 mmol), Λ -**RhInd** (6.6 mg, 4.0 mol%), *N*-Phenylpiperidine (96.8 mg, 3.0 eq) and anhydrous CaSO₄ (100 mg, 5% m/v) in anhydrous acetone (2.0 mL, 0.1 M) was stirred under nitrogen atmosphere for 24 hours with 24 W blue LEDs at room temperature, affording 45.5 mg (94% yield, colorless liquid) of (*R*)-**3g**. Enantiomeric excess was established by HPLC analysis using a Chiralpak IG column, ee = 95% (HPLC: 254 nm, *n*-hexane/isopropanol = 97:3, flow rate 1 mL/min, 25 °C, t_r (major) = 14.9 min, t_r (minor) = 14.1 min). $[\alpha]_D^{25} = -45.2^\circ$ (*c* 1.0, CH₂Cl₂).

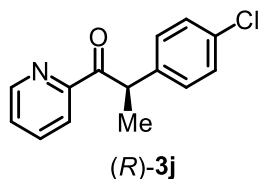


According to the **Method A**, the reaction of racemic **3h** (51.0 mg, 0.2 mmol), Λ -**RhInd** (6.6 mg, 4.0 mol%), *N*-phenylpiperidine (64.5 mg, 2.0 eq) and anhydrous CaSO₄ (100 mg, 5% m/v) in anhydrous acetone (2.0 mL, 0.1 M) was stirred under nitrogen atmosphere for 24 hours with 24 W blue LEDs at

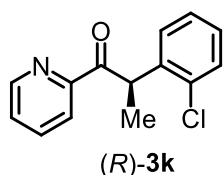
room temperature, affording 48.5 mg (95% yield, white solid) of (*R*)-**3h**. Enantiomeric excess was established by HPLC analysis using a Chiralpak OD-H column, ee = 96% (HPLC: 254 nm, *n*-hexane/isopropanol = 95:5, flow rate 1 mL/min, 25 °C, t_r (major) = 7.5 min, t_r (minor) = 11.3 min). $[\alpha]_D^{25} = -34.8^\circ$ (*c* 1.0, CH₂Cl₂).



According to the **Method A**, the reaction of racemic **3i** (58.0 mg, 0.2 mmol), Λ -**RhInd** (6.6 mg, 4.0 mol%), *N*-Phenylpiperidine (64.5 mg, 2.0 eq) and anhydrous CaSO₄ (100 mg, 5% m/v) in anhydrous acetone (2.0 mL) was stirred under nitrogen atmosphere for 24 hours with 24 W blue LEDs at room temperature, affording 54.3 mg (94% yield, white solid) of (*R*)-**3i**. Enantiomeric excess was established by HPLC analysis using a Chiralpak OD-H column, ee = 96% (HPLC: 254 nm, *n*-hexane/isopropanol = 99:1, flow rate 1 mL/min, 25 °C, t_r (major) = 6.6 min, t_r (minor) = 6.1 min). $[\alpha]_D^{25} = -22.4^\circ$ (*c* 1.0, CH₂Cl₂).

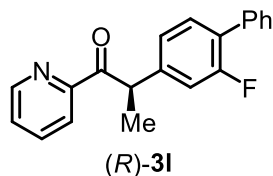


According to the **Method B**, the reaction of racemic **3j** (49.1 mg, 0.2 mmol), Λ -**RhInd** (6.6 mg, 4.0 mol%), *N*-phenylpiperidine (96.8 mg, 3.0 eq) and anhydrous CaSO₄ (100 mg, 5% m/v) in anhydrous acetone (2.0 mL) was stirred under nitrogen atmosphere for 24 hours with 24 W blue LEDs at room temperature, affording 42.6 mg (87% yield, white solid) of (*R*)-**3j**. Enantiomeric excess was established by HPLC analysis using a Chiralpak OD-H column, ee = 97% (HPLC: 254 nm, *n*-hexane/isopropanol = 99:1, flow rate 1 mL/min, 25 °C, t_r (major) = 6.5 min, t_r (minor) = 6.0 min). $[\alpha]_D^{25} = -29.2^\circ$ (*c* 1.0, CH₂Cl₂).

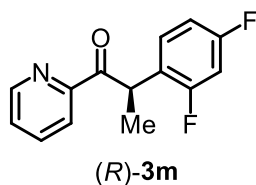


According to the **Method A**, the reaction of racemic **3k** (49.1 mg, 0.2 mmol), Λ -**RhInd** (6.6 mg, 4.0 mol%), *N*-phenylpiperidine (64.5 mg, 2.0 eq) and anhydrous CaSO₄ (100 mg, 5% m/v) in anhydrous acetone (2.0 mL, 0.1 M) was stirred under nitrogen atmosphere for 24 hours with 24 W blue LEDs at room temperature, affording 45.5 mg (93% yield, white solid) of (*R*)-**3k**. Enantiomeric excess was

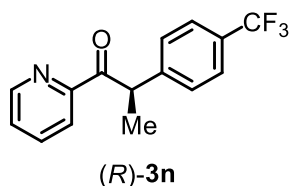
established by HPLC analysis using a Chiralpak OD-H column, ee = 91% (HPLC: 254 nm, *n*-hexane/isopropanol = 98:2, flow rate 1 mL/min, 25 °C, t_r (major) = 8.6 min, t_r (minor) = 7.2 min). $[\alpha]_D^{25} = -115.0^\circ$ (*c* 1.0, CH₂Cl₂).



According to the **Method B**, the reaction of **3l** (61.0 mg, 0.2 mmol), Λ -**RhInd** (6.6 mg, 4.0 mol%), *N*-phenylpiperidine (96.8 mg, 3.0 eq) and anhydrous CaSO₄ (100 mg, 5% m/v) in anhydrous acetone (2.0 mL) was stirred under nitrogen atmosphere for 24 hours with 24 W blue LEDs at room temperature, affording 56.6 mg (93% yield, white solid) of (*R*)-**3l**. Enantiomeric excess was established by HPLC analysis using a Chiralpak IG column, ee = 95% (HPLC: 254 nm, *n*-hexane/isopropanol = 98:2, flow rate 1 mL/min, 25 °C, t_r (major) = 10.1 min, t_r (minor) = 11.6min). $[\alpha]_D^{25} = -8.9^\circ$ (*c* 1.0, CH₂Cl₂).

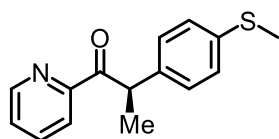


According to the **Method A**, the reaction of racemic **3m** (49.4 mg, 0.2 mmol), Λ -**RhInd** (6.6 mg, 4.0 mol%), *N*-phenylpiperidine (64.5 mg, 2.0 eq) and anhydrous CaSO₄ (100 mg, 5% m/v) in anhydrous acetone (2.0 mL) was stirred under nitrogen atmosphere for 24 hours with 24 W blue LEDs at room temperature, affording 43.9 mg (89% yield, pale yellow solid) of (*R*)-**3m**. Enantiomeric excess was established by HPLC analysis using a Chiralpak OD-H column, ee = 92% (HPLC: 254 nm, *n*-hexane/isopropanol = 99:1, flow rate 1 mL/min, 25 °C, t_r (major) = 6.9 min, t_r (minor) = 6.2 min). $[\alpha]_D^{25} = -55.7^\circ$ (*c* 1.0, CH₂Cl₂).



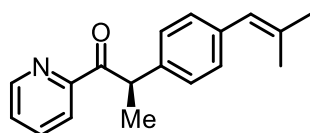
According to the **Method B**, the reaction of racemic **3n** (55.9 mg, 0.2 mmol), Λ -**RhInd** (6.6 mg, 4.0 mol%), *N*-phenylpiperidine (96.8 mg, 3.0 eq) and anhydrous CaSO₄ (100 mg, 5% m/v) in anhydrous acetone (2.0 mL) was stirred under nitrogen atmosphere for 24 hours with 24 W blue LEDs at room temperature, affording 38.5 mg (69% yield, white solid) of (*R*)-**3n**. Enantiomeric excess was established by HPLC analysis using a Chiralpak OD-H column, ee = 96% (HPLC: 254 nm, *n*-hexane/isopropanol = 99:1, flow rate 1 mL/min, 25 °C, t_r (major) = 5.9 min, t_r (minor) = 5.6 min). $[\alpha]_D^{25} = -26.5^\circ$ (*c* 1.0,

CH₂Cl₂).



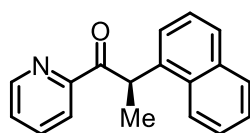
(*R*)-**3o**

According to the **Method B**, the reaction of racemic **3o** (51.5 mg, 0.2 mmol), Λ -**RhInd** (6.6 mg, 4.0 mol%), N-phenylpiperidine (96.8 mg, 3.0 eq) and anhydrous CaSO₄ (100 mg, 5% m/v) in anhydrous acetone (2.0 mL) was stirred under nitrogen atmosphere for 24 hours with 24 W blue LEDs at room temperature, affording 48.8 mg (95% yield, yellow solid) of (*R*)-**3o**. Enantiomeric excess was established by HPLC analysis using a Chiralpak IG column, ee = 97% (HPLC: 254 nm, *n*-hexane/isopropanol = 99:1, flow rate 1 mL/min, 25 °C, t_r (major) = 18.8 min, t_r (minor) = 17.8 min). [α]_D²⁵ = -27.9° (*c* 1.0, CH₂Cl₂).



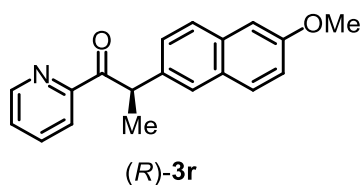
(*R*)-**3p**

According to the **Method B**, the reaction of racemic **3p** (53.1 mg, 0.2 mmol), Λ -**RhInd** (6.6 mg, 4.0 mol%), N-phenylpiperidine (96.8 mg, 3.0 eq) and anhydrous CaSO₄ (100 mg, 5% m/v) in anhydrous acetone (2.0 mL) was stirred under nitrogen atmosphere for 24 hours with 24 W blue LEDs at room temperature, affording 49.8 mg (94% yield, pale yellow liquid) of (*R*)-**3p**. Enantiomeric excess was established by HPLC analysis using a Chiralpak OD-H column, ee = 91% (HPLC: 254 nm, *n*-hexane/isopropanol = 99:1, flow rate 1 mL/min, 25 °C, t_r (major) = 6.2 min, t_r (minor) = 5.9 min). [α]_D²⁵ = -15.8° (*c* 1.0, CH₂Cl₂).

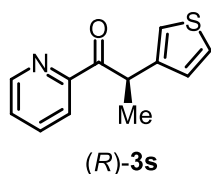


(*R*)-**3q**

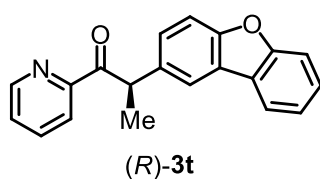
According to the **Method B**, the reaction of racemic **3q** (52.3 mg, 0.2 mmol), Λ -**RhInd** (6.6 mg, 4.0 mol%), N-phenylpiperidine (96.8 mg, 3.0 eq) and anhydrous CaSO₄ (100 mg, 5% m/v) in anhydrous acetone (2.0 mL) was stirred under nitrogen atmosphere for 24 hours with 24 W blue LEDs at room temperature, affording 45.9 mg (88% yield, pale yellow solid) of (*R*)-**3q**. Enantiomeric excess was established by HPLC analysis using a Chiralpak OD-H column, ee = 95% (HPLC: 254 nm, *n*-hexane/isopropanol = 97:3, flow rate 1 mL/min, 25 °C, t_r (major) = 9.4 min, t_r (minor) = 7.8 min). [α]_D²⁵ = -283.6° (*c* 1.0, CH₂Cl₂).



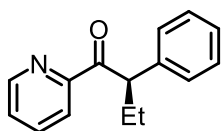
According to the **Method A**, the reaction of racemic **3r** (58.3 mg, 0.2 mmol), Λ -**RhInd** (6.6 mg, 4.0 mol%), N-phenylpiperidine (64.5 mg, 2.0 eq) and anhydrous CaSO_4 (100 mg, 5% m/v) in anhydrous acetone (2.0 mL) was stirred under nitrogen atmosphere for 24 hours with 24 W blue LEDs at room temperature, affording 54.7 mg (94% yield, white solid) of (*R*)-**3r**. Enantiomeric excess was established by HPLC analysis using a Chiralpak OD-H column, ee = 96% (HPLC: 254 nm, *n*-hexane/isopropanol = 95:5, flow rate 1 mL/min, 25 °C, t_r (major) = 7.7 min, t_r (minor) = 7.3 min). $[\alpha]_D^{25} = -44.5^\circ$ (*c* 1.0, CH_2Cl_2).



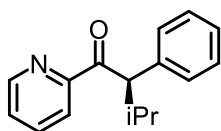
According to the **Method B**, the reaction of racemic **3s** (43.5 mg, 0.2 mmol), Λ -**RhInd** (6.6 mg, 4.0 mol%), N-phenylpiperidine (96.8 mg, 3.0 eq) and anhydrous CaSO_4 (100 mg, 5% m/v) in anhydrous acetone (2.0 mL) was stirred under nitrogen atmosphere for 24 hours with 24 W blue LEDs at room temperature, affording 40.4 mg (93% yield, colorless liquid) of (*R*)-**3s**. Enantiomeric excess was established by HPLC analysis using a Chiralpak OD-H column, ee = 86% (HPLC: 254 nm, *n*-hexane/isopropanol = 99:1, flow rate 1 mL/min, 25 °C, t_r (major) = 9.7 min, t_r (minor) = 7.8 min). $[\alpha]_D^{25} = +9.6^\circ$ (*c* 1.0, CH_2Cl_2).



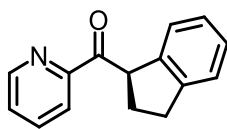
According to the **Method B**, the reaction of racemic **3t** (30.1 mg, 0.1 mmol), Λ -**RhInd** (6.6 mg, 4.0 mol%), N-phenylpiperidine (48.4mg, 3.0 eq) and anhydrous CaSO_4 (100 mg, 5% m/v) in anhydrous acetone (1.0 mL) was stirred under nitrogen atmosphere for 24 hours with 24 W blue LEDs at room temperature, affording 28.1 mg (93% yield, pale yellow solid) of (*R*)-**3t**. Enantiomeric excess was established by HPLC analysis using a Chiralpak OD-H column, ee = 95% (HPLC: 254 nm, *n*-hexane/isopropanol = 99:1, flow rate 1 mL/min, 25 °C, t_r (major) = 10.0 min, t_r (minor) = 8.7 min). $[\alpha]_D^{25} = -13.2^\circ$ (*c* 1.0, CH_2Cl_2).

**(R)-3u**

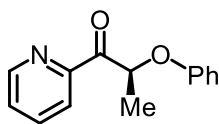
According to the **Method D**, the reaction of racemic **3u** (45.1 mg, 0.2 mmol), Λ -**RhS** (13.8 mg, 8.0 mol%), and *N,N*-diisopropyl-3,5-di-*tert*-butylbenzenemethanamine (182.0 mg, 3.0 eq) in anhydrous acetone (2.0 mL) was stirred under nitrogen atmosphere for 24 hours with 24 W blue LEDs at room temperature, affording 37.2 mg (83% yield, pale yellow solid) of **(R)-3u**. Enantiomeric excess was established by HPLC analysis using a Chiralpak IG column, ee = 87% (HPLC: 254 nm, *n*-hexane/isopropanol = 99:1, flow rate 1 mL/min, 25 °C, t_r (major) = 9.2 min, t_r (minor) = 8.5 min). $[\alpha]_D^{25} = -40.2^\circ$ (*c* 1.0, CH₂Cl₂).

**(R)-3v**

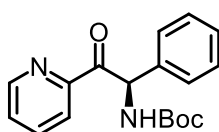
According to the **Method D**, the reaction of racemic **3v** (47.9 mg, 0.2 mmol), Λ -**RhS** (13.8 mg, 8.0 mol%), and *N,N*-diisopropyl-3,5-di-*tert*-butylbenzenemethanamine (182.0 mg, 3.0 eq) in anhydrous acetone (2.0 mL) was stirred under nitrogen atmosphere for 24 hours with 24 W blue LEDs at room temperature, affording 37.3 mg (78% yield, white solid) of **(R)-3v**. Enantiomeric excess was established by HPLC analysis using a Chiralpak IG column, ee = 89% (HPLC: 254 nm, *n*-hexane/isopropanol = 99:1, flow rate 1 mL/min, 25 °C, t_r (major) = 7.6 min, t_r (minor) = 7.2 min). $[\alpha]_D^{25} = -15.1^\circ$ (*c* 1.0, CH₂Cl₂).

**(R)-3w**

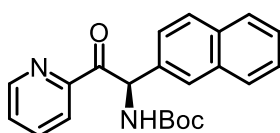
According to the **Method D**, the reaction of racemic **3w** (44.7 mg, 0.2 mmol), Λ -**RhS** (13.8 mg, 8.0 mol%), and *N,N*-diisopropyl-3,5-di-*tert*-butylbenzenemethanamine (182.0 mg, 3.0 eq) in anhydrous acetone (2.0 mL) was stirred under nitrogen atmosphere for 24 hours with 24 W blue LEDs at room temperature, affording 35.4 mg (79% yield, pale yellow solid) of **(R)-3w**. Enantiomeric excess was established by HPLC analysis using a Chiralpak OD-H column, ee = 86% (HPLC: 254 nm, *n*-hexane/isopropanol = 95:5, flow rate 1 mL/min, 25 °C, t_r (major) = 6.6 min, t_r (minor) = 8.6 min). $[\alpha]_D^{25} = -25.6^\circ$ (*c* 1.0, CH₂Cl₂).

(S)-**3x**

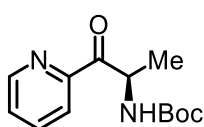
According to the **Method F**, the reaction of racemic **3x** (45.5 mg, 0.2 mmol), Λ -**RhS** (6.9 mg, 4.0 mol%) and N-phenylpiperidine (96.8 mg, 3.0 eq) in anhydrous acetone (2.0 mL) was stirred under nitrogen atmosphere for 24 hours with 24 W blue LEDs at room temperature, affording 34.1 mg (75% yield, white solid) of (S)-**3x**. Enantiomeric excess was established by HPLC analysis using a Chiralpak IG column, ee = 64% (HPLC: 254 nm, *n*-hexane/isopropanol = 90 : 10, flow rate 1 mL/min, 25 °C, t_r (major) = 8.7 min, t_r (minor) = 11.0 min). $[\alpha]_D^{25} = +24.2^\circ$ (*c* 1.0, CH₂Cl₂).

(R)-**3y**

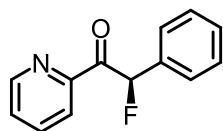
According to the **Method E**, the reaction of racemic **3y** (62.5 mg, 0.2 mmol), Λ -**RhInd** (6.6 mg, 4.0 mol%) and N-phenylazepane (105.2 mg, 3.0 eq) in anhydrous acetone (2.0 mL) was stirred under nitrogen atmosphere for 48 hours with 24 W blue LEDs at room temperature, affording 59.3 mg (95% yield, white solid) of (R)-**3y**. Enantiomeric excess was established by HPLC analysis using a Chiralpak IG column, ee = 92% (HPLC: 254 nm, *n*-hexane/isopropanol = 70:30, flow rate 1 mL/min, 25 °C, t_r (major) = 11.7 min, t_r (minor) = 10.5 min). $[\alpha]_D^{25} = -98.0^\circ$ (*c* 1.0, CH₂Cl₂).

(R)-**3z**

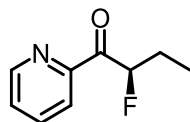
According to the **Method E**, the reaction of racemic **3z** (36.2 mg, 0.1 mmol), Λ -**RhInd** (3.3 mg, 4.0 mol%) and N-phenylazepane (52.6 mg, 3.0 eq) in anhydrous acetone (1.0 mL) was stirred under nitrogen atmosphere for 48 hours with 24 W blue LEDs at room temperature, affording 32.6 mg (90% yield, pale yellow solid) of (R)-**3z**. Enantiomeric excess was established by HPLC analysis using a Chiralpak IG column, ee = 85% (HPLC: 254 nm, *n*-hexane/isopropanol = 70:30, flow rate 1 mL/min, 25 °C, t_r (major) = 18.7 min, t_r (minor) = 13.6 min). $[\alpha]_D^{25} = -86.1^\circ$ (*c* 1.0, CH₂Cl₂).

(R)-**3aa**

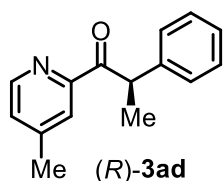
According to the **Method E**, the reaction of racemic **3aa** (25.0 mg, 0.1 mmol), Λ -**RhInd** (3.3 mg, 4.0 mol%) and N-phenylazepane (52.6 mg, 3.0 eq) in anhydrous acetone (1.0 mL) was stirred under nitrogen atmosphere for 48 hours with 24 W blue LEDs at room temperature, affording 20.5 mg (82% yield, white solid) of (*R*)-**3aa**. Enantiomeric excess was established by HPLC analysis using a Chiralpak OD-H column, ee = 85% (HPLC: 254 nm, *n*-hexane/isopropanol = 94:6, flow rate 1 mL/min, 25 °C, t_r (major) = 8.6 min, t_r (minor) = 6.7 min). $[\alpha]_D^{25} = +7.1^\circ$ (*c* 1.0, CH₂Cl₂).

(*R*)-**3ab**

According to the **Method B**, the reaction of racemic **3ab** (43.0 mg, 0.2 mmol), Λ -**RhInd** (6.6 mg, 4.0 mol%), N-phenylpiperidine (96.8 mg, 3.0 eq) and anhydrous CaSO₄ (100 mg, 5% m/v) in anhydrous acetone (1.0 mL) was stirred under nitrogen atmosphere for 48 hours with 24 W blue LEDs at room temperature, affording 39.7 mg (93% yield, white solid) of (*R*)-**3ab**. Enantiomeric excess was established by HPLC analysis using a Chiralpak OD-H column, ee = 72% (HPLC: 254 nm, *n*-hexane/isopropanol = 90 :10, flow rate 1 mL/min, 25 °C, t_r (major) = 9.6 min, t_r (minor) = 7.0 min). $[\alpha]_D^{25} = -94.2^\circ$ (*c* 1.0, CH₂Cl₂).

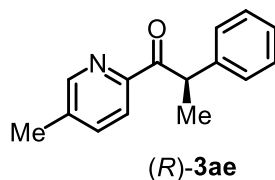
(*R*)-**3ac**

According to the **Method B**, the reaction of racemic **3ac** (33.4 mg, 0.2 mmol), Λ -**RhInd** (6.6 mg, 4.0 mol%), N-phenylpiperidine (96.8 mg, 3.0 eq) and anhydrous CaSO₄ (100 mg, 5% m/v) in anhydrous acetone (1.0 mL) was stirred under nitrogen atmosphere for 48 hours with 24 W blue LEDs at room temperature, affording 28.3 mg (85% yield, colorless liquid) of (*R*)-**3ac**. Enantiomeric excess was established by HPLC analysis using a Chiralpak OD-H column, ee = 40% (HPLC: 254 nm, *n*-hexane/isopropanol = 99 :1, flow rate 1 mL/min, 25 °C, t_r (major) = 8.2 min, t_r (minor) = 7.7 min). $[\alpha]_D^{25} = +4.7^\circ$ (*c* 0.3, CH₂Cl₂).

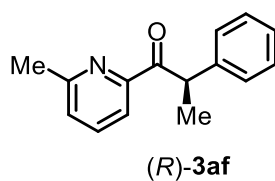
(*R*)-**3ad**

According to the **Method B**, the reaction of racemic **3ad** (45.1 mg, 0.2 mmol), Λ -**RhInd** (6.6 mg, 4.0 mol%), N-phenylpiperidine (96.8 mg, 3.0 eq) and anhydrous CaSO₄ (100 mg, 5% m/v) in anhydrous

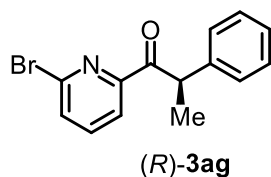
acetone (2.0 mL) was stirred under nitrogen atmosphere for 24 hours with 24 W blue LEDs at room temperature, affording 41.4 mg (92% yield, pale yellow liquid) of (*R*)-**3ad**. Enantiomeric excess was established by HPLC analysis using a Chiralpak OD-H column, ee = 93% (HPLC: 254 nm, *n*-hexane/isopropanol = 99:1, flow rate 1 mL/min, 25 °C, t_r (major) = 8.7 min, t_r (minor) = 8.0 min). $[\alpha]_D^{25} = -81.4^\circ$ (*c* 1.0, CH₂Cl₂).



According to the **Method B**, the reaction of racemic **3ae** (45.1 mg, 0.2 mmol), Λ -**RhInd** (6.6 mg, 4.0 mol%), *N*-phenylpiperidine (96.8 mg, 3.0 eq) and anhydrous CaSO₄ (100 mg, 5% m/v) in anhydrous acetone (2.0 mL) was stirred under nitrogen atmosphere for 24 hours with 24 W blue LEDs at room temperature, affording 39.6 mg (88% yield, white solid) of (*R*)-**3ae**. Enantiomeric excess was established by HPLC analysis using a Chiralpak OD-H column, ee = 89% (HPLC: 254 nm, *n*-hexane/isopropanol = 99:1, flow rate 1 mL/min, 25 °C, t_r (major) = 10.0 min, t_r (minor) = 8.7 min). $[\alpha]_D^{25} = -16.5^\circ$ (*c* 1.0, CH₂Cl₂).

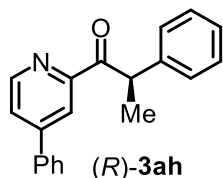


According to the **Method C**, the reaction of racemic **3af** (45.1 mg, 0.2 mmol), Λ -**RhInd** (13.2 mg, 8.0 mol%), *N*-phenylpiperidine (96.8 mg, 3.0 eq) and anhydrous CaSO₄ (100 mg, 5% m/v) in anhydrous acetone (2.0 mL) was stirred under nitrogen atmosphere for 24 hours with 24 W blue LEDs at room temperature, affording 36.3 mg (81% yield, pale yellow solid) of (*R*)-**3af**. Enantiomeric excess was established by HPLC analysis using a Chiralpak OD-H column, ee = 90% (HPLC: 254 nm, *n*-hexane/isopropanol = 99:1, flow rate 1 mL/min, 25 °C, t_r (major) = 7.1 min, t_r (minor) = 6.7 min). $[\alpha]_D^{25} = +17.6^\circ$ (*c* 1.0, CH₂Cl₂).

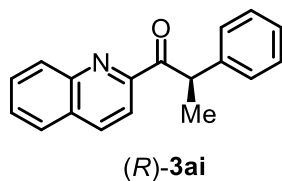


According to the **Method C**, the reaction of racemic **3ag** (58.0 mg, 0.2 mmol), Λ -**RhInd** (13.2mg, 8.0 mol%), *N*-phenylpiperidine (96.8 mg, 3.0 eq) and anhydrous CaSO₄ (100 mg, 5% m/v) in anhydrous acetone (2.0 mL, 0.1 M) was stirred under nitrogen atmosphere for 24 hours with 24 W blue LEDs at

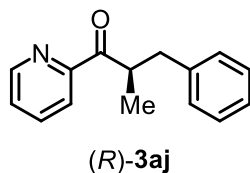
room temperature, affording 49.3 mg (85% yield, white solid) of (*R*)-**3ag**. Enantiomeric excess was established by HPLC analysis using a Chiralpak OD-H column, ee = 94% (HPLC: 254 nm, *n*-hexane/isopropanol = 98:2, flow rate 1 mL/min, 25 °C, t_r (major) = 8.0 min, t_r (minor) = 7.1 min). $[\alpha]_D^{25} = +115.9^\circ$ (*c* 1.0, CH₂Cl₂).



According to the **Method B**, the reaction of racemic **3ah** (57.5 mg, 0.2 mmol), Λ -**RhInd** (6.6 mg, 4.0 mol%), *N*-phenylpiperidine (96.8 mg, 3.0 eq) and anhydrous CaSO₄ (100 mg, 5% m/v) in anhydrous acetone (2.0 mL) was stirred under nitrogen atmosphere for 24 hours with 24 W blue LEDs at room temperature, affording 53.9 mg (94% yield, white solid) of (*R*)-**3ah**. Enantiomeric excess was established by HPLC analysis using a Chiralpak OD-H column, ee = 88% (HPLC: 254 nm, *n*-hexane/isopropanol = 95:5, flow rate 1 mL/min, 25 °C, t_r (major) = 8.0 min, t_r (minor) = 6.5 min). $[\alpha]_D^{25} = -162.2^\circ$ (*c* 1.0, CH₂Cl₂).



According to the **Method B**, the reaction of racemic **3ai** (52.3 mg, 0.2 mmol), Λ -**RhInd** (6.6 mg, 4.0 mol%), *N*-phenylpiperidine (96.8 mg, 3.0 eq) and anhydrous CaSO₄ (100 mg, 5% m/v) in anhydrous acetone (2.0 mL) was stirred under nitrogen atmosphere for 24 hours with 24 W blue LEDs at room temperature, affording 47.8 mg (92% yield, pale yellow solid) of (*R*)-**3ai**. Enantiomeric excess was established by HPLC analysis using a Chiralpak OD-H column, ee = 87% (HPLC: 254 nm, *n*-hexane/isopropanol = 98:2, flow rate 1 mL/min, 25 °C, t_r (major) = 7.2 min, t_r (minor) = 6.4 min). $[\alpha]_D^{25} = +254.3^\circ$ (*c* 1.0, CH₂Cl₂).



According to the **Method G**, the reaction of racemic **3aj** (45.0 mg, 0.2 mmol), Λ -**RhInd** (6.6 mg, 4.0 mol%) and DIPEA (77.6 mg, 3.0 eq) in anhydrous acetone (2.0 mL) was stirred under nitrogen atmosphere for 24 hours with 24 W blue LEDs at room temperature, affording 33.8 mg (75% yield, colorless liquid) of (*R*)-**3aj**. Enantiomeric excess was established by HPLC analysis using a Chiralpak

OD-H column, ee = 42% (HPLC: 254 nm, *n*-hexane/isopropanol = 98:2, flow rate 0.5 ml/min, 25 °C, t_r (major) = 16.6min, t_r (minor) = 14.7 min). $[\alpha]_D^{25} = +22.2^\circ$ (*c* 0.5, CH₂Cl₂).

4.3.4 Mechanistic Experiments

1) Absorption Spectra

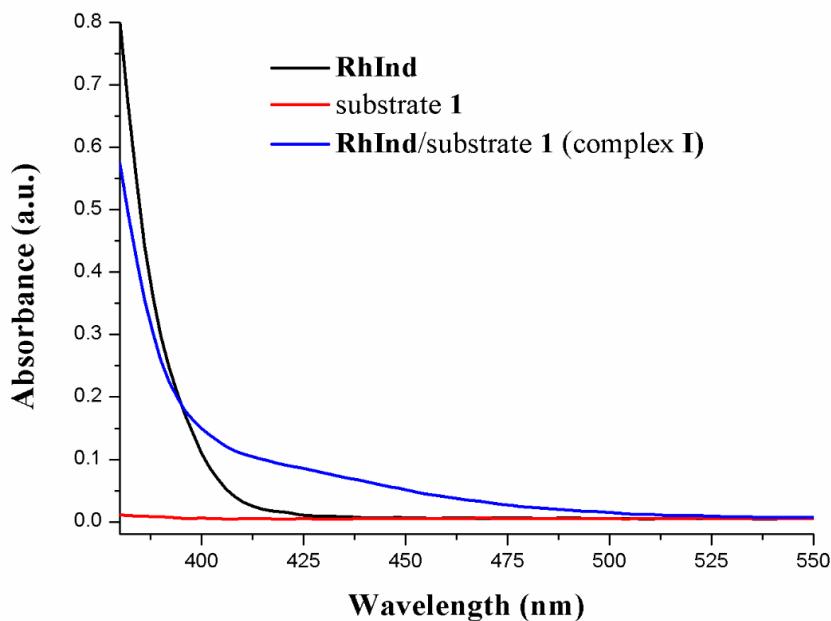


Figure 51. UV/Vis-absorbance measurements. UV/Vis absorption spectra of substrate **1**, catalyst **RhInd**, and the substrate-coordinated catalyst **RhInd/substrate 1 (complex I)**. Recorded in acetone at concentrations of 0.2 mM.

2) Cyclic Voltammetry

Cyclic voltammetry was carried out on a BAS C3 Cell Stand and a BAS 100 series Electrochemical Analyzer using a platinum disk anode (2.0 mm diameter) and a platinum wire cathode (0.5 mm diameter) at r.t. in acetonitrile containing 0.1 M Bu₄NBF₄. Potentials were referred to a saturated Ag/AgCl reference electrode. Before each experiment the surface of the anode was polished followed by thorough rinsing with distilled water. The solution was purged with nitrogen before each measurement. See **Figure 52** for the results.

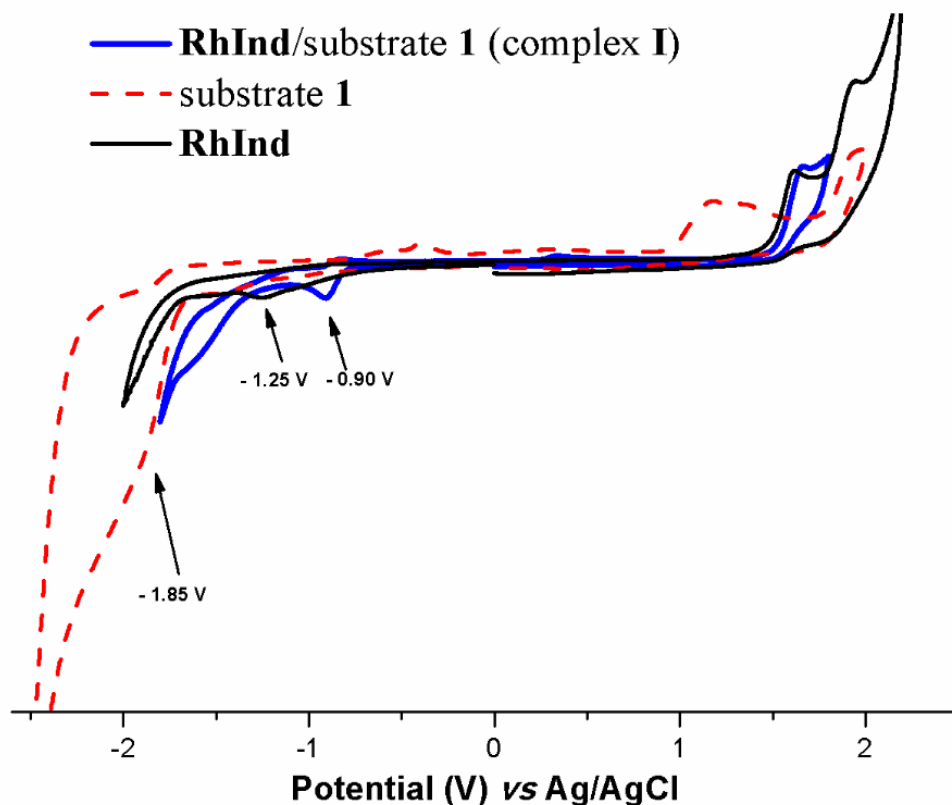
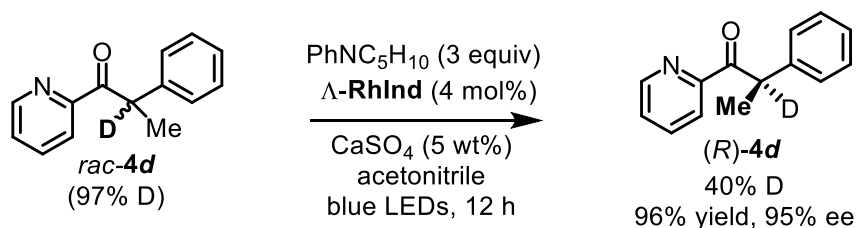


Figure 52. Cyclic voltammetry. Cyclic voltammograms of substrate **1**, the catalyst **RhInd**, and the substrate-coordinated catalyst **RhInd/substrate 1** (complex **I**). Measured in CH_2Cl_2 (0.6 mM) containing $n\text{Bu}_4\text{NBF}_4$ (0.1 M) at a scan rate = 0.1 V/s.

3) Retaining deuteration at the chiral center



An oven-dried 10 mL Schlenk tube was charged with *rac-4d* (97% D, 21.2 mg, 0.1 mmol, 1.0 eq), $\Delta\text{-RhInd}$ (3.3 mg, 0.004 mmol, 4.0 mol%), N-phenylpiperidine (48.4 mg, 0.3 mmol, 3.0 eq) and anhydrous CaSO_4 (50 mg, 5% m/v). Then, acetone (max. 0.01% water, purchased from AppliChem GmbH) (1.0 mL) was added via syringe. The reaction mixture was degassed via freeze-pump-thaw for three cycles. Subsequent, the vial was sealed and placed approximately 10 cm away from the 24 W blue LEDs. After stirring for 12 hours, the mixture was diluted with CH_2Cl_2 . The combined organic solutions were concentrated under reduced pressure and the mixture purified by flash chromatography on silica gel (*n*-hexane/ EtOAc=50:1 to 10:1) to afford the pure non-racemic product. The enantiomeric excess was determined by HPLC analysis on a chiral stationary phase.

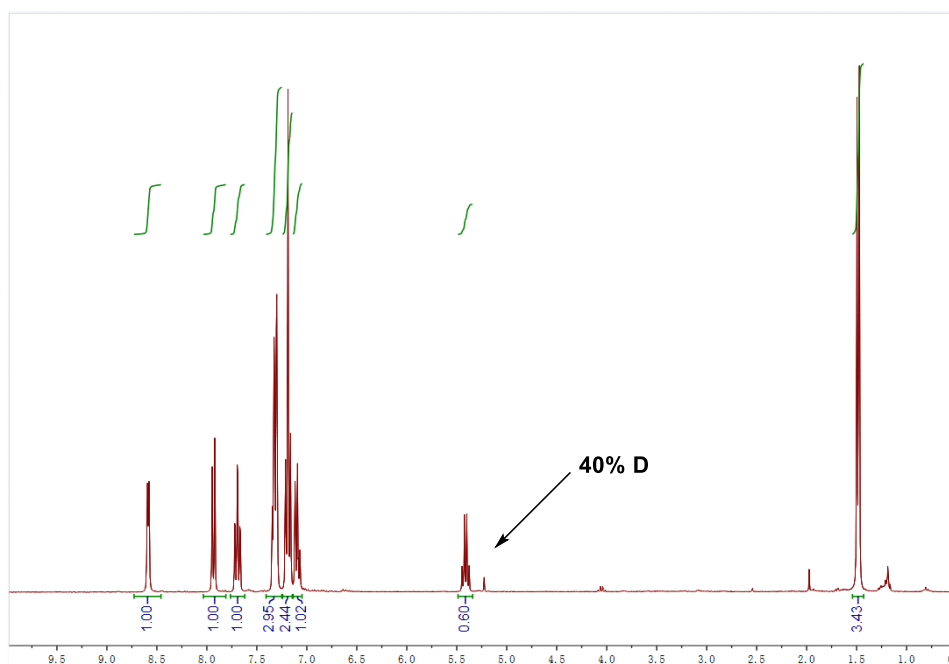
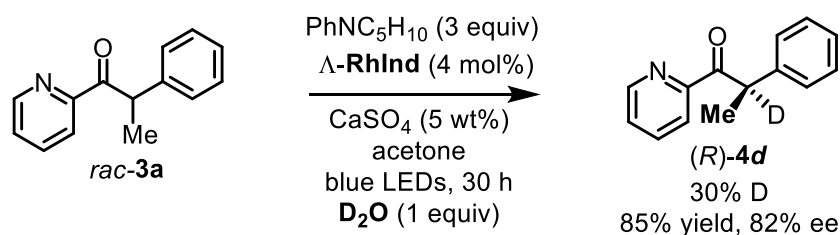


Figure 53. ^1H NMR analysis of the deuterated (*R*)-**4d** when use deuterated *rac*-**4d** as the starting material.

4) Introduction of deuterium at the chiral center



An oven-dried 10 mL Schlenk tube was charged with *rac*-**3a** (21.1 mg, 0.1 mmol, 1.0 eq), Δ -**RhInd** (3.3 mg, 0.04 mmol, 4.0 mol%) and N-phenylpiperidine (48.4 mg, 0.3 mmol, 3.0 eq). Then, a mixture of acetone (1.0 ml) including D_2O (2.0 mg) was added via syringe. The reaction mixture was degassed via freeze-pump-thaw for three cycles. Subsequent, the vial was sealed and placed approximately 10 cm away from the 24 W blue LEDs. After stirring for 30 hours, the mixture was diluted with CH_2Cl_2 . The combined organic solutions were concentrated under reduced pressure and the mixture was purified by flash chromatography on silica gel (*n*-hexane/ EtOAc=50:1 to 10:1) to afford the pure non-racemic product. The enantiomeric excess was determined by HPLC analysis on a chiral stationary phase.

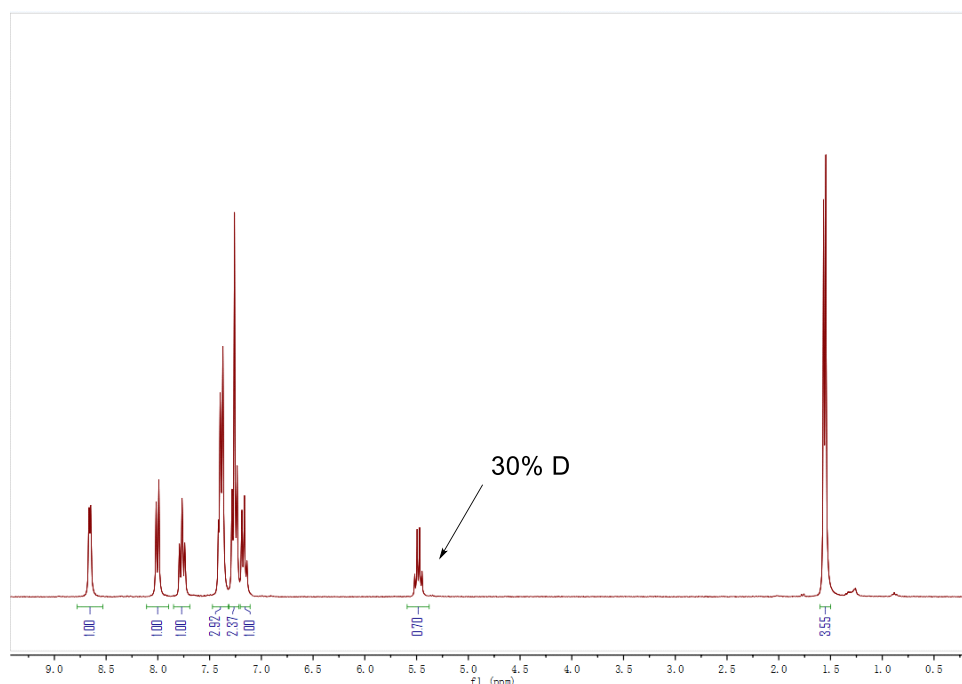
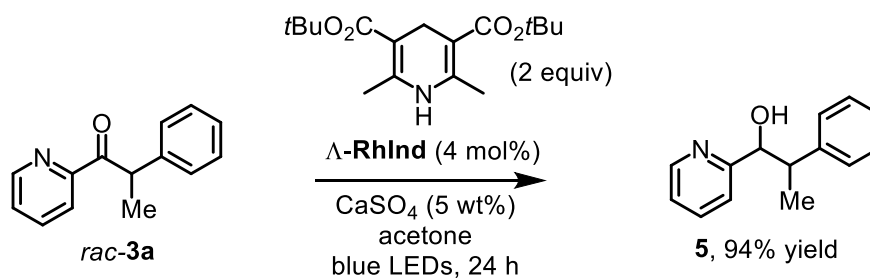


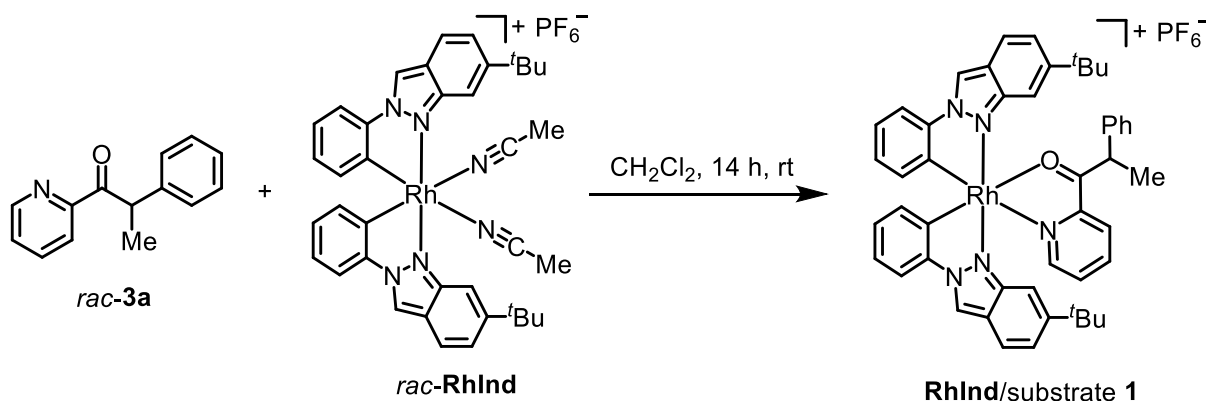
Figure 54. ^1H NMR analysis of the deuterated (*R*)-**4d** when add 1 equiv D_2O .

5) Hantzsch ester as an alternative reducing agent



An oven-dried 10 mL Schlenk tube was charged with *rac*-**3a** (21.1 mg, 0.1 mmol, 1.0 eq), $\Delta\text{-RhInd}$ (3.3 mg, 0.04 mmol, 4.0 mol%), Hantzsch ester (61.9 mg, 0.2 mmol, 2.0 eq) and anhydrous CaSO_4 (50 mg, 5% m/v). Then, acetone (max. 0.01% water, purchased from AppliChem GmbH) (1.0 mL) was added via syringe. The reaction mixture was degassed via freeze-pump-thaw for three cycles. After the mixture was thoroughly degassed, the vial was sealed and positioned at approximately 10 cm away from a 24 W blue LEDs lamp. After stirring for 24 hours, the mixture was diluted with CH_2Cl_2 . The combined organic solutions were concentrated under reduced pressure and the mixture was purified by flash chromatography on silica gel (*n*-hexane/ EtOAc=10:1 to 2:1) to afford the pure product as a white solid. ^1H NMR (300 MHz, CDCl_3) δ 8.39 (d, J = 4.8 Hz, 1H), 7.52 (td, J = 7.7, 1.4 Hz, 1H), 7.24 – 7.02 (m, 6H), 6.96 (d, J = 7.8 Hz, 1H), 4.80 (d, J = 5.6 Hz, 1H), 3.29 – 3.07 (m, 1H), 1.20 (d, J = 7.1 Hz, 3H).

6) Synthesis of racemic RhInd/substrate complex for cyclic voltammetry



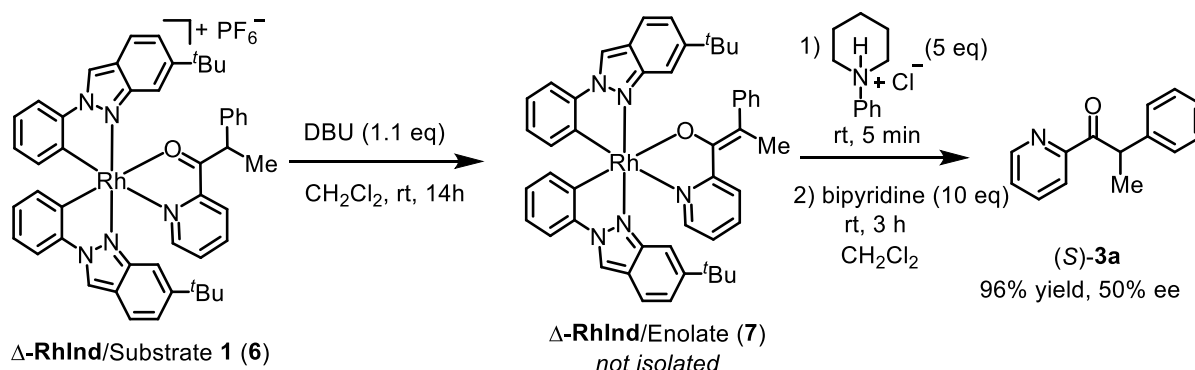
Racemic substrate **3a** (26.4 mg, 0.12 mmol, 2.5 eq.) and racemic **RhInd** (41.4 mg, 0.05 mmol, 1.0 eq.) in CH_2Cl_2 (1 mL) were stirred at room temperature for 14 h. Then, the solvent was removed under reduced pressure and the residue was redissolved in CH_2Cl_2 (1 mL). The resulting mixture was stirred for another 30 min and the solvent was removed (this procedure was repeated for 2 times). Afterwards, Et_2O was added to the residue and the precipitate was filtered, washed with Et_2O to afford the complex **RhInd/substrate 3a** (42.1 mg, 0.04 mmol, 88% yield) as an orange solid.

^1H NMR (300 MHz, CD_2Cl_2): δ = 8.87 (s, 1H), 8.82 (s, 1H), 8.62 (d, J = 8.0 Hz, 1H), 8.29-8.15 (m, 2H), 7.81 (dd, J = 8.9, 8.5 Hz, 2H), 7.72-7.62 (m, 3H), 7.39 (dd, J = 9.0, 1.3 Hz, 1H), 7.28-7.14 (m, 3H), 7.08 (s, 1H), 6.94 (t, J = 7.2 Hz, 1H), 6.90-6.77 (m, 2H), 6.76-6.62 (m, 4H), 6.06 (dd, J = 22.3, 7.6 Hz, 2H), 5.26 (s, 1H), 5.07 (q, J = 6.6 Hz, 1H), 1.55 (d, J = 6.6 Hz, 3H), 1.34 (s, 9H), 0.69 (s, 9H).

^{13}C NMR (75 MHz, CD_2Cl_2) δ 209.6, 154.2, 154.0, 151.7, 150.8, 148.1, 146.3, 145.9, 144.6, 144.2, 142.9, 141.6, 140.9, 137.8, 135.7, 134.5, 131.8, 130.7, 129.5, 128.2, 127.9, 127.6, 127.3, 124.9, 124.8, 123.8, 123.5, 121.4, 121.0, 120.9, 120.8, 114.4, 113.9, 107.9, 107.3, 52.8, 48.8, 35.6, 35.0, 30.8, 30.4, 18.6.

HRMS (ESI, m/z) calcd for $\text{C}_{48}\text{H}_{47}\text{N}_5\text{ORh}$ $[\text{M}]^+$: 812.2830, found: 812.2849.

7) Enantioselective protonation of rhodium enolate complex



A rhodium substrate complex from Δ -**RhInd** and racemic substrate **3a** was synthesized following the procedure above (Section 5.4). To a solution of Δ -**RhInd**/substrate **3a** (38.3 mg, 0.04 mmol) in CH_2Cl_2 (1.0 mL) was added DBU (6.6 μL , 0.044 mmol, 1.1 eq.) under nitrogen atmosphere to generate the complex Δ -**RhInd**/enolate *in situ*. The resulting mixture was stirred for 14 h at room temperature. Then,

the HCl salt of N-phenylpiperidine (39.5 mg, 0.2 mmol, 5 eq.) was added. The mixture was stirred for 5 min at room temperature. Afterwards, bipyridine (62.5 mg, 0.4 mmol, 10 eq.) was added to the mixture and stirred for another 3 h. The solvent was removed in vacuo and the mixture was purified by column chromatography on silica gel (*n*-hexane/EtOAc 10:1) to afford 8.1 mg (0.037 mmol, 96%) of the non-racemic ketone (*S*)-**3a** with 50% ee.

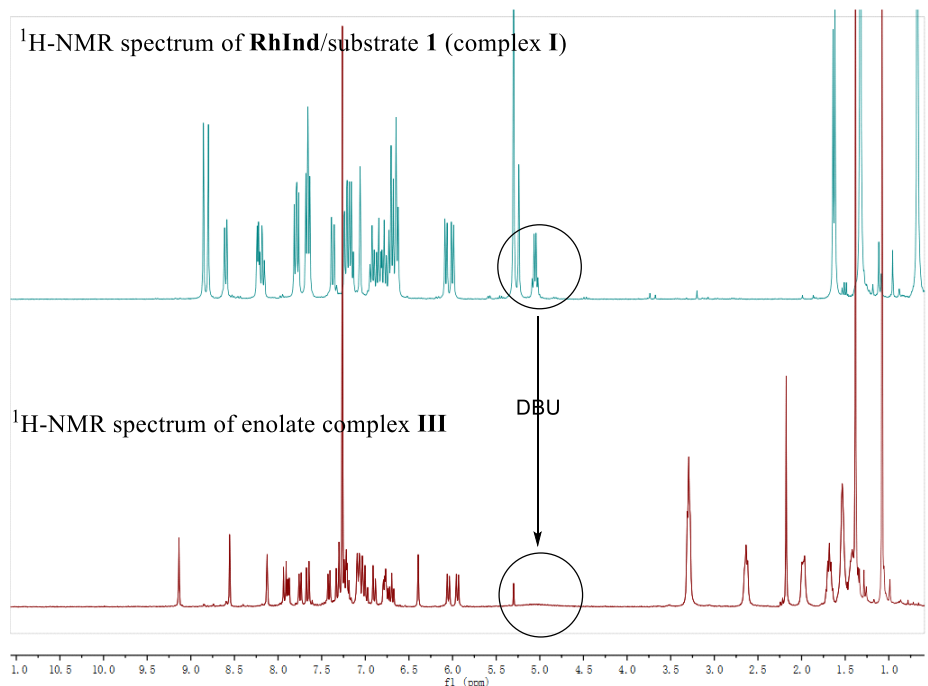
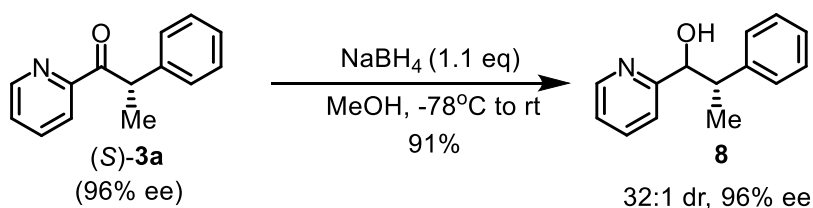


Figure 55. ^1H NMR spectrum of **RhInd**/substrate **3a** and enolate complex **III**.

4.3.5 Follow-Up Chemistry



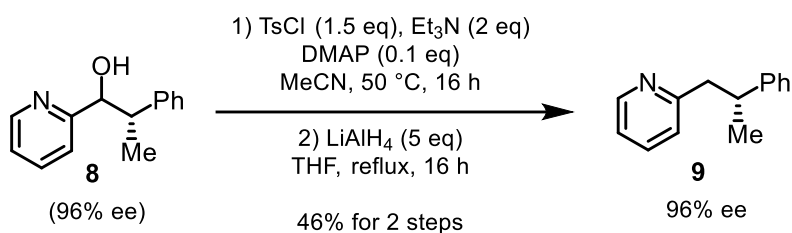
A solution of the NaBH_4 (13.8 mg, 0.33 mmol, 1.1 eq) in methanol (3.0 mL) was placed in a dry ice/acetone bath. After cooling to -78°C , a solution of (*S*)-**3a** (63.4 mg, 0.3 mmol, 1.0 eq) in THF (1.0 mL) was added dropwise at -78°C . The reaction mixture was warmed to room temperature. After completion, the reaction was quenched by addition of saturated aqueous NH_4Cl (2 mL) and was extracted with ethyl acetate for three times. The combined organic layer was dried over anhydrous Na_2SO_4 . After filtration, the solvent was removed under reduced pressure, and the residue was purified by column chromatography on silica gel (ethyl acetate/hexane = 1:2) to give the alcohol as a white solid (58.3 mg, 0.27 mmol, 91% yield) with 32:1 dr and 96% ee. HPLC: Daicel Chiralcel OD-H,

*i*PrOH/hexane = 3/97, 1.0 mL/min, 25 °C, 254 nm; $t_1 = 15.1$ min, $t_2 = 20.7$ min. $[\alpha]_D^{25} = -90.0$ (c 1.0, CH₂Cl₂).

¹H NMR (500 MHz, CDCl₃) δ 8.53 – 8.45 (m, 1H), 7.62 (td, $J = 7.7, 1.8$ Hz, 1H), 7.29 – 7.12 (m, 6H), 7.06 (d, $J = 7.9$ Hz, 1H), 4.90 (d, $J = 5.5$ Hz, 1H), 3.86 (s, 1H), 3.32 – 3.22 (m, 1H), 1.31 (d, $J = 7.1$ Hz, 3H).

¹³C NMR (75 MHz, CDCl₃) δ 160.4, 148.1, 142.2, 136.1, 128.3, 128.1, 126.5, 122.3, 121.5, 77.6, 46.8, 17.1.

HRMS (ESI, m/z) calcd for C₁₄H₁₆NO [M+H]⁺: 214.1226, found: 210.1230.

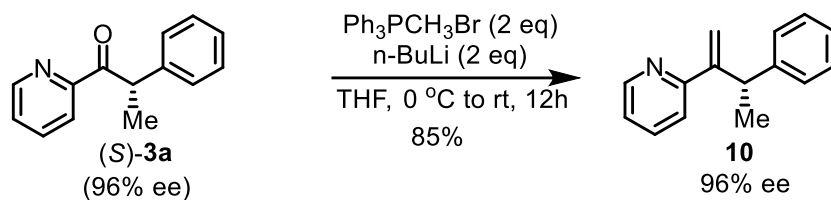


To a solution of alcohol (19.0 mg, 0.09 mmol, 96% ee) in MeCN (2.0 mL) was added TsCl (28.6 mg, 0.15 mmol, 1.5 eq), DMAP (1.2 mg, 0.01 mmol) and Et₃N (28 μ L, 0.2 mmol) successively. The reaction mixture was stirred at 50 °C for 16 hours. After completion, the solvent was removed under reduced pressure and the residue was redissolved in THF (2.0 mL). LiAlH₄ (19 mg, 0.5 mmol) was added and the reaction mixture was refluxed under N₂ atmosphere for 16 hours. After completion, the reaction mixture was cooled to 0 °C and was quenched by addition of ice water until the evolution of hydrogen gas ceased. Aqueous NaOH (3 M, 5.0 mL) was added and the reaction mixture was extracted with ethyl acetate for three times. The combined organic layer was washed with brine and was dried over anhydrous Na₂SO₄. After filtration, the solvent was removed under reduced pressure, and the residue was purified by column chromatography on silica gel (eluted with ethyl acetate/hexane = 1:3) to give the target product as a colorless oil (8.1 mg, 0.04 mmol, 46% yield for 2 steps) with 96% ee. HPLC: Daicel Chiralcel OD-H, *i*PrOH/hexane = 10/90, 1.0 mL/min, 25 °C, 254 nm; $t_1 = 5.6$ min, $t_2 = 7.2$ min. $[\alpha]_D^{25} = -60.3$ (c 0.5, CH₂Cl₂).

¹H NMR (300 MHz, CDCl₃) δ 1.27 (d, $J = 7.0$ Hz, 3H), 2.98 (dd, $J = 13.2, 8.2$ Hz, 1H), 3.08 (dd, $J = 13.2, 6.9$ Hz, 1H), 3.21-3.37 (m, 1H), 6.93 (d, $J = 7.8$ Hz, 1H), 7.07 (dd, $J = 7.5, 5.0$ Hz, 1H), 7.12-7.23 (m, 3H), 7.23-7.31 (m, 2H), 7.49 (td, $J = 7.8, 1.8$ Hz, 1H), 8.47-8.62 (m, 1H).

¹³C NMR (75 MHz, CDCl₃) δ 21.4, 40.4, 47.2, 121.0, 123.6, 126.0, 127.0, 128.3, 135.9, 146.7, 149.2, 160.6.

The ¹H and ¹³C NMR data match those reported in the reference.⁷

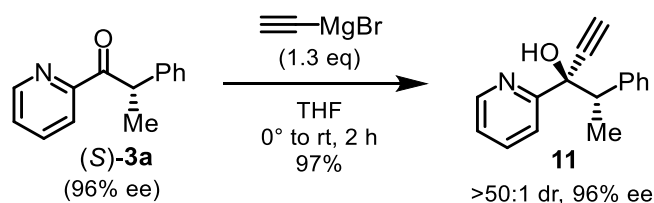


To a flask charged with methyltriphenylphosphonium bromide (143 mg, 0.4 mmol) in 4.0 mL of anhydrous THF at 0 °C was added *n*-butyllithium (0.25 mL, 1.6 M in hexanes, 0.4 mmol). The reaction was allowed to warm to room temperature spontaneously and then stirred for 1 h. The compound (*S*)-**1** (42.25 mg, 0.2 mmol) in anhydrous THF (1.0 mL) was added dropwise, and the reaction was stirred for 12 h at room temperature. After being quenched with saturated aqueous NH_4Cl , the mixture was extracted with ethyl acetate for three times. The combined organic layer was washed with brine and was dried over anhydrous Na_2SO_4 . After filtration, the solvent was removed under reduced pressure, and the residue was purified by column chromatography on silica gel (ethyl acetate/hexane = 1:3) to afford the desired product as a white solid (35.6 mg, 0.17 mmol, 85% yield) with 96% ee. The procedure was adapted and modified from a previous report.⁸ HPLC: Daicel Chiralcel OD-H, *i*PrOH/hexane = 3/97, 1.0 mL/min, 25 °C, 254 nm; $t_1 = 6.2$ min, $t_2 = 9.6$ min. $[\alpha]_{\text{D}}^{25} = +75.9$ (c 1.0, CH_2Cl_2).

^1H NMR (300 MHz, CDCl_3) δ 8.42 (d, $J = 4.7$ Hz, 1H), 7.46 – 7.35 (m, 1H), 7.24 – 7.08 (m, 5H), 6.98 (ddd, $J = 10.2, 7.4, 5.8$ Hz, 1H), 5.73 (s, 1H), 5.21 (s, 1H), 4.36 (q, $J = 7.1$ Hz, 1H), 1.39 (d, $J = 7.1$ Hz, 3H).

^{13}C NMR (75 MHz, CDCl_3) δ 158.9, 152.4, 148.7, 145.2, 136.2, 128.2, 127.7, 125.9, 122.0, 121.2, 115.1, 41.7, 21.41.

HRMS (ESI, m/z) calcd for $\text{C}_{15}\text{H}_{16}\text{N}$ $[\text{M}+\text{H}]^+$: 210.1277, found: 210.1281.



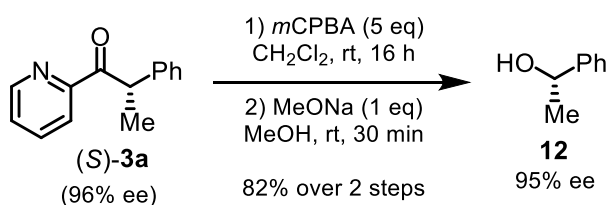
To a solution of compound (*S*)-**1** (15.8 mg, 0.075 mmol, 96% ee) in THF (1.5 mL) at 0 °C under N_2 atmosphere was added a solution of ethynylmagnesium bromide (0.5 M in THF, 0.2 mL, 0.1 mmol) dropwise. The reaction mixture was warmed to room temperature and stirred for 2 hours. After completion, the reaction was quenched by addition of saturated aqueous NH_4Cl (2.0 mL). The mixture was diluted with water (5.0 mL) and was extracted with ethyl acetate for three times. The combined organic layer was washed with brine and was dried over anhydrous Na_2SO_4 . After filtration, the solvent was removed under reduced pressure, and the residue was purified by column chromatography on silica gel (eluted with ethyl acetate/hexane = 1:5) to give the desired product as a colorless oil (17.3 mg, 0.073 mmol, 97% yield) with >50:1 dr and 96% ee. HPLC: Agilent HPLC 1260, Daicel Chiralpak IG,

*i*PrOH/hexane = 10/90, 1.0 mL/min, 25 °C, 254 nm; $t_1 = 9.4$ min, $t_2 = 16.8$ min. $[\alpha]_D^{25} = -59.5$ (c 0.5, CH₂Cl₂).

¹H NMR (300 MHz, CDCl₃) δ 1.60 (d, $J = 7.1$ Hz, 3H), 2.63 (s, 1H), 3.32 (q, $J = 7.1$ Hz, 1H), 5.24-5.42 (br, 1H), 7.00-7.07 (m, 2H), 7.07-7.11 (m, 3H), 7.11-7.16 (m, 1H), 7.57-7.64 (m, 1H), 7.64-7.73 (m, 1H), 8.23-8.32 (m, 1H).

¹³C NMR (75 MHz, CDCl₃) δ 16.4, 51.5, 73.5, 74.6, 85.8, 121.3, 122.6, 126.5, 127.4, 129.1, 136.6, 140.4, 146.8, 159.5.

HRMS (ESI, m/z) calcd for C₁₆H₁₆NO [M+H]⁺: 238.1226; found: 238.1229.

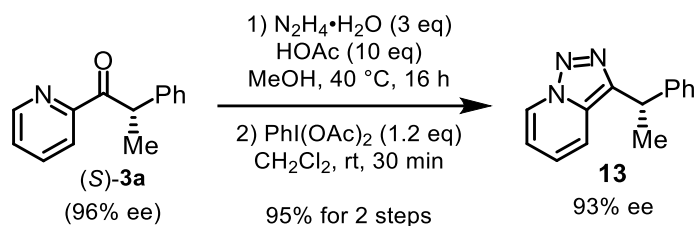


To a solution of (*S*)-**1** (52.8 mg, 0.25 mmol, 96% ee) in CH₂Cl₂ (5.0 mL) was added *m*CPBA (308 mg, 70%, 1.25 mmol) in one portion at room temperature. The reaction mixture was stirred at room temperature for 16 hours. After completion, the reaction mixture was diluted with ethyl acetate (20 mL) and was washed successively with saturated aqueous NaHCO₃ and brine. The organic layer was dried over anhydrous Na₂SO₄. After filtration, the solvent was removed under reduced pressure and the residue was redissolved in MeOH (5.0 mL), to which MeONa (13 mg, 0.25 mmol) was added and the mixture was stirred at room temperature for 30 min. Then the reaction mixture was diluted with ethyl acetate (20 mL) and was washed with water and brine and was dried over anhydrous Na₂SO₄. After filtration, the solvent was removed under reduced pressure and the residue was purified by column chromatography on silica gel (eluted with ethyl acetate/hexane = 1:5) to give the desired product as a colorless oil (25.0 mg, 0.21 mmol, 82% yield for 2 steps) with 95% ee. HPLC: Daicel Chiralcel OD-H, *i*PrOH/hexane = 10/90, 1.0 mL/min, 25 °C, 254 nm; $t_1 = 6.0$ min, $t_2 = 6.7$ min. $[\alpha]_D^{25} = -23.6$ (c 1.0, CH₂Cl₂).

¹H NMR (300 MHz, CDCl₃) δ 1.50 (d, $J = 6.5$ Hz, 3H), 1.85-1.95 (br, 1H), 4.90 (q, $J = 6.5$ Hz 1H), 7.24-7.31 (m, 1H), 7.31-7.44 (m, 4H).

¹³C NMR (75 MHz, CDCl₃) δ 25.1, 70.4, 125.4, 127.4, 128.5, 145.8.

The ¹H and ¹³C NMR data match those reported in the reference.⁹

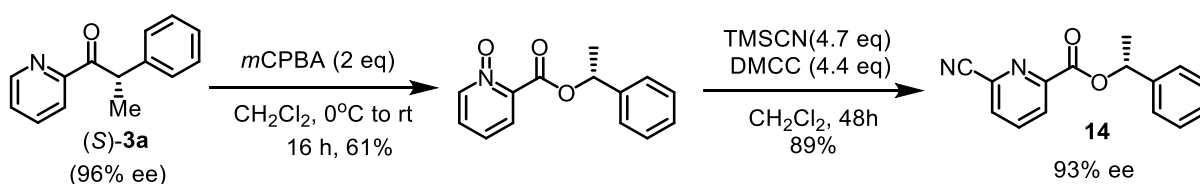


To a solution of (*S*)-**1** (16.9 mg, 0.08 mmol, 96% ee) in MeOH (1.5 mL) was added HOAc (46 μL , 0.8 mmol) and $\text{N}_2\text{H}_4 \cdot \text{H}_2\text{O}$ (80%, 15 μL , 0.24 mmol). The reaction mixture was stirred at 40 °C for 16 hours. After completion, the reaction mixture was diluted with ethyl acetate (20 mL) and was washed successively with saturated aqueous NaHCO_3 and brine. The organic layer was dried over anhydrous Na_2SO_4 . After filtration, the solvent was removed under reduced pressure and the residue was redissolved in CH_2Cl_2 (1.5 mL), to which $\text{PhI}(\text{OAc})_2$ (31 mg, 0.096 mmol) was added and the mixture was stirred at room temperature for 30 min. After completion, the solvent was removed under reduced pressure and the residue was purified by column chromatography on silica gel (eluted with ethyl acetate/hexane = 1:2) to give the desired product as a colorless oil (17.0 mg, 0.076 mmol, 95% yield for 2 steps) with 93% ee. HPLC: Daicel Chiralpak IG, *i*PrOH/hexane = 20/80, 1.0 mL/min, 25 °C, 254 nm; $t_1 = 14.5$ min, $t_2 = 16.2$ min. $[\alpha]_{\text{D}}^{25} = +30.5$ (*c* 1.0, CH_2Cl_2).

$^1\text{H NMR}$ (300 MHz, CDCl_3) δ 1.90 (d, $J = 7.3$ Hz, 3H), 4.56 (q, $J = 7.3$ Hz, 1H), 6.85 (t, $J = 6.9$ Hz, 1H), 6.99 (dd, $J = 9.0, 6.6$ Hz, 1H), 7.15 (d, $J = 9.0$ Hz, 1H), 7.18-7.25 (m, 1H), 7.25-7.40 (m, 4H), 8.63 (d, $J = 7.1$ Hz, 1H).

$^{13}\text{C NMR}$ (75 MHz, CDCl_3) δ 21.2, 37.4, 114.9, 117.9, 123.7, 125.1, 126.5, 127.4, 128.6, 130.9, 141.8, 144.6.

HRMS (ESI, *m/z*) calcd for $[\text{C}_{14}\text{H}_{13}\text{N}_3\text{Na}]^+$ ($\text{M}+\text{Na}$) $^+$: 246.1002; found: 246.1005.



First step: Oxidation of (*S*)-**1** with *m*-chloroperbenzoic acid (188 mg, percent purity = 55%, 0.6 mmol) was added to a solution of (*S*)-**1** (63.4 mg, 0.3 mmol) in CH_2Cl_2 (3.0 mL) at 0 °C. The mixture was stirred at room temperature until completion (monitored by TLC). After that, the reaction was quenched by addition of saturated aqueous NaHCO_3 . The mixture was extracted with CH_2Cl_2 for three times. The combined organic layer was washed with brine and was dried over anhydrous Na_2SO_4 . After filtration, the solvent was removed under reduced pressure, and the residue was purified by column chromatography on silica gel (ethyl acetate/MeOH = 5:1) to give the pyridine oxide as a colorless oil (44.3 mg, 0.182 mmol, 61%).

Second step: Dimethylcarbamyl chloride (57 μL , 0.62 mmol) was added to a solution of the pyridine oxide synthesized in the previous step (34 mg, 0.14 mmol) and cyanotrimethylsilane (83 μL , 0.66 mmol)

in CH₂Cl₂ (0.8 mL) at 0 °C under nitrogen. The reaction mixture was stirred for 48 h. After that, the mixture was extracted with EtOAc for three times. The combined organic layer was washed with brine and was dried over anhydrous Na₂SO₄. After filtration, the solvent was removed under reduced pressure, and the residue was purified by column chromatography on silica gel (ethyl acetate/ hexane = 5:1) to give the desired product as a white solid (31.5 mg, 0.125 mmol, 89%). The procedure was adapted and modified from a previous report.¹⁰ $[\alpha]_{\text{D}}^{25} = +37.3$ (*c* 1.0, CH₂Cl₂).

¹H NMR (300 MHz, CDCl₃) δ 8.29 (dd, *J* = 7.9, 0.9 Hz, 1H), 7.99 (t, *J* = 7.9 Hz, 1H), 7.85 (dd, *J* = 7.7, 0.9 Hz, 1H), 7.53 – 7.43 (m, 2H), 7.42 – 7.28 (m, 3H), 6.20 (q, *J* = 6.6 Hz, 1H), 1.74 (d, *J* = 6.6 Hz, 3H).

¹³C NMR (75 MHz, CDCl₃) δ 162.8, 150.0, 140.8, 138.2, 134.1, 131.0, 128.6, 128.3, 127.8, 126.2, 116.4, 74.8, 22.1.

HRMS (ESI, *m/z*) calcd for C₁₅H₁₂N₂NaO₂ [M+Na]⁺: 275.0791, found: 275.0800.

4.3.6 Single Crystal X-Ray Analysis of Compound (*R*)-3I

A suitable crystal of C₂₀H₁₆FNO was selected under inert oil and mounted using a MiTeGen loop. Intensity data of the crystal were recorded with a STADIVARI diffractometer (Stoe & Cie). The diffractometer was operated with Cu-K α radiation (1.54186 Å, microfocus source) and equipped with a Dectris PILATUS 300K detector. Evaluation, integration and reduction of the diffraction data was carried out using the X-Area software suite.¹¹ Multi-scan and numerical absorption corrections were applied with the LANA and X-RED32 modules of the X-Area software suite.^{12,13} The structure was solved using dual-space methods (SHELXT-2018/2) and refined against *F*² (SHELXL-2018/3 using ShelXle interface).^{14,15,16} All non-hydrogen atoms were refined with anisotropic displacement parameters. The hydrogen atoms were refined using the “riding model” approach with isotropic displacement parameters 1.2 times (1.5 times for the methyl groups) of that of the preceding carbon atom. The fluorine atom was found to be slightly disordered (5 % probability at the second position) between the two positions corresponding to the ring rotation around the C7–C9 bond. CCDC 2081804 contains the supplementary crystallographic data for this paper. These data can be obtained free of charge from The Cambridge Crystallographic Data Centre via www.ccdc.cam.ac.uk/structures.

Table 4. Selected crystallographic data and details of the structure determination for C₂₀H₁₆FNO.

Identification code	ZCH013
Empirical formula	C ₂₀ H ₁₆ FNO
Molar mass / g·mol ⁻¹	305.34
Space group (No.)	<i>P</i> 2 ₁ 2 ₁ 2 ₁ (19)
<i>a</i> / Å	11.0908(2)
<i>b</i> / Å	11.5946(2)
<i>c</i> / Å	11.9725(2)
<i>V</i> / Å ³	1539.58(5)
<i>Z</i>	4
$\rho_{calc.}$ / g·cm ⁻³	1.317
μ / mm ⁻¹	0.723
Color	colorless
Crystal habitus	block
Crystal size / mm ³	0.249 x 0.248 x 0.196
<i>T</i> / K	100
λ / Å	1.54186 (Cu-K α)
θ range / °	5.311 to 76.052
Range of Miller indices	-13 ≤ <i>h</i> ≤ 12 -12 ≤ <i>k</i> ≤ 14 -15 ≤ <i>l</i> ≤ 12
Absorption correction	multi-scan and numerical
<i>T</i> _{min} , <i>T</i> _{max}	0.5404, 0.8693
<i>R</i> _{int} , <i>R</i> _{σ}	0.0179, 0.0104
Completeness of the data set	0.999
No. of measured reflections	17762
No. of independent reflections	3167
No. of parameters	220
No. of restraints	0
<i>S</i> (all data)	1.020
<i>R</i> (<i>F</i>) (<i>I</i> ≥ 2σ(<i>I</i>), all data)	0.0276, 0.0282
<i>wR</i> (<i>F</i> ²) (<i>I</i> ≥ 2σ(<i>I</i>), all data)	0.0754, 0.0760
Extinction coefficient	0.0039(5)
Flack parameter <i>x</i>	-0.04(6)
$\Delta\rho_{max}$, $\Delta\rho_{min}$ / e·Å ⁻³	0.196, -0.126

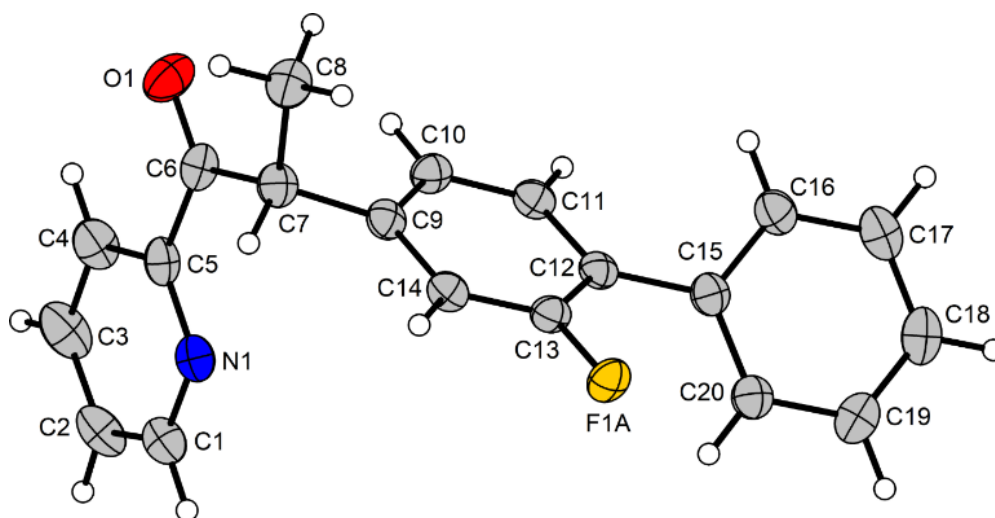


Figure 56. X-ray crystallography. Crystal structure of the deracemized compound (*R*)-**31**. The disordered fluorine atom is shown on the position with its major probability. Displacement ellipsoids are shown at 50% probability level at 100 K. The hydrogen atoms are shown with arbitrary radii.

Reference

1. H. A. Duong, R. E. Gilligan, M. L. Cooke, R. J. Phipps, M. J. Gaunt, *Angew. Chem. Int. Ed.* **2011**, *50*, 463.
2. A. O. Adeniji, M. J. Uddin, T. Zang, D. Tamae, P. Wangtra-kuldee, L. J. Marnett, T. M. Penning, *J. Med. Chem.* **2016**, *59*, 7431.
3. J. F. Eaddy, III, D. Heyer, S. R. Katamreddy, M. T. Martin, M. S. McClure, A. S. Randhawa, V. Samano, J. A. Ray, WO 2005033056, 14 April 2005.
4. A. Recio, J. A. Tunge, *Org. Lett.* **2009**, *11*, 5630.
5. H. Yang, N. Huo, P. Yang, H. Pei, H. Lv and X.-M. Zhang, *Org. Lett.* **2015**, *17*, 4144.
6. C. Sabot, K. A. Kumar, C. Antheaume and C. Mioskowski, *J. Org. Chem.* **2007**, *72*, 5001.
7. P. Zhang, D. Huang and T. R. Newhouse, *J. Am. Chem. Soc.* **2020**, *142*, 1757.
8. J. Li, J.-Z. Chen, W. Jiao, G.-Q. Wang, Y. Li, X. Cheng and G.-G. Li, *J. Org. Chem.* **2016**, *81*, 9992.
9. C. Ayya Swamy, P. A. Varenikov, G. de Ruiter, *Chem. Eur. J.* **2020**, *26*, 2333.
10. S. Barroso, G. Blay, J. R. Pedro, *Org. Lett.* **2007**, *9*, 1983.
11. *X-Area*, STOE & Cie GmbH, Darmstadt, Germany, **2018**.
12. *LANA - Laue Analyzer*, STOE & Cie GmbH, Darmstadt, Germany, **2019**.
13. *X-RED32*, STOE & Cie GmbH, Darmstadt, Germany, **2018**.
14. G. M. Sheldrick, *Acta Crystallogr., Sect. A: Found. Adv.* **2015**, *71*, 3–8.
15. G. M. Sheldrick, *Acta Crystallogr., Sect. C: Struct. Chem.* **2015**, *71*, 3–8.
16. C. B. Hübschle, G. M. Sheldrick, B. Dittrich, *J. Appl. Crystallogr.* **2011**, *44*, 1281.

Chapter 5: Appendices

5.1 List of Abbreviations

$^1\text{H NMR}$	proton nuclear magnetic resonance spectroscopy
$^{13}\text{C NMR}$	carbon nuclear magnetic resonance spectroscopy
$^9\text{F NMR}$	fluorine nuclear magnetic resonance spectroscopy
δ	chemical shift
J	coupling constant
br	broad
s	singlet
d	doublet
t	triplet
q	quartet
m	multiplet
ppm	parts per million
aq	aqueous
Ar	Aryl-group
bpy	2,2'-bipyridine
$\text{CH}_2\text{Cl}_2/\text{DCM}$	dichloromethane
CD_2Cl_2	dideuteromethylenechloride
CHCl_3	chloroform
CDCl_3	deuteriochloroform
$\text{CH}_3\text{CN}/\text{MeCN}$	acetonitrile
conc	concentrated
DMAP	4-dimethylaminopyridine
DMF	dimethylformamide
DMSO	dimethyl sulfoxide
dr	diastereomeric ratio
ee	enantiomeric excesses
Et_2O	diethyl ether
Et_3N	triethyl amine
EtOAc	ethyl acetate
HAT	hydrogen atom transfer
h	hour(s)
HPLC	high performance liquid chromatography
HRMS	high resolution mass spectrometry
IR spectra	infrared spectra
Ir	iridium

Chapter 5. Appendices

Rh	rhodium
L	liter(s)
M	mol/liter
<i>m</i>	meta-
min	minute(s)
mL	milliliter(s)
mmol	millimole
MS	mass spectroscopy
N ₂	nitrogen
Ph	phenyl
ppm	parts per million
<i>rac</i>	racemate
rt	room temperature
TFA	trifluoroacetic acid
THF	tetrahydrofuran
TLC	thin layer chromatography

5.2 List of Figures

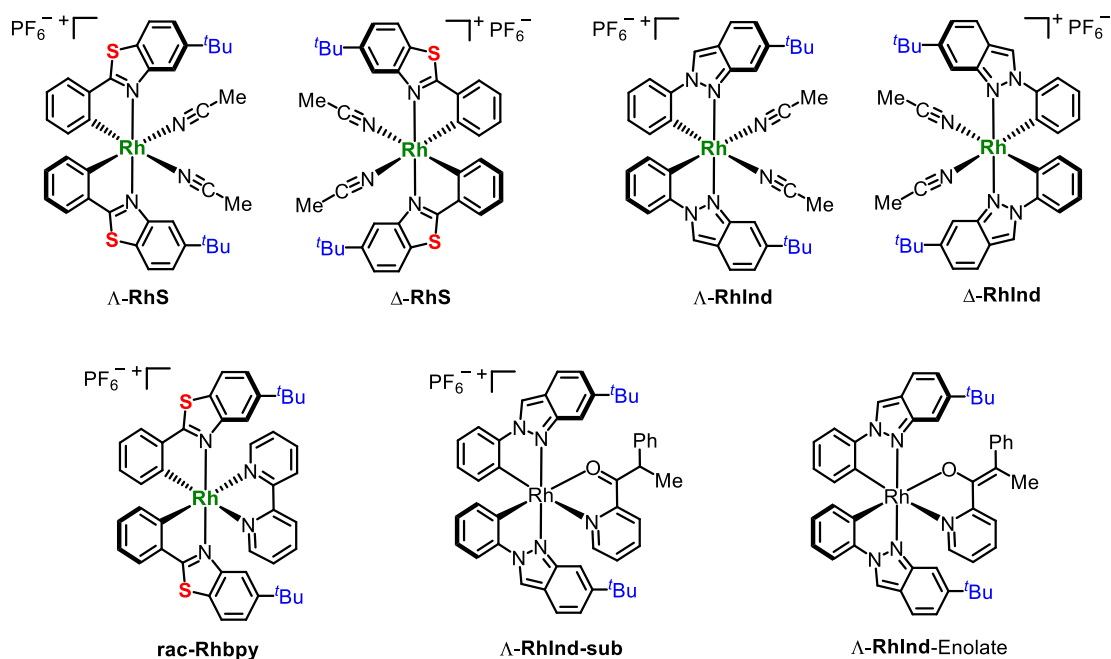
Figure 1. Photocatalysts possible quenching pathways. ISC = intersystem crossing.	1
Figure 2. Substrate activation through photoinduced intermolecular HAT promoted through a direct or indirect photocatalytic approach.	2
Figure 3. Representative direct HAT photocatalysts and representative indirect HAT reagents.	3
Figure 4. Photoinduced enantioselective alkynylation of C(sp ³)–H bonds, TBS = <i>tert</i> -butyldimethylsilyl.	4
Figure 5. sp ³ C–H arylation and alkylation enabled by the synergy of triplet excited ketones and nickel catalysts.	5
Figure 6. Proposed mechanism for selective C(sp ³)–H functionalization.	6
Figure 7. A radical Smiles rearrangement promoted by neutral eosin Y.	7
Figure 8. The fluorination of unactivated C(sp ³)–H by UO ₂ ²⁺ and NFSI.	8
Figure 9. Diacetyl as a direct HAT photosensitizer in Minisci alkylation.	9
Figure 10. Photoinduced C–H alkylation of alcohols.	10
Figure 11. Photoinduced C–H arylation through photoredox, quinuclidine, and nickel catalysis.	11
Figure 12. C–H activation in alkanes through the action of photogenerated amidyl radical.	12
Figure 13. Arylation of C(sp ³)–H bonds through the action of photogenerated sulfonamidyl radical.	13
Figure 14. Electrophotocatalytic arylation of ether.	14
Figure 15. Photoinduced arylation of ethers using persulfate as an indirect HAT reagent.	15
Figure 16. The nitrate radical induced oxidation of alkynes and alcohols.	16
Figure 17. The difunctionalization of simple alkenes for the synthesis of α,β-epoxy ketones.	17
Figure 18. Photoinduced C(sp ³)–H trifluoromethylthiolation using benzoate salt as an indirect HAT catalyst.	18
Figure 19. Photoinduced C(sp ³)–H amination using alcohols as indirect HAT catalyst.	19
Figure 20. Photoinduced allylic arylation with triisopropylsilanethiol as an indirect HAT catalyst. ...	20
Figure 21. Photoinduced C–H alkylation of heteroarenes with alcohols as the alkylating reagents. ...	21
Figure 22. C(sp ³)–H cross-coupling enabled by the catalytic generation of chlorine radicals by nickel and photoredox catalysis.	22
Figure 23. Hydrogen atom transfer reactions via photoredox catalyzed chlorine radical generation. .	23
Figure 24. C(sp ³)–H cross-coupling enabled by the catalytic generation of bromine radical by nickel and photoredox catalysis.	24
Figure 25. Enantioselective α-amino C(sp ³)–H acylation enabled by the catalytic generation of bromine radical by nickel and photoredox catalysis.	25
Figure 26. α-functionalization of boronate complexes via trifluoromethyl radicals.	26
Figure 27. Photoredox-catalyzed remote C(sp ³)–H alkylation via an amidyl radical.	27
Figure 28. Photocatalytic iminyl radical-mediated γ-alkylation of α-iminoxy-acids.	28
Figure 29. Visible-light-induced allylation and alkylation of remote C(sp ³)–H bonds of alcohols.	29
Figure 30. Photoredox catalyzed C(sp ²)-radical mediated remote C(sp ³)–H vinylation.	30
Figure 31. Photoredox catalyzed 1,6-carboalkylation of alkenes.	31
Figure 32. Previous reports and this design for asymmetric photocatalysis by intramolecular hydrogen atom transfer.	34
Figure 33. Substrate scope. Standard conditions (entry 4 of Table 1) were applied if not indicated otherwise. Modified reaction conditions were used for obtaining products 2m , 2s , and 2u . ^[a] Catalyst loading of 8 mol% was used to increase the ee. ^[b] Reduced substrate concentration of 0.005 M was used to improve the yield. ^[c] Photolysis with weaker blue LEDs (3 W, 420 nm) for 10 h afforded an improved yield. ^[d] 1,2-Dichloroethane was used as the solvent which provided a higher ee.	36
Figure 34. Proposed mechanism.	37
Figure 35. Mechanistic experiments. UV/Vis-absorption spectra measured in CH ₂ Cl ₂ (0.05 mm).	38
Figure 36. Computational study. a) Computed free energy diagram of the photoinduced HAT/hetero-Diels-Alder cascade reaction catalyzed by Δ-RhS. b) Calculated transition states for the intramolecular hetero-Diels-Alder reaction leading to major and minor product enantiomers. Energies are in kcal/mol, and interatomic distances are in ångströms. Hydrogen atoms are omitted for clarity. c) Two different calculated triplet excited states, II-1 and II-2 , for the Rh-bound substrate. Interatomic distances denoted in ångströms. Hydrogens are omitted for clarity. Spin densities on atoms are shown with red italic numbers.	40

Figure 37. Subjected the compound 2d to reductive ozonolysis.	41
Figure 38. Previous work on light-driven deracemization, most established strategy for α -functionalization of carbonyls and the methods of synthesizing chiral α -tertiary carbonyl compounds by catalytic asymmetric protonation.	44
Figure 39. Catalytic deracemization of carbonyl compounds in α -position: motivation, mechanistic plan and realization.	46
Figure 40. Substrate scope with pyridylketones bearing an aryl group at the stereocenter. Py = 2-pyridyl. Standard reaction conditions according to Table 2, entry 14. ^a Deviation from standard reaction conditions: 3.0 equivalents of <i>N</i> -phenylpiperidine (B5) instead. The absolute configuration of compound (R)- 3I was determined by X-ray crystallography (CCDC 2081804).	50
Figure 41. Expanded substrate scope. The combination of catalyst and base varied for optimal results. ^a Λ -RhS (8.0 mol%) as catalyst and 3,5-(<i>t</i> Bu) ₂ PhCH ₂ N(<i>i</i> Pr) ₂ (3.0 equiv) as base. ^b Λ -RhS (4.0 mol%) as catalyst and <i>N</i> -phenylpiperidine as base (3.0 equiv). ^c Λ -RhInd (4.0 mol%) as catalyst and <i>N</i> -phenylazepane as base (3.0 equiv). ^d Λ -RhInd (4.0 mol%) as catalyst and <i>N</i> -phenylpiperidine (3.0 equiv) as base. ^e Λ -RhInd (8.0 mol%) as catalyst and <i>N</i> -phenylpiperidine (3.0 equiv) as base. ^f Λ -RhInd (4.0 mol%) as catalyst and <i>N,N</i> -diisopropylethylamine (3.0 equiv) as base.	51
Figure 42. Proposed mechanism for the developed photoderacemization.	52
Figure 43. Supporting mechanistic experiments. bpy = 2,2'-bipyridine.	54
Figure 44. Computational study. (a) Calculated free energy diagram of the Λ -RhInd-catalyzed conversion of (<i>S</i>)- 3a into (<i>R</i>)- 3a at the ω B97X-D/def2-TZVPP-SDD(Rh), SMD (acetone)//B3LYP-D3BJ/def2-SVP-LANL2DZ(Rh) level of theory. (b) Calculated geometries and relative free energies (kcal/mol) of intermediates. Interatomic distances are shown in ångströms (Å).	55
Figure 45. Follow-up chemistry. Conversions starting from compound (<i>S</i>)- 3a	56
Figure 46. Asymmetric photorearrangement to benzo-[d]cyclopropa[b]pyranones involving intramolecular hydrogen atom transfer.	59
Figure 47. Photoinduced deracemization of carbonyl compounds via photoredox deprotonation and enantioselective protonation.	60
Figure 48. Emission spectrum of the 24 W blue LEDs lamp use in this study. Picture from Christian P. Haas.	64
Figure 49. UV/Vis absorption spectra of 1d (0.05 mM), RhS (0.05 mM) and RhS-1d (0.05 mM). ...	88
Figure 50. Crystal structure of 2k	93
Figure 51. UV/Vis-absorbance measurements. UV/Vis absorption spectra of substrate 1 , catalyst RhInd , and the substrate-coordinated catalyst RhInd /substrate 1 (complex I). Recorded in acetone at concentrations of 0.2 mM.	134
Figure 52. Cyclic voltammetry. Cyclic voltammograms of substrate 1 , the catalyst RhInd , and the substrate-coordinated catalyst RhInd /substrate 1 (complex I). Measured in CH ₂ Cl ₂ (0.6 mM) containing <i>n</i> Bu ₄ NBF ₄ (0.1 M) at a scan rate = 0.1 V/s.	135
Figure 53. ¹ H NMR analysis of the deuterated (<i>R</i>)- 4d when use deuterated rac- 4d as the starting material.	136
Figure 54. ¹ H NMR analysis of the deuterated (<i>R</i>)- 4d when add 1 equiv D ₂ O.	137
Figure 55. ¹ H NMR spectrum of RhInd /substrate 3a and enolate complex III	139
Figure 56. X-ray crystallography. Crystal structure of the deracemized compound (<i>R</i>)- 3I . The disordered fluorine atom is shown on the position with its major probability. Displacement ellipsoids are shown at 50% probability level at 100 K. The hydrogen atoms are shown with arbitrary radii.	146

5.3 List of Tables

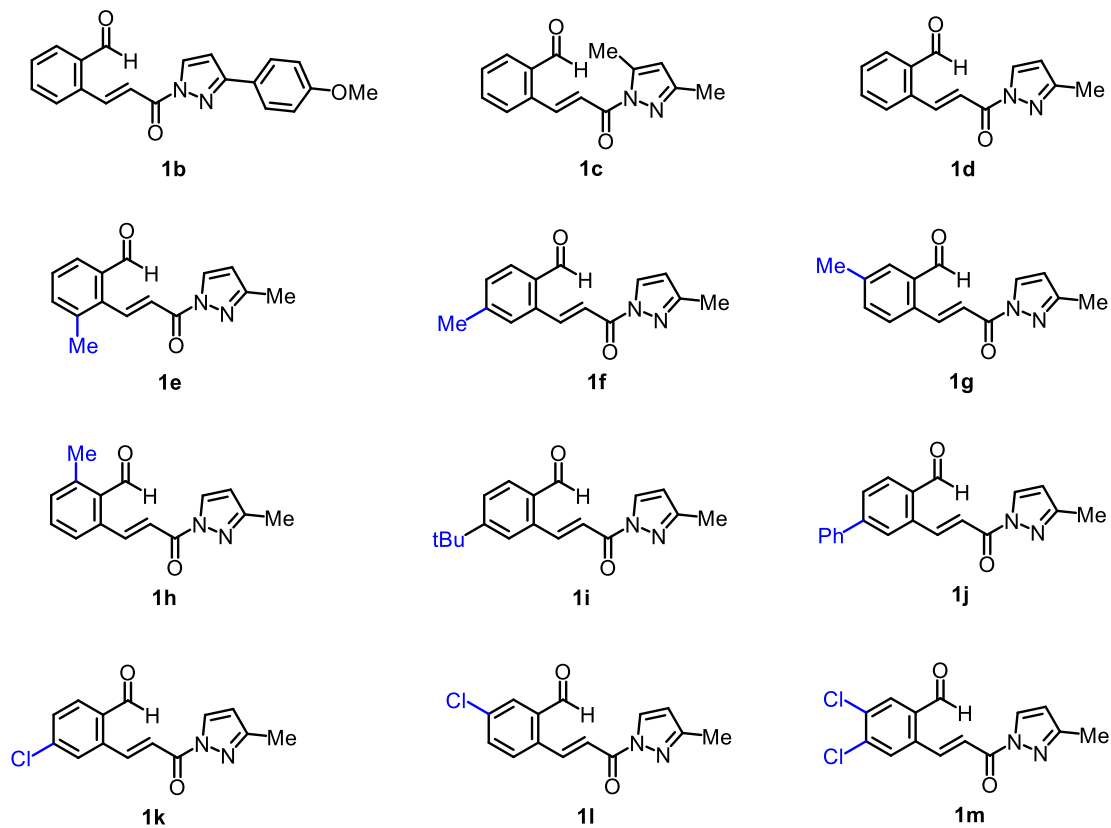
Table 1. Initial experiments and optimization of reaction conditions ^[a]	35
Table 2. Initial experiments and optimization. ^a	48
Table 3. Crystal data and structure refinement for 2k	94
Table 4. Selected crystallographic data and details of the structure determination for C ₂₀ H ₁₆ FNO. ...	145

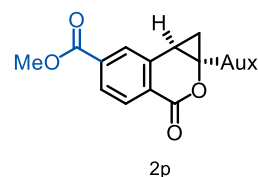
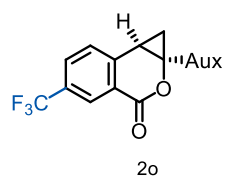
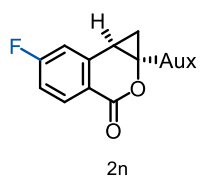
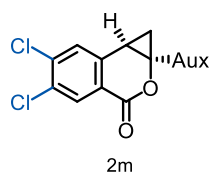
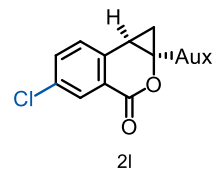
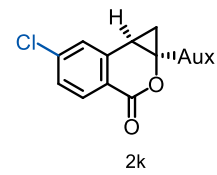
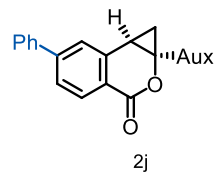
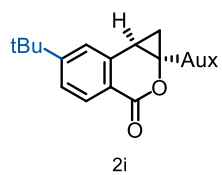
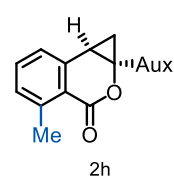
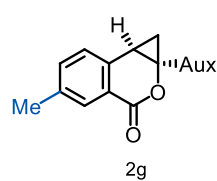
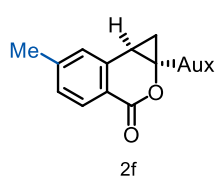
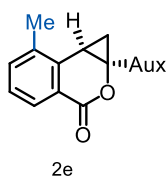
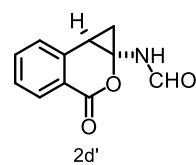
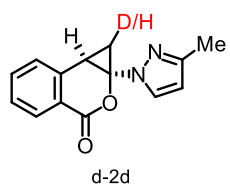
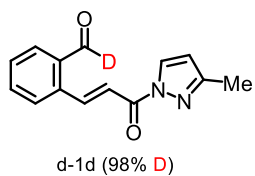
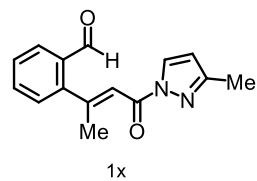
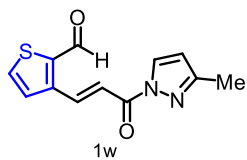
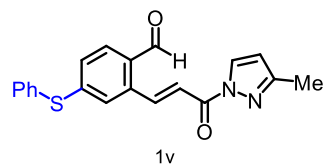
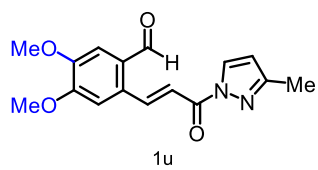
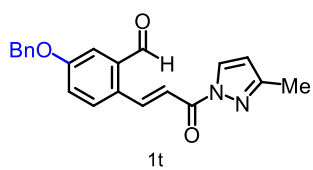
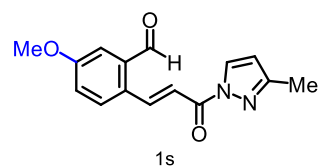
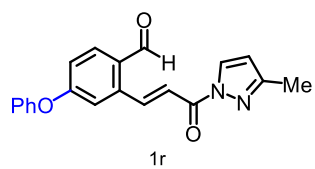
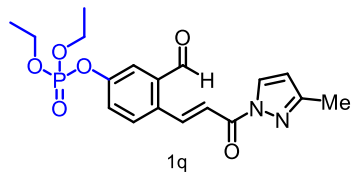
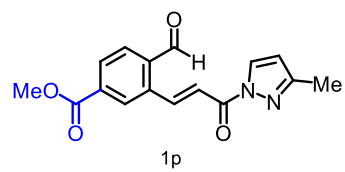
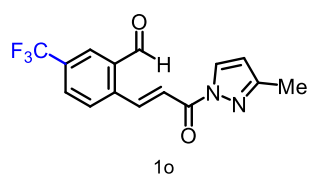
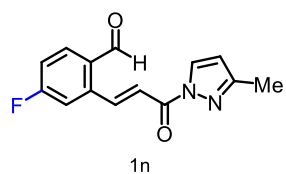
5.4 List of Organometallic Complexes

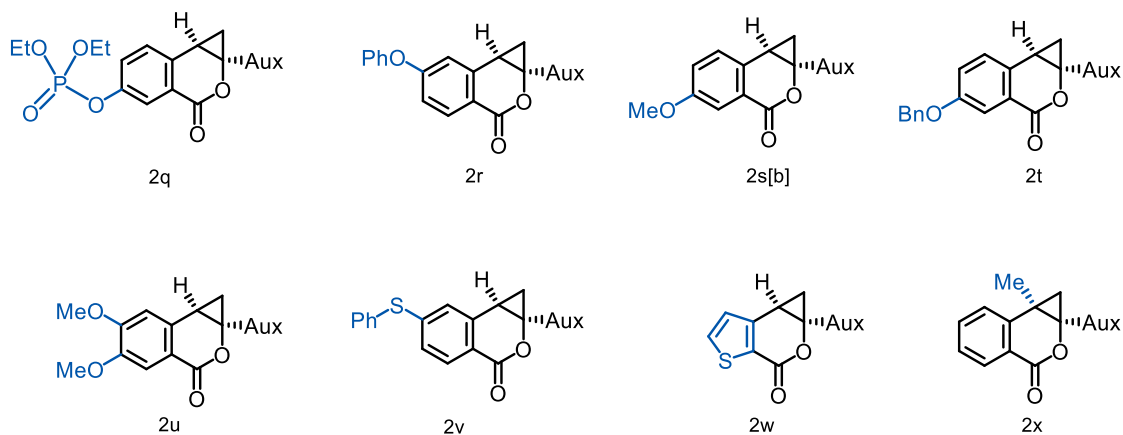


5.5 List of Organic Compounds

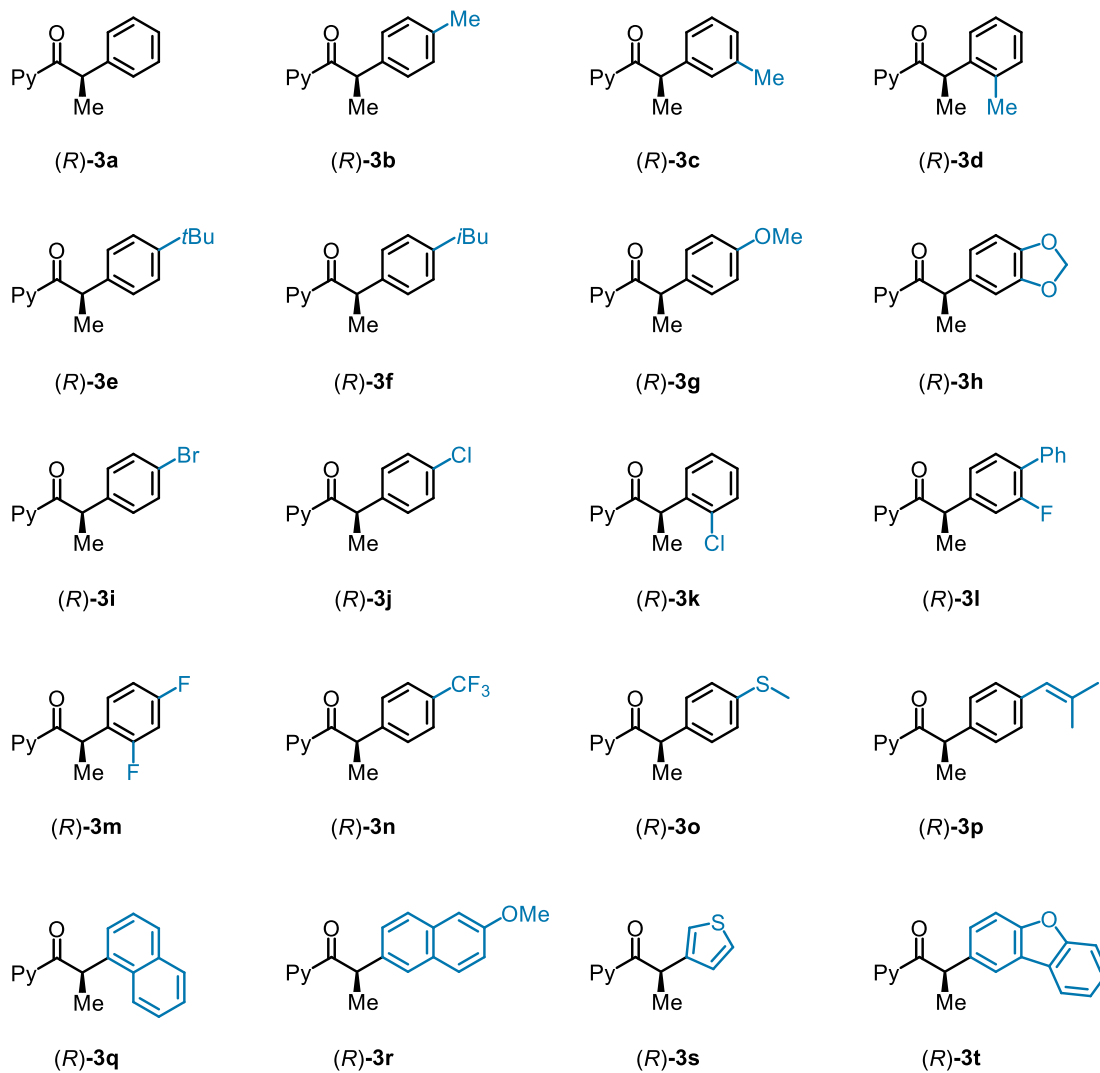
(1) Chapter 2.1 and its Experimental Part

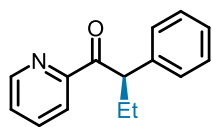




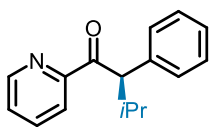


(2) Chapter 2.2 and its Experimental Part

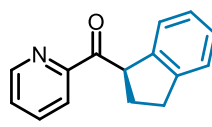




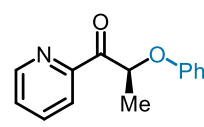
(R)-3u



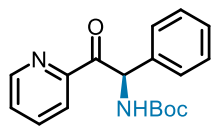
(R)-3v



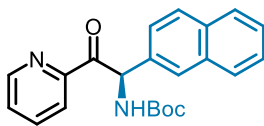
(R)-3w



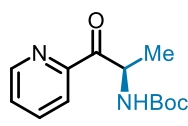
(S)-3x



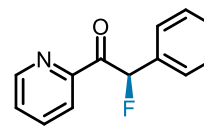
(R)-3y



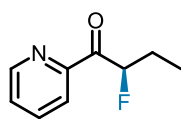
(R)-3z



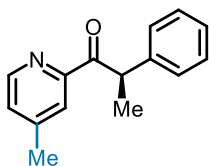
(R)-3aa



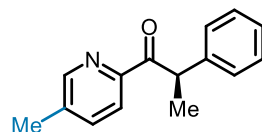
(R)-3ab



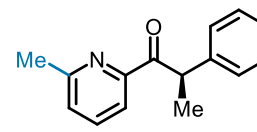
(R)-3ac



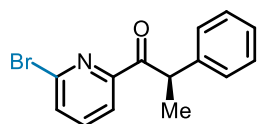
(R)-3ad



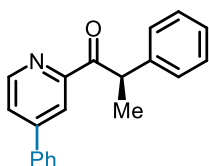
(R)-3ae



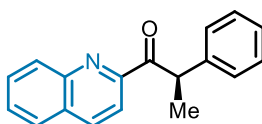
(R)-3af



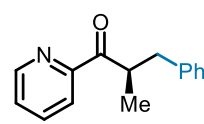
(R)-3ag



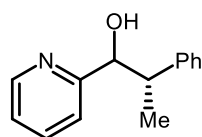
(R)-3ah



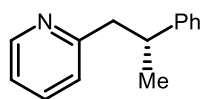
(R)-3ai



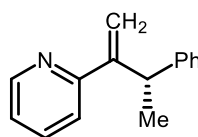
(R)-3aj



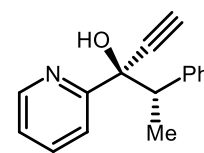
8



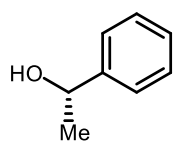
9



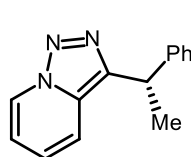
10



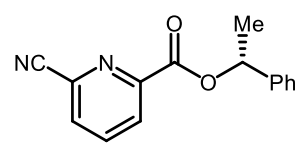
11



12

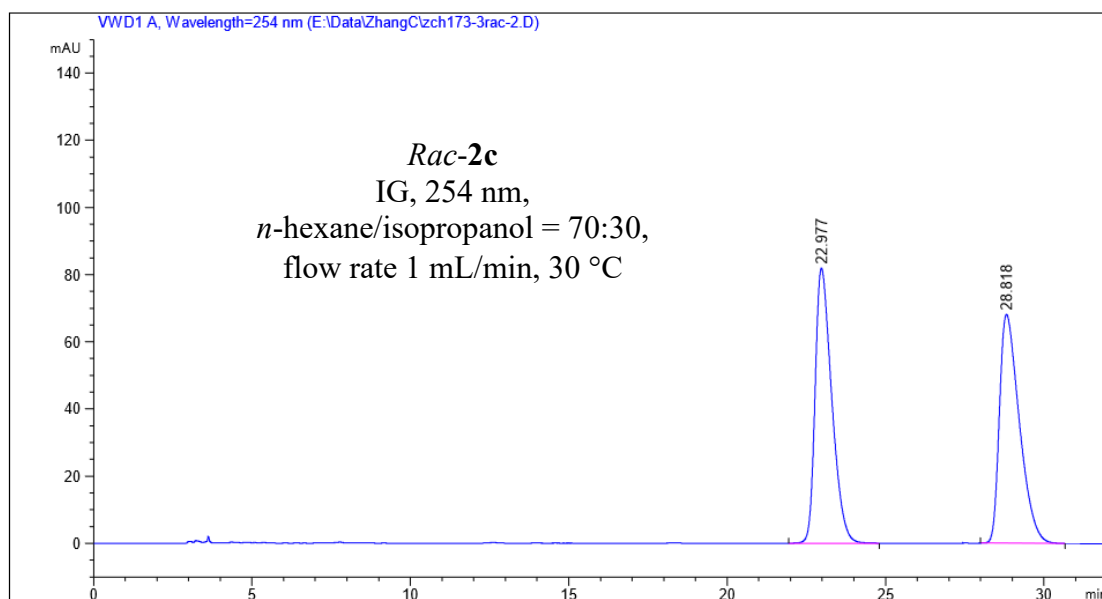


13

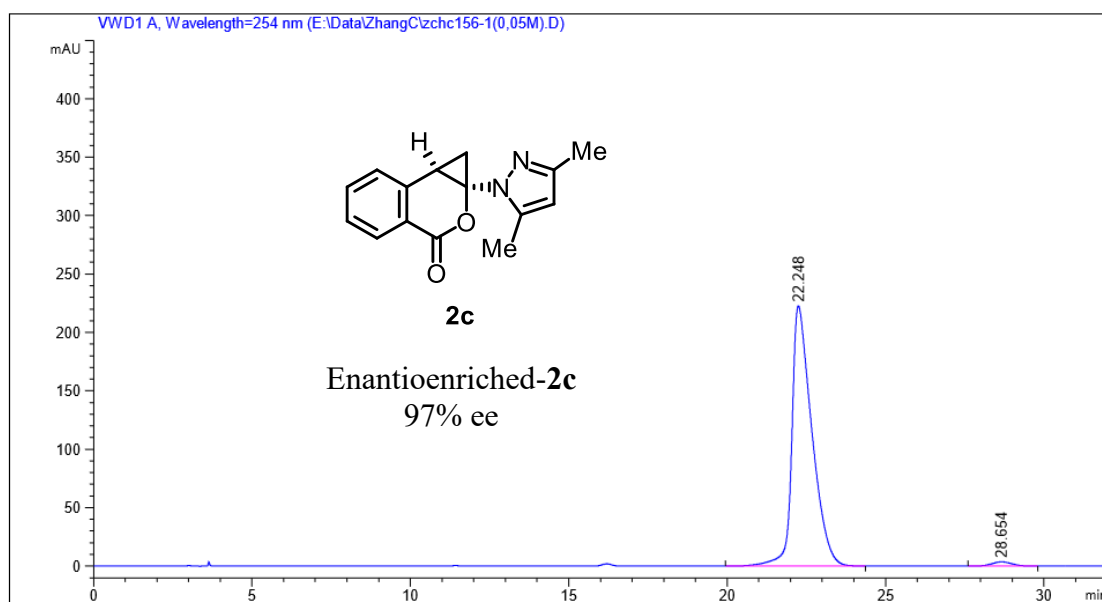


14

5.6 Enantiomeric Excess for Catalytic Reactions

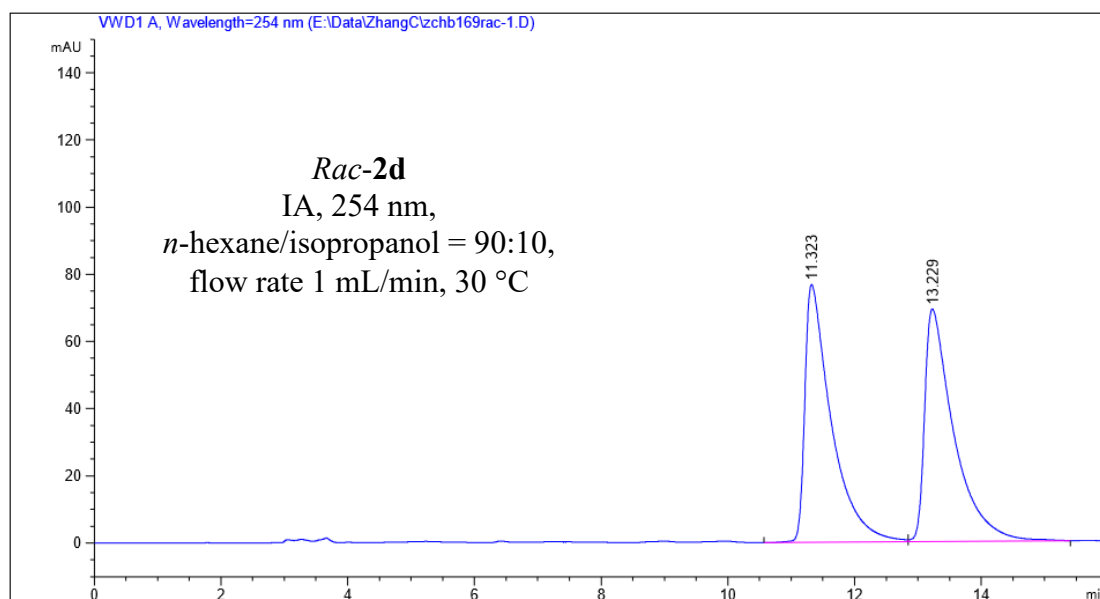


Peak #	RetTime [min]	Type	Width [min]	Area [mAU*s]	Height [mAU]	Area %
1	22.977	BB	0.5535	2979.61060	81.89731	50.0061
2	28.818	BB	0.6671	2978.88550	68.12800	49.9939

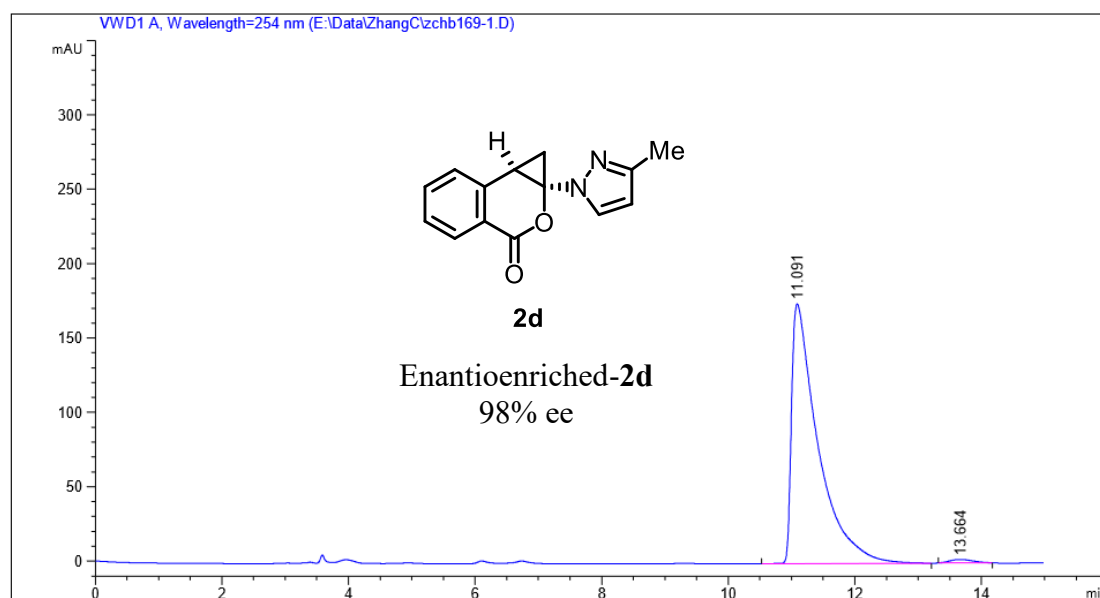


Peak #	RetTime [min]	Type	Width [min]	Area [mAU*s]	Height [mAU]	Area %
1	22.248	BB	0.6476	9784.43750	222.70468	98.3834
2	28.654	BB	0.6538	160.77577	3.62973	1.6166

Figure 57. HPLC traces of *rac-2c* (reference) and enantioenriched-**2c**.

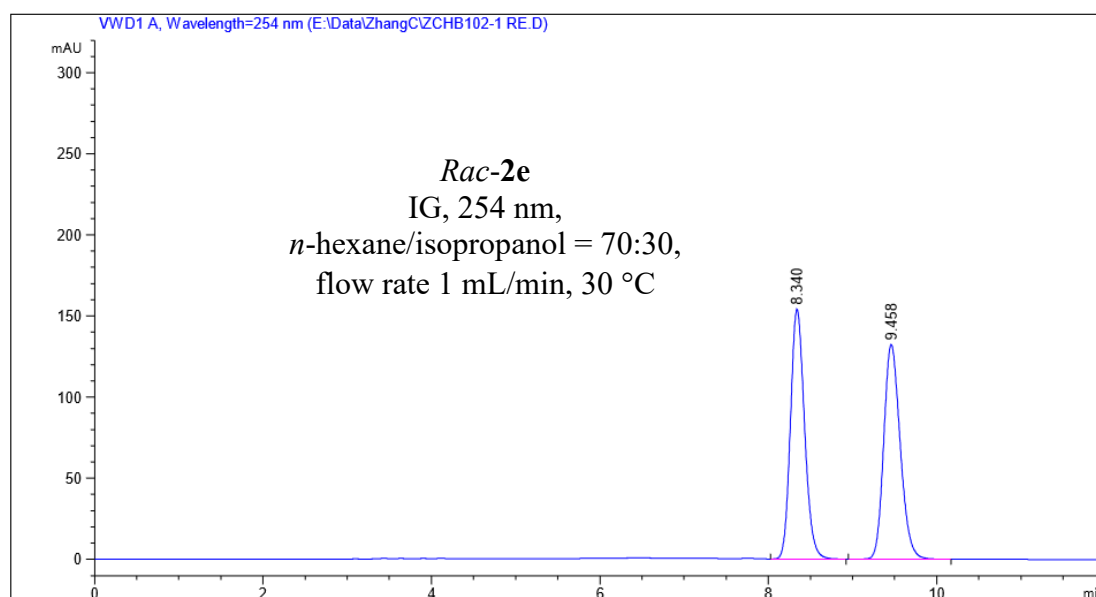


Peak #	RetTime [min]	Type	Width [min]	Area [mAU*s]	Height [mAU]	Area %
1	11.323	BV	0.4124	2225.82007	76.74575	50.1317
2	13.229	VB	0.4569	2214.12891	69.26335	49.8683

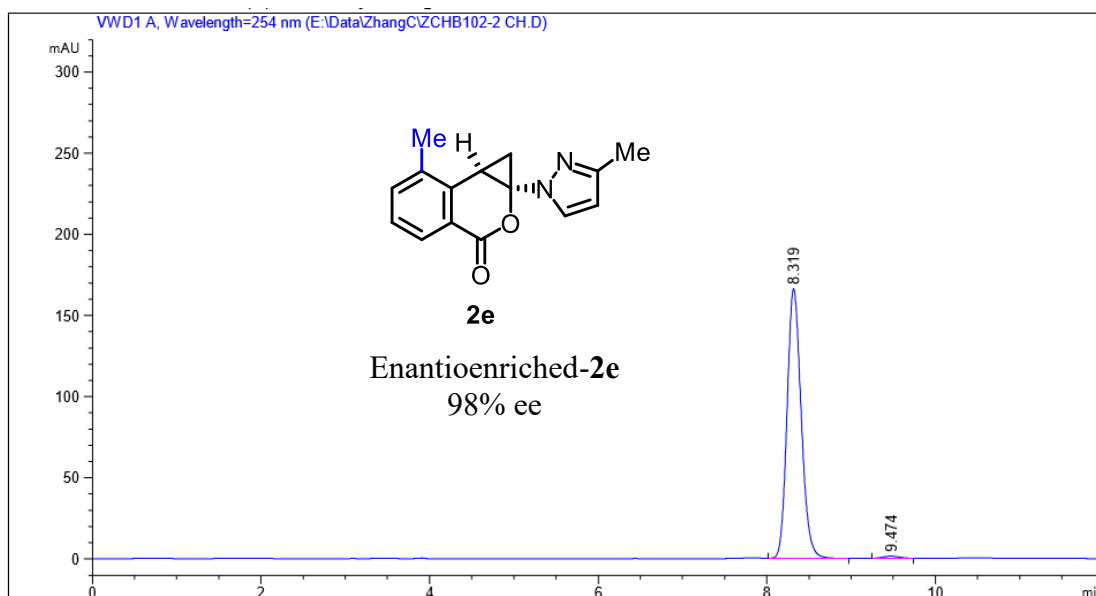


Peak #	RetTime [min]	Type	Width [min]	Area [mAU*s]	Height [mAU]	Area %
1	11.091	BB	0.4071	5040.97607	174.48216	98.9862
2	13.664	MM R	0.3904	51.62853	2.20416	1.0138

Figure 58. HPLC traces of *rac*-**2d** (reference) and enantioenriched-**2d**.

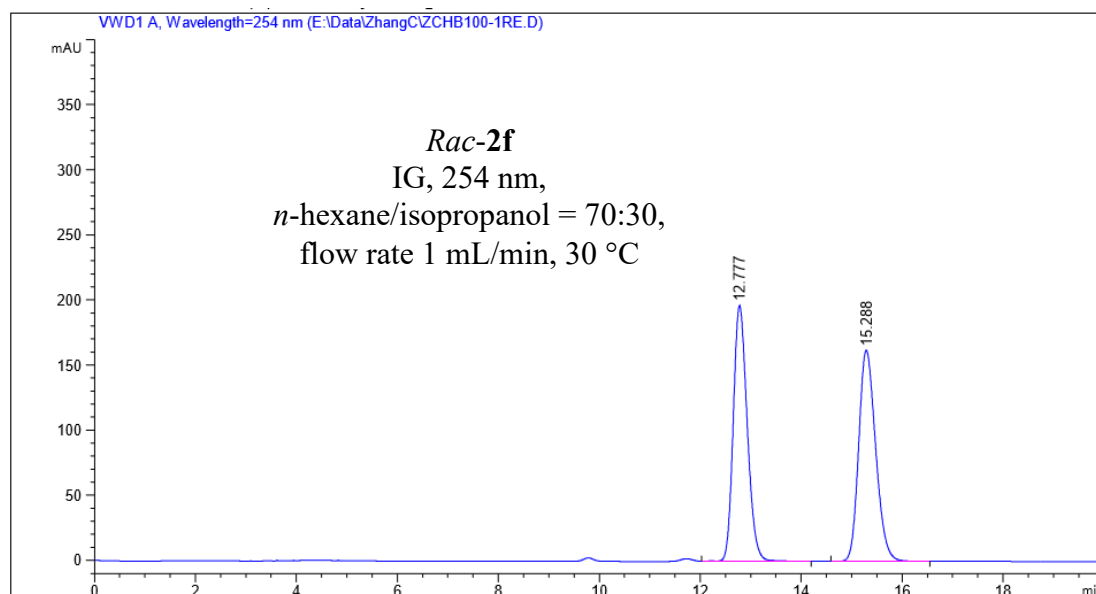


Peak #	RetTime [min]	Type	Width [min]	Area [mAU*s]	Height [mAU]	Area %
1	8.340	BB	0.1798	1793.07068	154.08856	49.9079
2	9.458	BB	0.2107	1799.68884	132.33784	50.0921

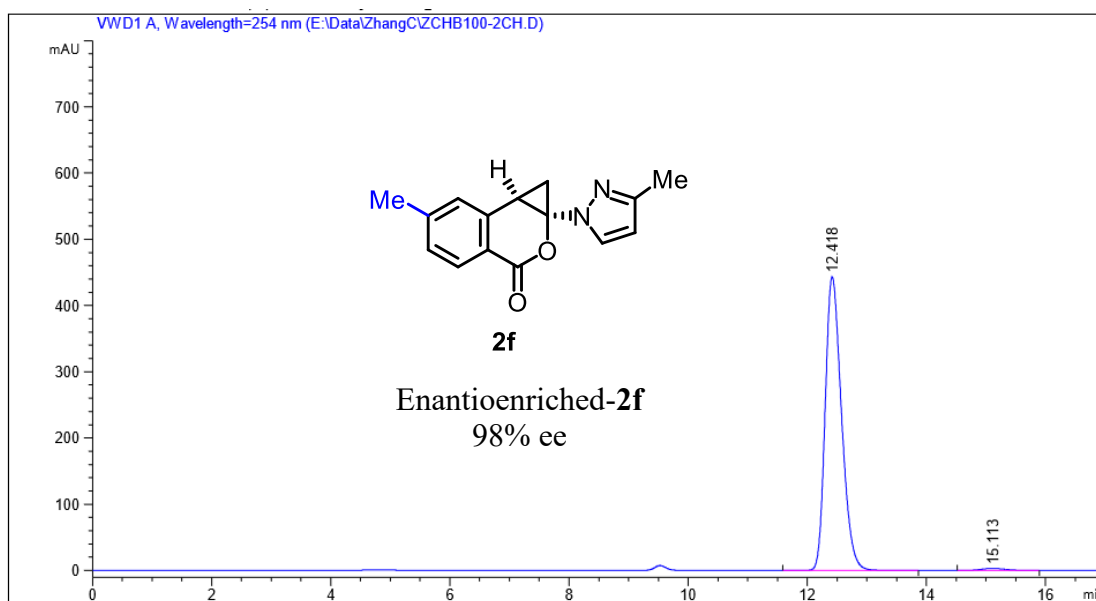


Peak #	RetTime [min]	Type	Width [min]	Area [mAU*s]	Height [mAU]	Area %
1	8.319	BB	0.1794	1926.47522	165.99669	99.0420
2	9.474	MM R	0.2234	18.63387	1.38997	0.9580

Figure 59. HPLC traces of *rac-2e* (reference) and enantioenriched-**2e**.

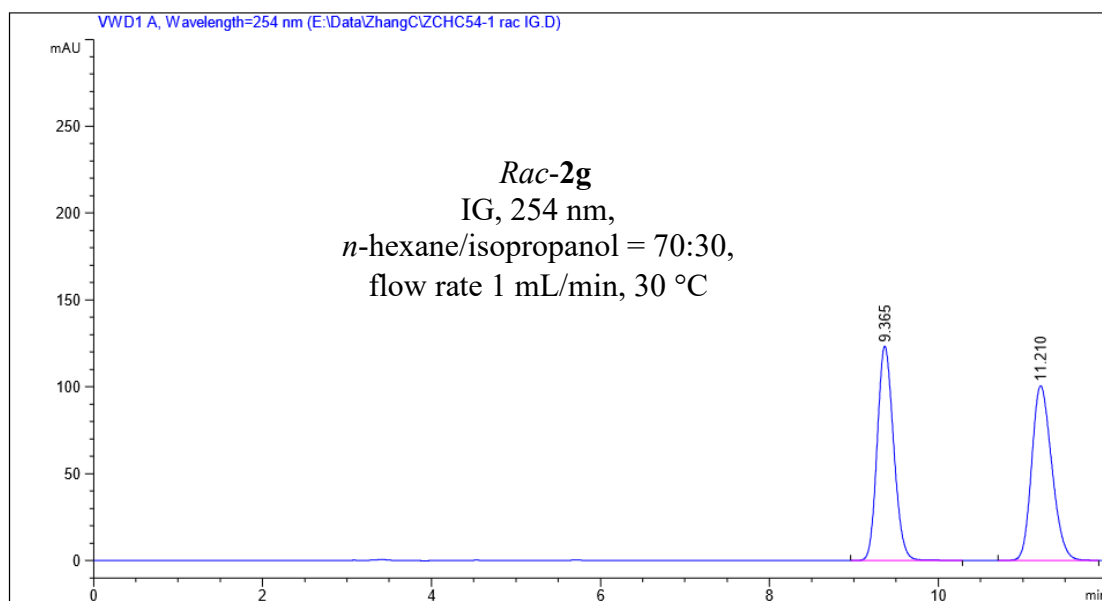


Peak #	RetTime [min]	Type	Width [min]	Area [mAU*s]	Height [mAU]	Area %
1	12.777	VB R	0.2982	3774.15698	196.41737	49.9179
2	15.288	BB	0.3614	3786.57324	162.14777	50.0821

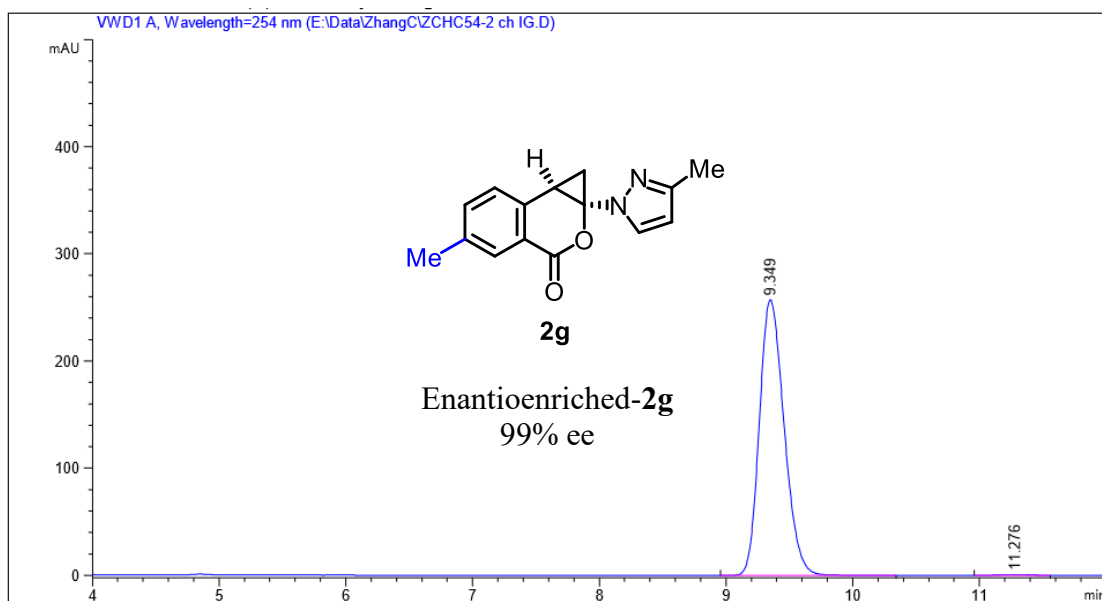


Peak #	RetTime [min]	Type	Width [min]	Area [mAU*s]	Height [mAU]	Area %
1	12.418	BB	0.2940	8436.13184	443.40787	98.9299
2	15.113	BB	0.4308	91.25233	3.18932	1.0701

Figure 60. HPLC traces of *rac*-3f (reference) and enantioenriched-3f.

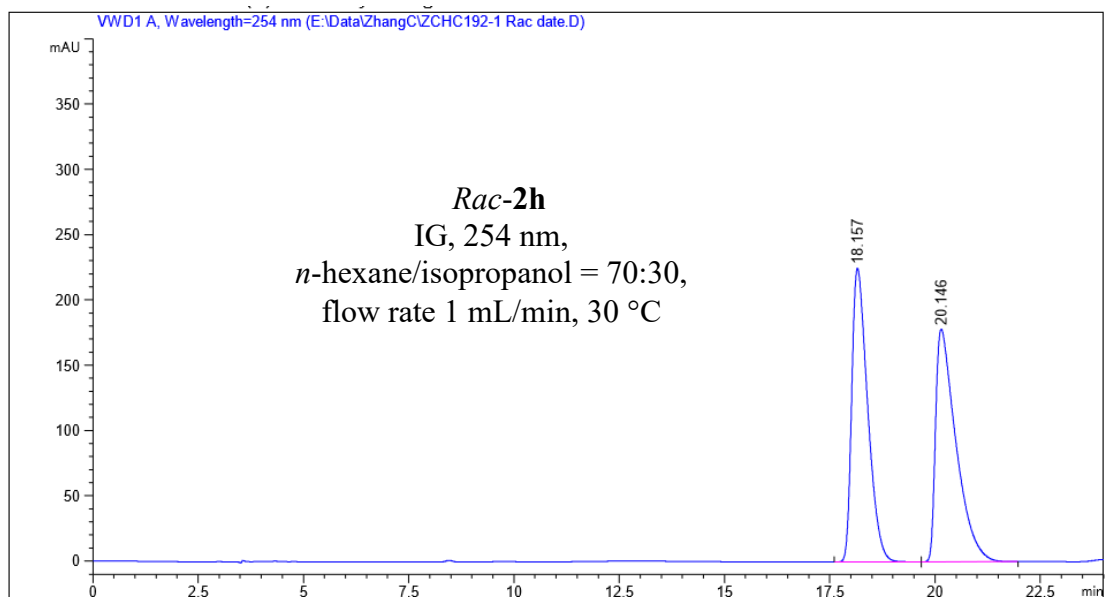


Peak #	RetTime [min]	Type	Width [min]	Area [mAU*s]	Height [mAU]	Area %
1	9.365	BB	0.2104	1663.66113	123.32854	50.0027
2	11.210	BB	0.2569	1663.48364	100.58227	49.9973

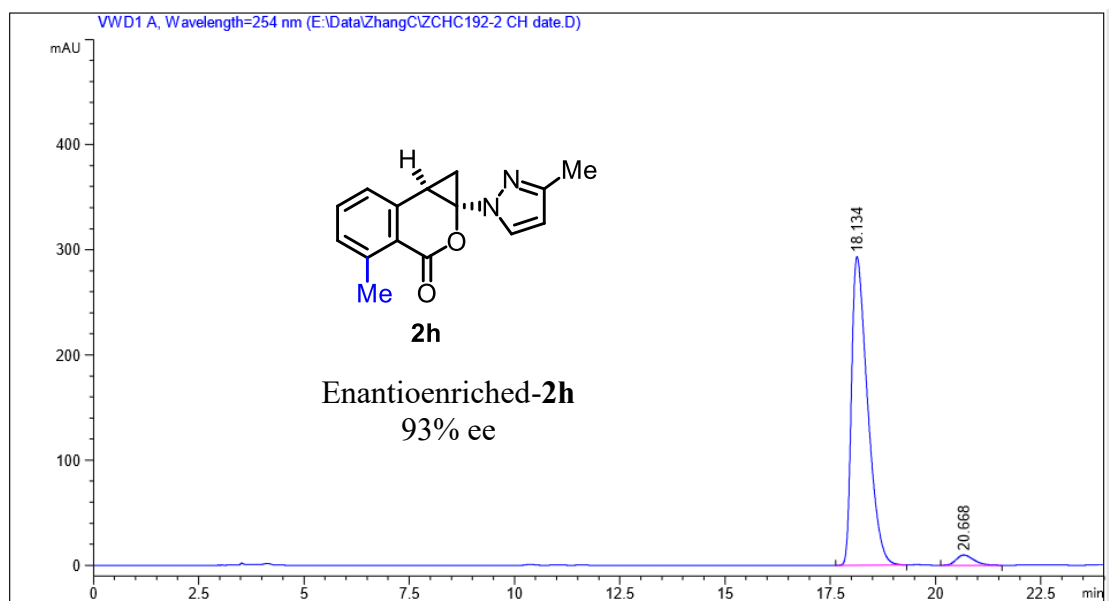


Peak #	RetTime [min]	Type	Width [min]	Area [mAU*s]	Height [mAU]	Area %
1	9.349	BB	0.2113	3489.33691	257.17743	99.4878
2	11.276	MM R	0.2706	17.96380	1.10643	0.5122

Figure 61. HPLC traces of *rac-2g*(reference) and enantioenriched-**2g**.

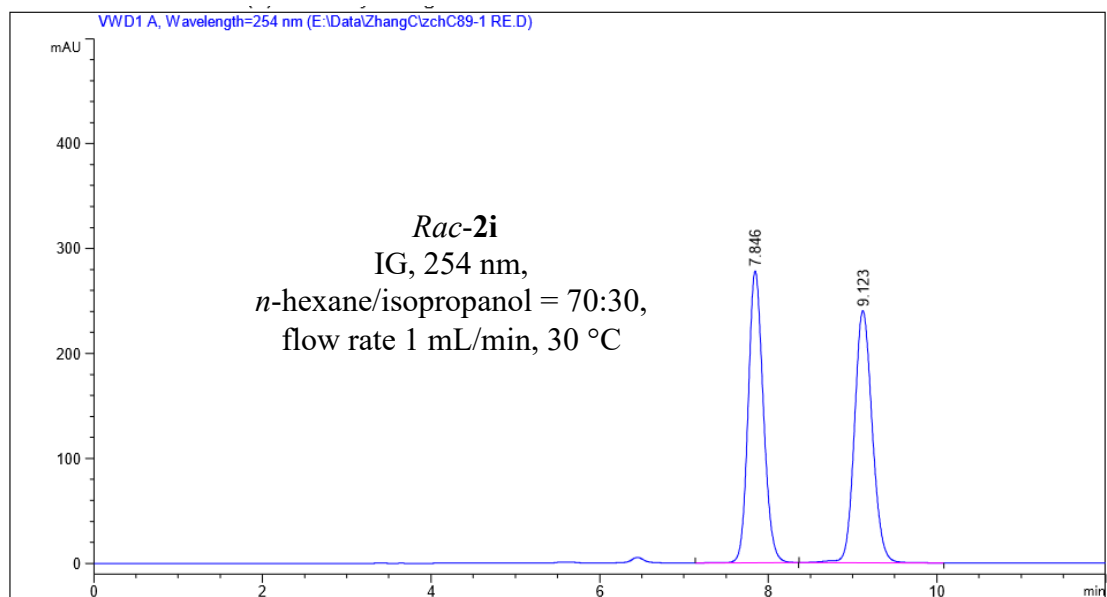


Peak #	RetTime [min]	Type	Width [min]	Area [mAU*s]	Height [mAU]	Area %
1	18.157	BB	0.4023	5905.54395	224.90198	49.5951
2	20.146	BB	0.4960	6001.98193	178.15488	50.4049

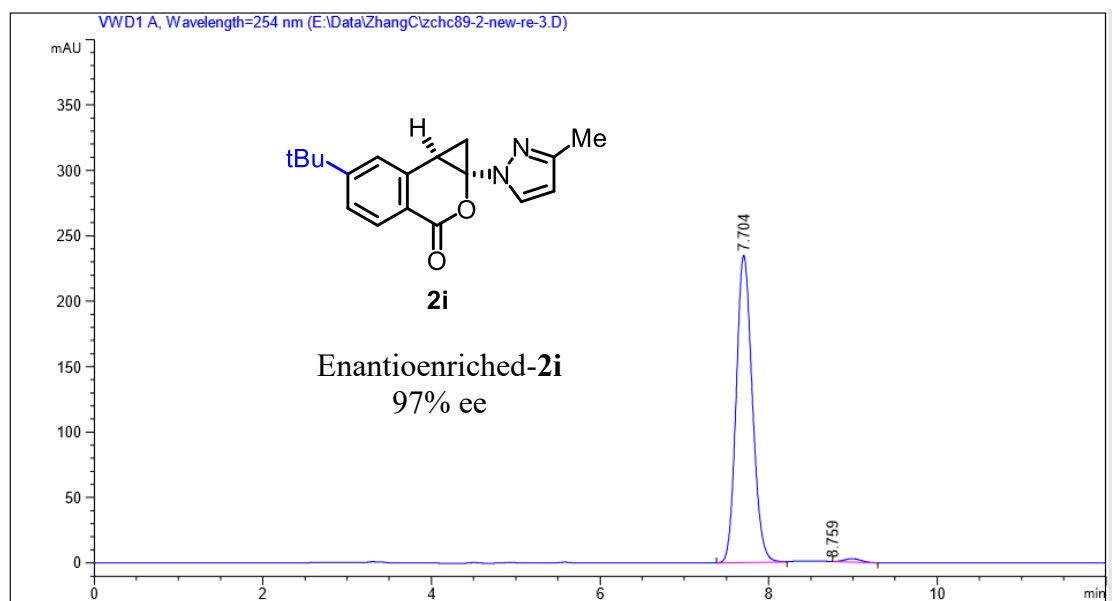


Peak #	RetTime [min]	Type	Width [min]	Area [mAU*s]	Height [mAU]	Area %
1	18.134	BB	0.4022	7775.54395	293.34097	96.5046
2	20.668	BB	0.4451	281.63449	9.77737	3.4954

Figure 62. HPLC traces of *rac*-**2h** (reference) and enantioenriched-**2h**.

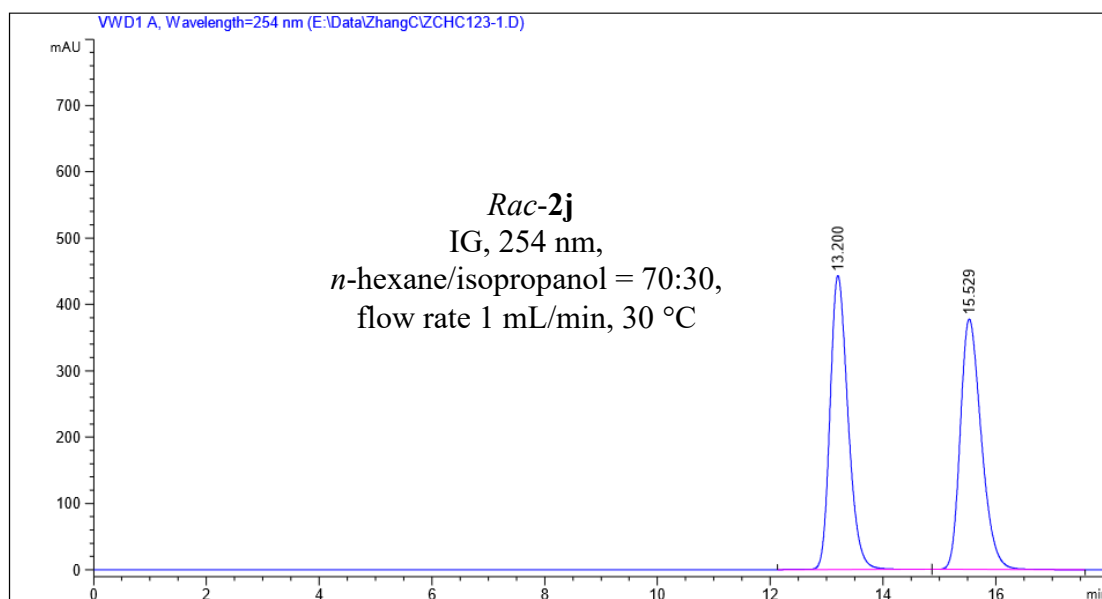


Peak #	RetTime [min]	Type	Width [min]	Area [mAU*s]	Height [mAU]	Area %
1	7.846	BB	0.1924	3466.36865	278.11047	49.6205
2	9.123	BB	0.2258	3519.38721	240.33003	50.3795

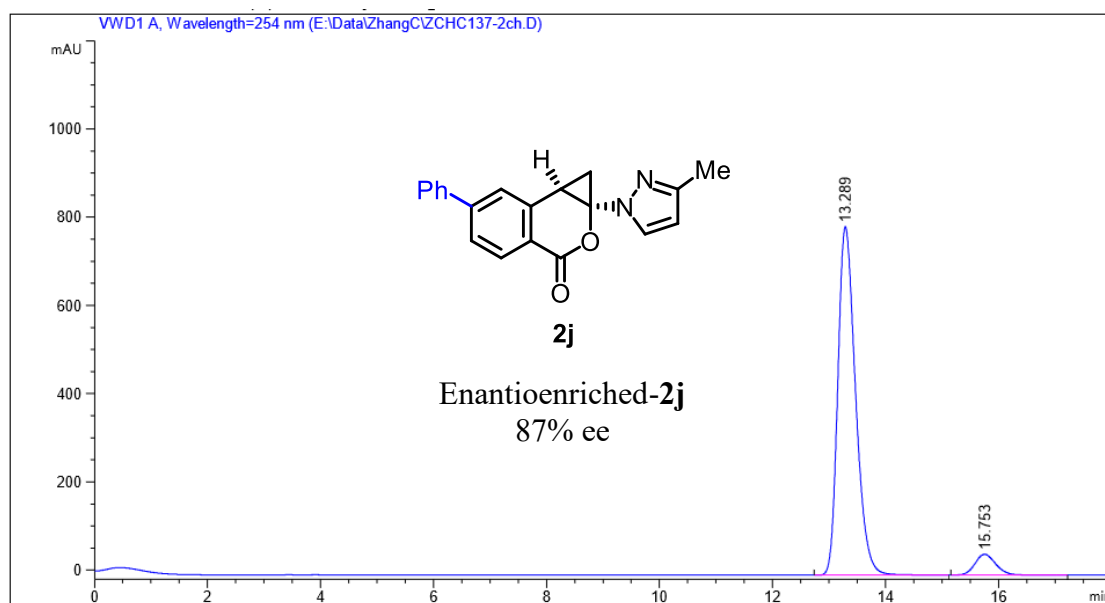


Peak #	RetTime [min]	Type	Width [min]	Area [mAU*s]	Height [mAU]	Area %
1	7.704	MM R	0.2209	3108.72559	234.59273	98.6889
2	8.759	MM R	0.2442	41.30056	9.76071e-2	1.3111

Figure 63. HPLC traces of *rac*-3i (reference) and enantioenriched-3i.

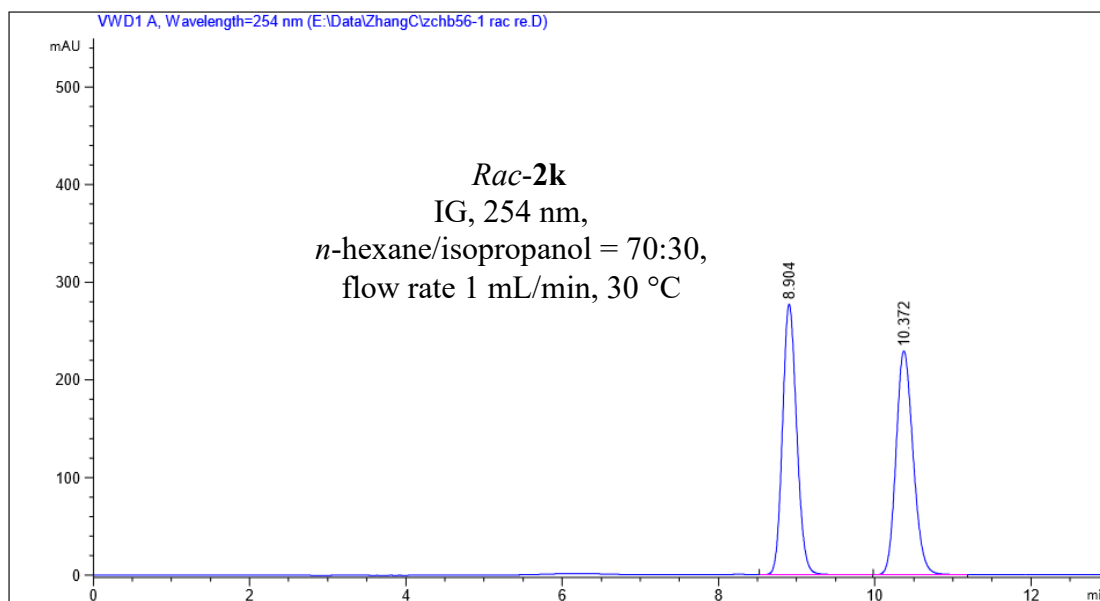


Peak #	RetTime [min]	Type	Width [min]	Area [mAU*s]	Height [mAU]	Area %
1	13.200	BB	0.3402	9766.34570	443.05759	49.9644
2	15.529	BB	0.3992	9780.28223	377.62646	50.0356

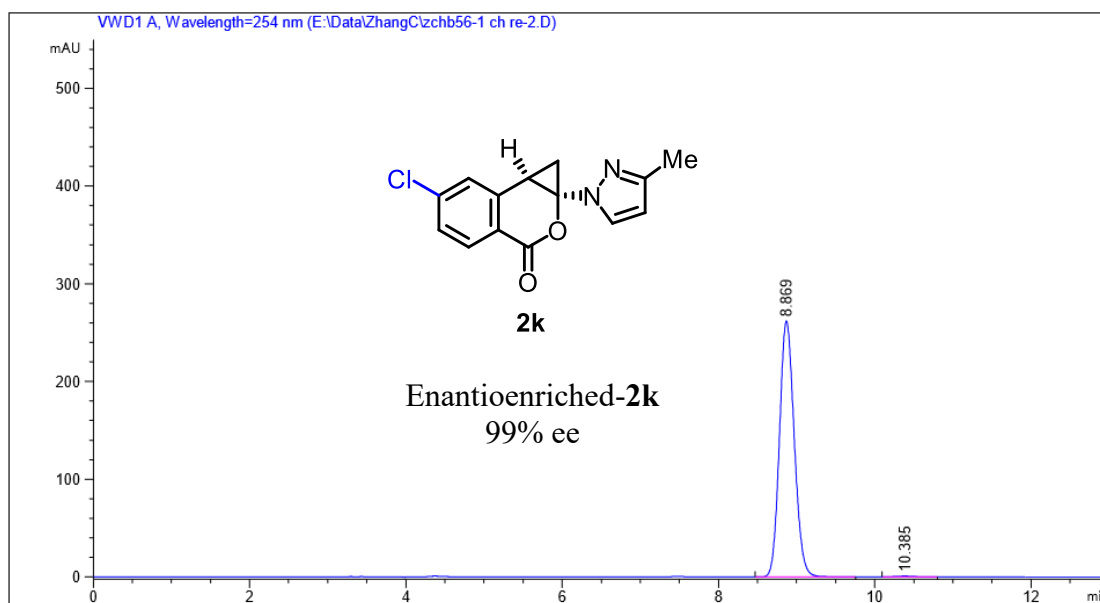


Peak #	RetTime [min]	Type	Width [min]	Area [mAU*s]	Height [mAU]	Area %
1	13.289	BB	0.3345	1.71598e4	789.77032	93.4318
2	15.753	BB	0.3966	1206.32202	46.97213	6.5682

Figure 64. HPLC traces of *rac*-2j (reference) and enantioenriched-2j.

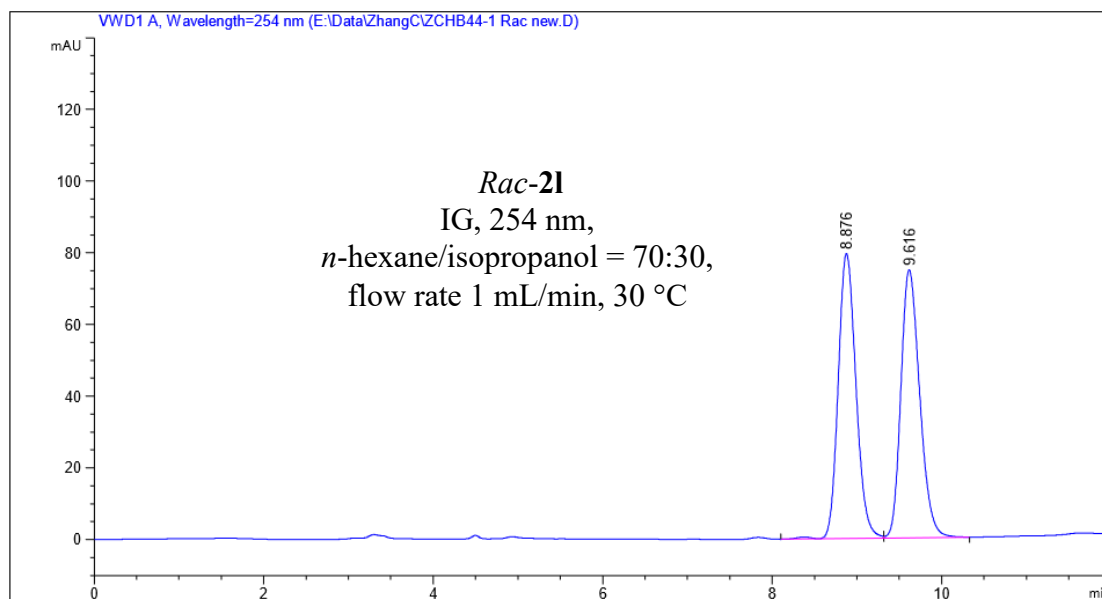


Peak #	RetTime [min]	Type	Width [min]	Area [mAU*s]	Height [mAU]	Area %
1	8.904	BB	0.1959	3492.03174	277.35123	50.0877
2	10.372	BB	0.2350	3479.79639	229.31519	49.9123

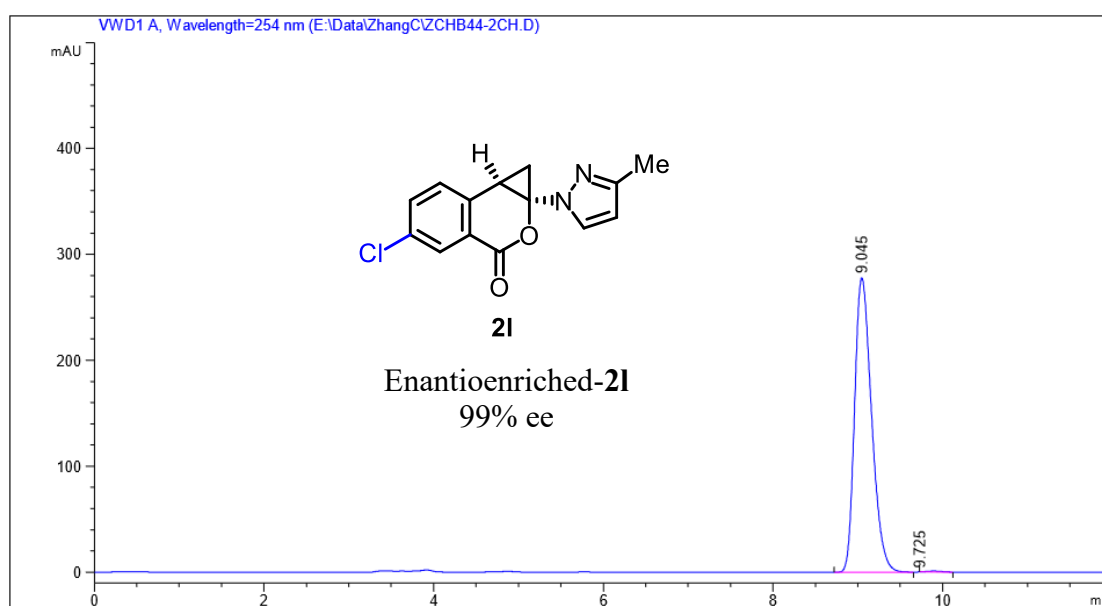


Peak #	RetTime [min]	Type	Width [min]	Area [mAU*s]	Height [mAU]	Area %
1	8.869	BB	0.2044	3443.49976	261.85419	99.6375
2	10.385	MM R	0.2553	12.52755	8.17778e-1	0.3625

Figure 65. HPLC traces of *rac*-2k (reference) and enantioenriched-2k.

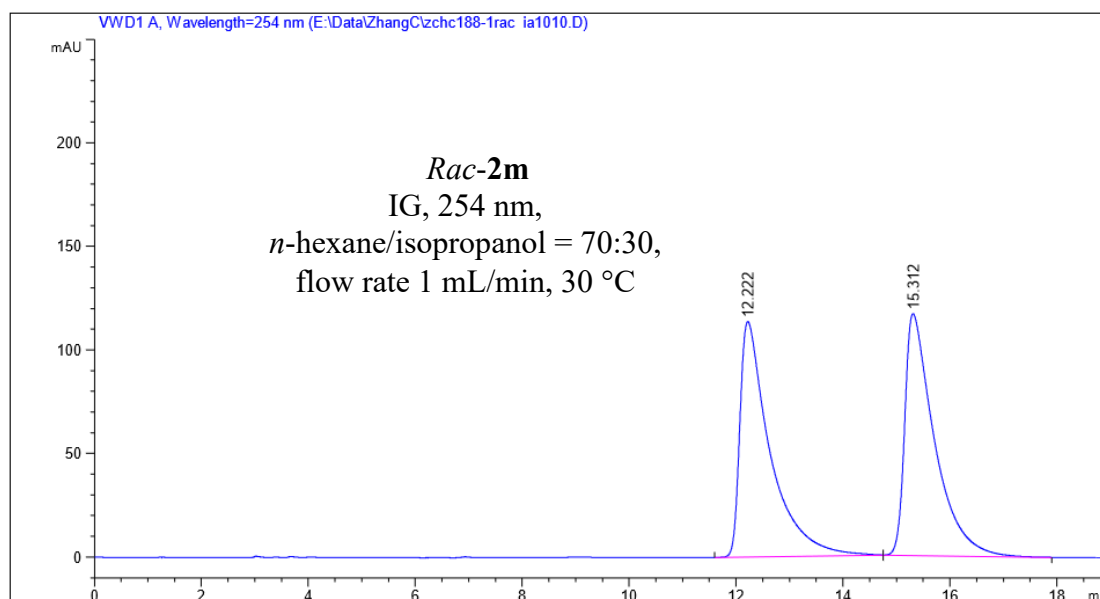


Peak #	RetTime [min]	Type	Width [min]	Area [mAU*s]	Height [mAU]	Area %
1	8.876	VR	0.2262	1160.02649	79.53937	50.1496
2	9.616	VB	0.2389	1153.10596	74.77422	49.8504

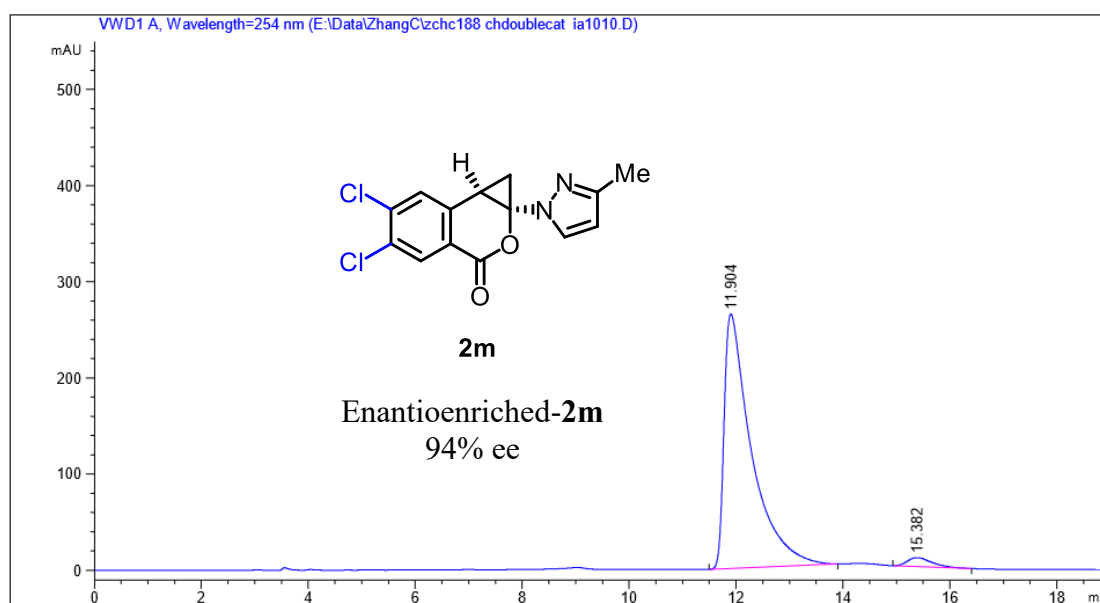


Peak #	RetTime [min]	Type	Width [min]	Area [mAU*s]	Height [mAU]	Area %
1	9.045	BB	0.2151	3862.32788	278.02325	99.7020
2	9.725	MM R	0.2106	11.54380	1.79939e-1	0.2980

Figure 66. HPLC traces of *rac*-21 (reference) and enantioenriched-21.

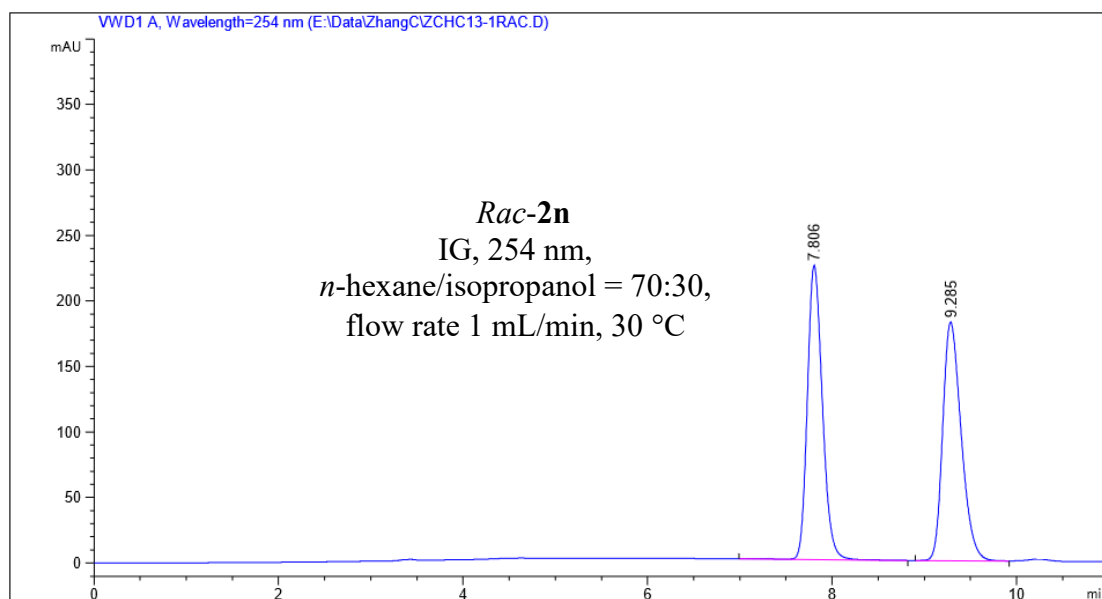


Peak #	RetTime [min]	Type	Width [min]	Area [mAU*s]	Height [mAU]	Area %
1	12.222	BB	0.5566	4448.68311	113.67832	49.7797
2	15.312	BB	0.5515	4488.05713	116.73502	50.2203

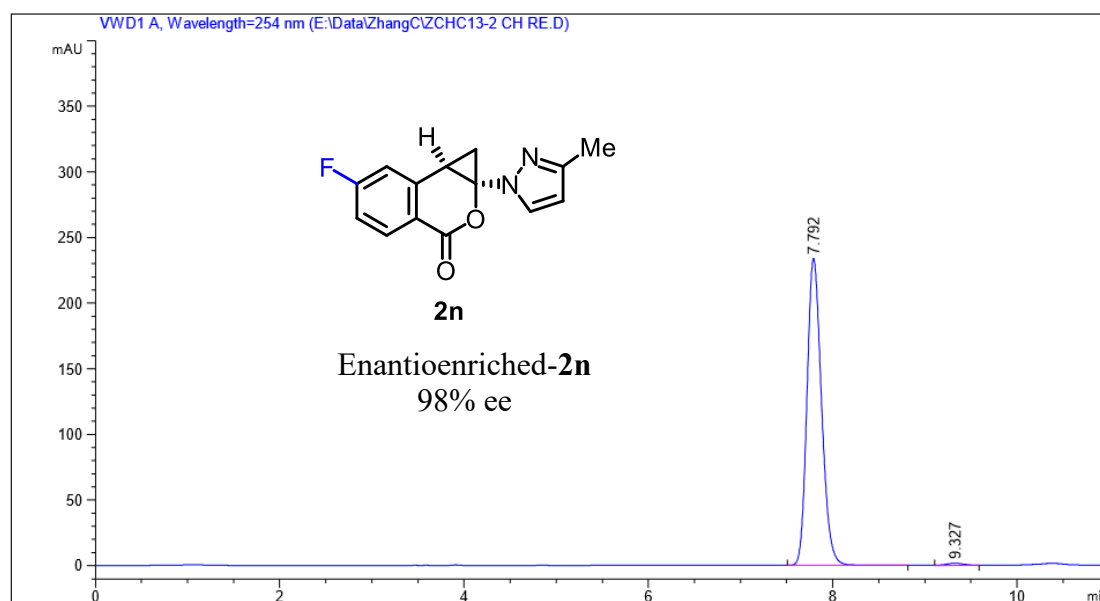


Peak #	RetTime [min]	Type	Width [min]	Area [mAU*s]	Height [mAU]	Area %
1	11.904	BB	0.5035	9401.01953	264.62875	96.9234
2	15.382	BB	0.4789	298.41223	9.33634	3.0766

Figure 67. HPLC traces of *rac*-2m (reference) and enantioenriched-2m.

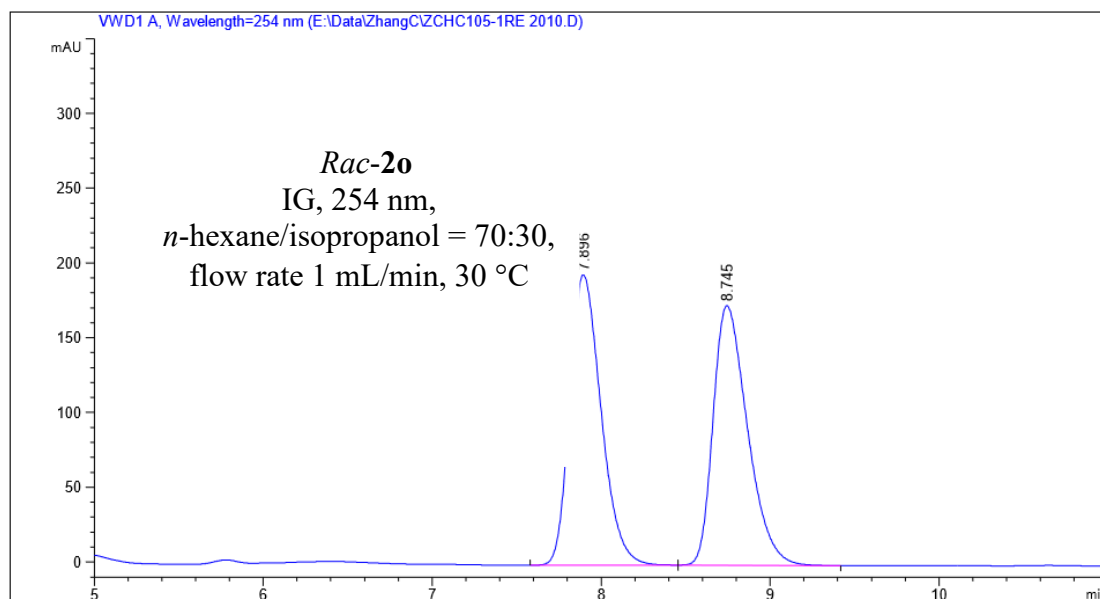


Peak #	RetTime [min]	Type	Width [min]	Area [mAU*s]	Height [mAU]	Area %
1	7.806	VB R	0.1749	2537.19629	224.48799	50.1048
2	9.285	BB	0.2140	2526.58276	181.91887	49.8952

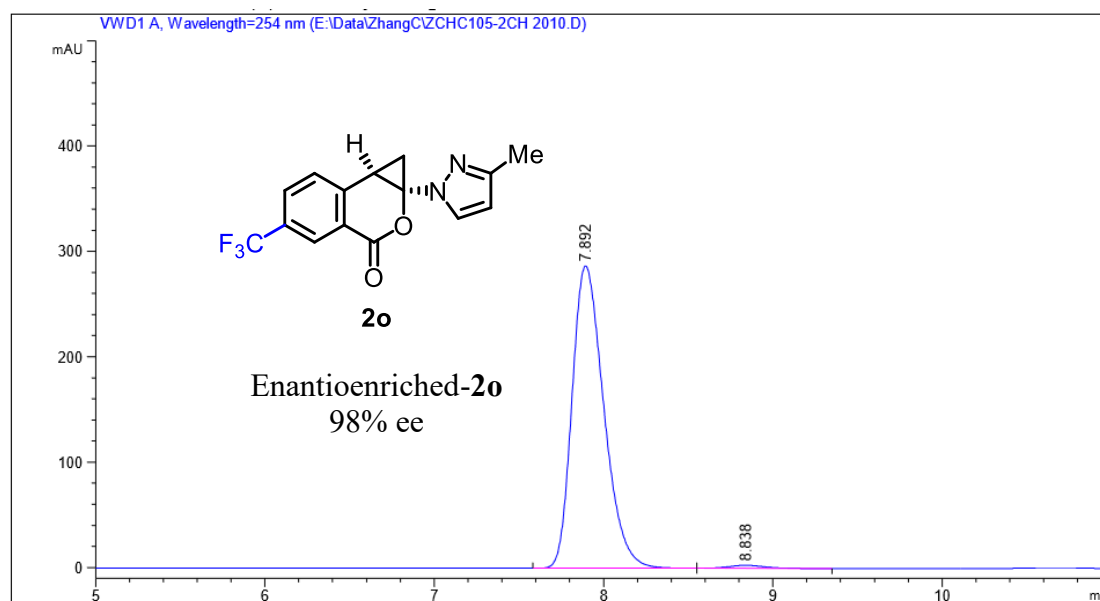


Peak #	RetTime [min]	Type	Width [min]	Area [mAU*s]	Height [mAU]	Area %
1	7.792	BB	0.1684	2551.47803	233.70763	99.0664
2	9.327	MM R	0.2341	24.04582	1.71208	0.9336

Figure 68. HPLC traces of *rac*-**2n** (reference) and enantioenriched-**2n**.

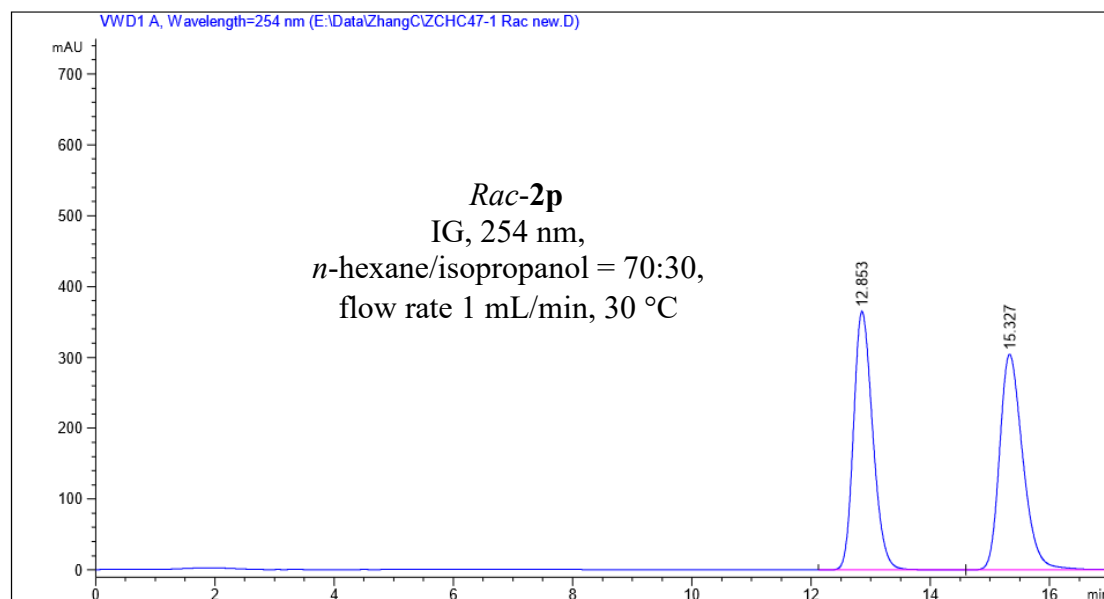


Peak #	RetTime [min]	Type	Width [min]	Area [mAU*s]	Height [mAU]	Area %
1	7.896	BB	0.2006	2505.06934	194.05273	50.5498
2	8.745	BB	0.2178	2450.57837	173.51668	49.4502

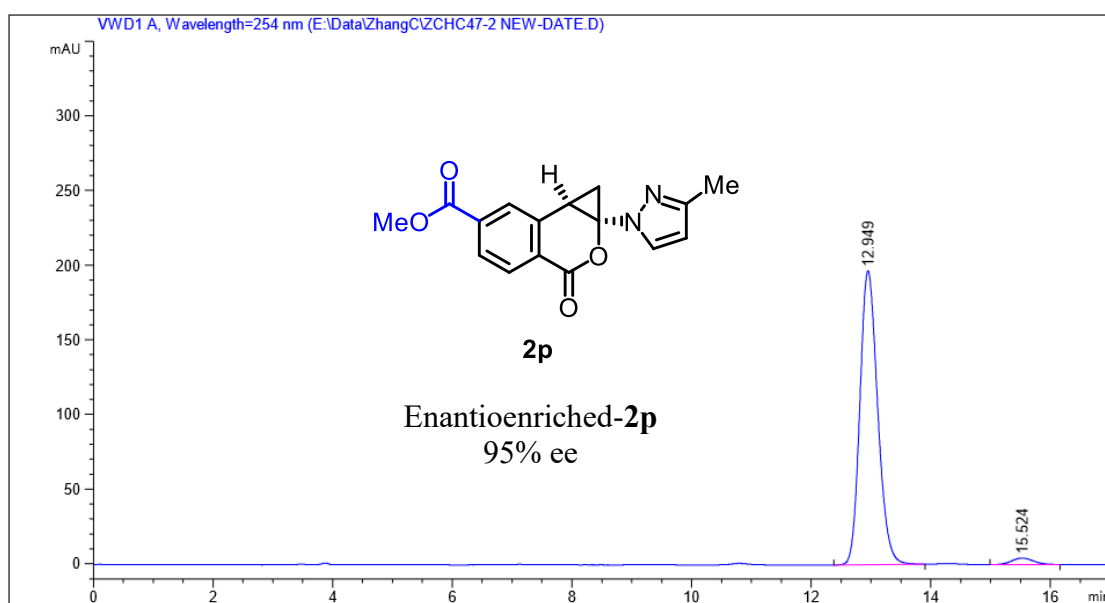


Peak #	RetTime [min]	Type	Width [min]	Area [mAU*s]	Height [mAU]	Area %
1	7.892	BB	0.2029	3735.50537	286.95105	98.9736
2	8.838	BB	0.2143	38.73763	2.78442	1.0264

Figure 69. HPLC traces of *rac*-3o (reference) and enantioenriched-3o.

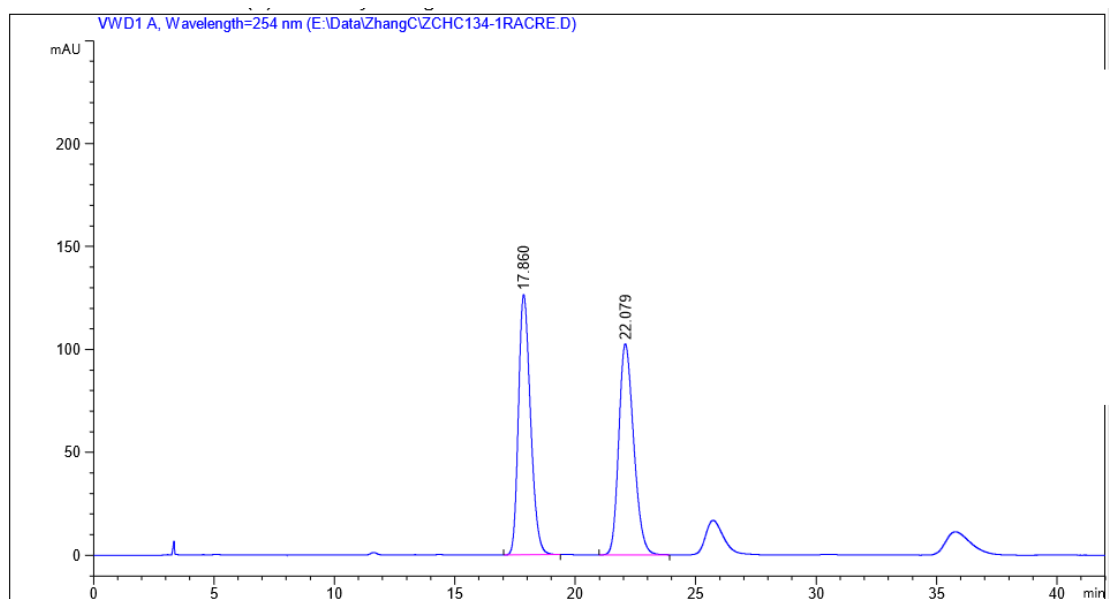


Peak #	RetTime [min]	Type	Width [min]	Area [mAU*s]	Height [mAU]	Area %
1	12.853	BB	0.3458	8157.29150	364.85648	49.8039
2	15.327	BB	0.4152	8221.52539	304.33069	50.1961

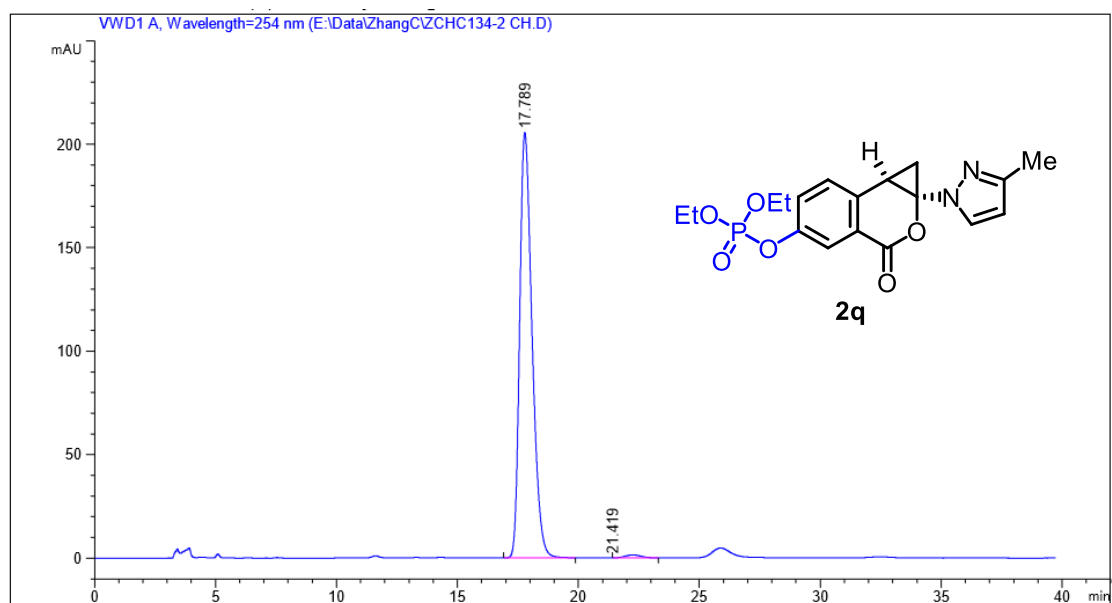


Peak #	RetTime [min]	Type	Width [min]	Area [mAU*s]	Height [mAU]	Area %
1	12.949	BB	0.3185	4055.63745	196.77440	97.3888
2	15.524	BB	0.3932	108.74123	4.32648	2.6112

Figure 70. HPLC traces of *rac*-3p (reference) and enantioenriched-3p.

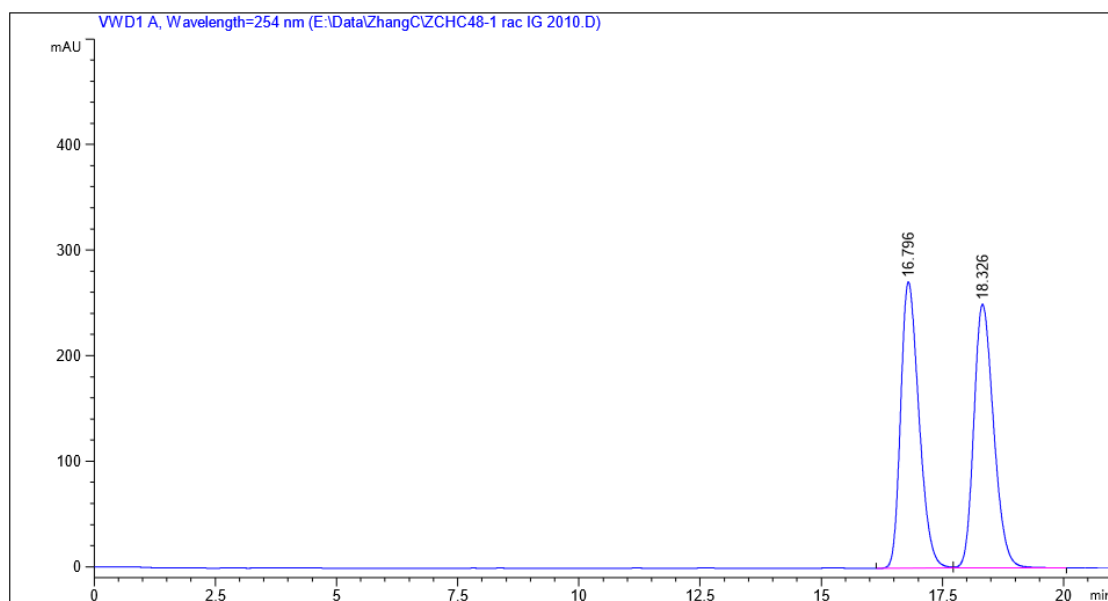


Peak #	RetTime [min]	Type	Width [min]	Area [mAU*s]	Height [mAU]	Area %
1	17.860	BB	0.5369	4387.67773	126.41782	49.8905
2	22.079	BB	0.6659	4406.94043	102.44596	50.1095

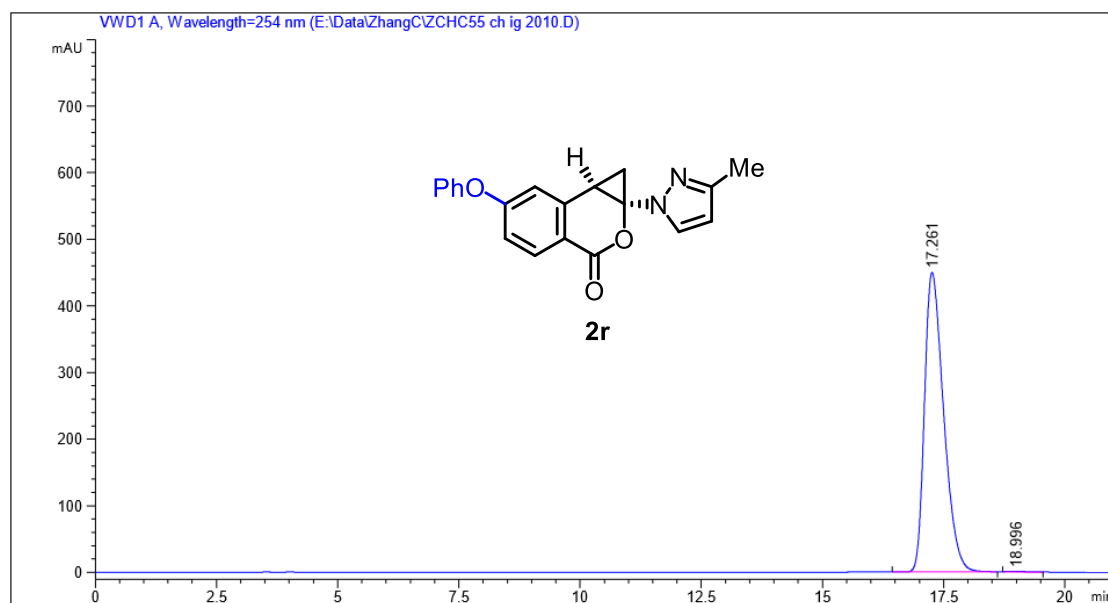


Peak #	RetTime [min]	Type	Width [min]	Area [mAU*s]	Height [mAU]	Area %
1	17.789	BB	0.5449	7288.47852	205.41814	99.0127
2	21.419	MM R	0.7986	72.67489	8.06024e-2	0.9873

Figure 71. HPLC traces of *rac*-**2q** (reference) and enantioenriched-**2q**.

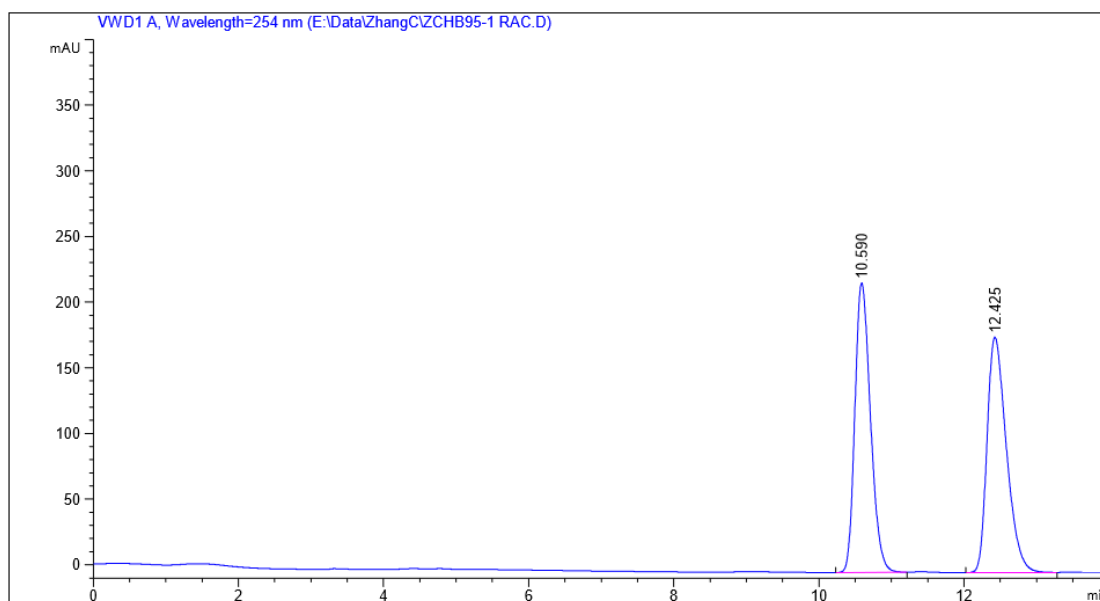


Peak #	RetTime [min]	Type	Width [min]	Area [mAU*s]	Height [mAU]	Area %
1	16.796	BV	0.4048	7102.92627	271.00607	50.0146
2	18.326	VB	0.4406	7098.77979	249.73477	49.9854

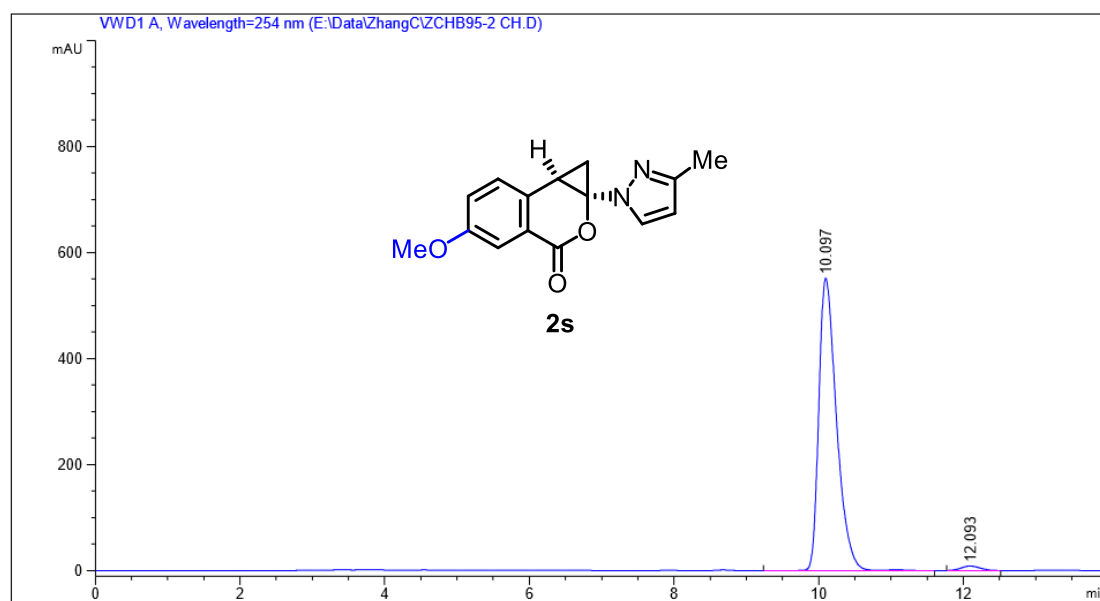


Peak #	RetTime [min]	Type	Width [min]	Area [mAU*s]	Height [mAU]	Area %
1	17.261	BB	0.4222	1.23337e4	449.42337	99.7899
2	18.996	MM R	0.4889	25.96144	8.84971e-1	0.2101

Figure 72. HPLC traces of *rac*-**2r** (reference) and enantioenriched-**2r**.

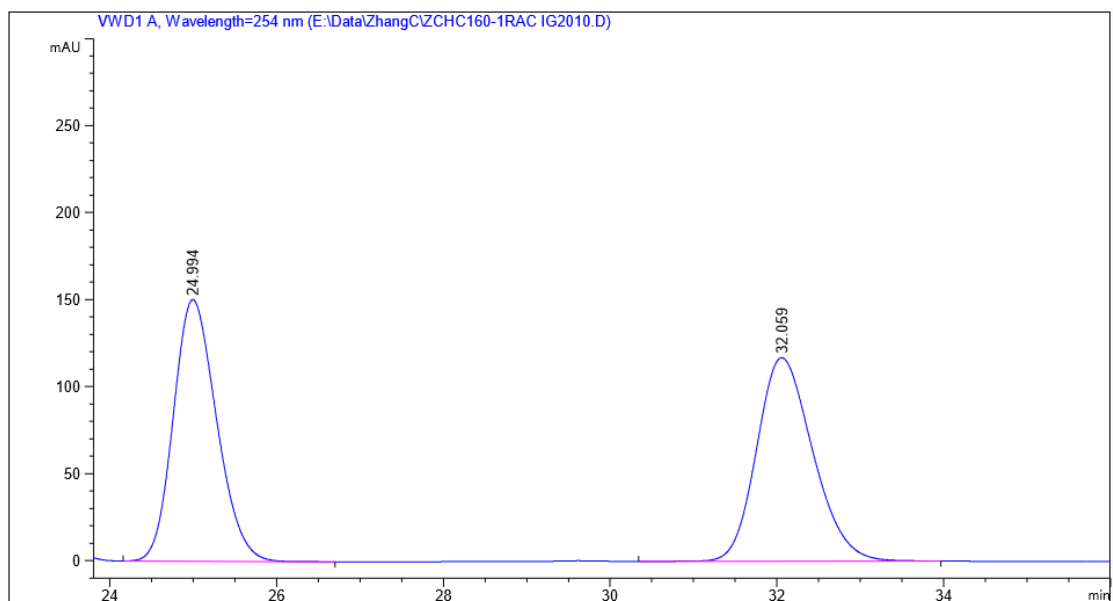


Peak #	RetTime [min]	Type	Width [min]	Area [mAU*s]	Height [mAU]	Area %
1	10.590	BB	0.2313	3291.04199	220.31030	49.7880
2	12.425	BB	0.2853	3319.07153	179.05035	50.2120

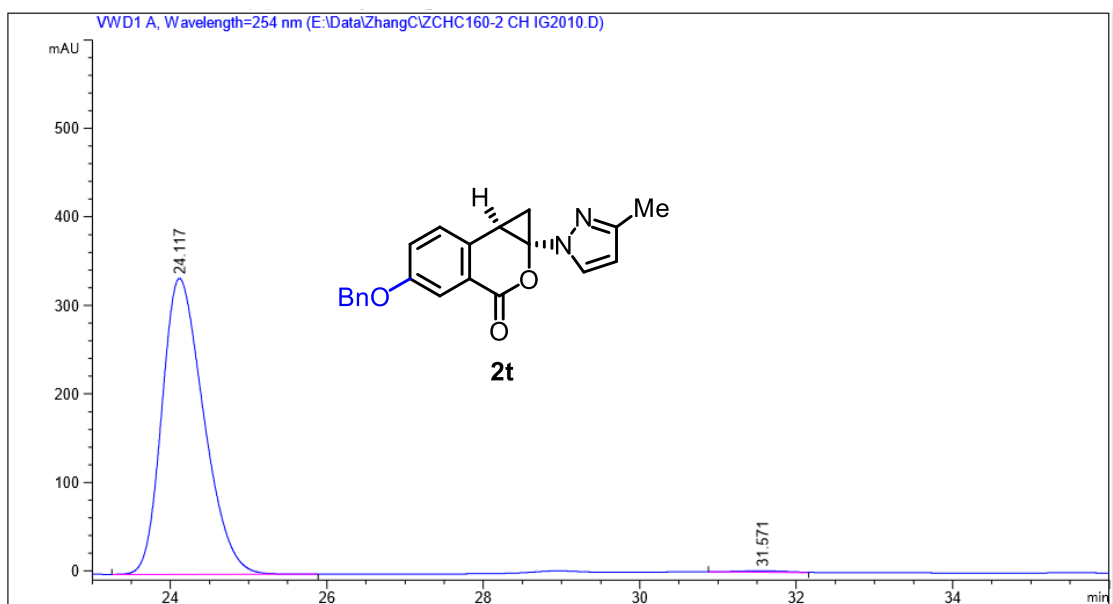


Peak #	RetTime [min]	Type	Width [min]	Area [mAU*s]	Height [mAU]	Area %
1	10.097	BV R	0.2604	9374.54492	551.29944	98.3124
2	12.093	MM R	0.3104	160.92104	8.63974	1.6876

Figure 73. HPLC traces of *rac*-2s (reference) and enantioenriched-2s.

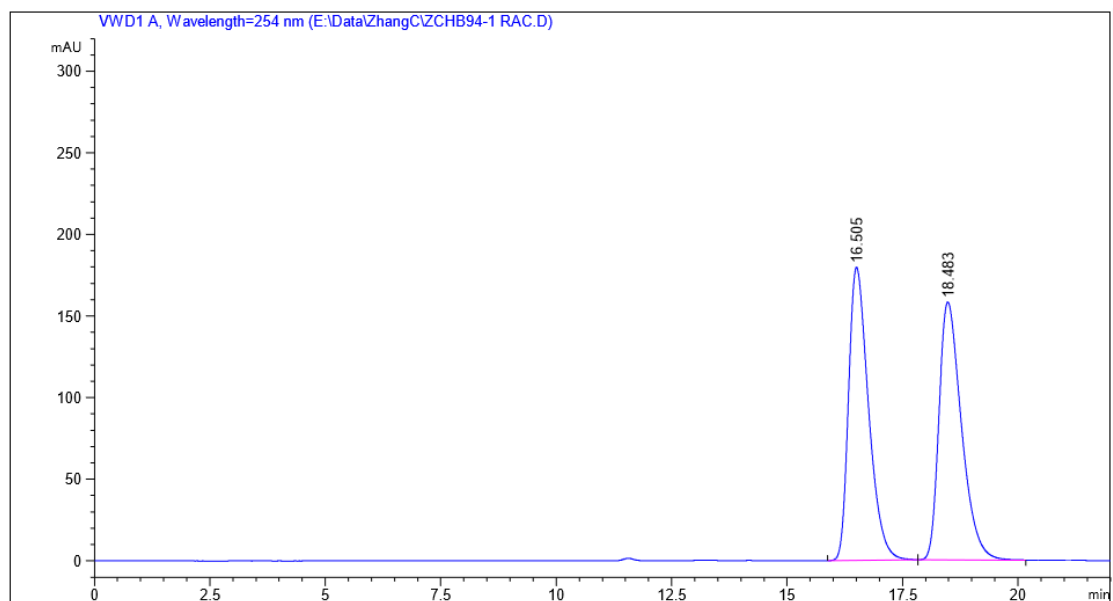


Peak #	RetTime [min]	Type	Width [min]	Area [mAU*s]	Height [mAU]	Area %
1	24.994	BB	0.5606	5421.60596	150.39987	49.7735
2	32.059	BB	0.7196	5470.93848	116.99458	50.2265

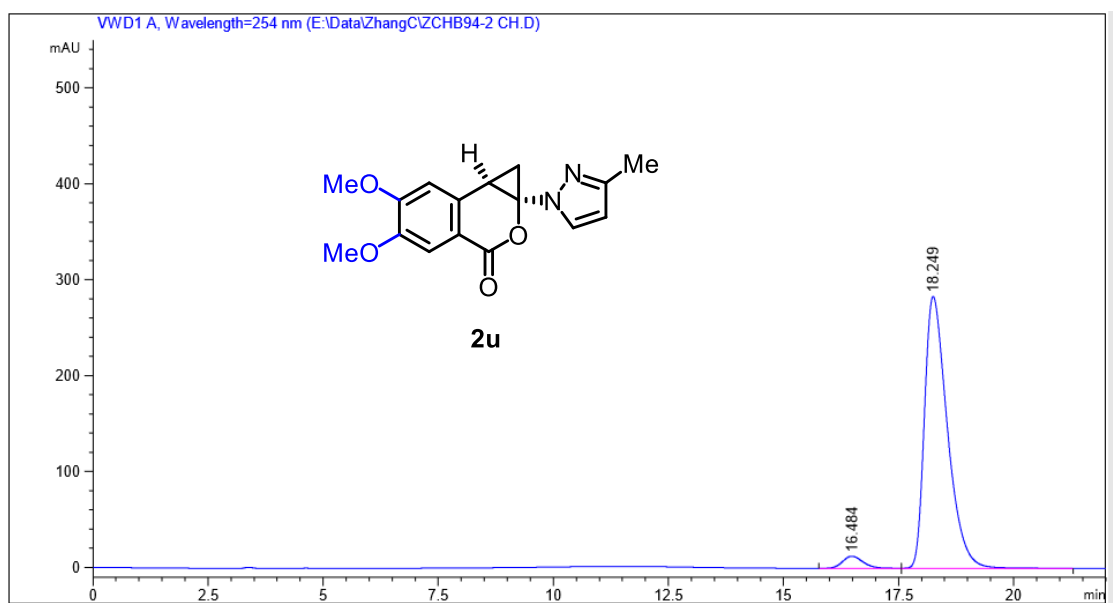


Peak #	RetTime [min]	Type	Width [min]	Area [mAU*s]	Height [mAU]	Area %
1	24.117	BB	0.5741	1.23797e4	334.23798	99.4269
2	31.571	MM R	0.7281	71.35336	1.63322	0.5731

Figure 74. HPLC traces of *rac*-**2t** (reference) and enantioenriched-**2t**.

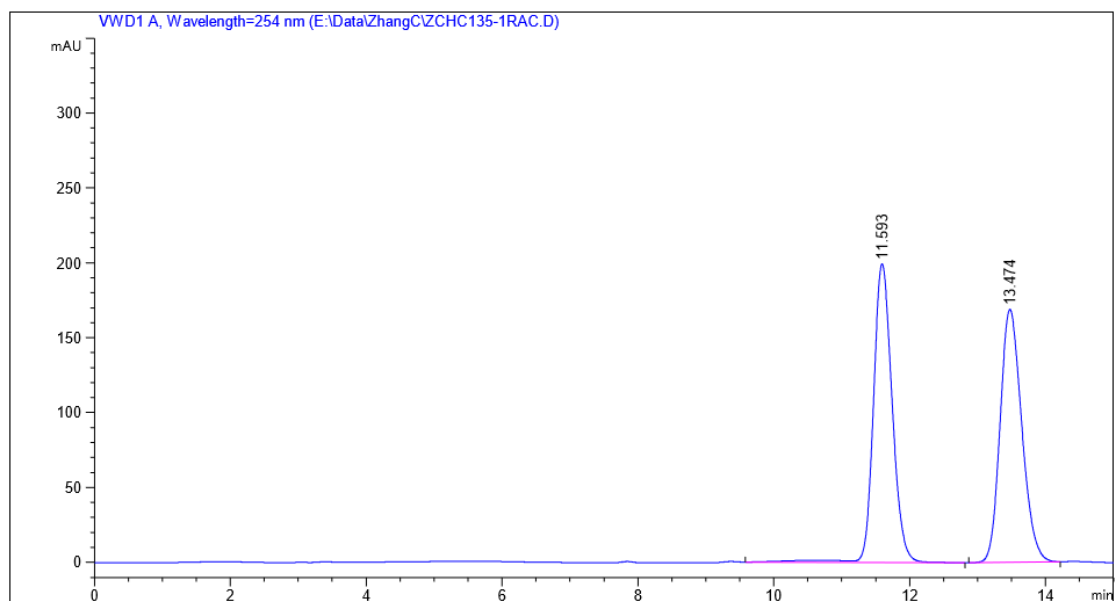


Peak #	RetTime [min]	Type	Width [min]	Area [mAU*s]	Height [mAU]	Area %
1	16.505	BB	0.4588	5380.72656	179.47021	50.1306
2	18.483	BB	0.5174	5352.68750	157.93256	49.8694

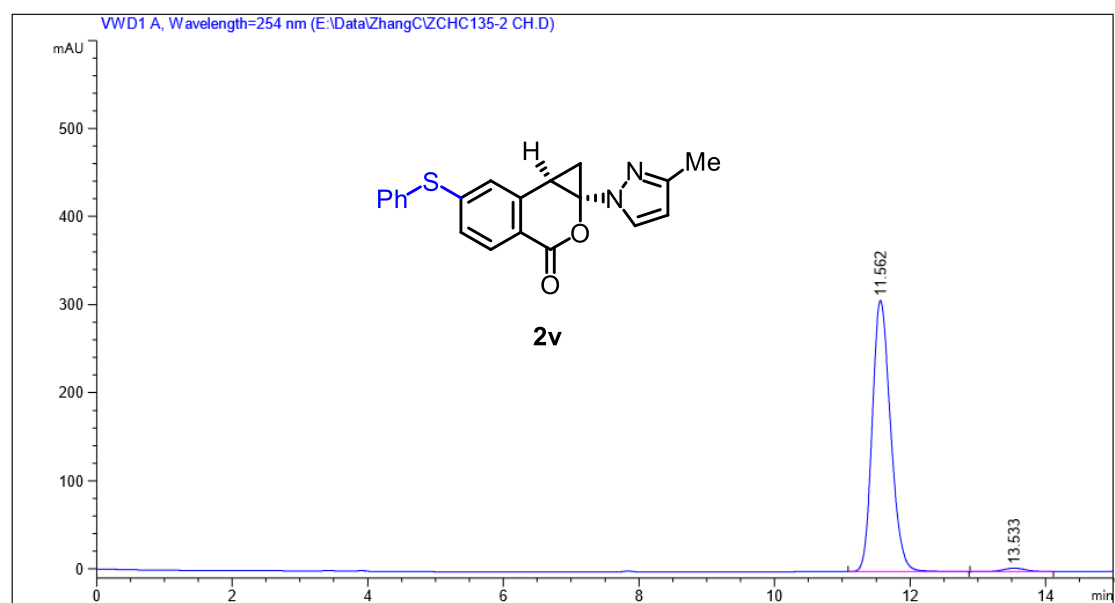


Peak #	RetTime [min]	Type	Width [min]	Area [mAU*s]	Height [mAU]	Area %
1	16.484	BB	0.4691	384.54355	12.59762	3.7803
2	18.249	BB	0.5269	9787.79980	283.42166	96.2197

Figure 75. HPLC traces of *rac*-**2u** (reference) and enantioenriched-**2u**.

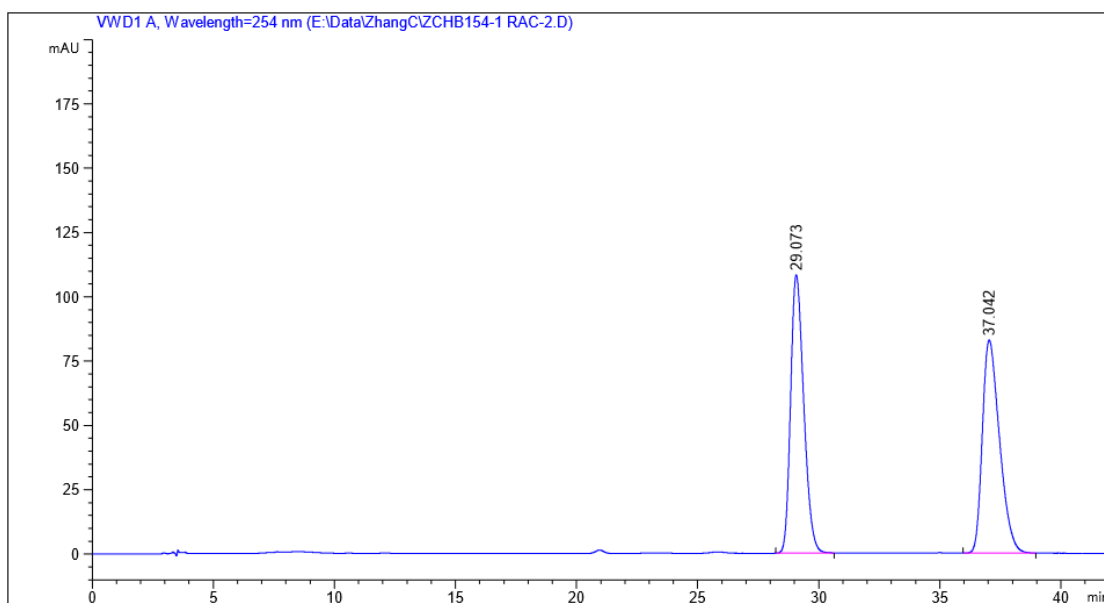


Peak #	RetTime [min]	Type	Width [min]	Area [mAU*s]	Height [mAU]	Area %
1	11.593	VB R	0.2968	3842.61255	199.43239	50.7350
2	13.474	BB	0.3430	3731.27930	168.71753	49.2650

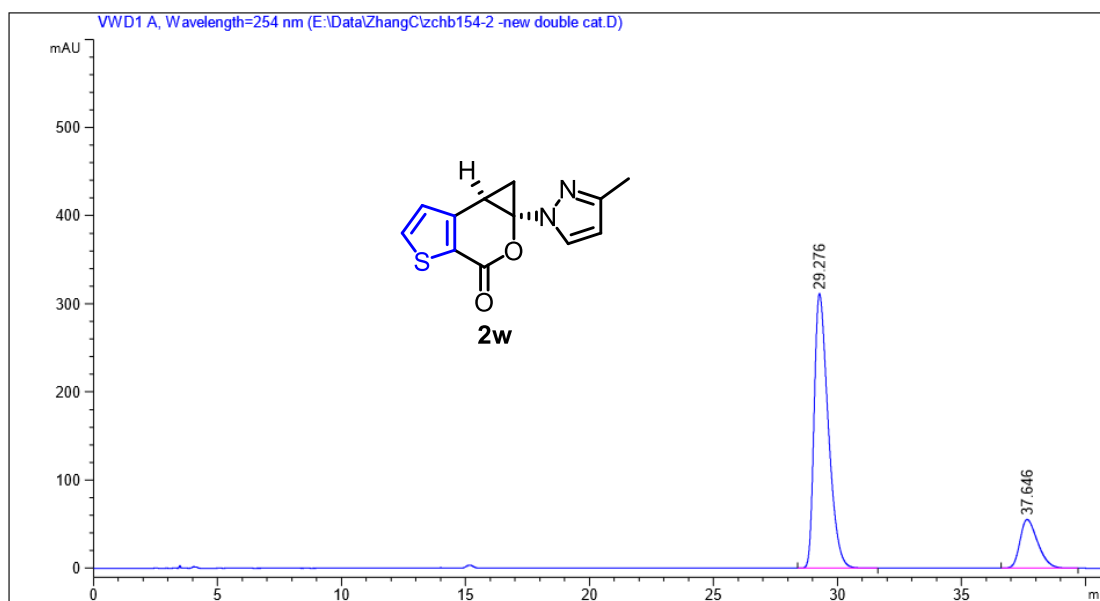


Peak #	RetTime [min]	Type	Width [min]	Area [mAU*s]	Height [mAU]	Area %
1	11.562	BB	0.2911	5776.92920	307.59854	98.4293
2	13.533	BB	0.3549	92.18547	3.96974	1.5707

Figure 76. HPLC traces of *rac*-**2v** (reference) and enantioenriched-**2v**.

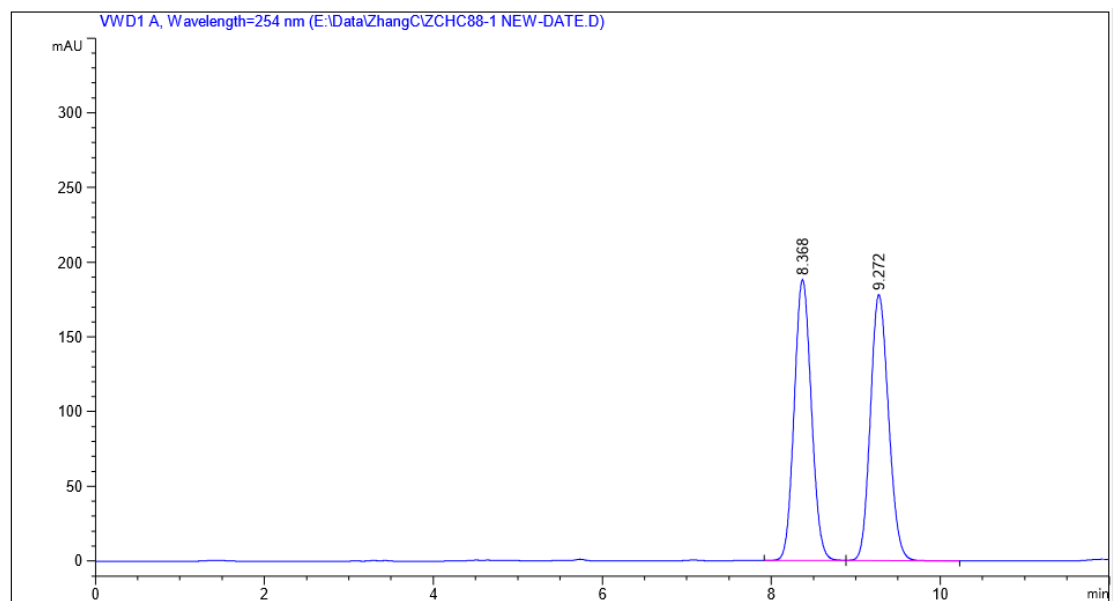


Peak #	RetTime [min]	Type	Width [min]	Area [mAU*s]	Height [mAU]	Area %
1	29.073	BB	0.5828	4078.68433	108.19929	49.9950
2	37.042	BB	0.7458	4079.50464	82.80291	50.0050

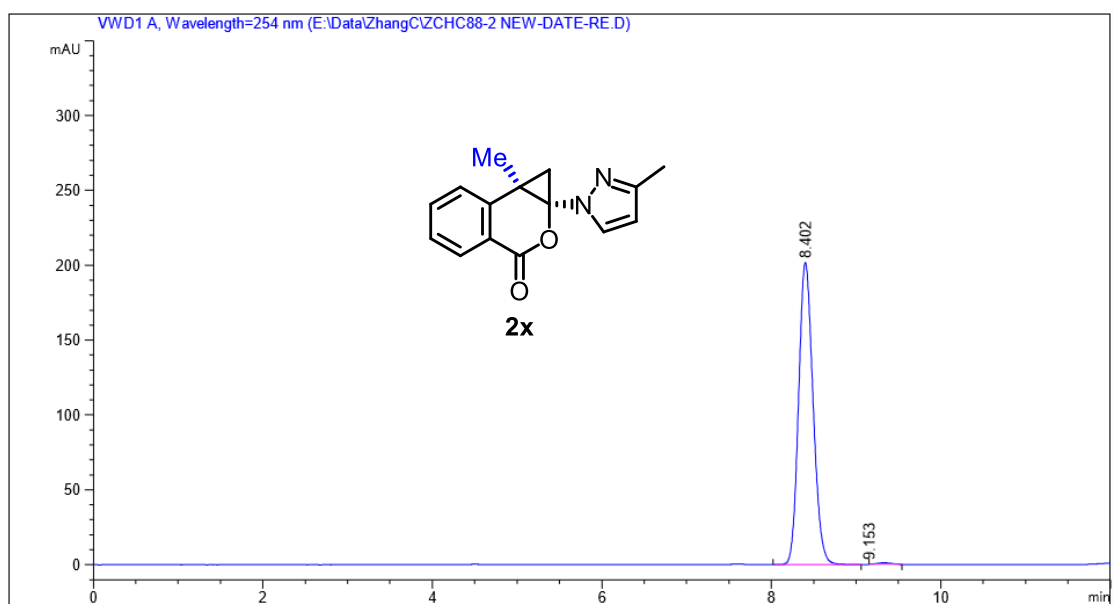


Peak #	RetTime [min]	Type	Width [min]	Area [mAU*s]	Height [mAU]	Area %
1	29.276	BB	0.5992	1.22602e4	311.49890	81.7737
2	37.646	BB	0.7563	2732.63843	55.12400	18.2263

Figure 77. HPLC traces of *rac*-**2w** (reference) and enantioenriched-**2w**.



Peak #	RetTime [min]	Type	Width [min]	Area [mAU*s]	Height [mAU]	Area %
1	8.368	BB	0.2212	2644.54858	187.89316	48.9033
2	9.272	BB	0.2330	2652.57080	177.85101	49.0516



Peak #	RetTime [min]	Type	Width [min]	Area [mAU*s]	Height [mAU]	Area %
1	8.402	BB	0.1842	2388.76611	201.66414	99.5267
2	9.153	MM R	0.1874	11.35977	2.68166e-2	0.4733

Figure 78. HPLC traces of *rac*-2x (reference) and enantioenriched-2x.

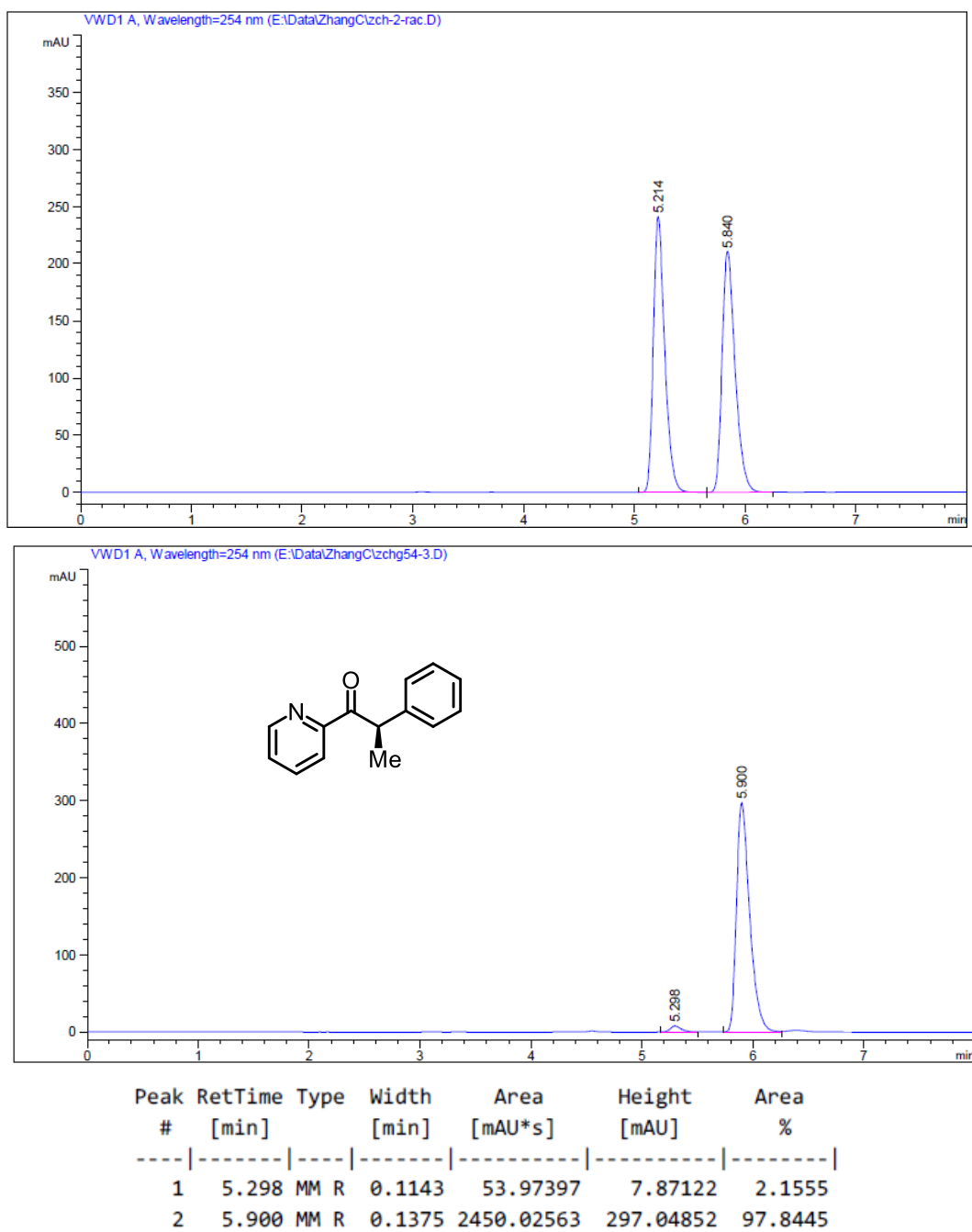


Figure 79. HPLC traces (Daicel Chiralpak OD-H column) of *rac*-**3a** (reference) and (*R*)-**3a**.

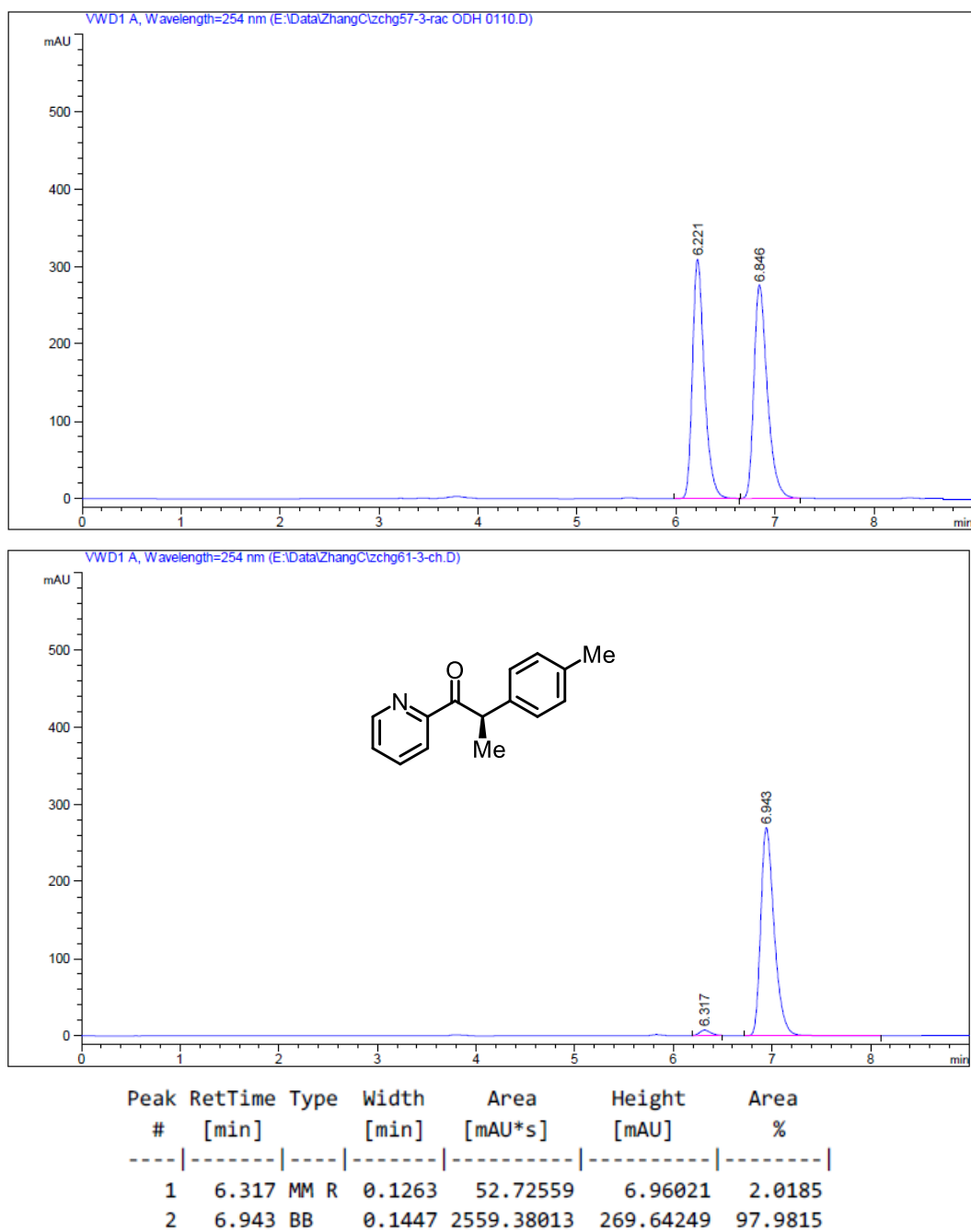


Figure 80. HPLC traces (Daicel Chiralpak OD-H column) of *rac*-**3b** (reference) and (*R*)-**3b**.

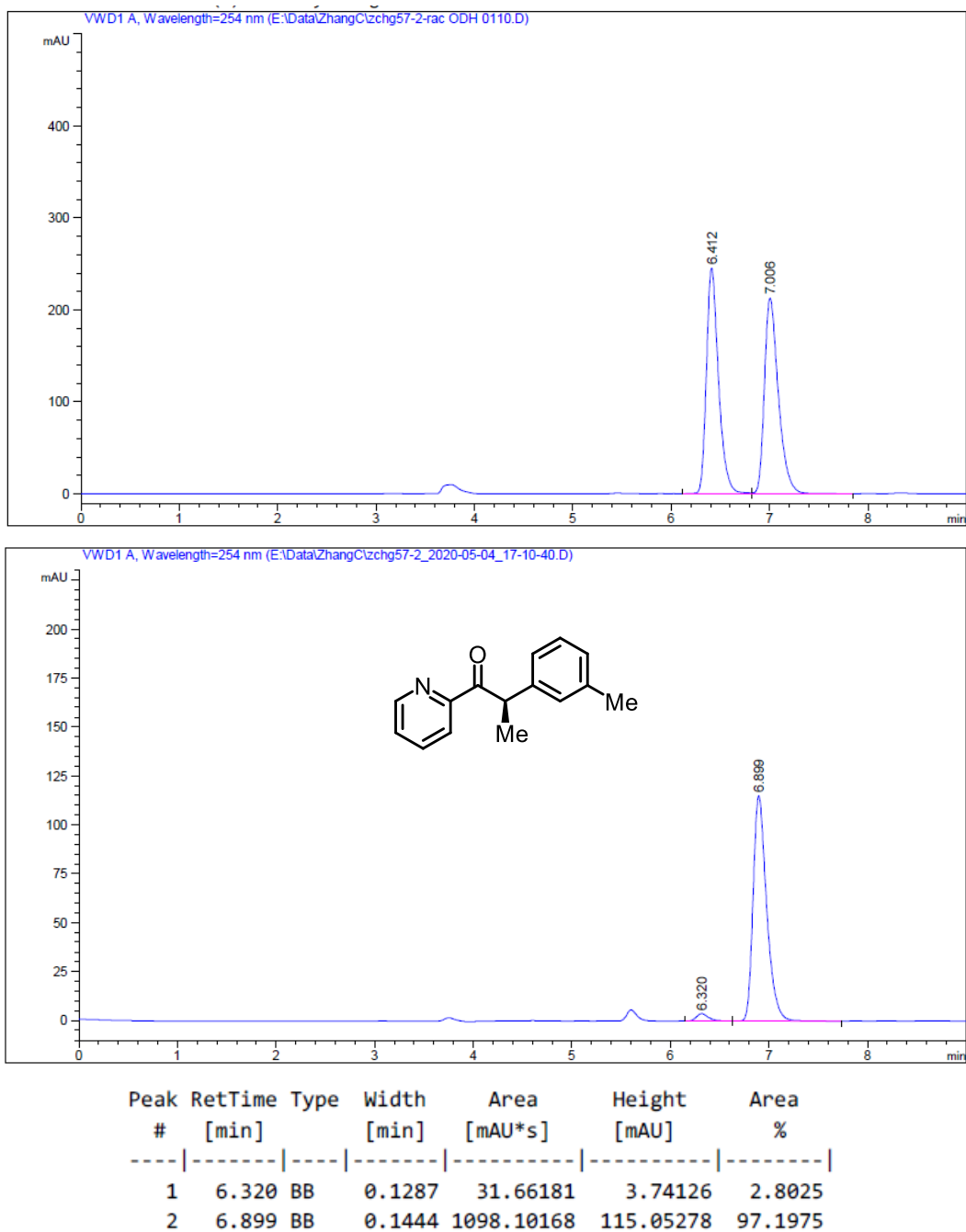


Figure 81. HPLC traces (Daicel Chiralpak OD-H column) of *rac*-**3c** (reference) and (*R*)-**3c**.

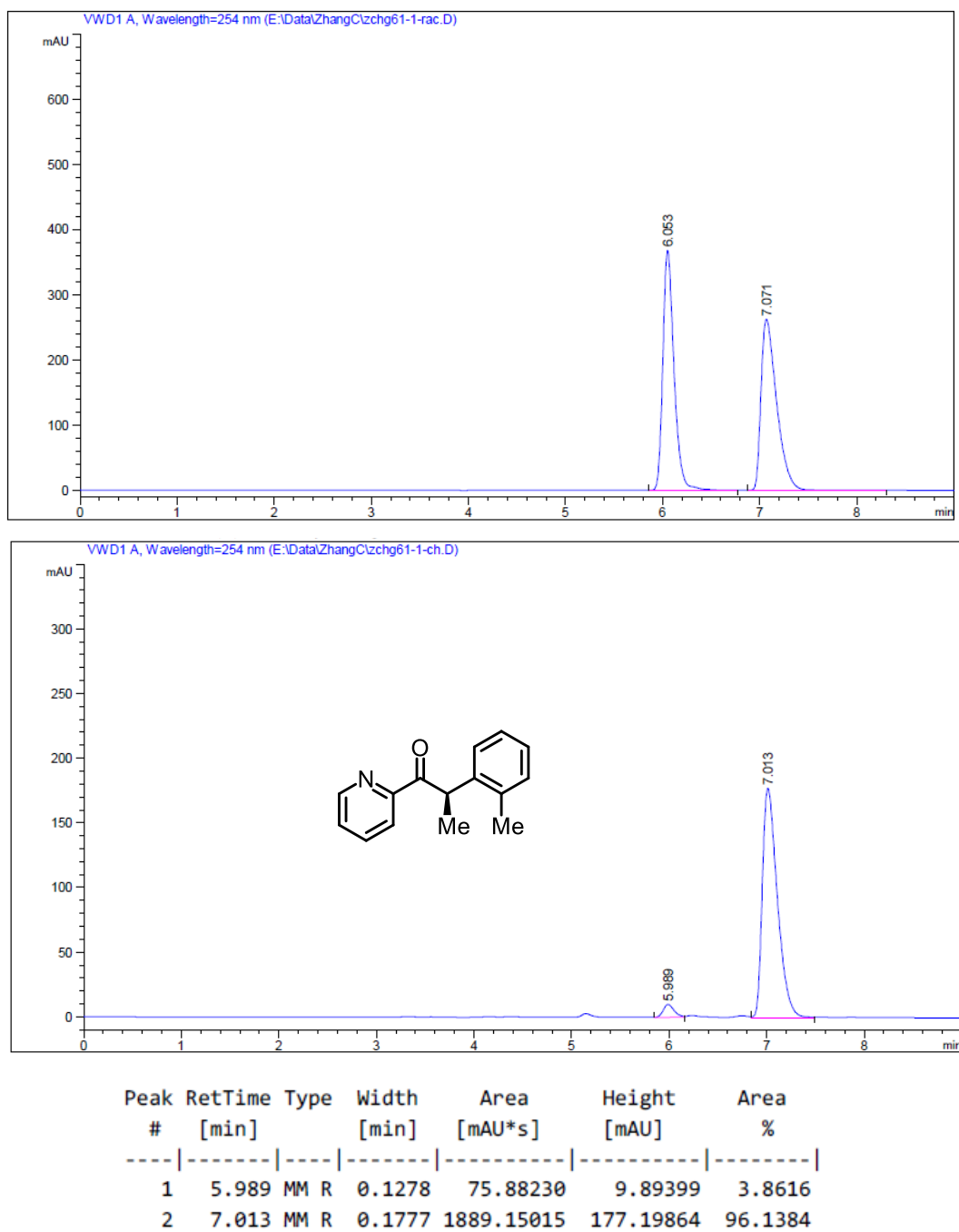


Figure 82. HPLC traces (Daicel Chiralpak OD-H column) of *rac*-**3d** (reference) and (*R*)-**3d**.

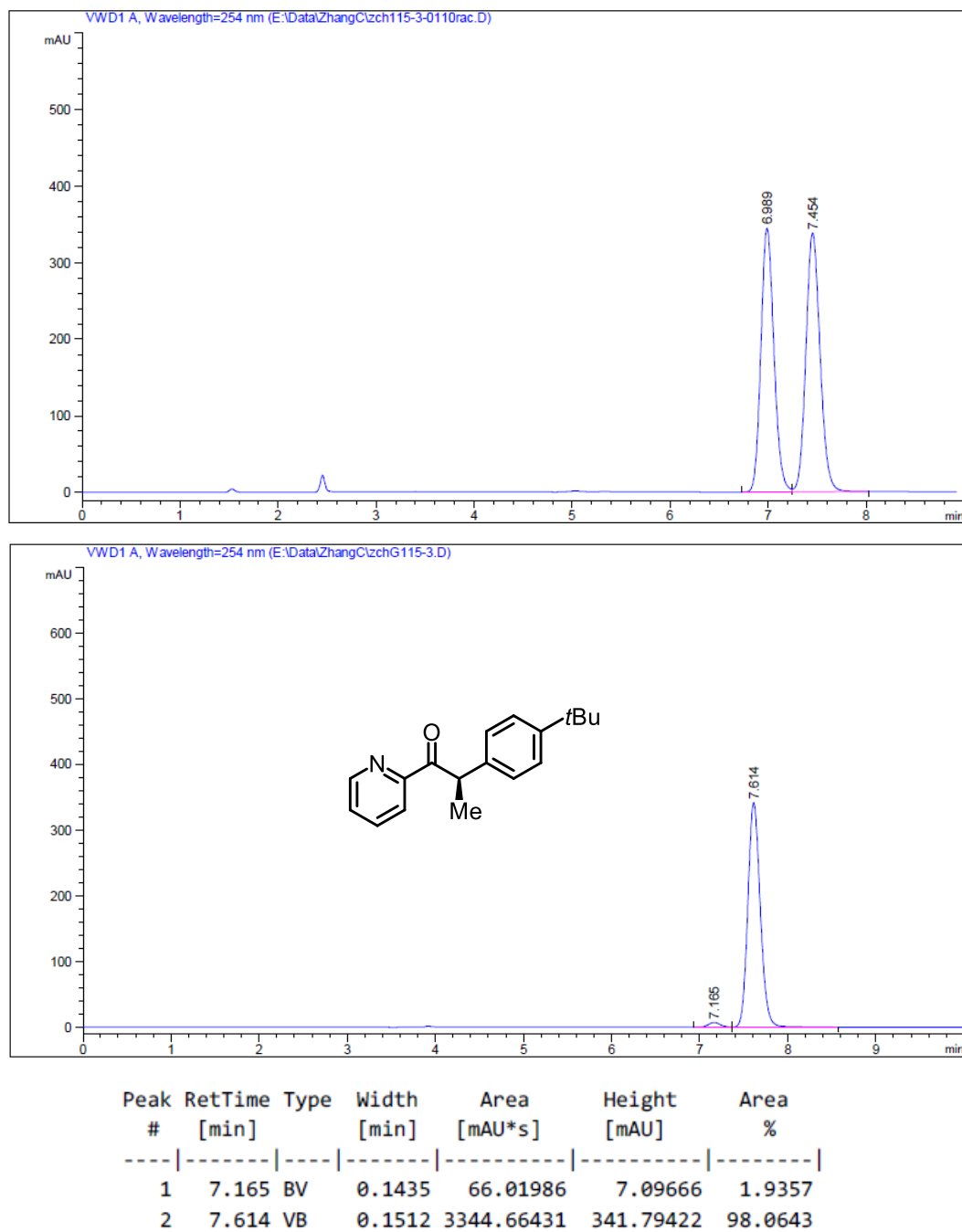


Figure 83. HPLC traces (Daicel Chiralpak IG column) of *rac*-**3e** (reference) and (*R*)-**3e**.

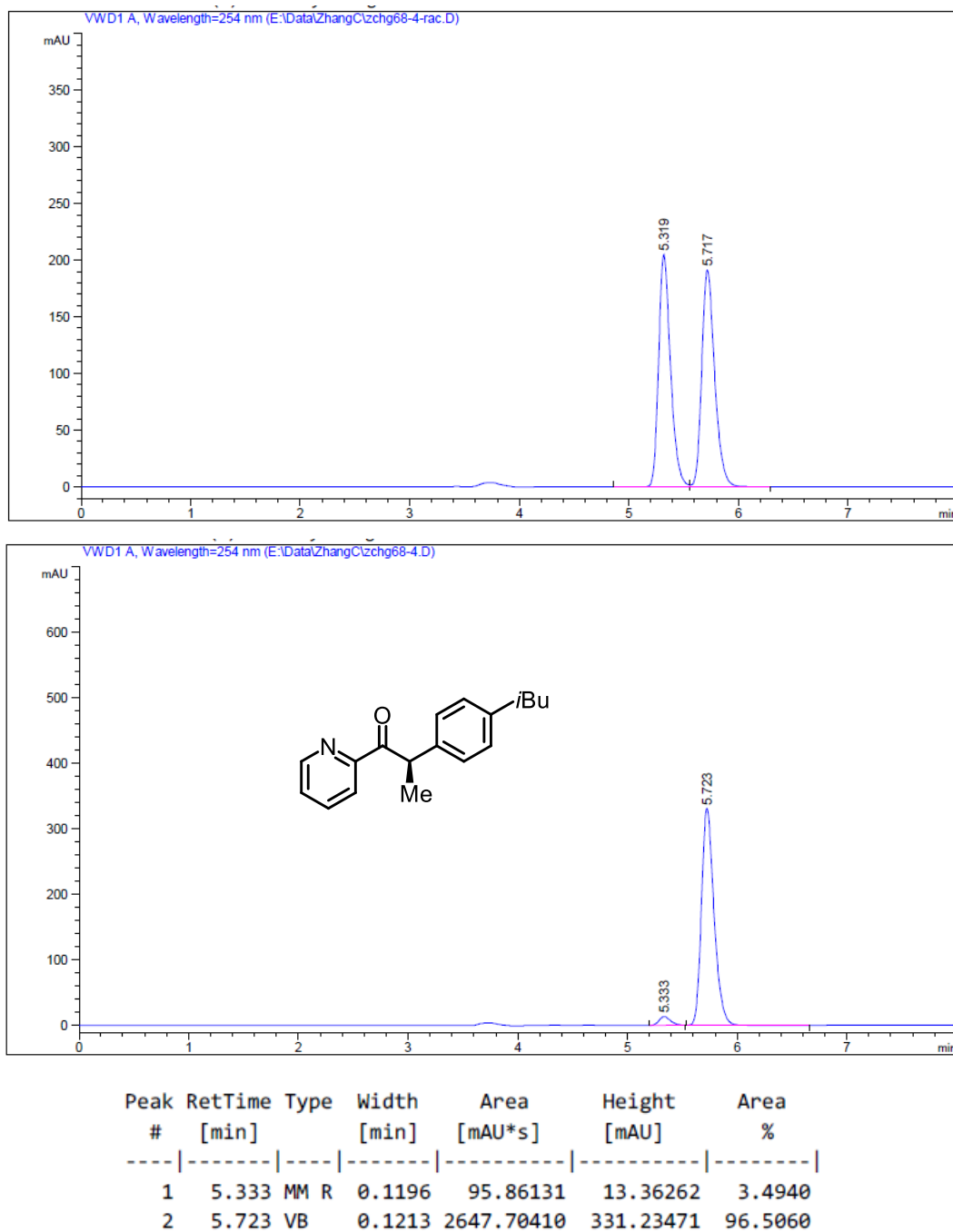


Figure 84. HPLC traces (Daicel Chiralpak OD-H column) of *rac*-**3f** (reference) and (*R*)-**3f**.

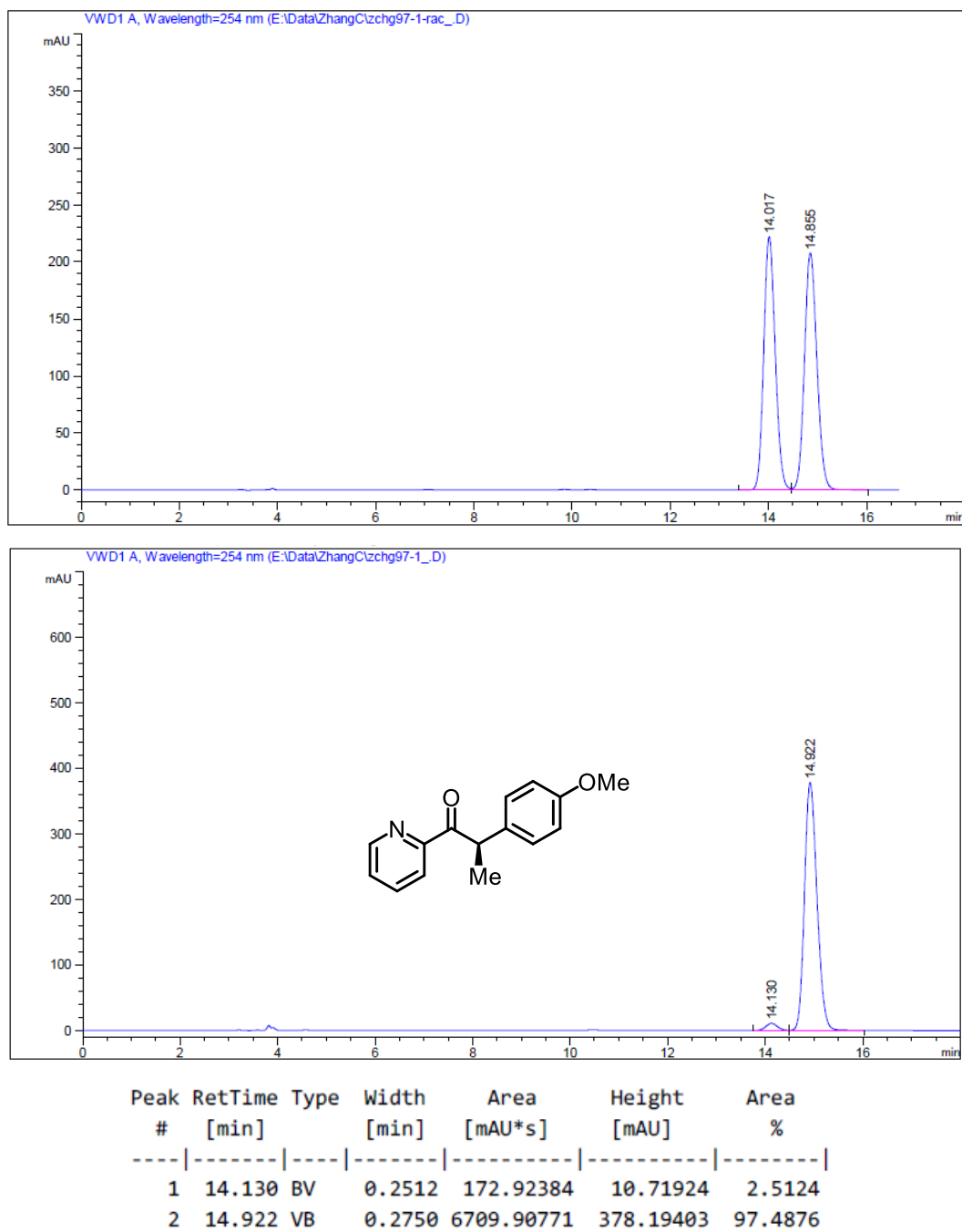


Figure 85. HPLC traces (Daicel Chiralpak IG column) of *rac*-3g (reference) and (*R*)-3g.

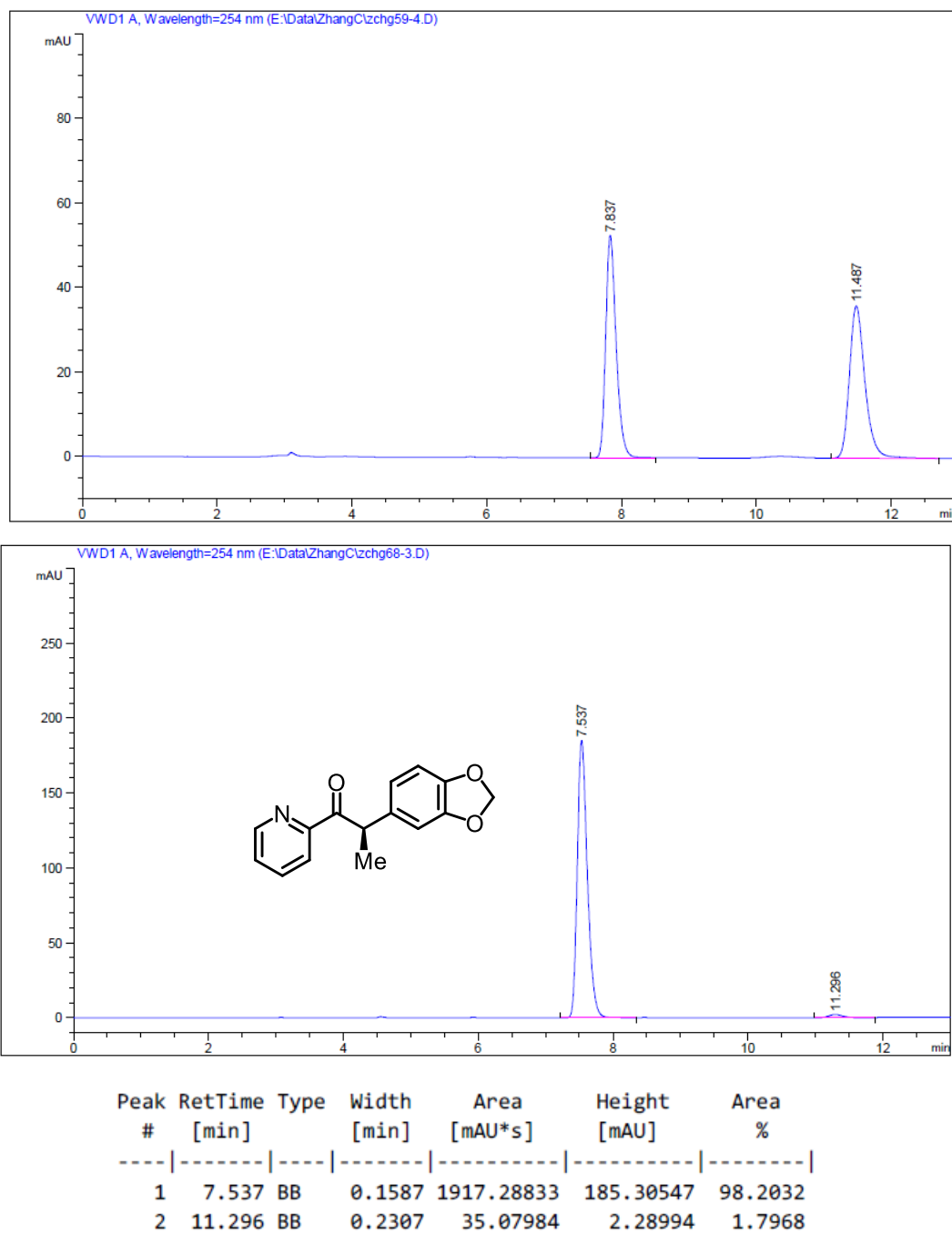


Figure 86. HPLC traces (Daicel Chiralpak OD-H column) of *rac*-**3h** (reference) and (*R*)-**3h**.

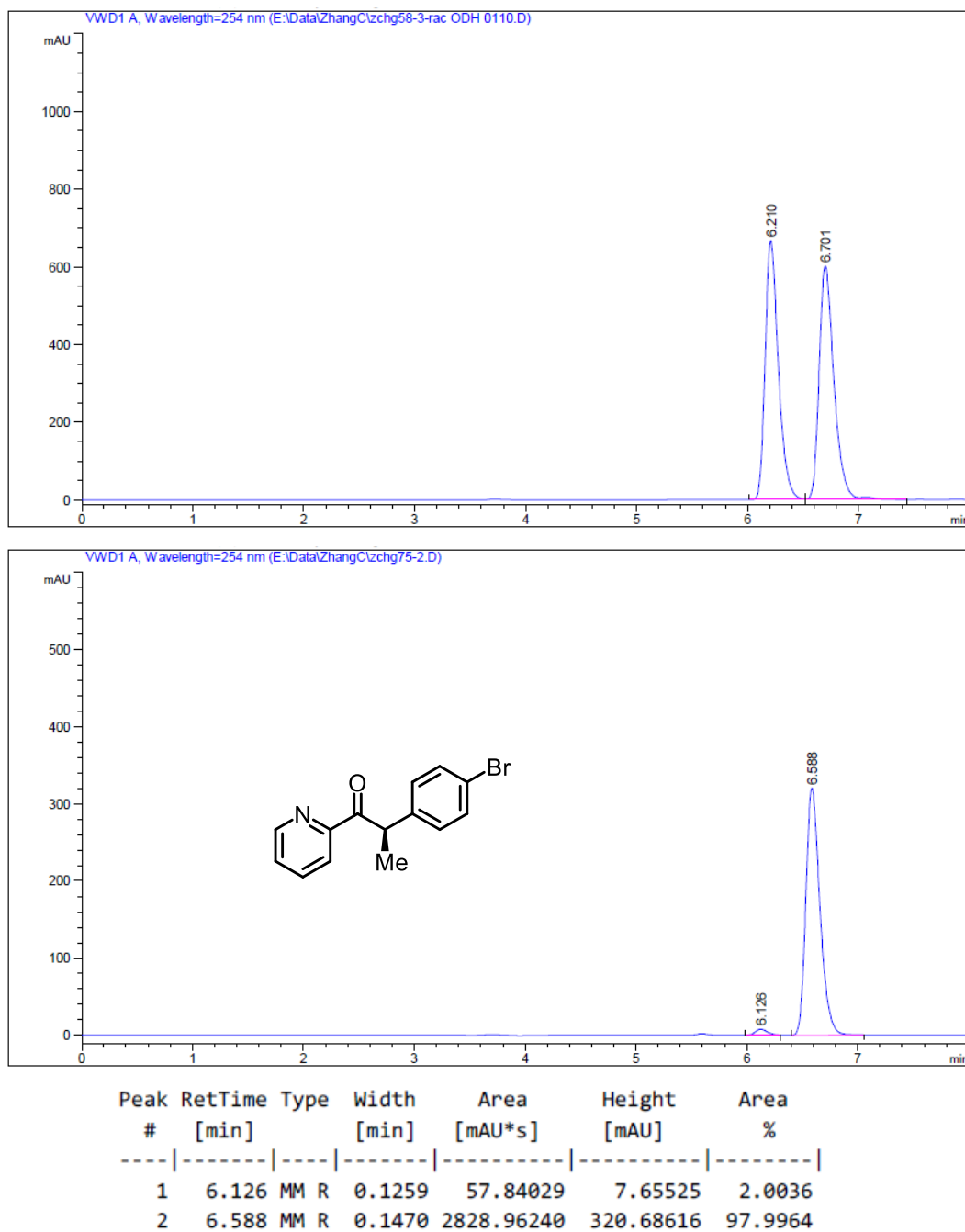


Figure 87. HPLC traces (Daicel Chiralpak OD-H column) of *rac*-**3i** (reference) and (*R*)-**3i**.

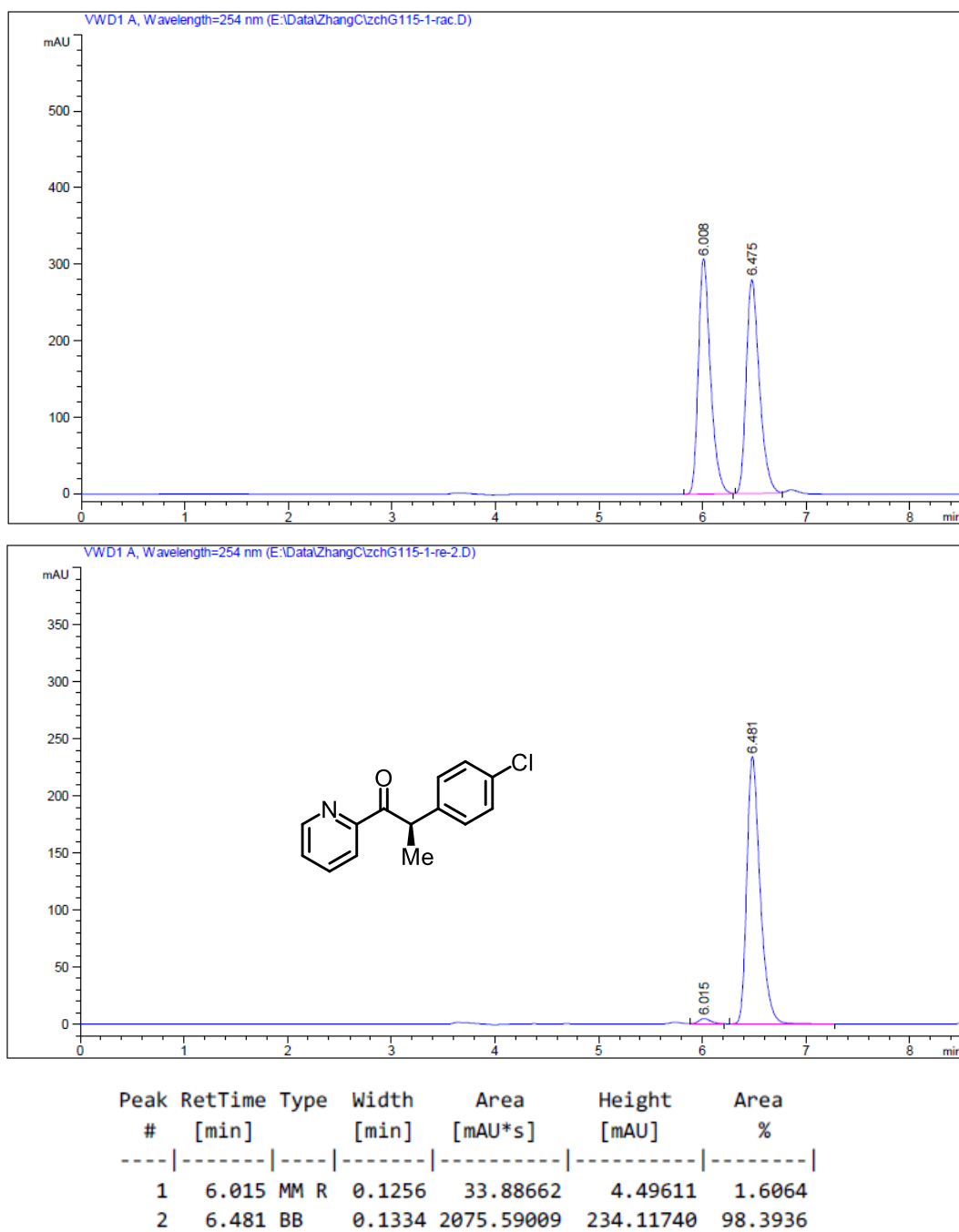


Figure 88. HPLC traces (Daicel Chiralpak OD-H column) of *rac*-**3j** (reference) and (*R*)-**3j**.

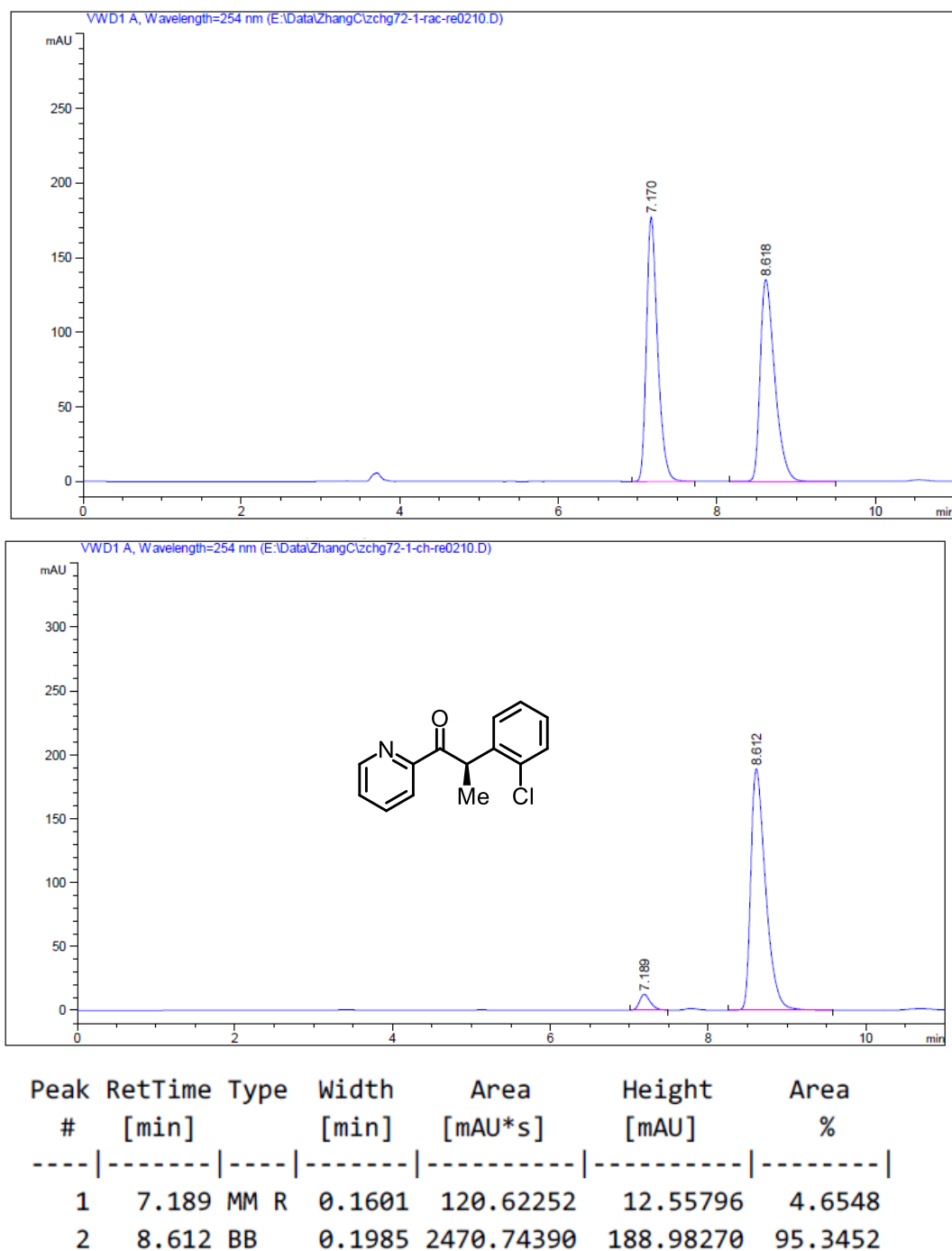


Figure 89. HPLC traces (Daicel Chiralpak OD-H column) of *rac*-**3k** (reference) and (*R*)-**3k**.

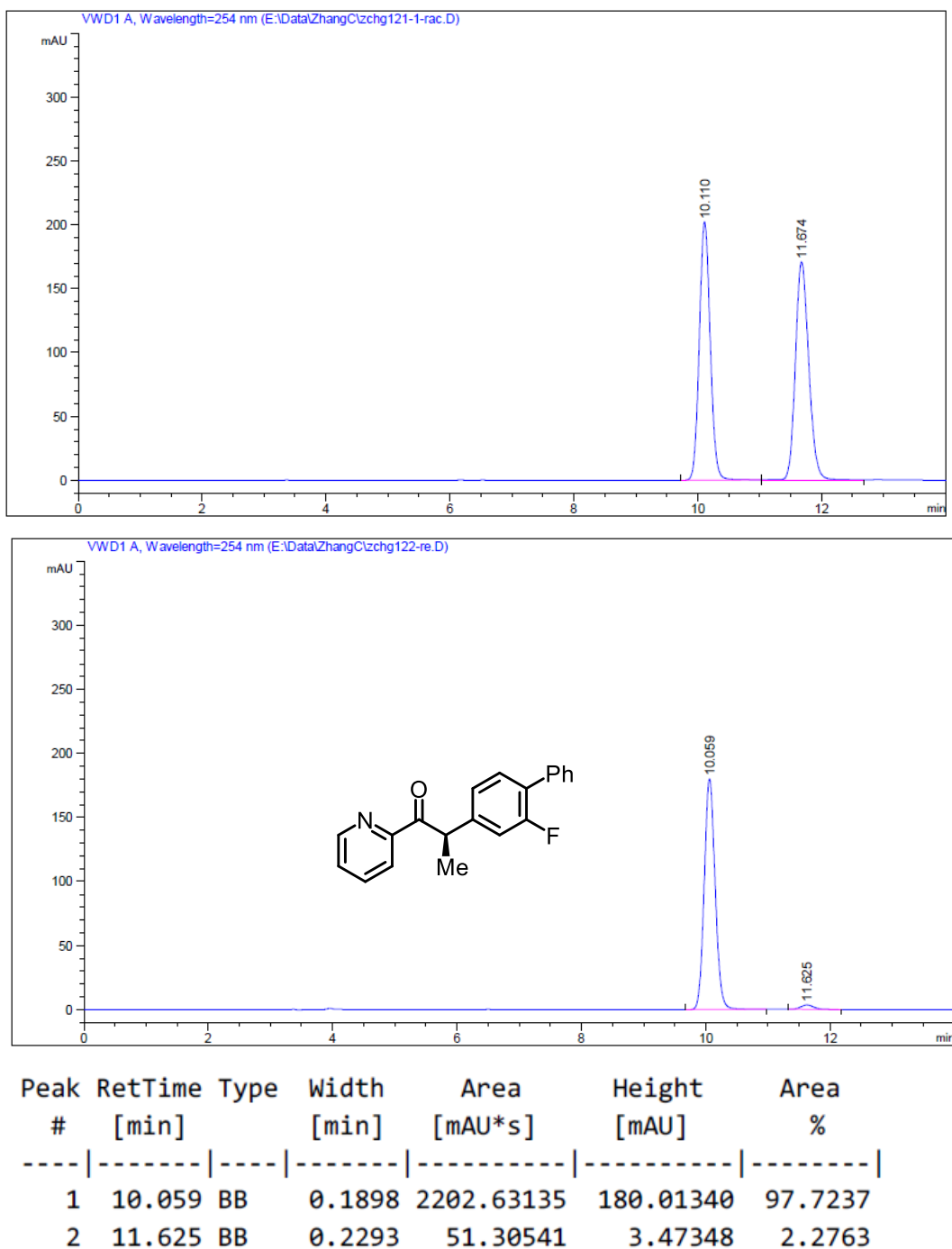


Figure 90. HPLC traces (Daicel Chiralpak IG column) of *rac*-**3I** (reference) and (*R*)-**3I**.

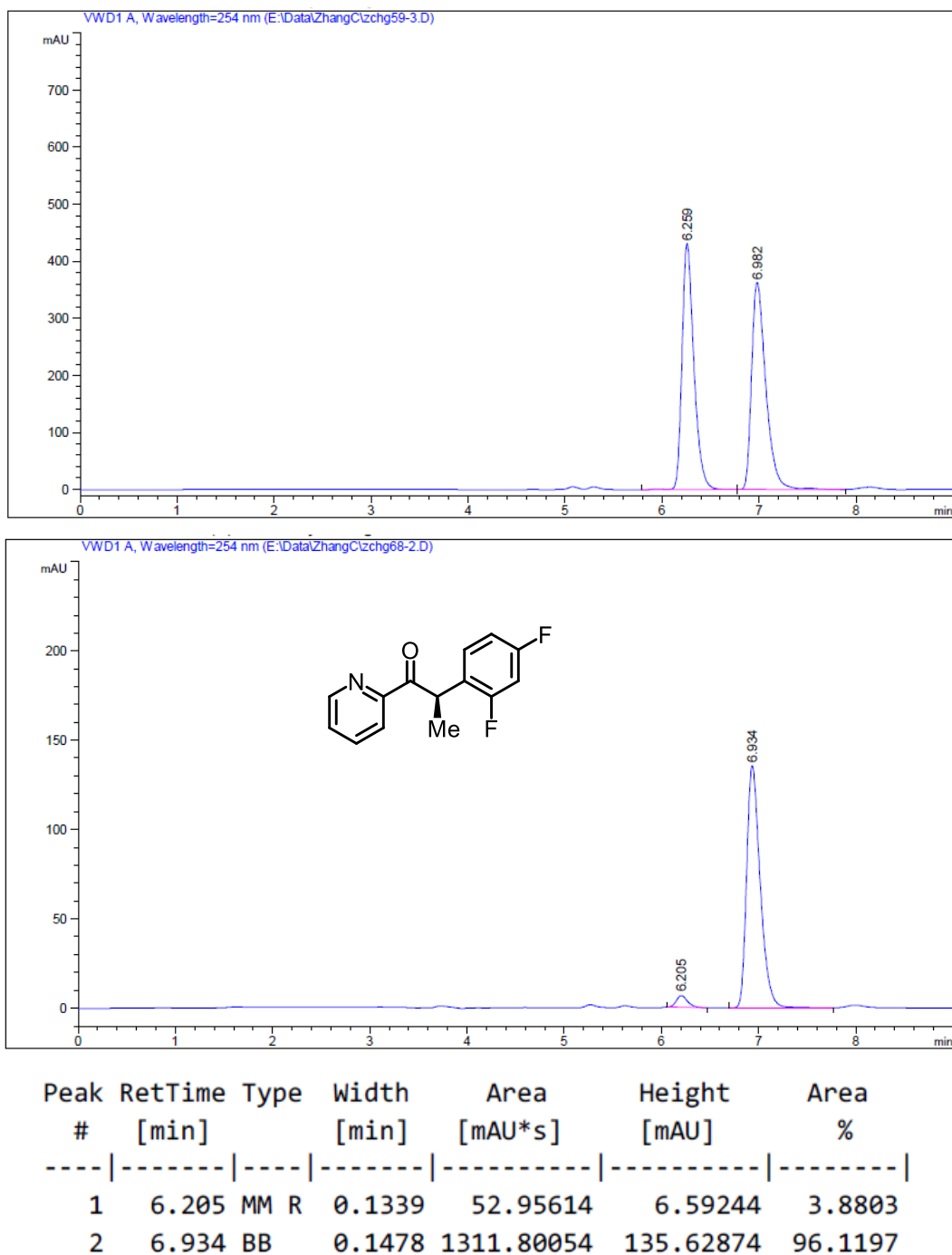


Figure 91. HPLC traces (Daicel Chiralpak OD-H column) of *rac*-**3m** (reference) and (*R*)-**3m**.

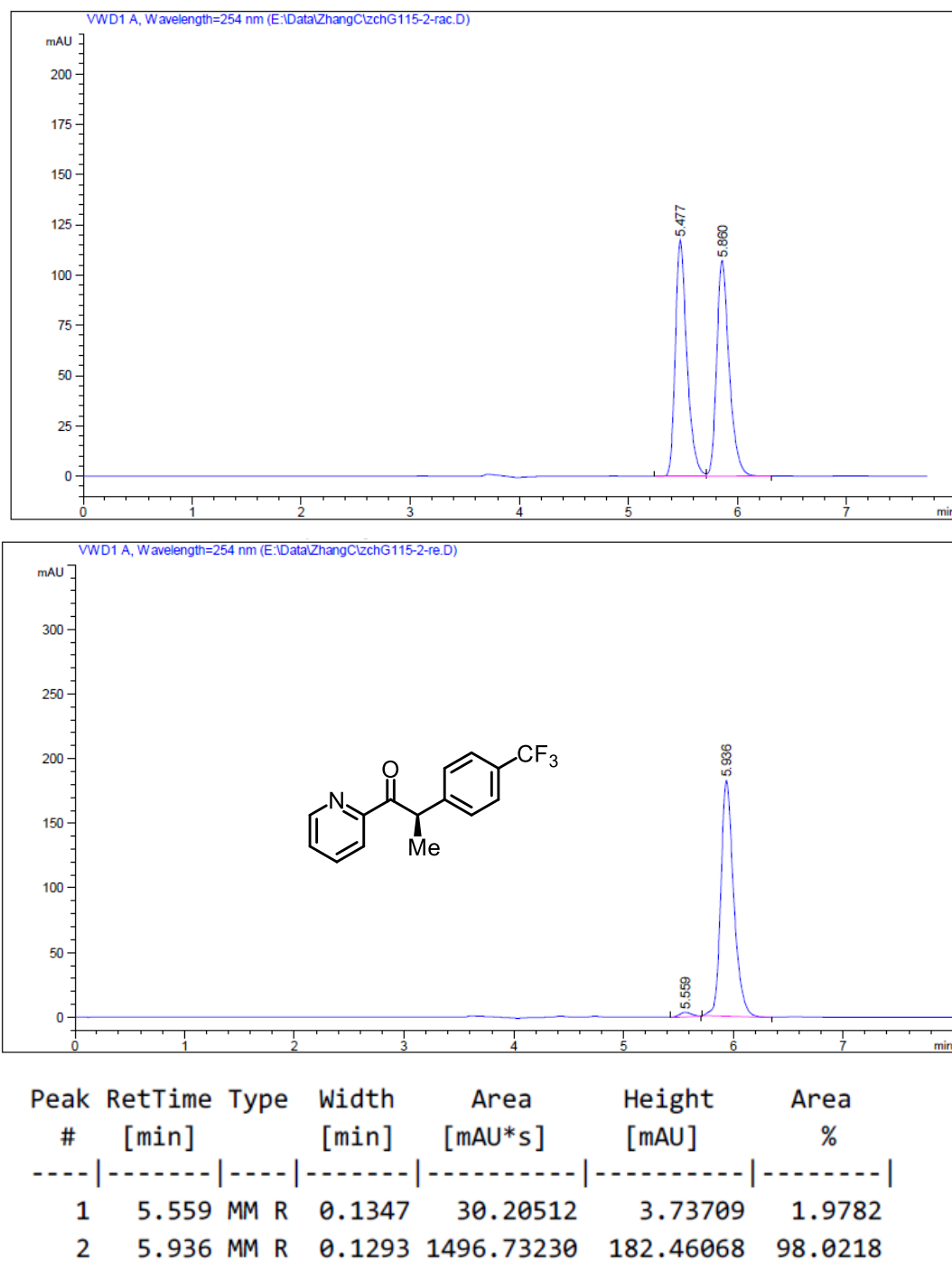
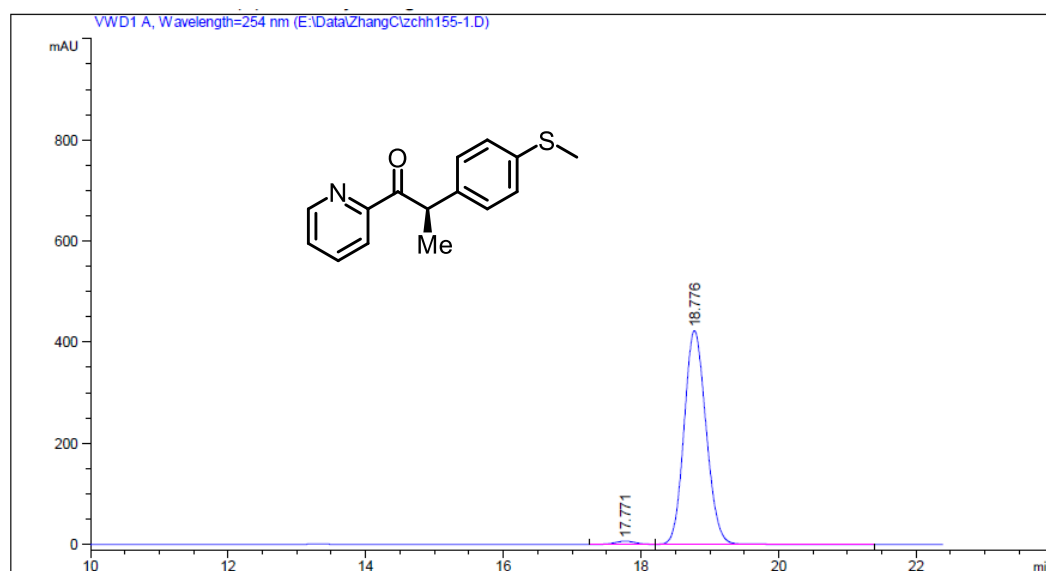
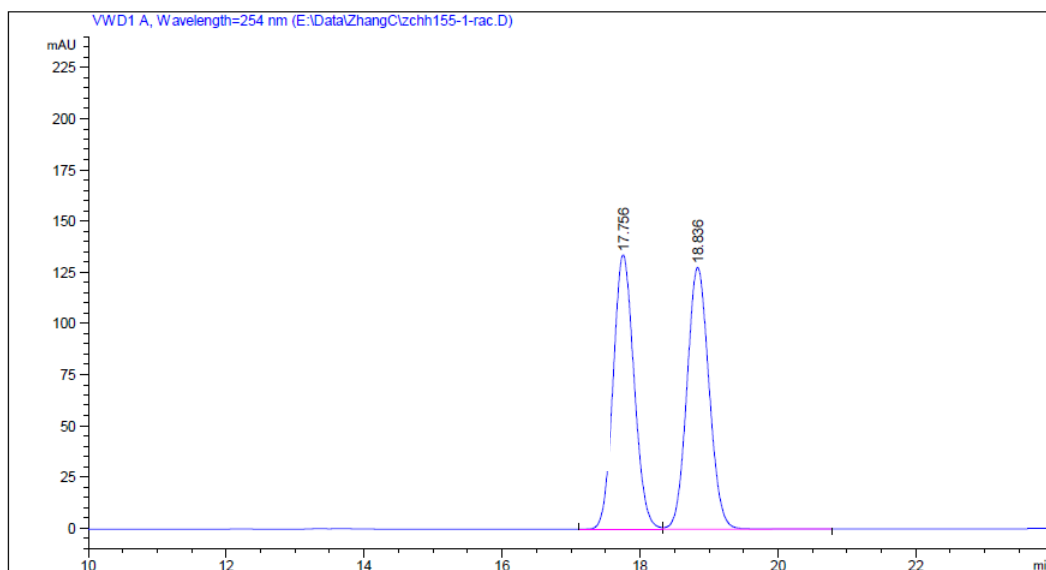
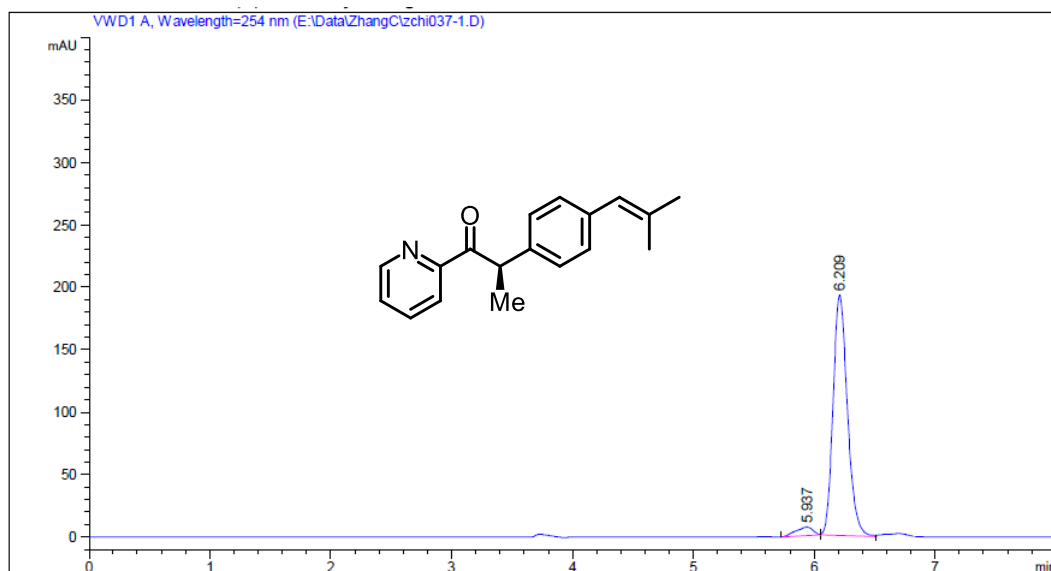
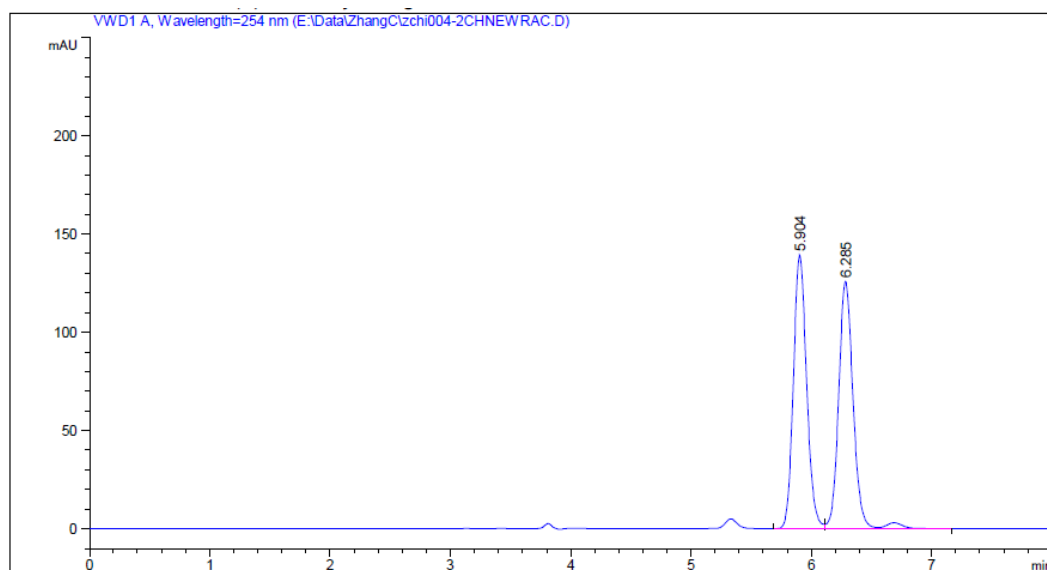


Figure 92. HPLC traces (Daicel Chiralpak OD-H column) of *rac*-**3n** (reference) and (*R*)-**3n**.



Peak #	RetTime [min]	Type	Width [min]	Area [mAU*s]	Height [mAU]	Area %
1	17.771	BV	0.3215	128.09239	6.21334	1.3490
2	18.776	VB	0.3457	9367.56738	422.46283	98.6510

Figure 93. HPLC traces (Daicel Chiralpak IG column) of *rac*-**3o** (reference) and (*R*)-**3o**.



Peak #	RetTime [min]	Type	Width [min]	Area [mAU*s]	Height [mAU]	Area %
1	5.937	MM R	0.1680	69.63528	6.90890	4.2142
2	6.209	MM R	0.1370	1582.74414	192.53546	95.7858

Figure 94. HPLC traces (Daicel Chiralpak OD-H column) of *rac*-**3p** (reference) and (*R*)-**3p**.

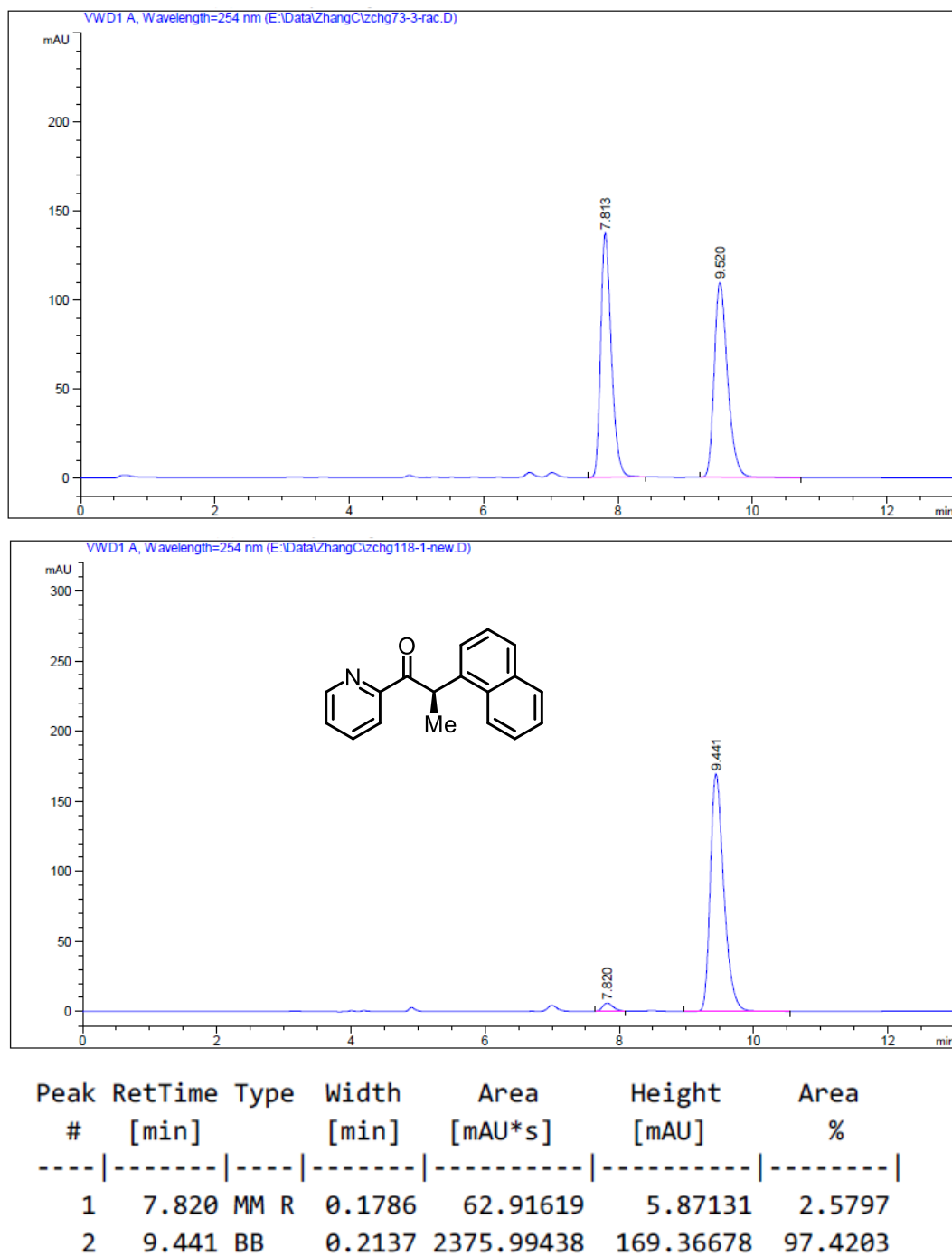
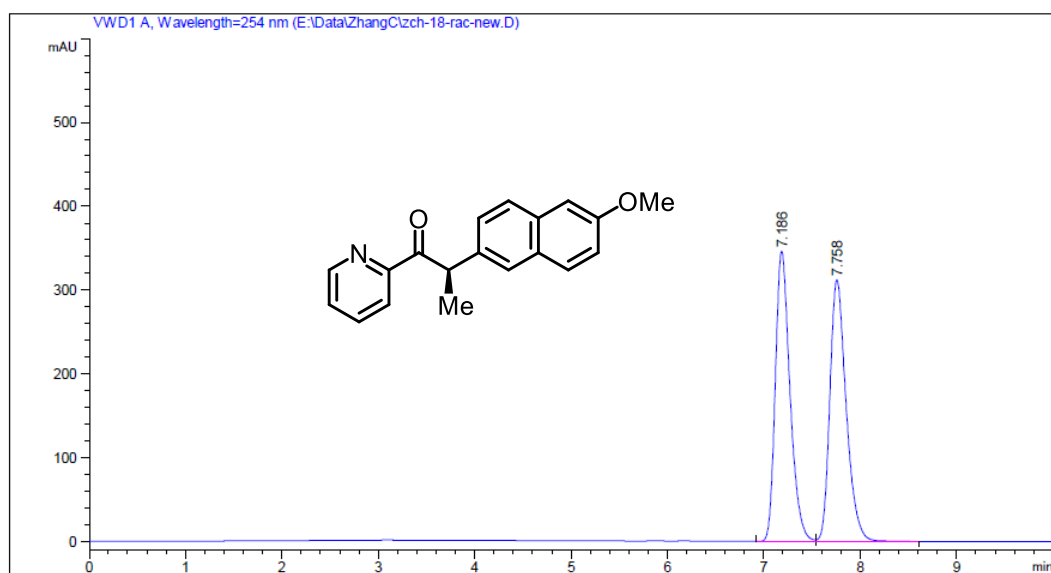
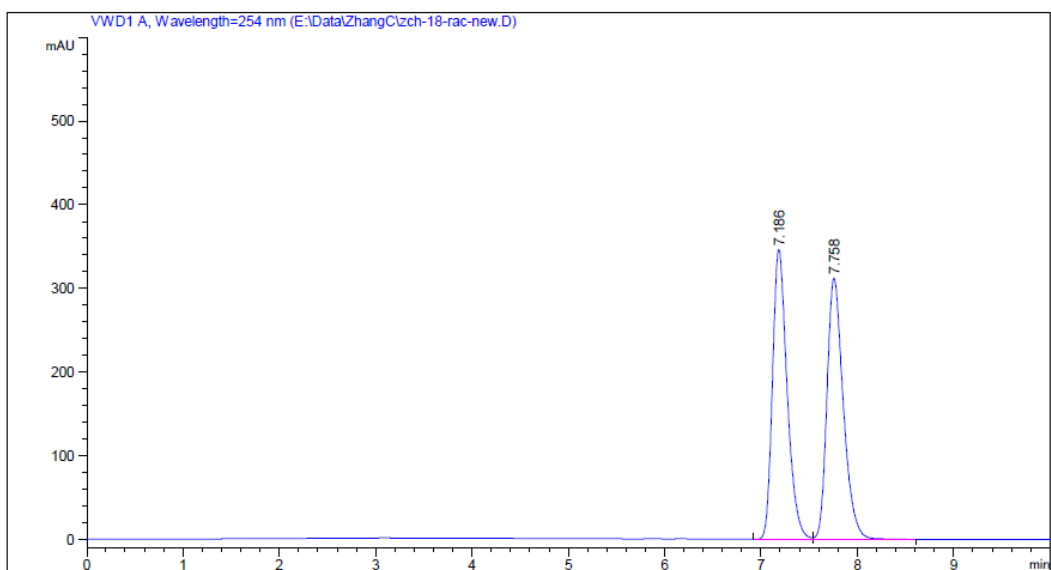


Figure 95. HPLC traces (Daicel Chiralpak OD-H column) of *rac*-**3q** (reference) and (*R*)-**3q**.



Peak #	RetTime [min]	Type	Width [min]	Area [mAU*s]	Height [mAU]	Area %
1	7.255	MM R	0.1626	56.96895	5.83815	2.0997
2	7.723	VB	0.1754	2656.27710	232.34747	97.9003

Figure 96. HPLC traces (Daicel Chiralpak OD-H column) of *rac*-**3r** (reference) and (*R*)-**3r**.

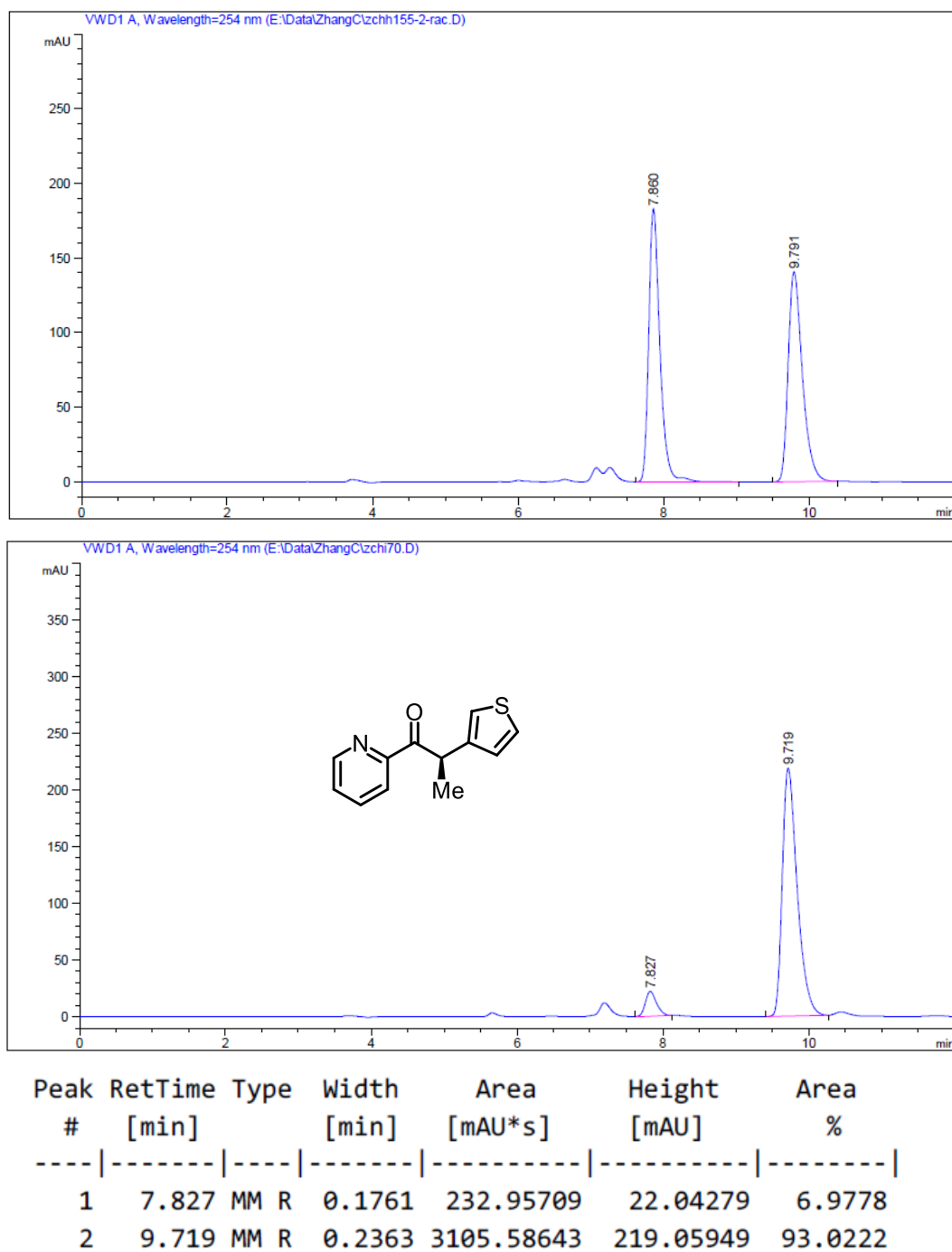


Figure 97. HPLC traces (Daicel Chiralpak OD-H column) of *rac*-**3s** (reference) and (*R*)-**3s**.

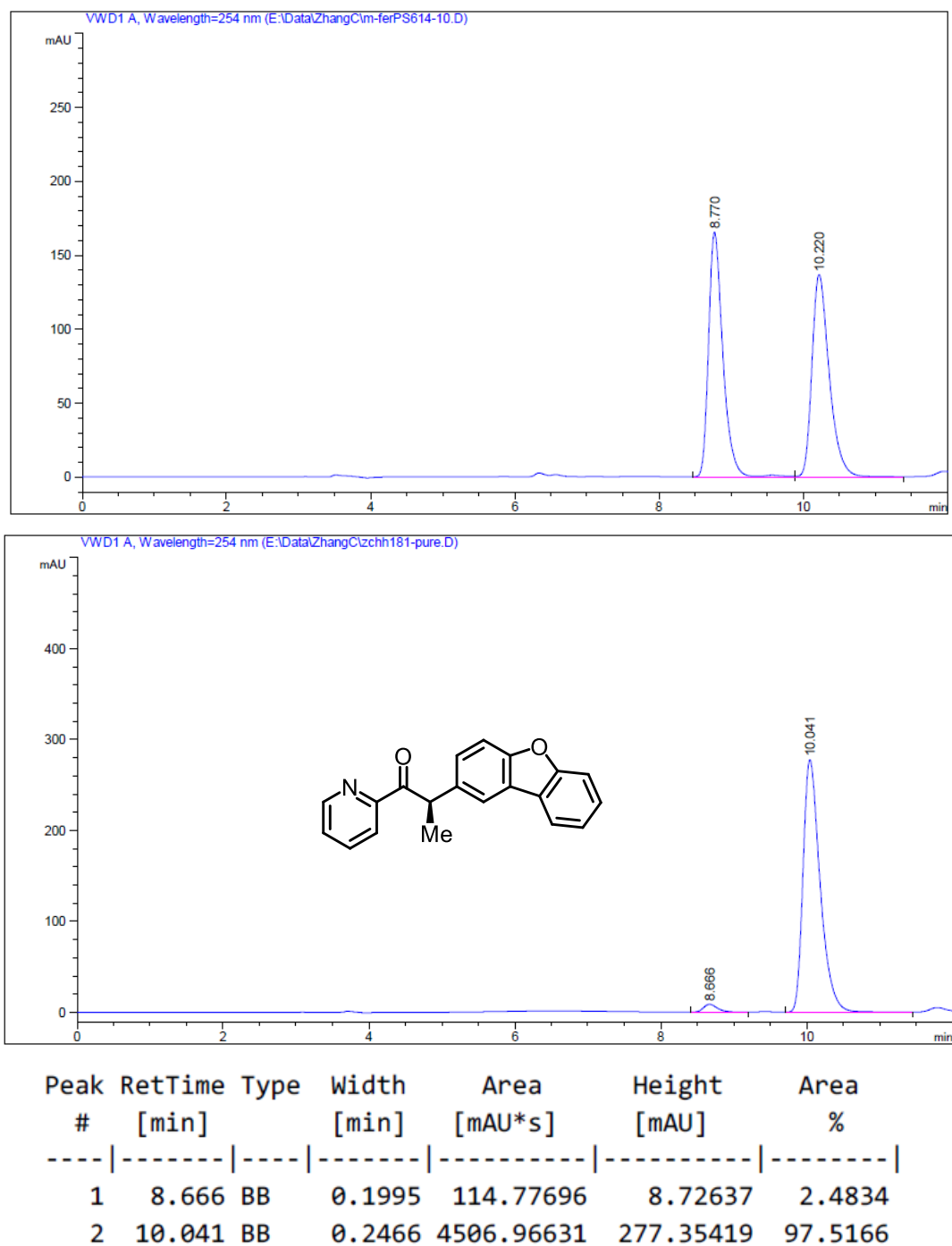
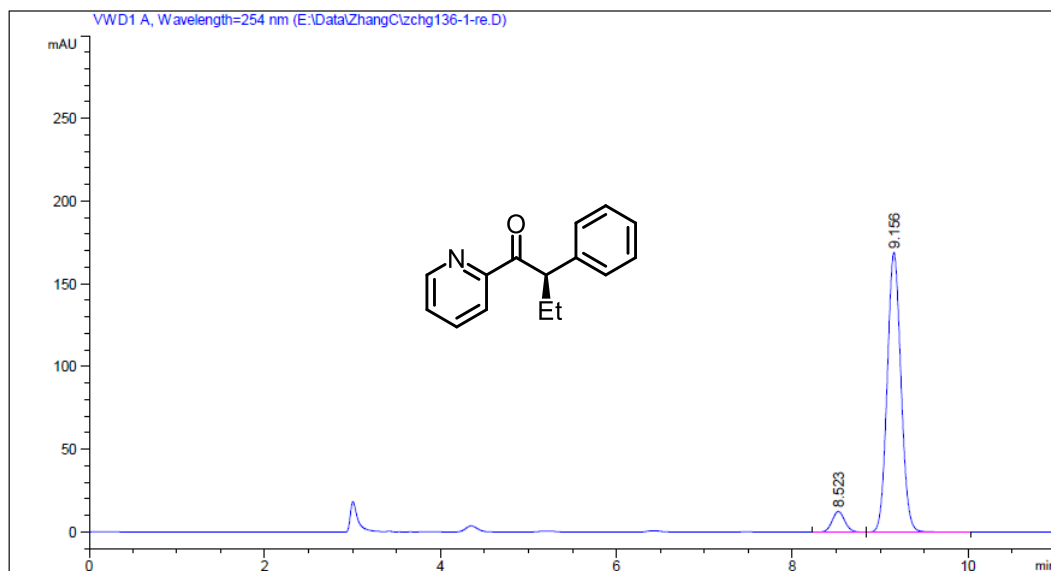
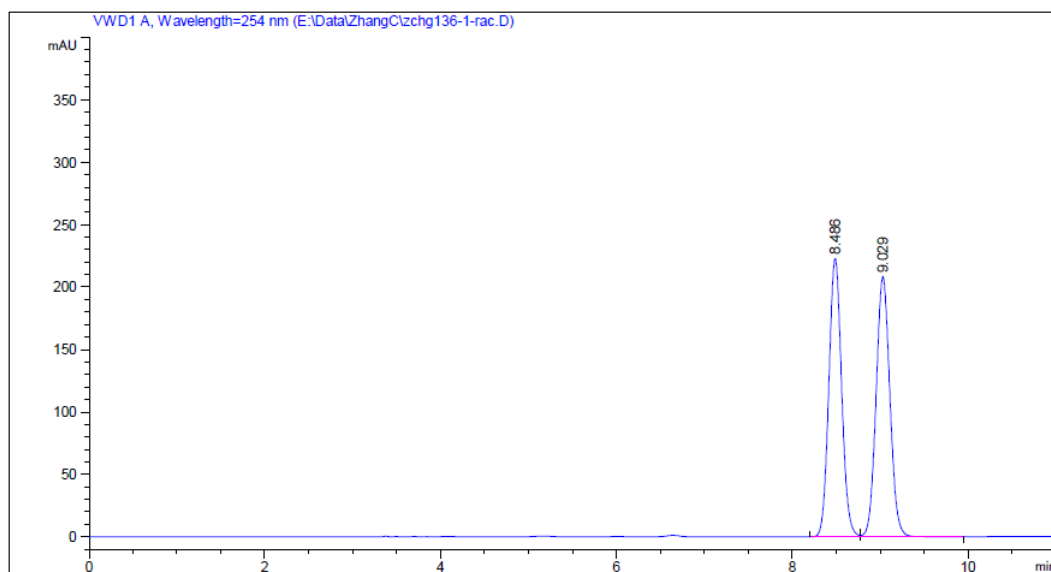


Figure 98. HPLC traces (Daicel Chiralpak OD-H column) of *rac*-**3t** (reference) and (*R*)-**3t**.



Peak #	RetTime [min]	Type	Width [min]	Area [mAU*s]	Height [mAU]	Area %
1	8.523	BV	0.1570	126.64478	12.52324	6.4251
2	9.156	VB	0.1702	1844.43628	169.20724	93.5749

Figure 99. HPLC traces (Daicel Chiralpak IG column) of *rac*-**21** (reference) and (*R*)-**21**.

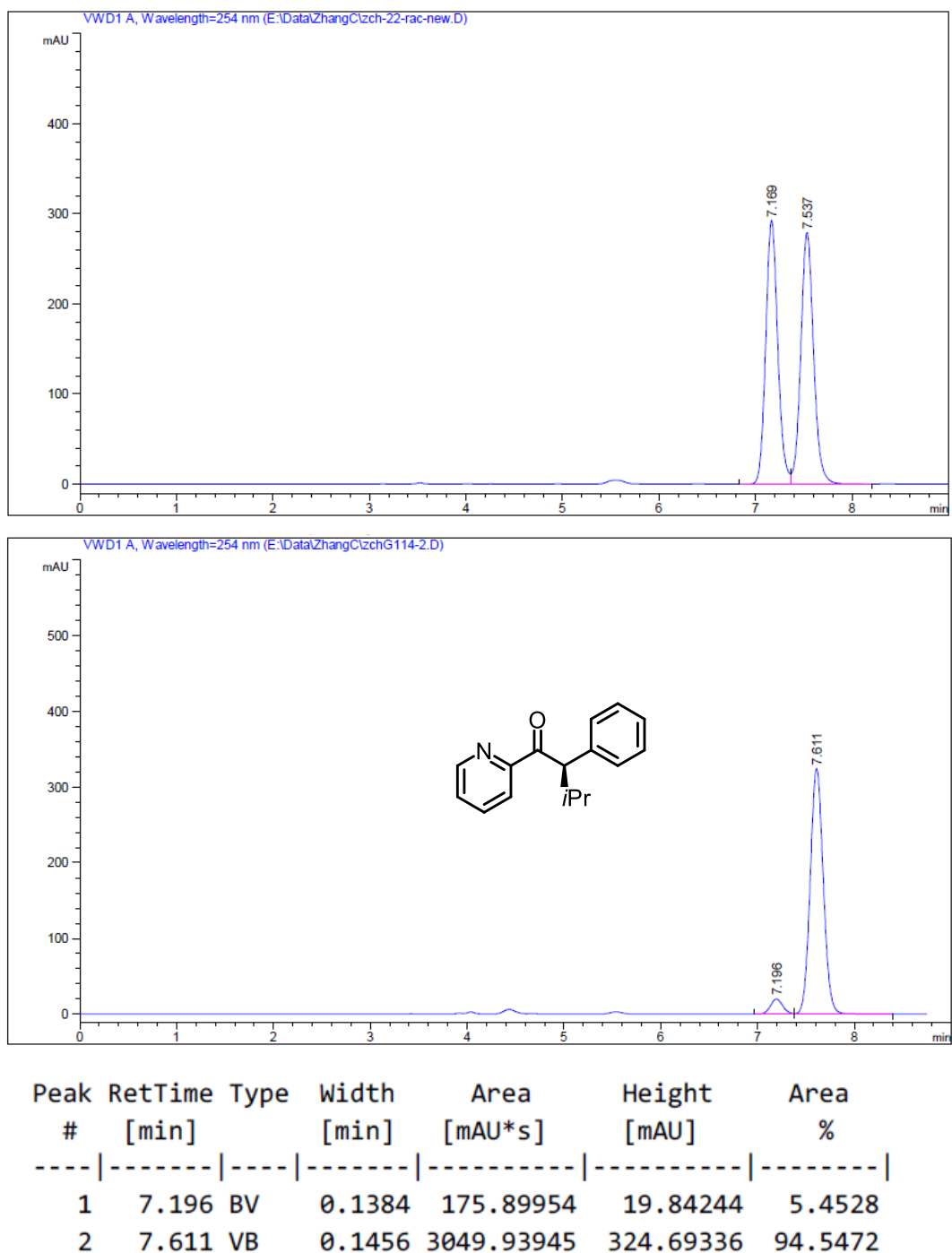


Figure 100. HPLC traces (Daicel Chiralpak IG column) of *rac*-**3v** (reference) and (*R*)-**3v**.

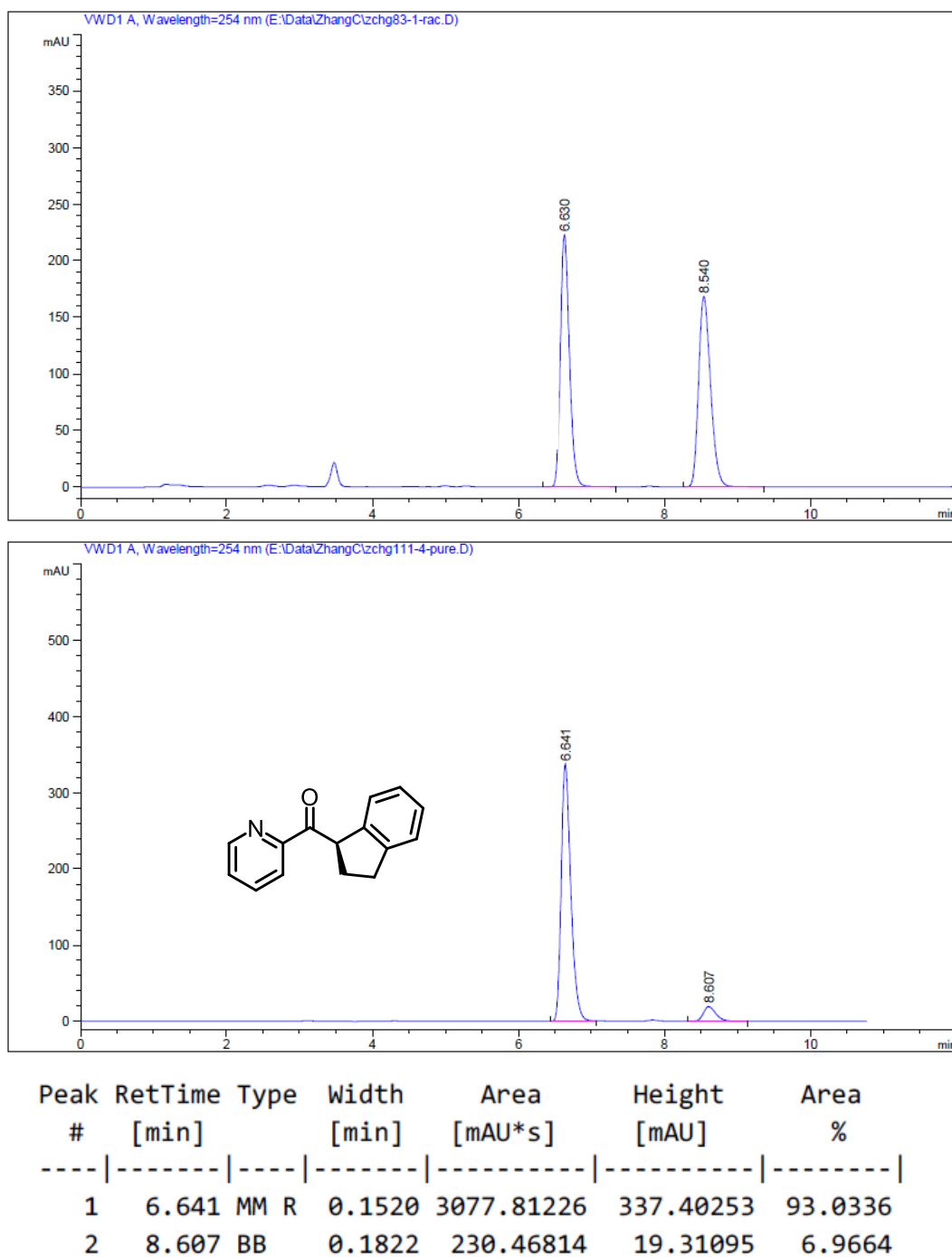
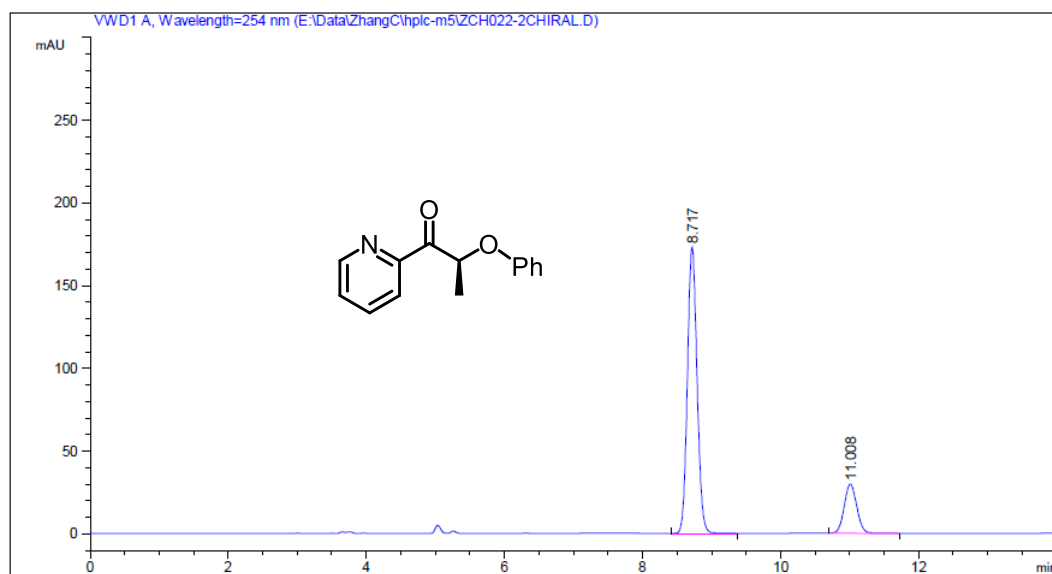
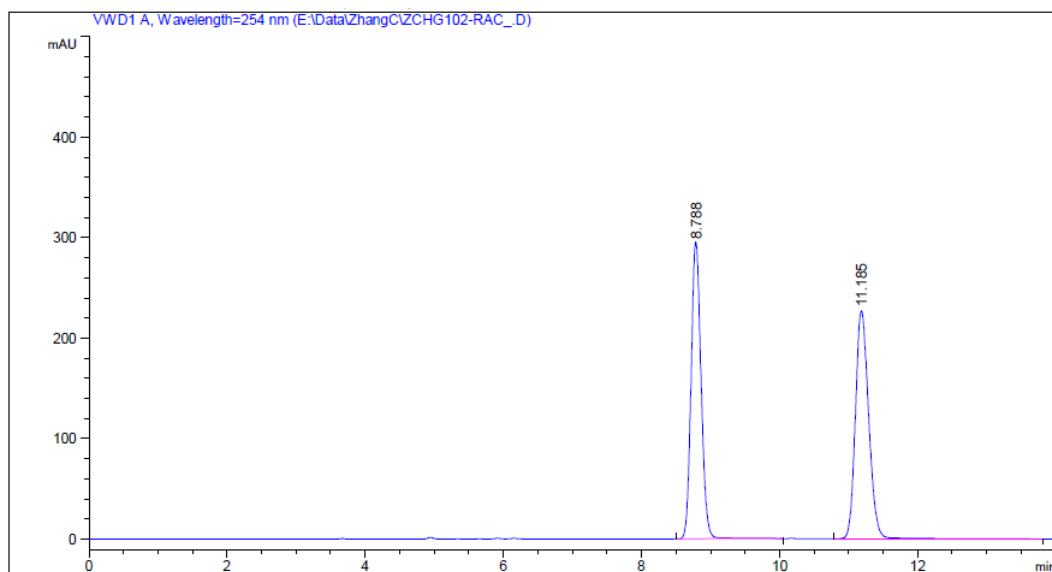
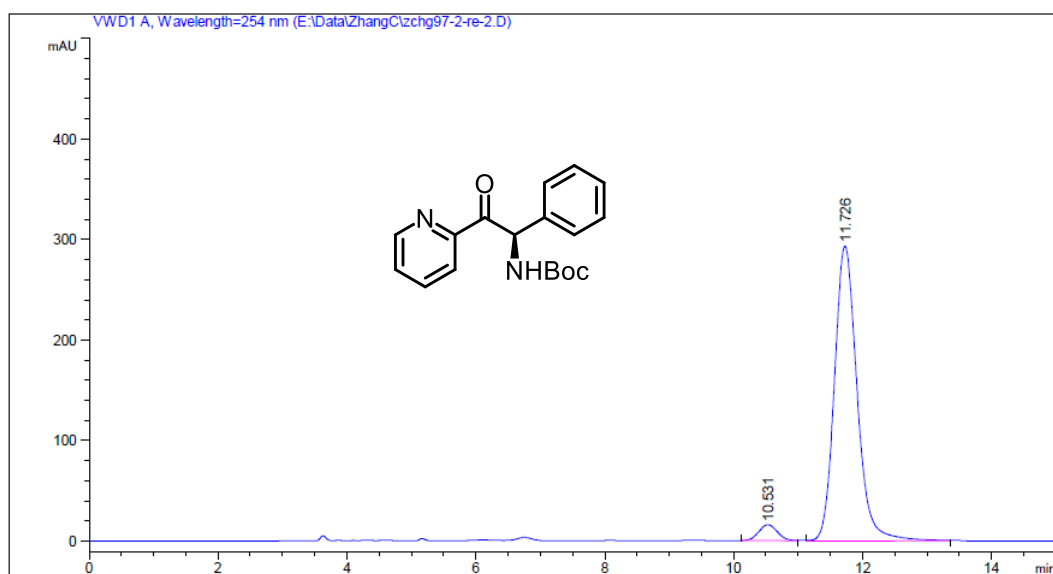
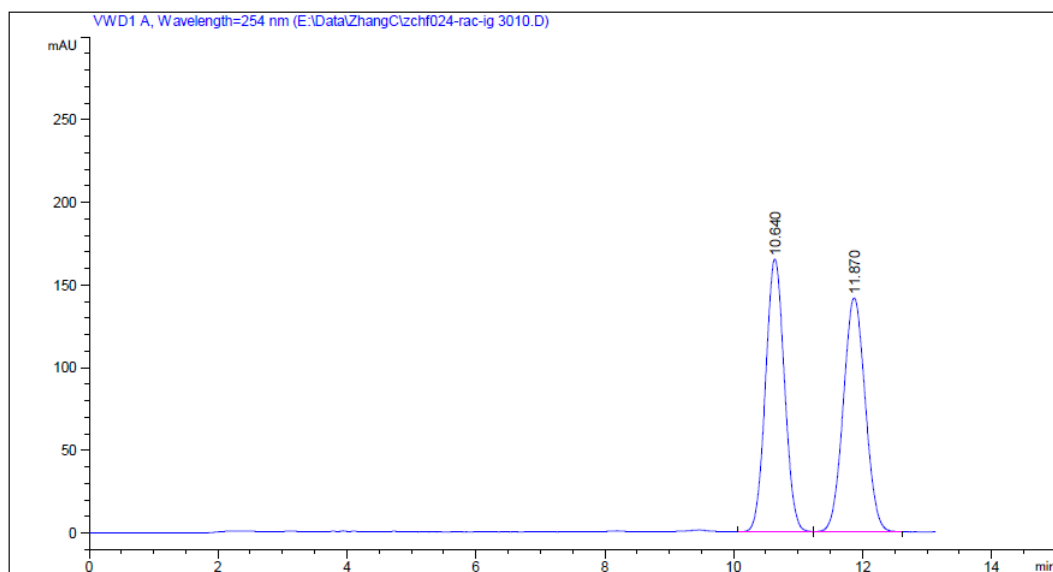


Figure 101. HPLC traces (Daicel Chiralpak OD-H column) of *rac*-**3w** (reference) and (*R*)-**3w**.



Peak #	RetTime [min]	Type	Width [min]	Area mAU *s	Height [mAU]	Area %
1	8.717	BB	0.1494	1676.38525	173.10094	81.9129
2	11.008	BB	0.1937	370.16037	29.64959	18.0871

Figure 102. HPLC traces (Daicel Chiralpak IG column) of *rac*-**3x** (reference) and (*S*)-**3x**.



Peak #	RetTime [min]	Type	Width [min]	Area [mAU*s]	Height [mAU]	Area %
1	10.531	MM R	0.3293	309.06665	15.64463	4.1429
2	11.726	MM R	0.3216	7151.03662	293.28226	95.8571

Figure 103. HPLC traces (Daicel Chiralpak IG column) of *rac*-**3y** (reference) and (*R*)-**3y**.

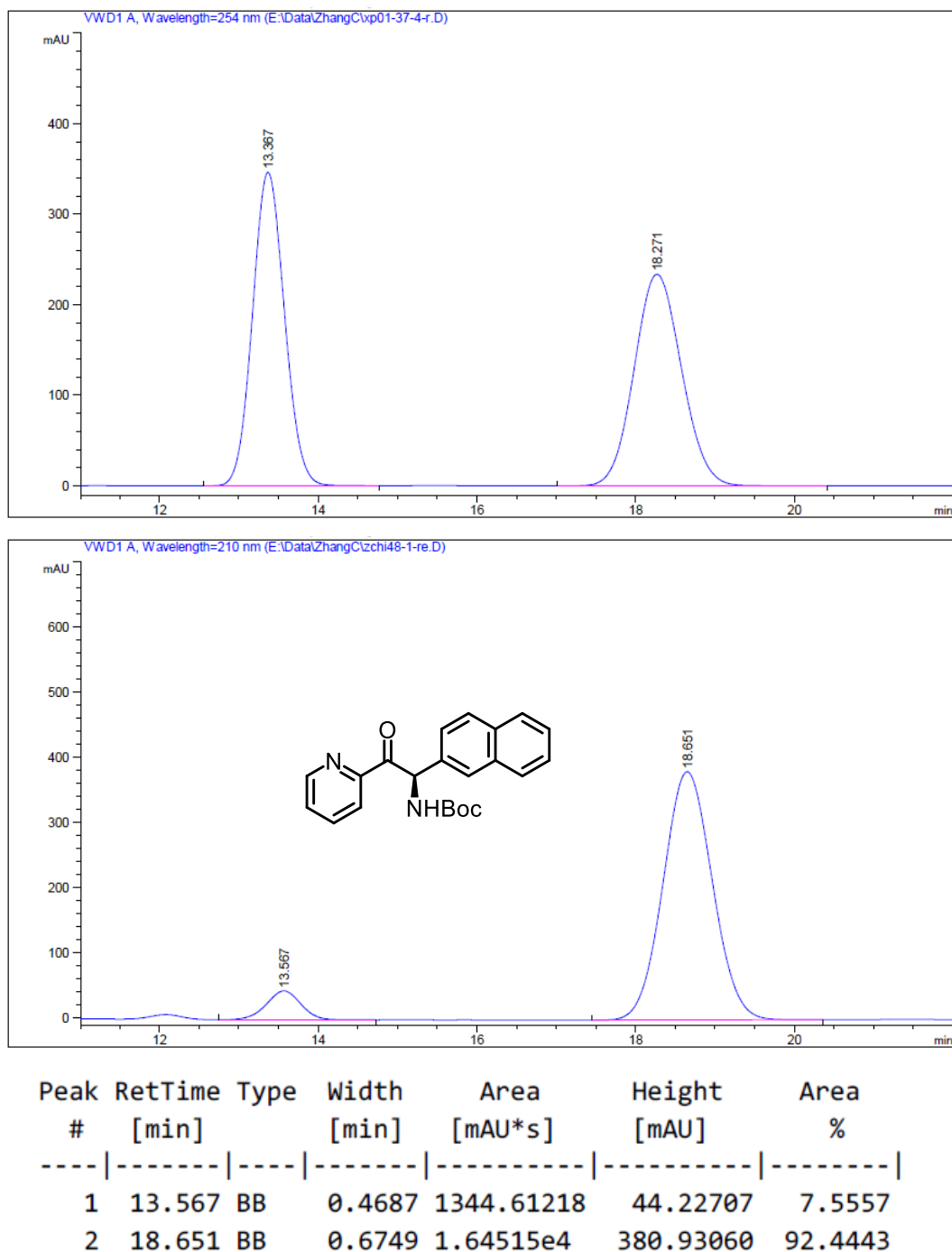
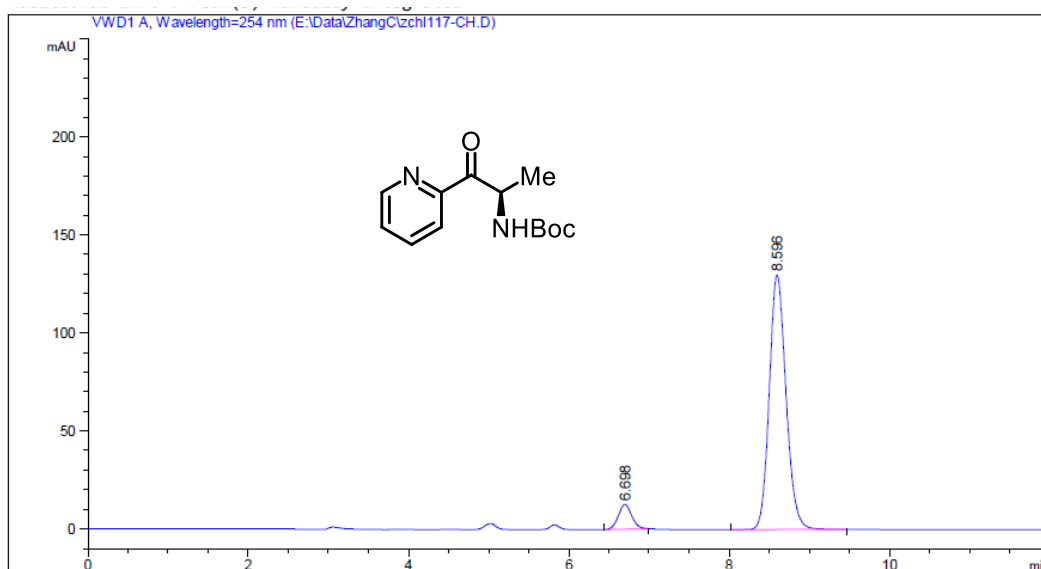
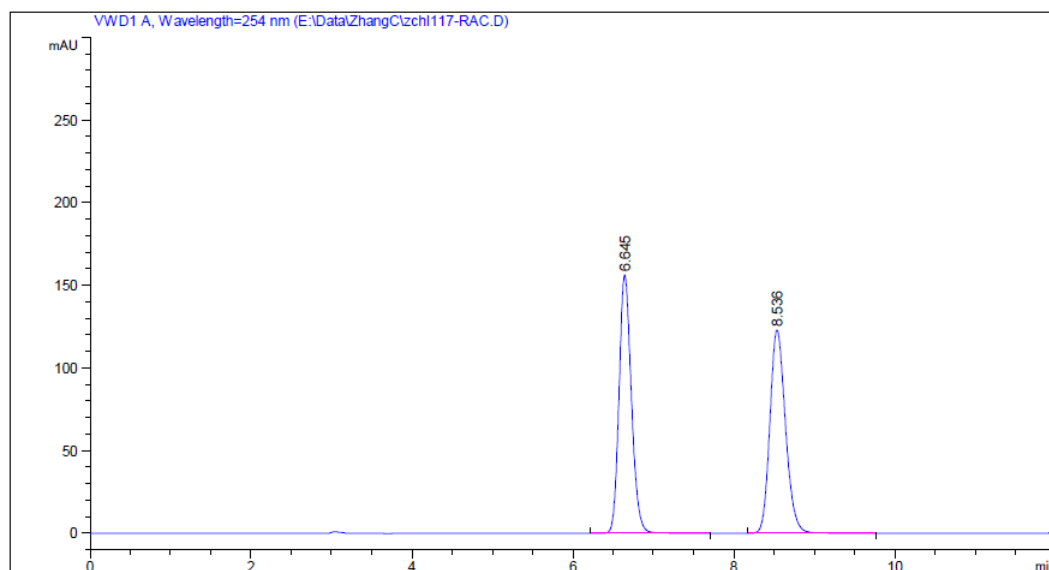


Figure 104. HPLC traces (Daicel Chiralpak IG column) of *rac*-**3z** (reference) and (*R*)-**3z**.



Peak #	RetTime [min]	Type	Width [min]	Area [mAU*s]	Height [mAU]	Area %
1	6.698	MM R	0.1949	147.86514	12.64326	7.2715
2	8.596	BB	0.2234	1885.61194	129.89323	92.7285

Figure 105. HPLC traces (Daicel Chiralpak OD-H column) of *rac*-**3aa** (reference) and (*R*)-**3aa**.

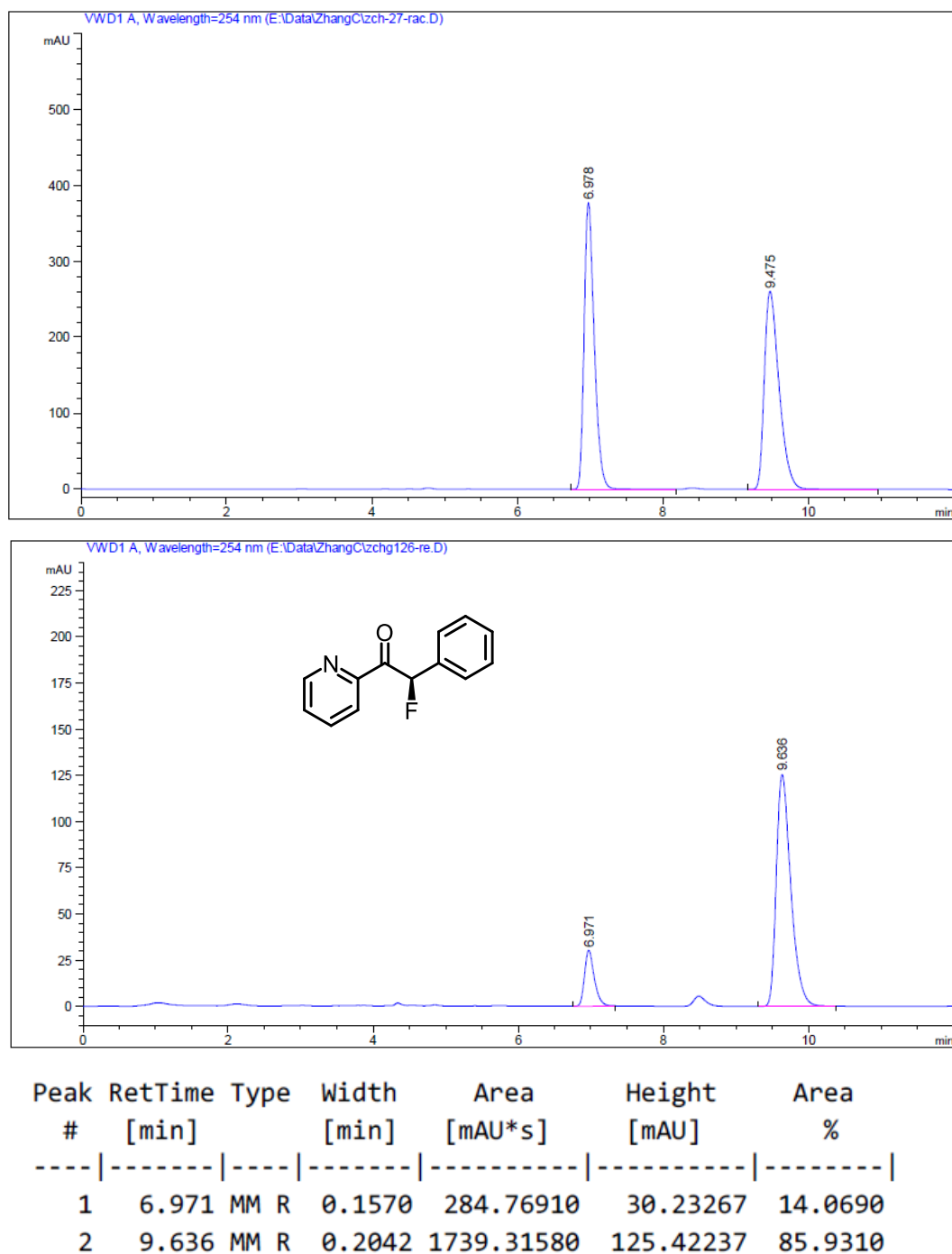


Figure 106. HPLC traces (Daicel Chiralpak OD-H column) of *rac*-**3ab** (reference) and (*R*)-**3ab**.

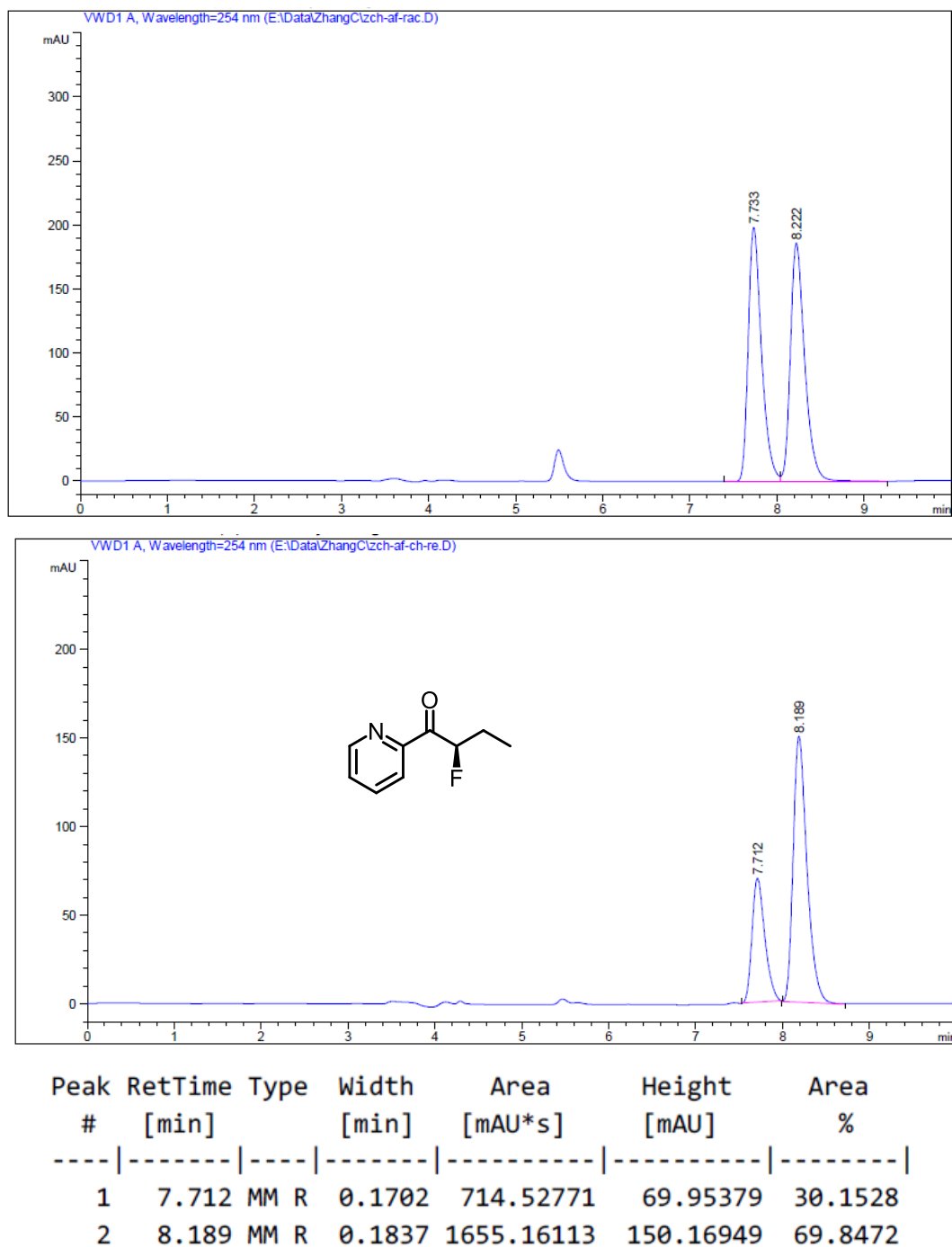


Figure 107. HPLC traces (Daicel Chiralpak OD-H column) of *rac*-**3ac** (reference) and (*R*)-**3ac**.

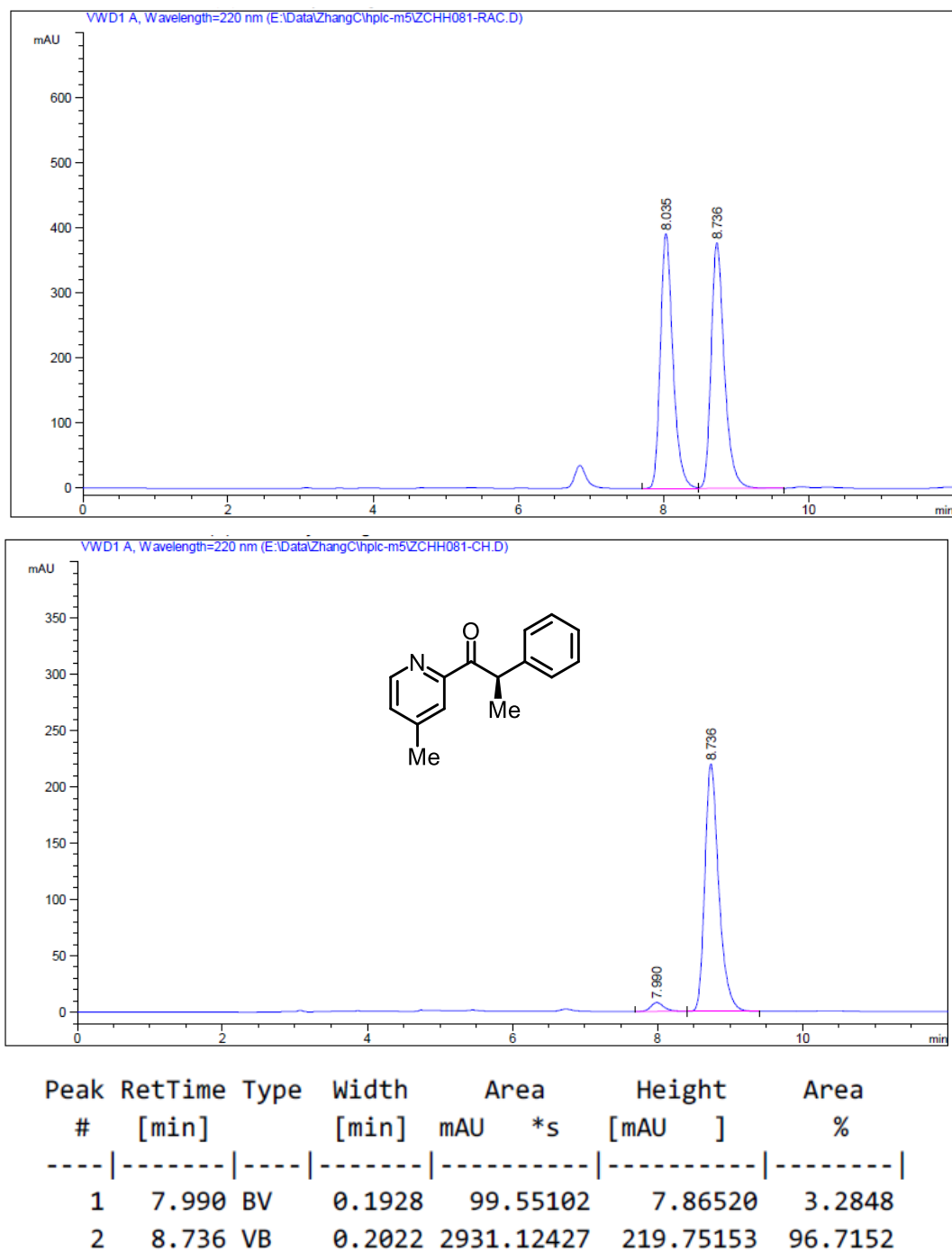
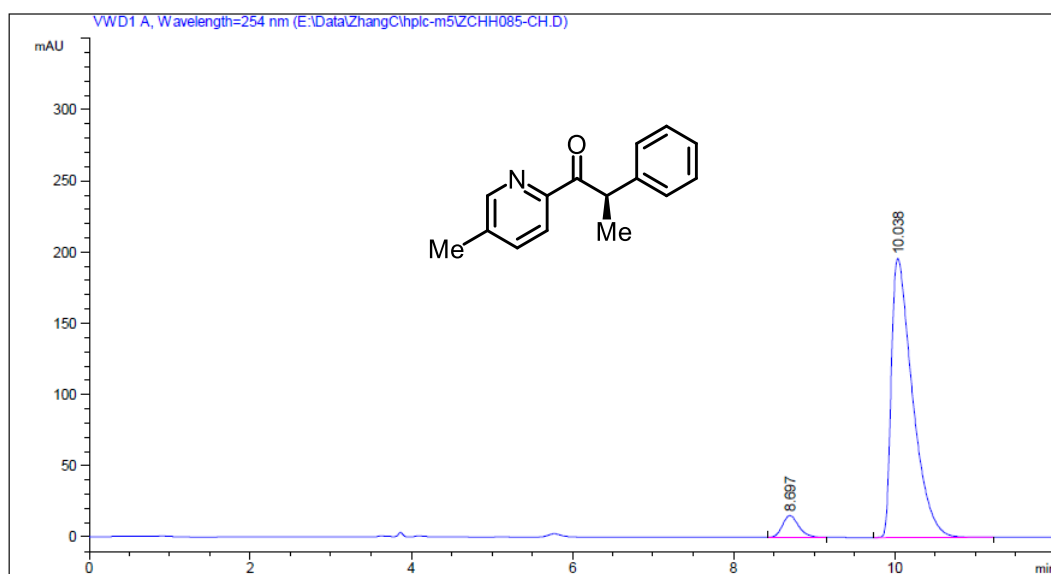
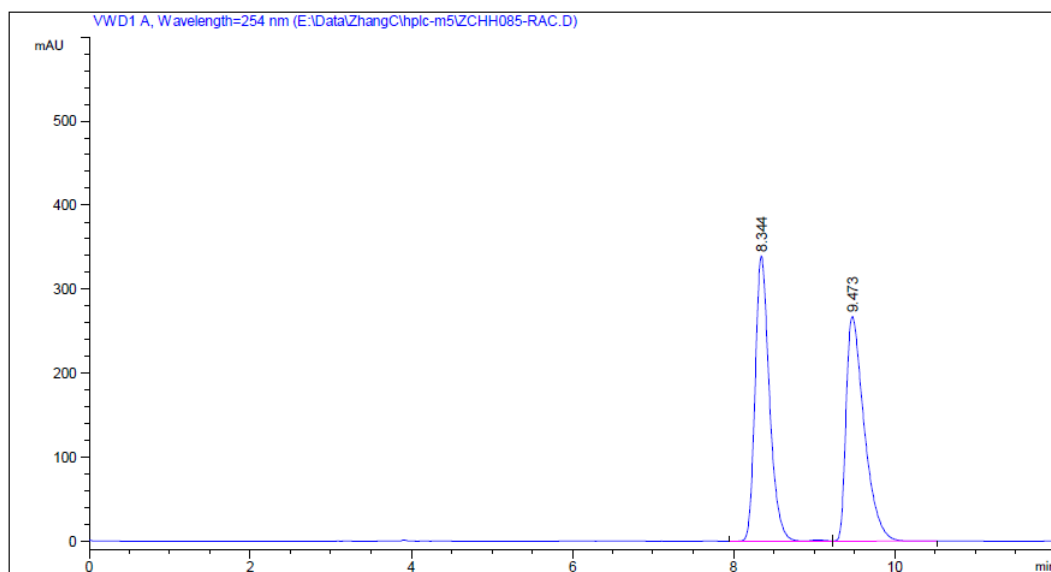
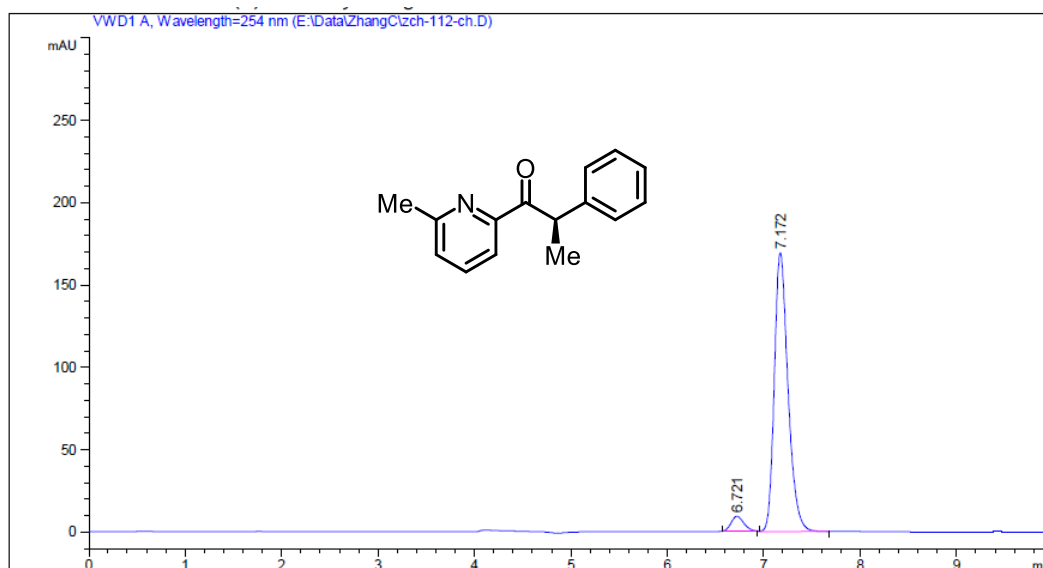
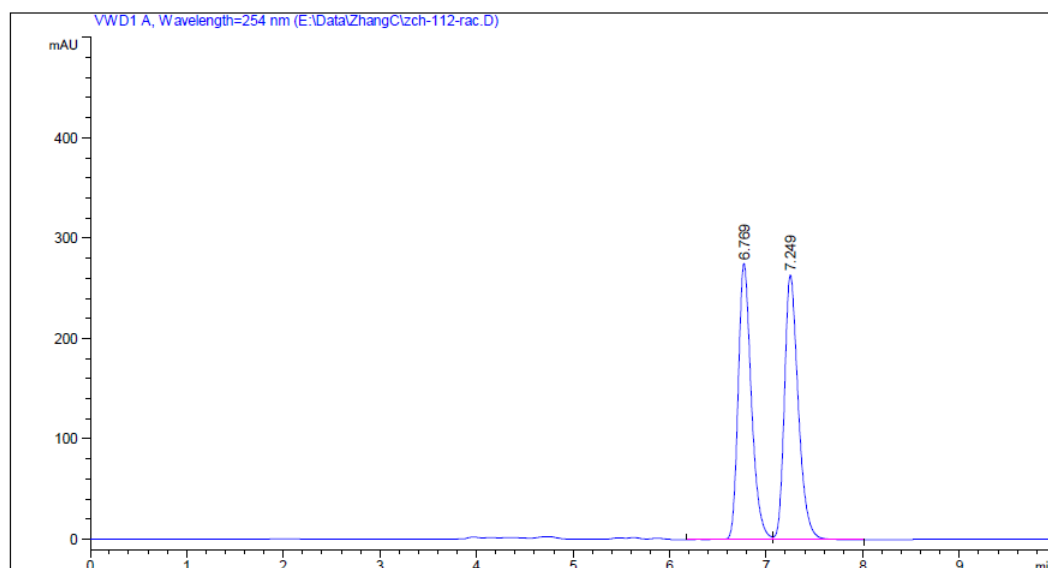


Figure 108. HPLC traces (Daicel Chiralpak OD-H column) of *rac*-**3ad** (reference) and (*R*)-**3ad**.



Peak #	RetTime [min]	Type	Width [min]	Area mAU *s	Height [mAU]	Area %
1	8.697	MM R	0.2308	210.64880	15.21007	5.5802
2	10.038	BB	0.2718	3564.26807	196.02168	94.4198

Figure 109. HPLC traces (Daicel Chiralpak OD-H column) of *rac*-**3ae** (reference) and (*R*)-**3ae**.



Peak #	RetTime [min]	Type	Width [min]	Area [mAU*s]	Height [mAU]	Area %
1	6.721	MM R	0.1542	85.16660	9.20549	4.8461
2	7.172	VB	0.1512	1672.26965	169.41795	95.1539

Figure 110. HPLC traces (Daicel Chiralpak OD-H column) of *rac*-32 (reference) and (*R*)-32.

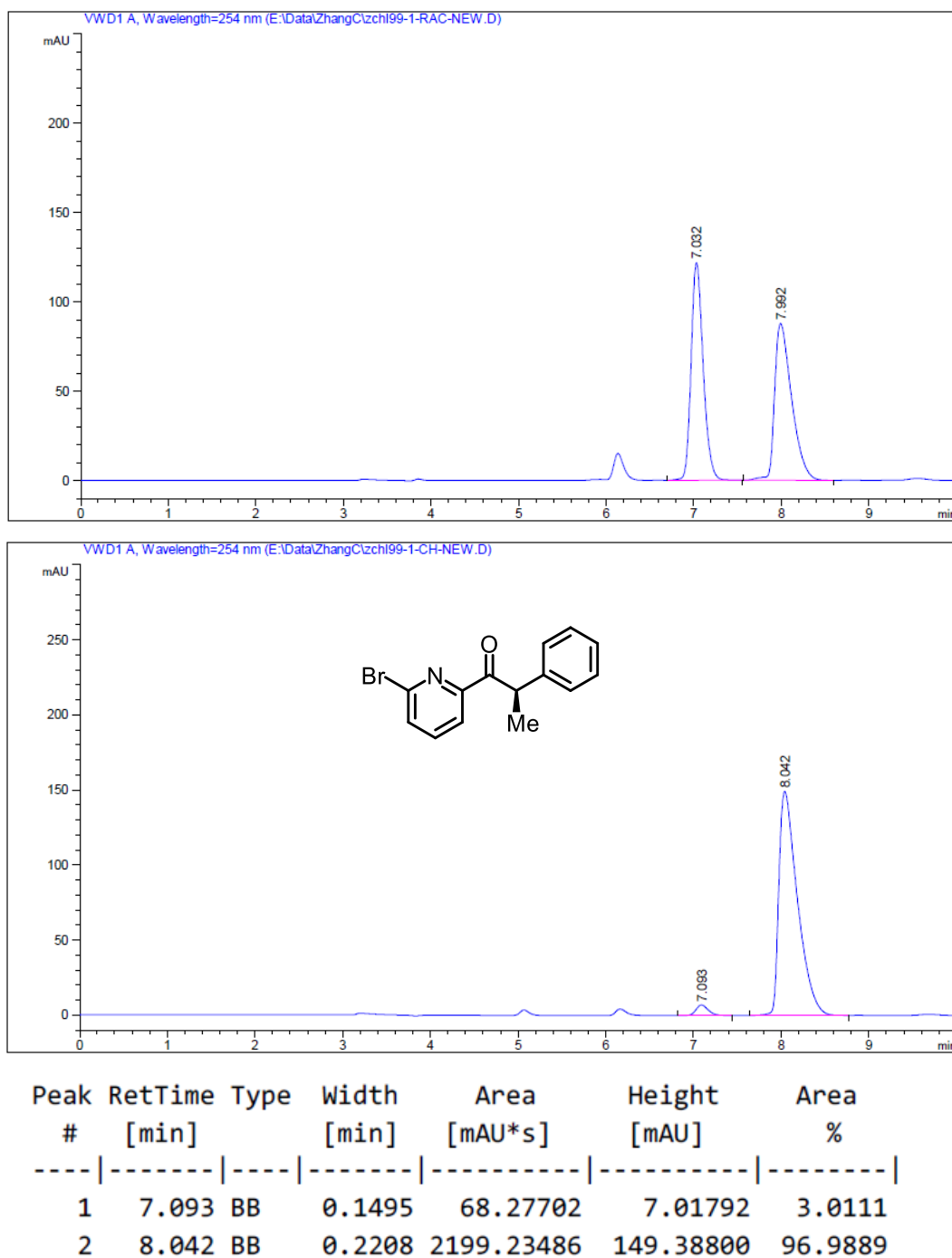


Figure 111. HPLC traces (Daicel Chiralpak OD-H column) of *rac*-**3ag** (reference) and (*R*)-**3ag**.

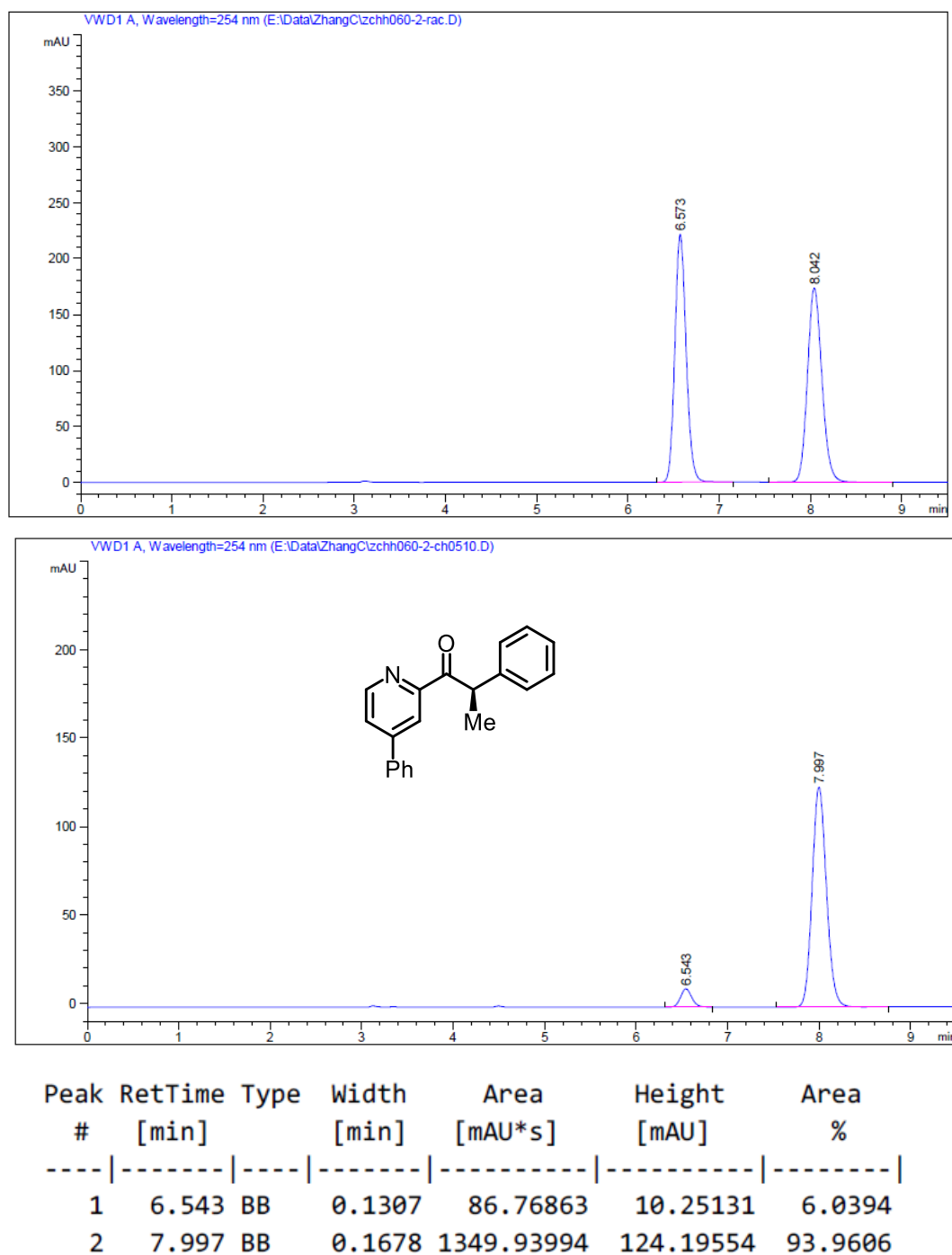
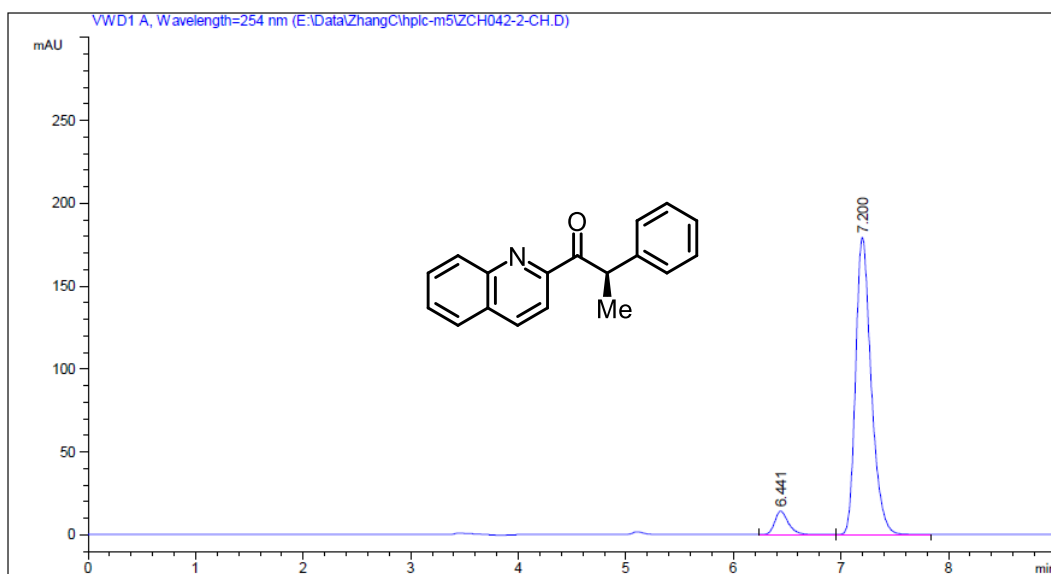
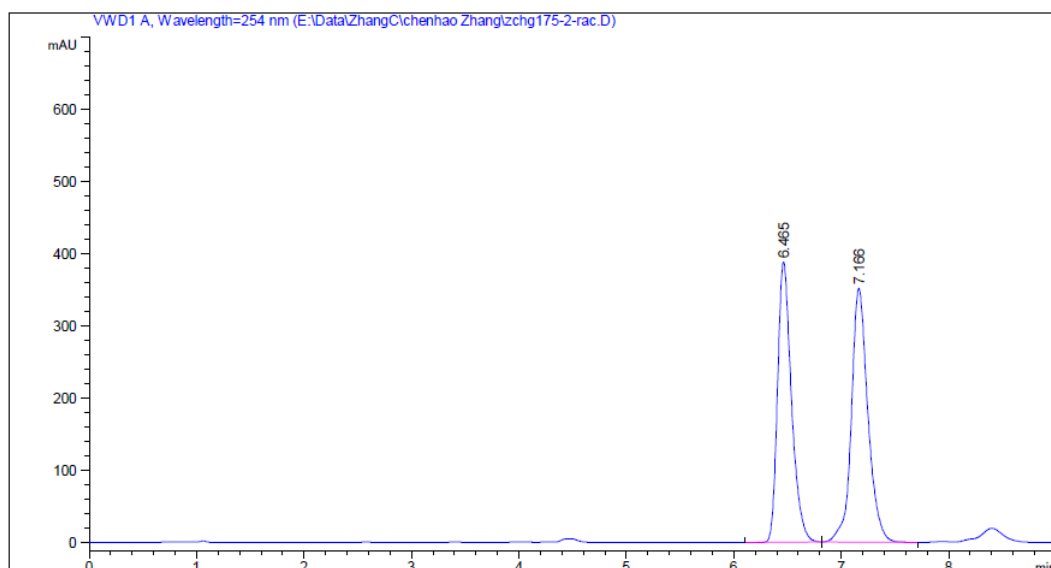


Figure 112. HPLC traces (Daicel Chiralpak OD-H column) of *rac*-**3ah** (reference) and (*R*)-**3ah**.



Peak #	RetTime [min]	Type	Width [min]	Area mAU *s	Height [mAU]	Area %
1	6.441	BB	0.1326	123.19801	14.08253	6.3985
2	7.200	BB	0.1521	1802.21704	179.46565	93.6015

Figure 113. HPLC traces (Daicel Chiralpak OD-H column) of *rac*-**3ai** (reference) and (*R*)-**3ai**.

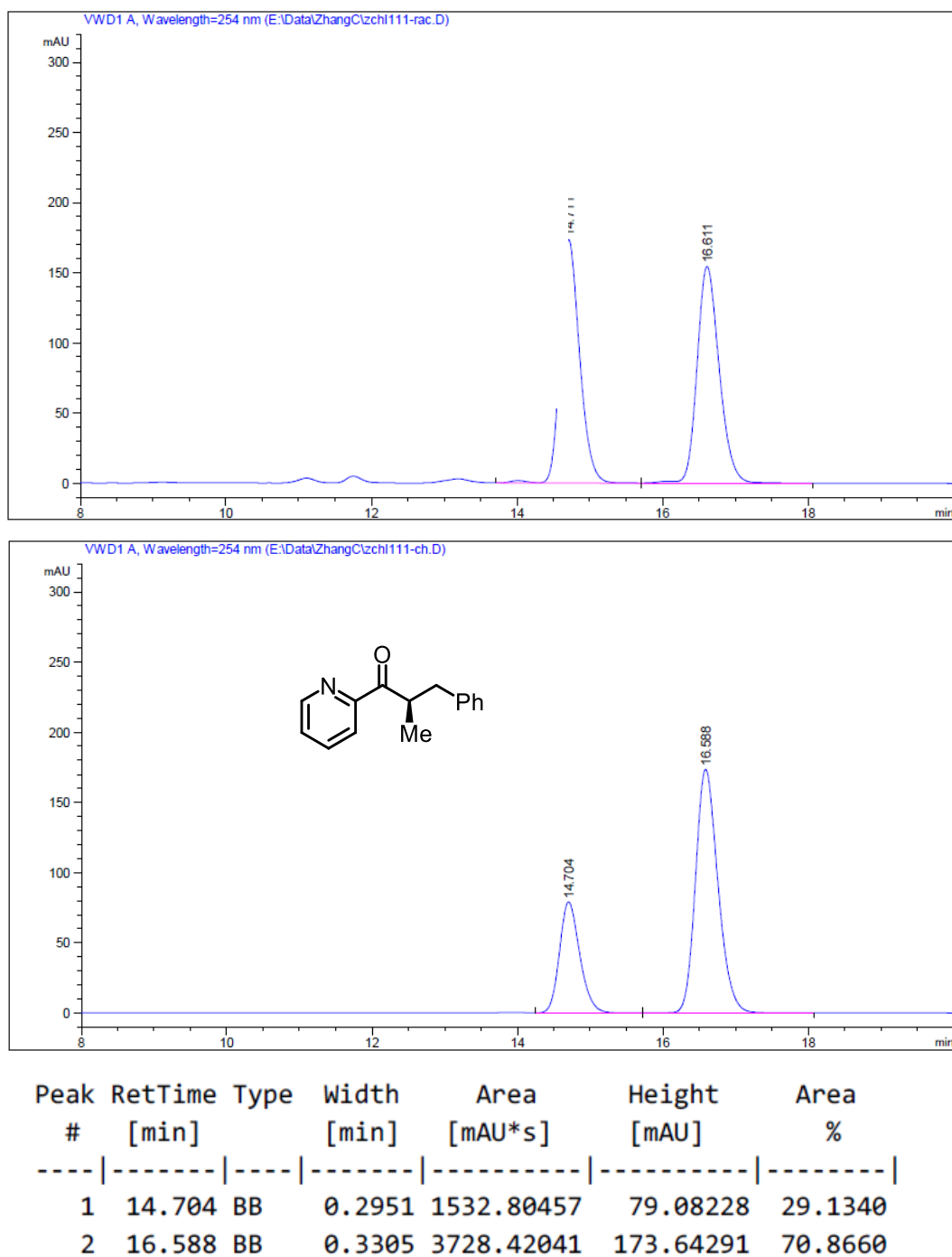
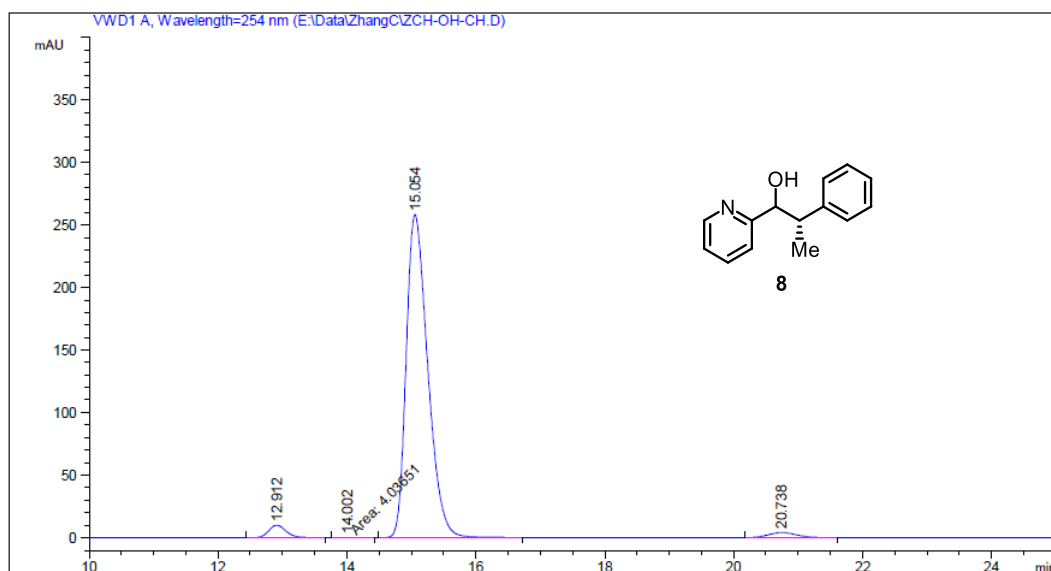
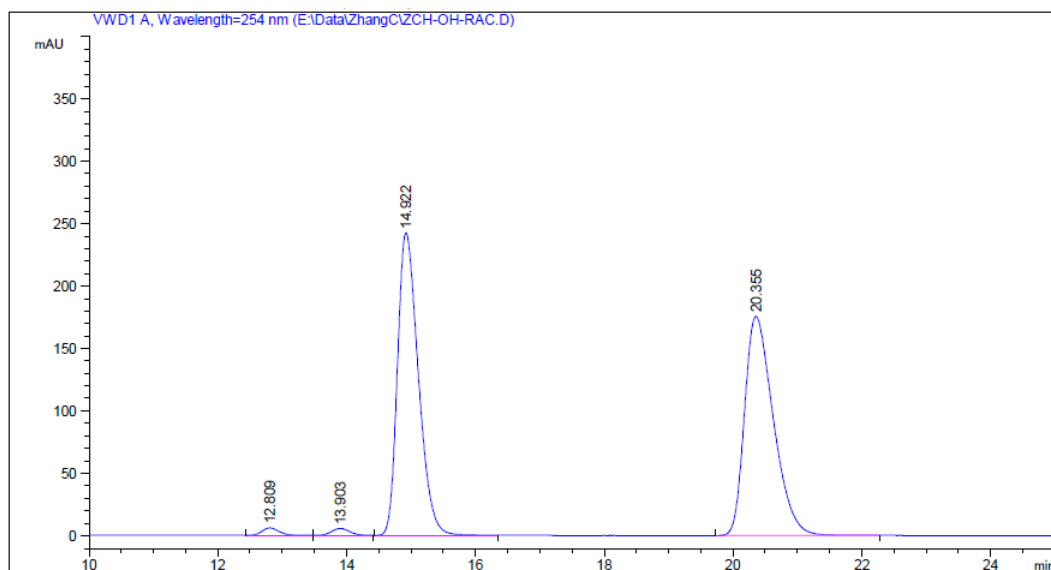
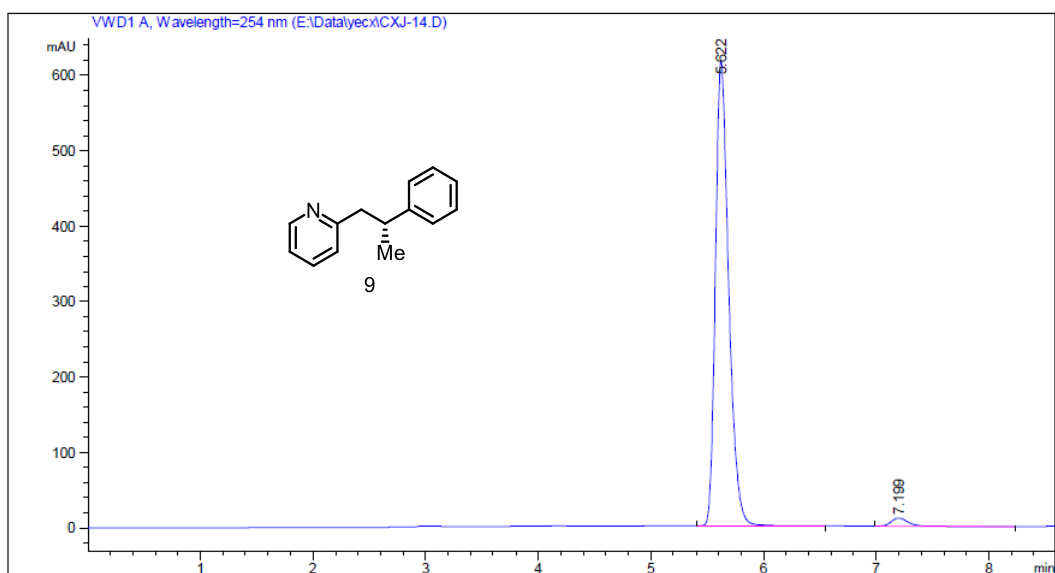
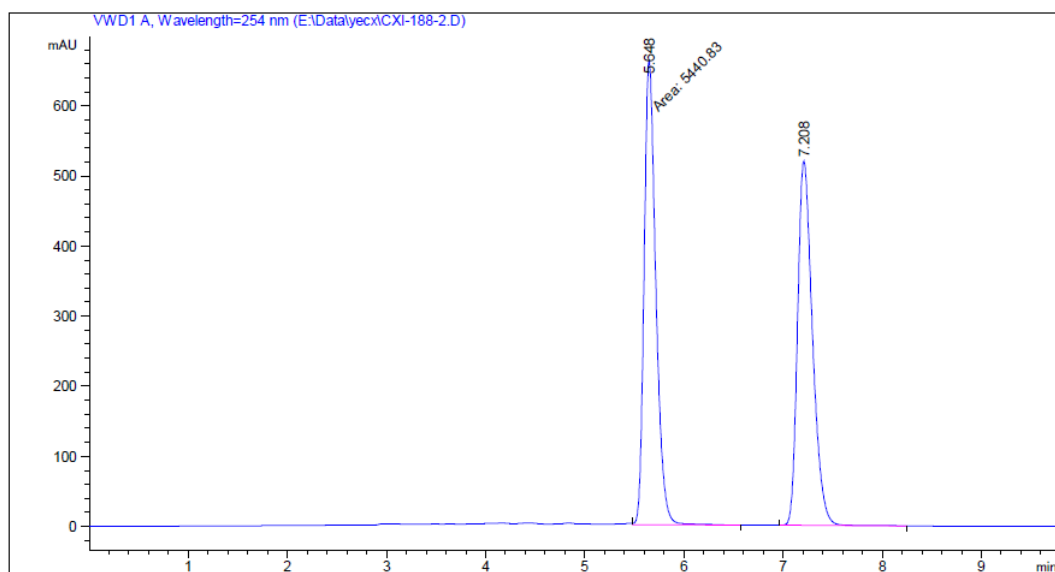


Figure 114. HPLC traces (Daicel Chiralpak OD-H column) of *rac*-**3aj** (reference) and (*R*)-**3aj**.



Peak #	RetTime [min]	Type	Width [min]	Area mAU *s	Height [mAU]	Area %
1	12.912	BB	0.2892	186.07779	9.96534	2.9652
2	14.002	MM	0.2724	2.27889	1.39413e-1	0.0363
3	15.054	BB	0.3570	5966.67969	258.20642	95.0804
4	20.738	BB	0.4587	120.36990	3.95232	1.9181

Figure 115. HPLC traces (Daicel Chiralpak OD-H column) of *rac*-**8** (reference) and non-racemic-**8**.



Peak #	RetTime [min]	Type	Width [min]	Area [mAU*s]	Height [mAU]	Area %
1	5.622	BB	0.1247	5052.66016	615.72833	97.8150
2	7.199	BBA	0.1580	112.86551	10.88473	2.1850

Figure 116. HPLC traces (Daicel Chiralpak OD-H column) of *rac*-**9** (reference) and non-racemic-**9**.

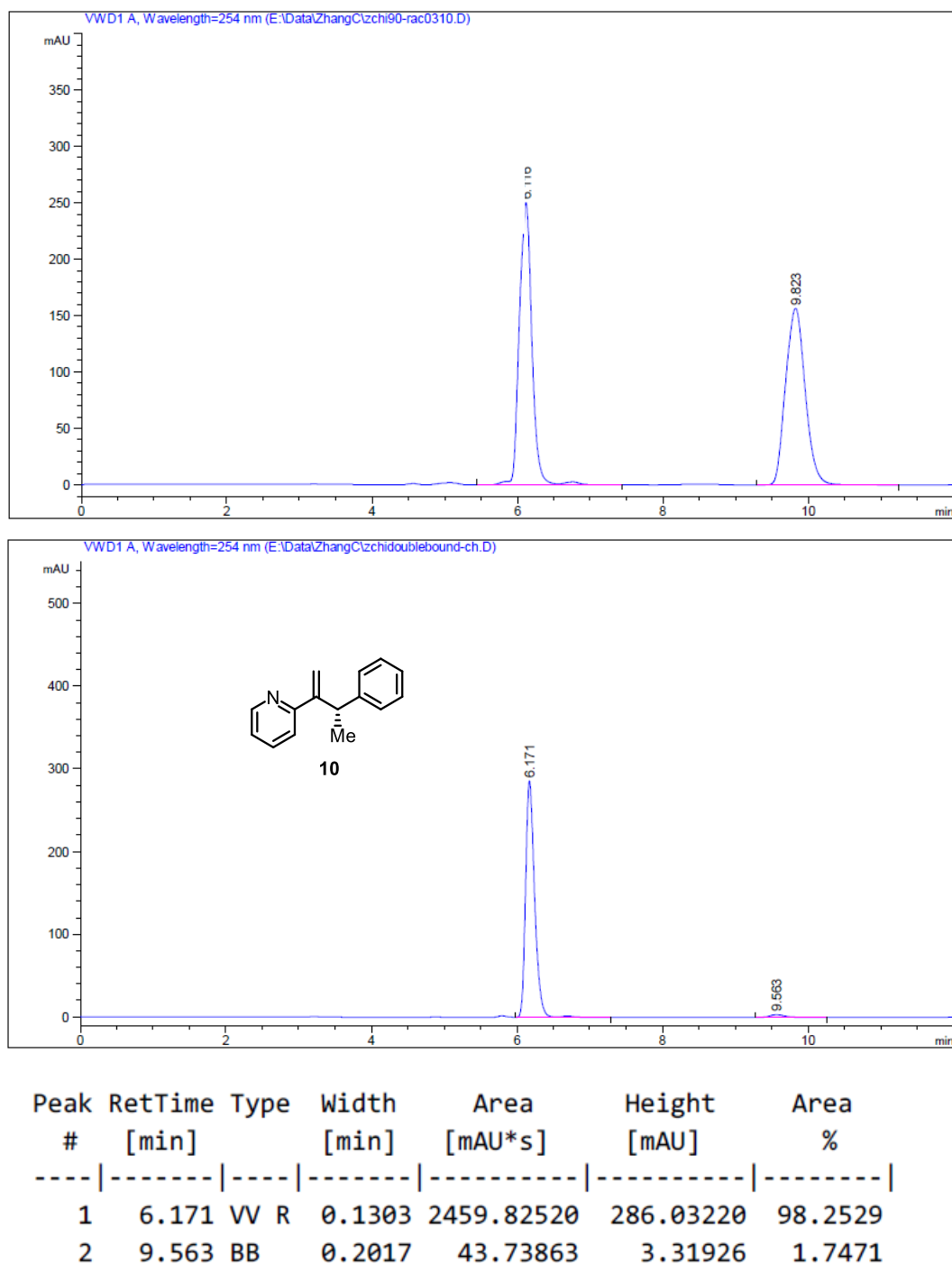
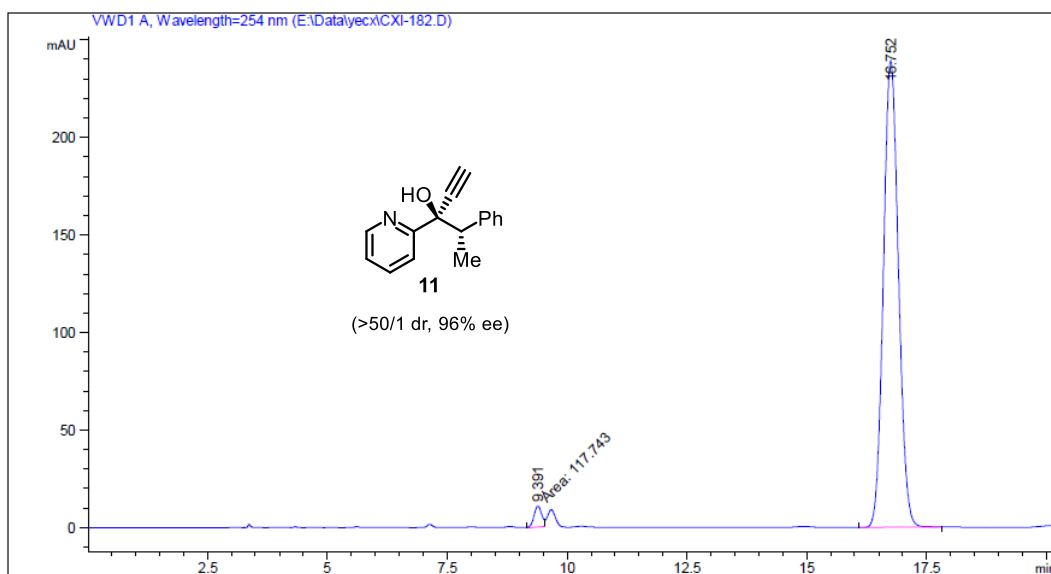
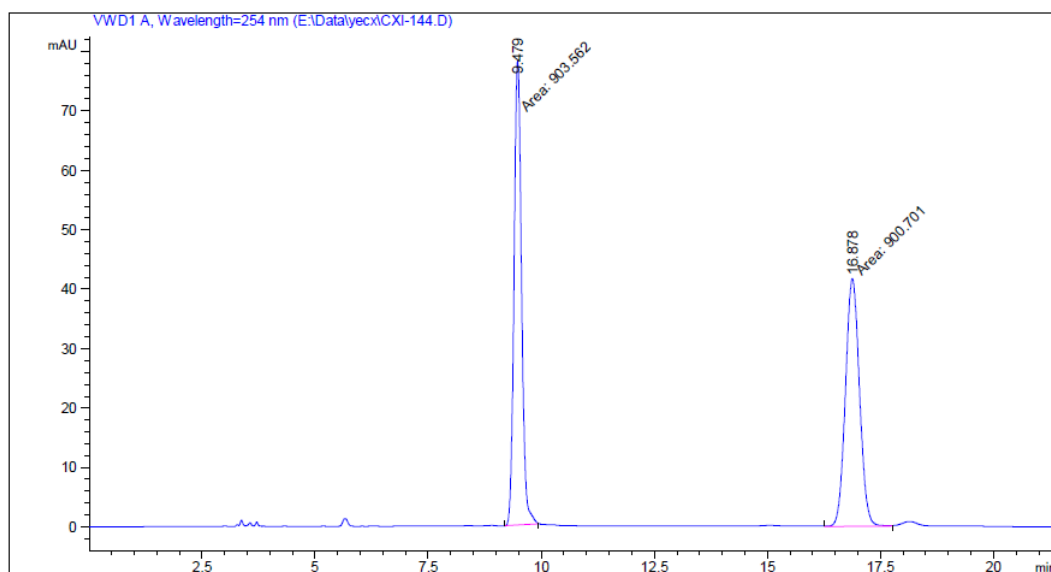
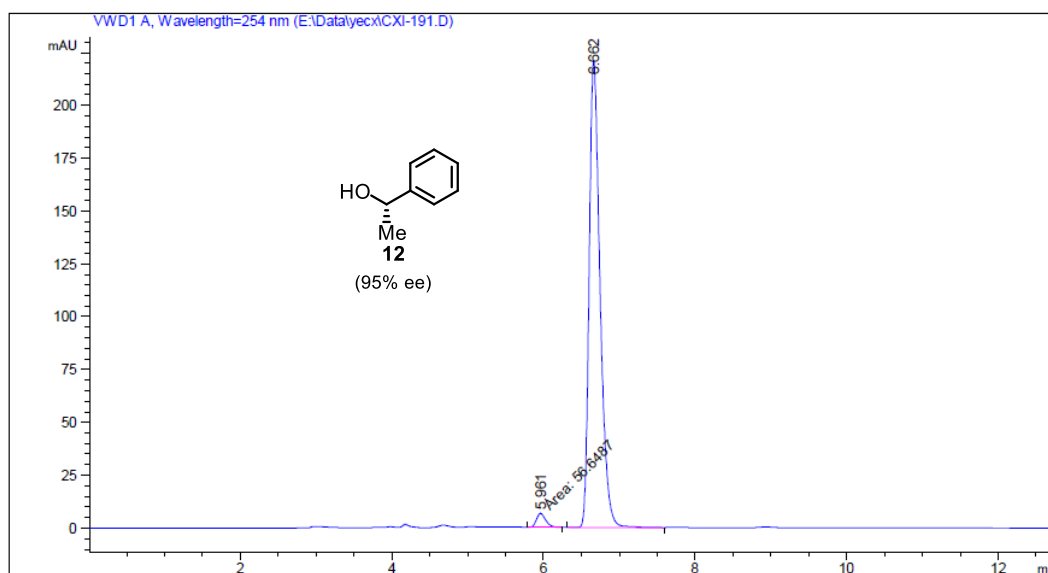
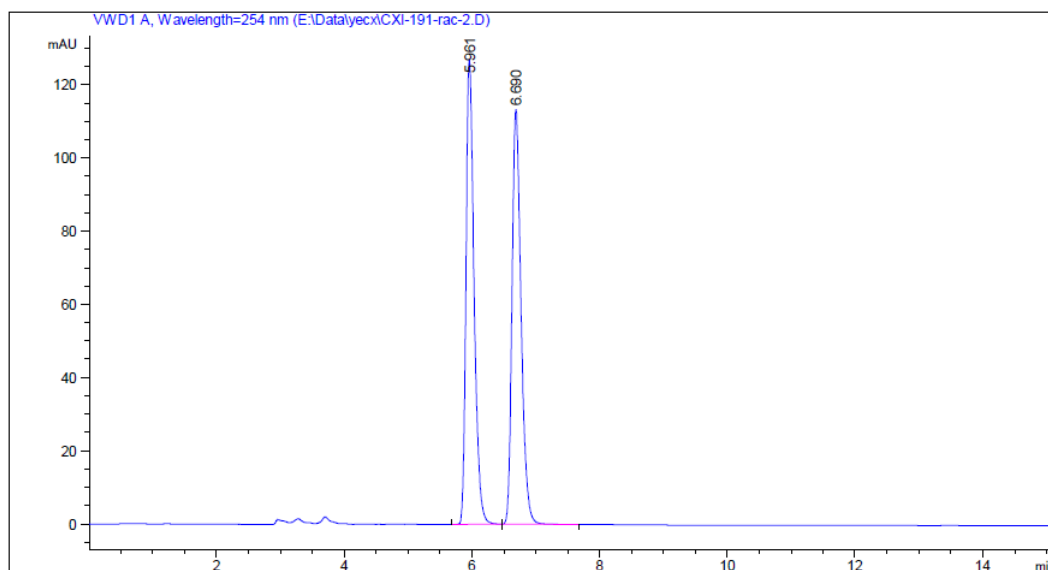


Figure 117. HPLC traces (Daicel Chiralpak OD-H column) of *rac*-**10** (reference) and non-racemic-**10**.



Peak #	RetTime [min]	Type	Width [min]	Area [mAU*s]	Height [mAU]	Area %
1	9.391	MM	0.1831	117.74312	10.71546	2.2069
2	16.752	BB	0.3396	5217.52539	239.09282	97.7931

Figure 118. HPLC traces (Daicel Chiralpak IG column) of *rac*-**11** (reference) and non-racemic-**11**.



Peak #	RetTime [min]	Type	Width [min]	Area [mAU*s]	Height [mAU]	Area %
1	5.961	MM	0.1428	56.64866	6.61145	2.5027
2	6.662	BB	0.1517	2206.82568	220.60466	97.4973

Figure 119. HPLC traces (Daicel Chiralpak OD-H column) of *rac*-**12** (reference) and non-racemic-**12**.

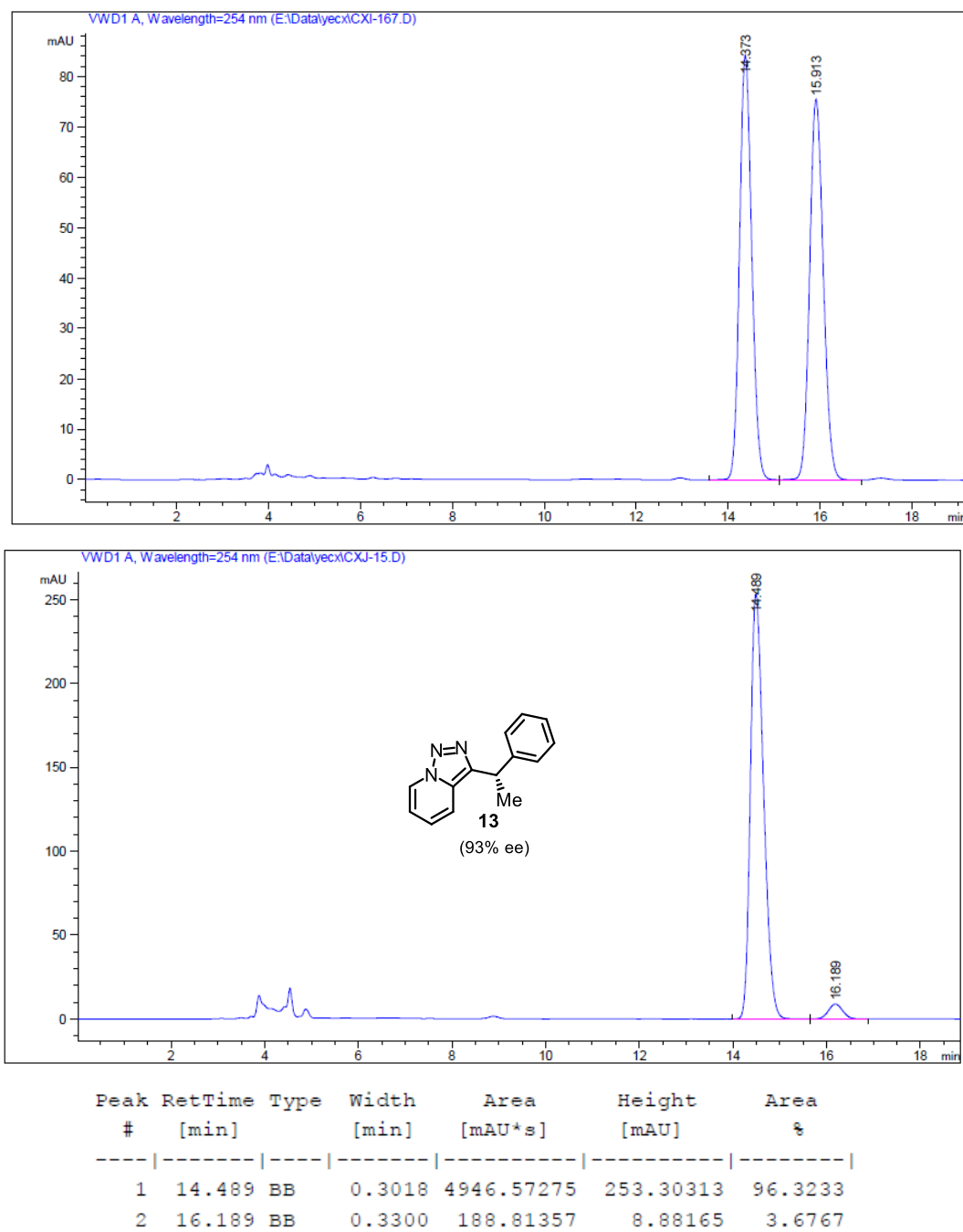


Figure 120. HPLC traces (Daicel Chiralpak IG column) of *rac*-**13** (reference) and non-racemic-**13**.

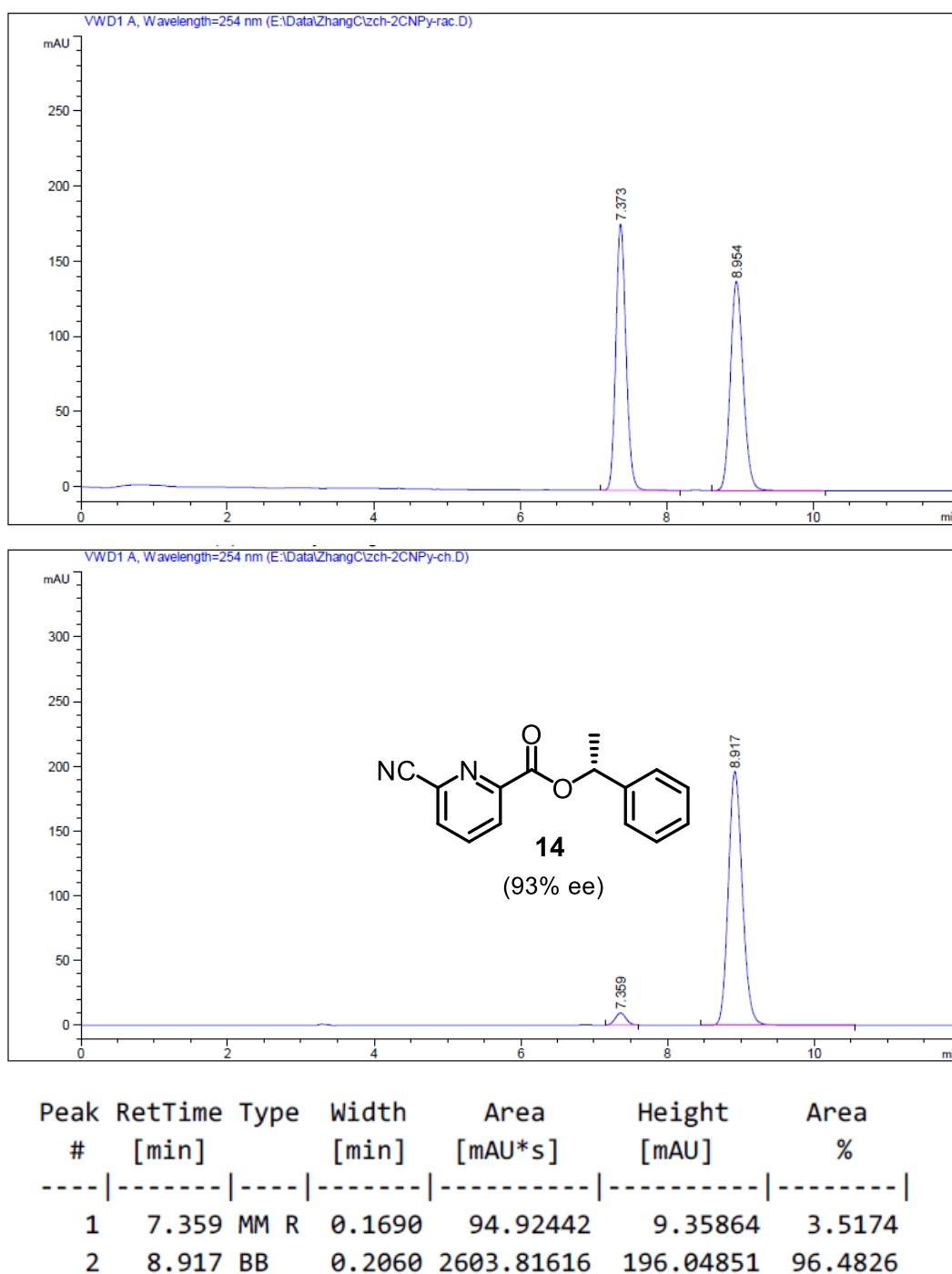
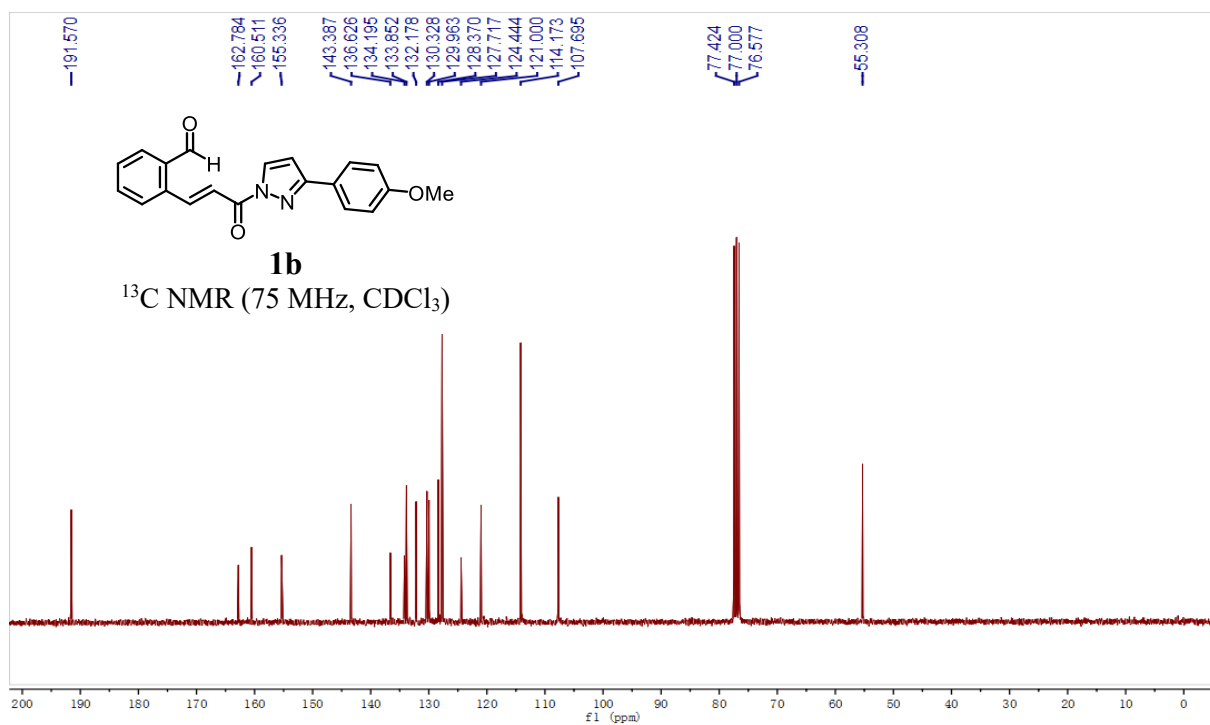
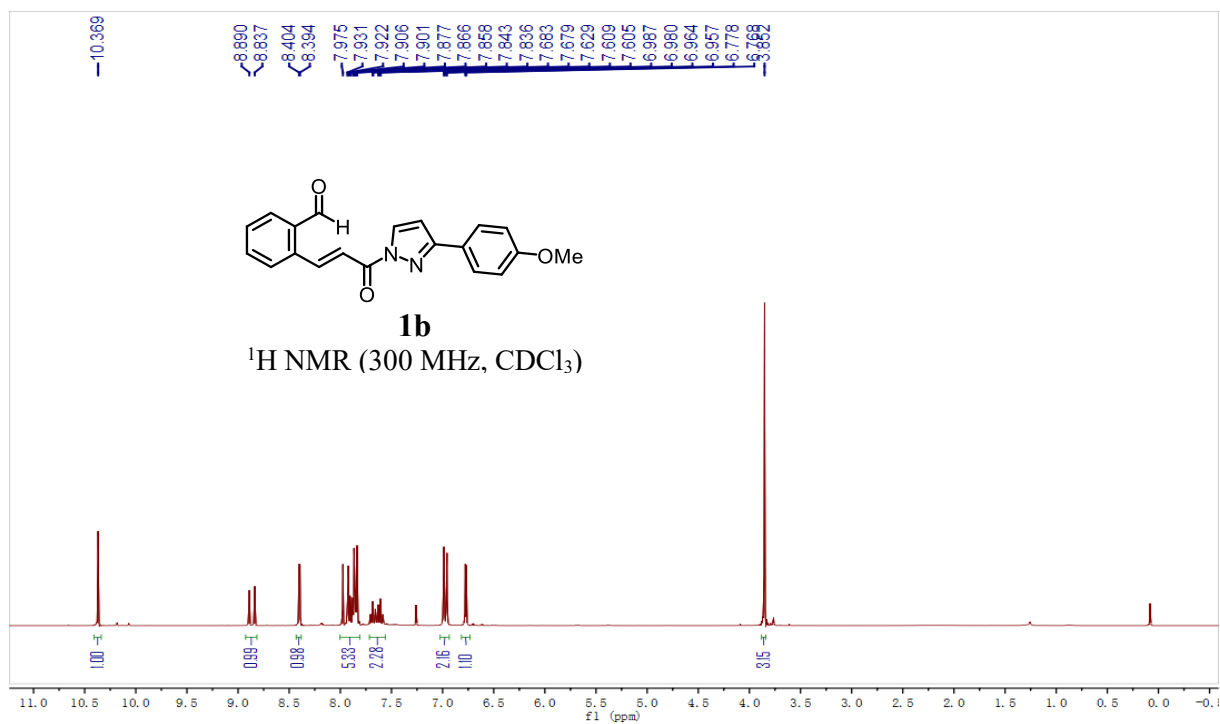
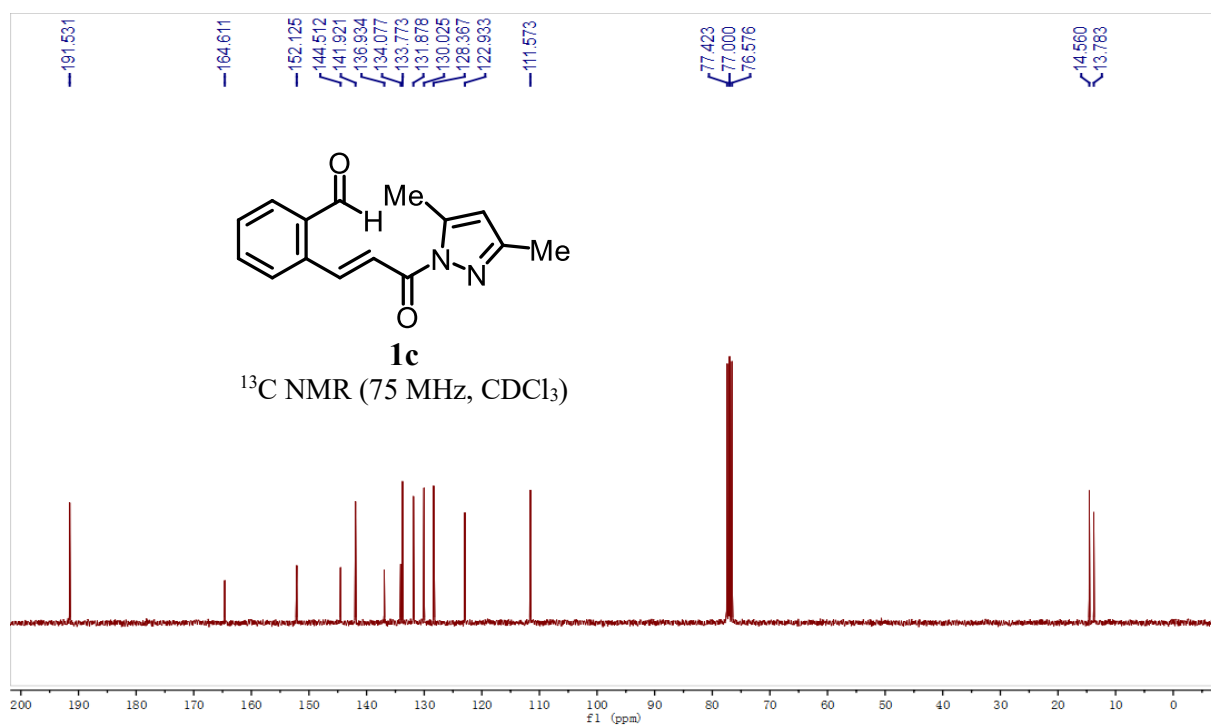
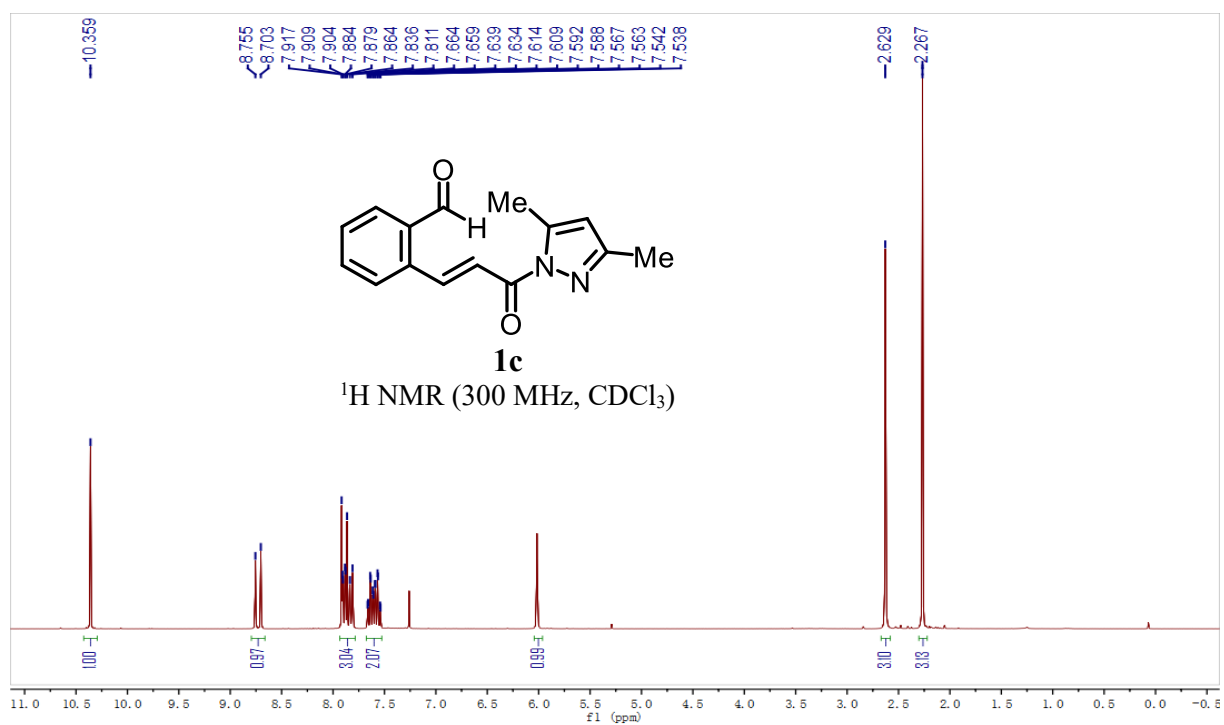


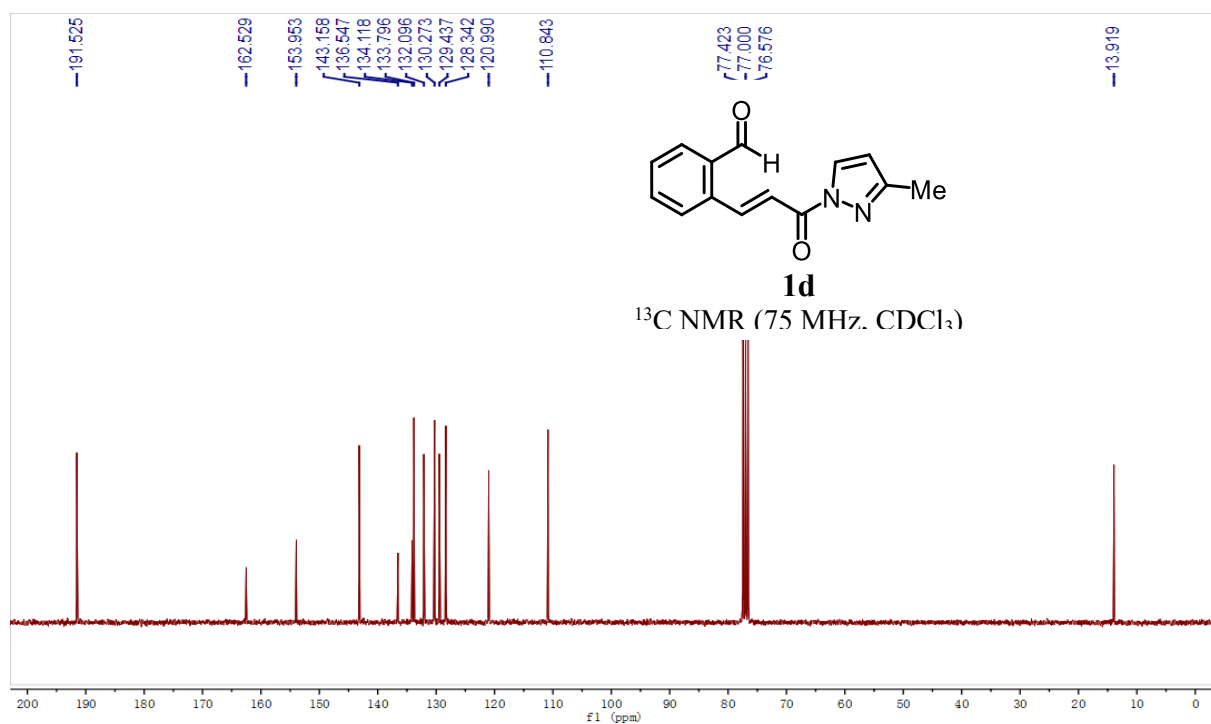
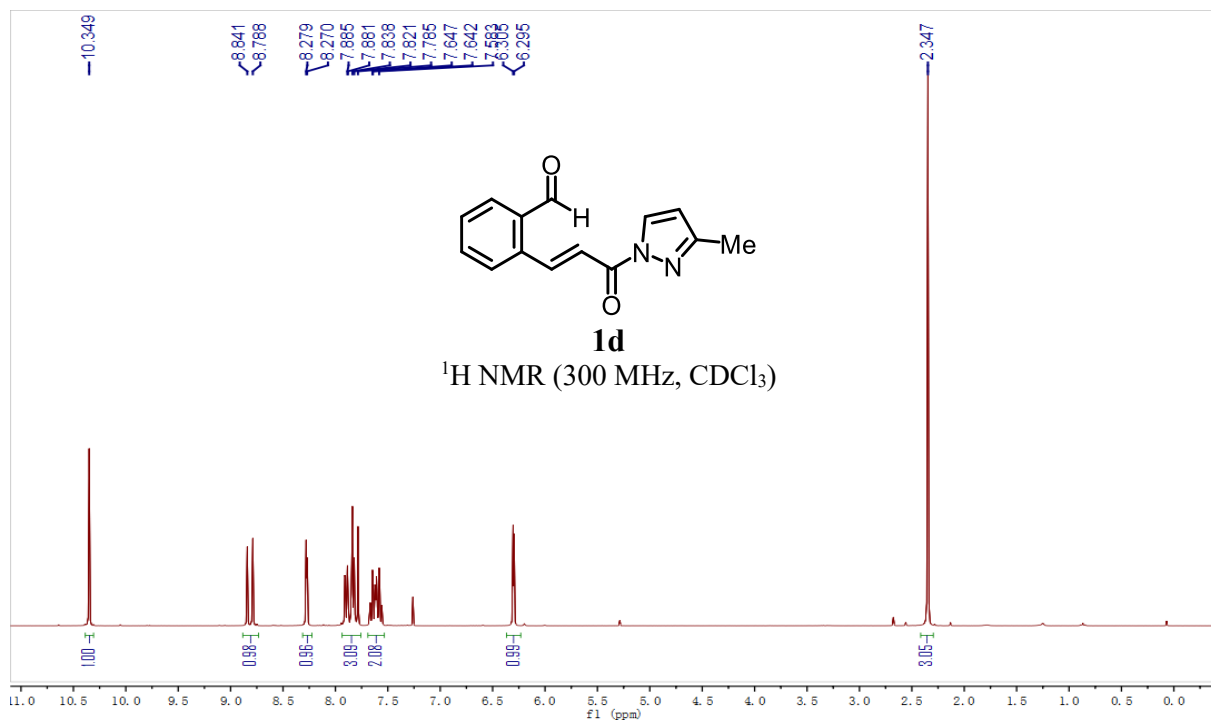
Figure 121. HPLC traces (Daicel Chiralpak IG column) of *rac*-**14** (reference) and non-racemic-**14**.

5.7 List of NMR Spectra of New Complexes

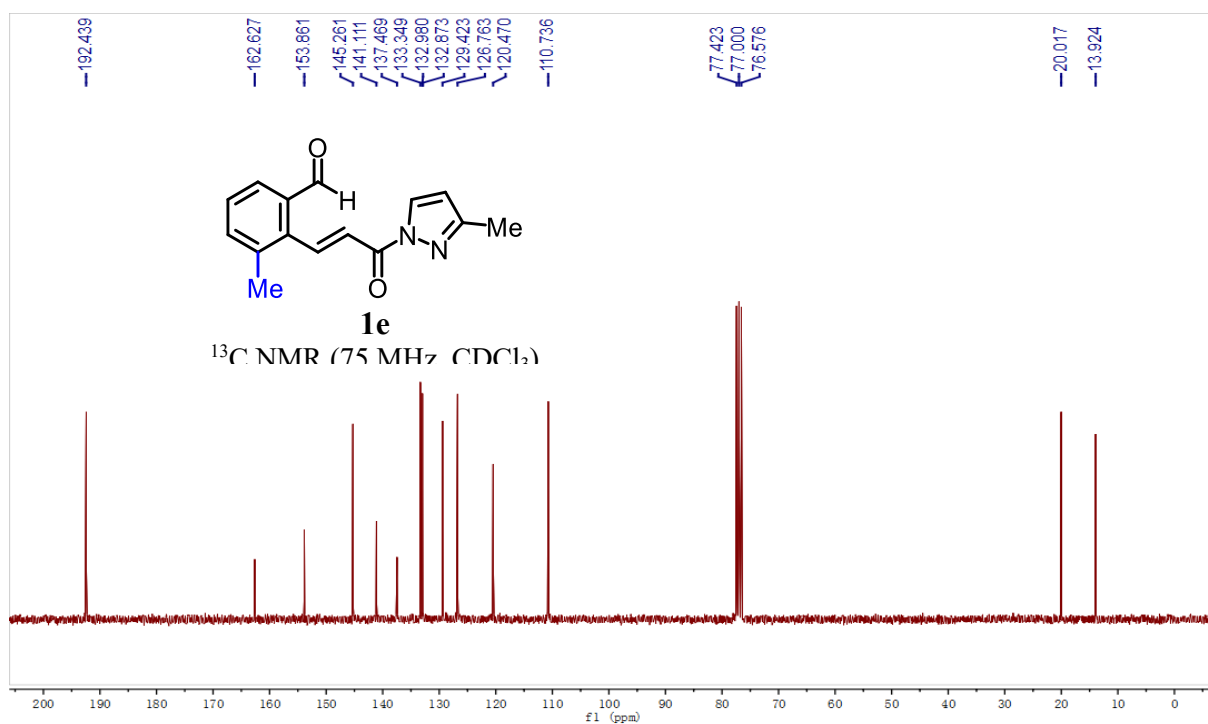
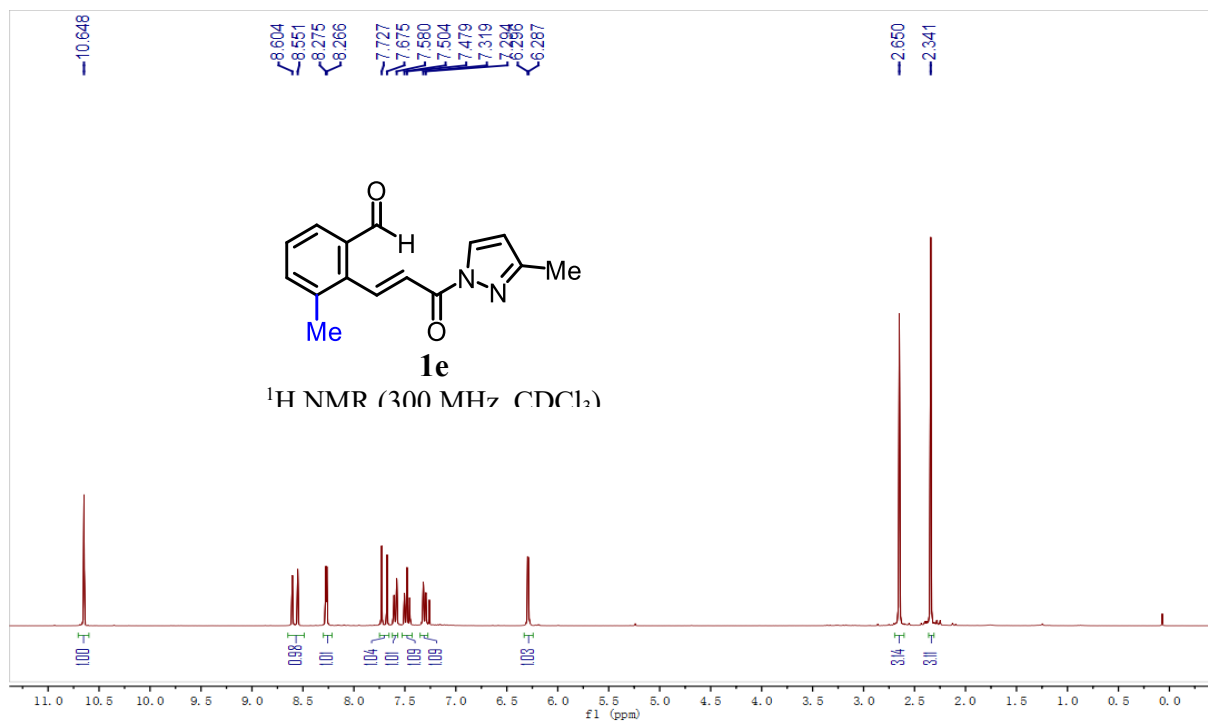


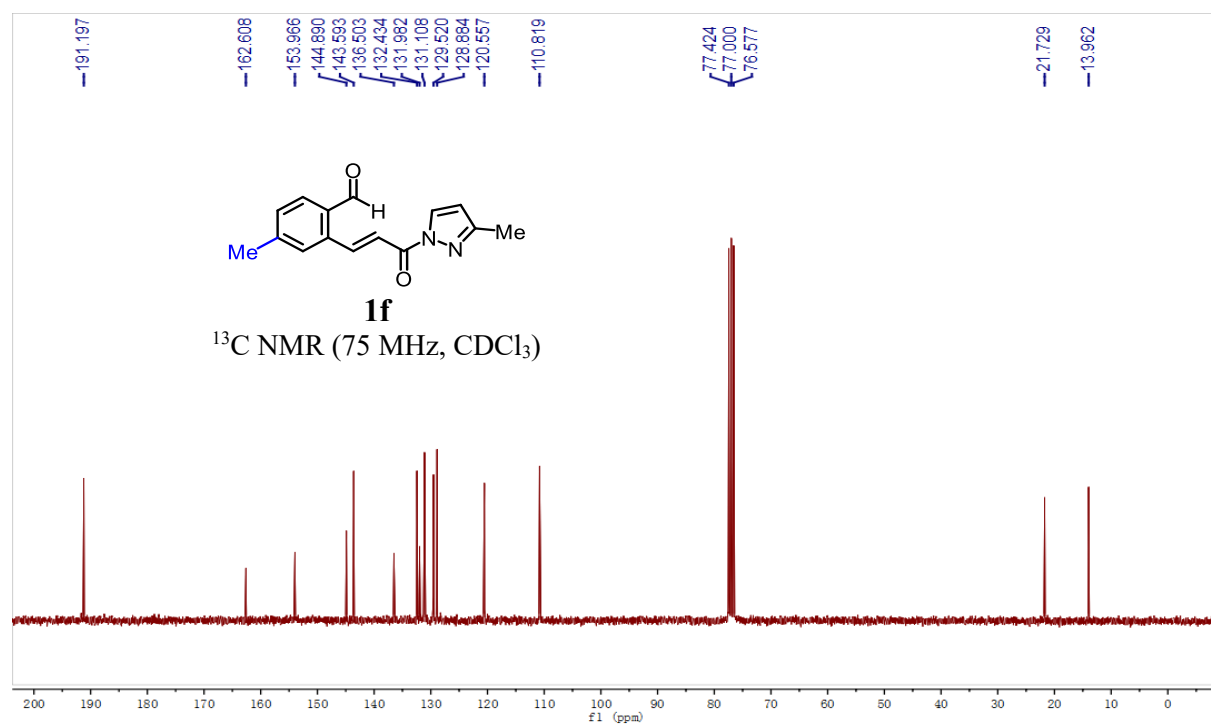
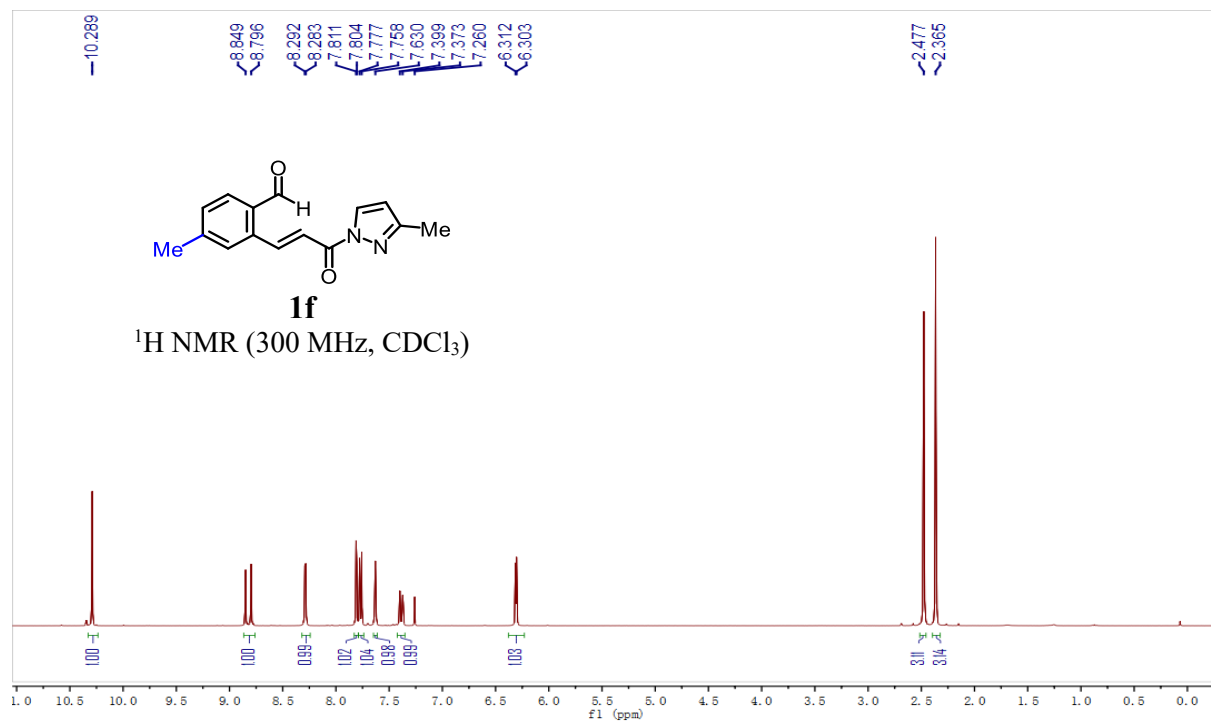
Chapter 5. Appendices

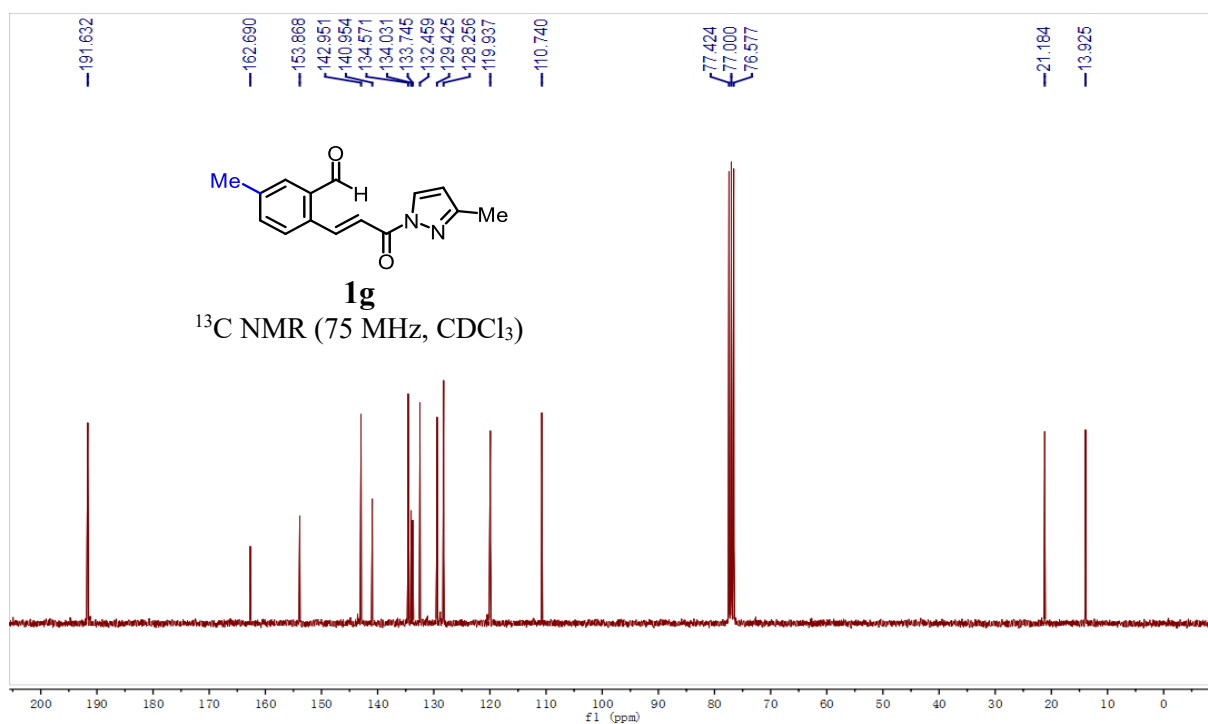
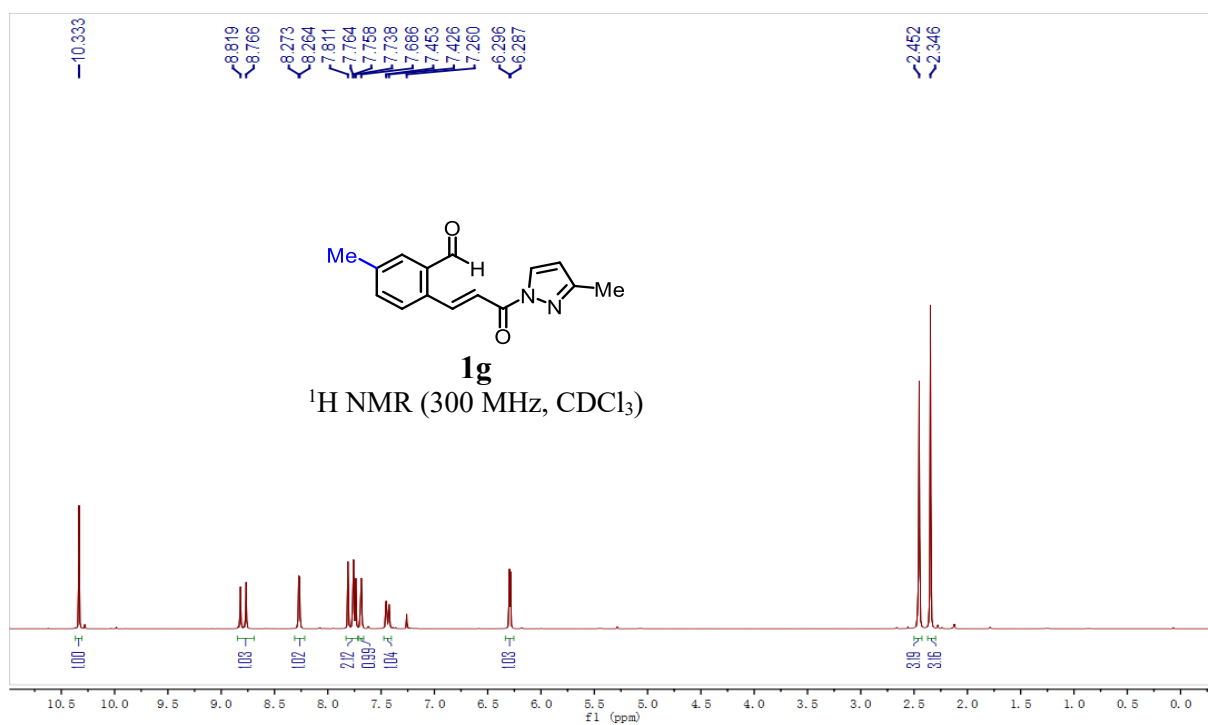


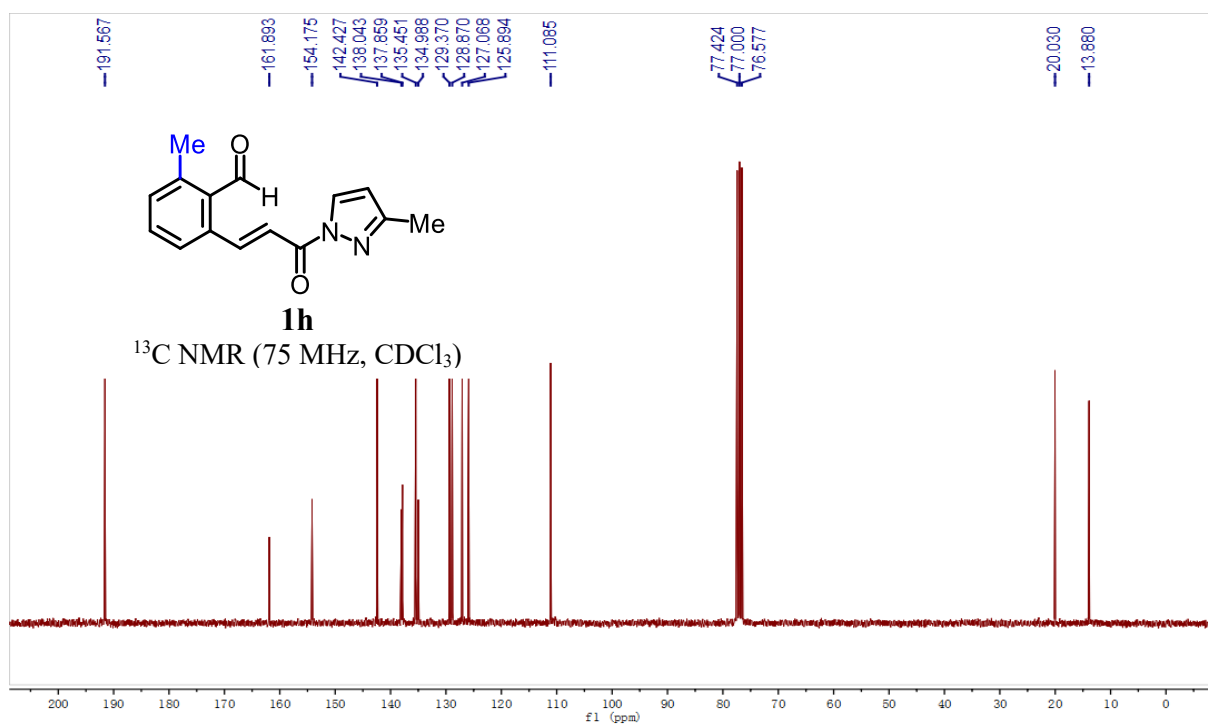
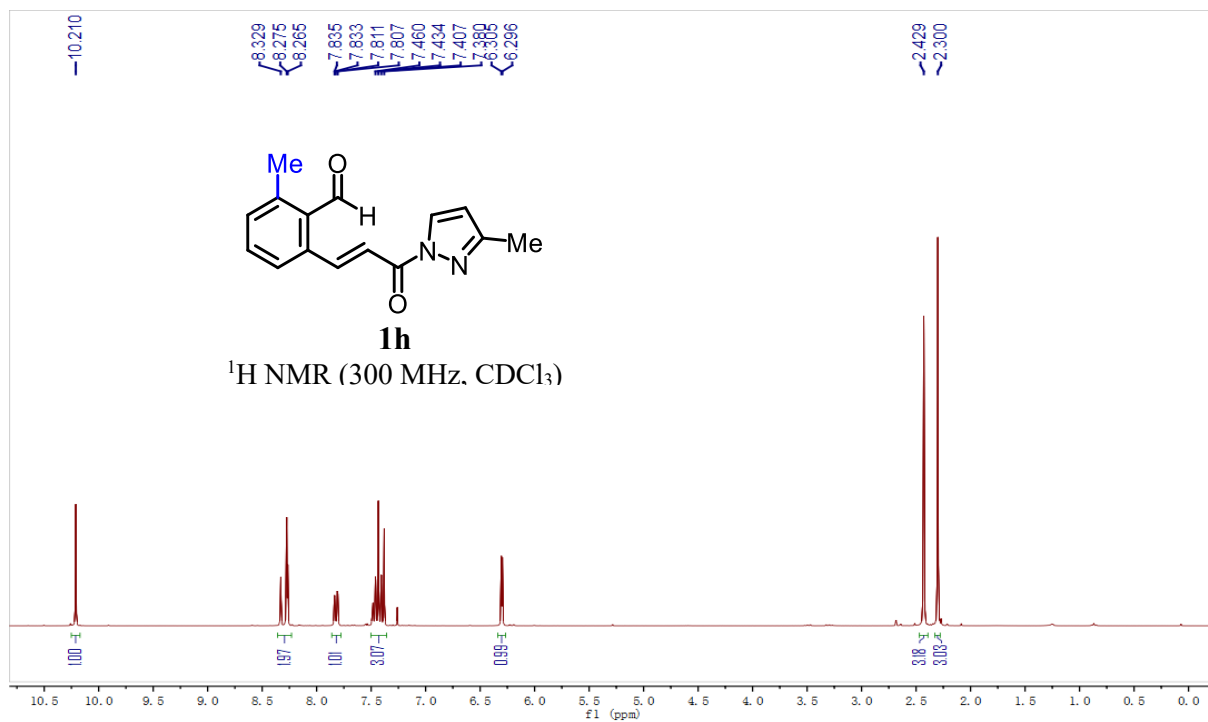


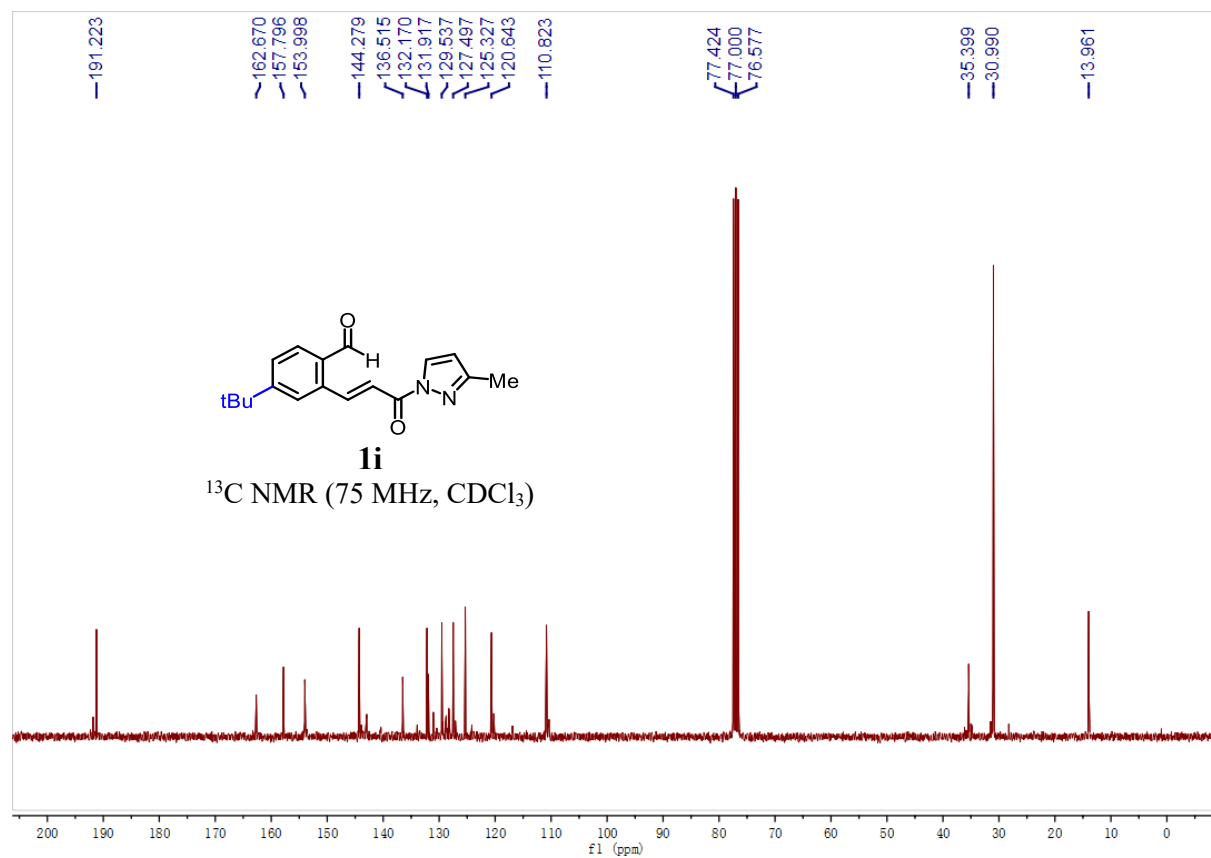
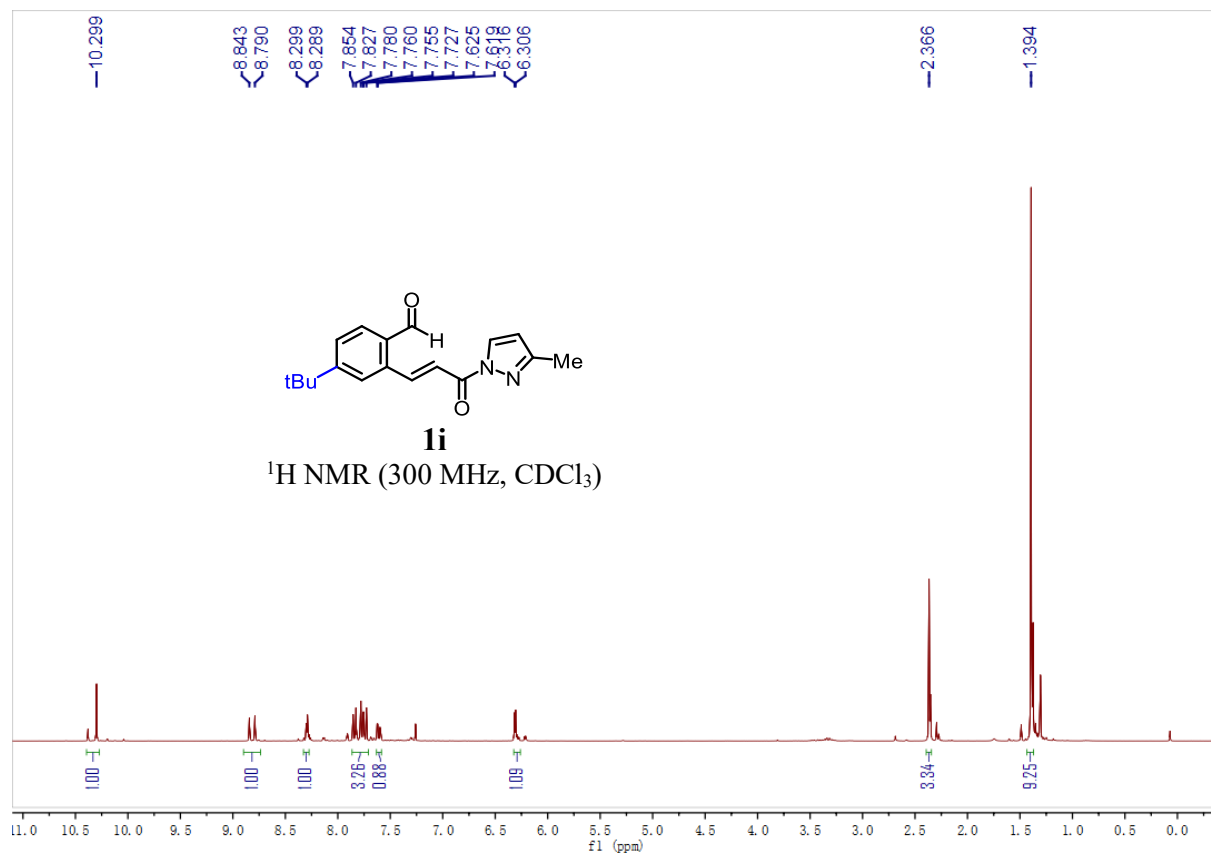
Chapter 5. Appendices

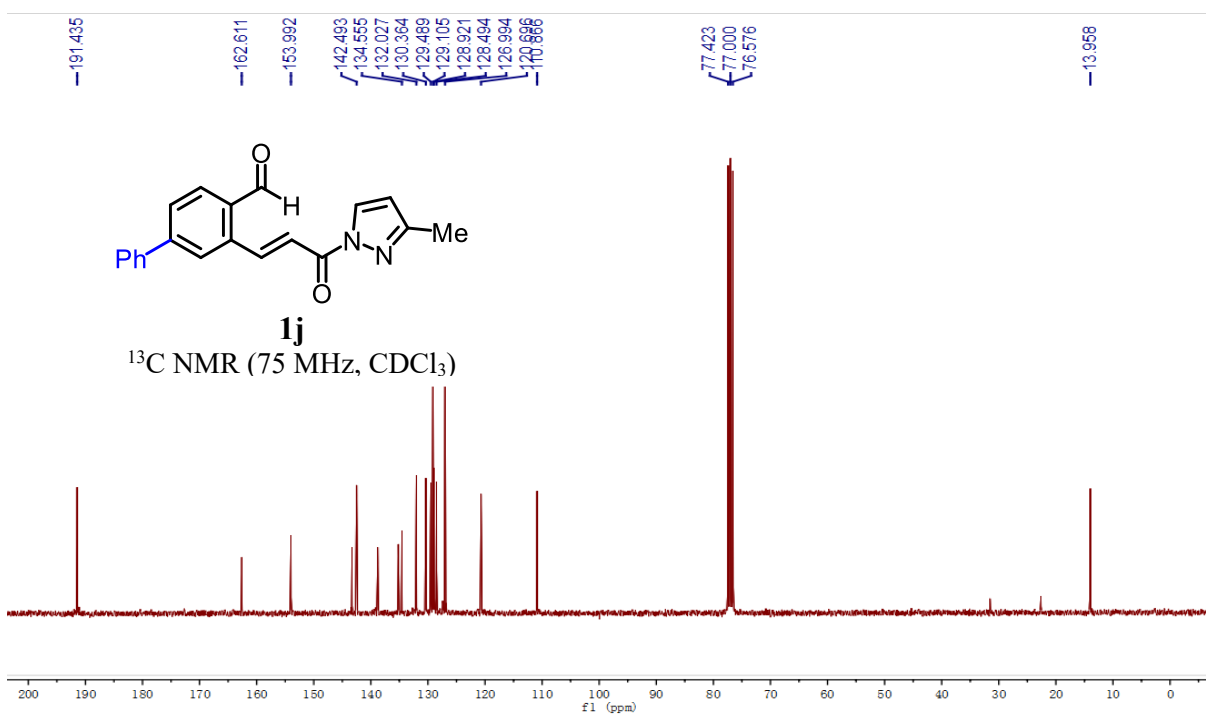
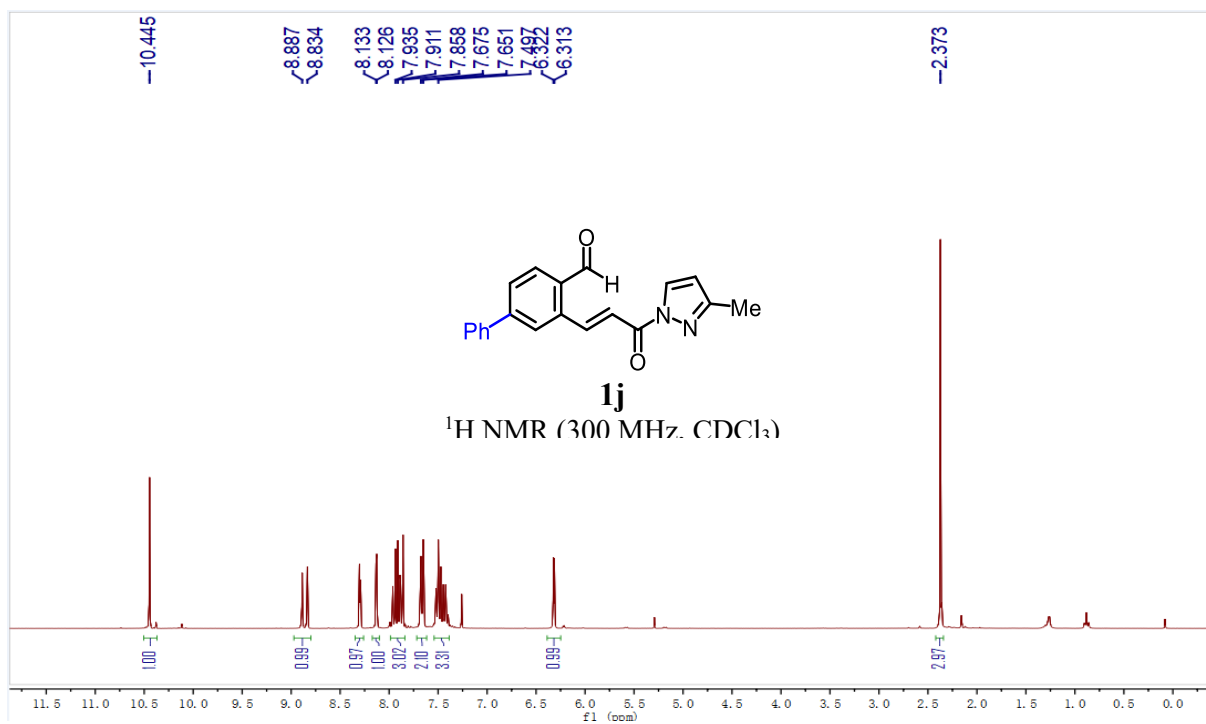




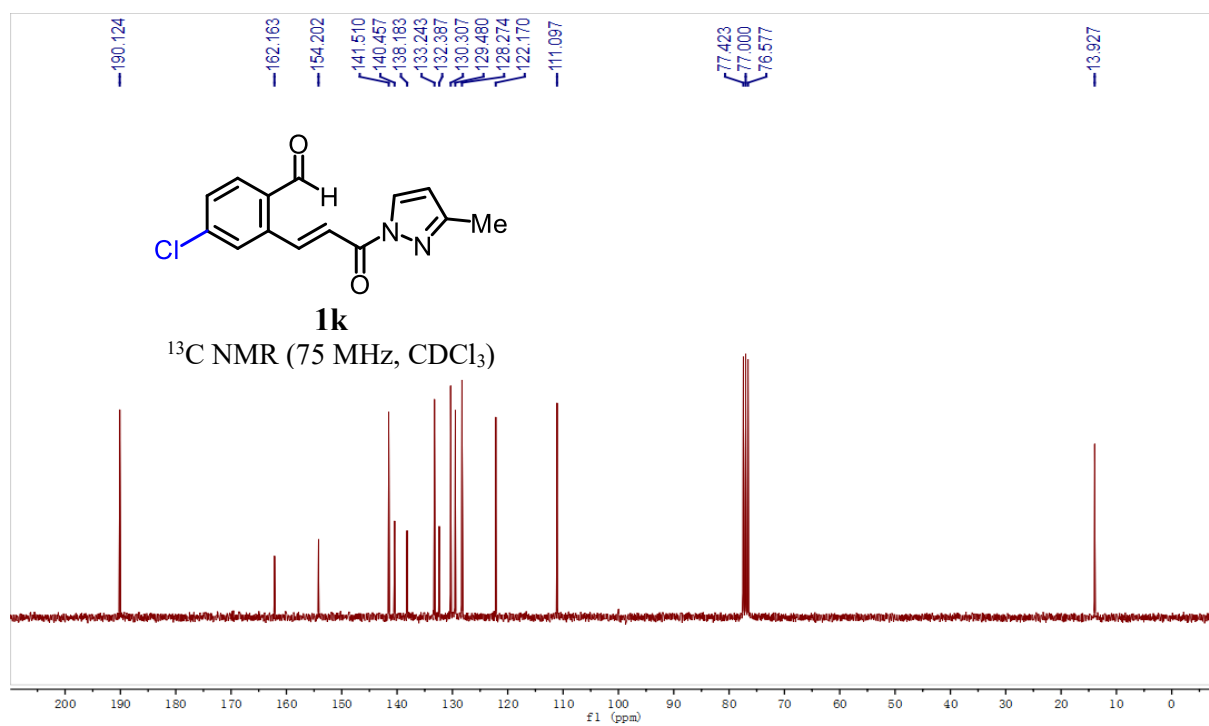
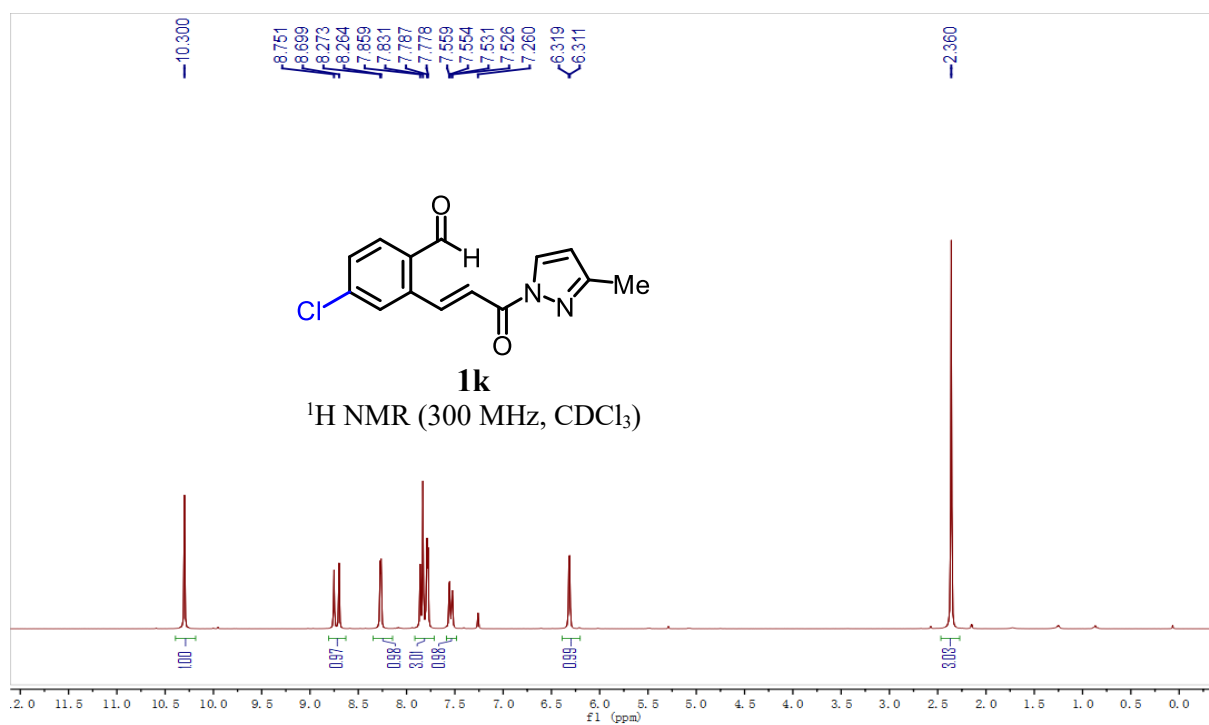


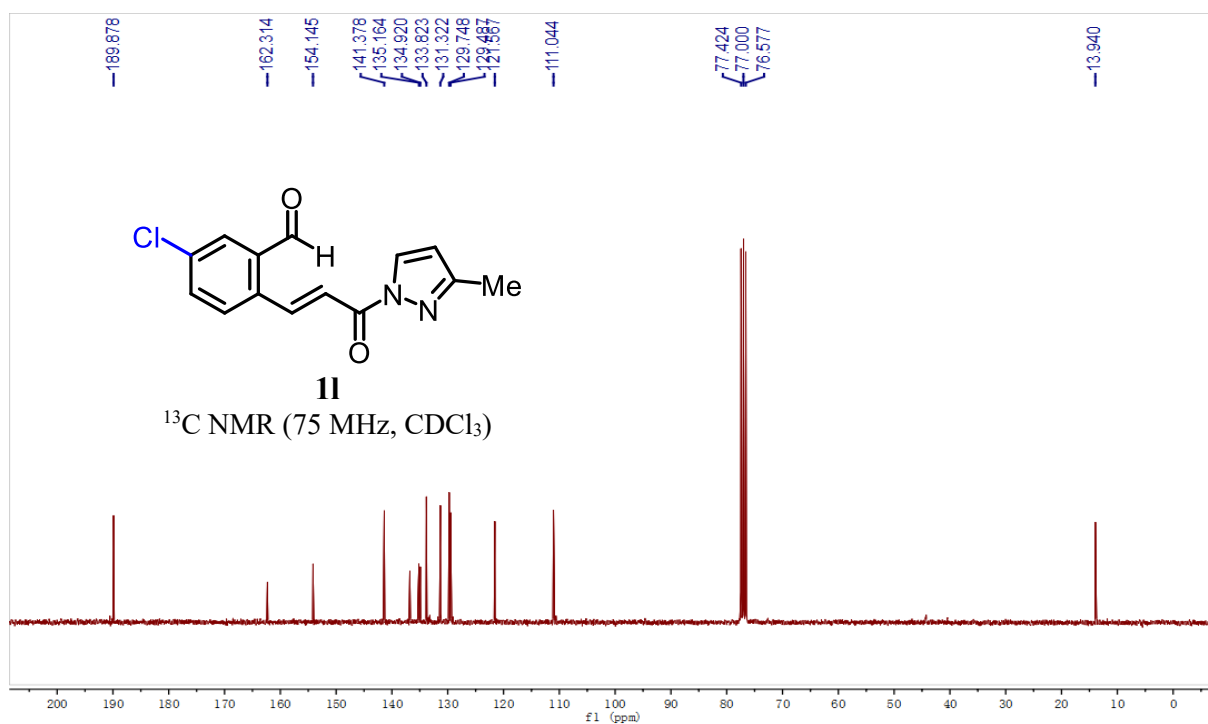
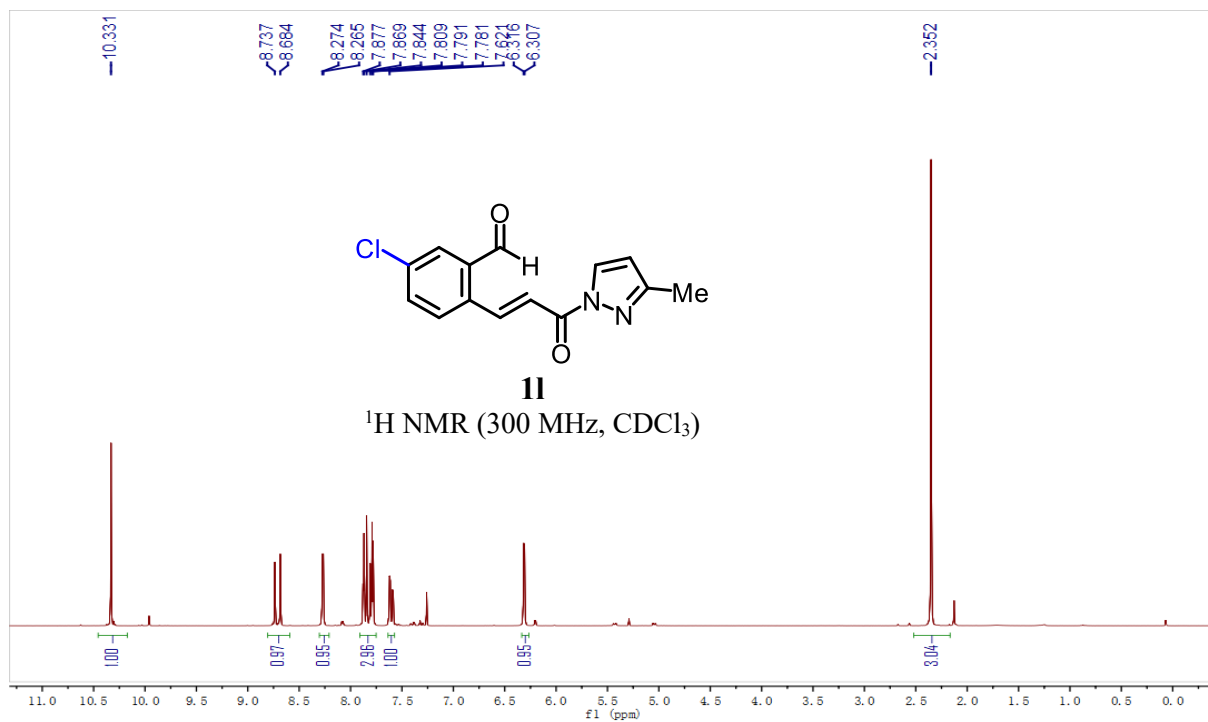




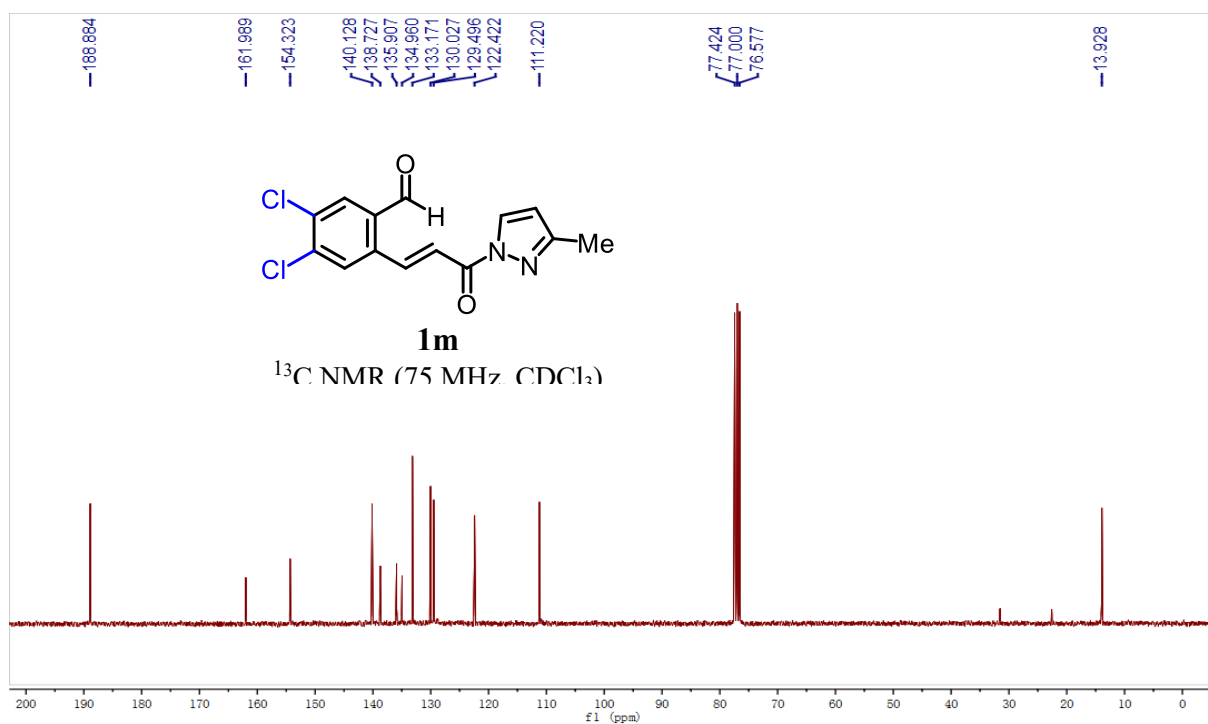
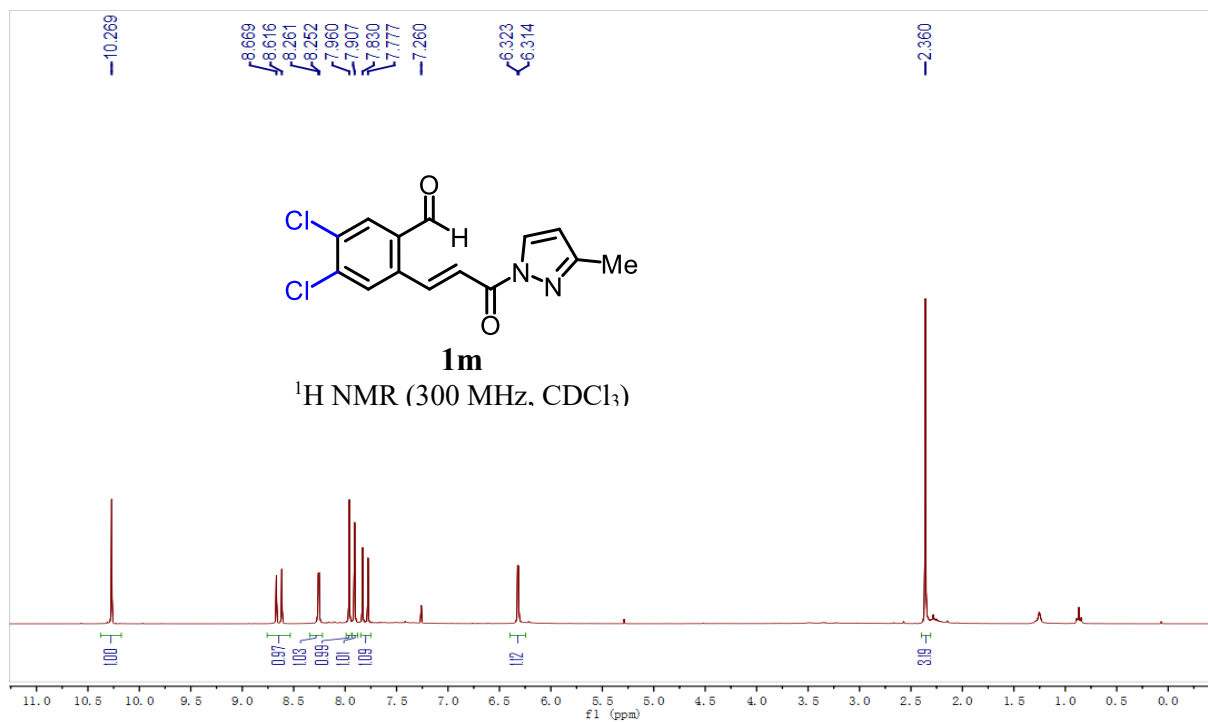


Chapter 5. Appendices

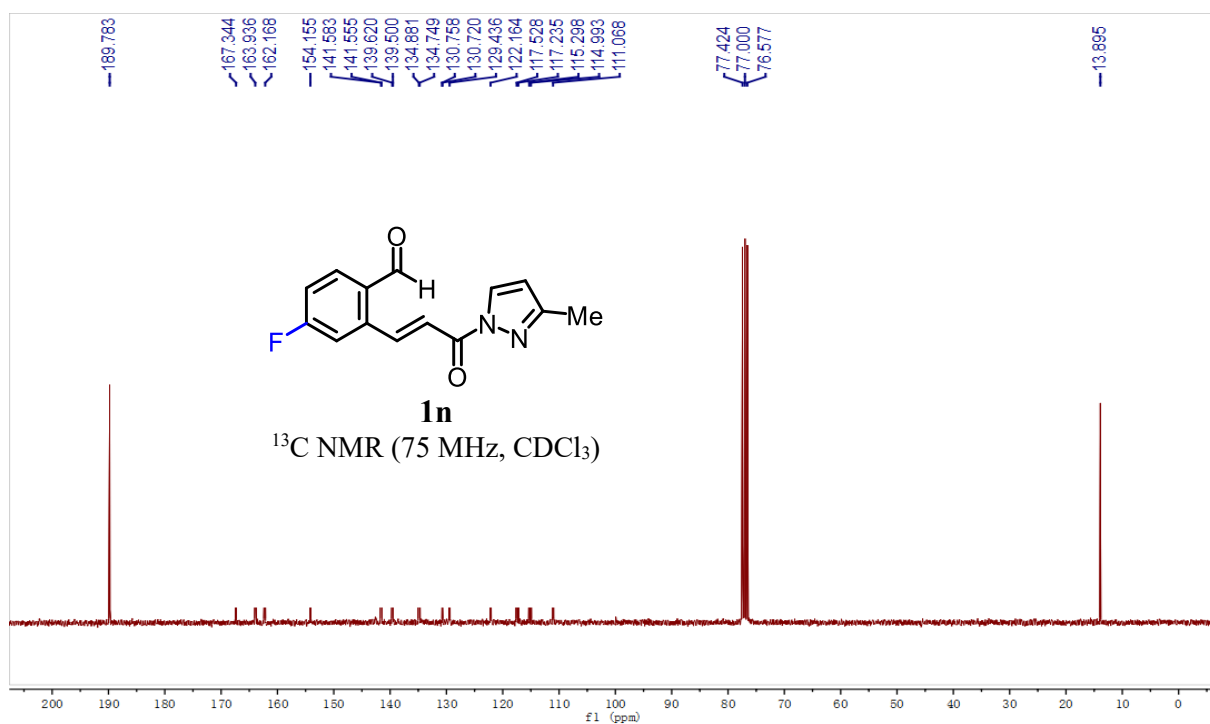
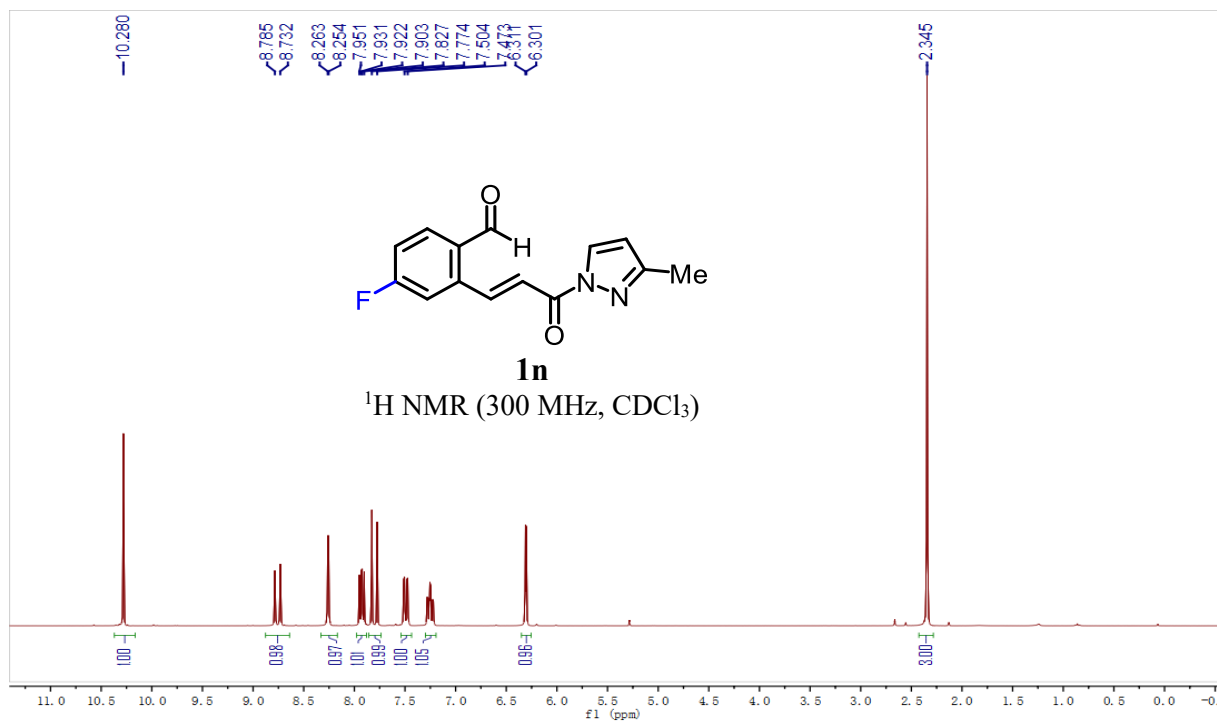




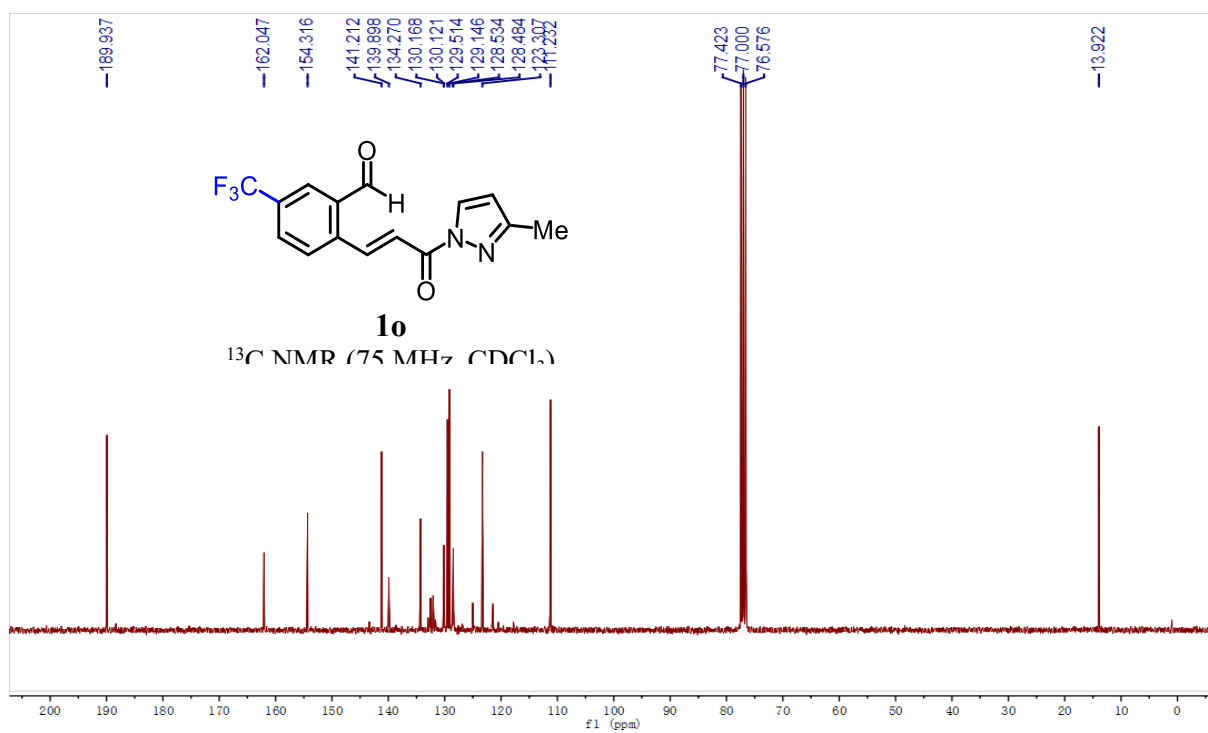
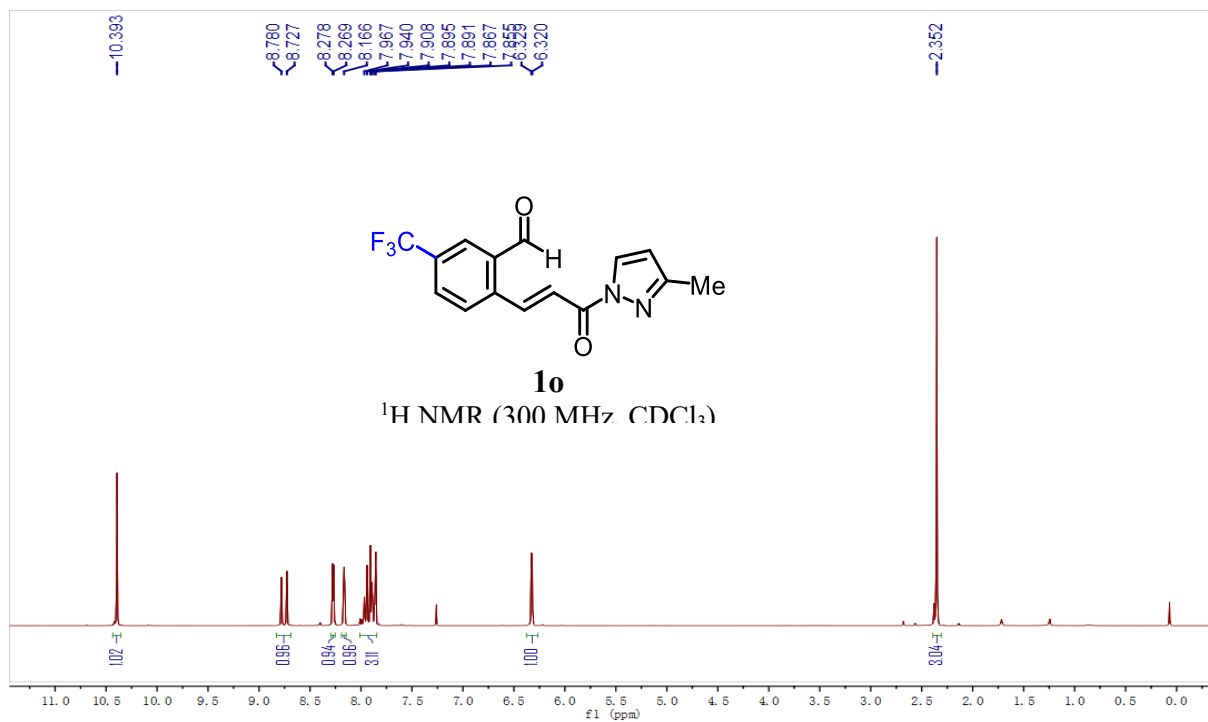
Chapter 5. Appendices



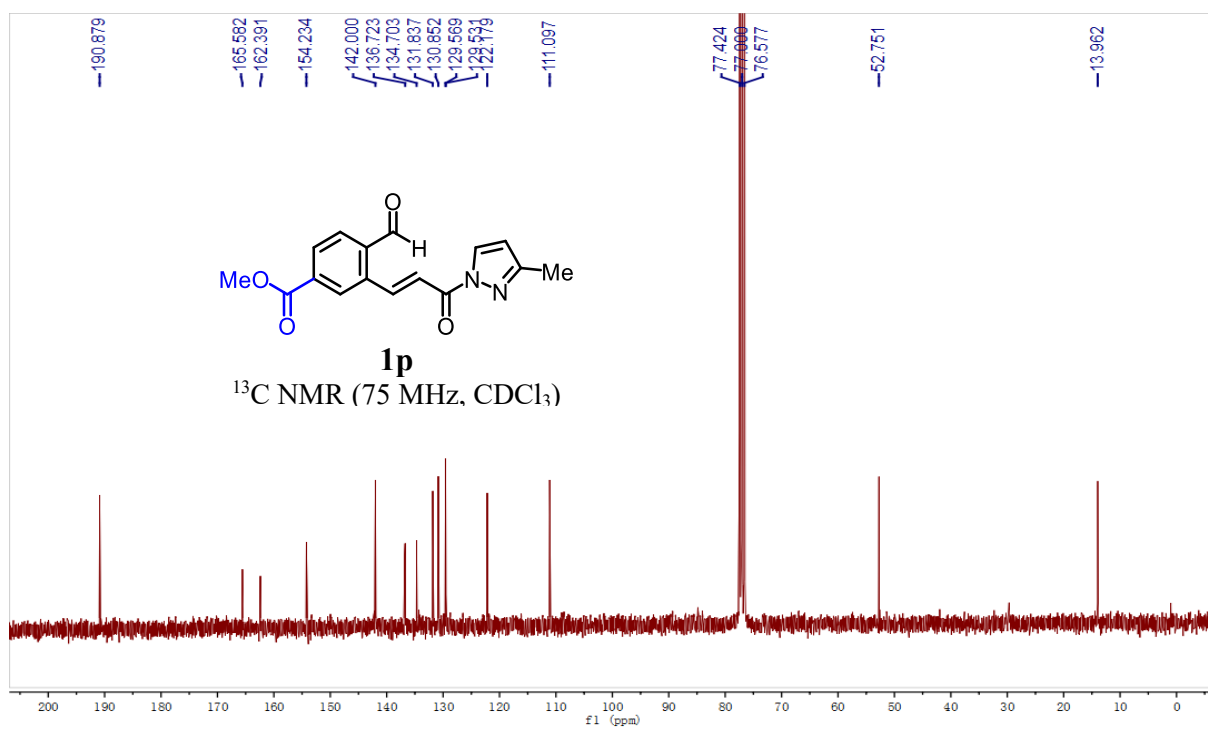
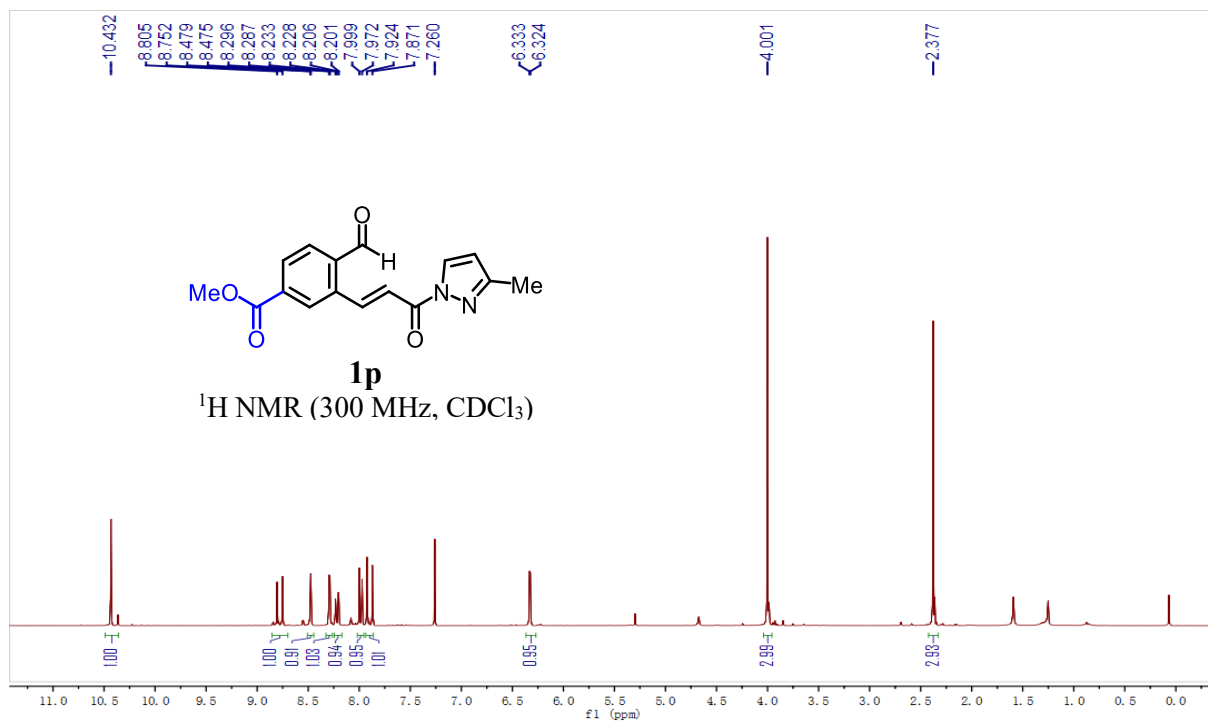
Chapter 5. Appendices

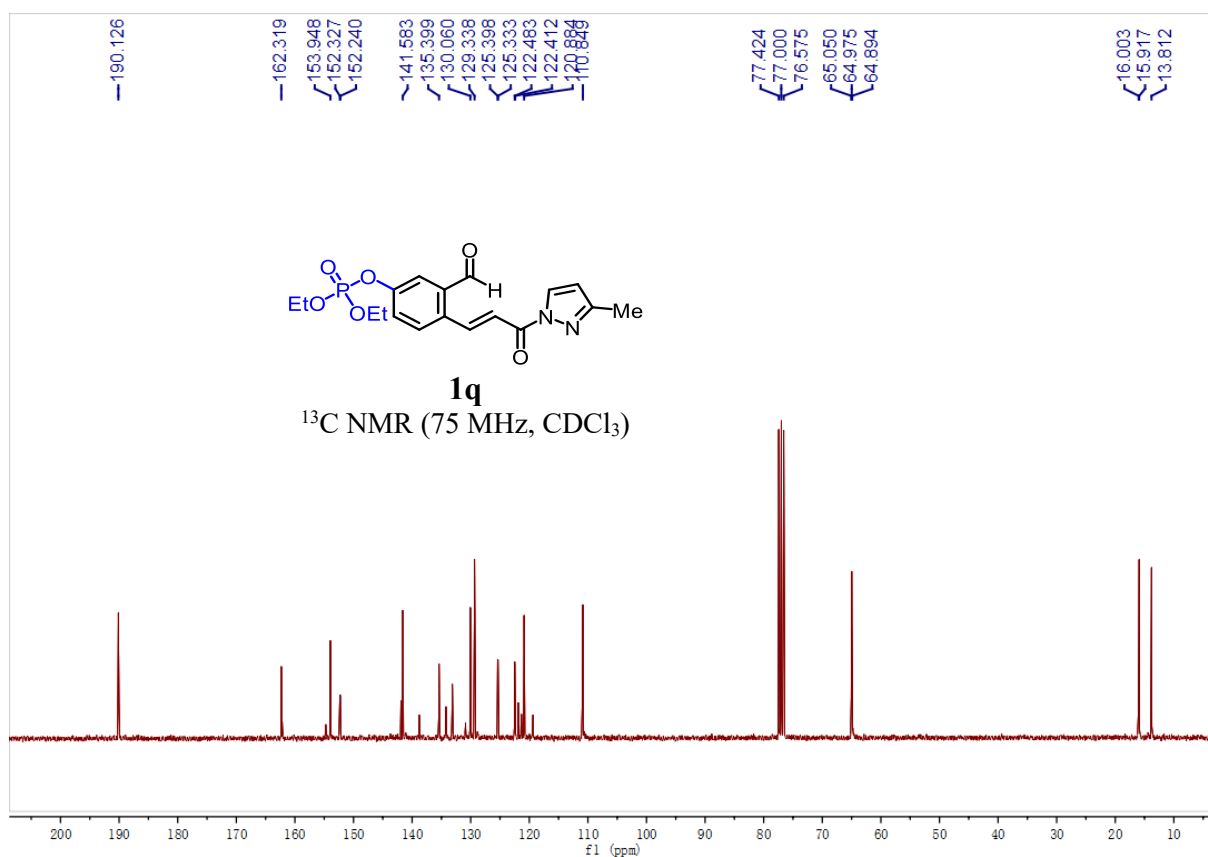
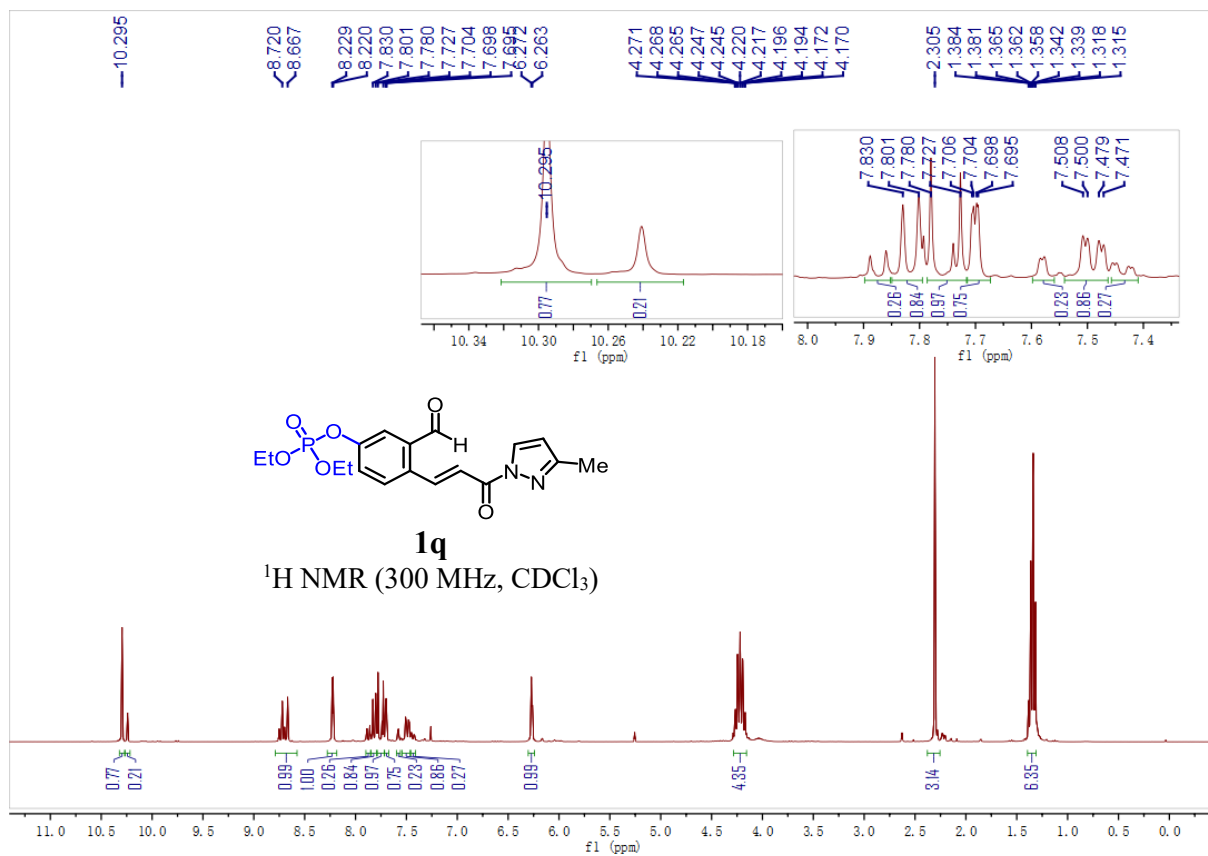


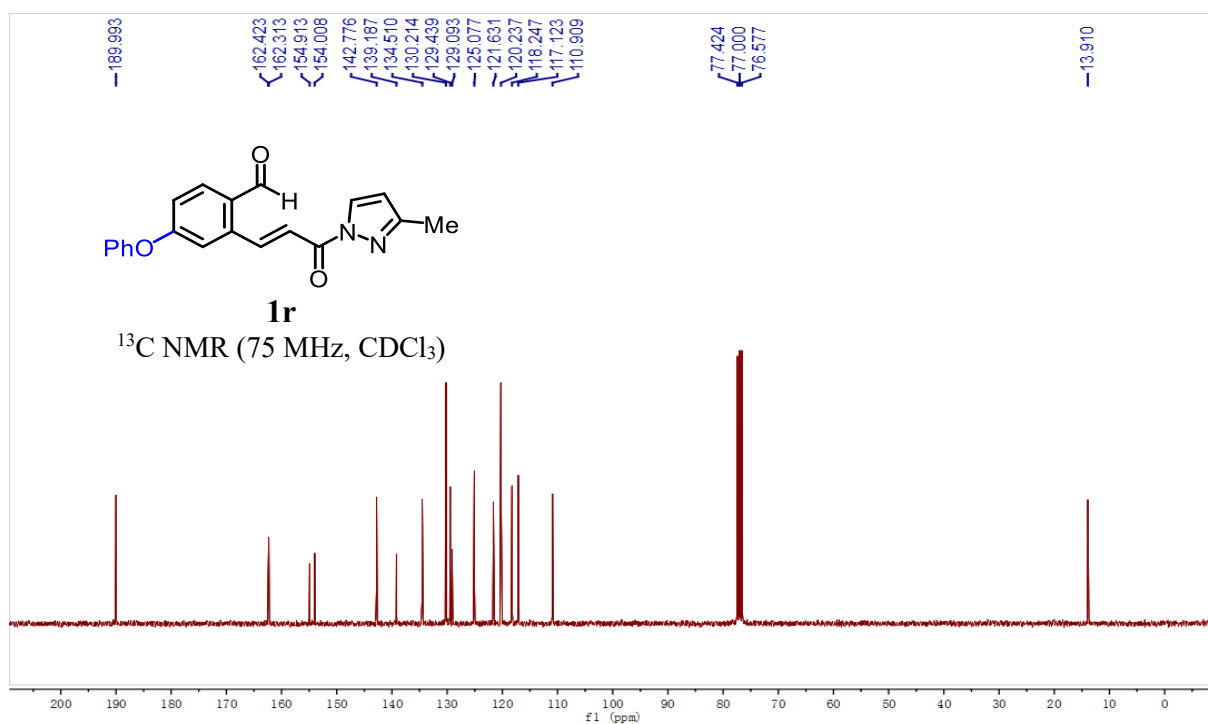
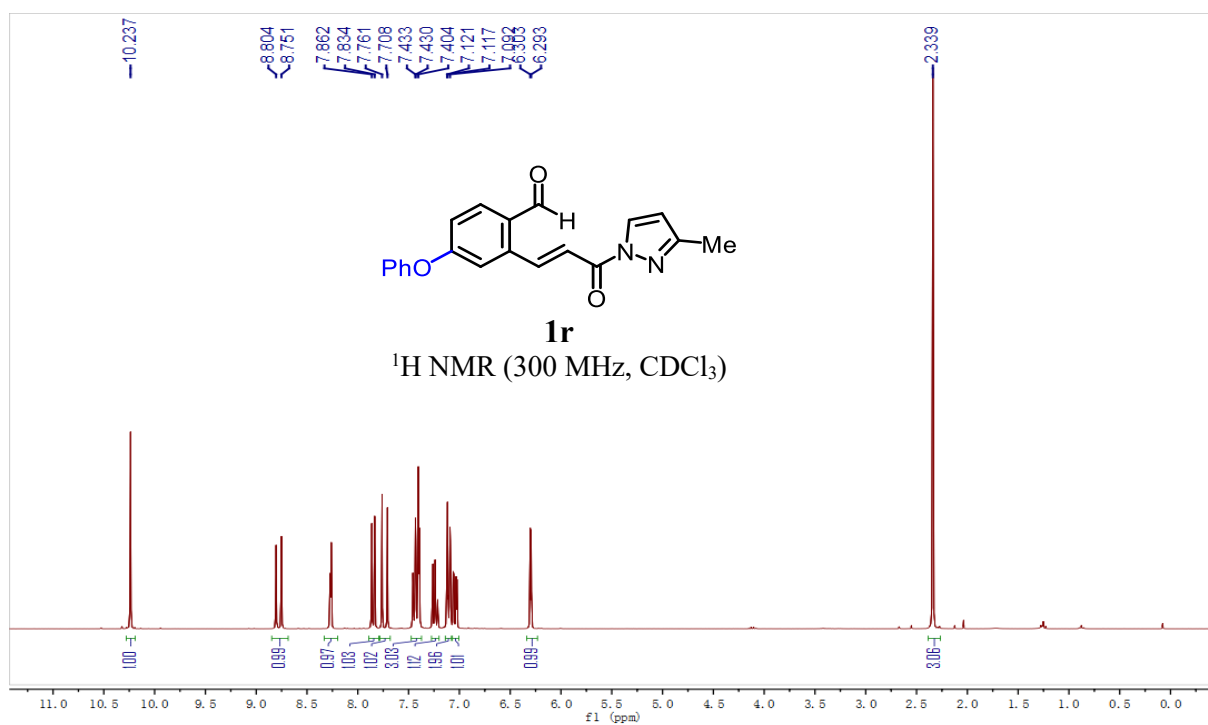
Chapter 5. Appendices



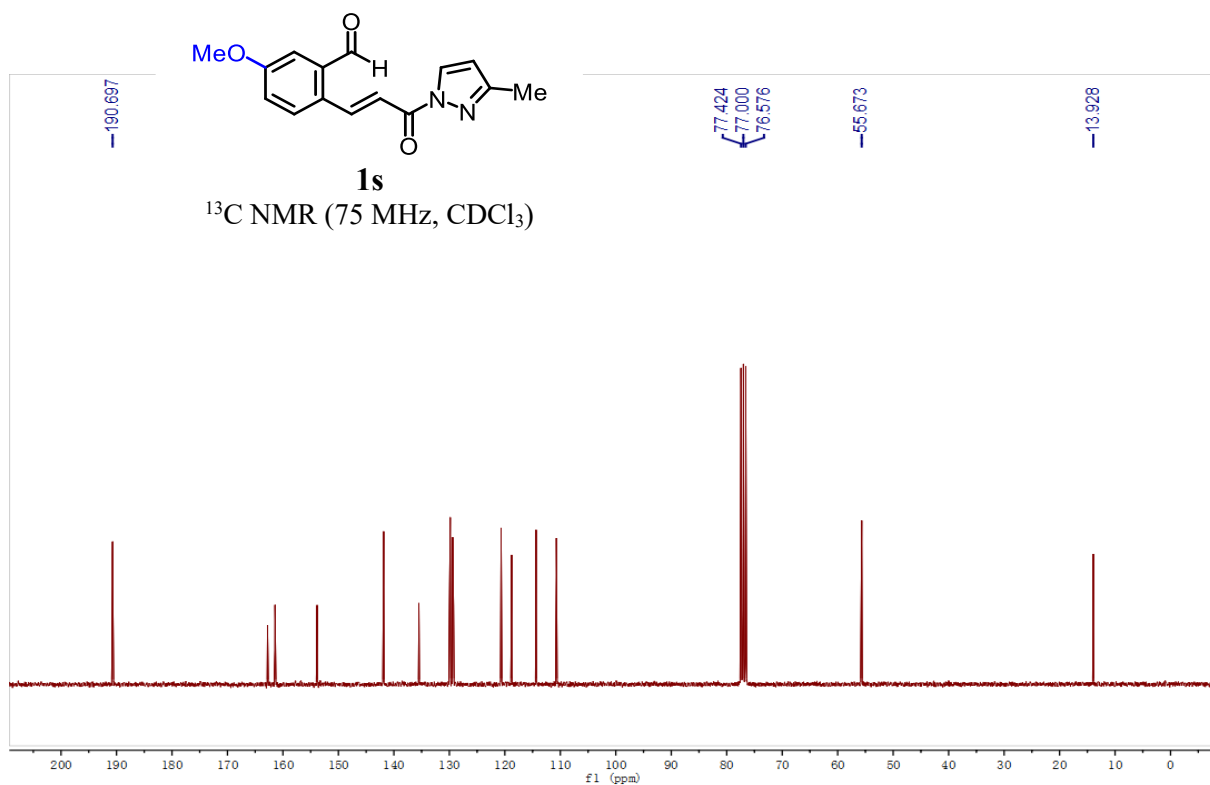
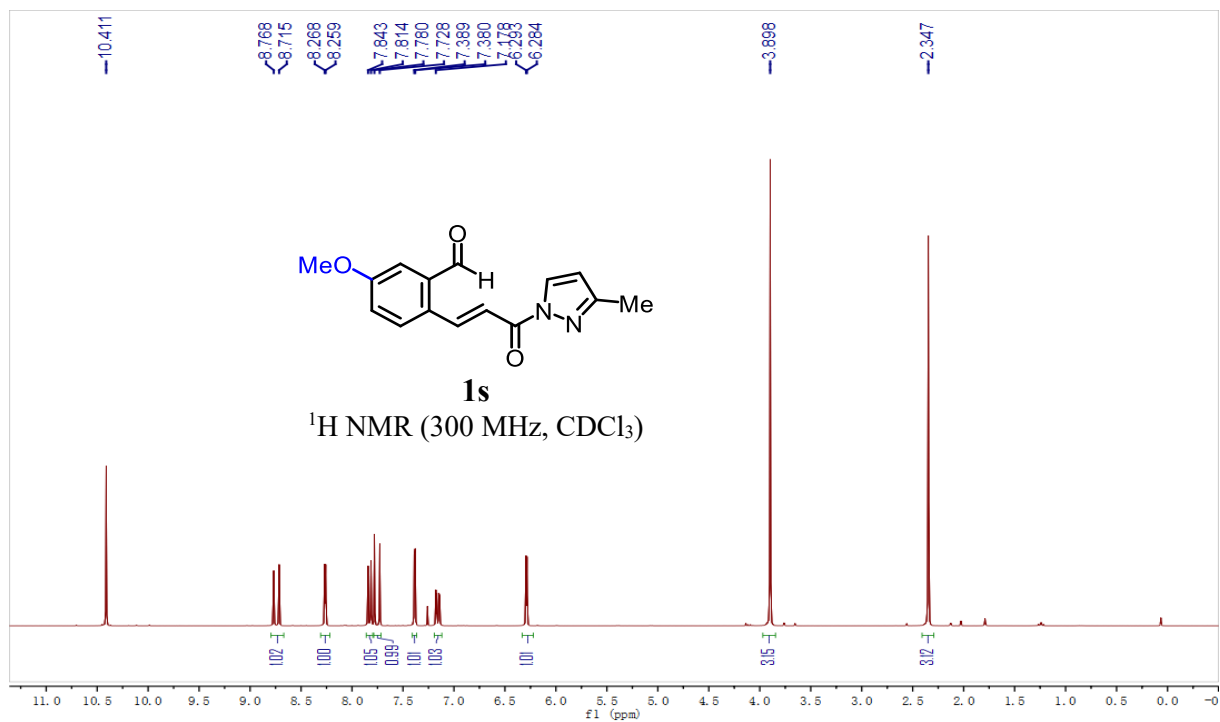
Chapter 5. Appendices

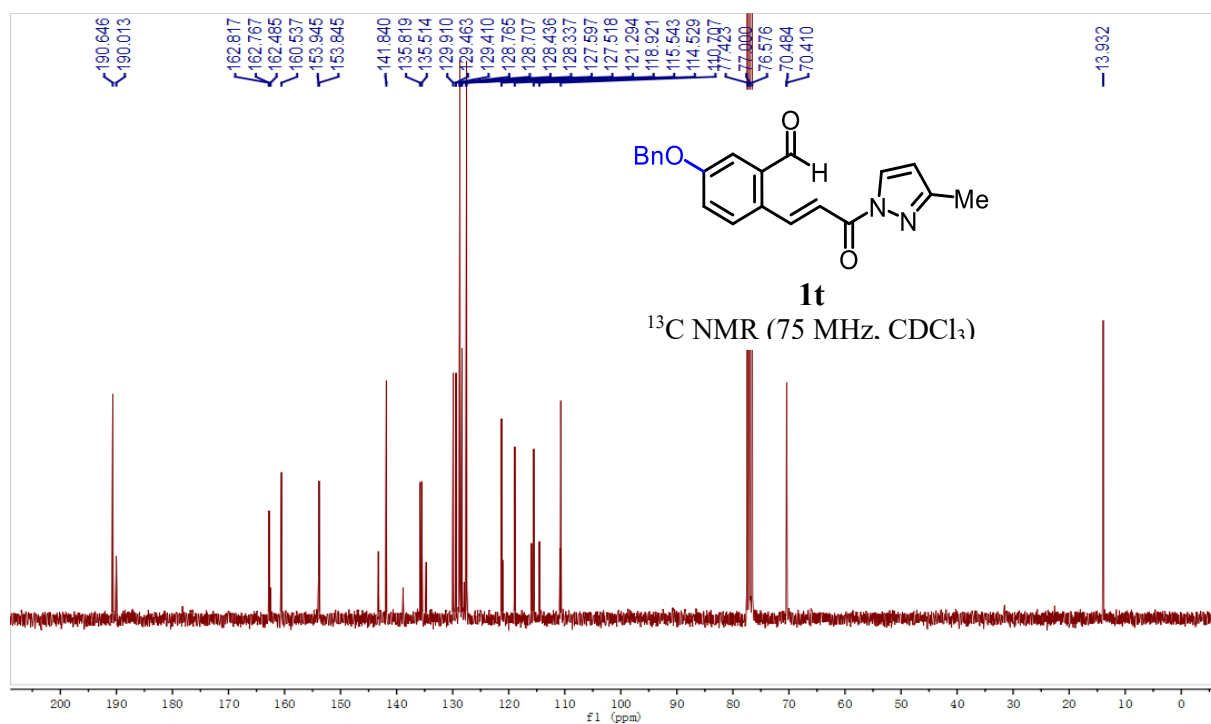
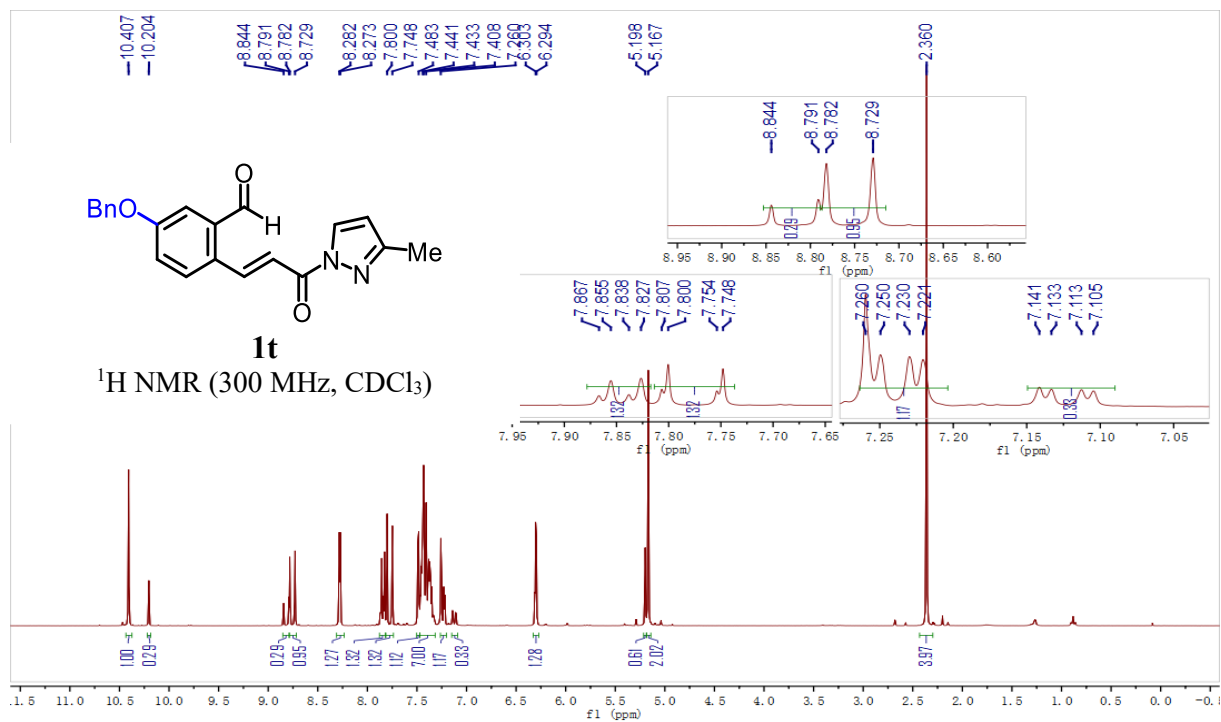


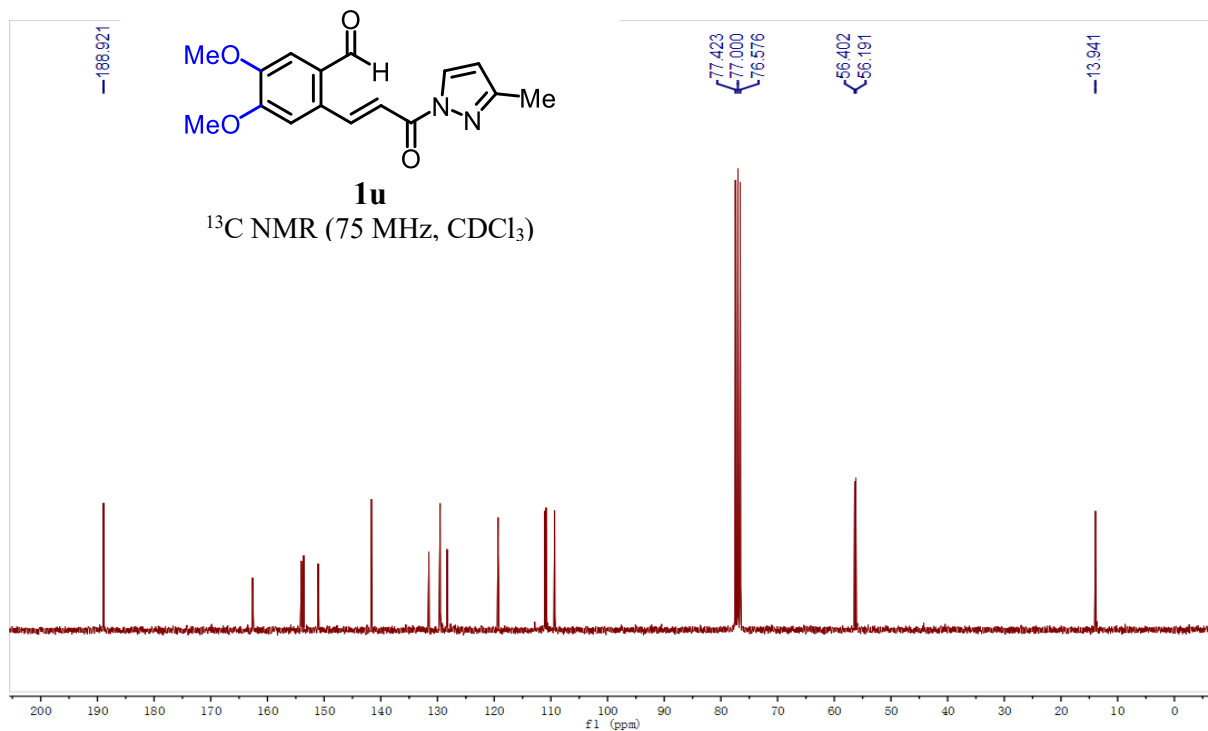
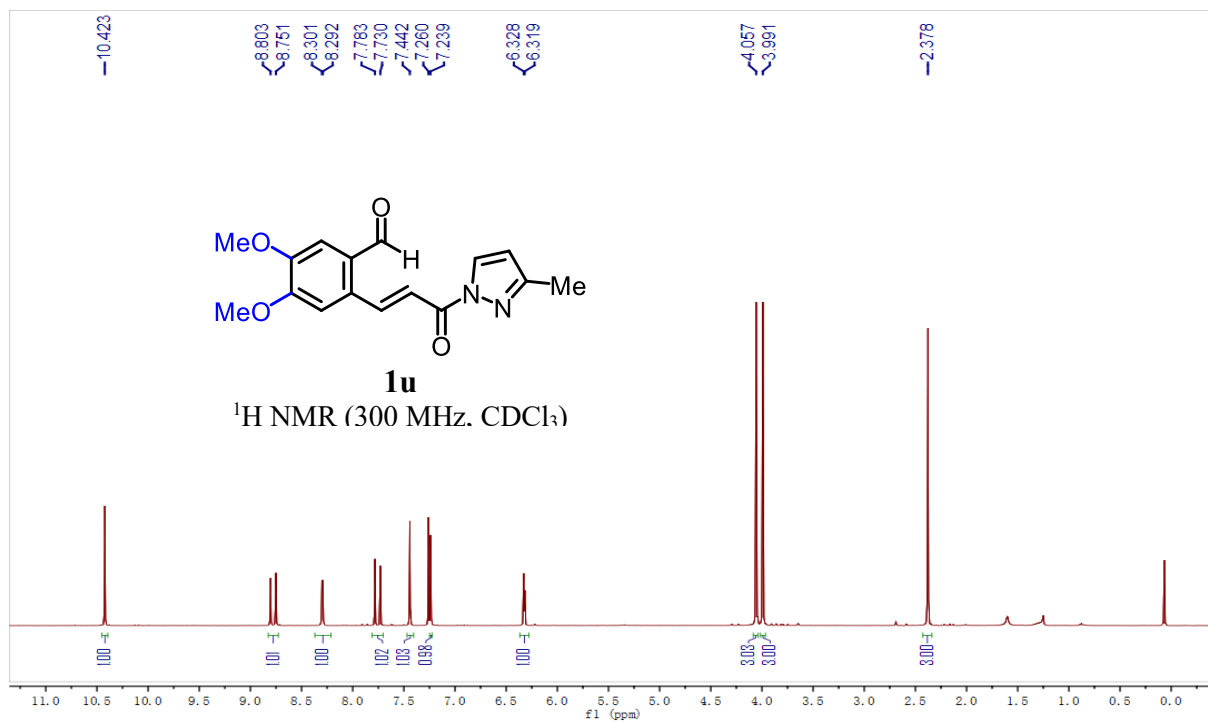




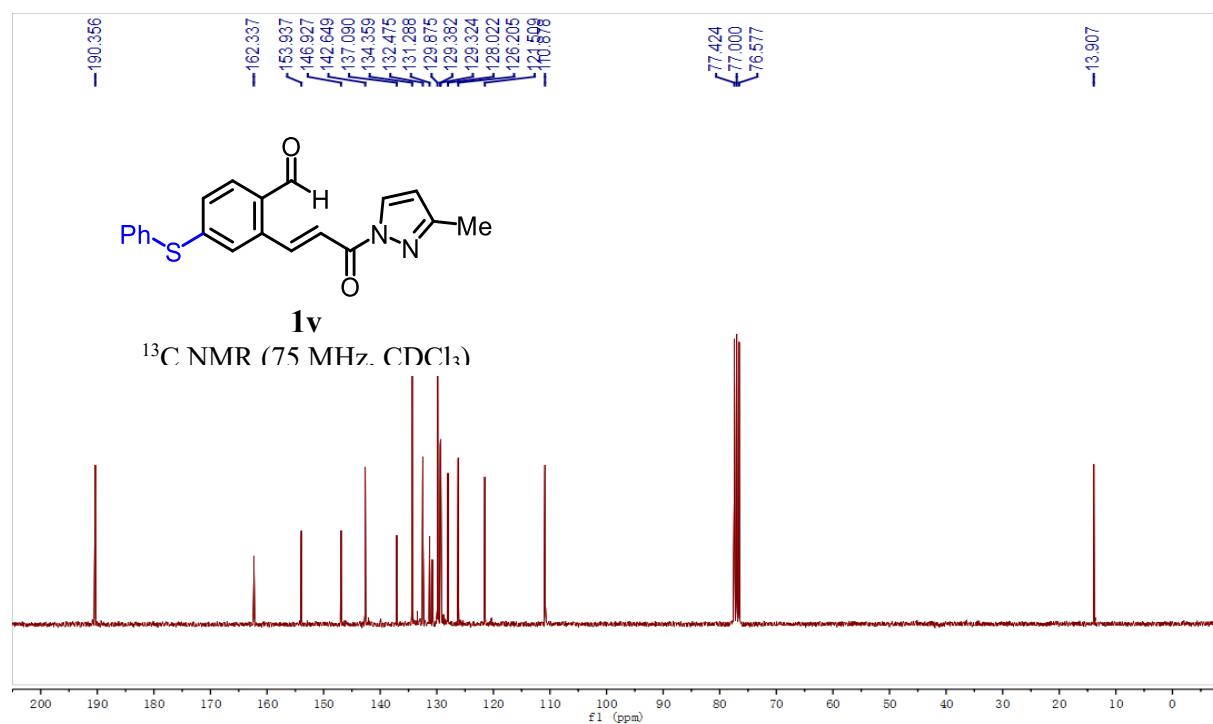
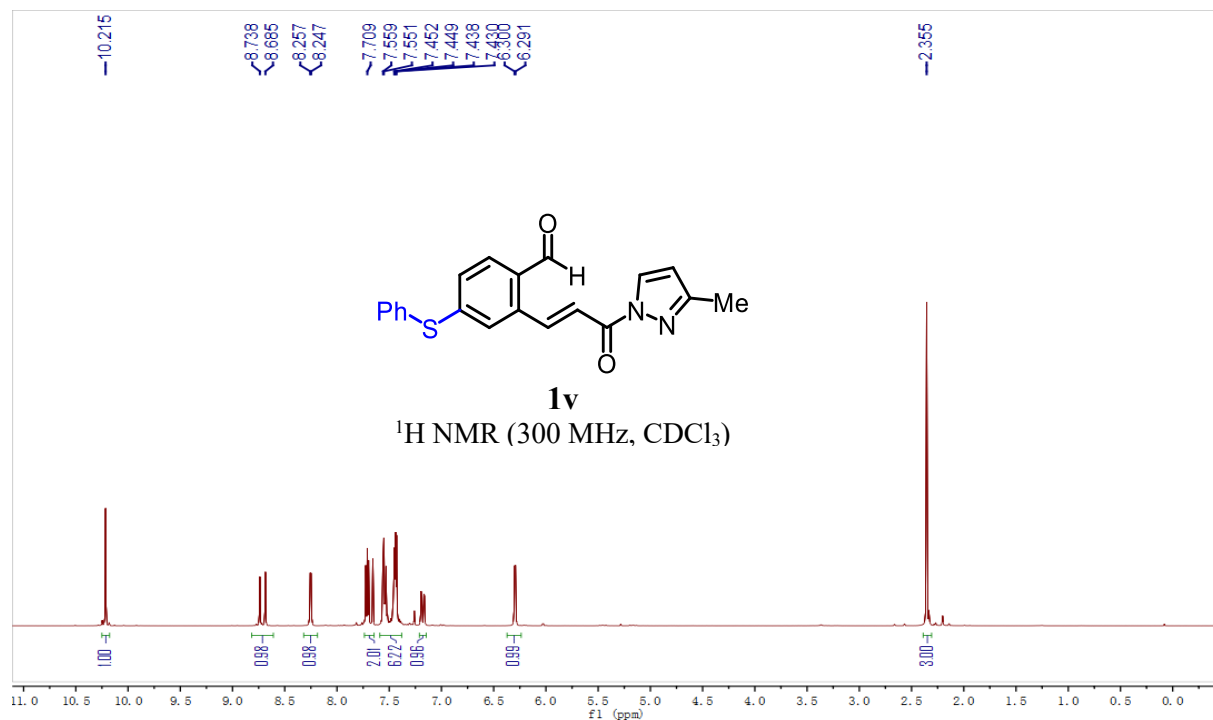
Chapter 5. Appendices



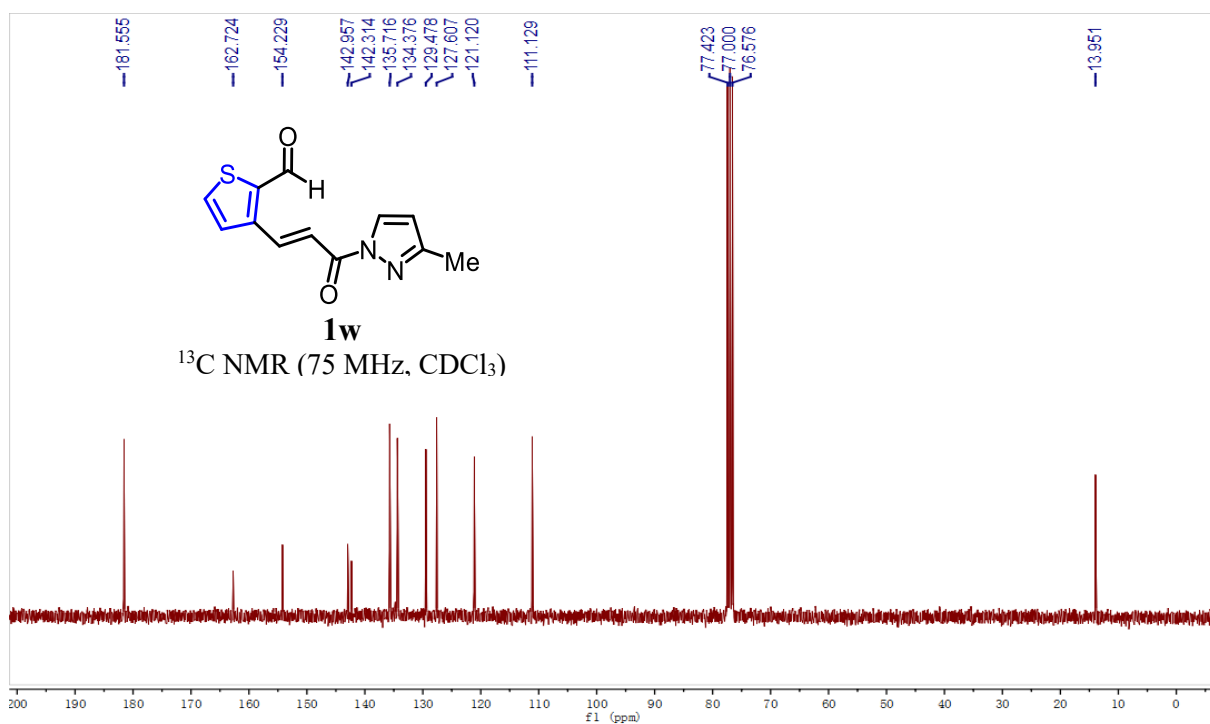
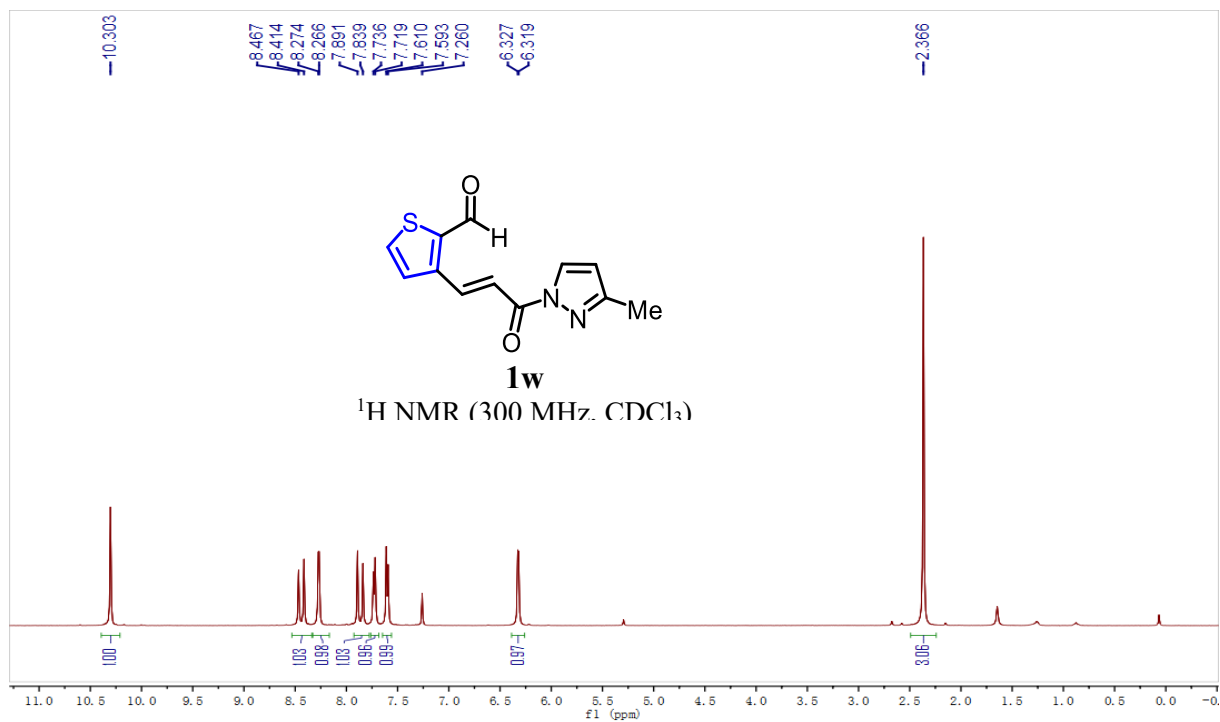




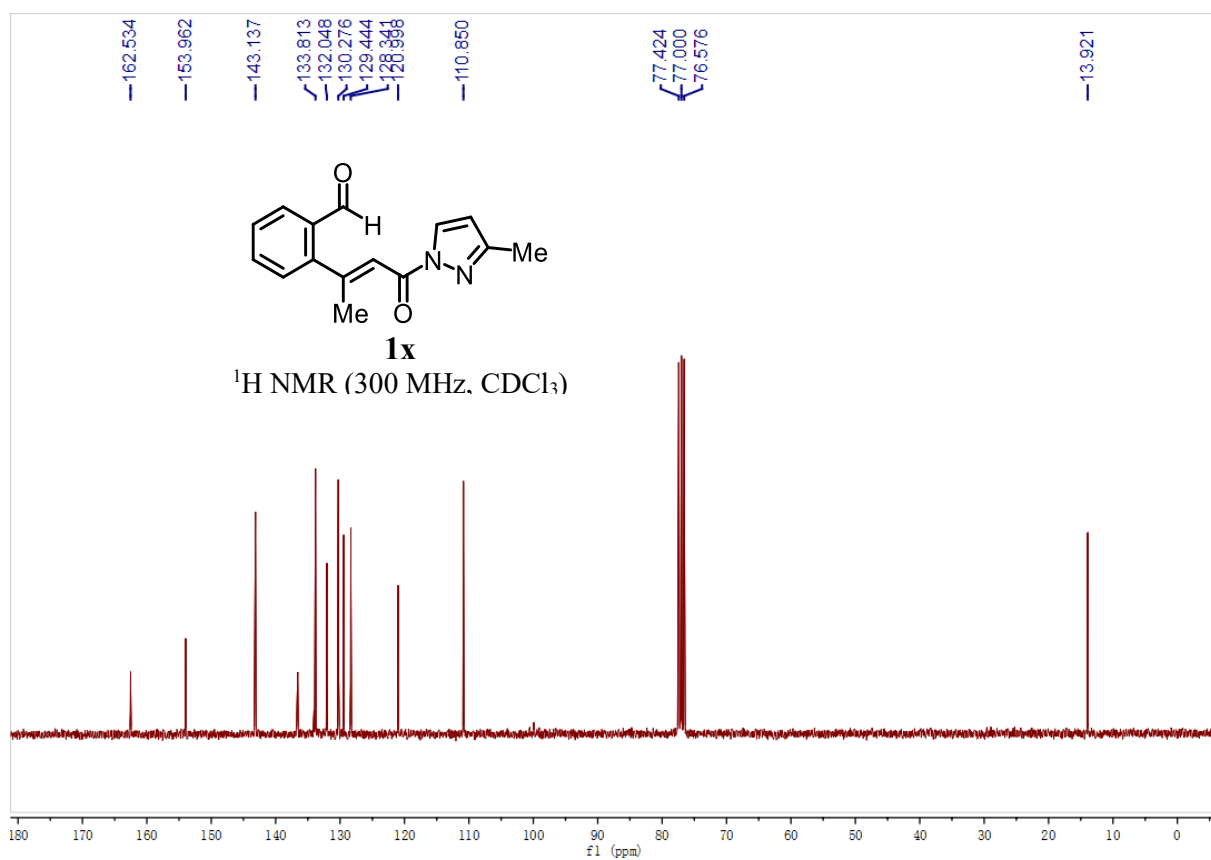
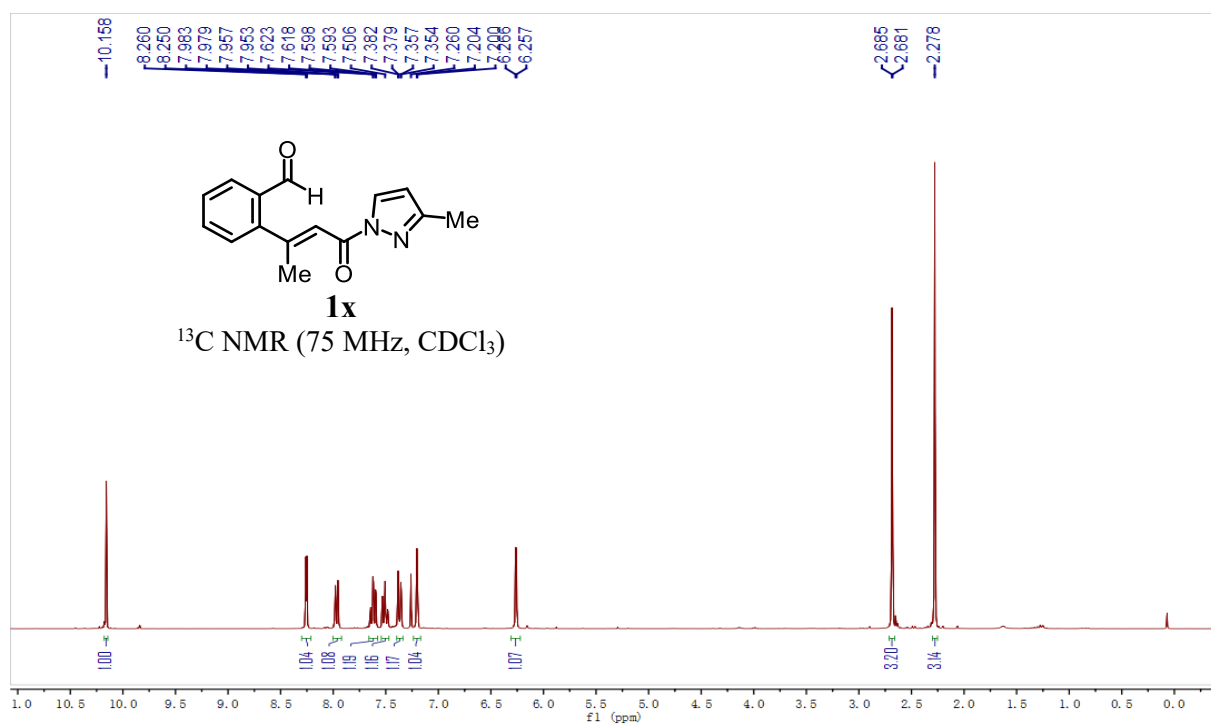
Chapter 5. Appendices

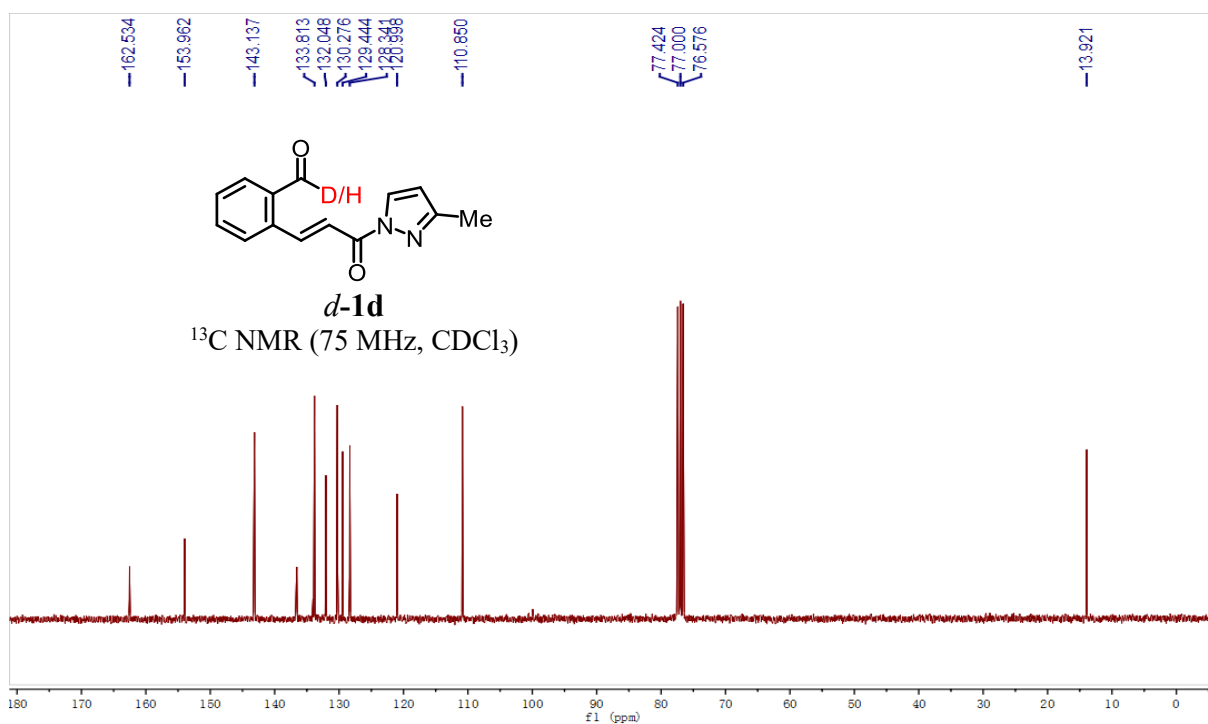
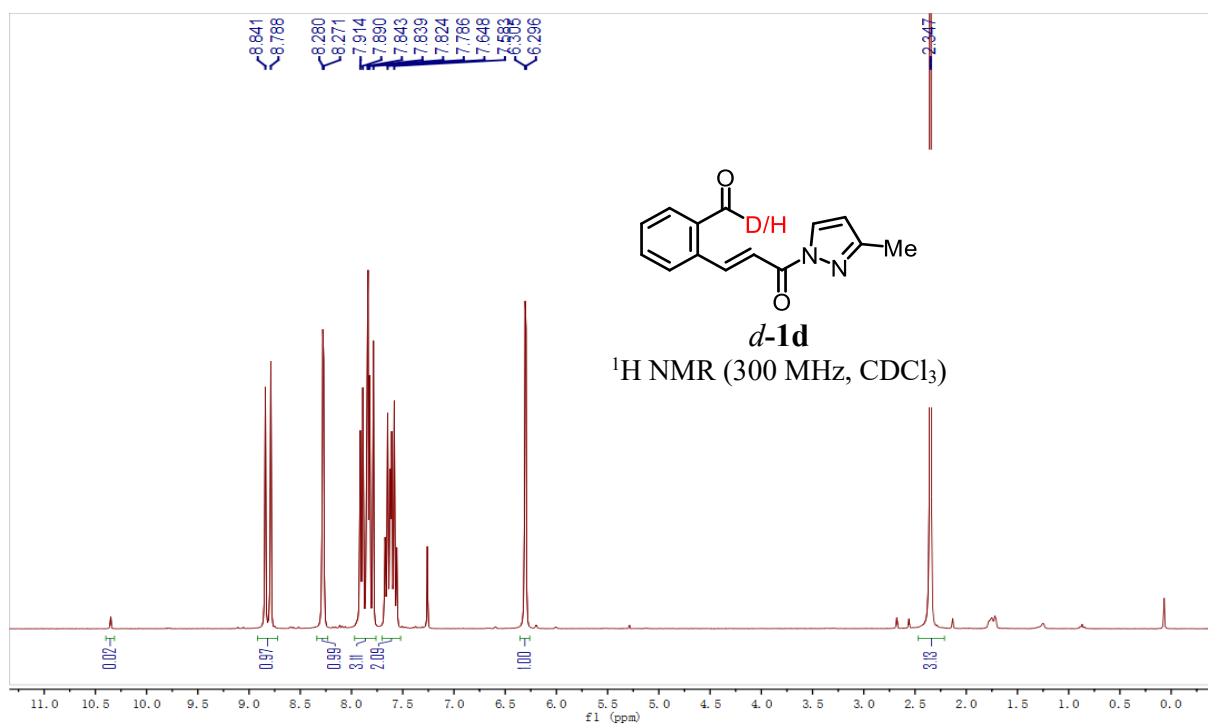


Chapter 5. Appendices

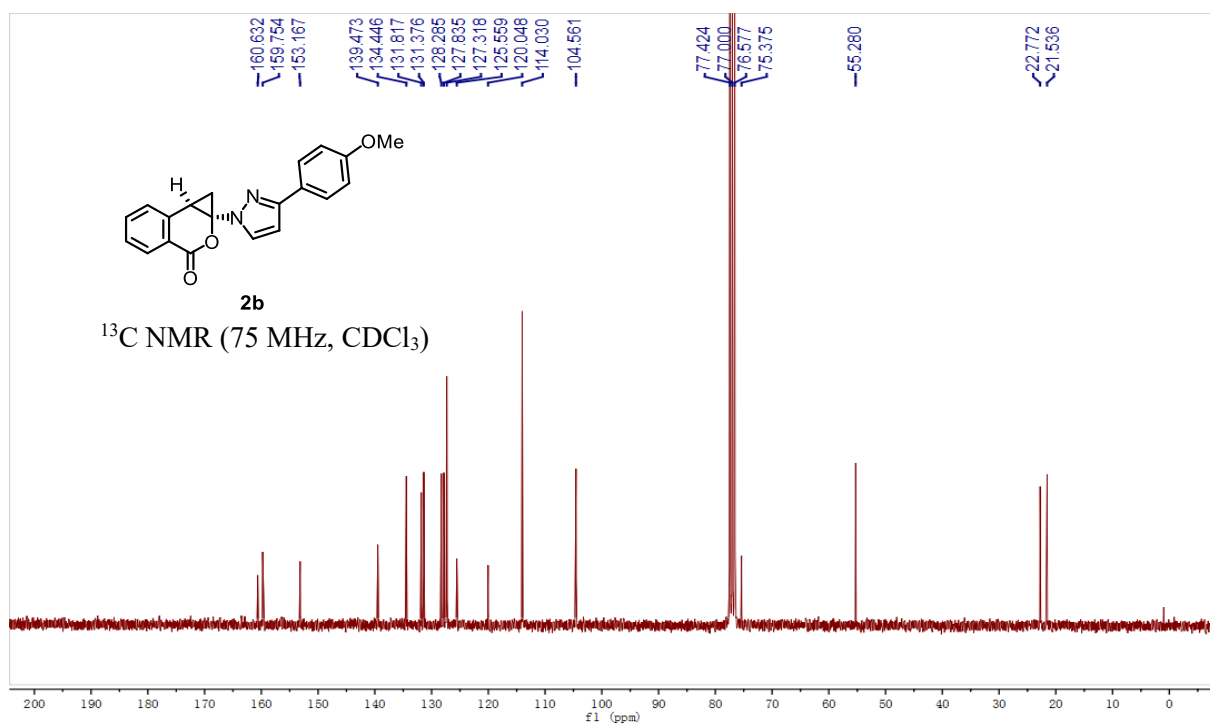
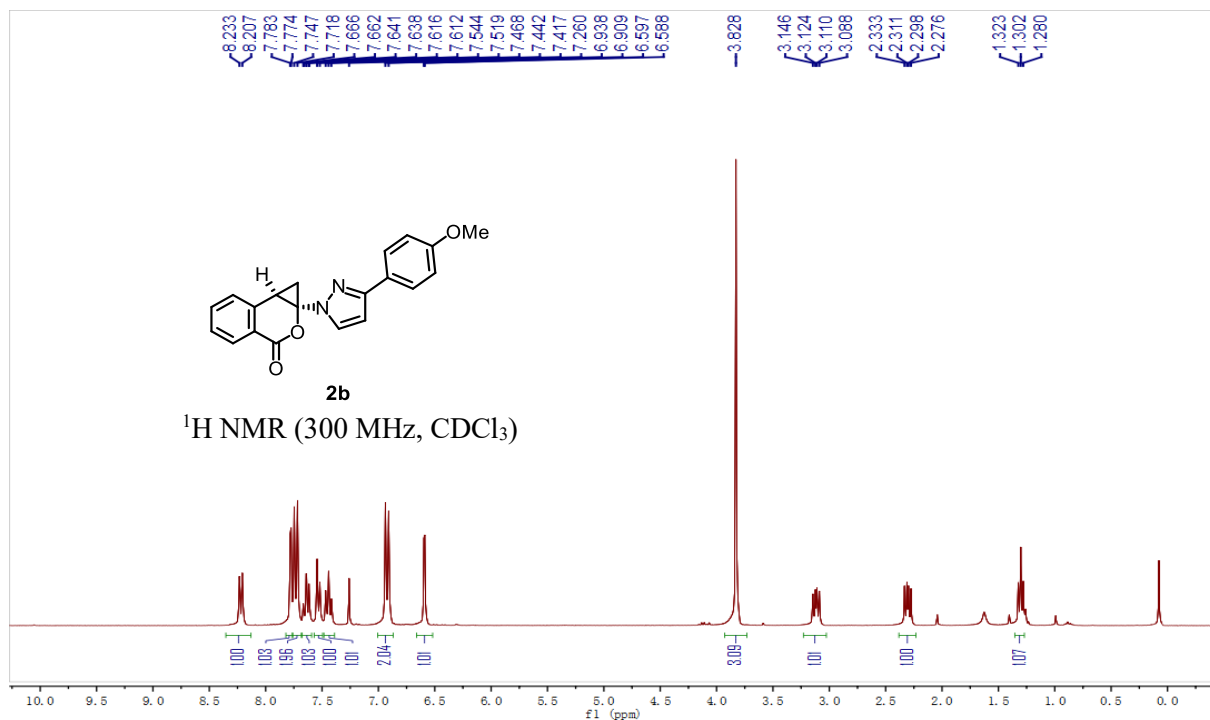


Chapter 5. Appendices

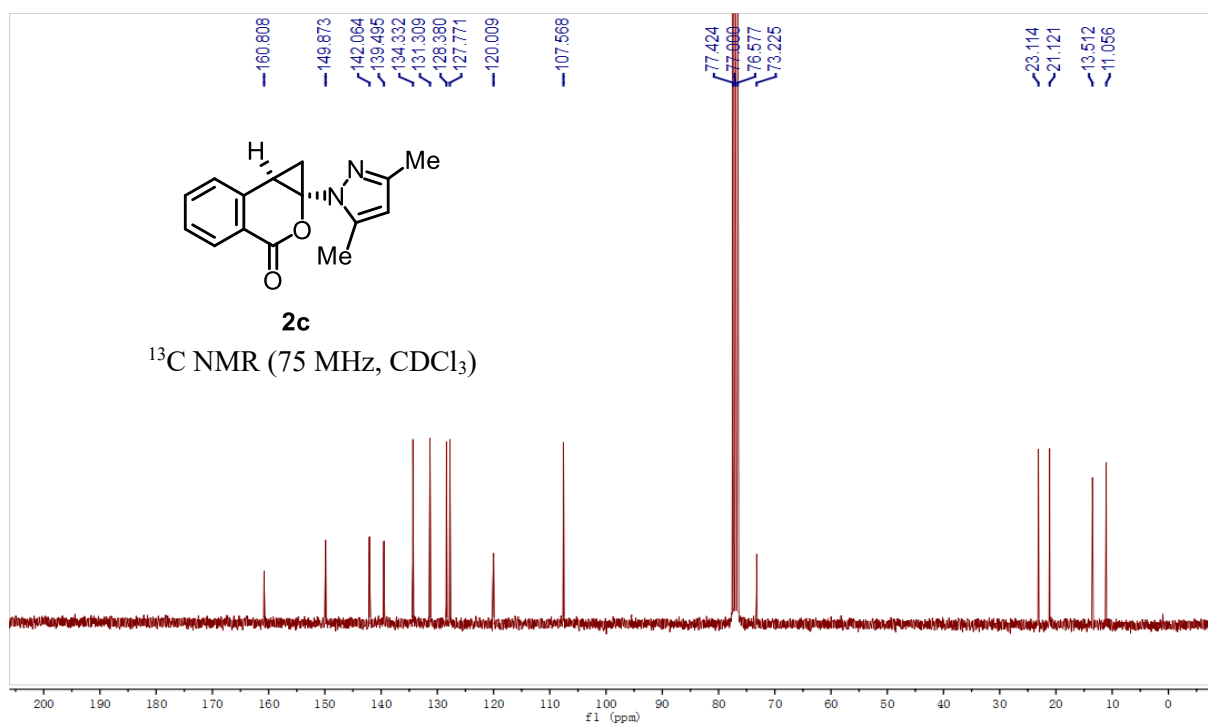
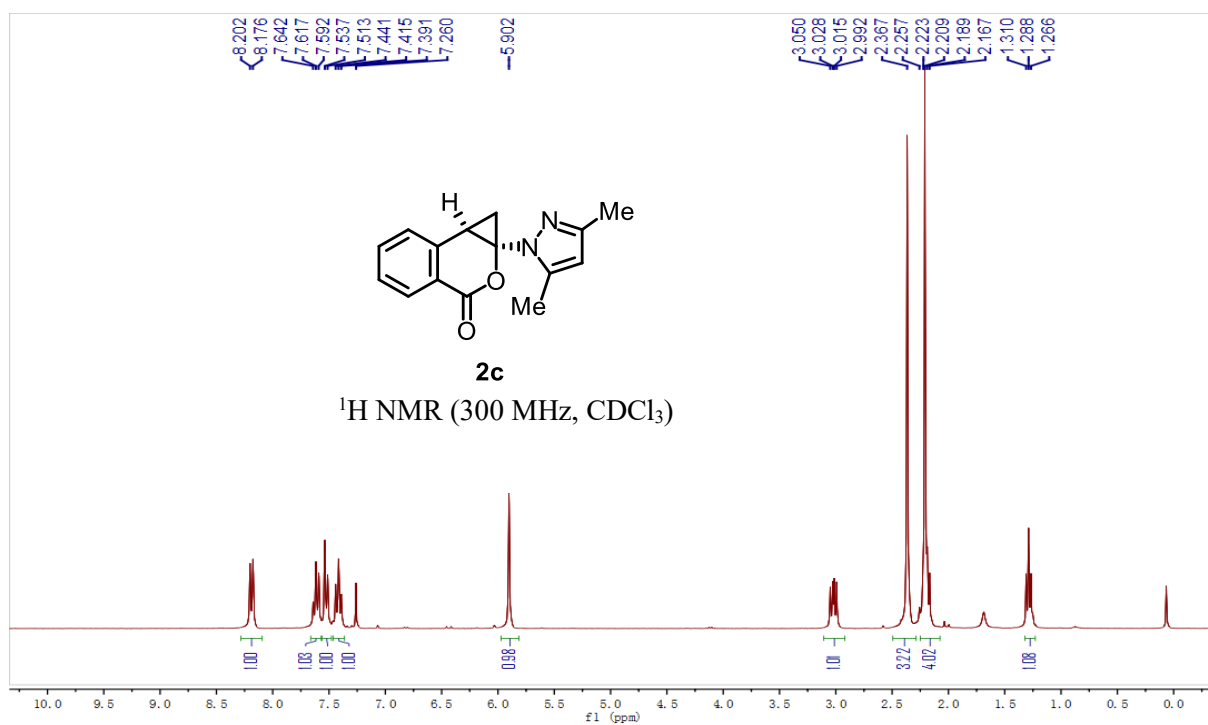




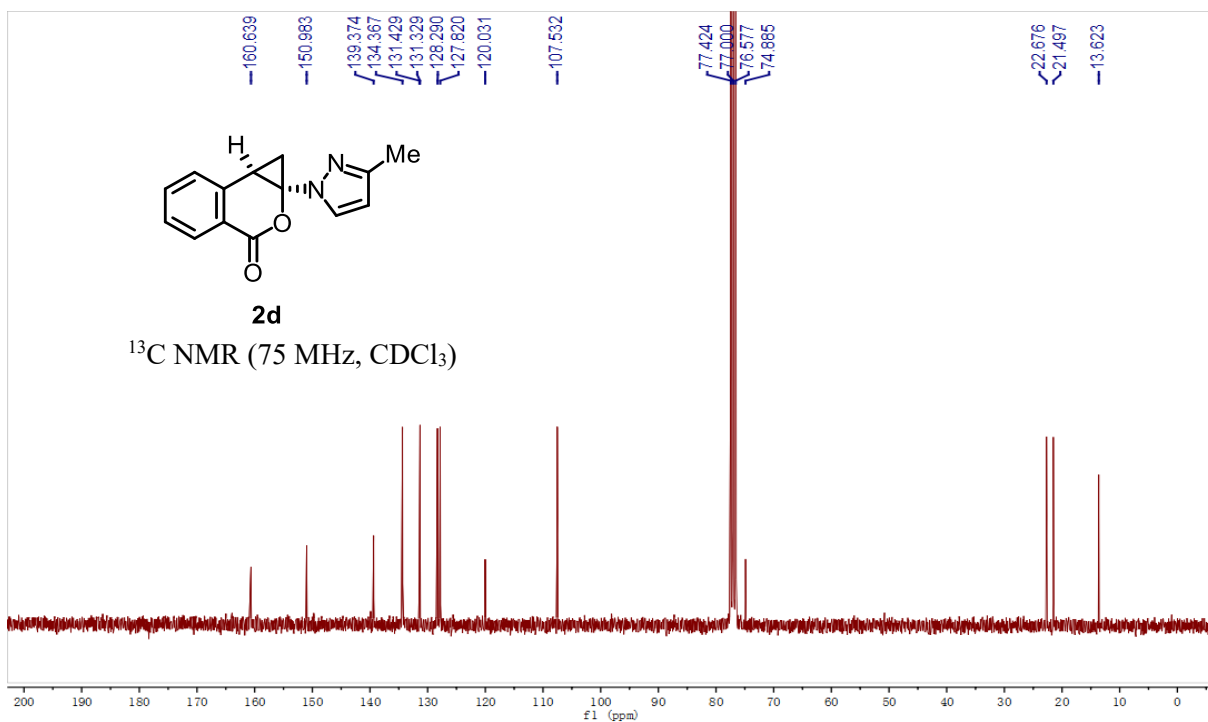
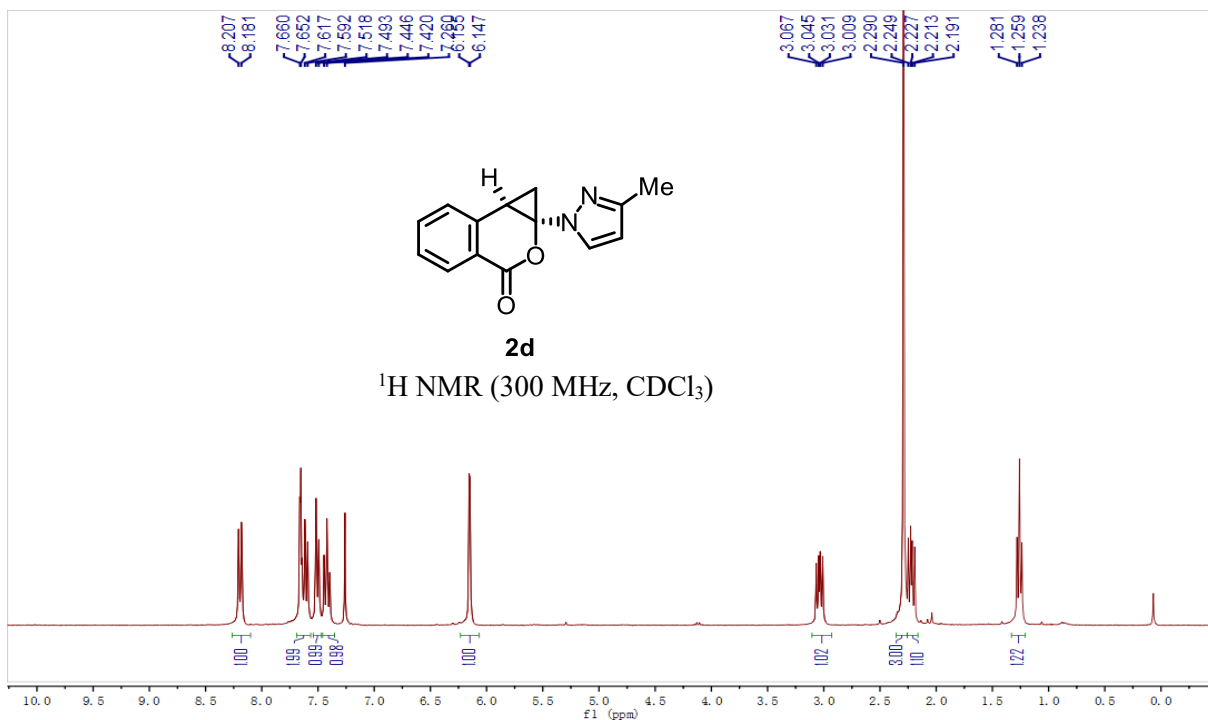
Chapter 5. Appendices



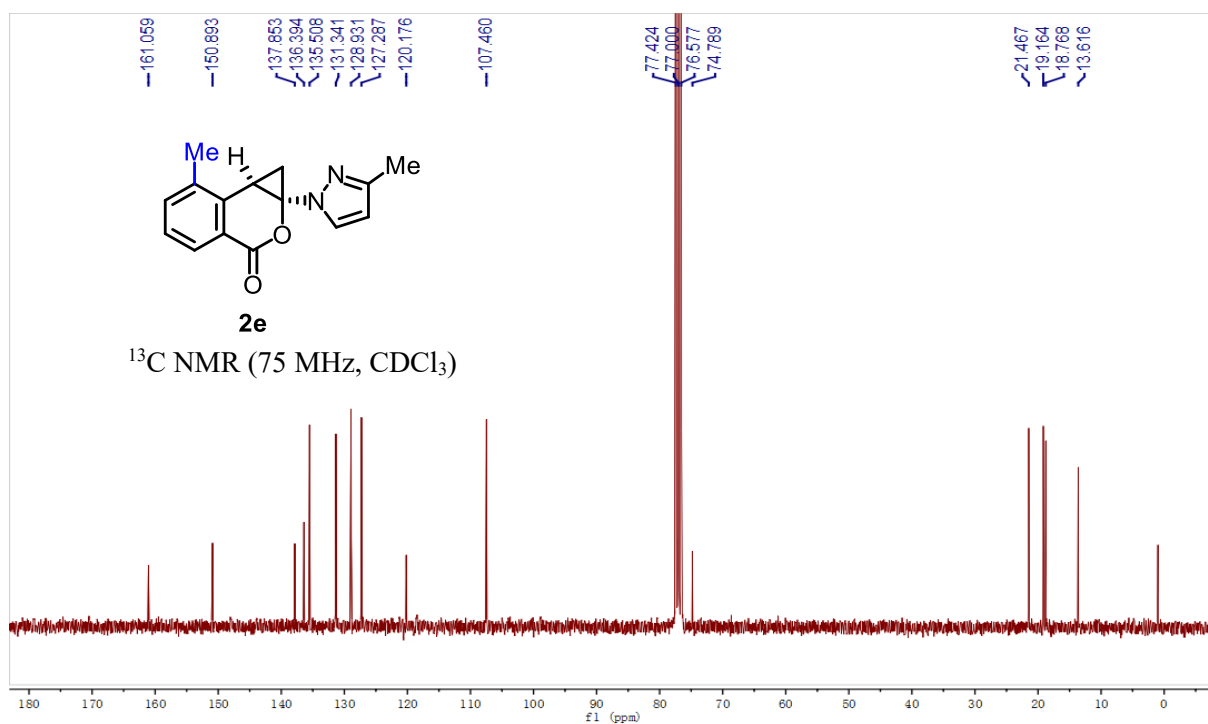
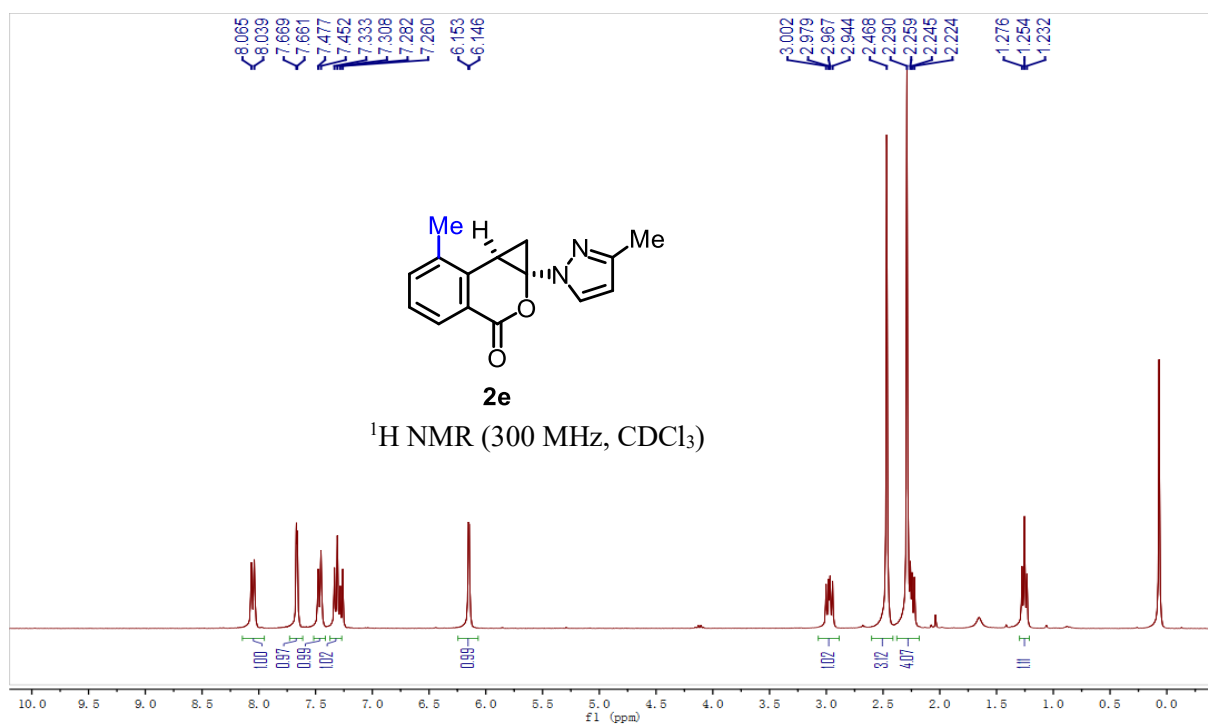
Chapter 5. Appendices



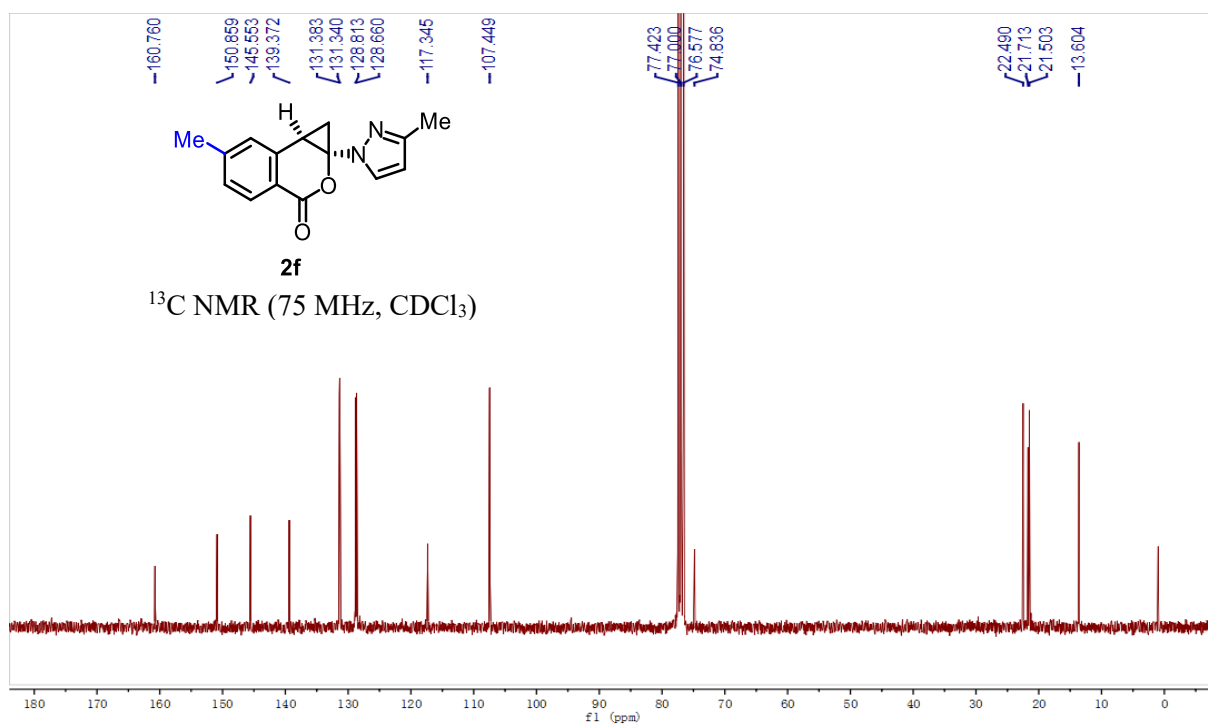
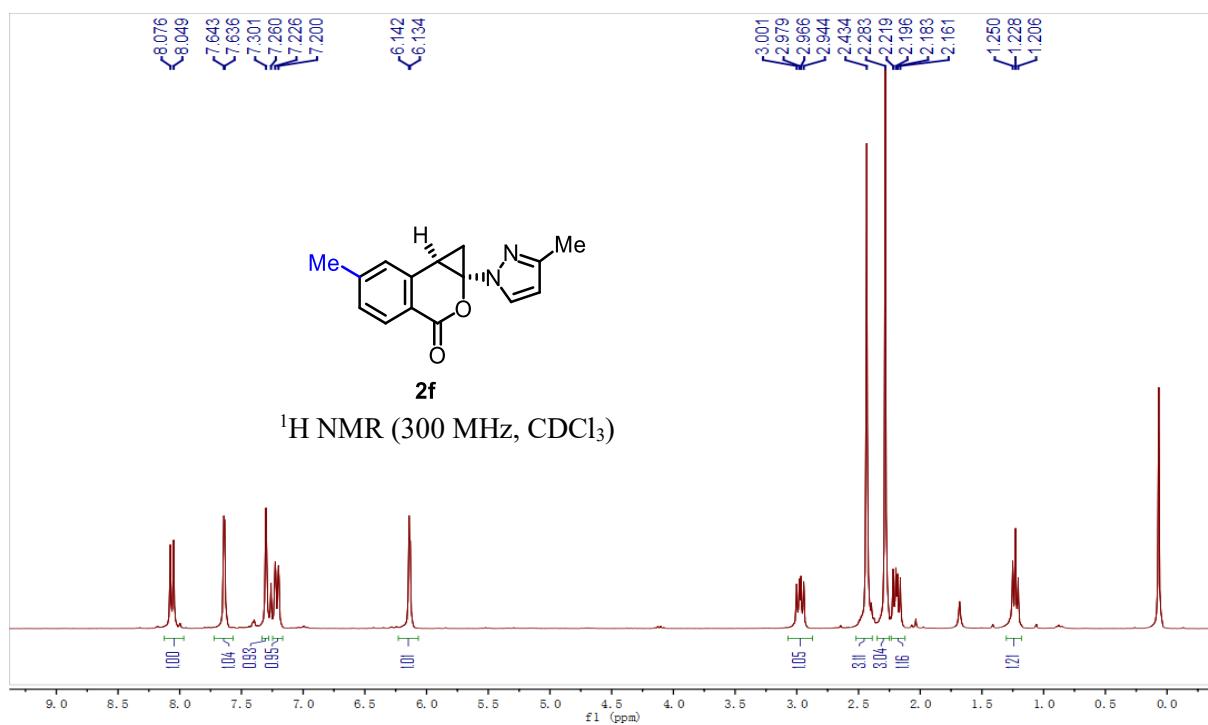
Chapter 5. Appendices

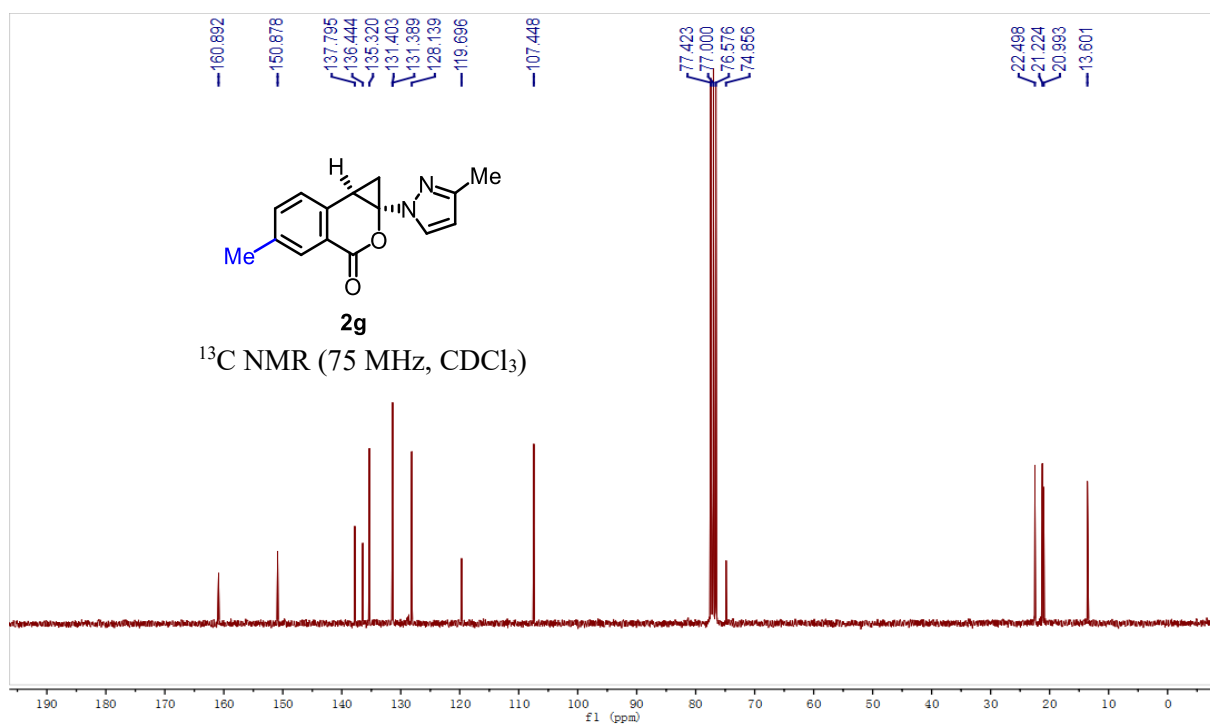
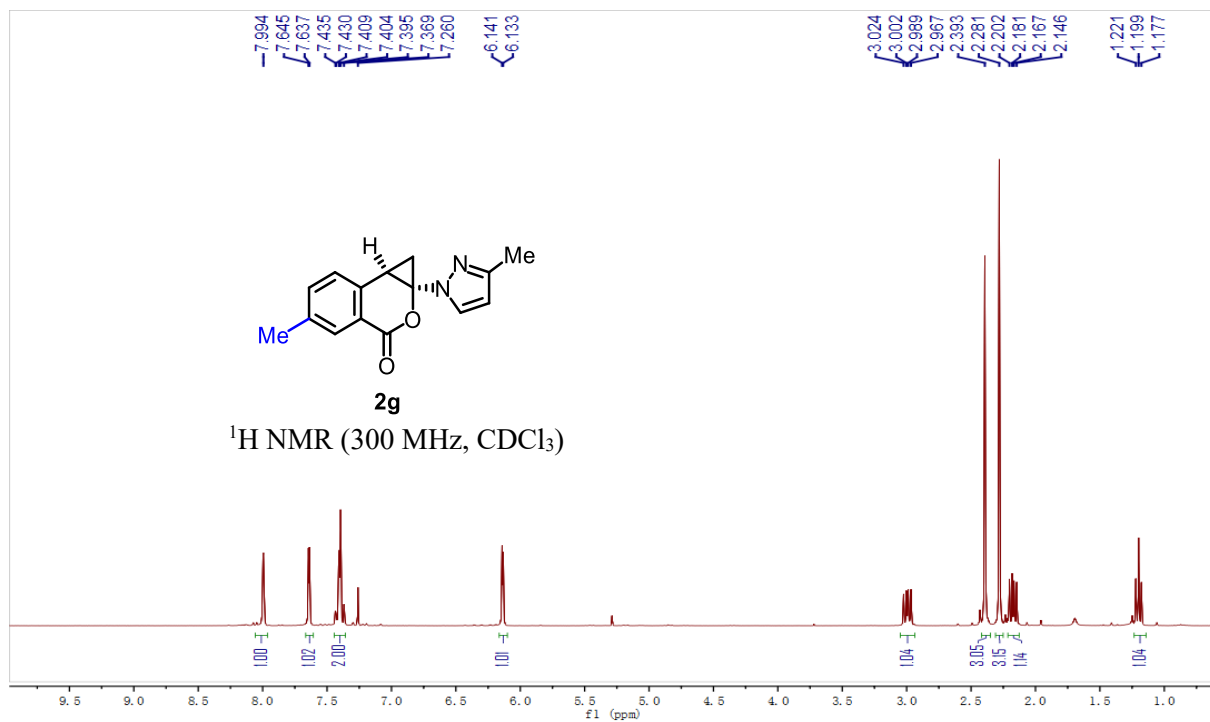


Chapter 5. Appendices

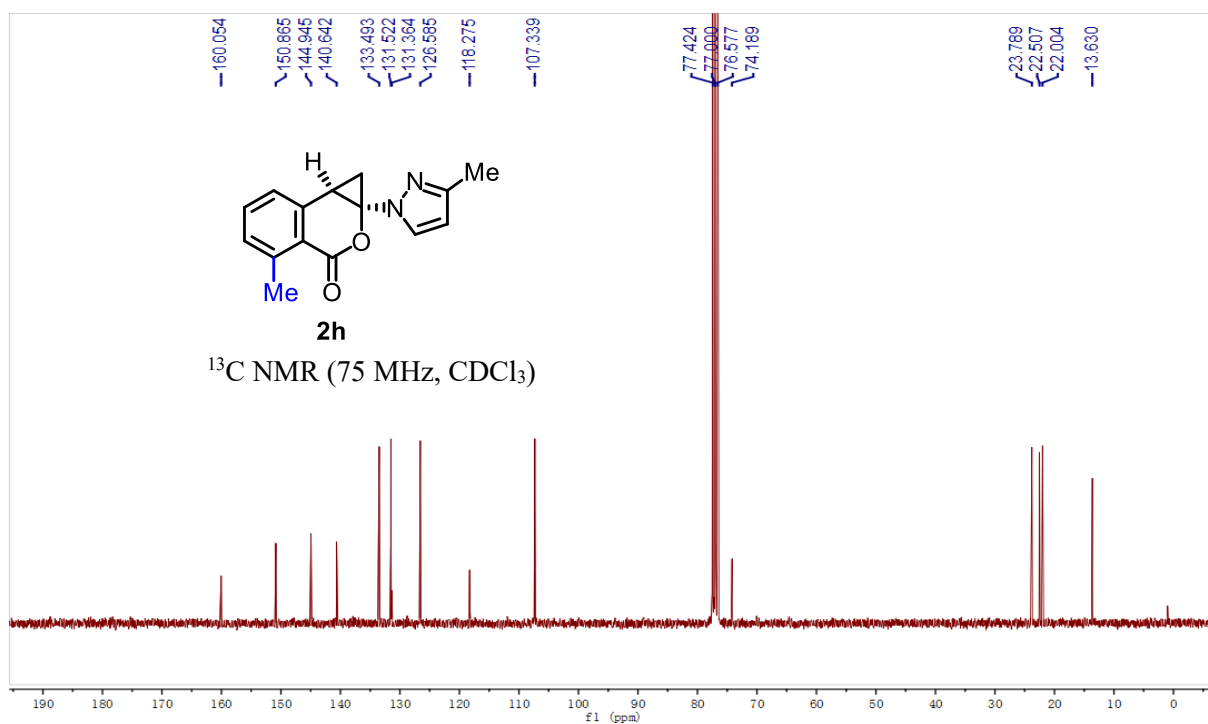
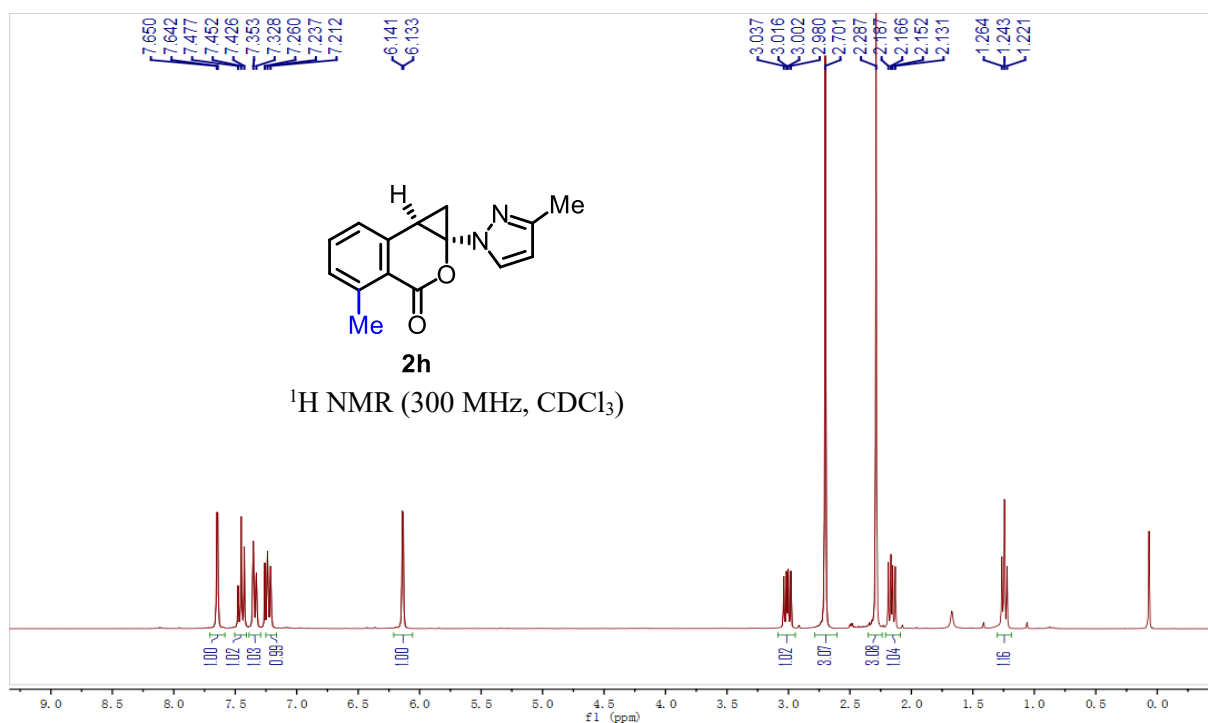


Chapter 5. Appendices

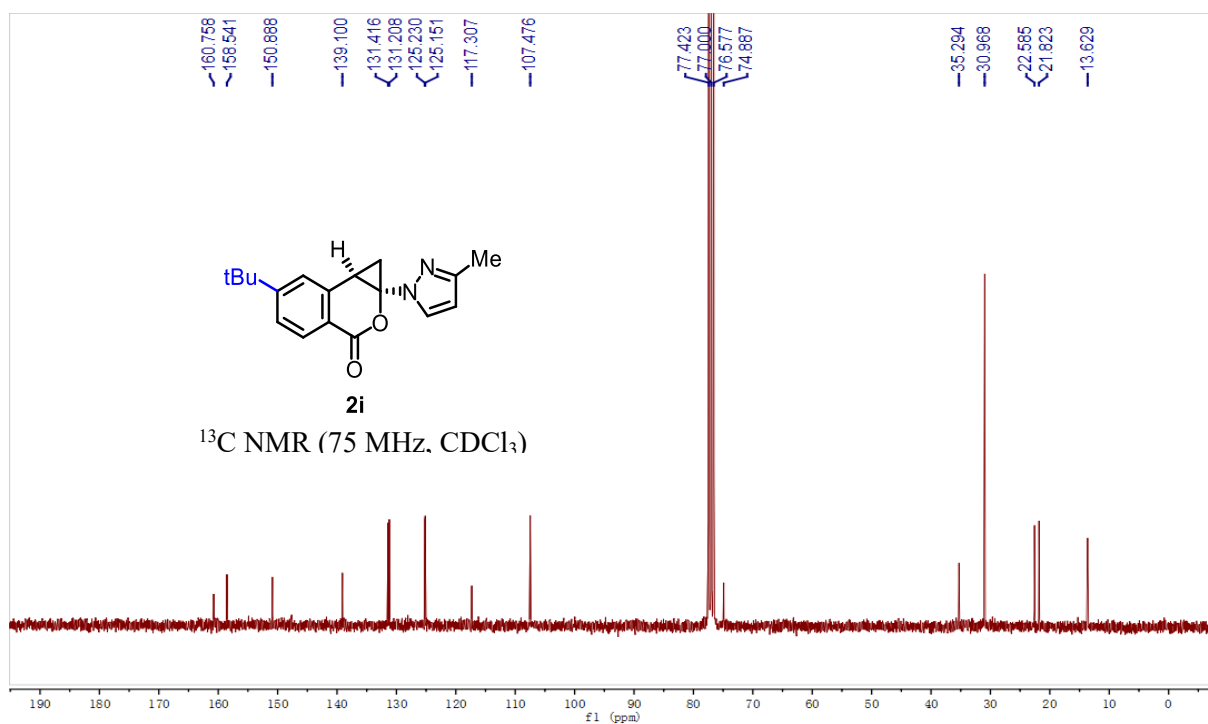
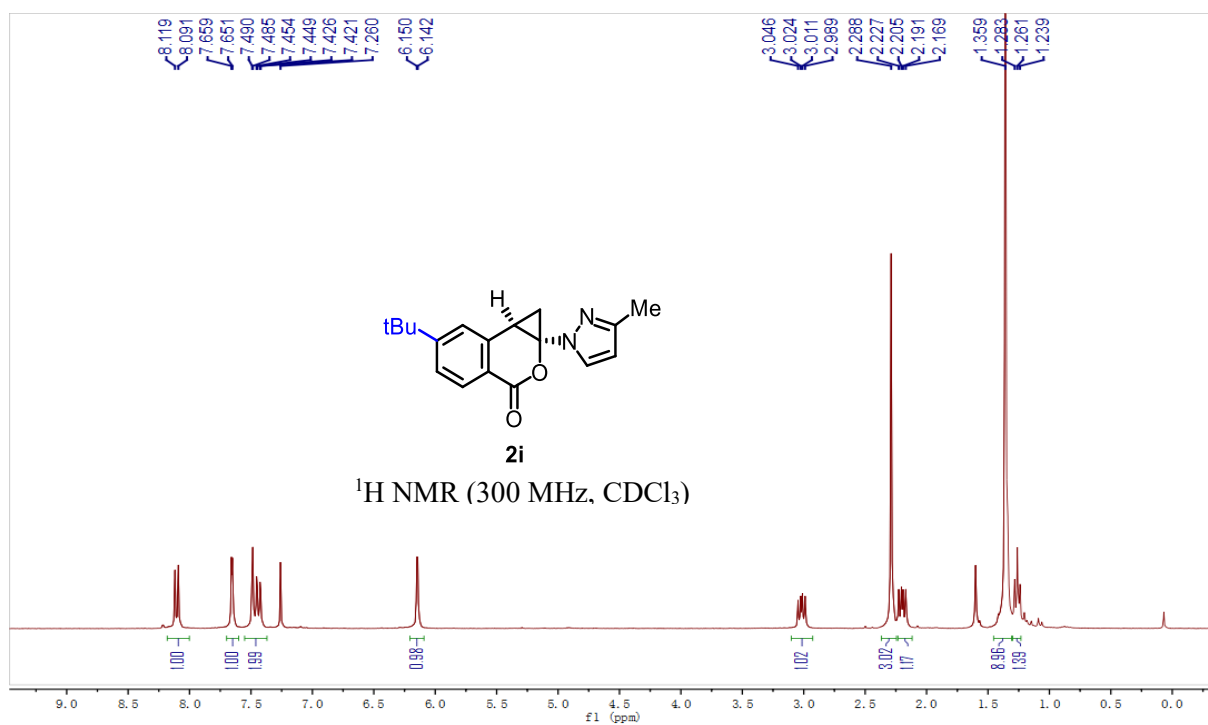




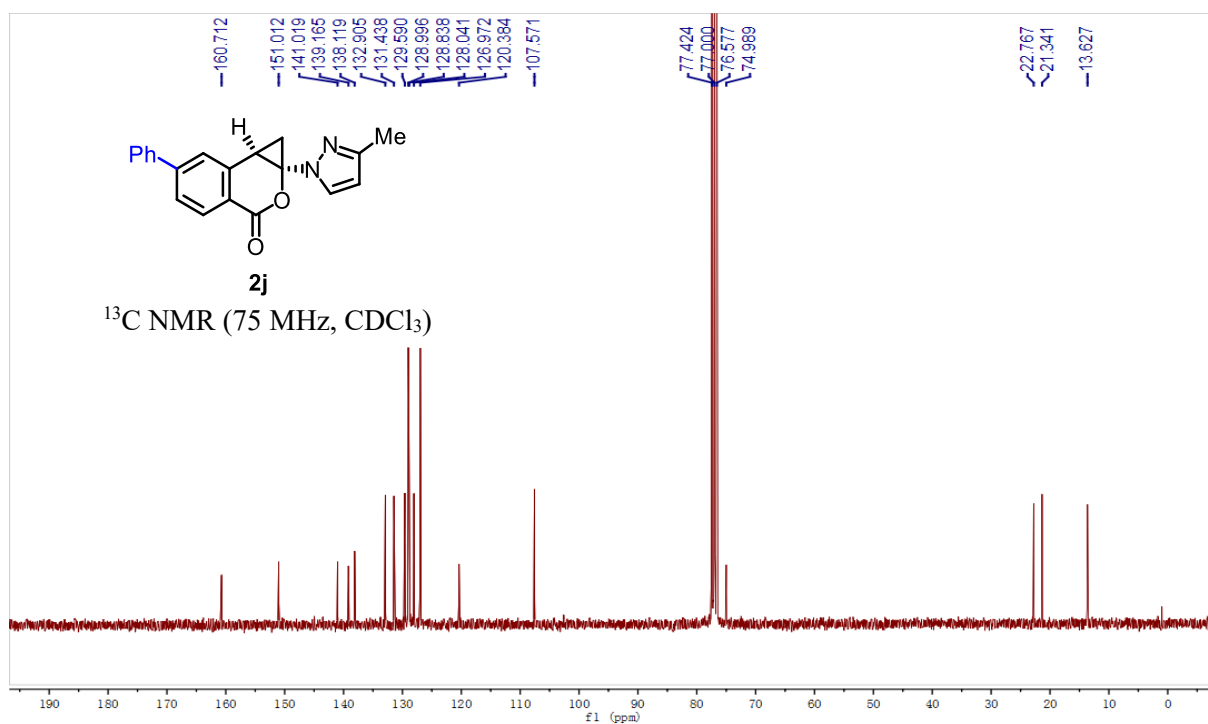
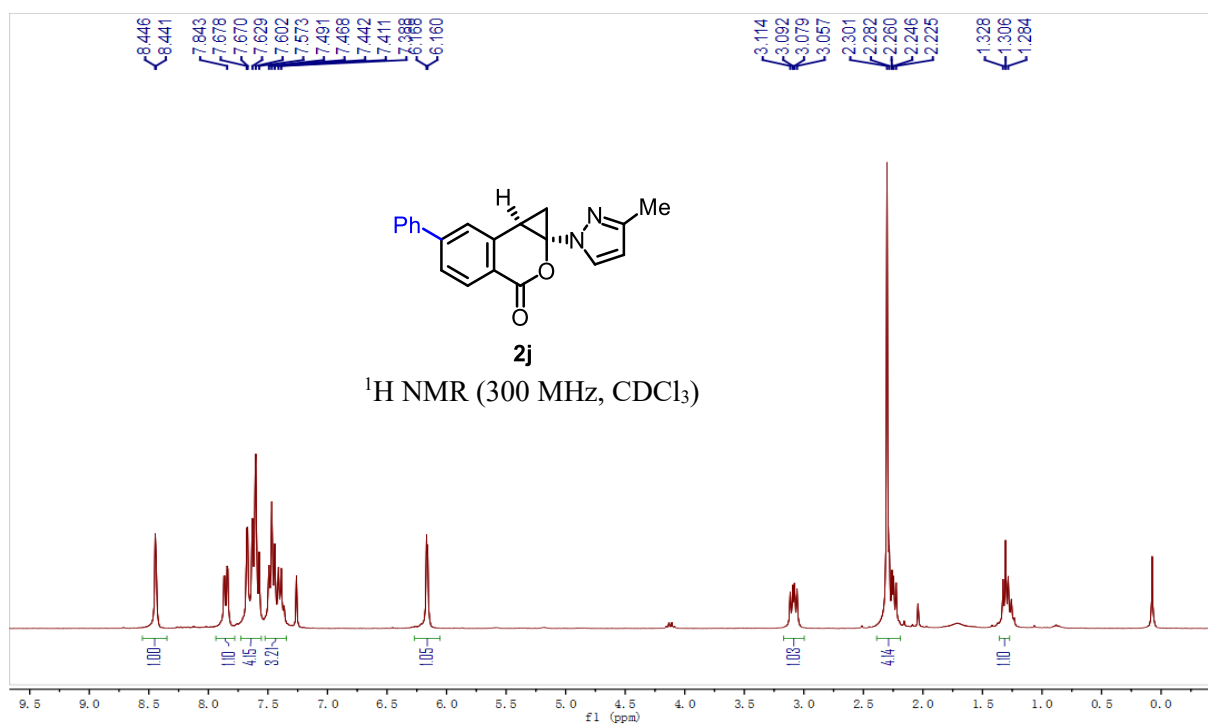
Chapter 5. Appendices



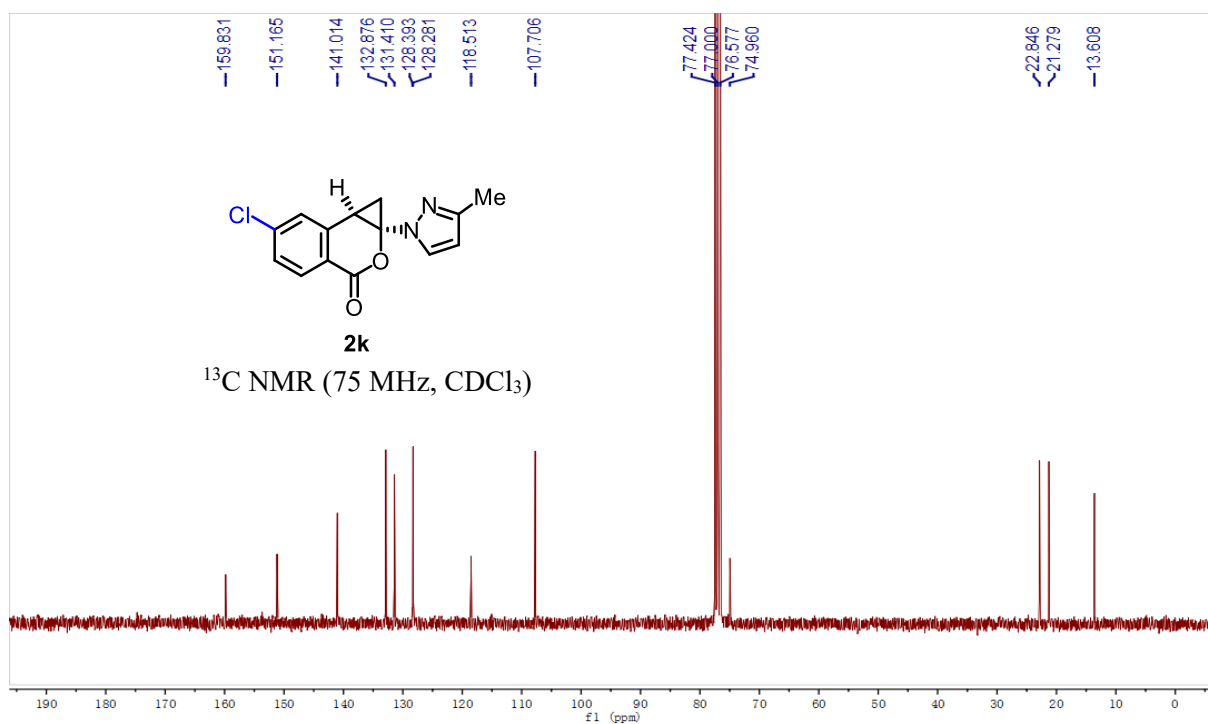
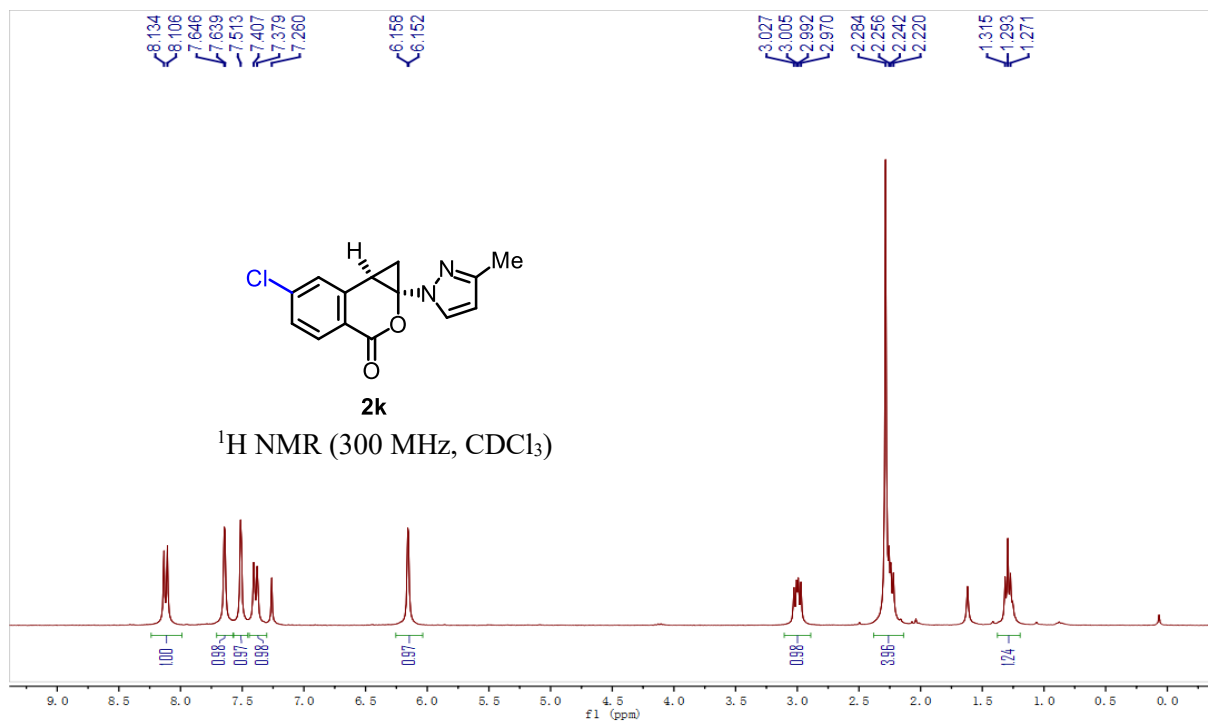
Chapter 5. Appendices



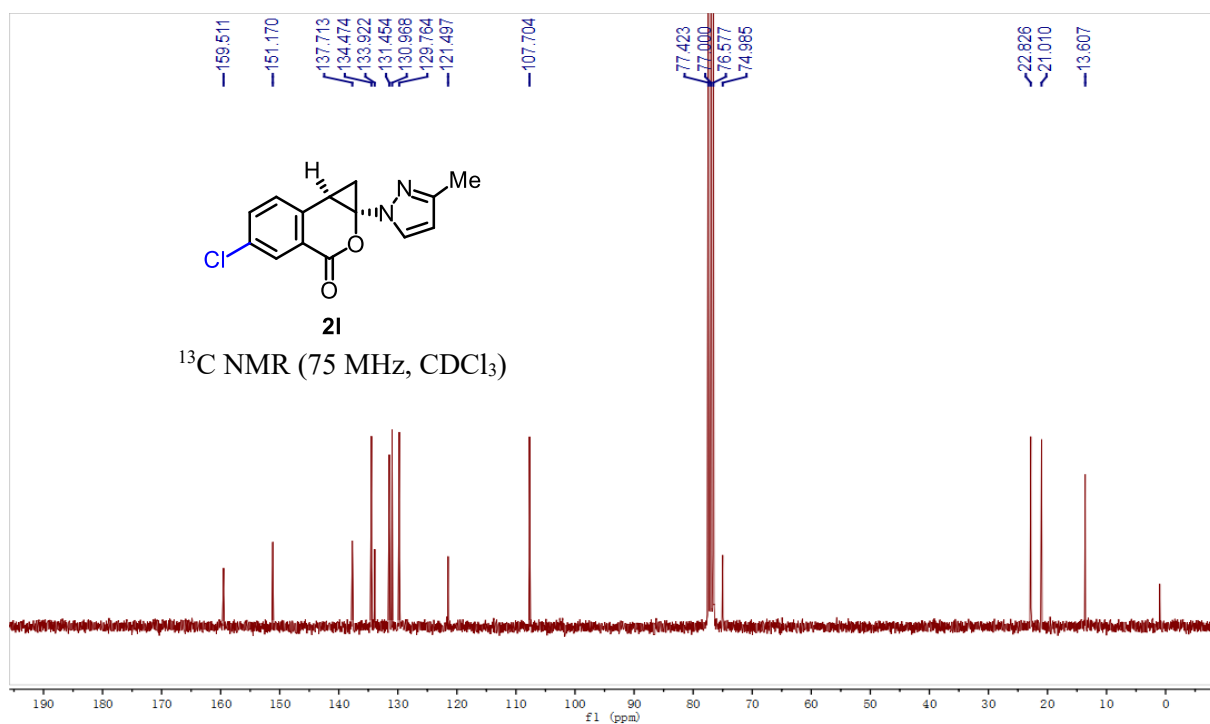
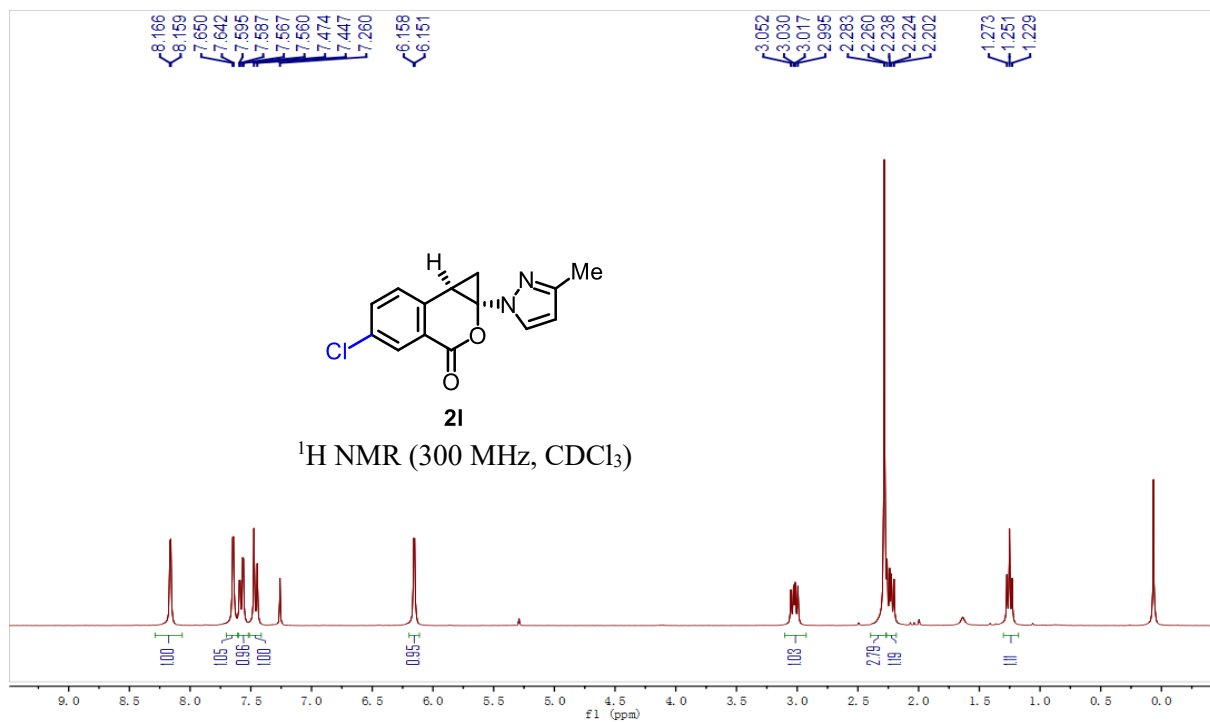
Chapter 5. Appendices



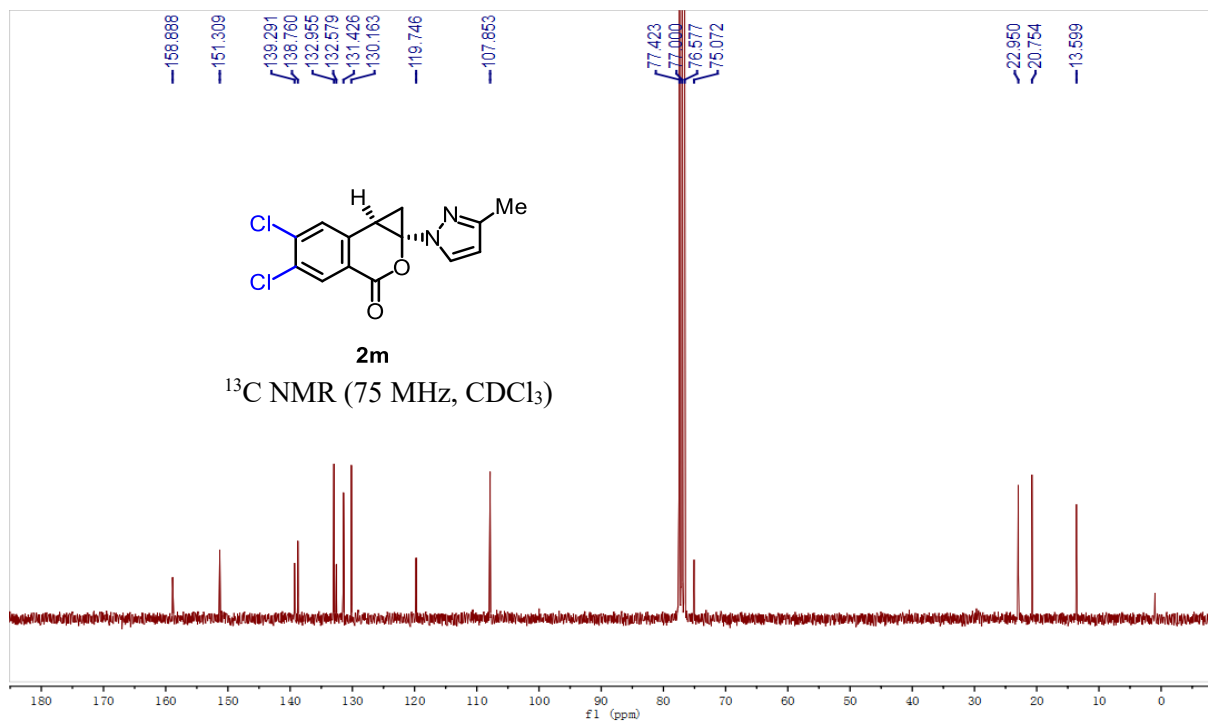
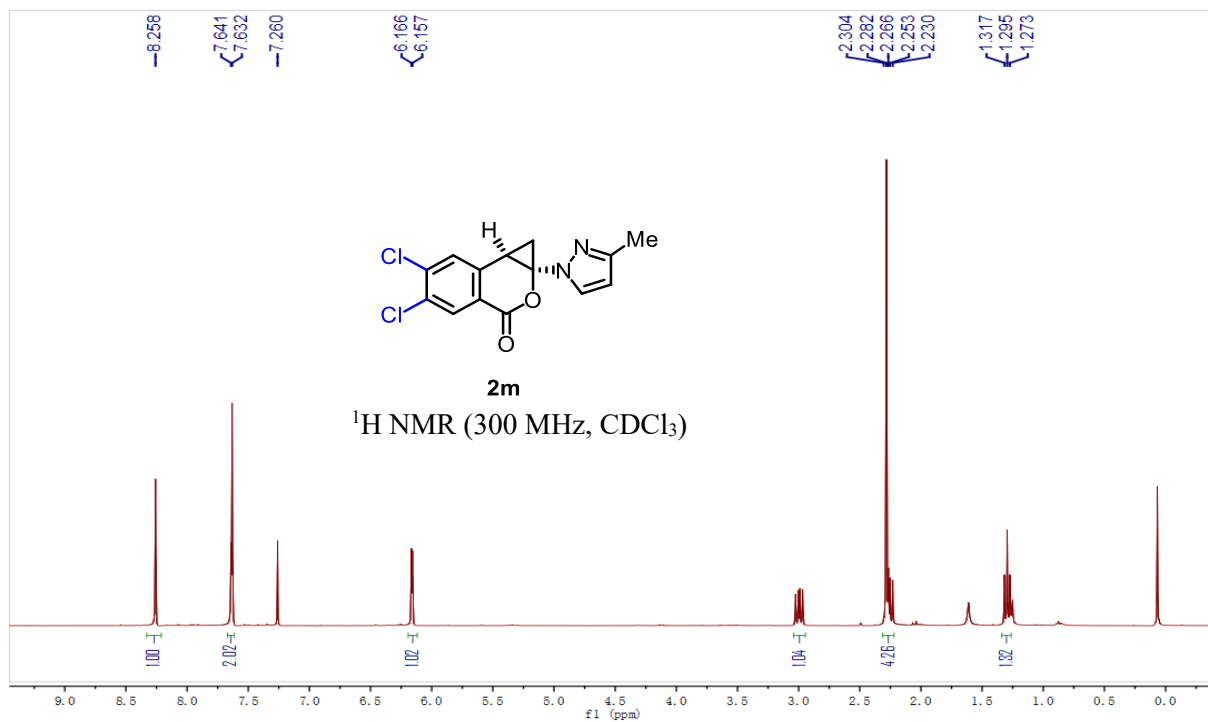
Chapter 5. Appendices

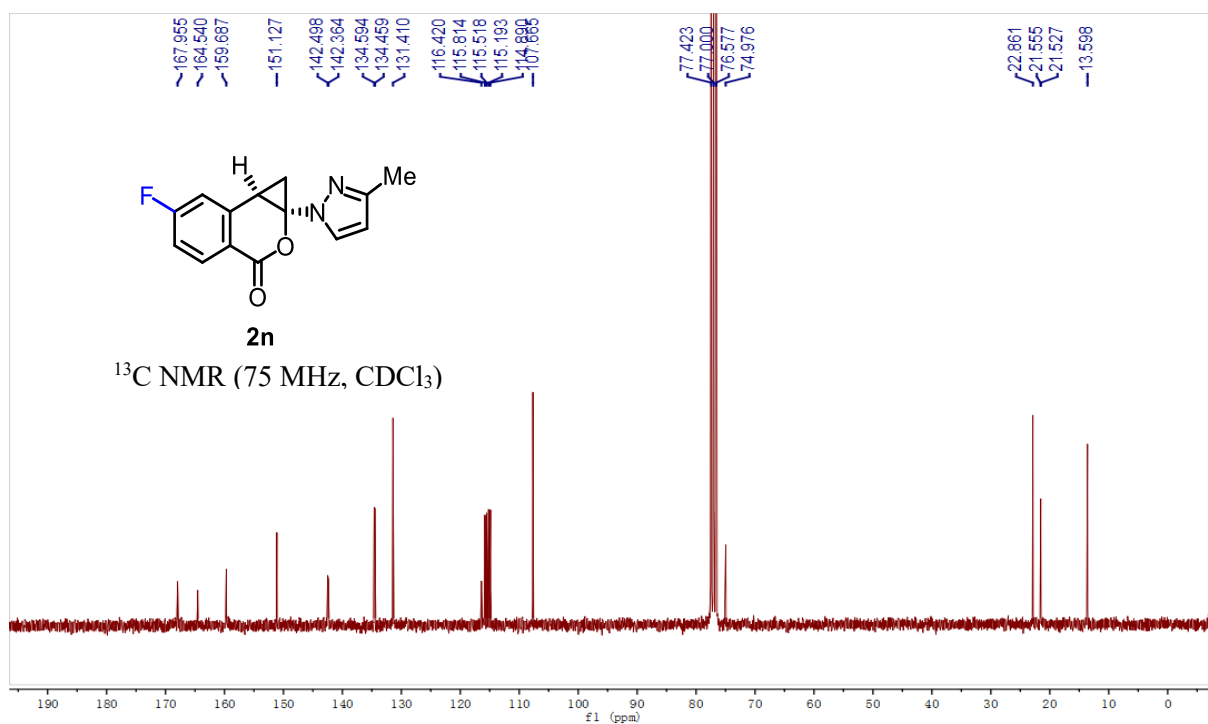
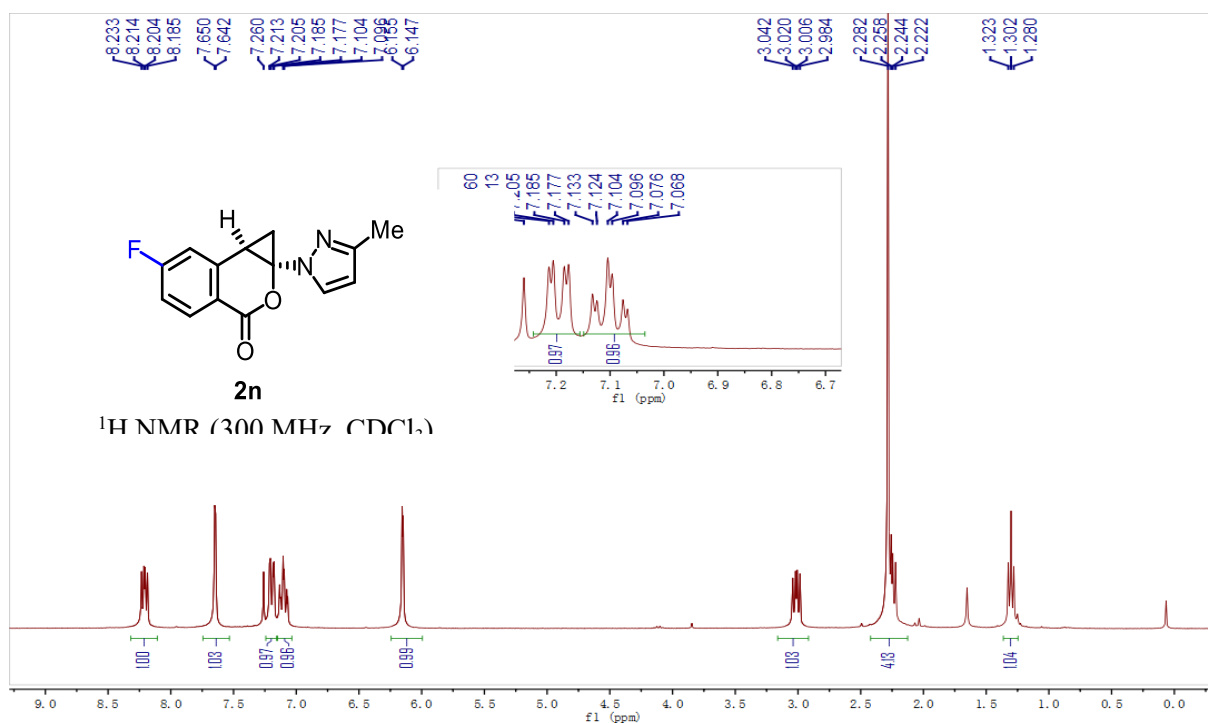


Chapter 5. Appendices

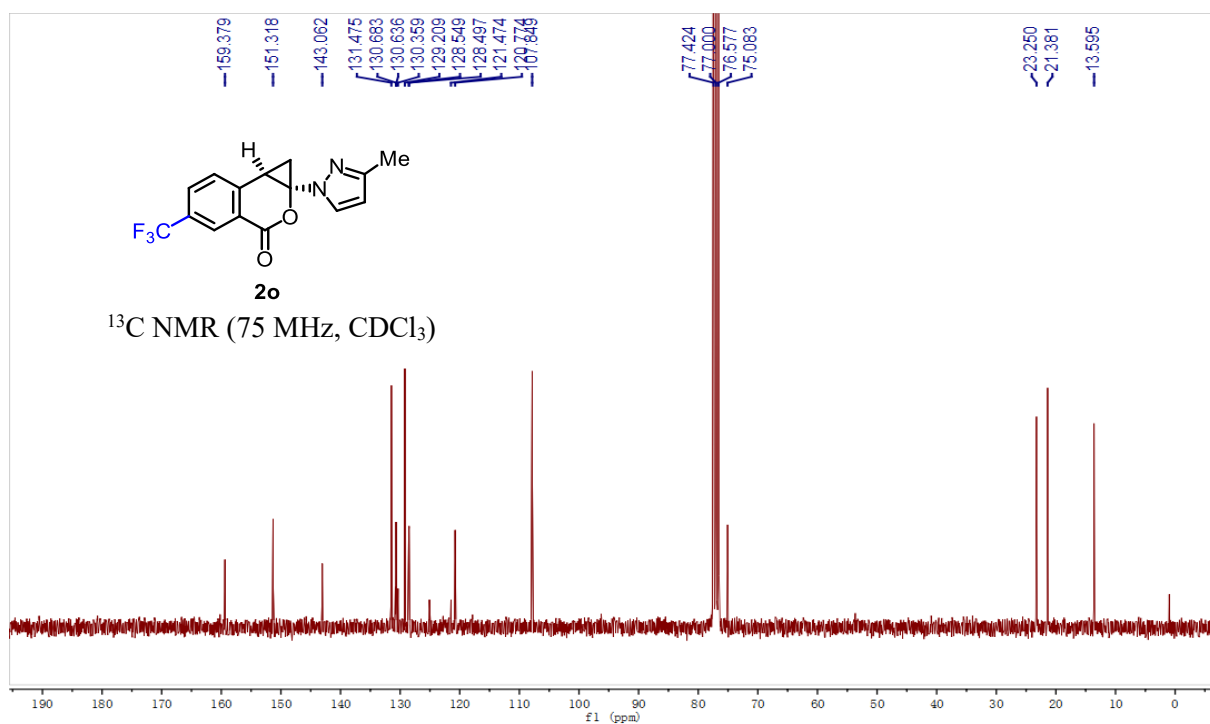
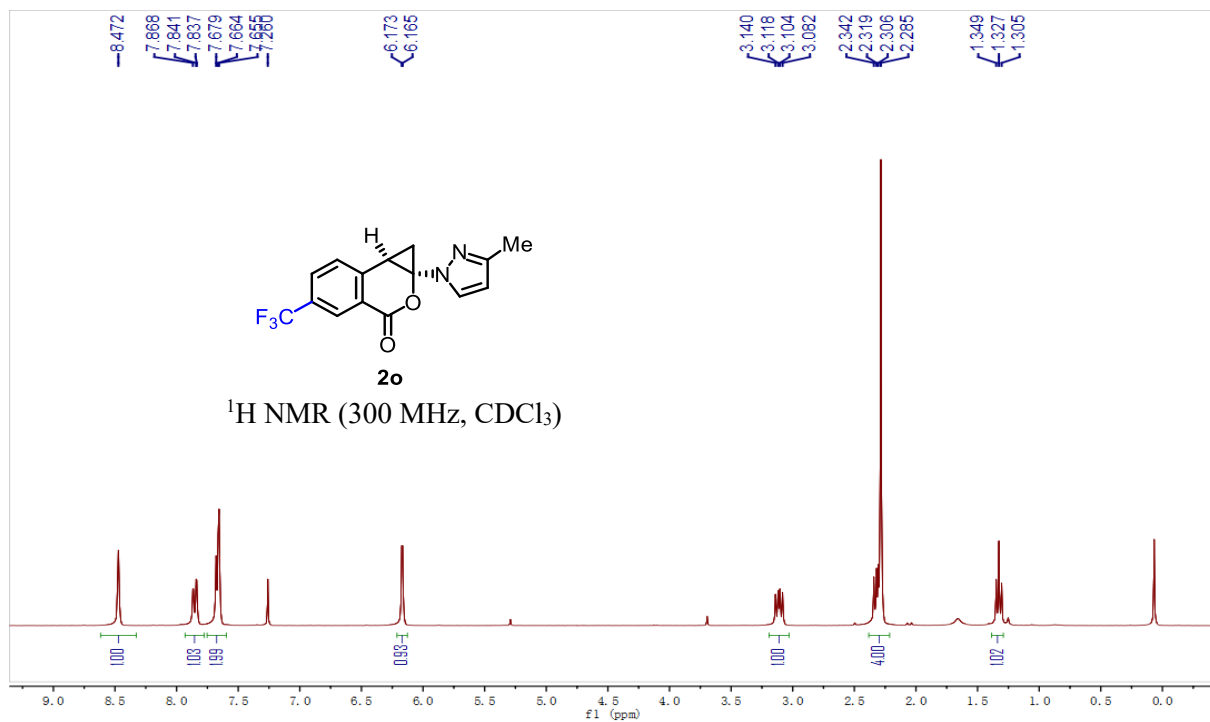


Chapter 5. Appendices

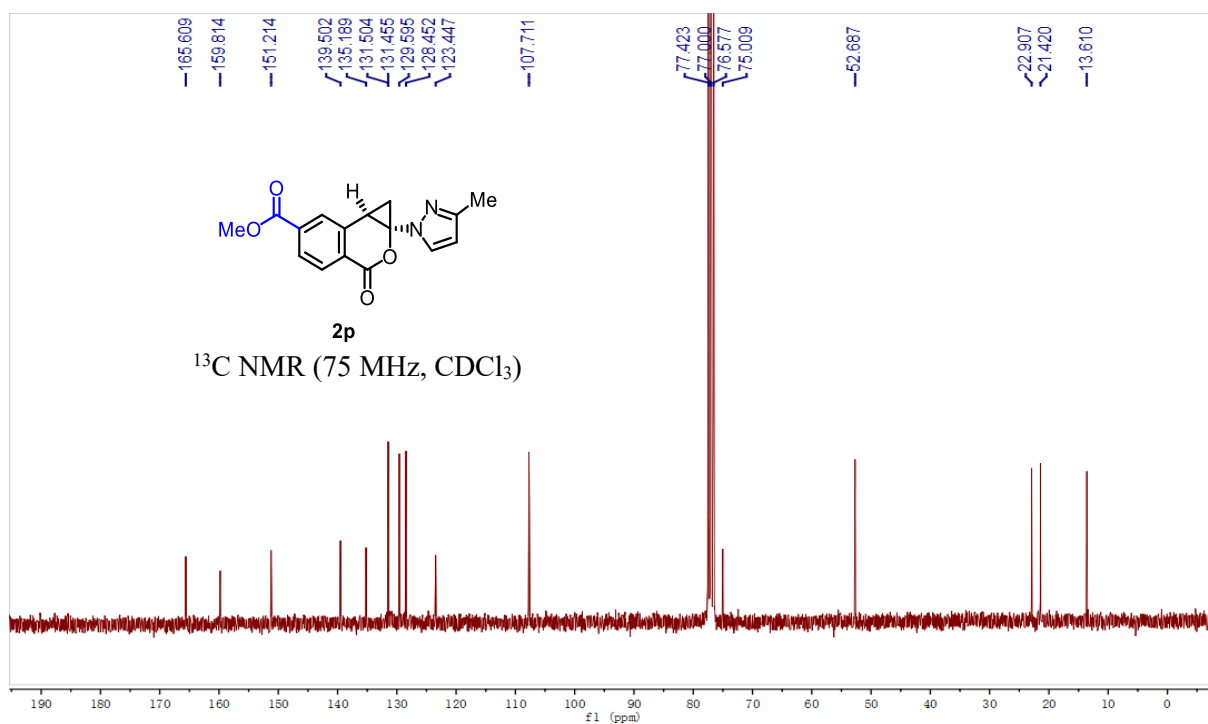
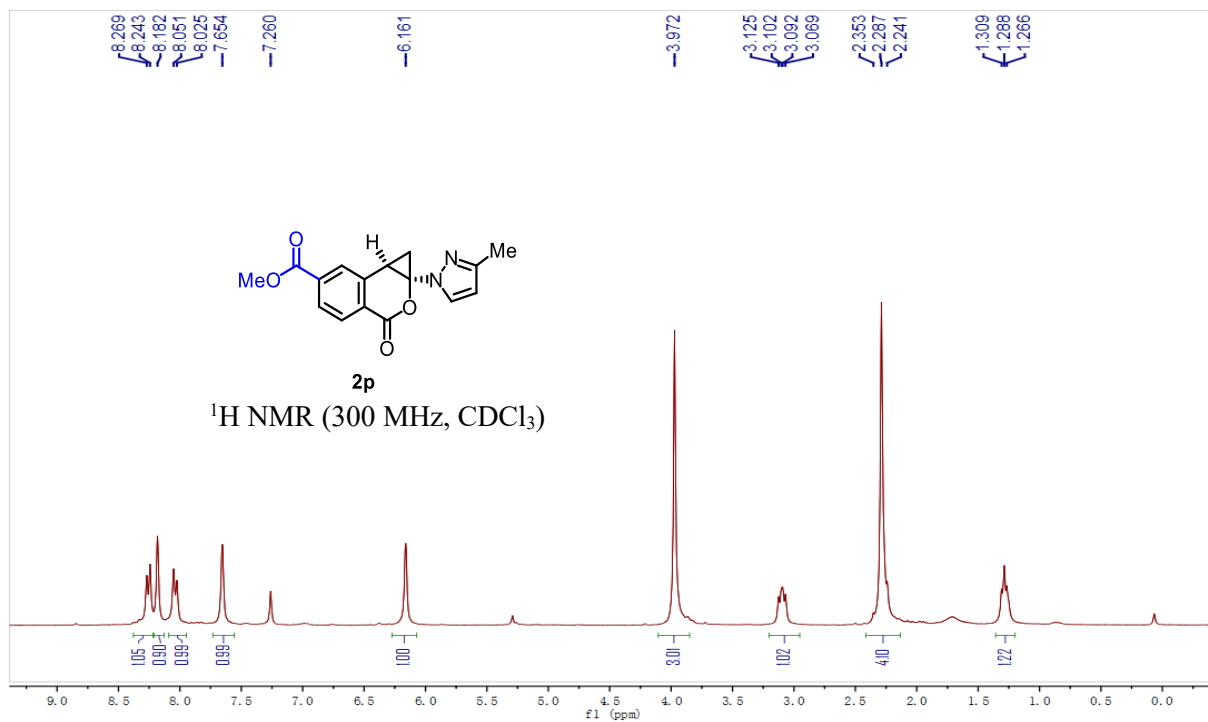




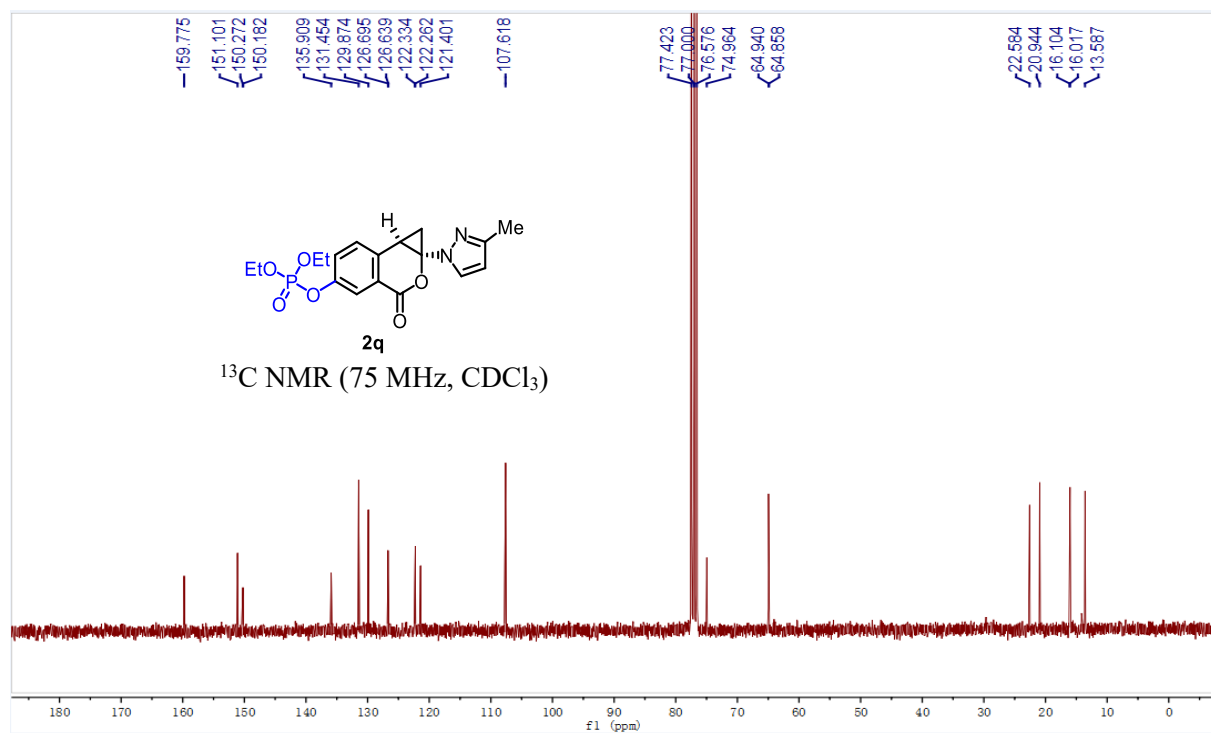
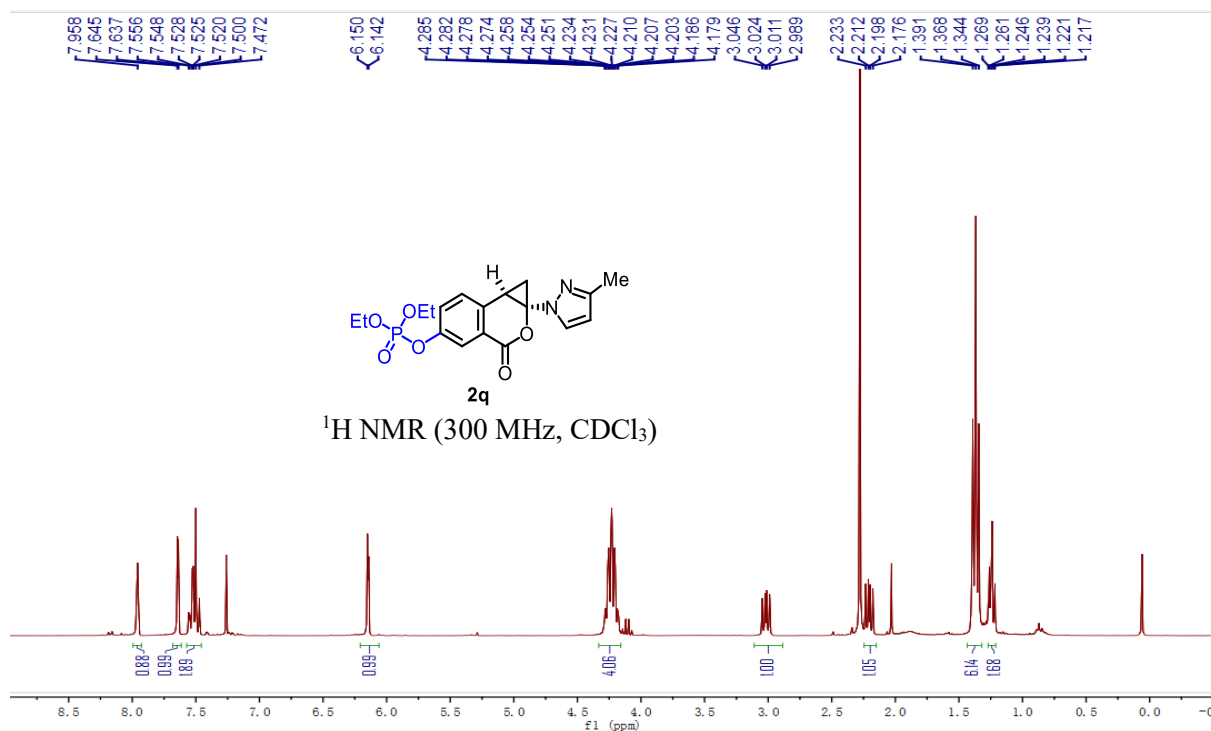
Chapter 5. Appendices



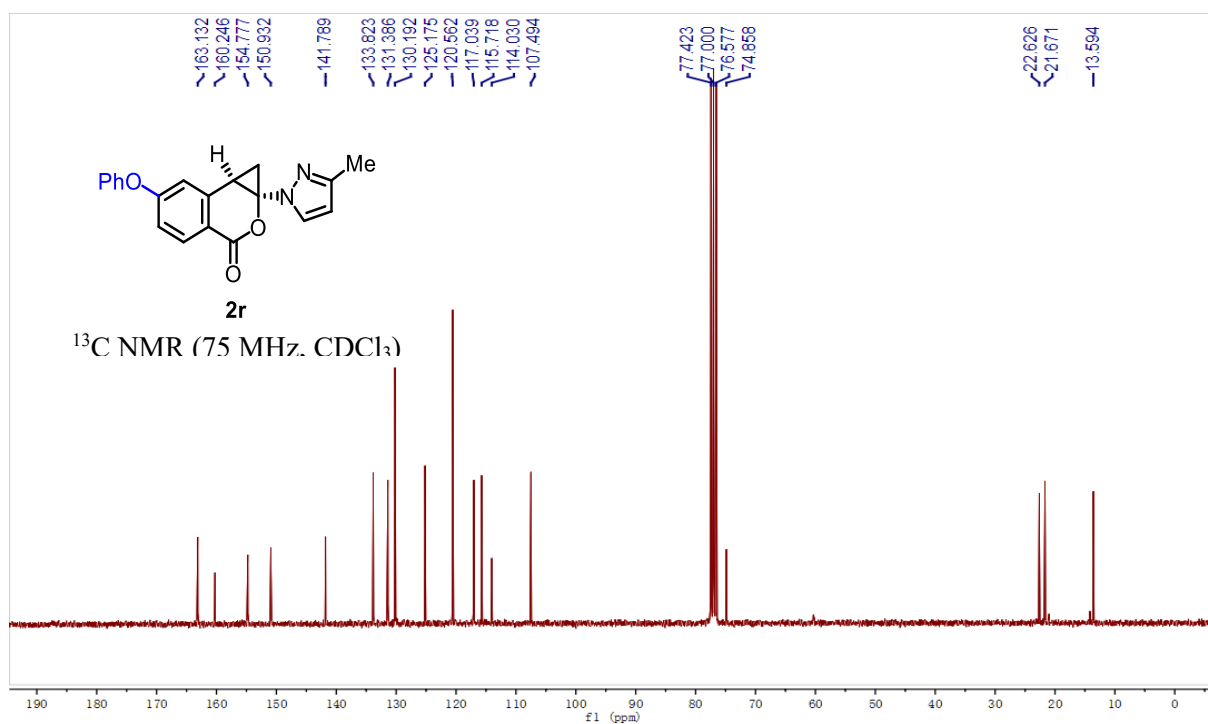
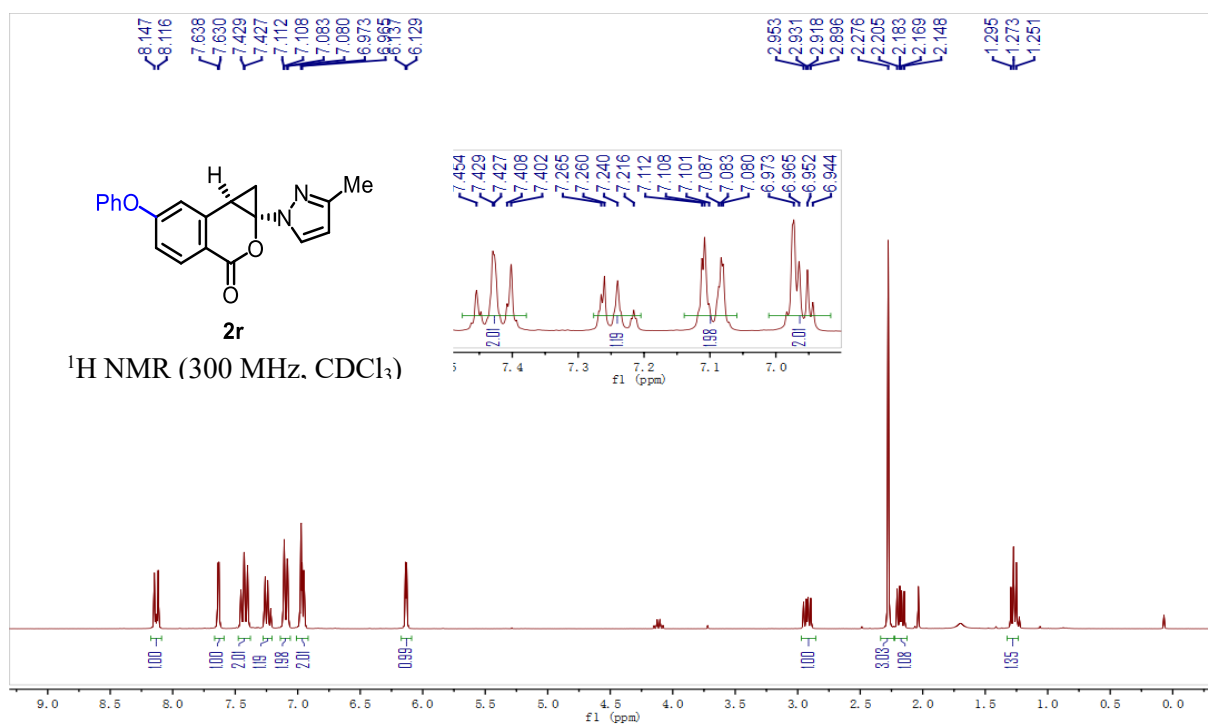
Chapter 5. Appendices



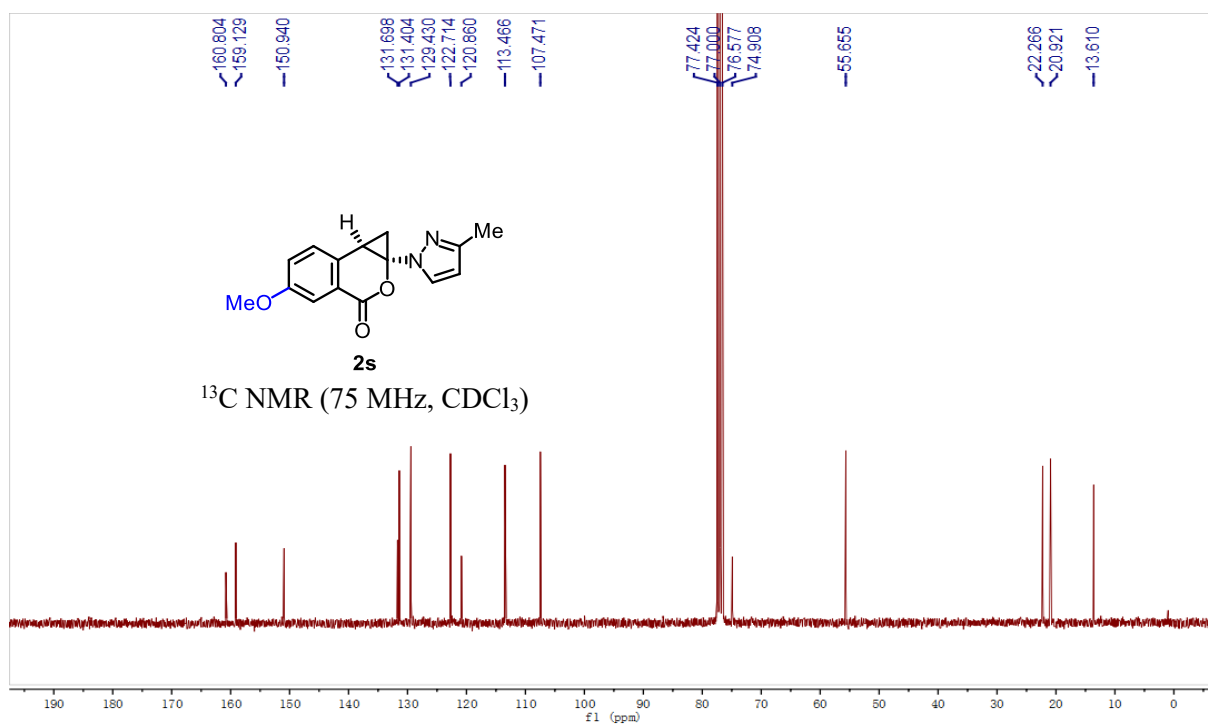
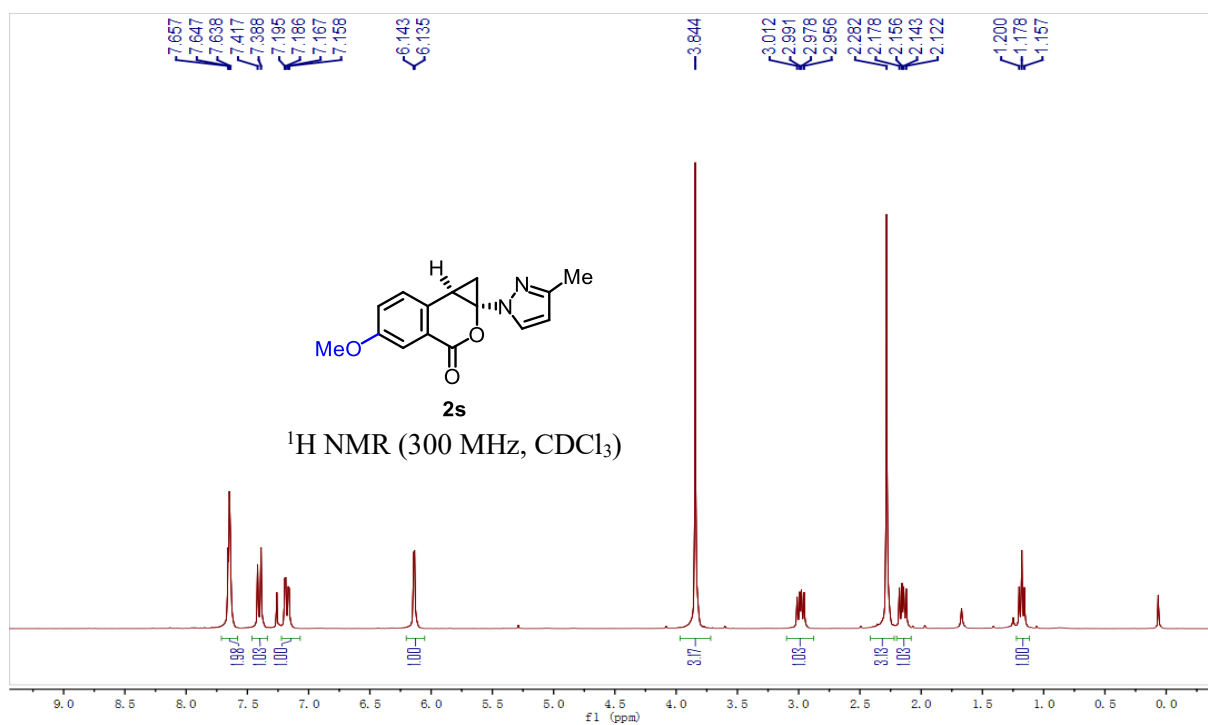
Chapter 5. Appendices



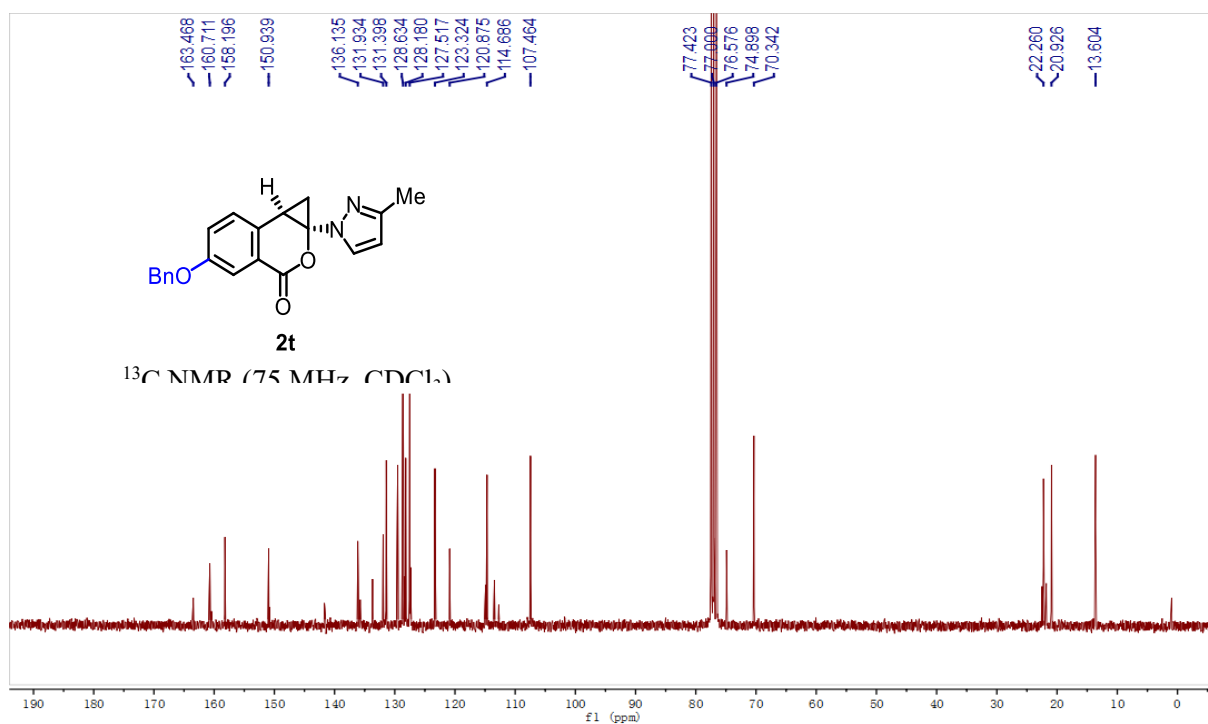
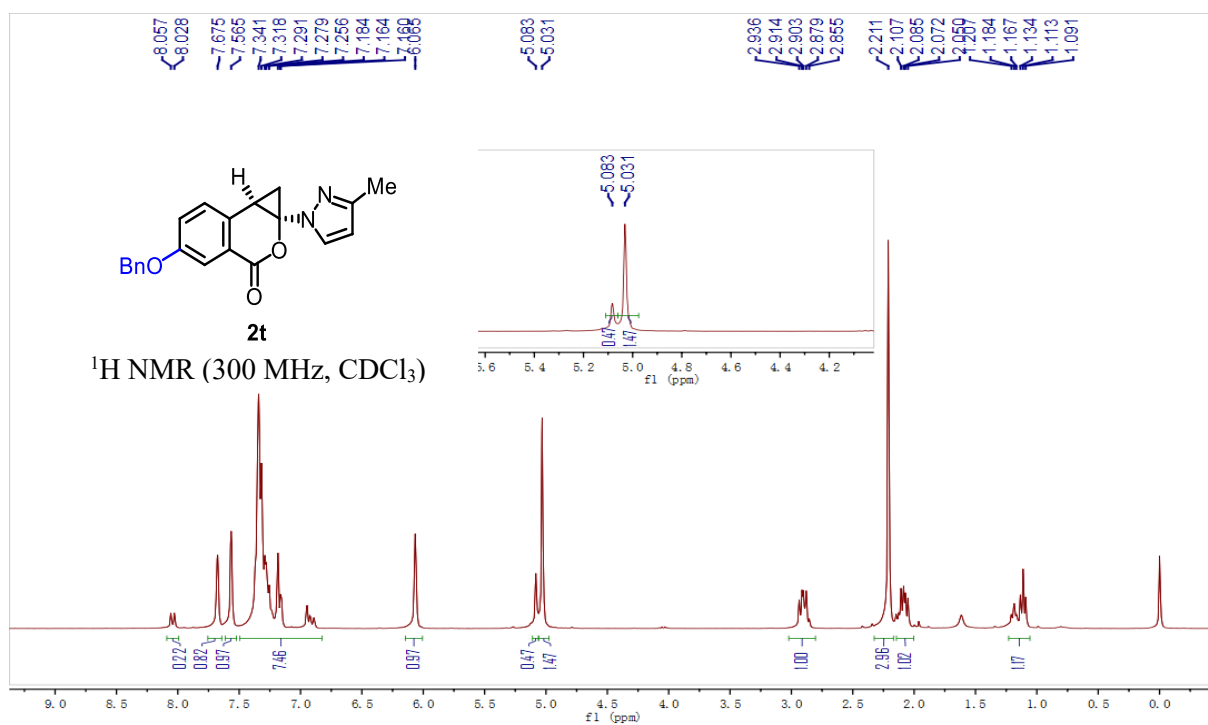
Chapter 5. Appendices



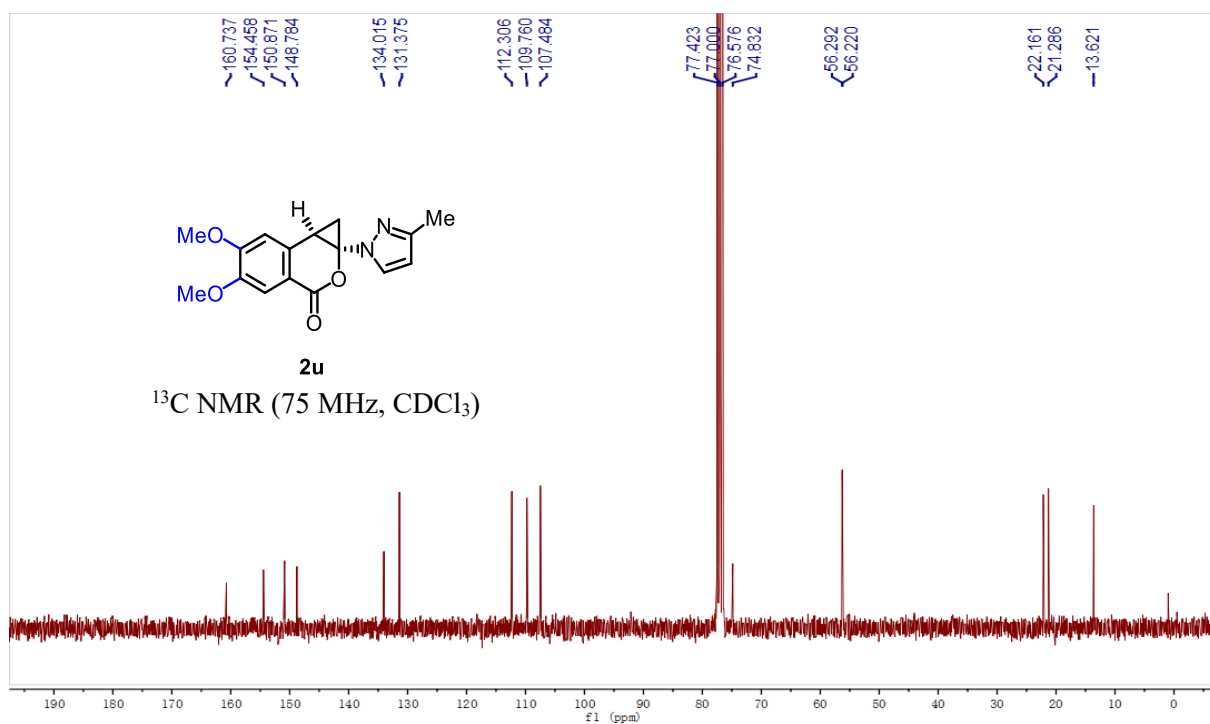
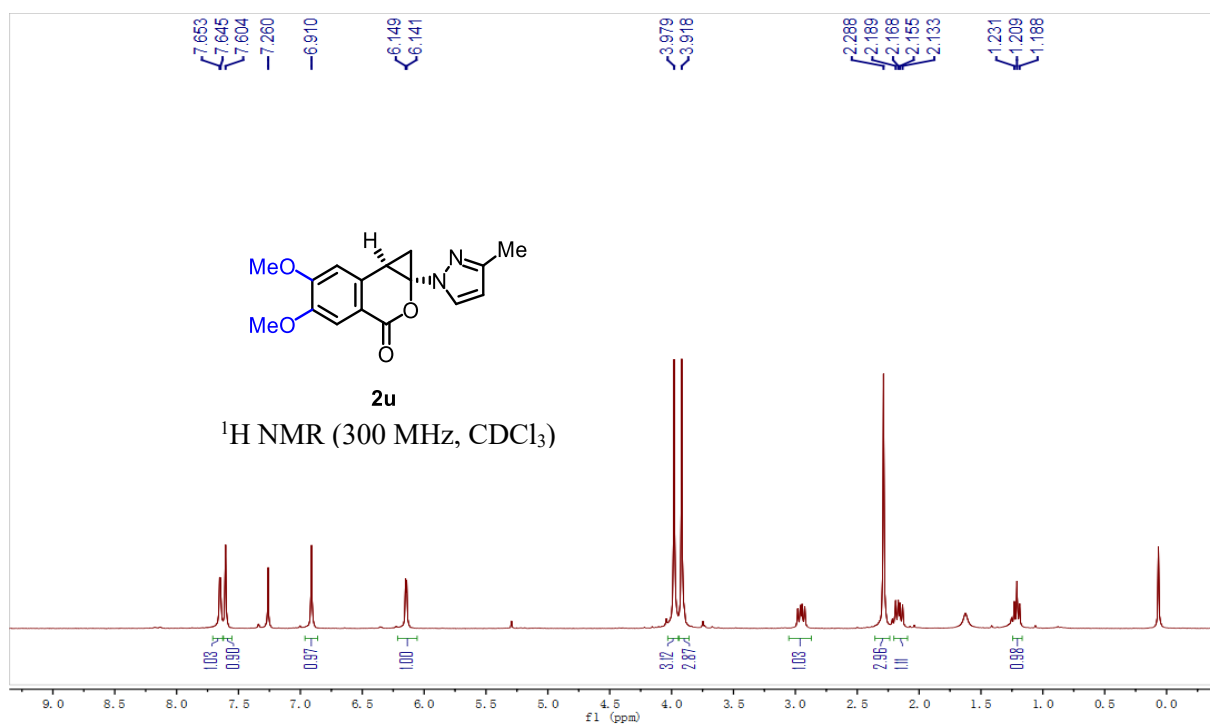
Chapter 5. Appendices



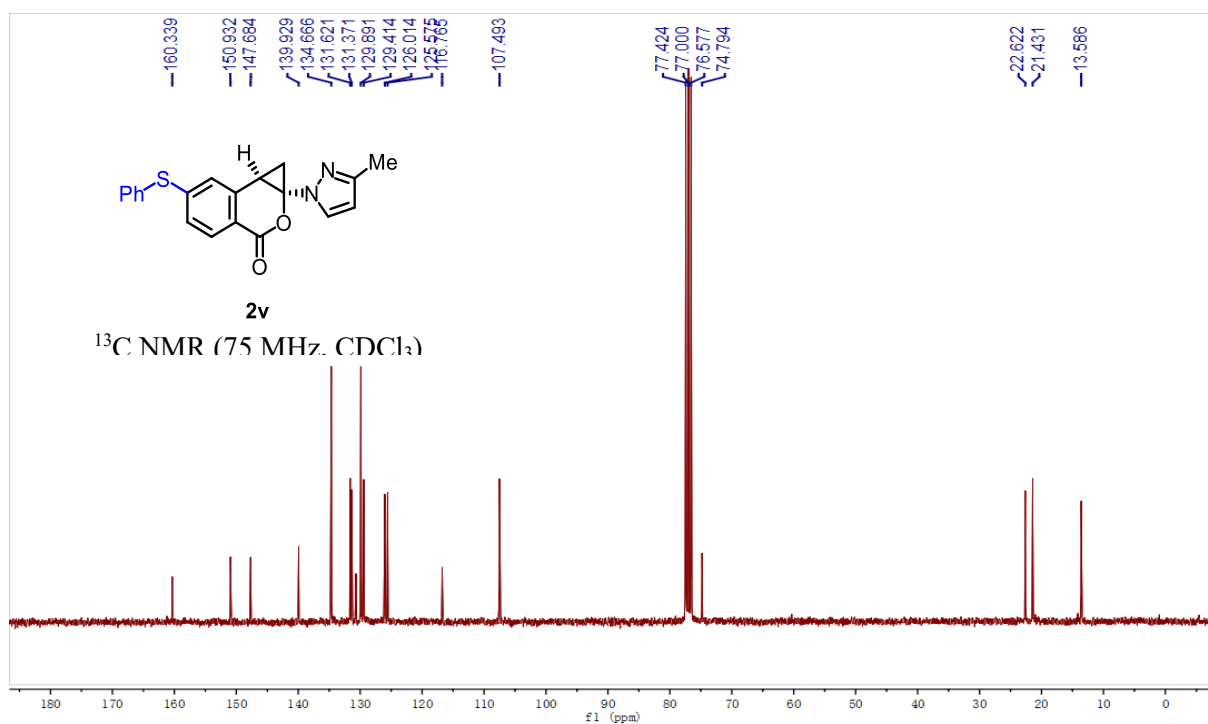
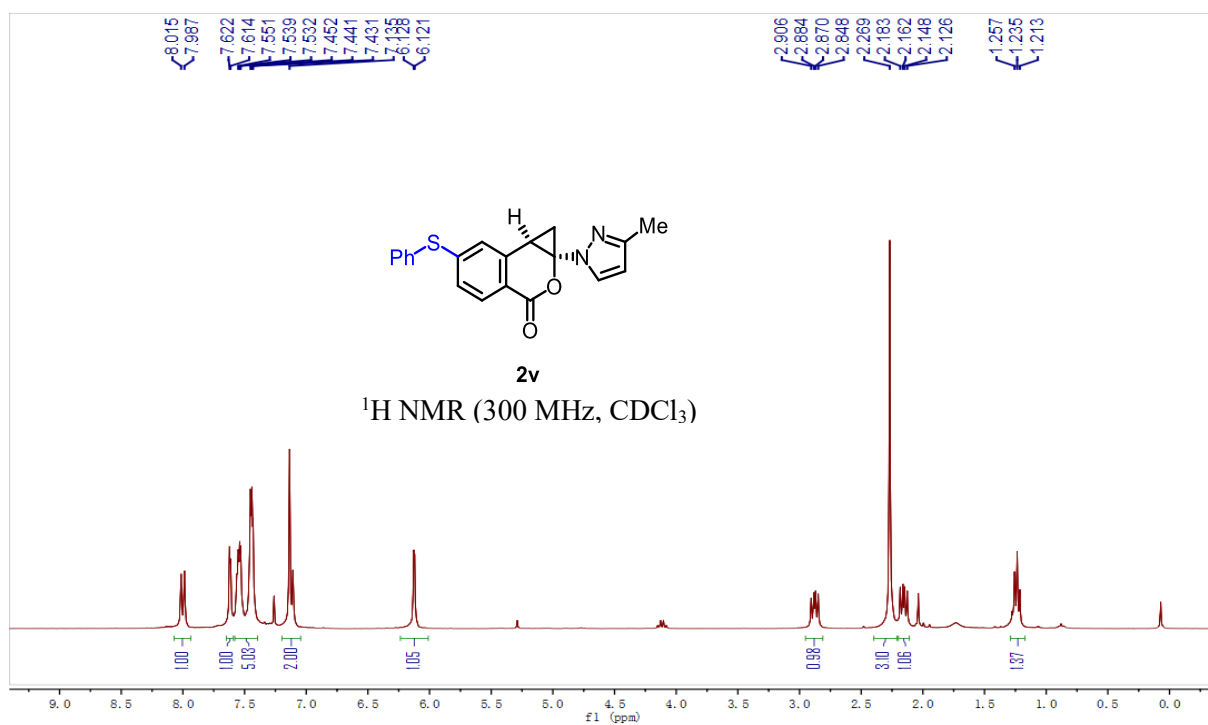
Chapter 5. Appendices



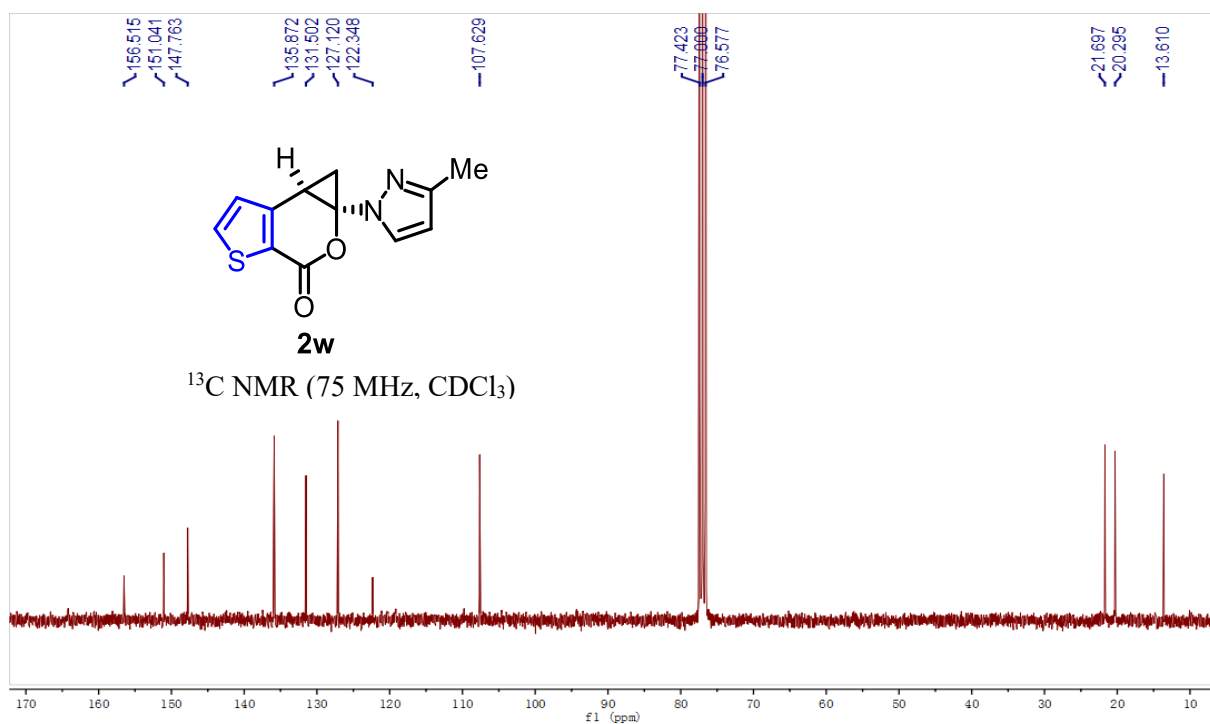
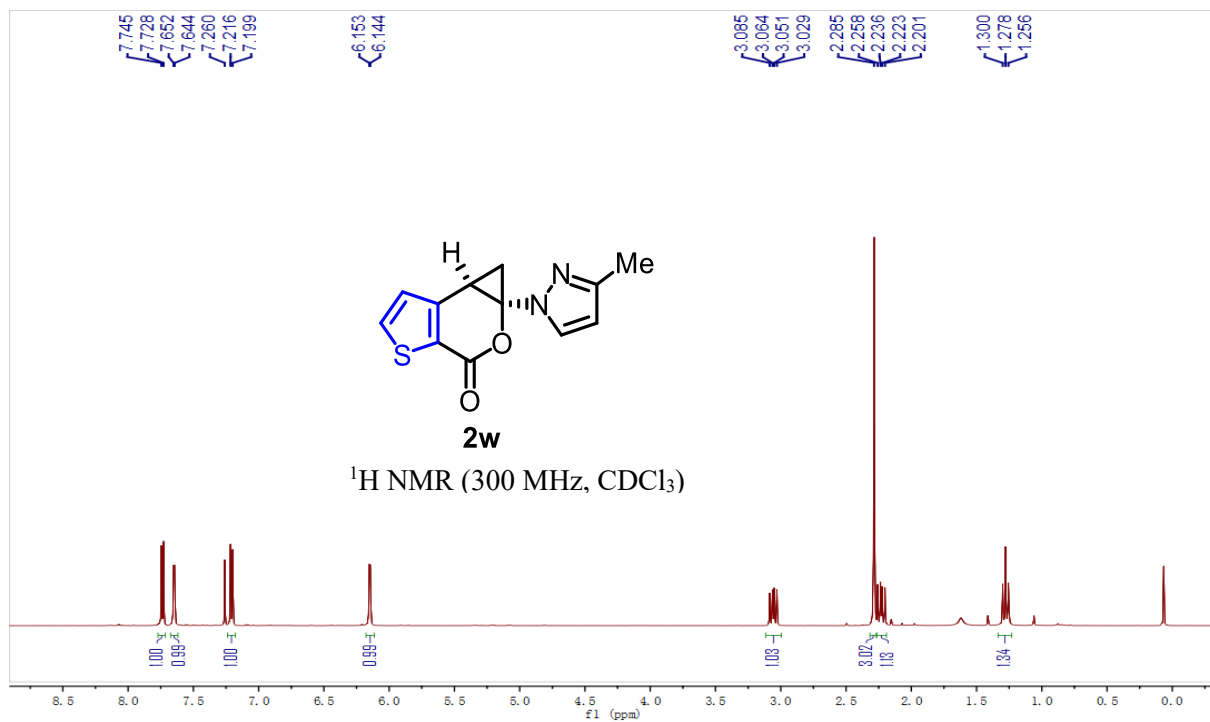
Chapter 5. Appendices



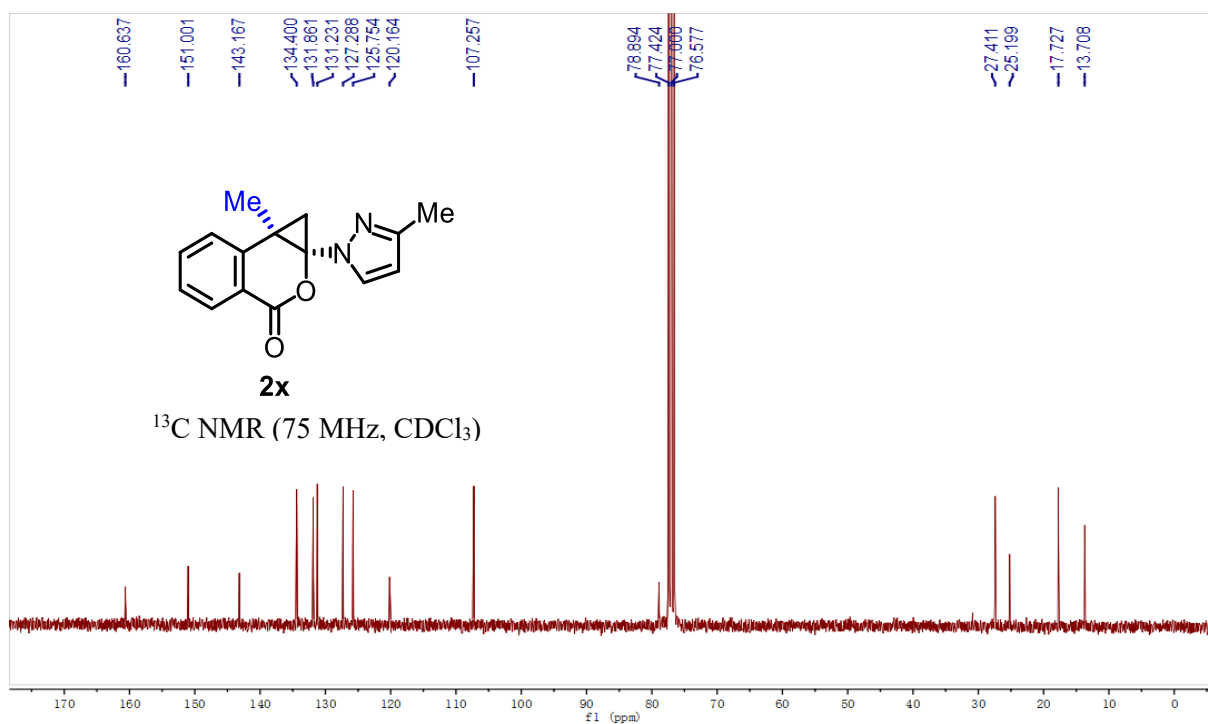
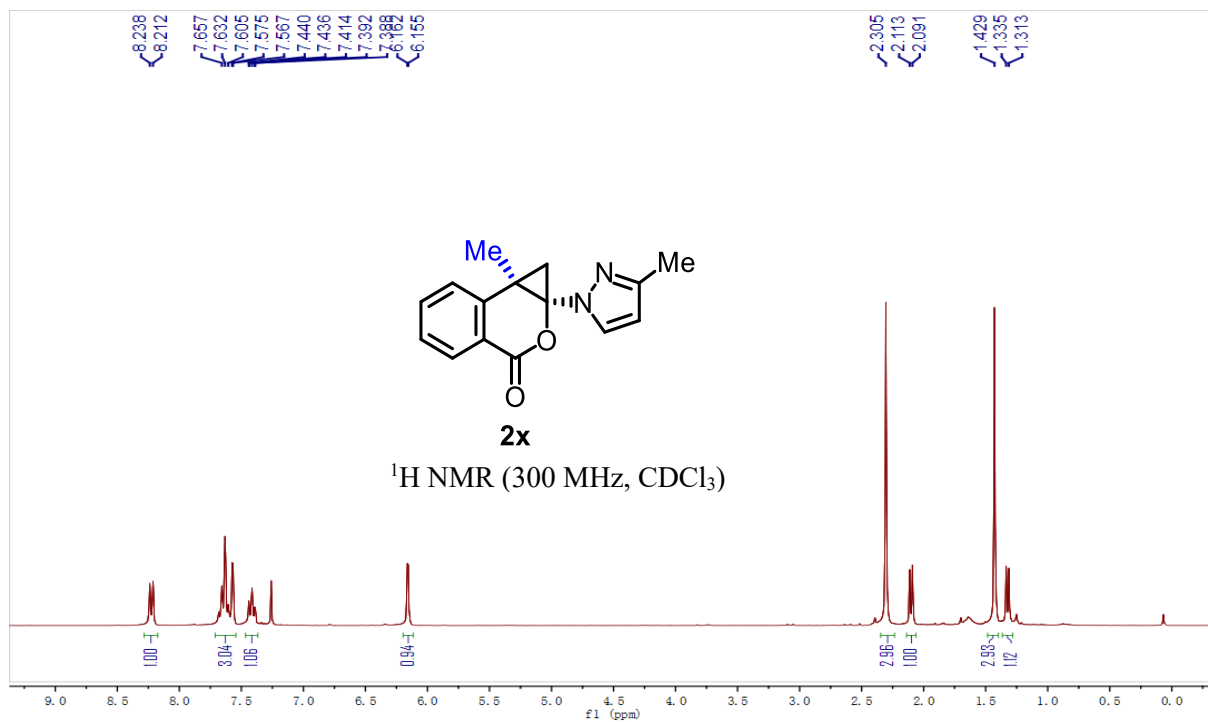
Chapter 5. Appendices

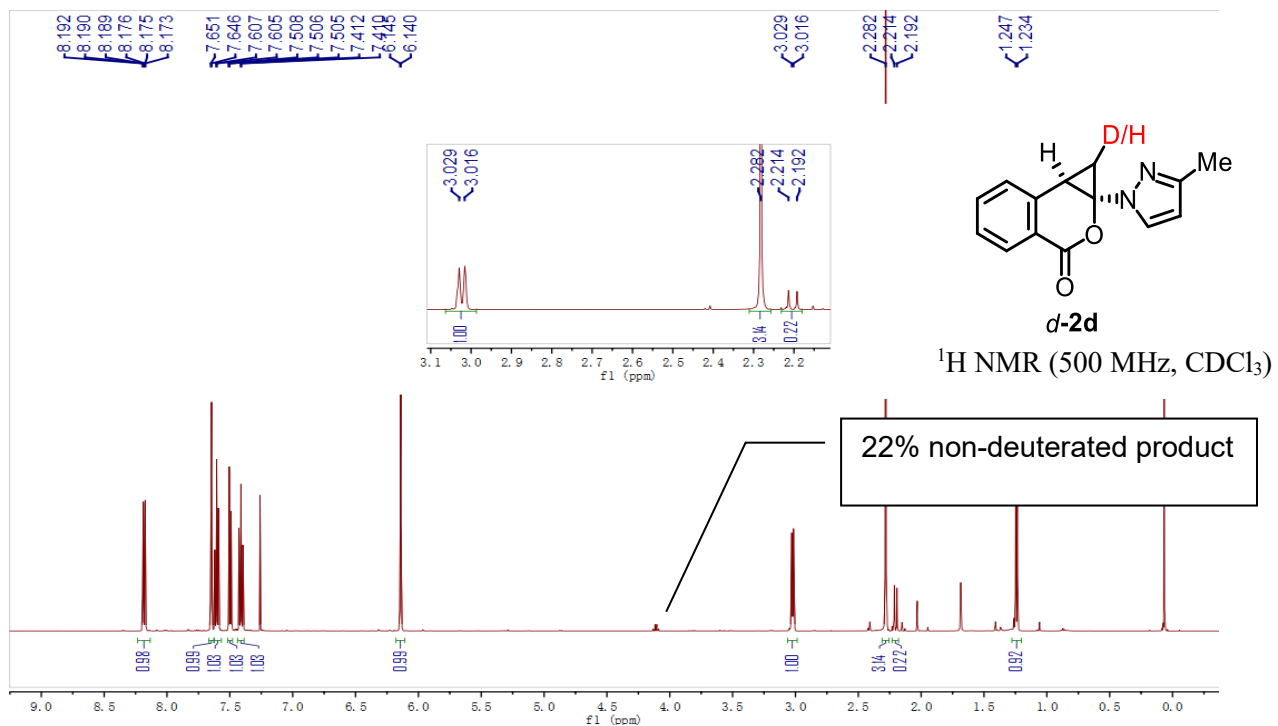


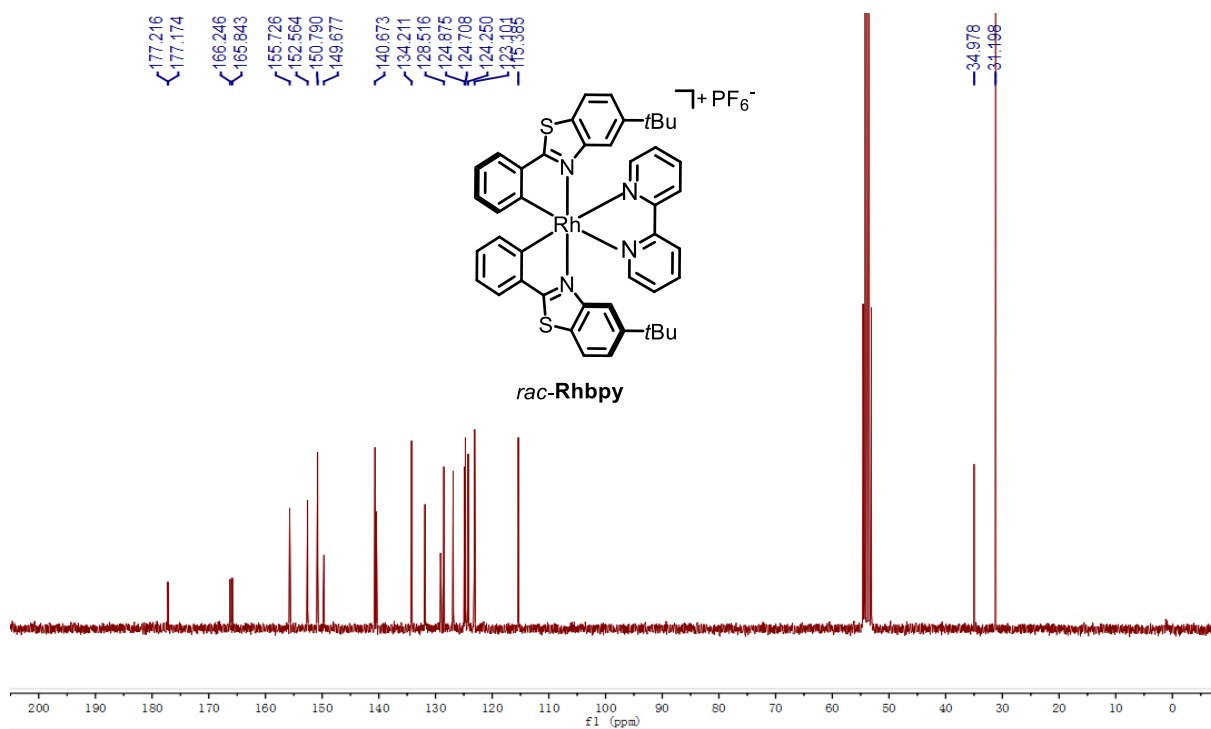
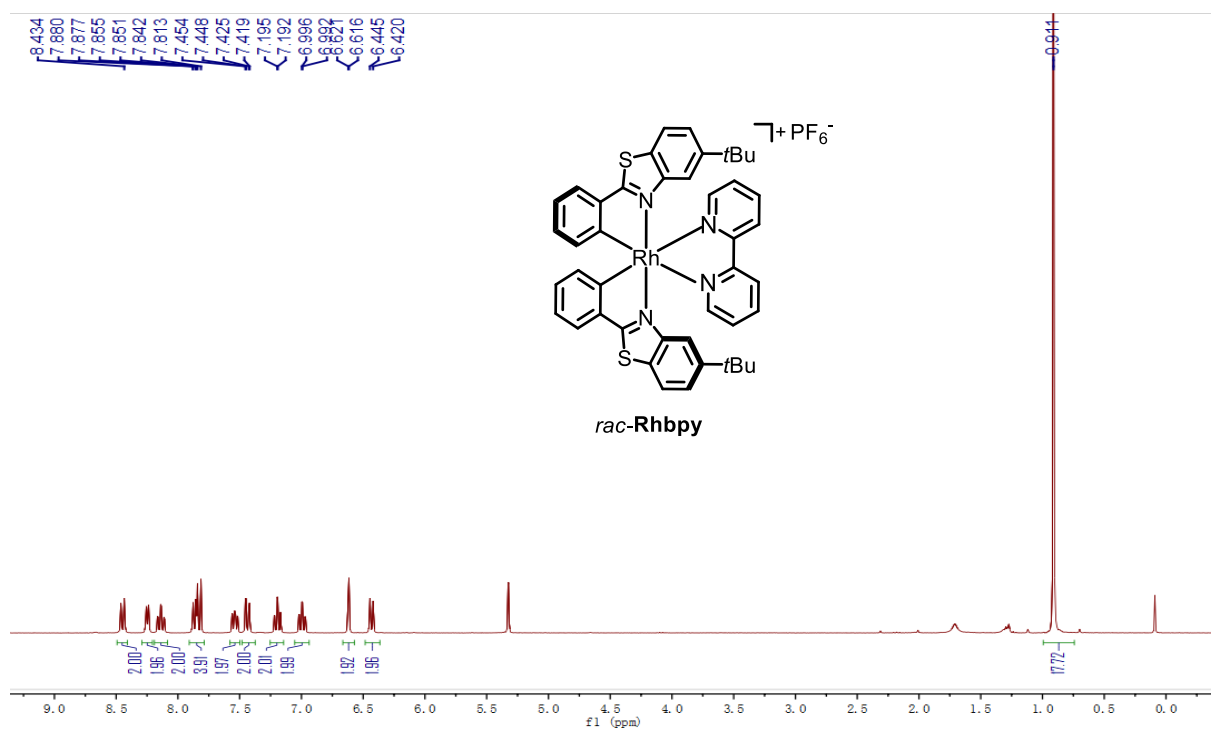
Chapter 5. Appendices



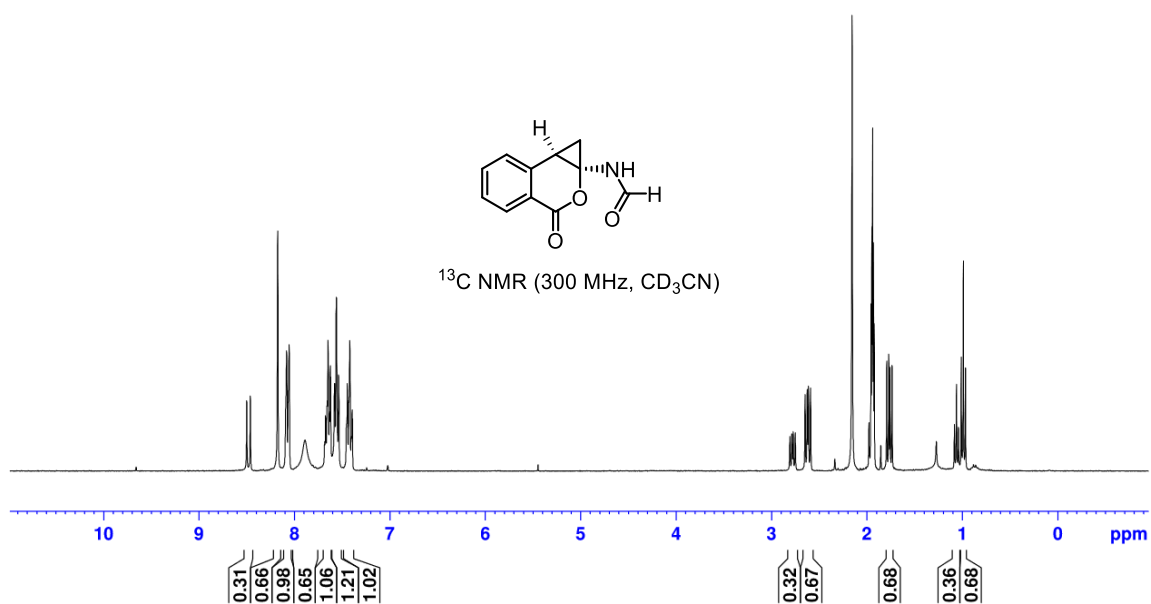
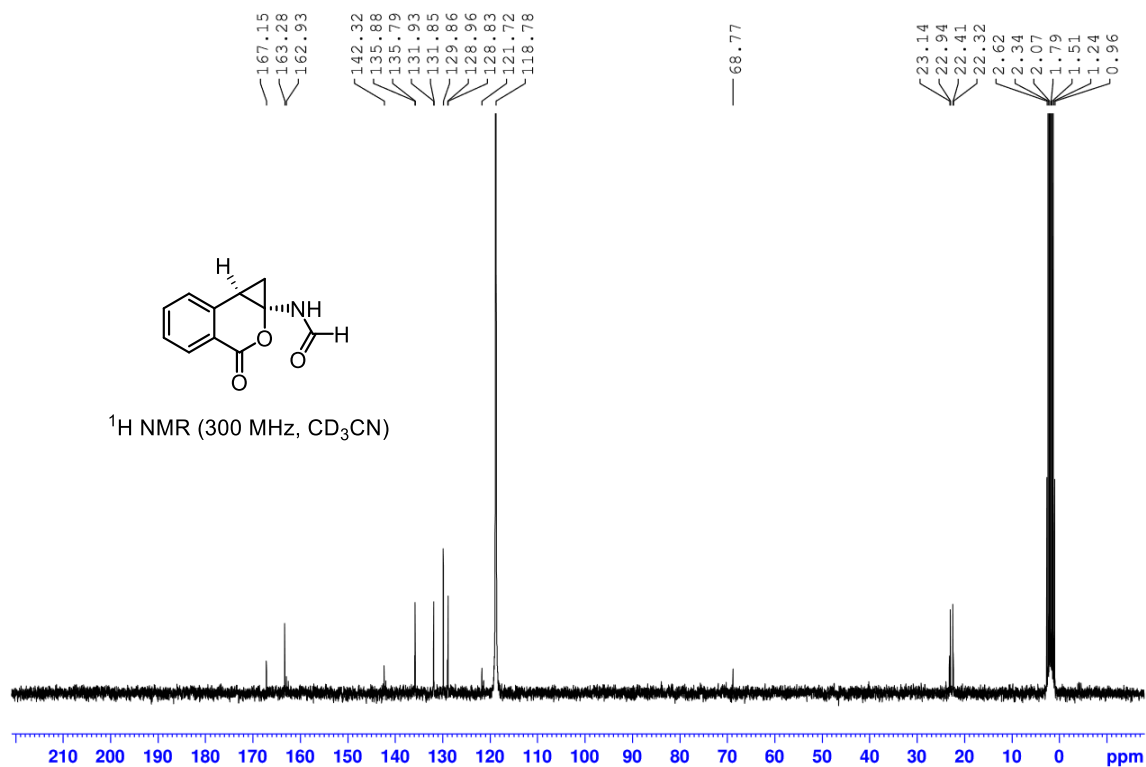
Chapter 5. Appendices

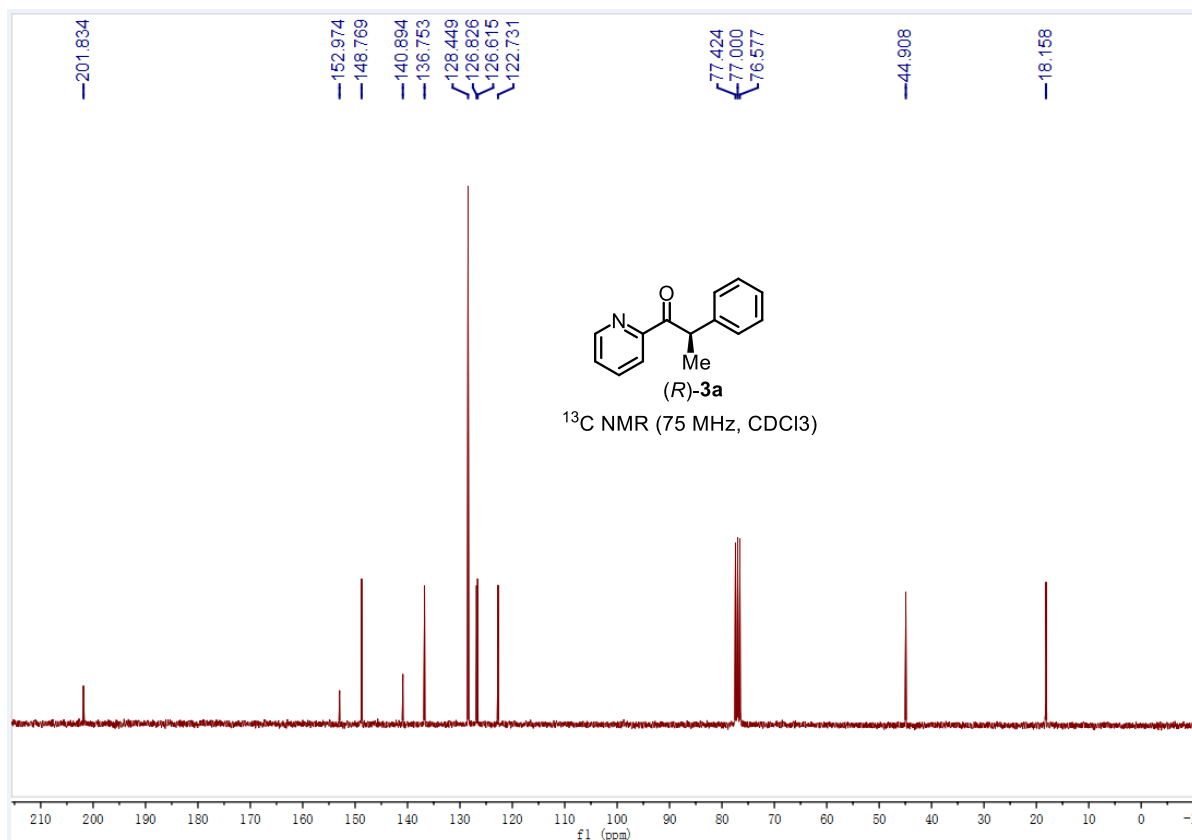
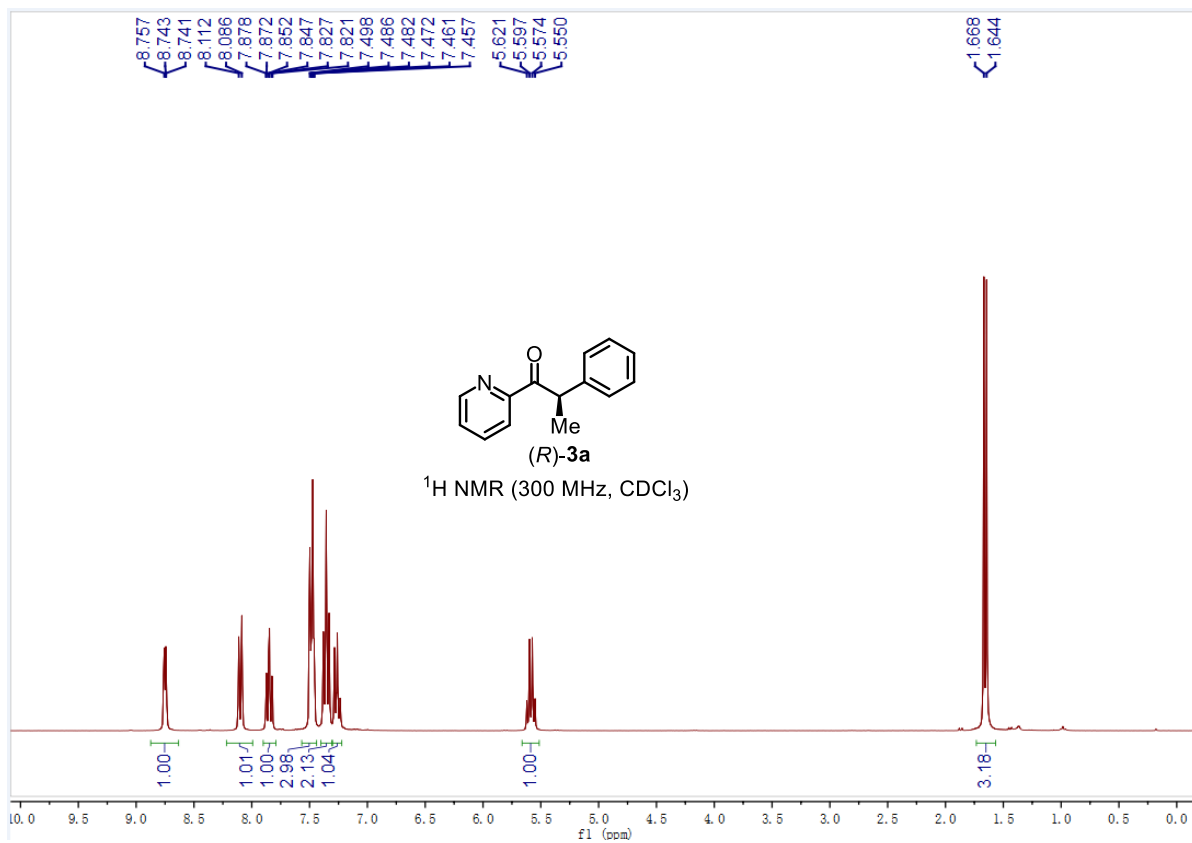




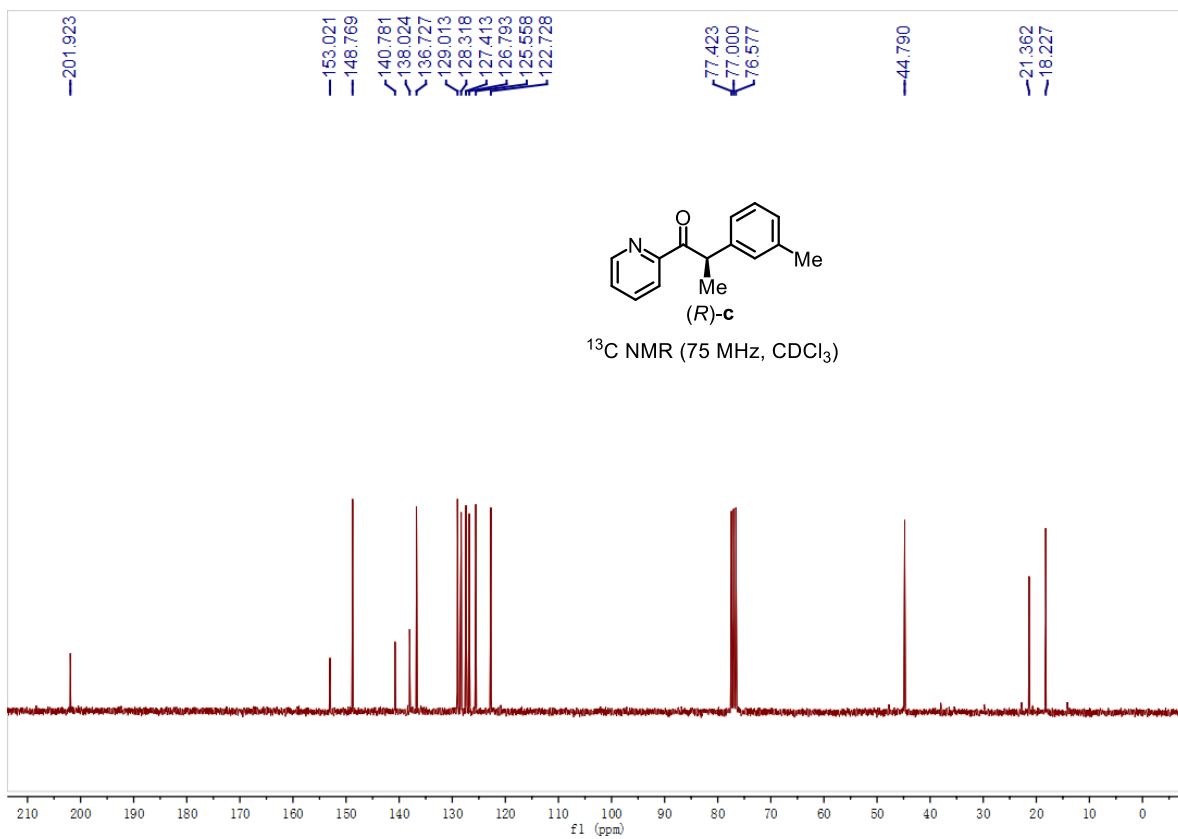
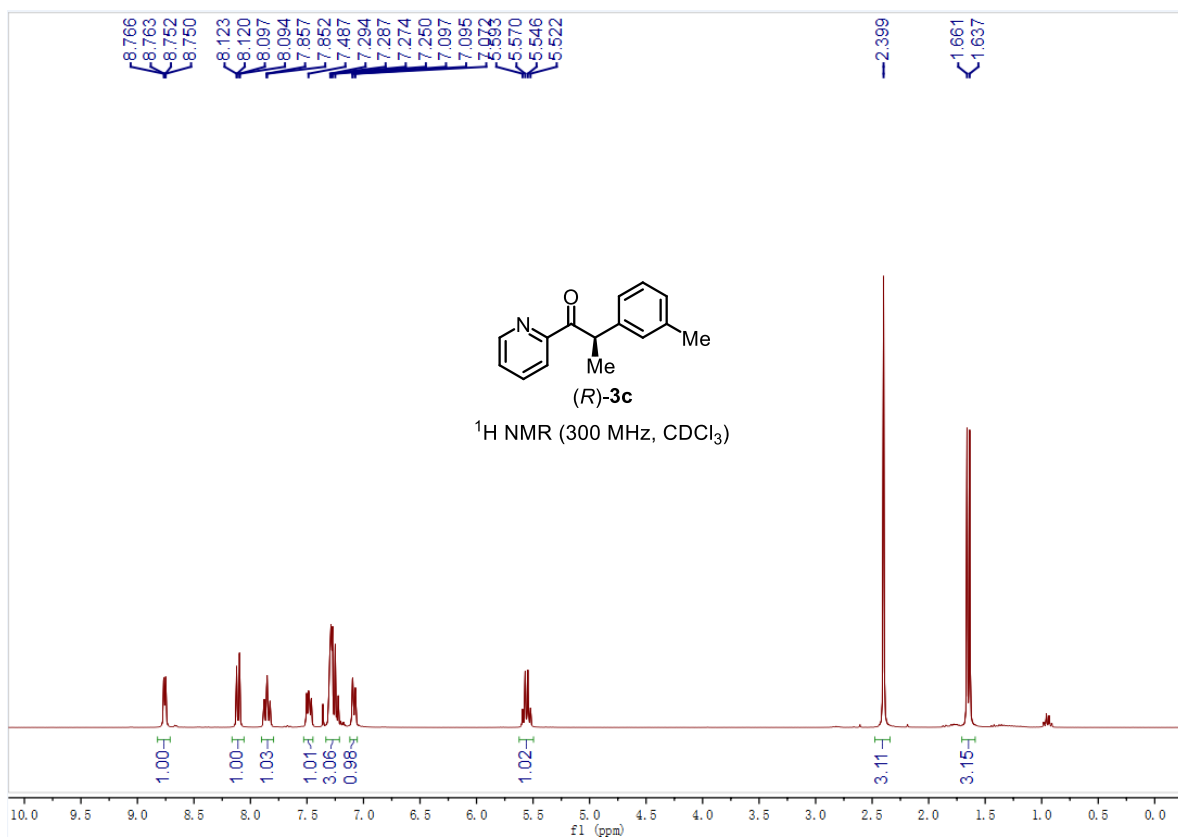


Chapter 5. Appendices

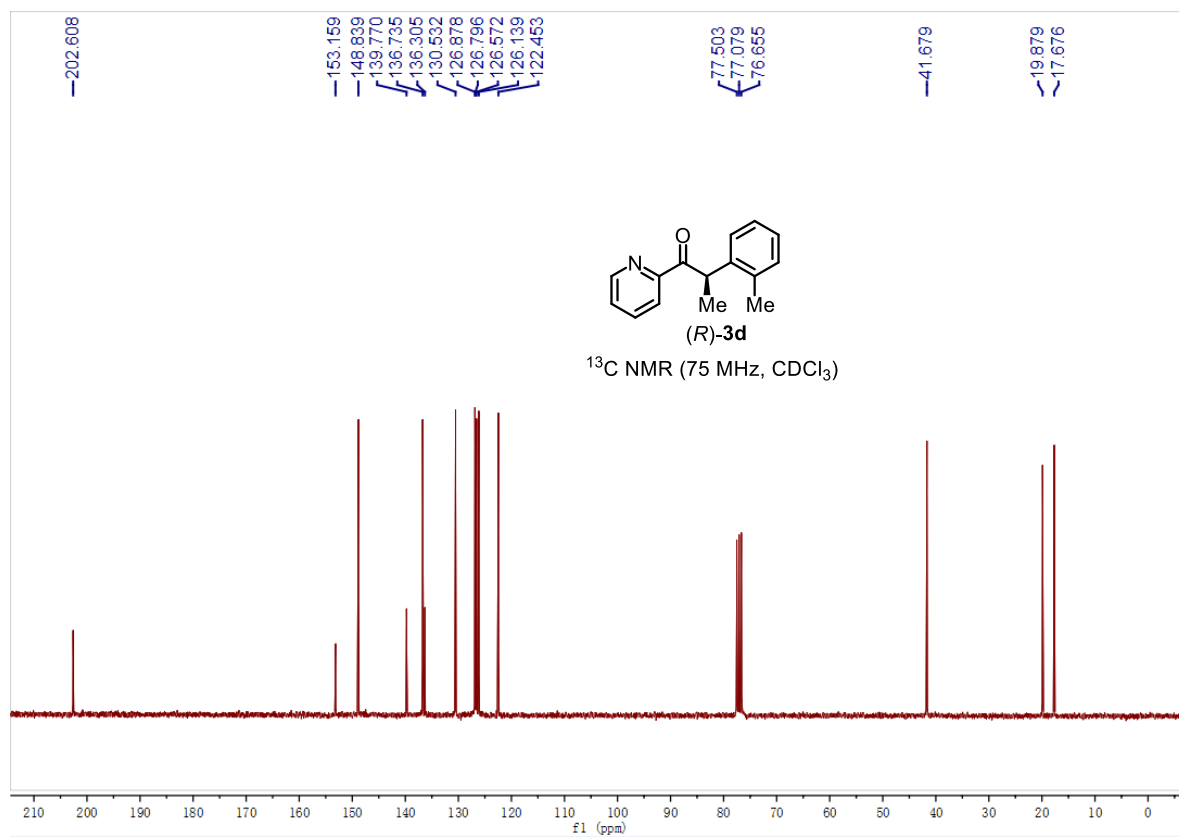
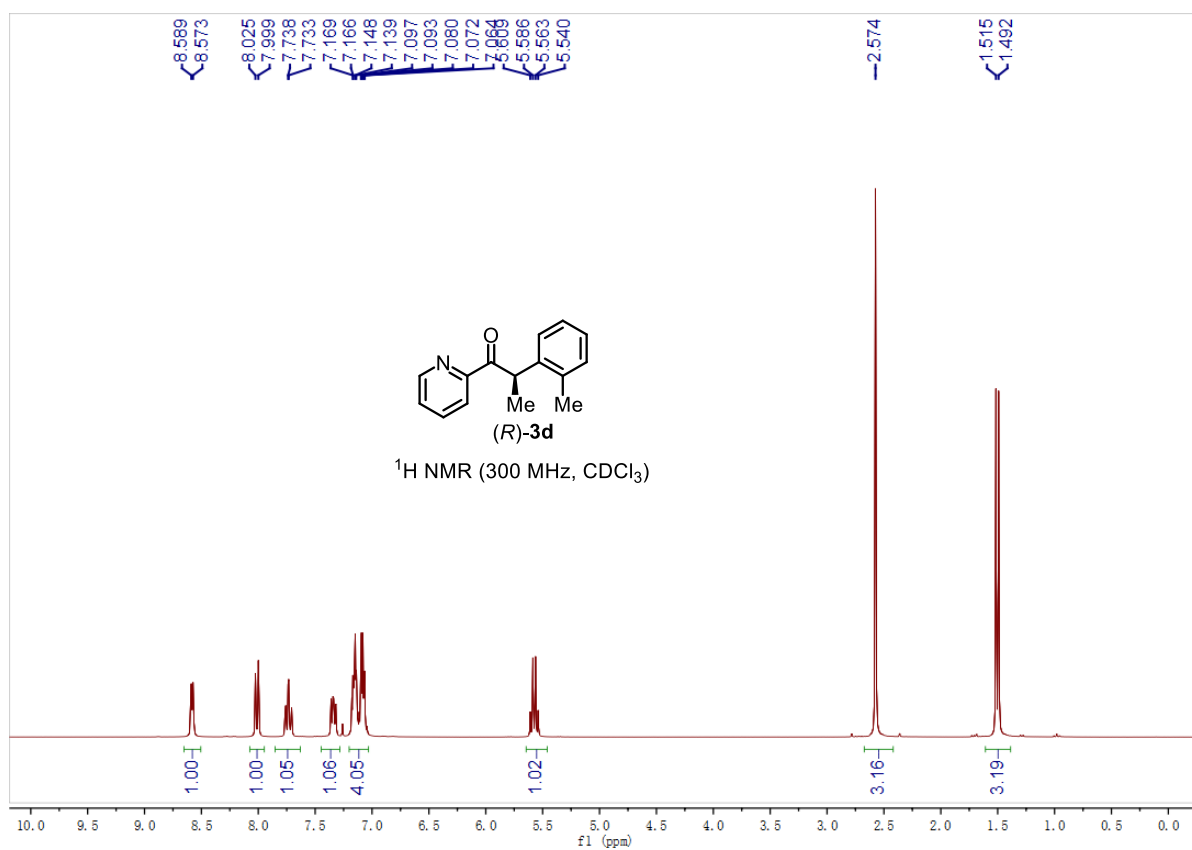




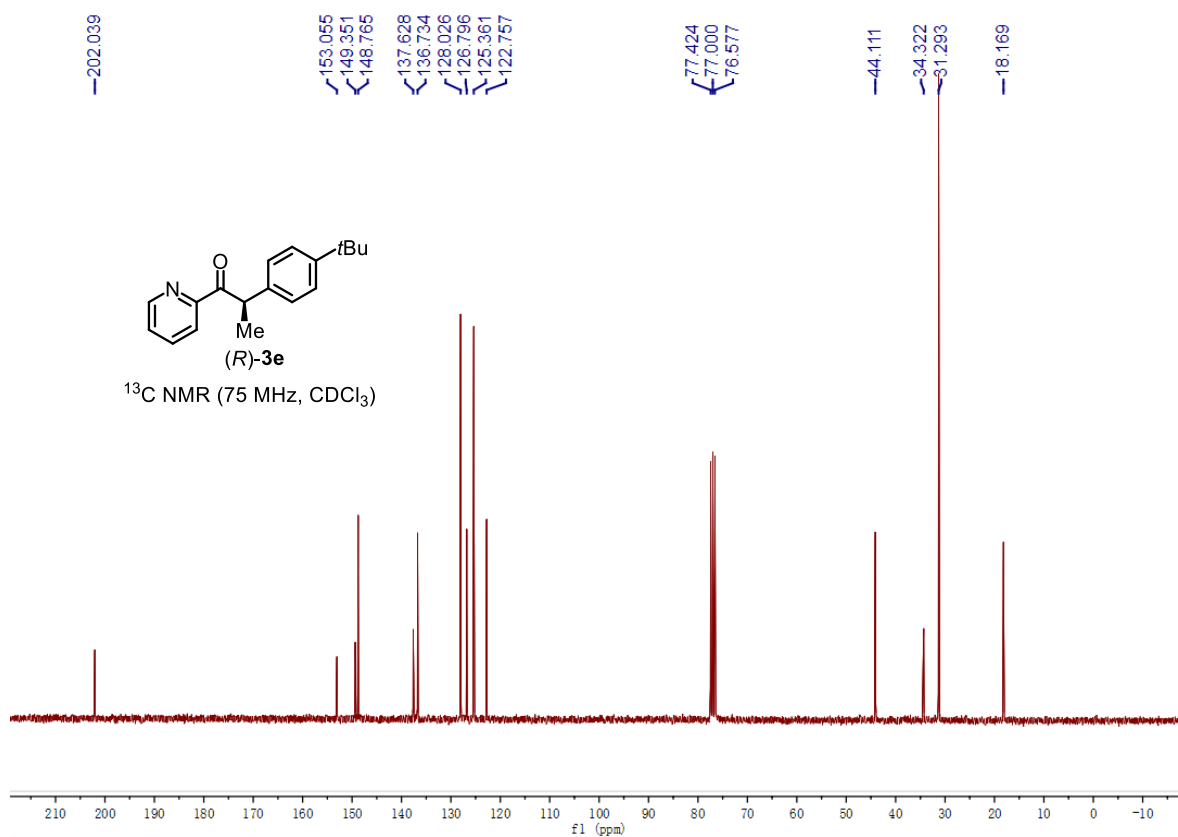
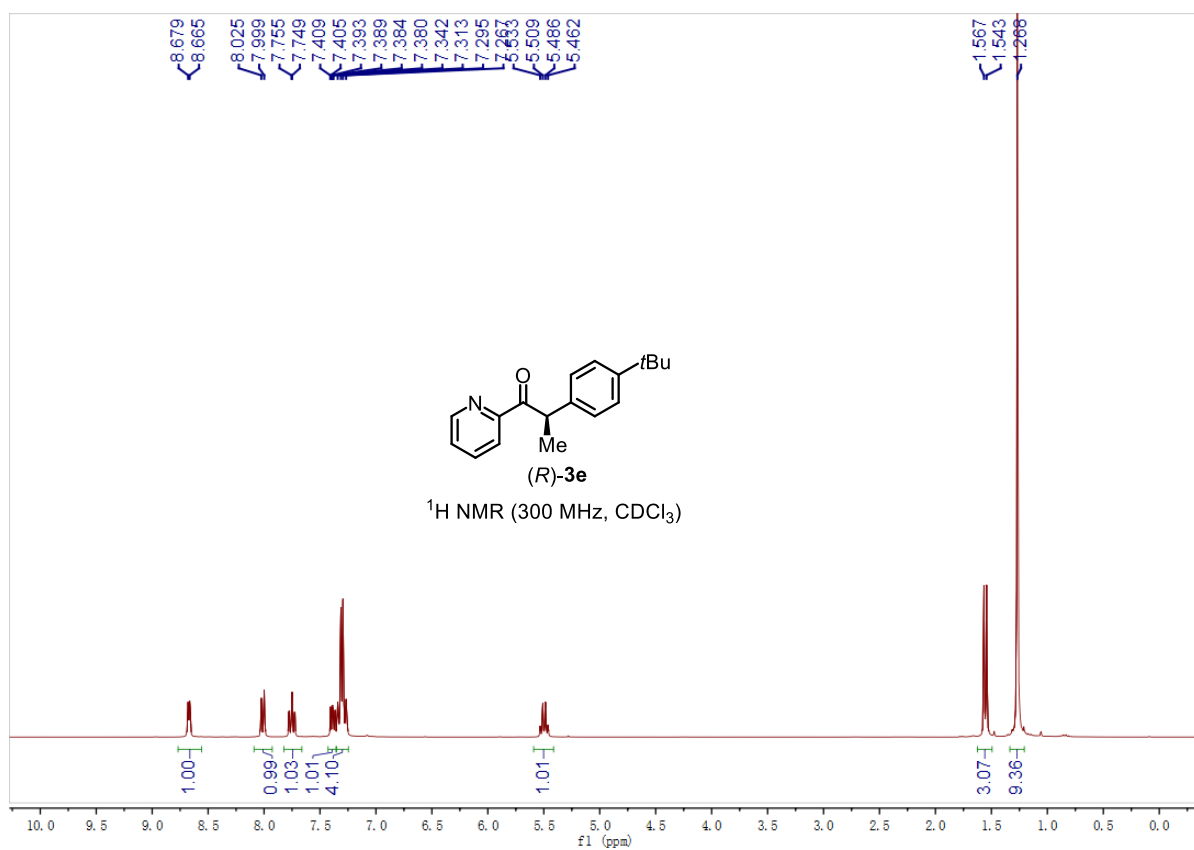
Chapter 5. Appendices



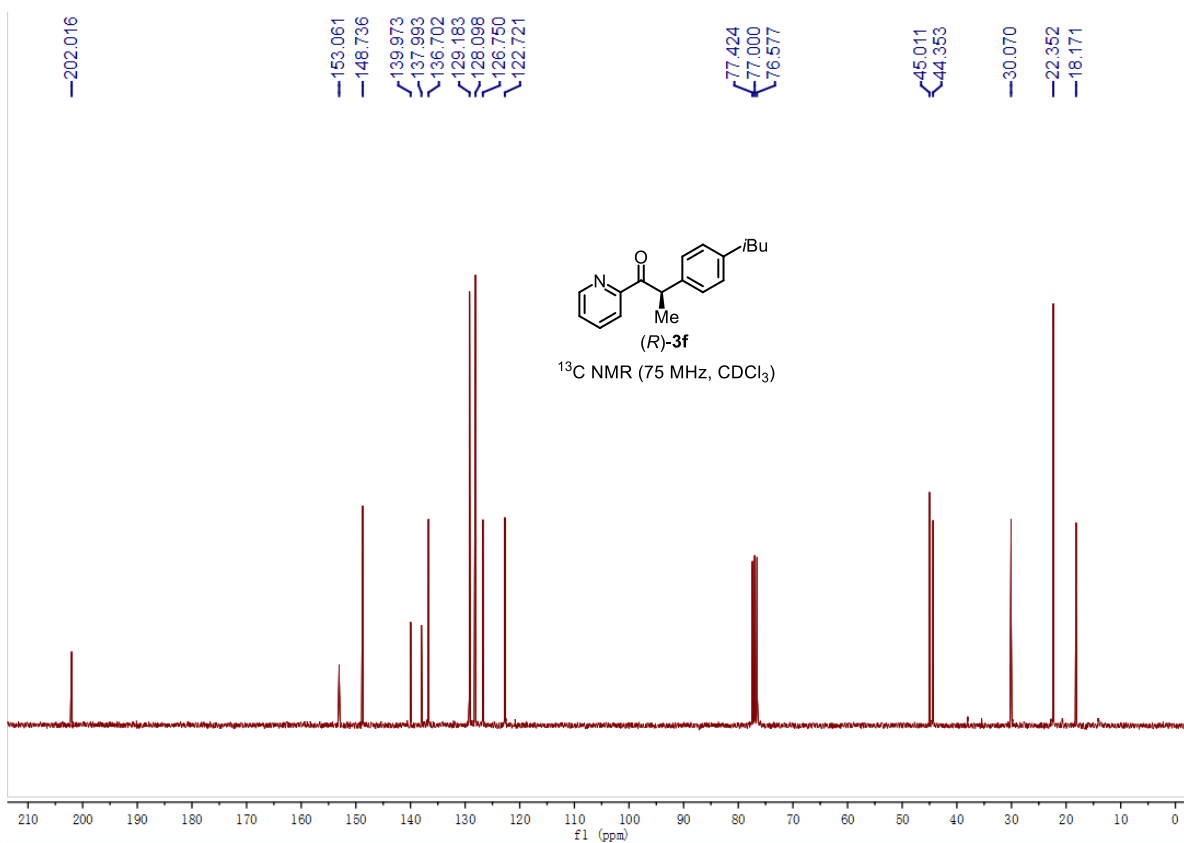
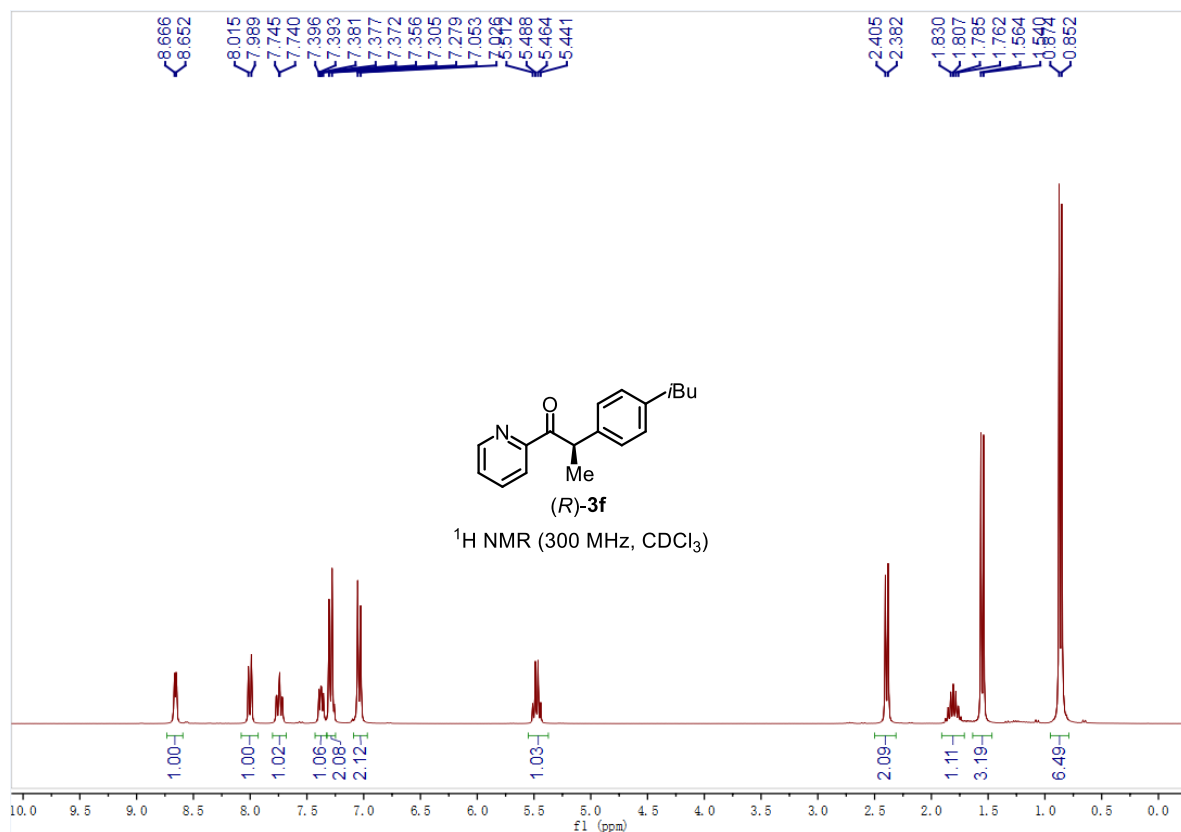
Chapter 5. Appendices



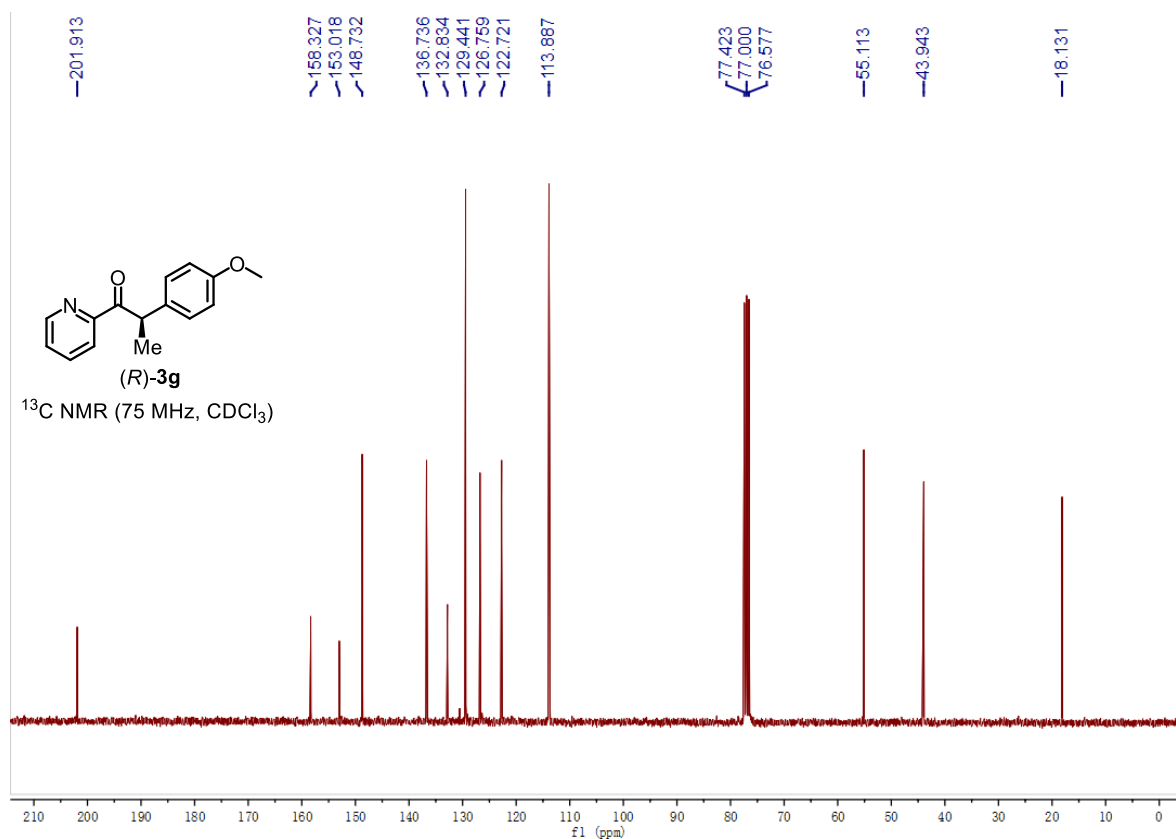
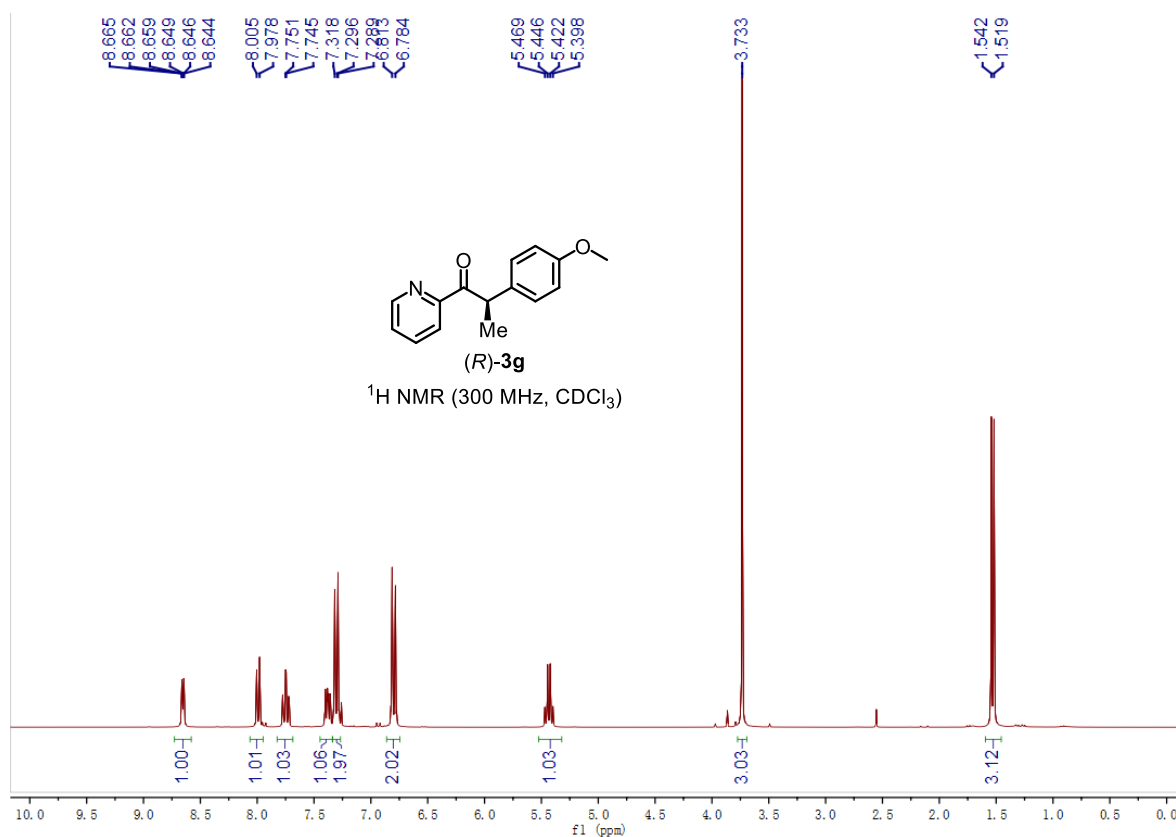
Chapter 5. Appendices

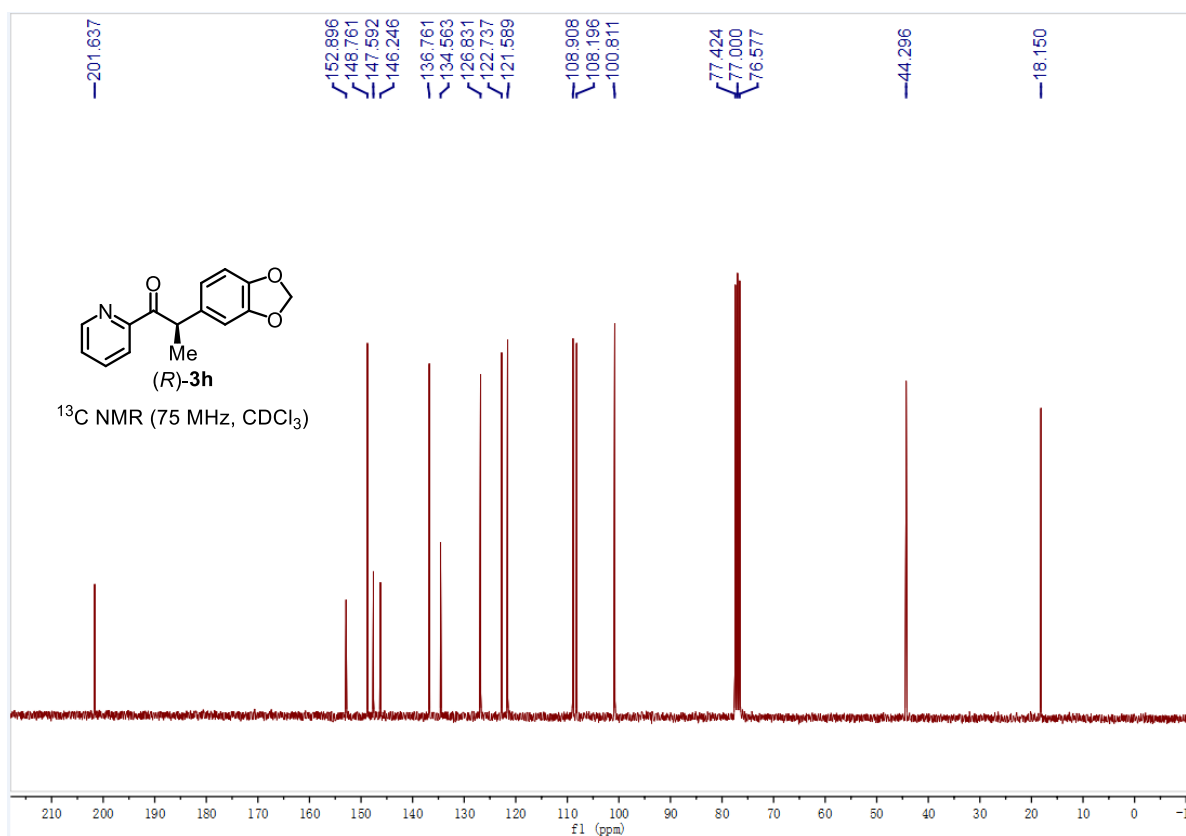
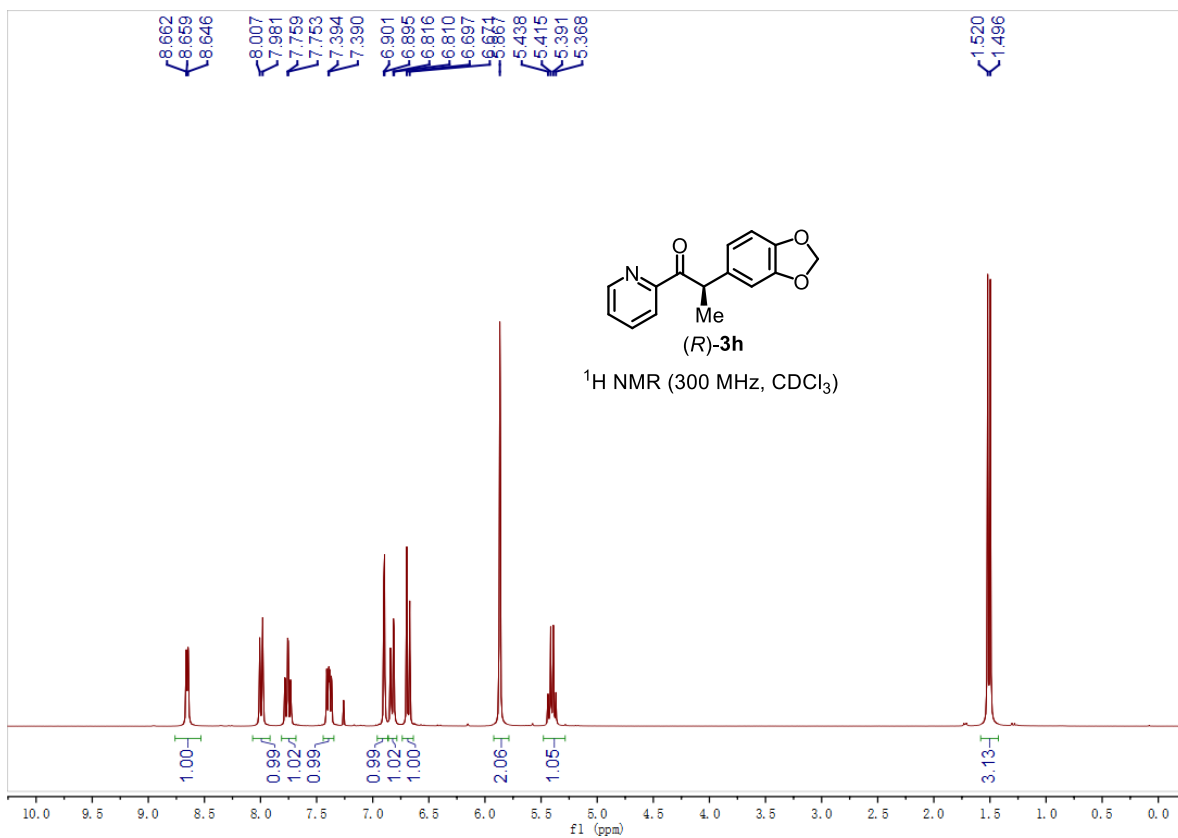


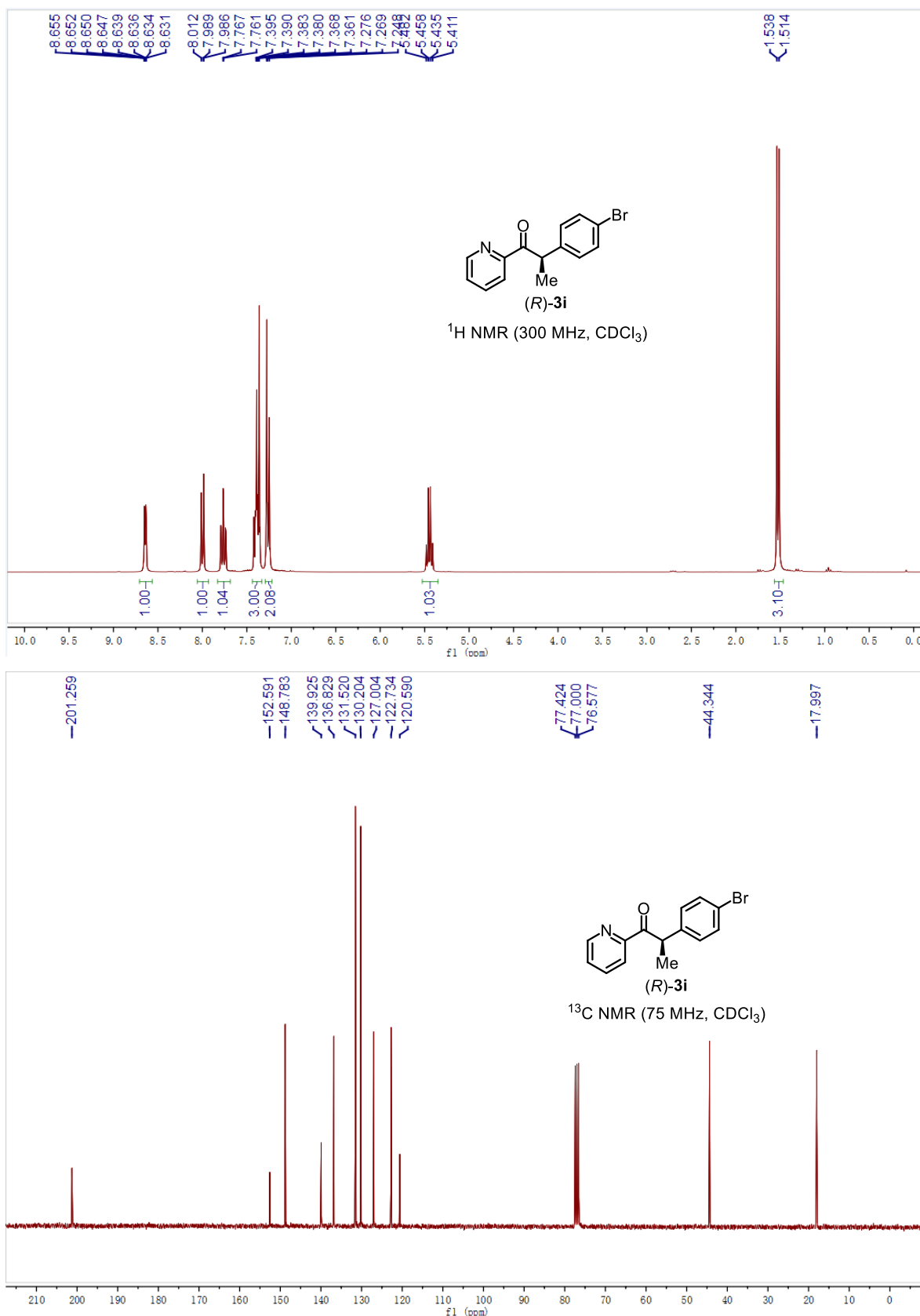
Chapter 5. Appendices



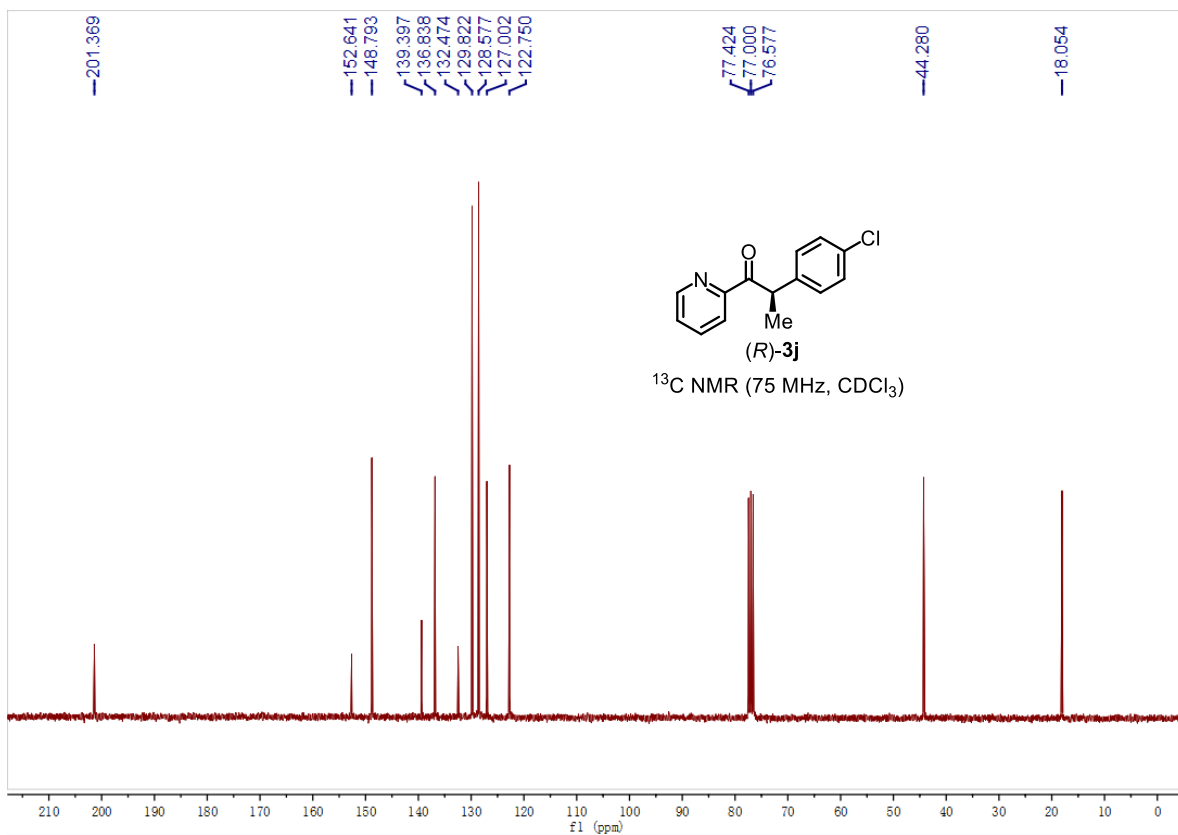
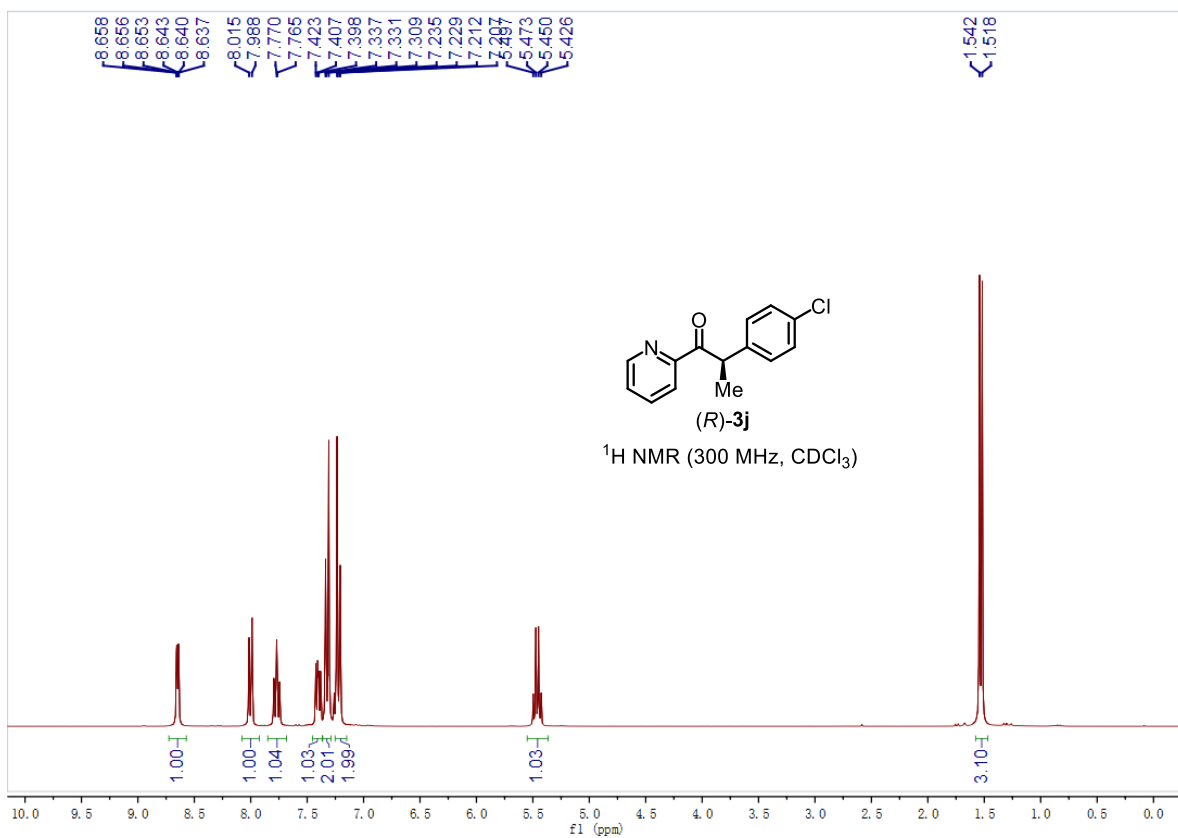
Chapter 5. Appendices

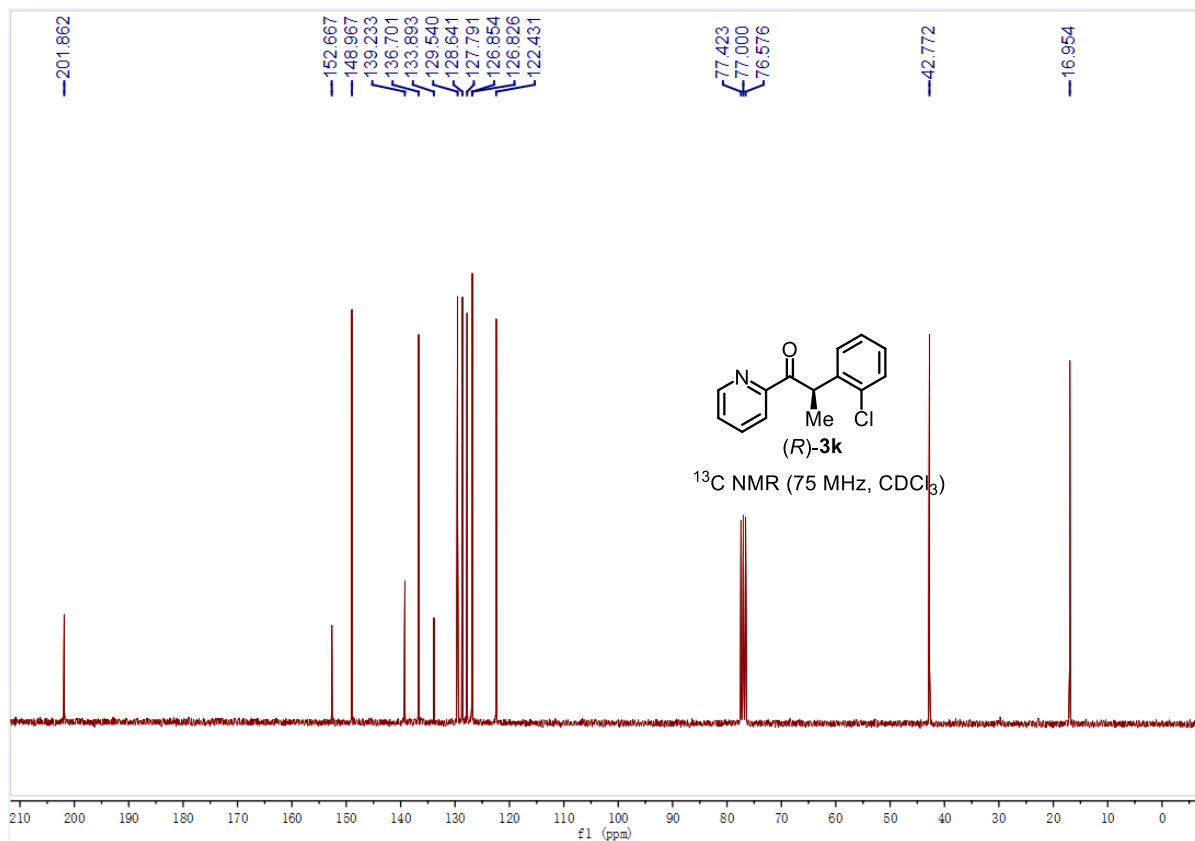
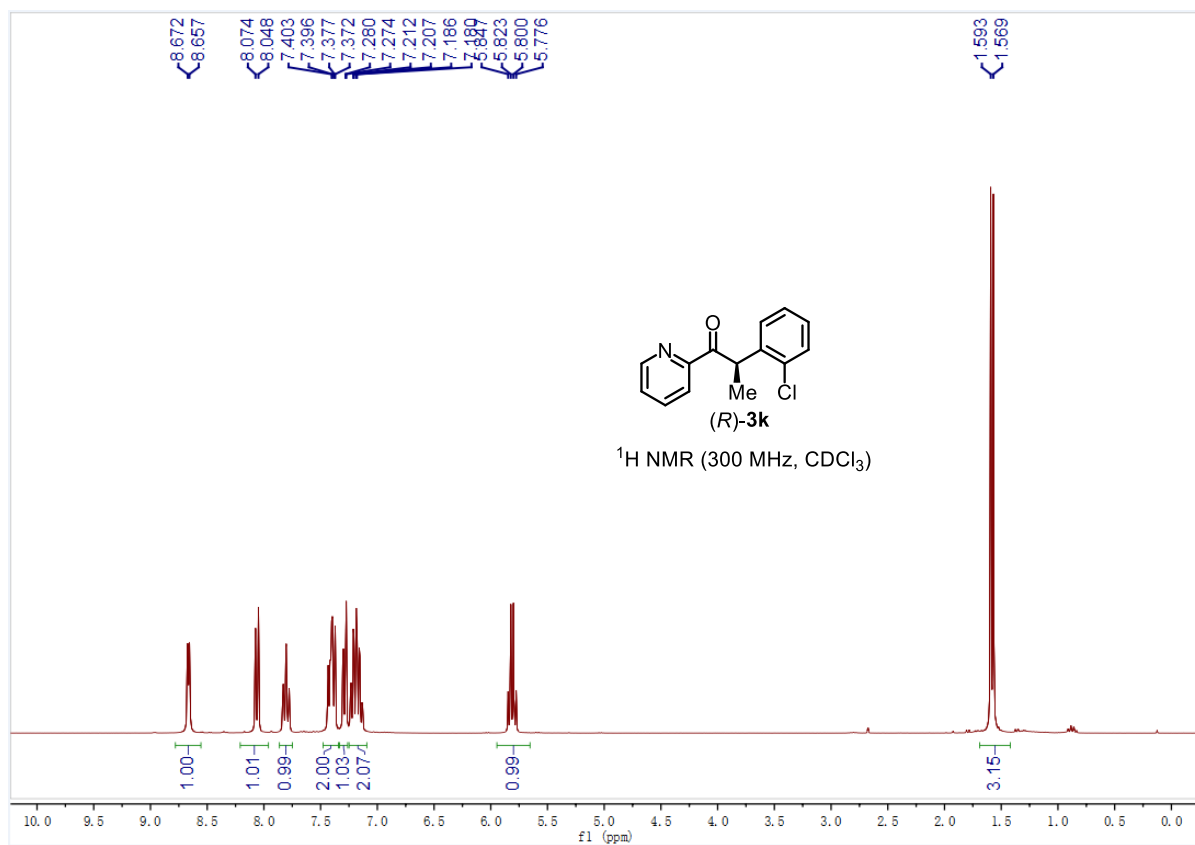




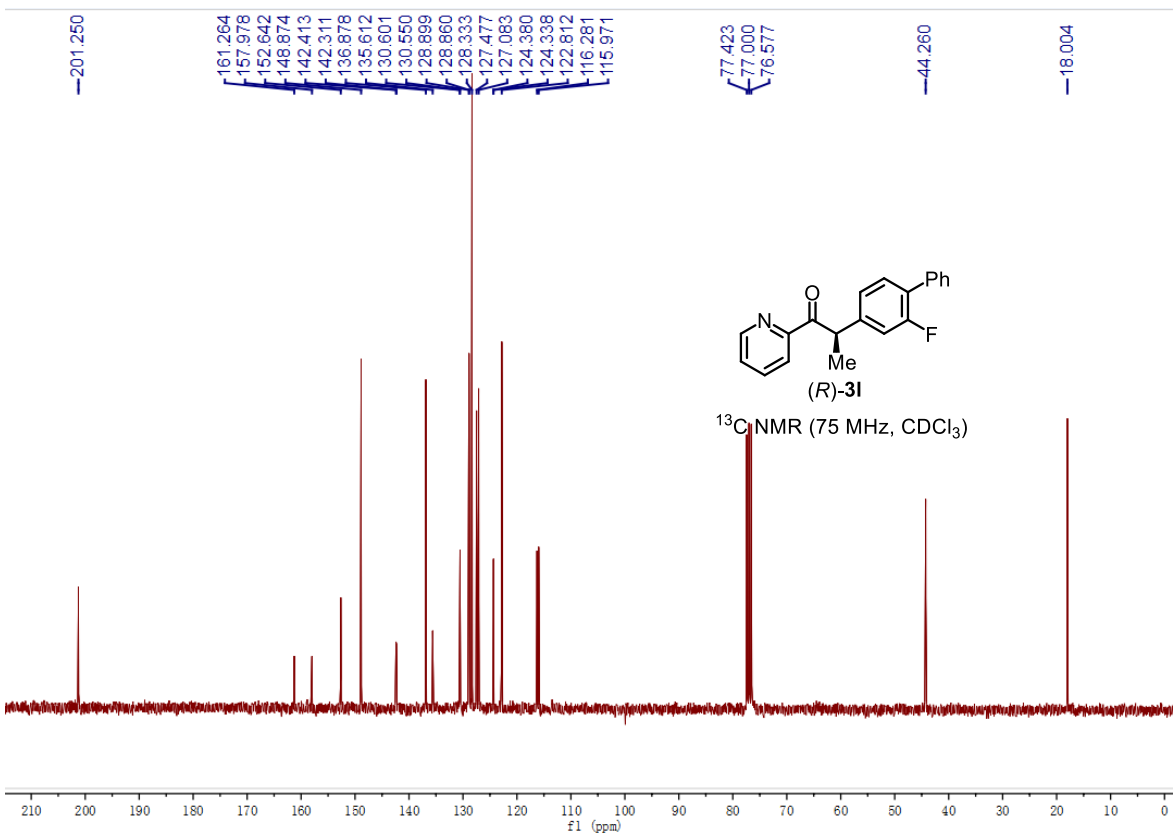
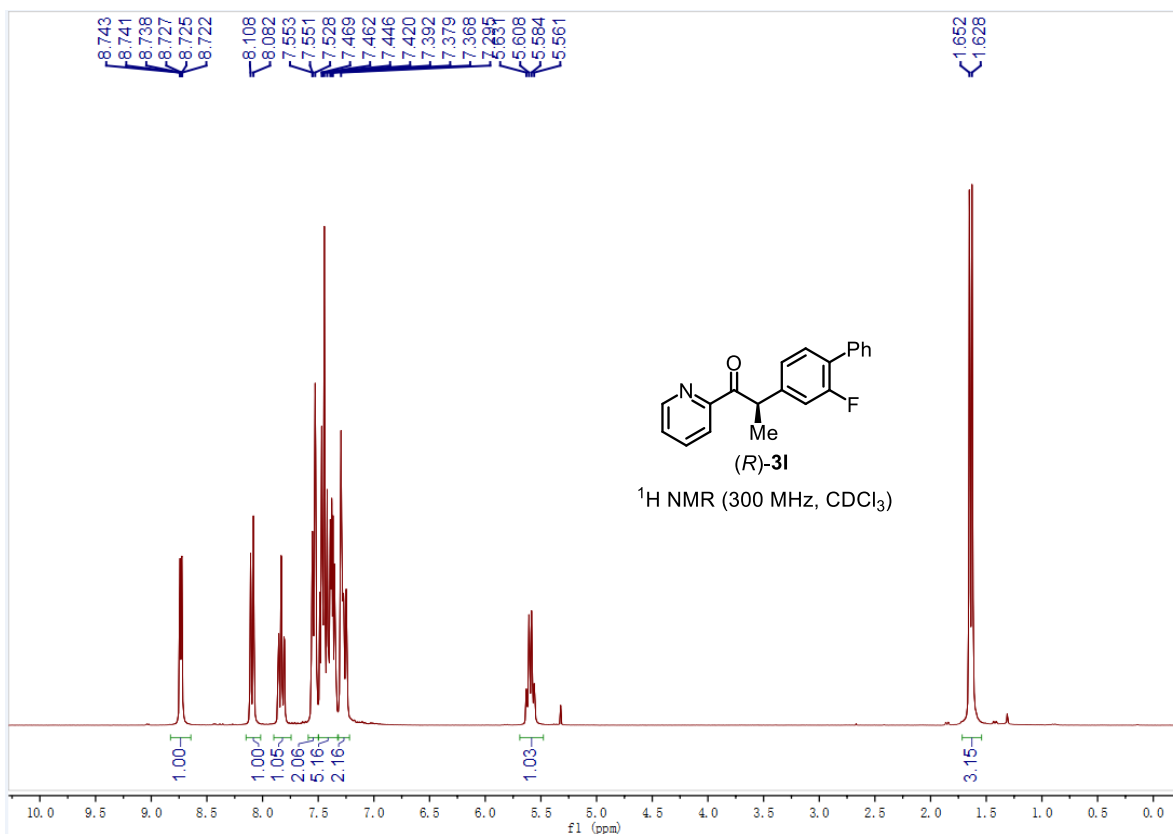


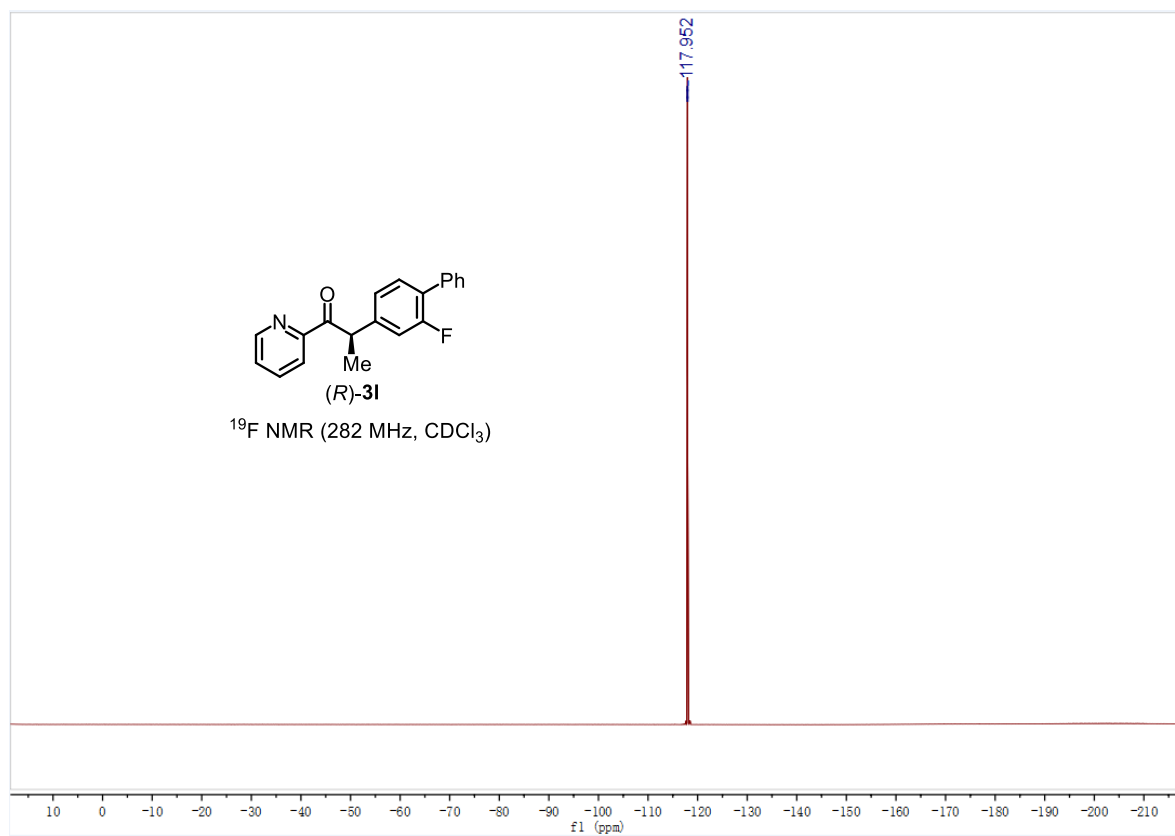
Chapter 5. Appendices



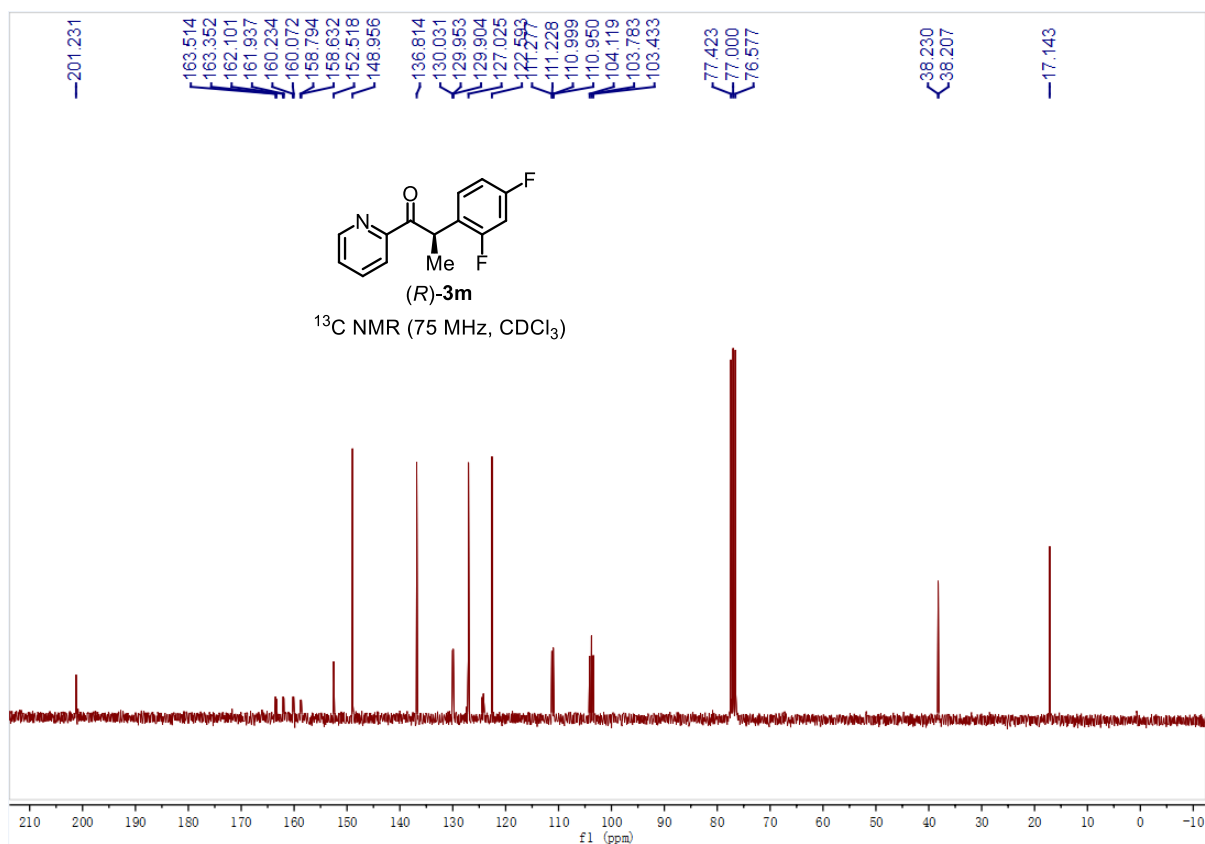
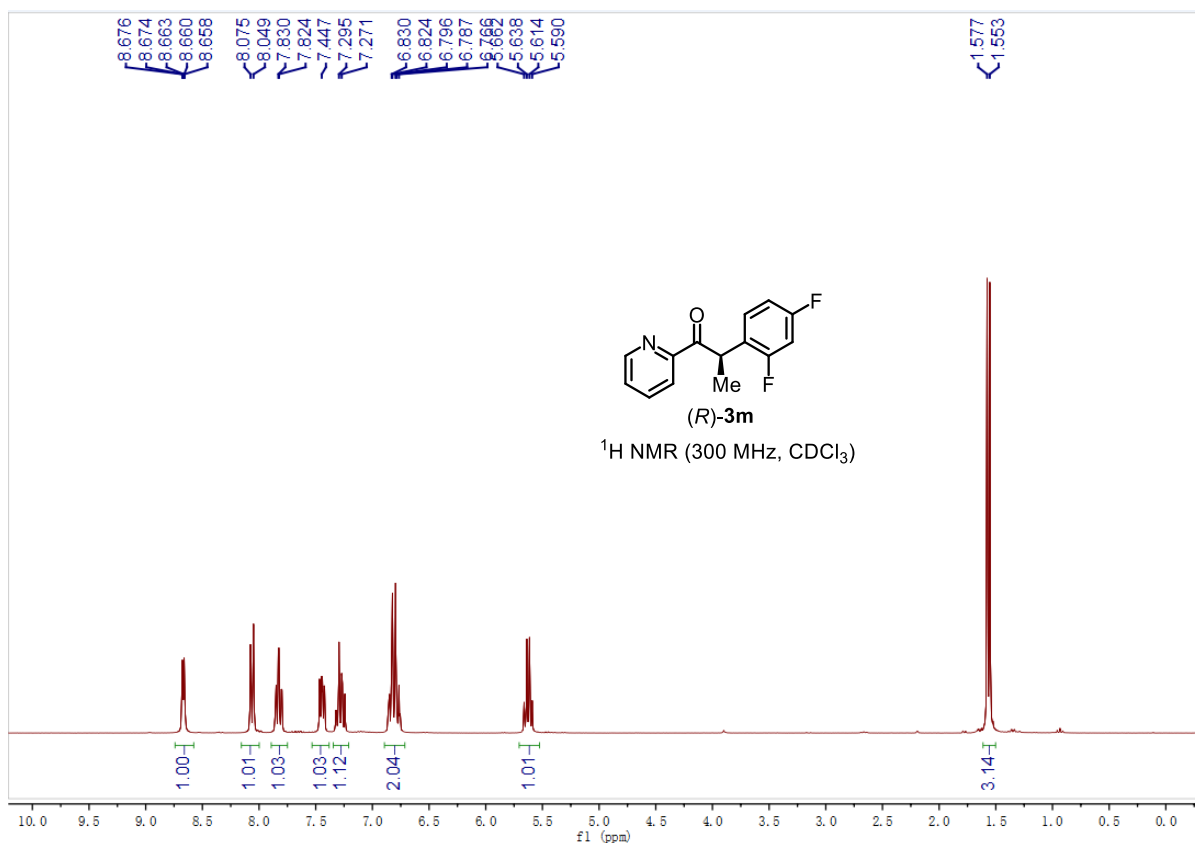


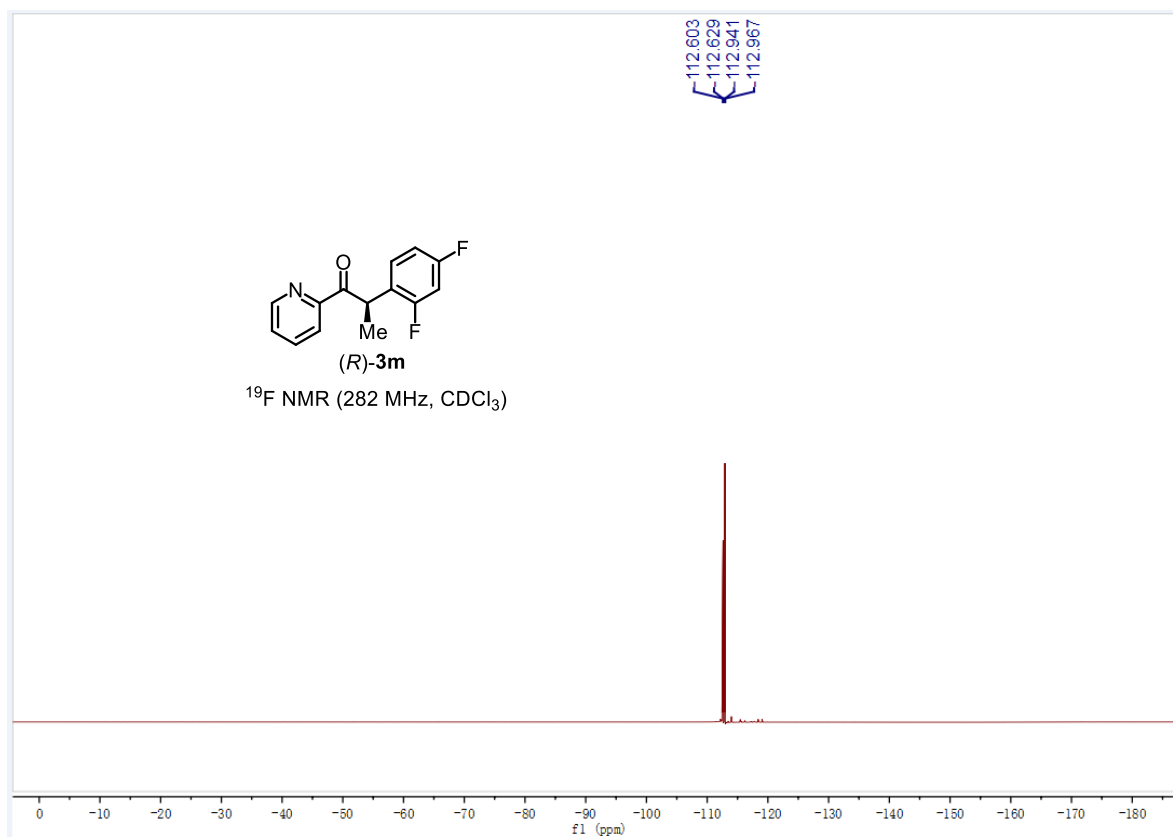
Chapter 5. Appendices

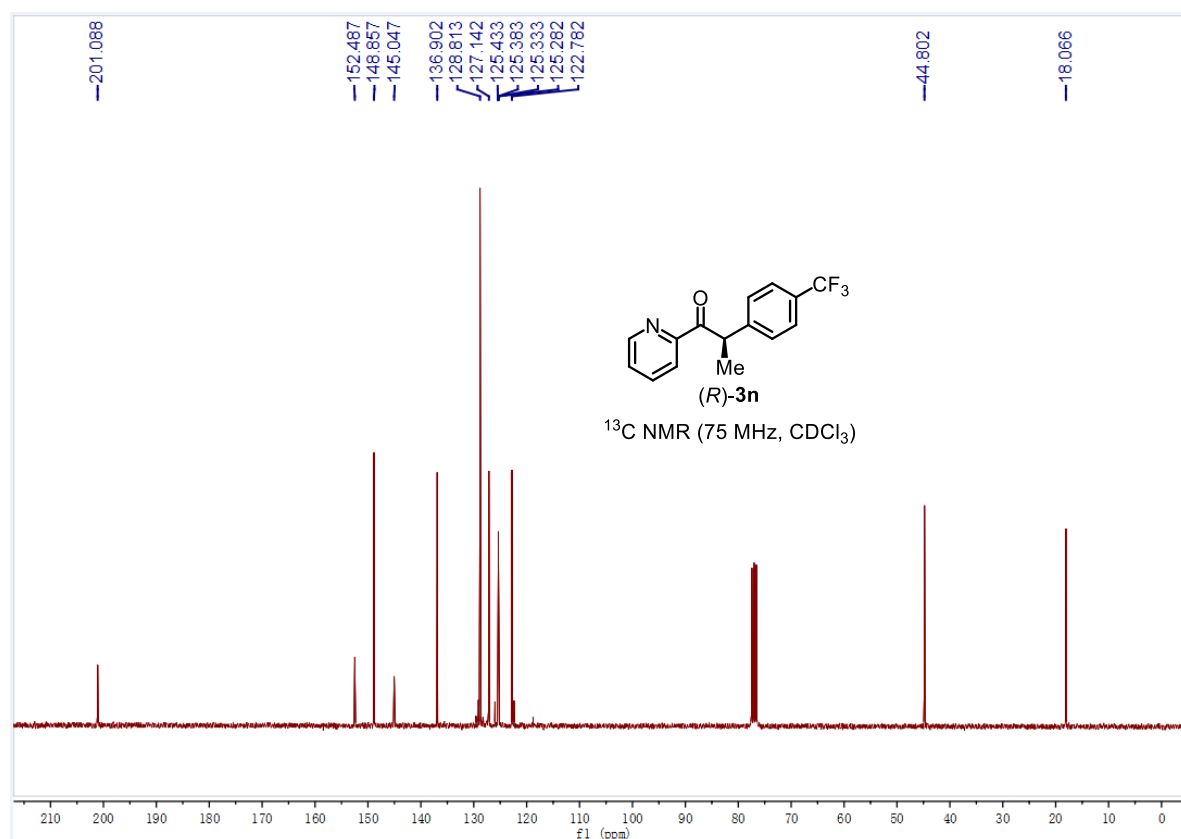
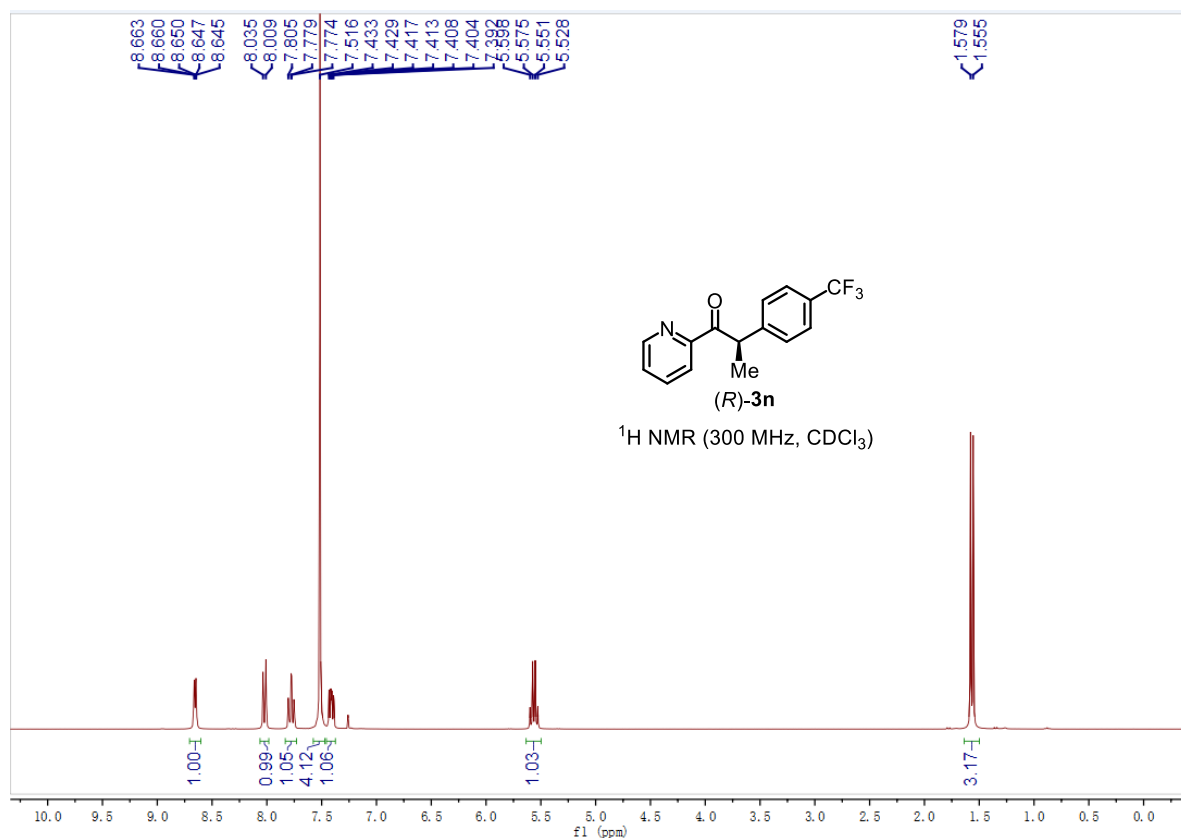


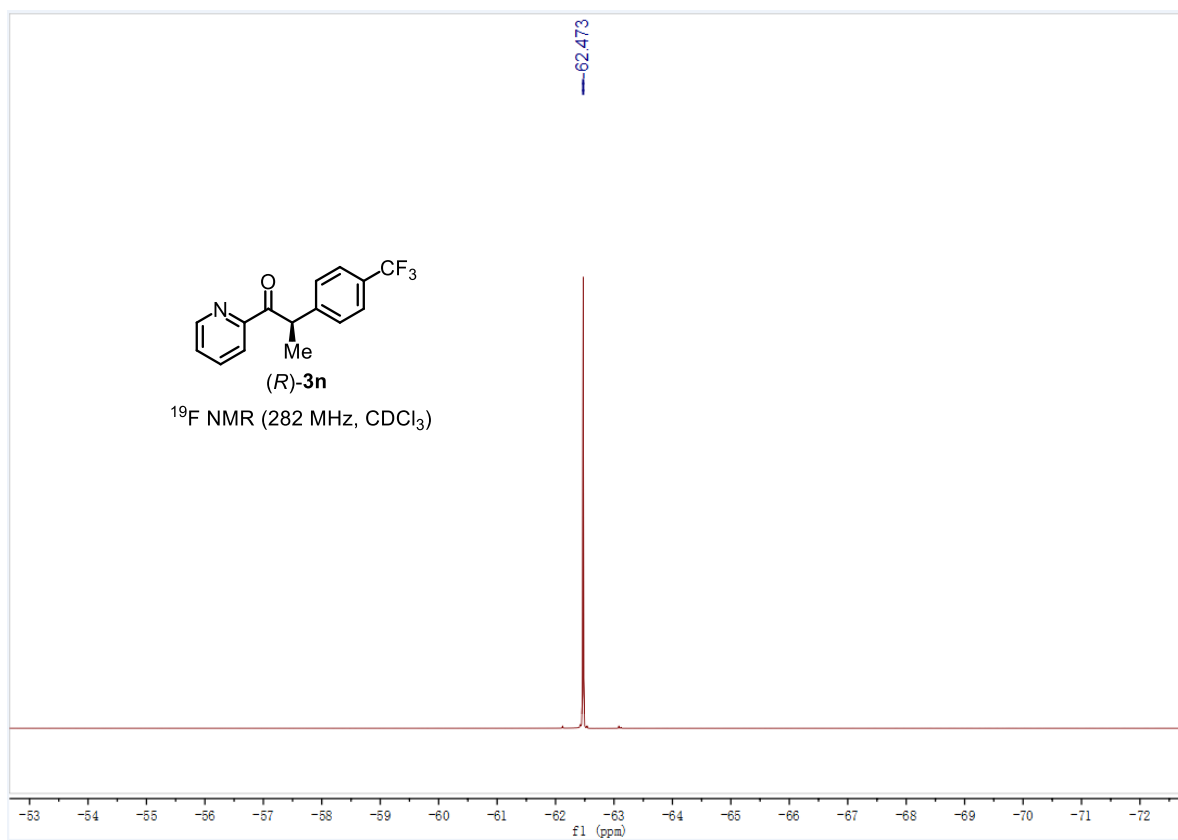


Chapter 5. Appendices

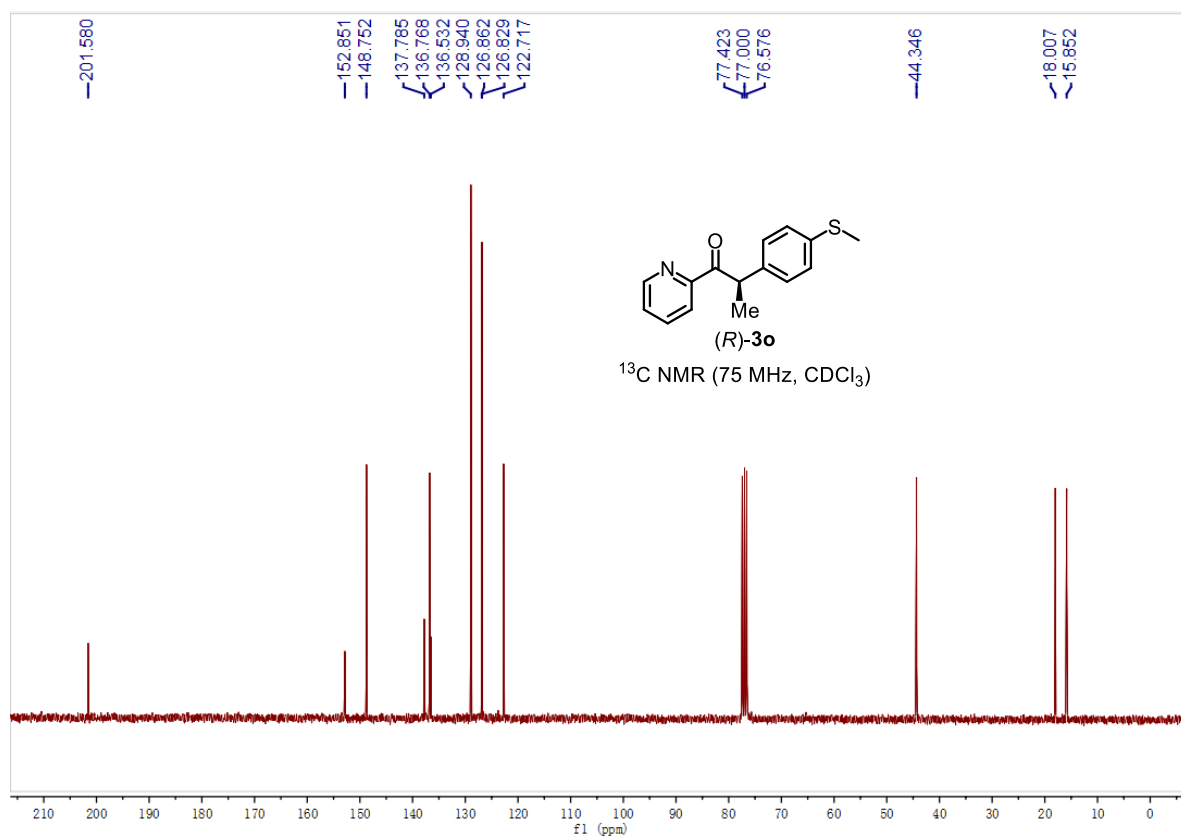
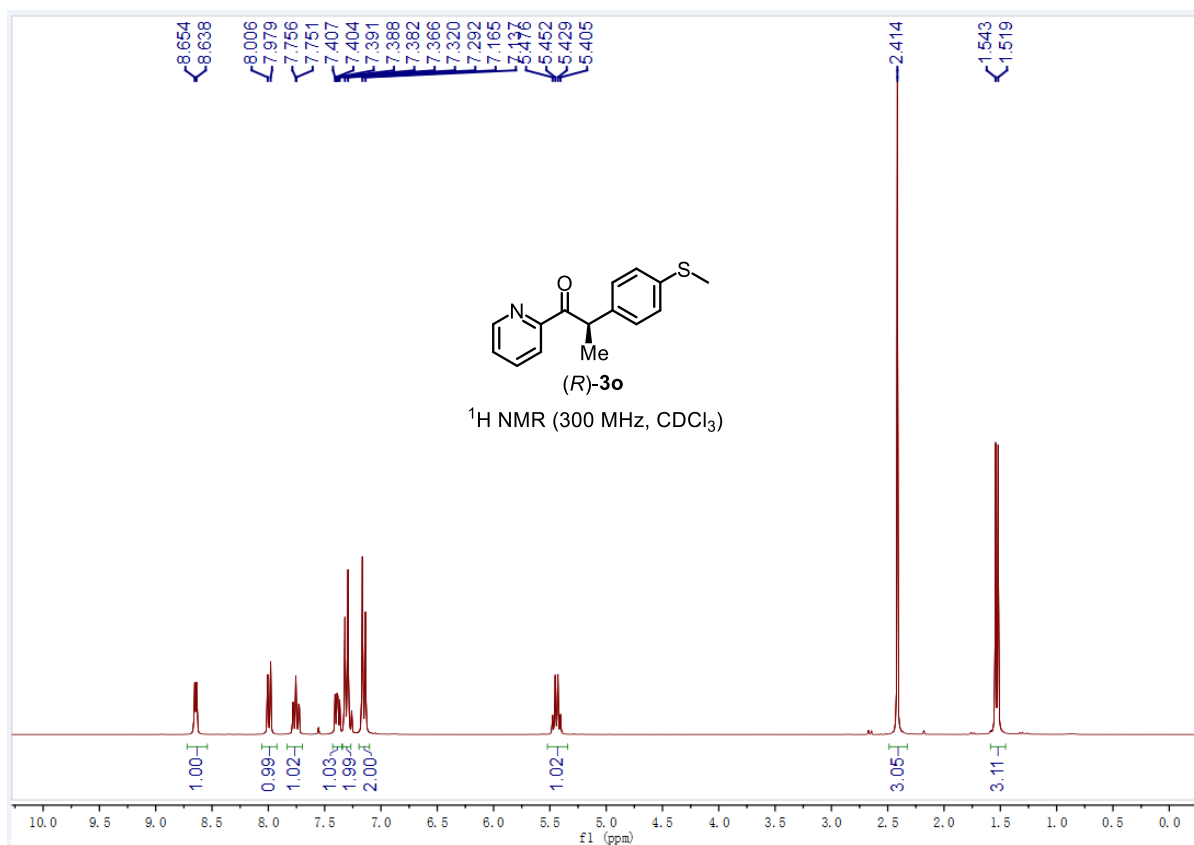




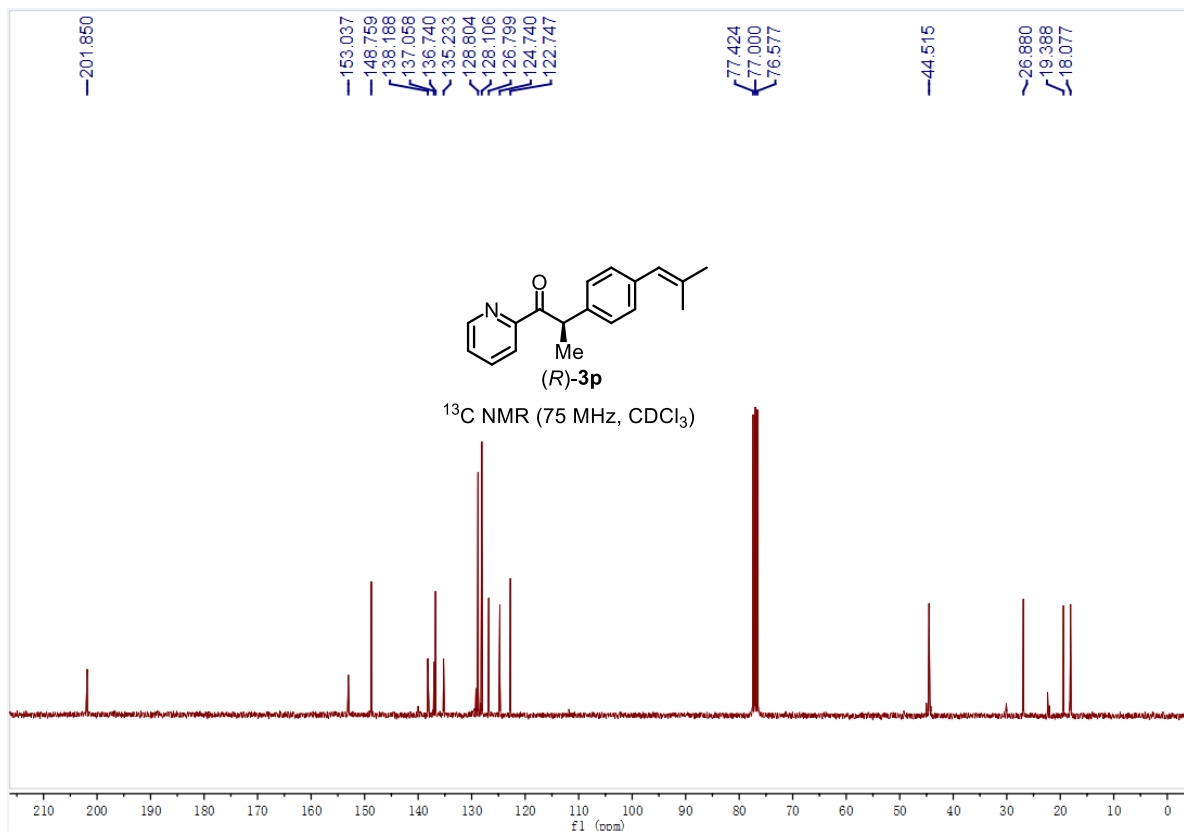
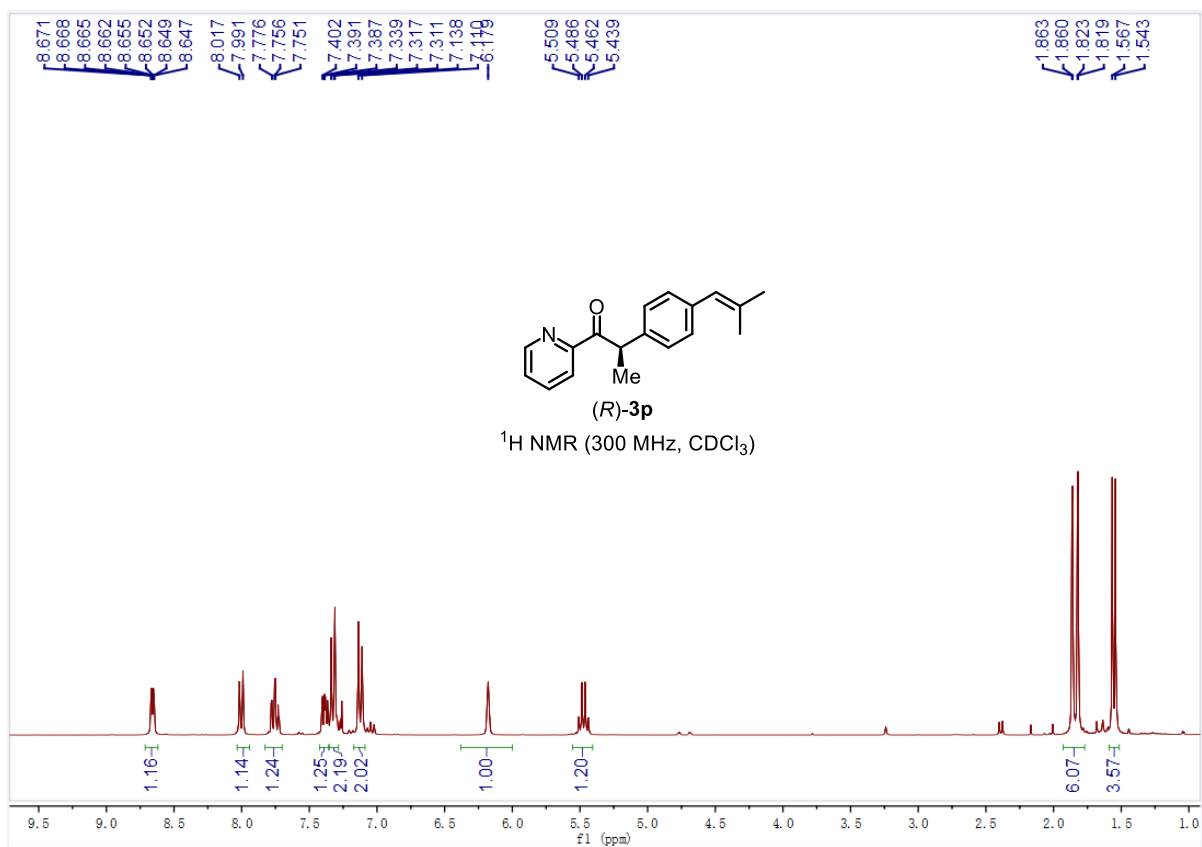




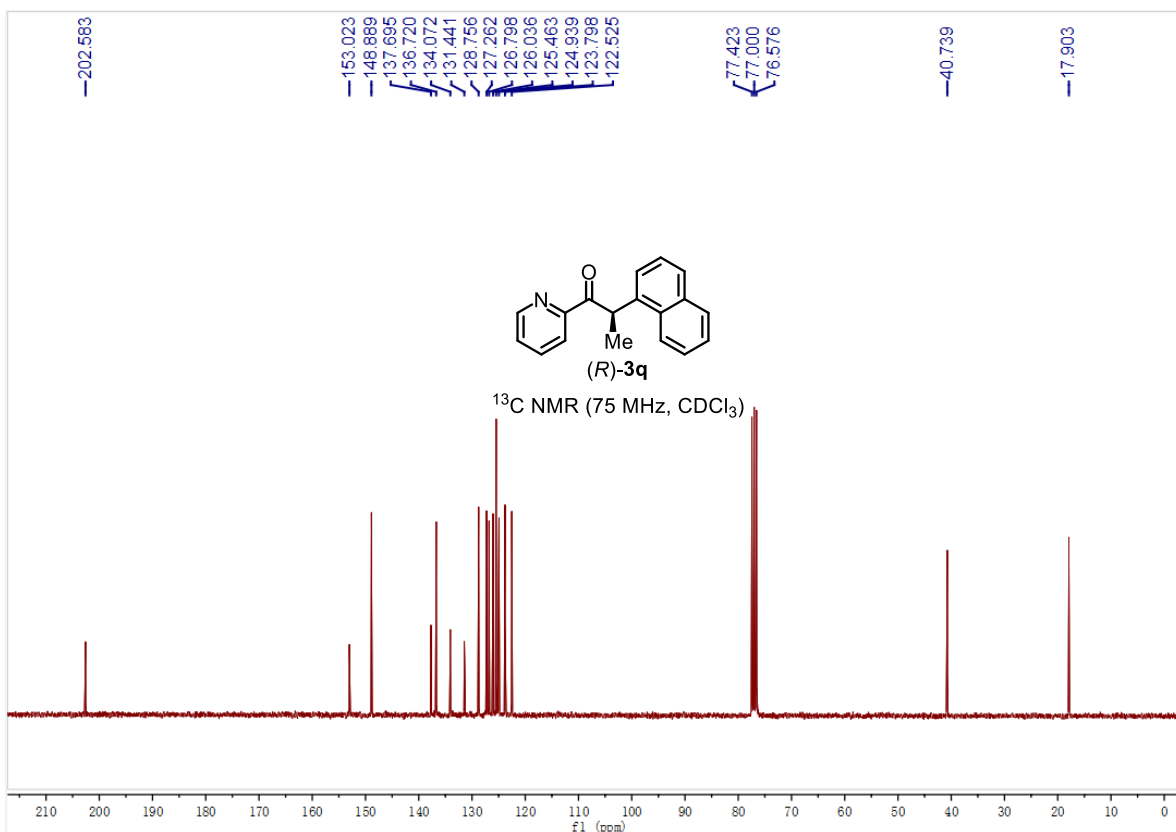
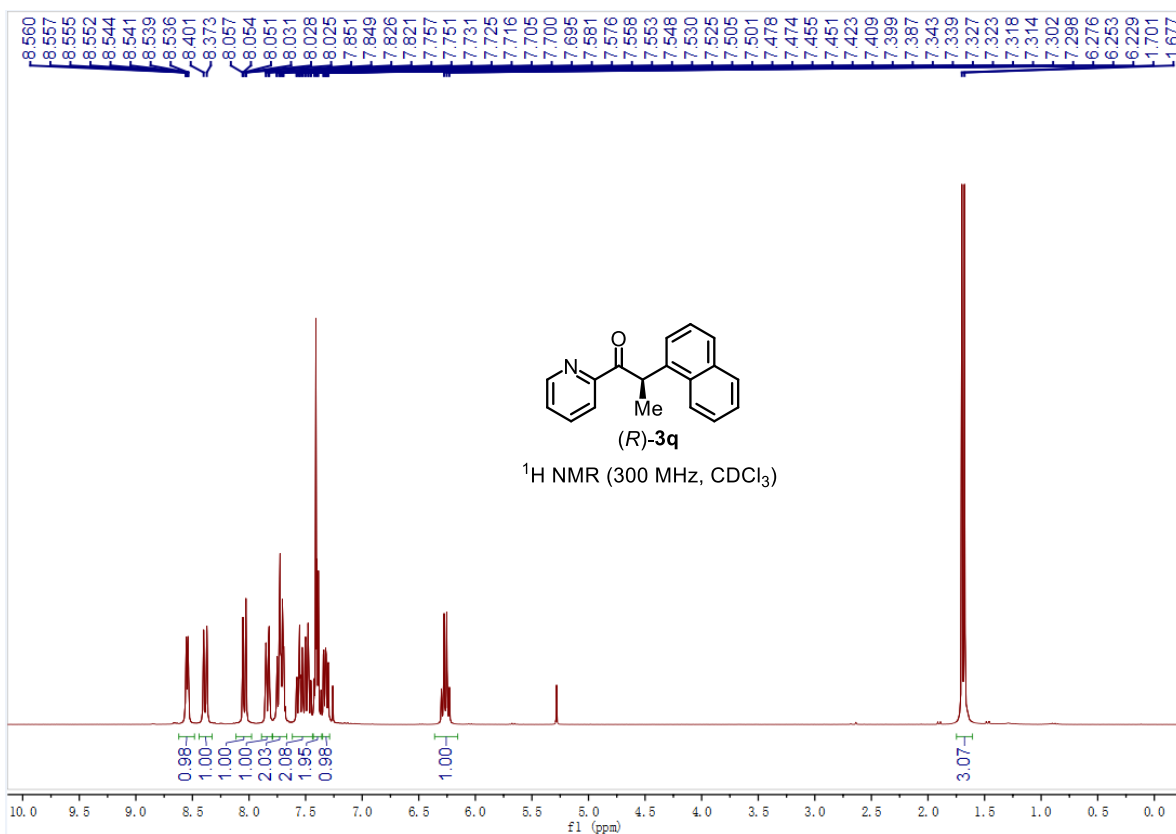
Chapter 5. Appendices

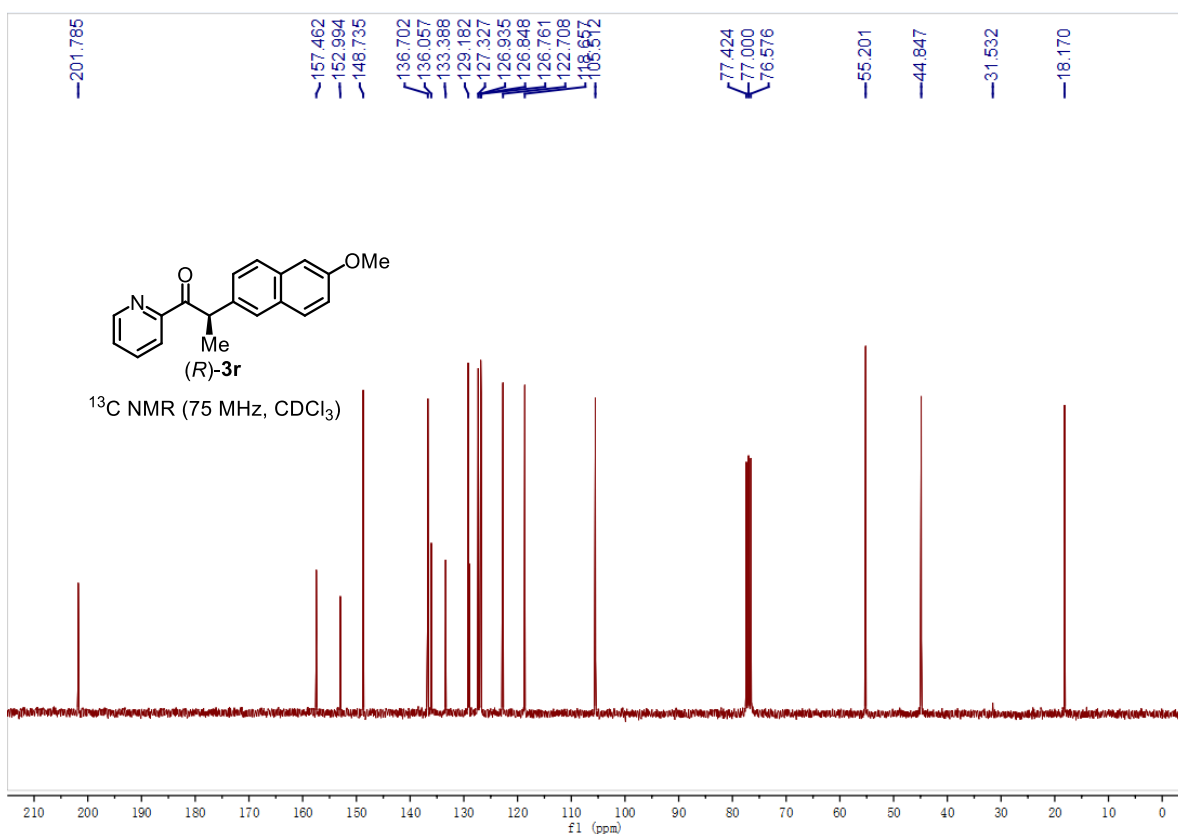
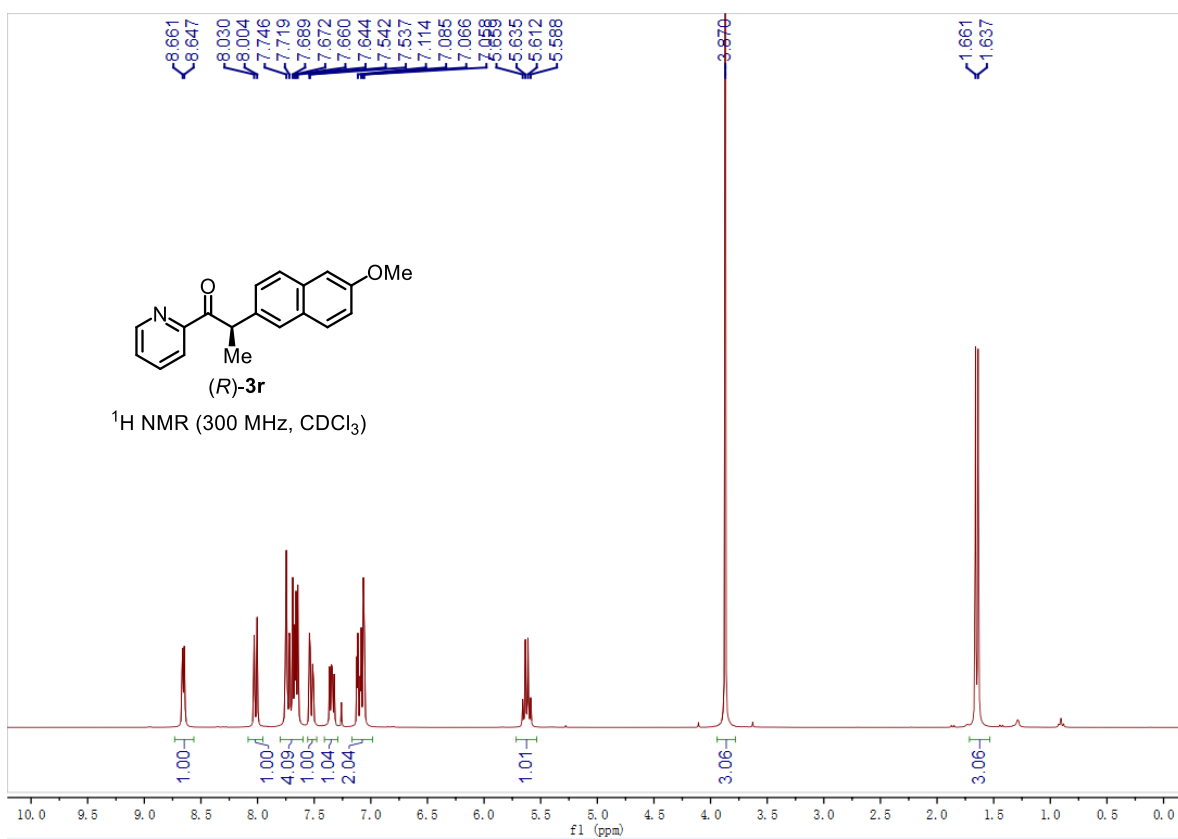


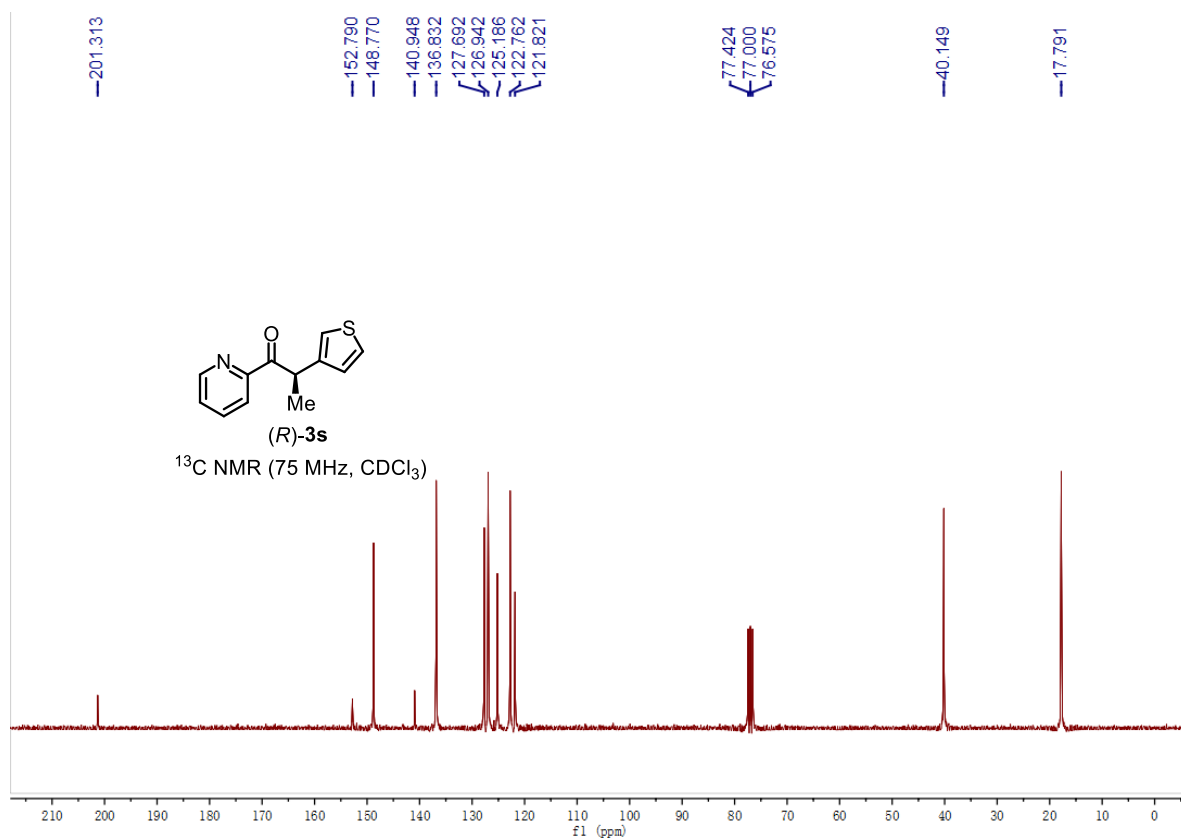
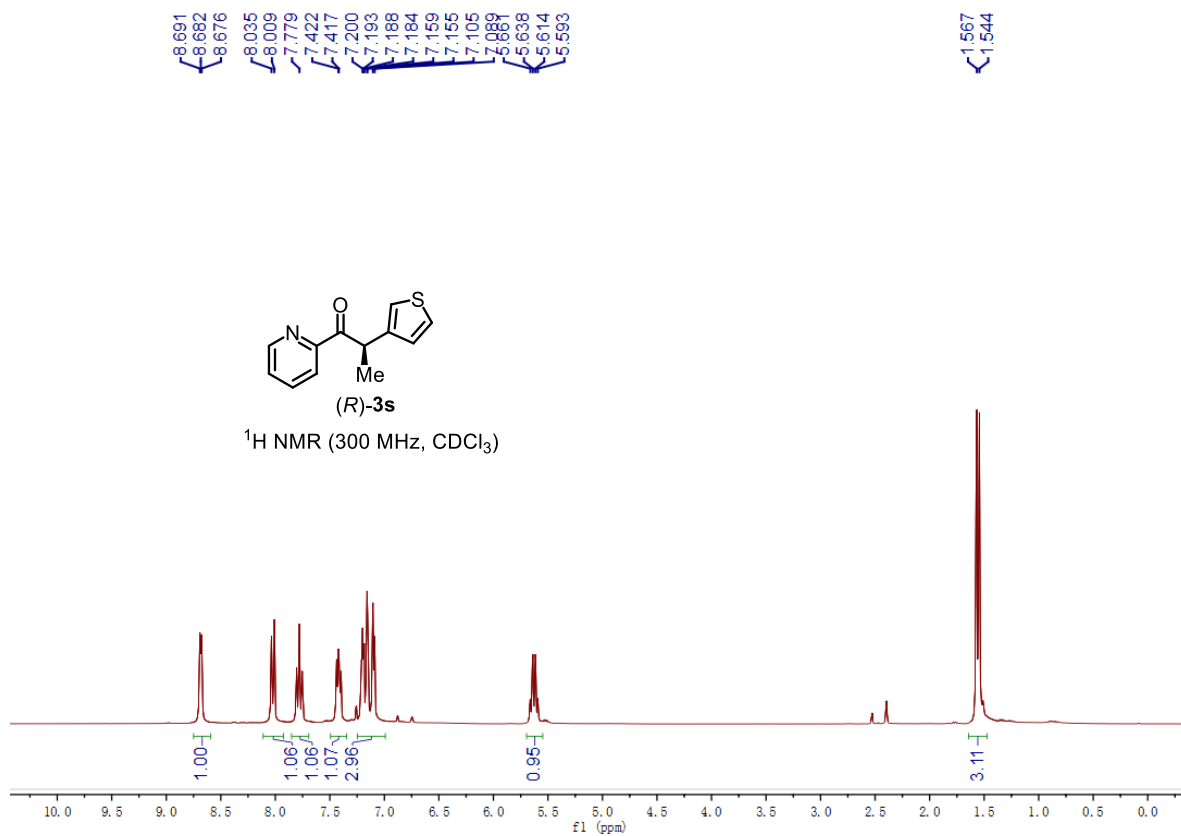
Chapter 5. Appendices

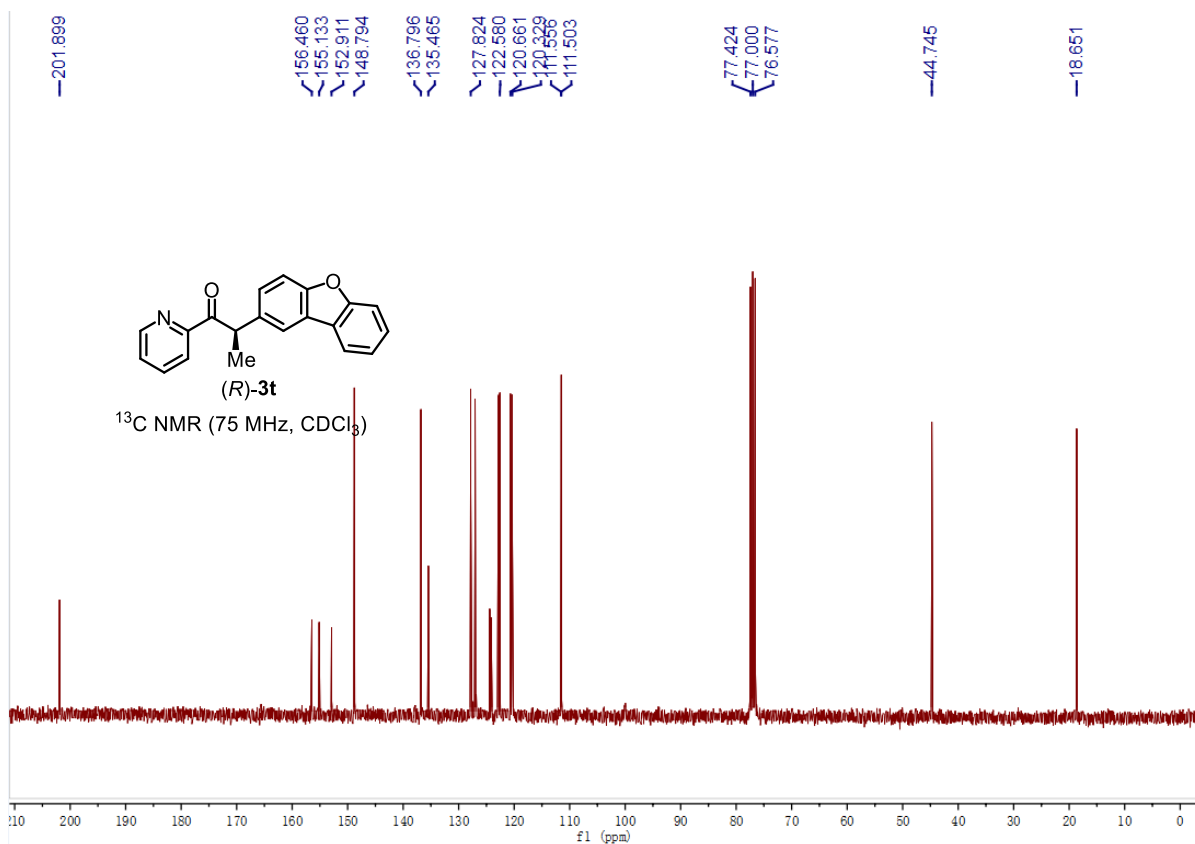
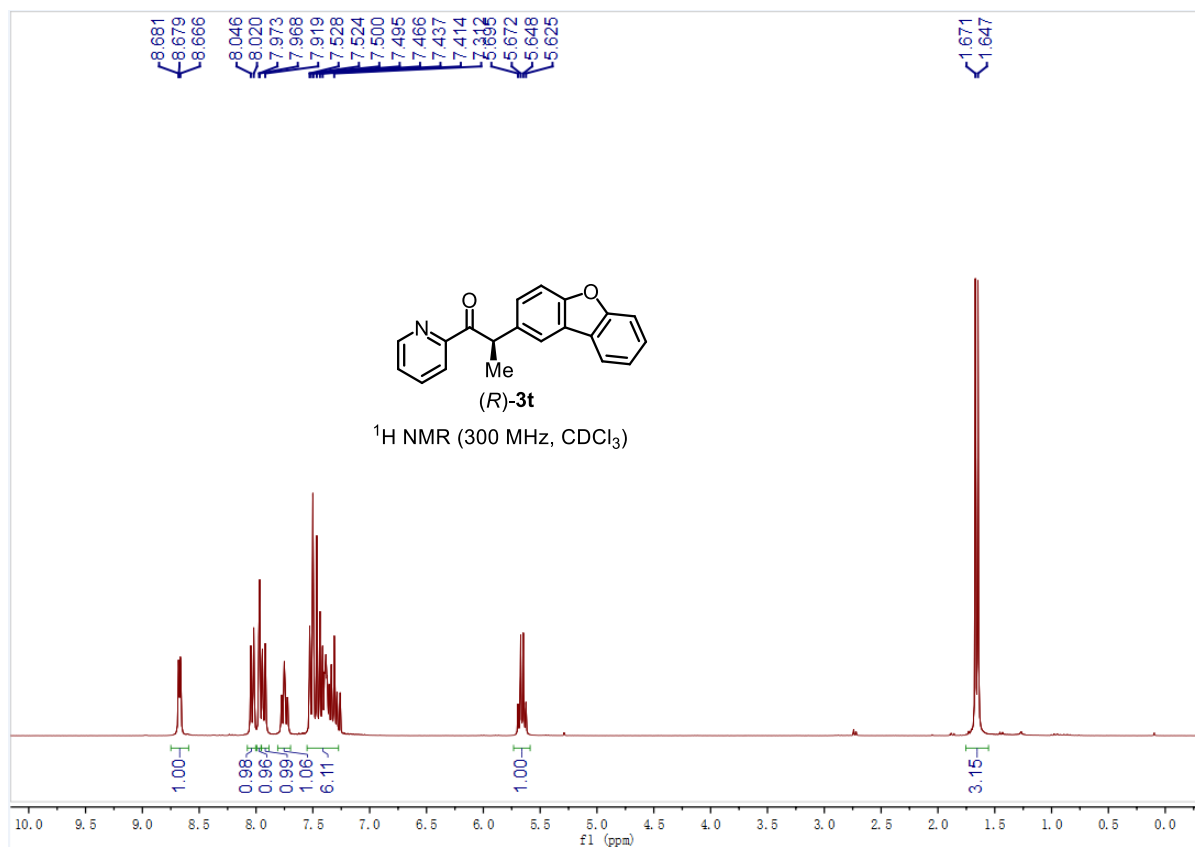


Chapter 5. Appendices

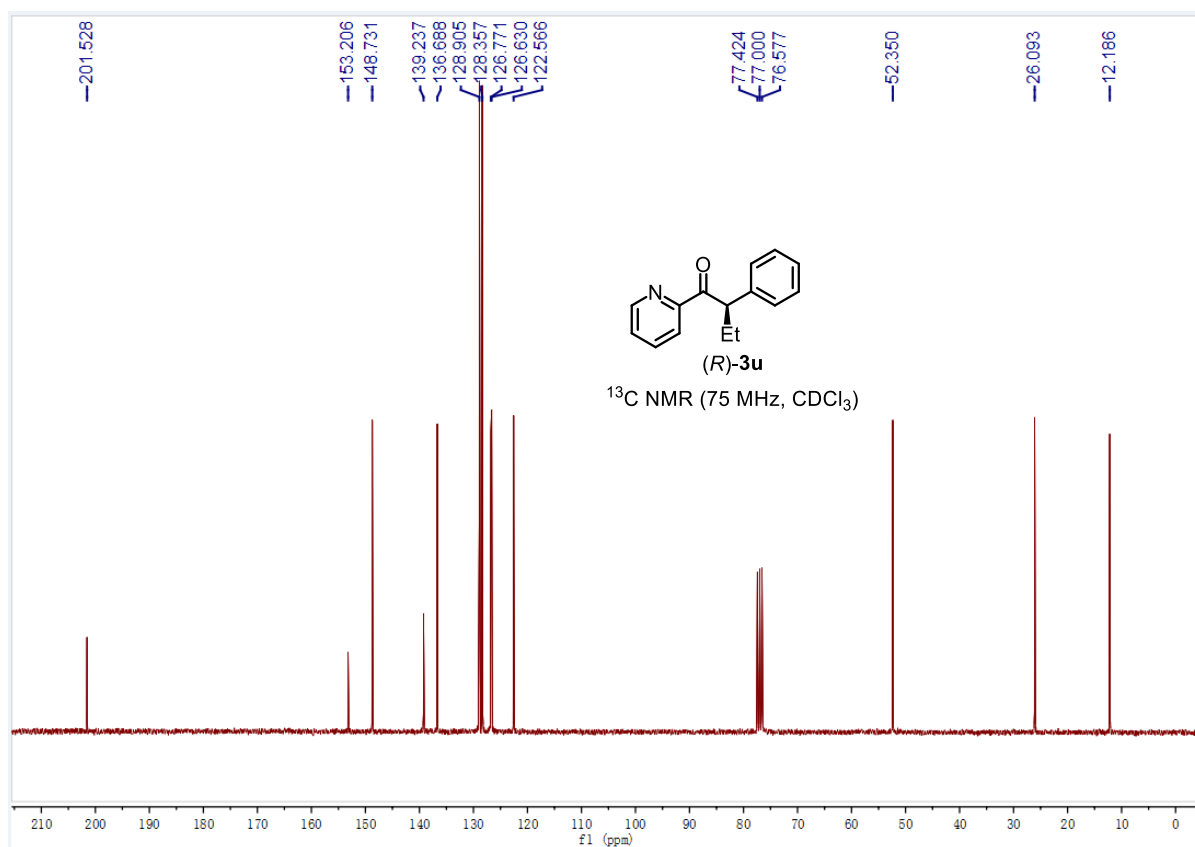
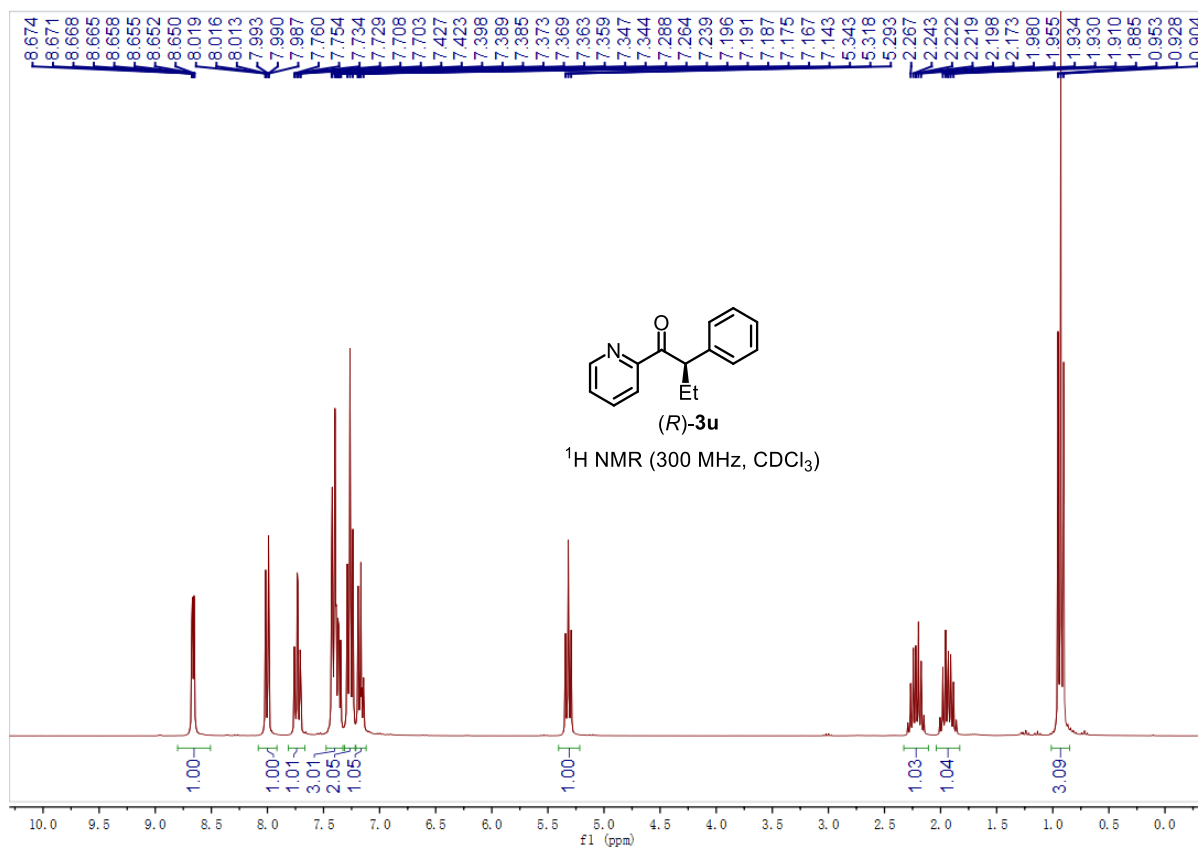




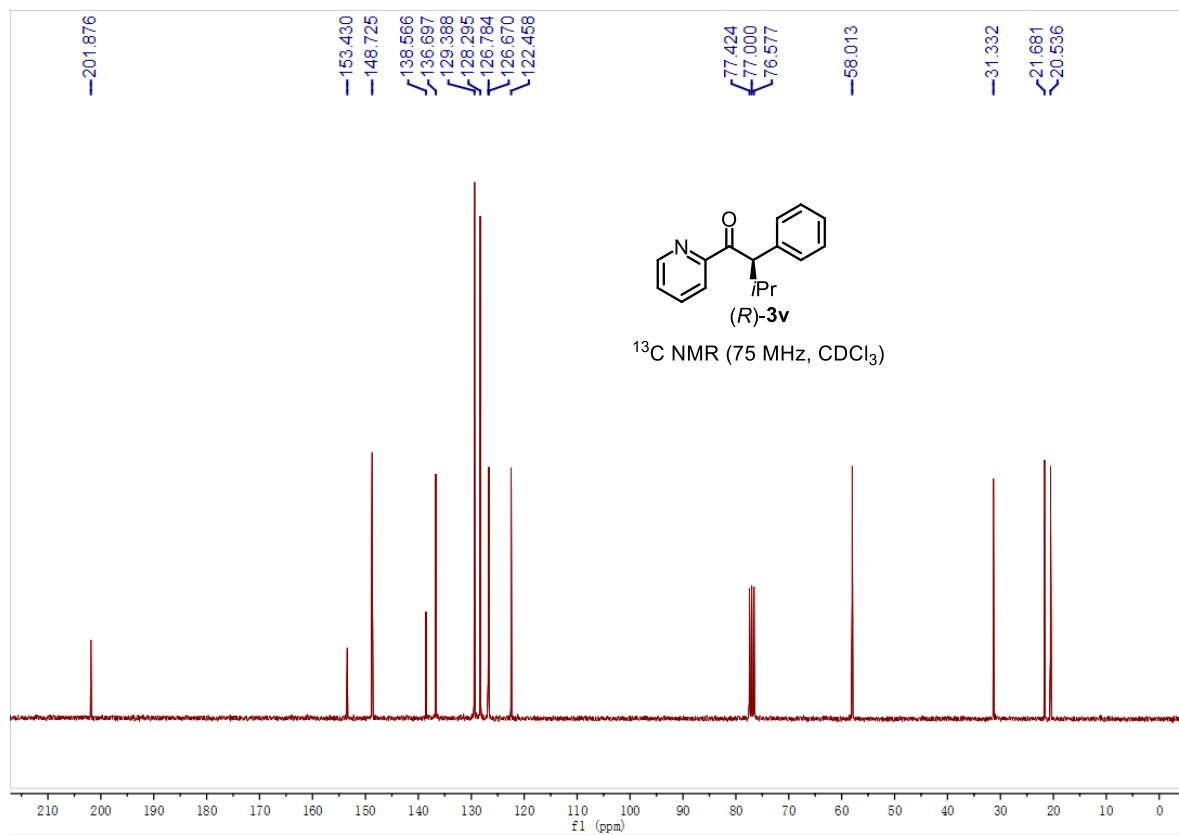
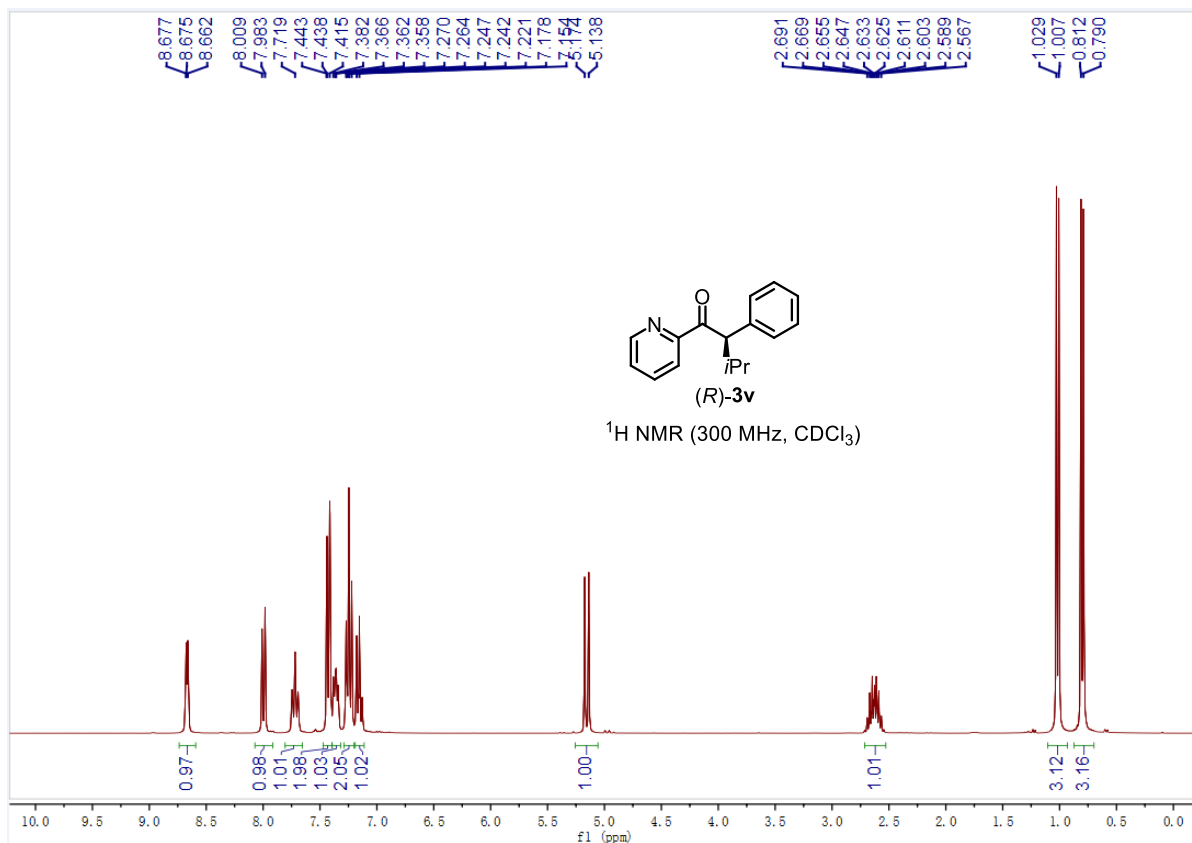




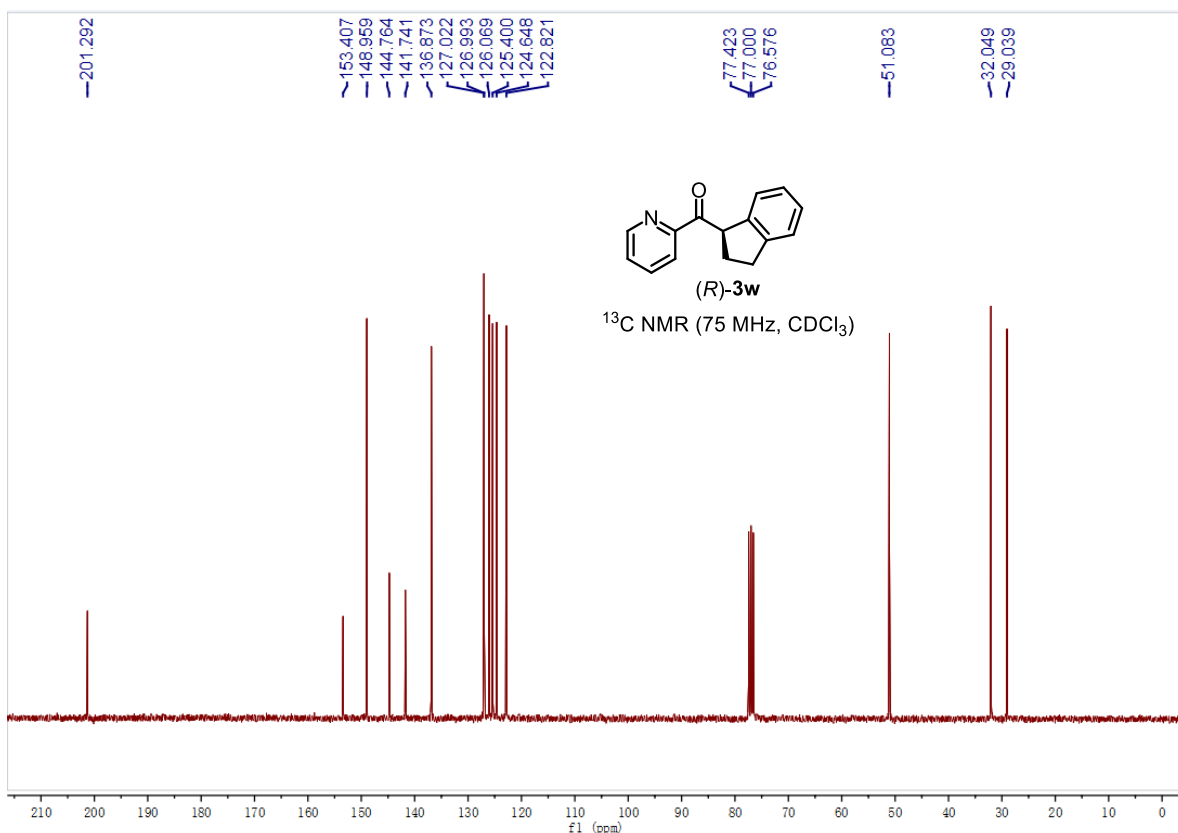
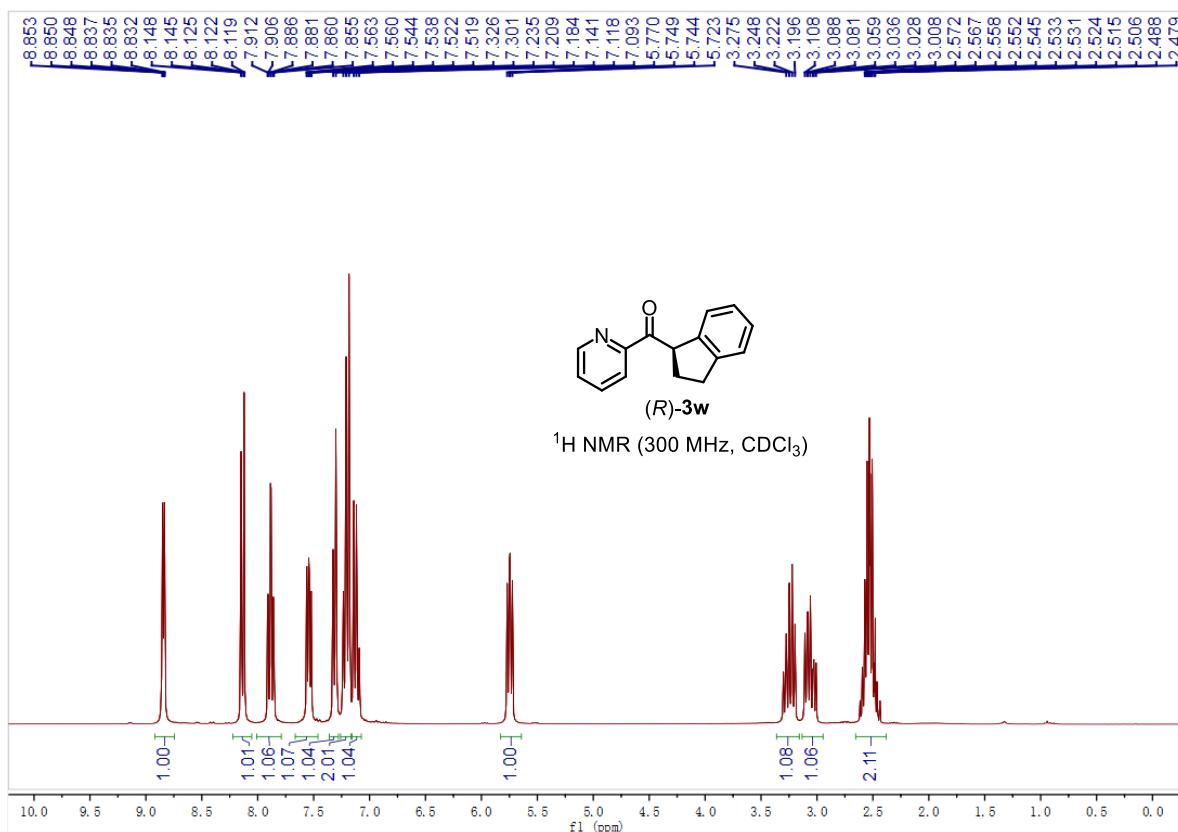
Chapter 5. Appendices



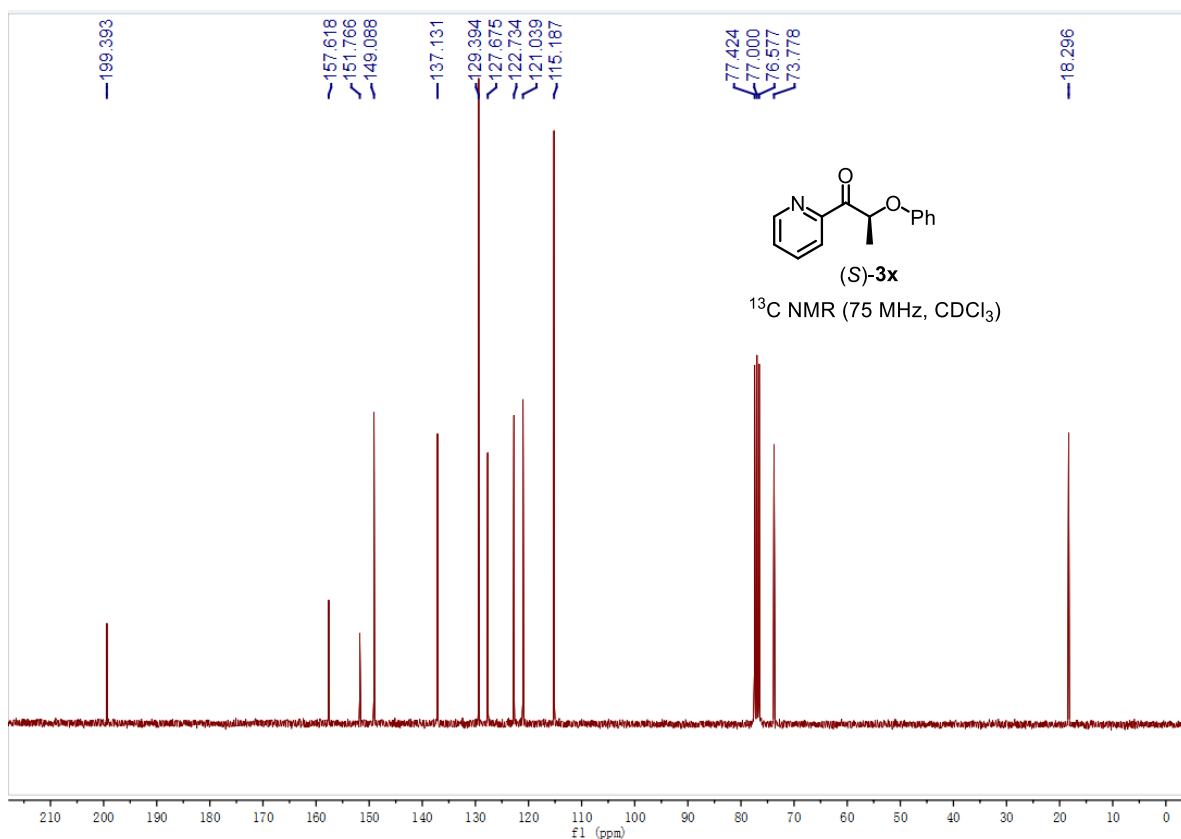
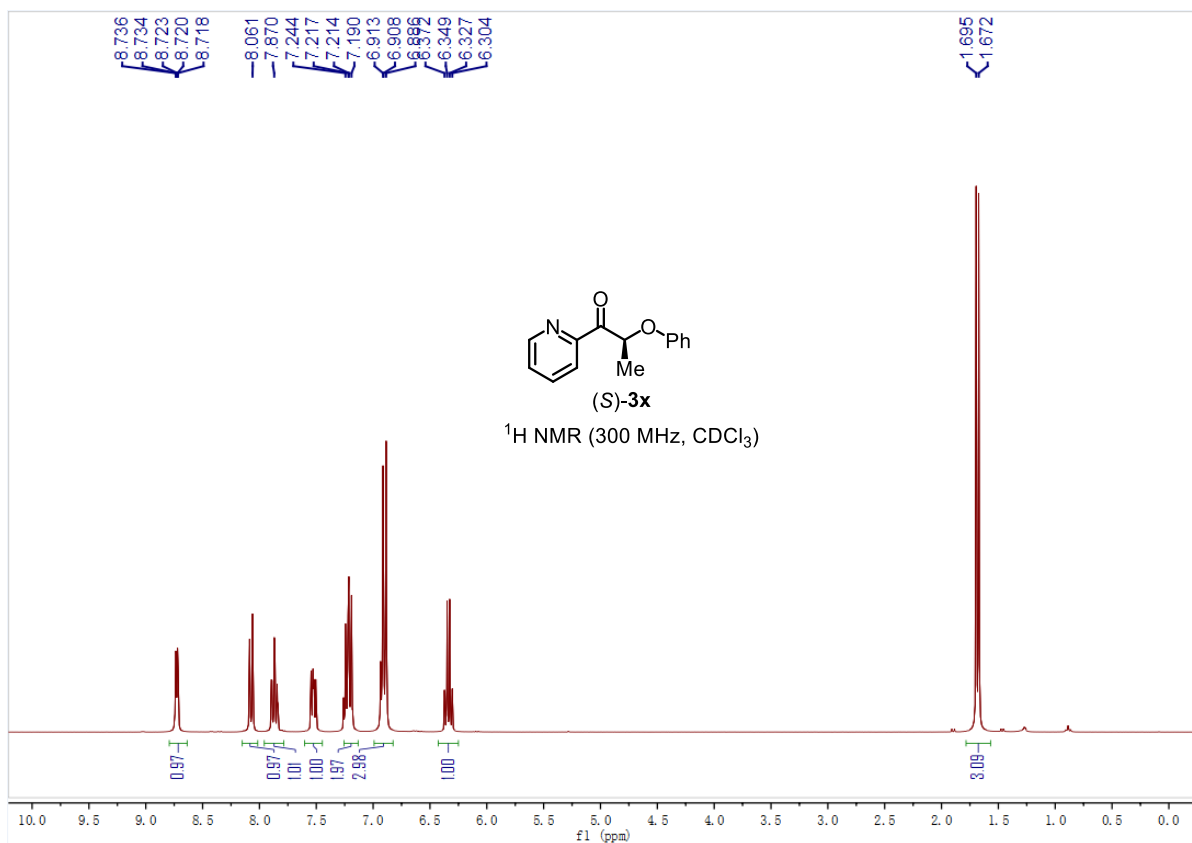
Chapter 5. Appendices

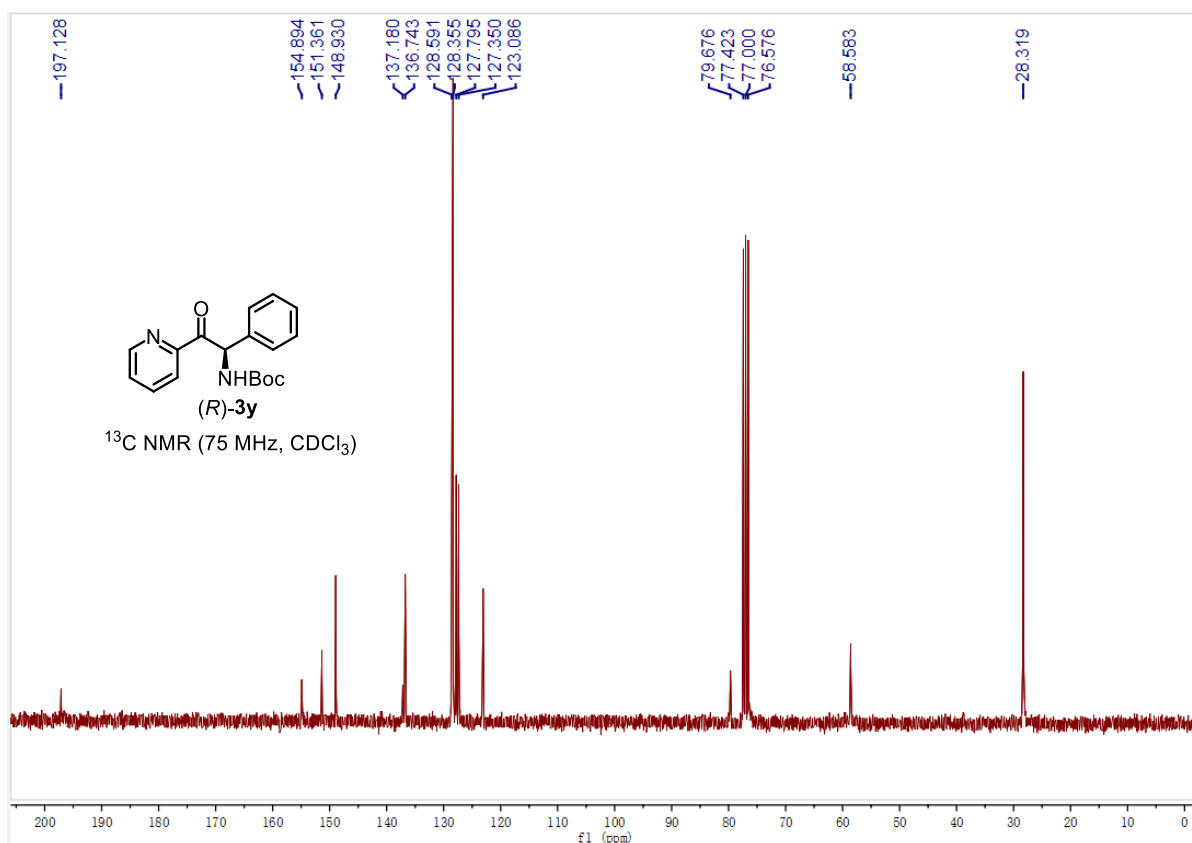
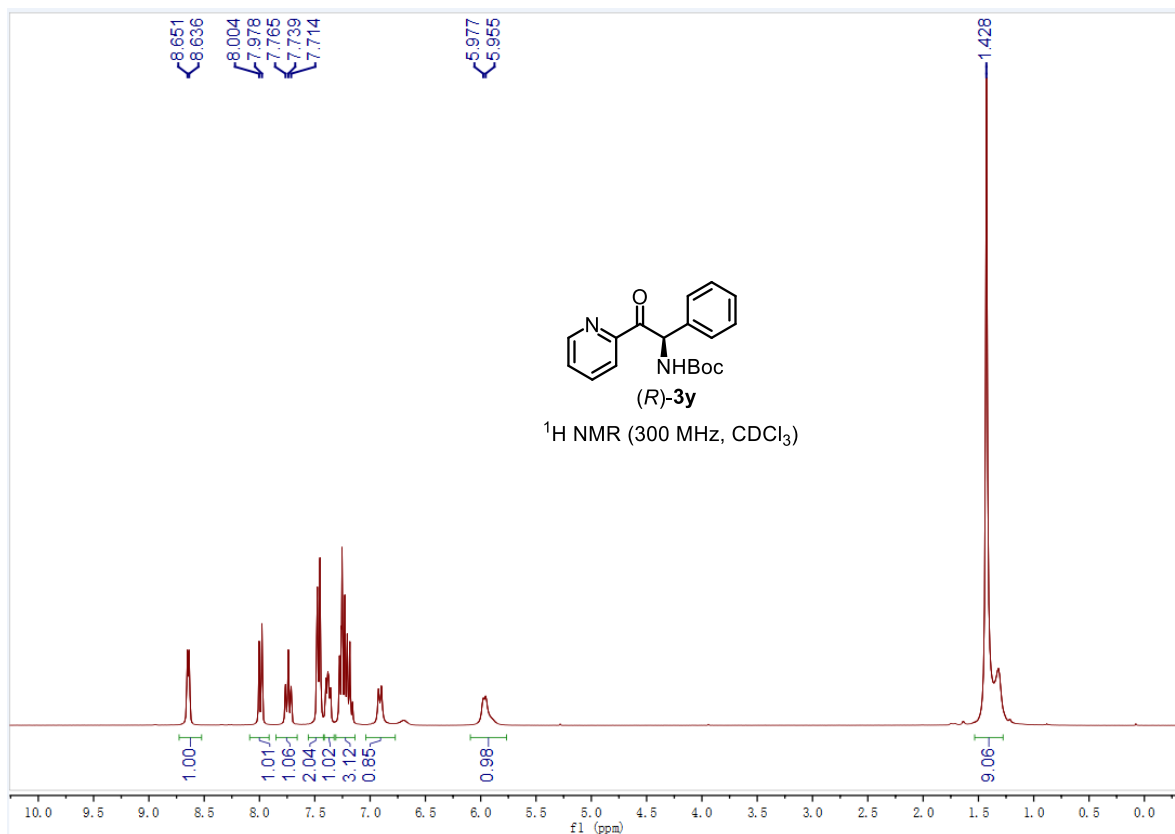


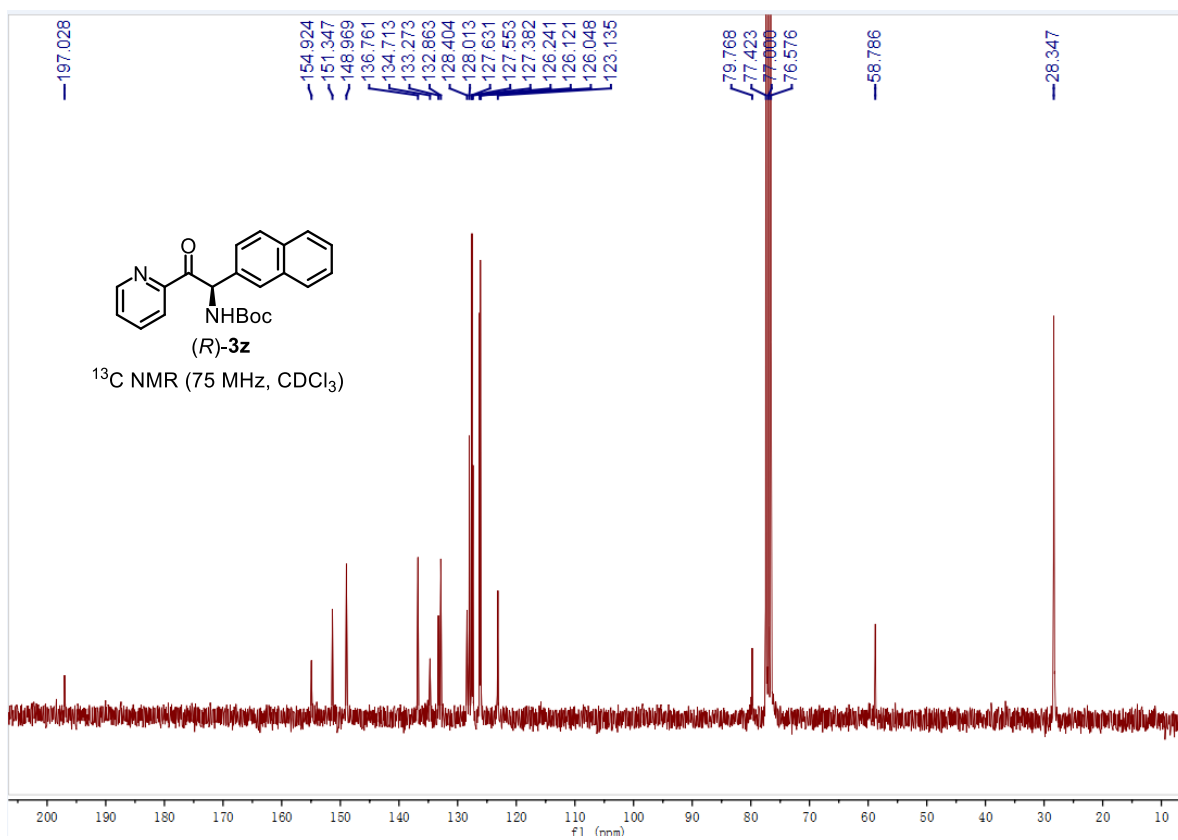
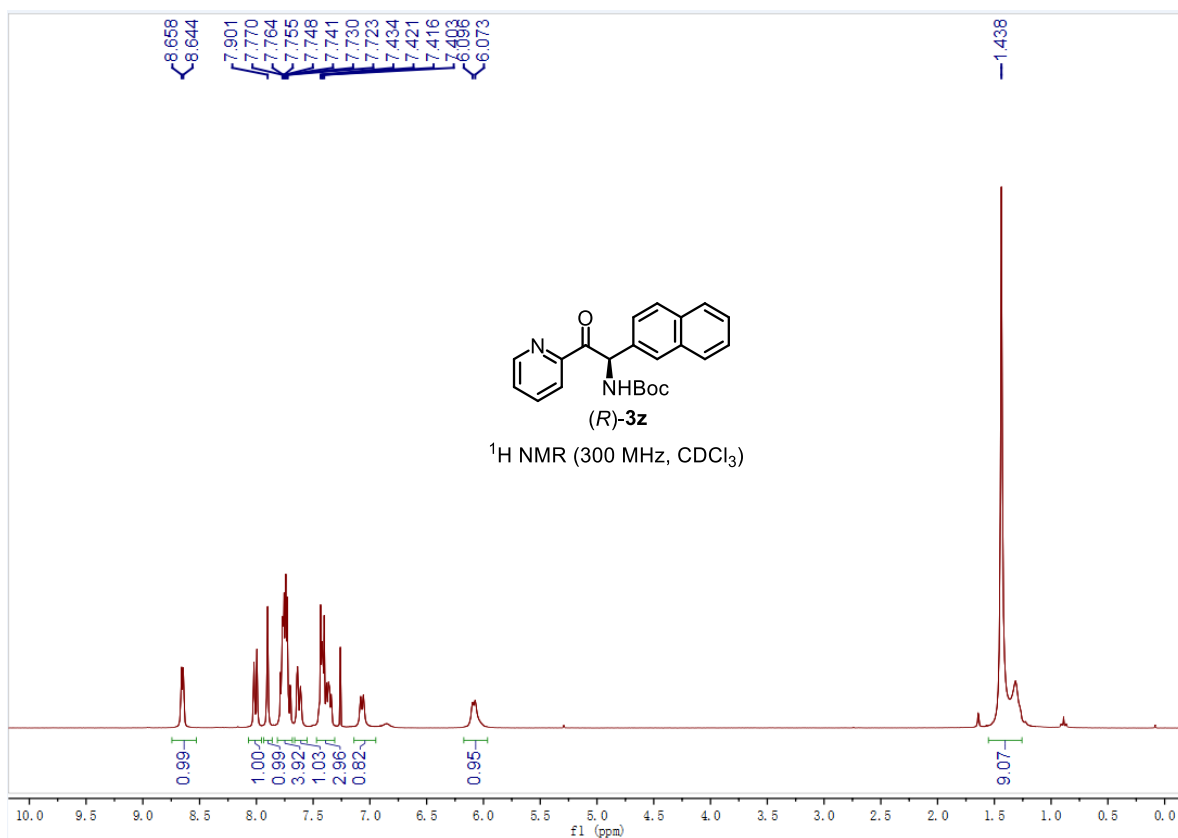
Chapter 5. Appendices

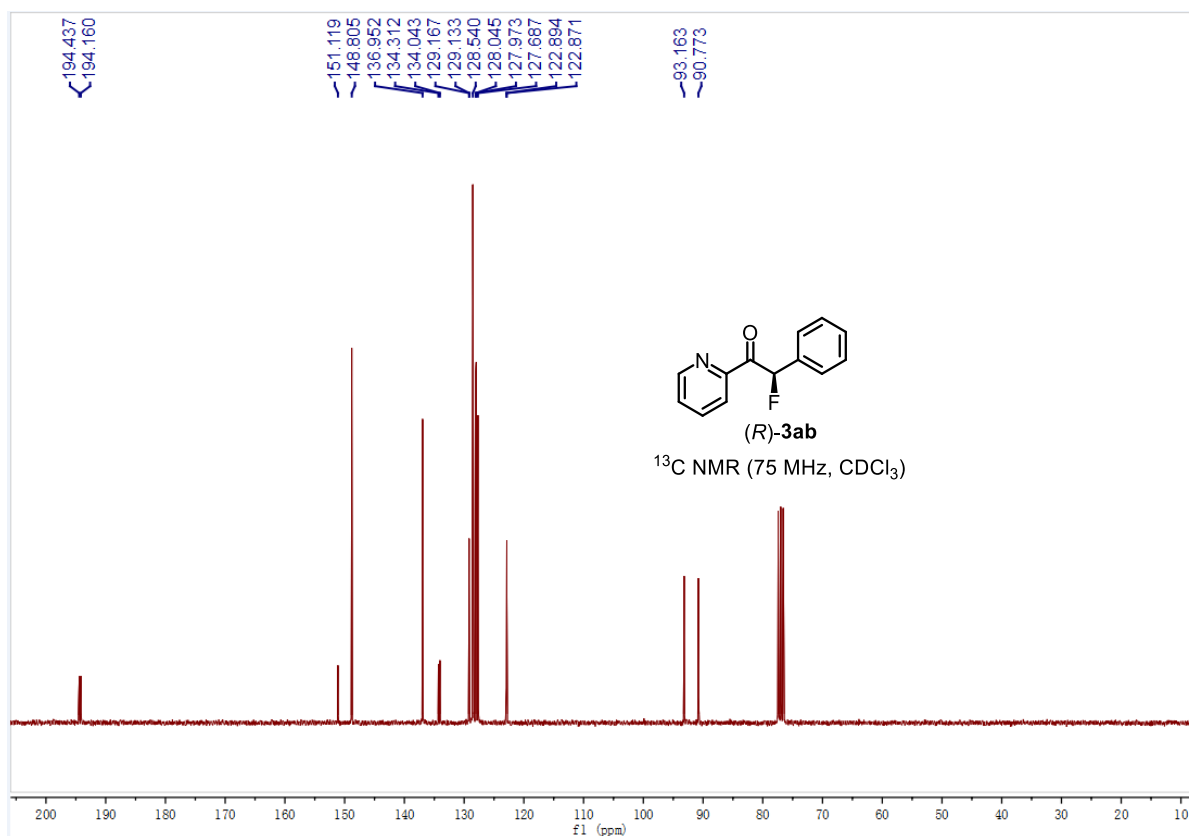
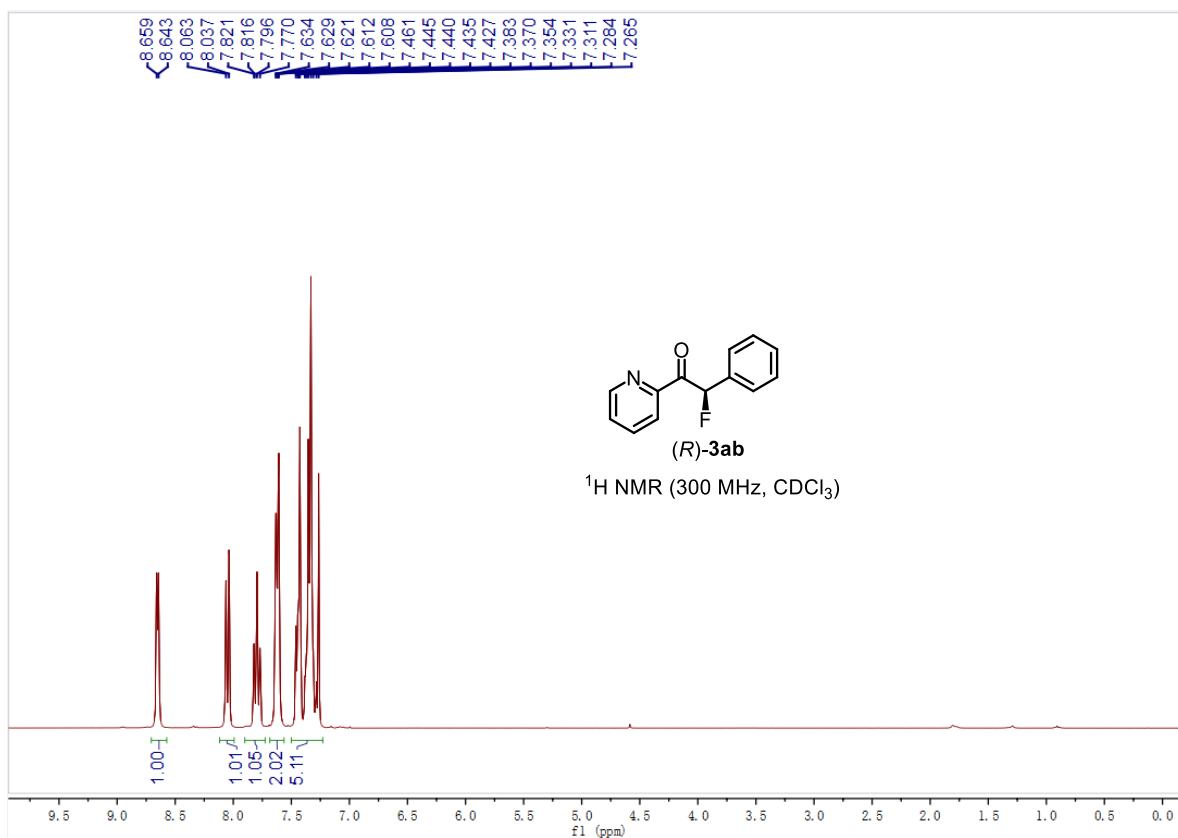


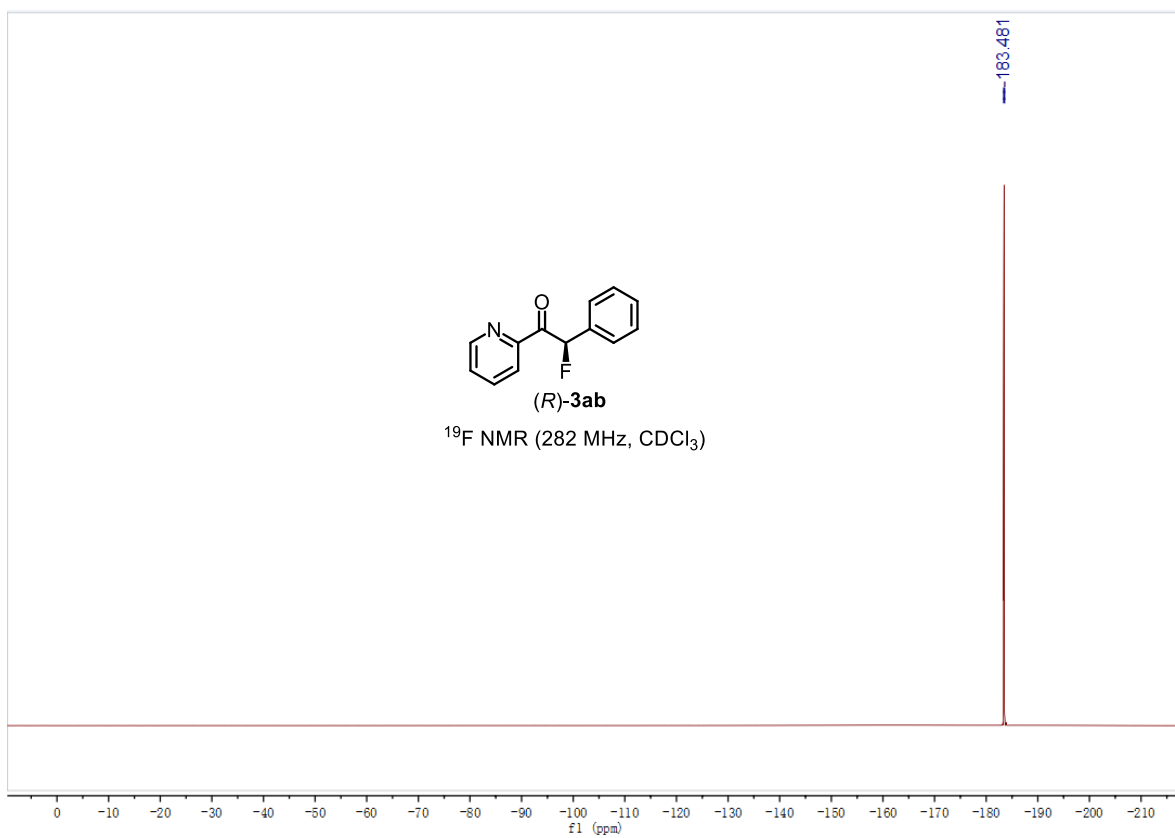
Chapter 5. Appendices



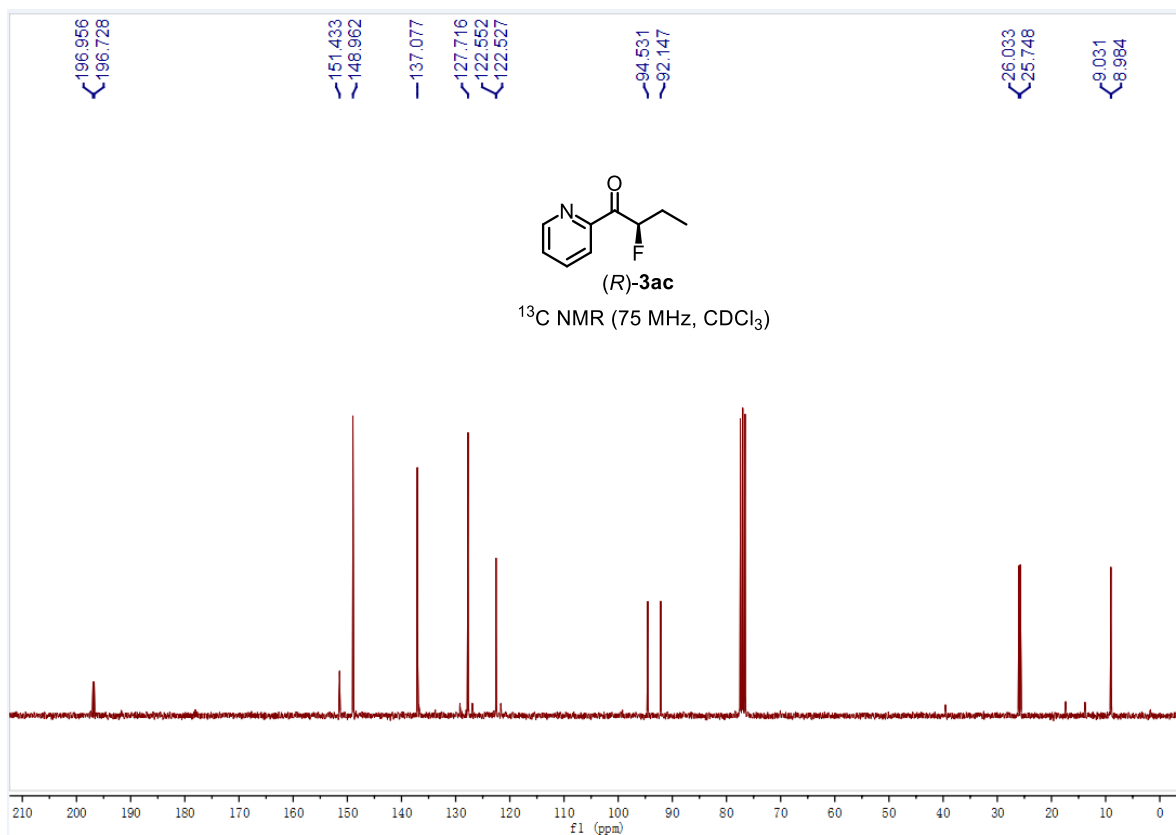
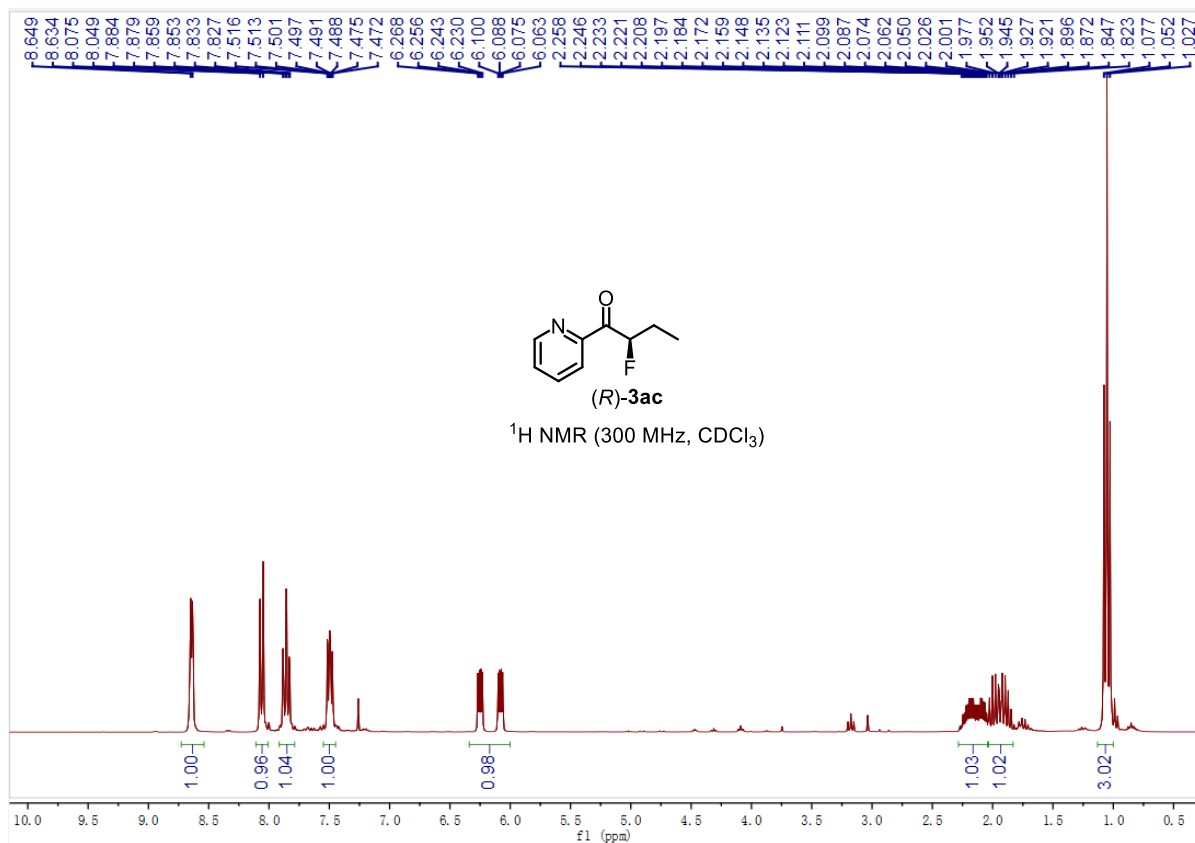


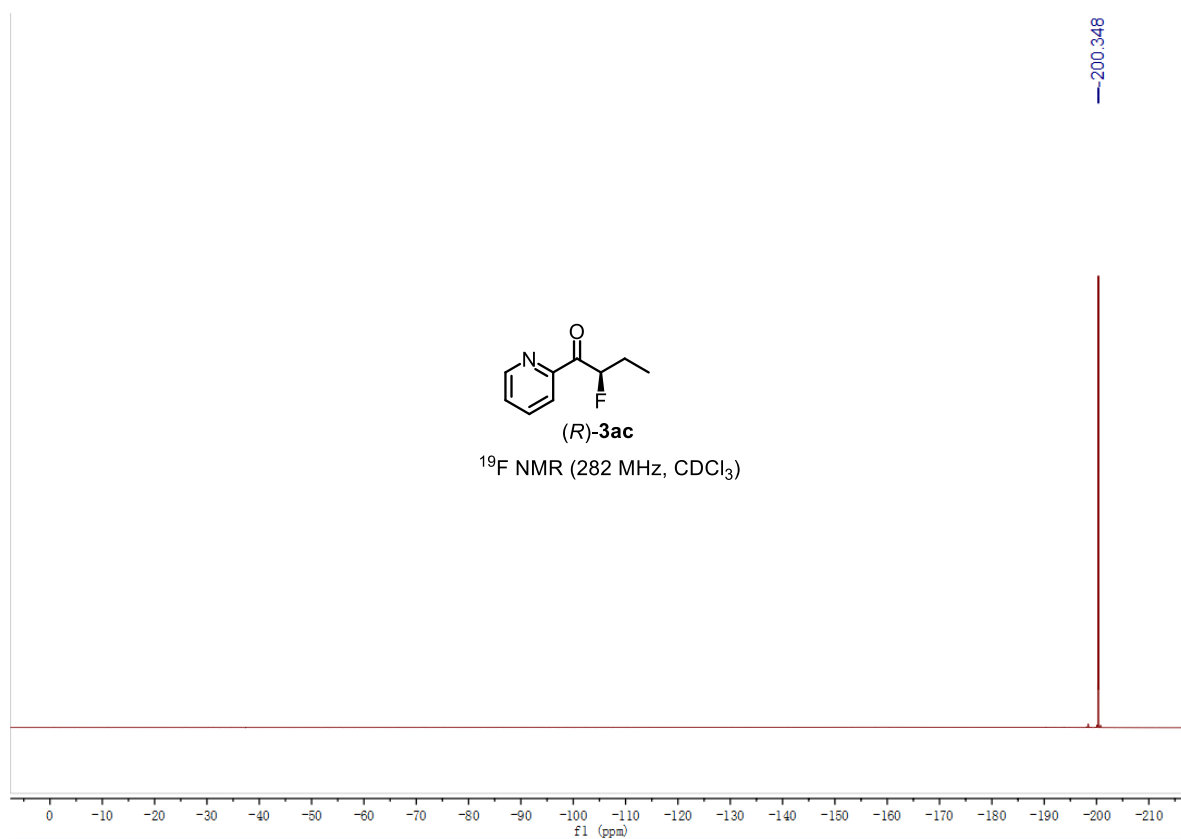




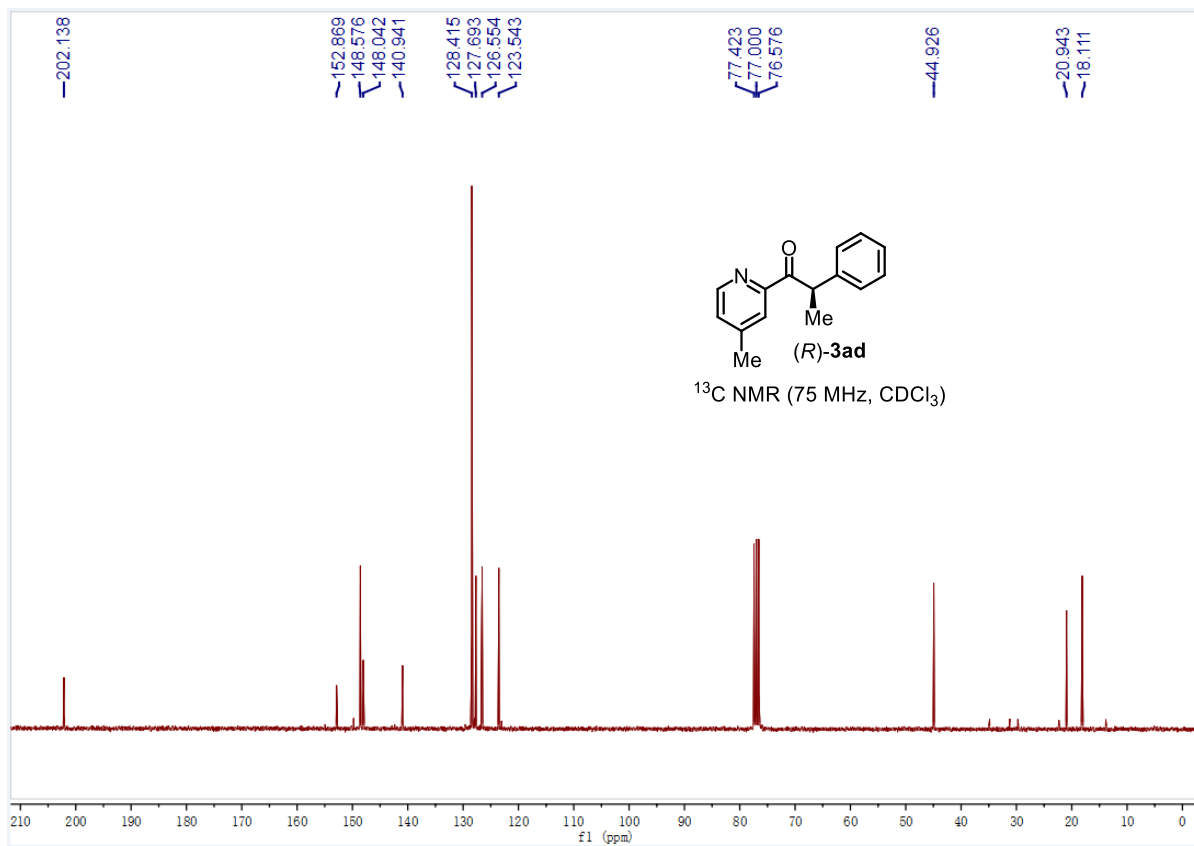
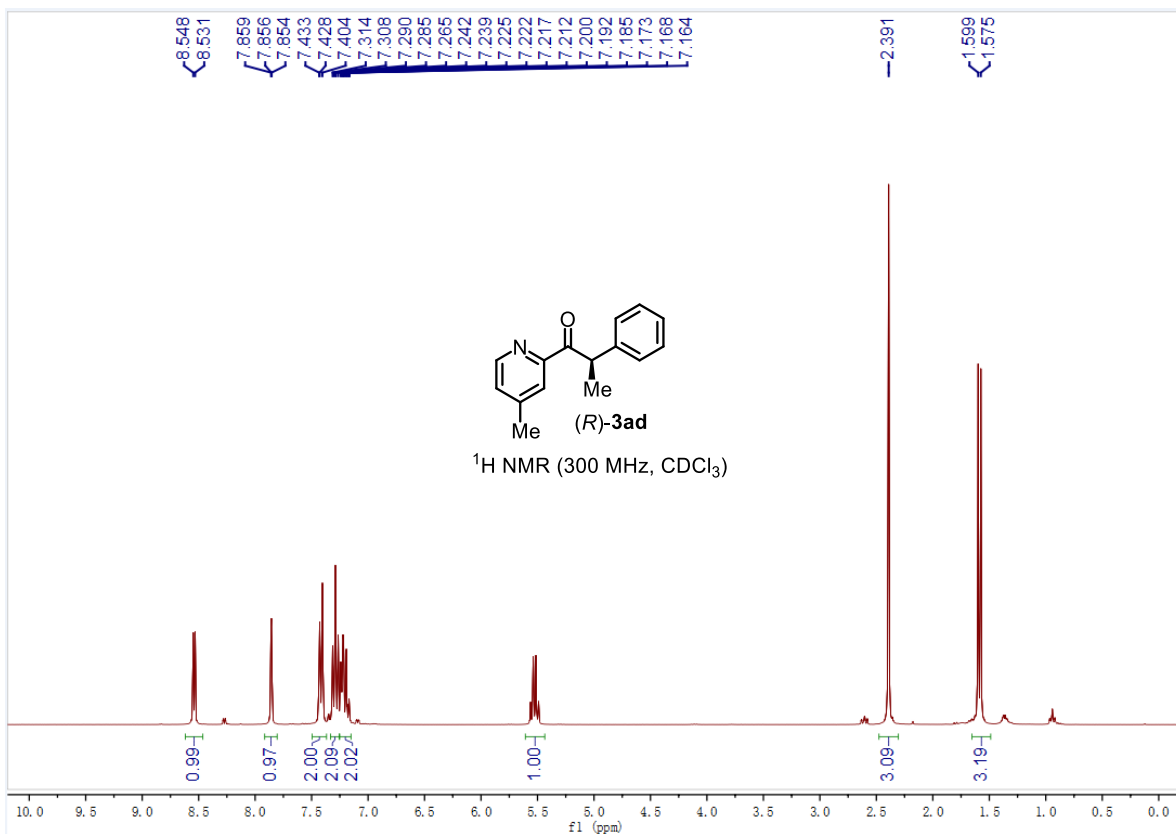


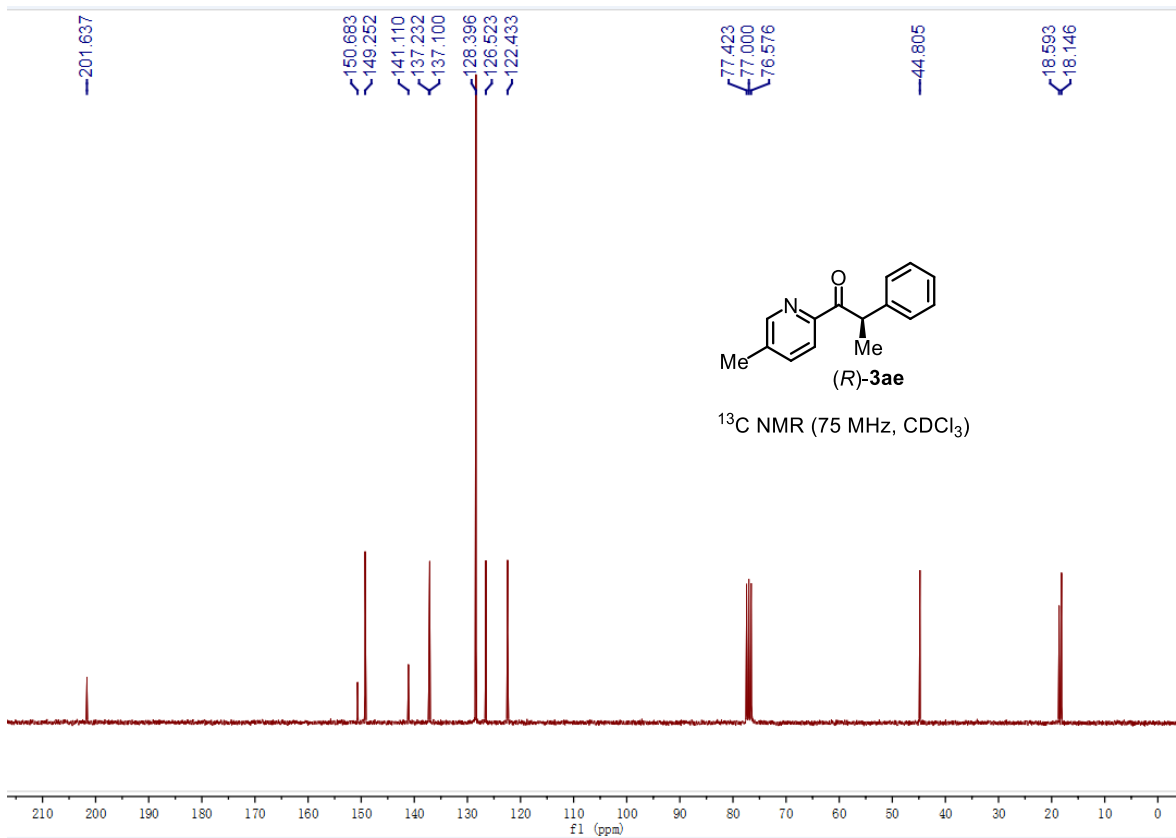
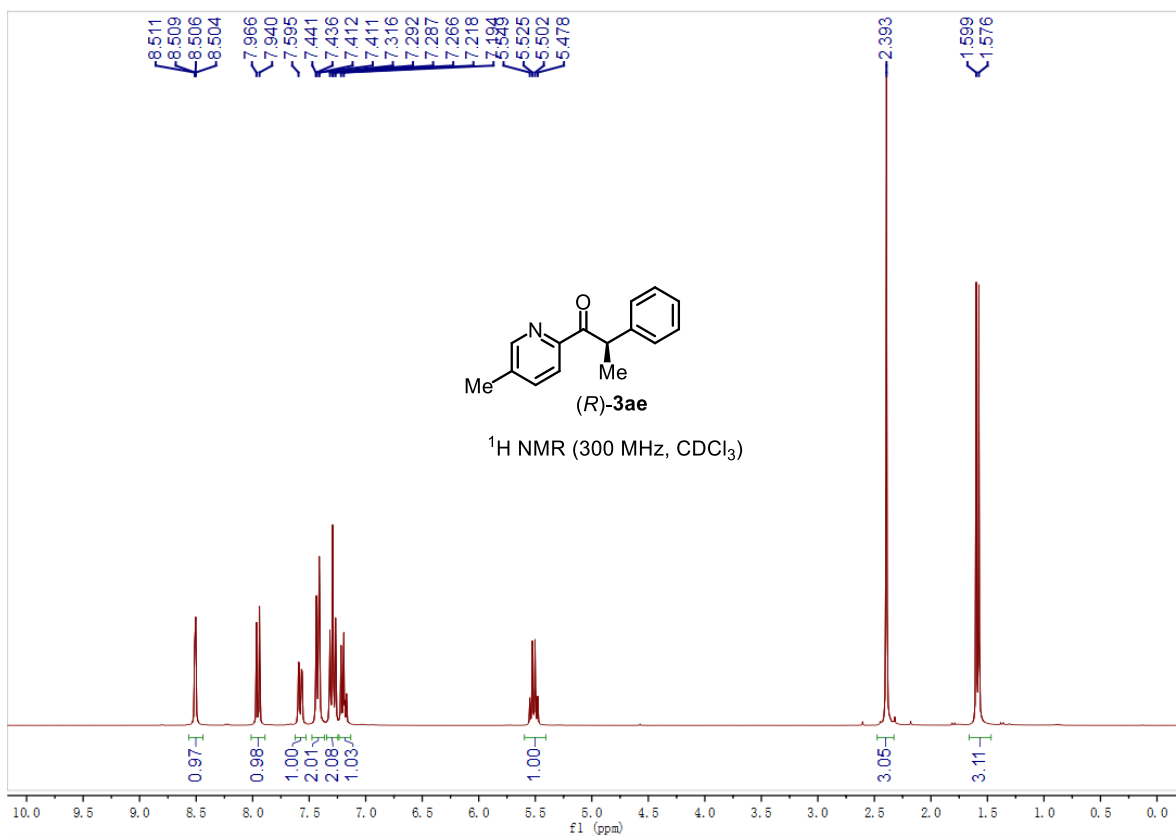
Chapter 5. Appendices

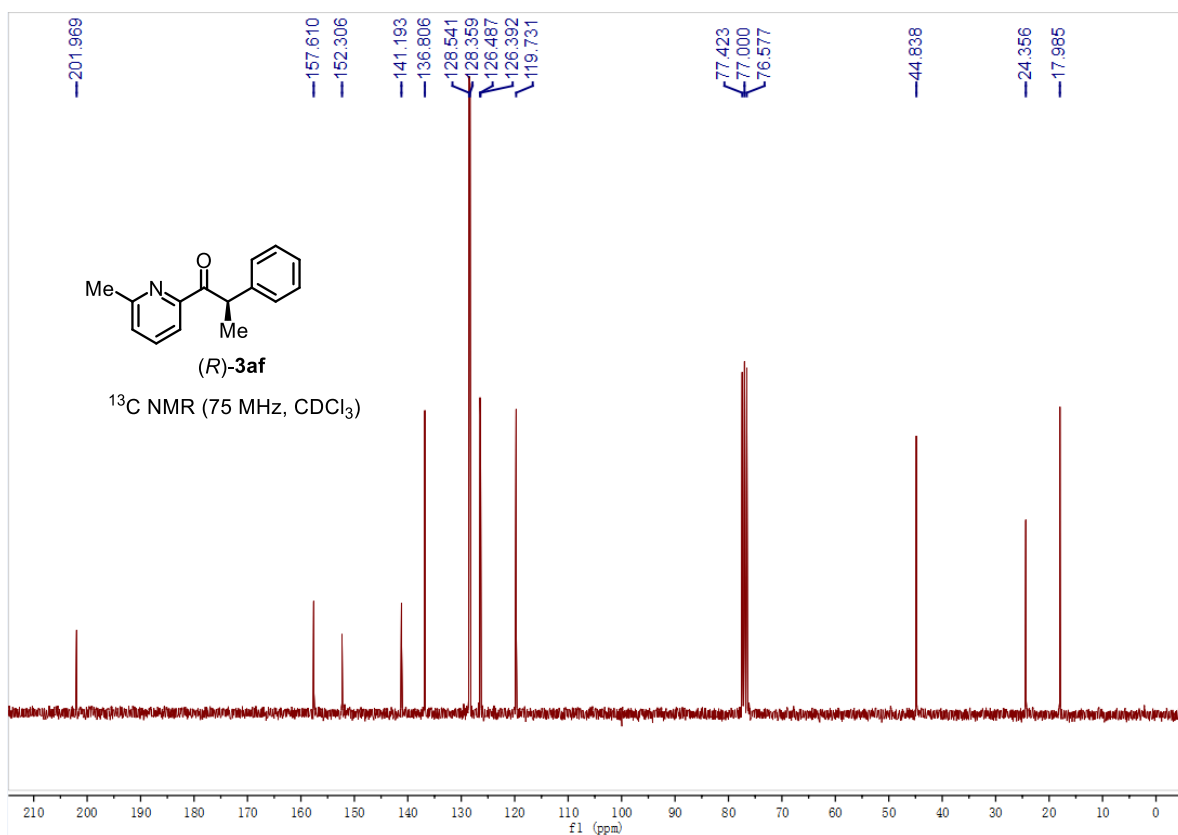
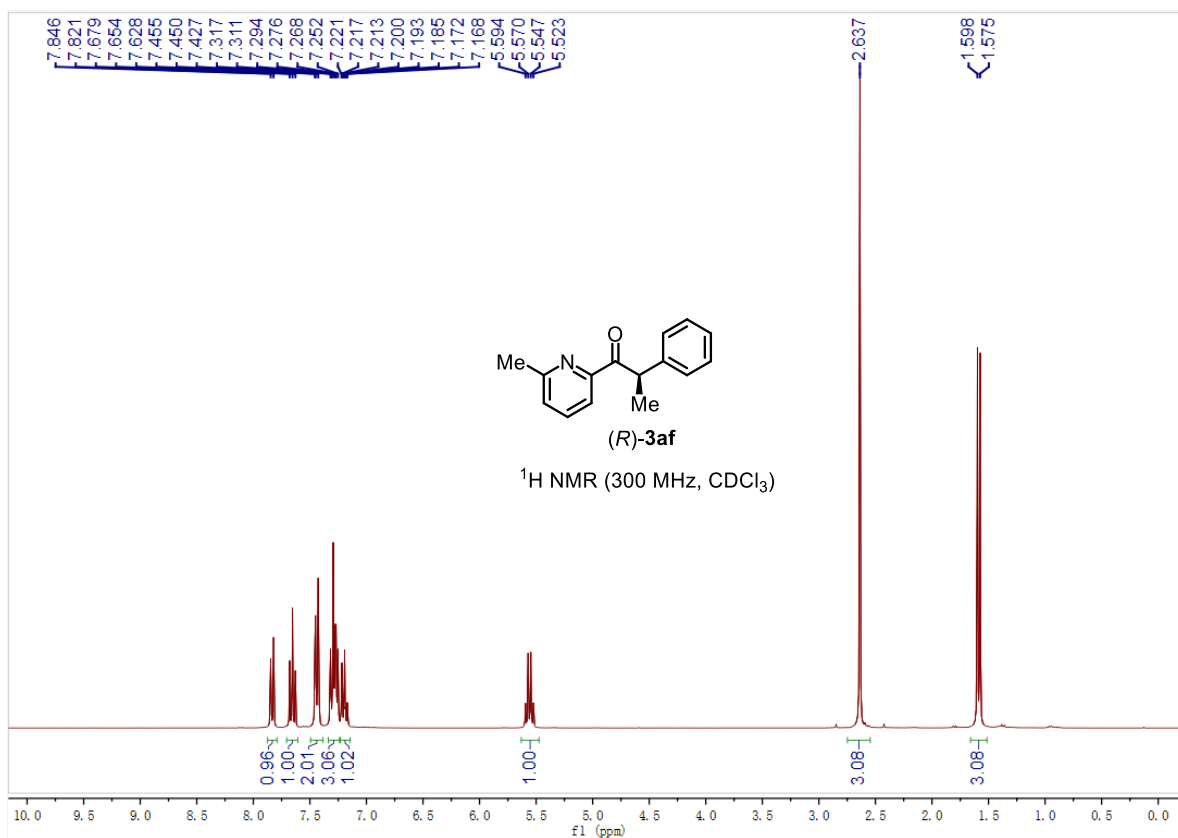




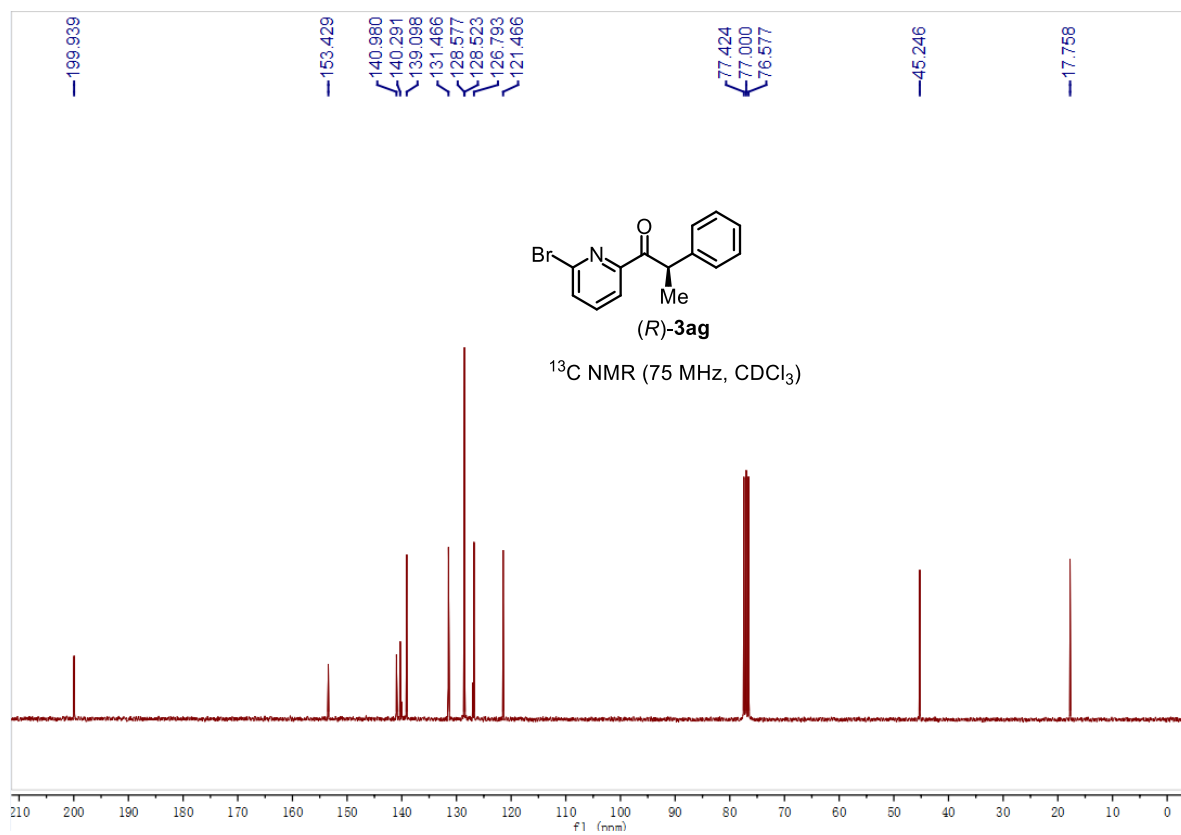
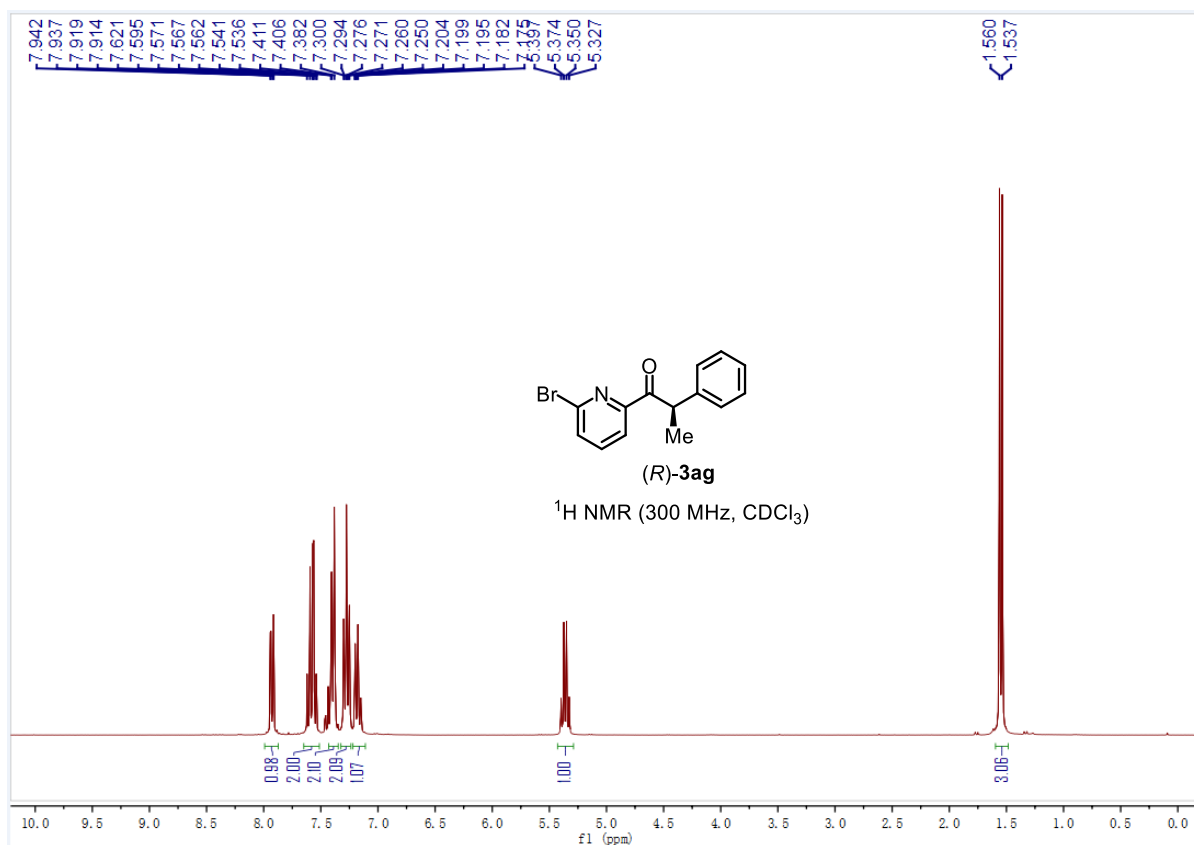
Chapter 5. Appendices



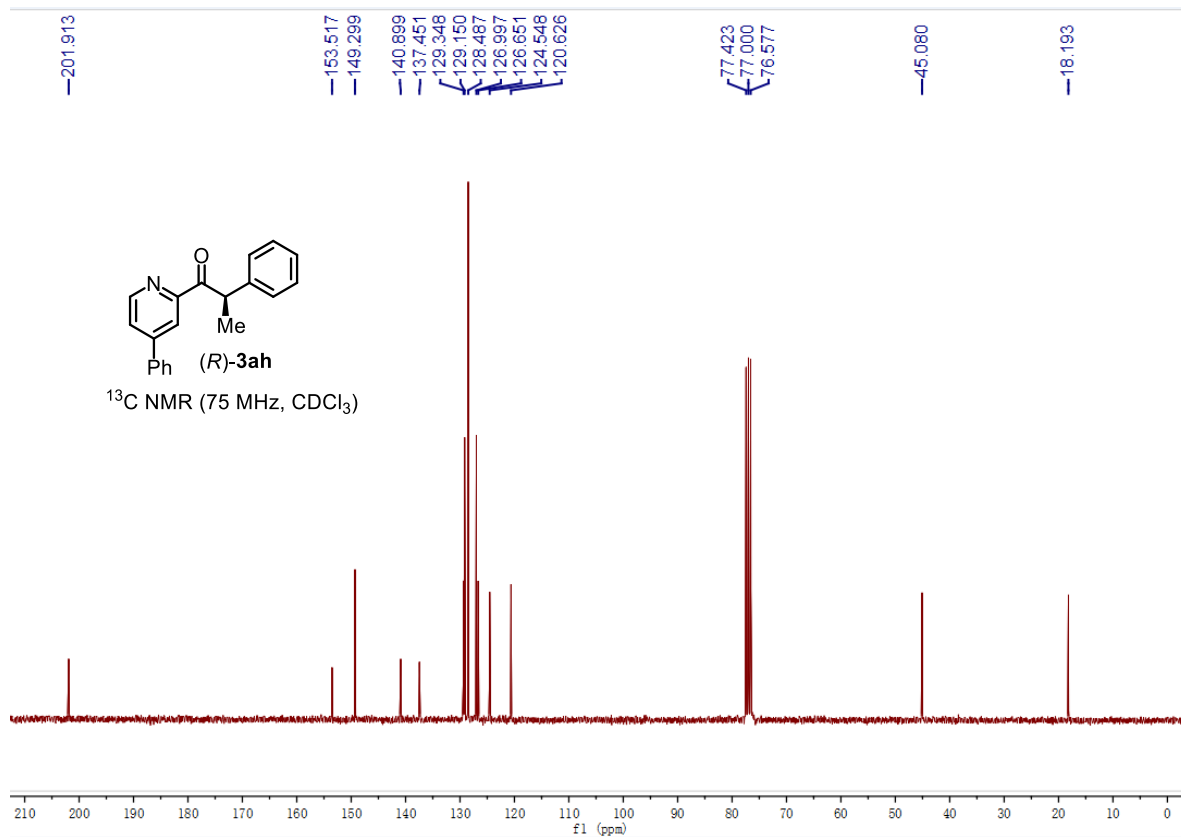
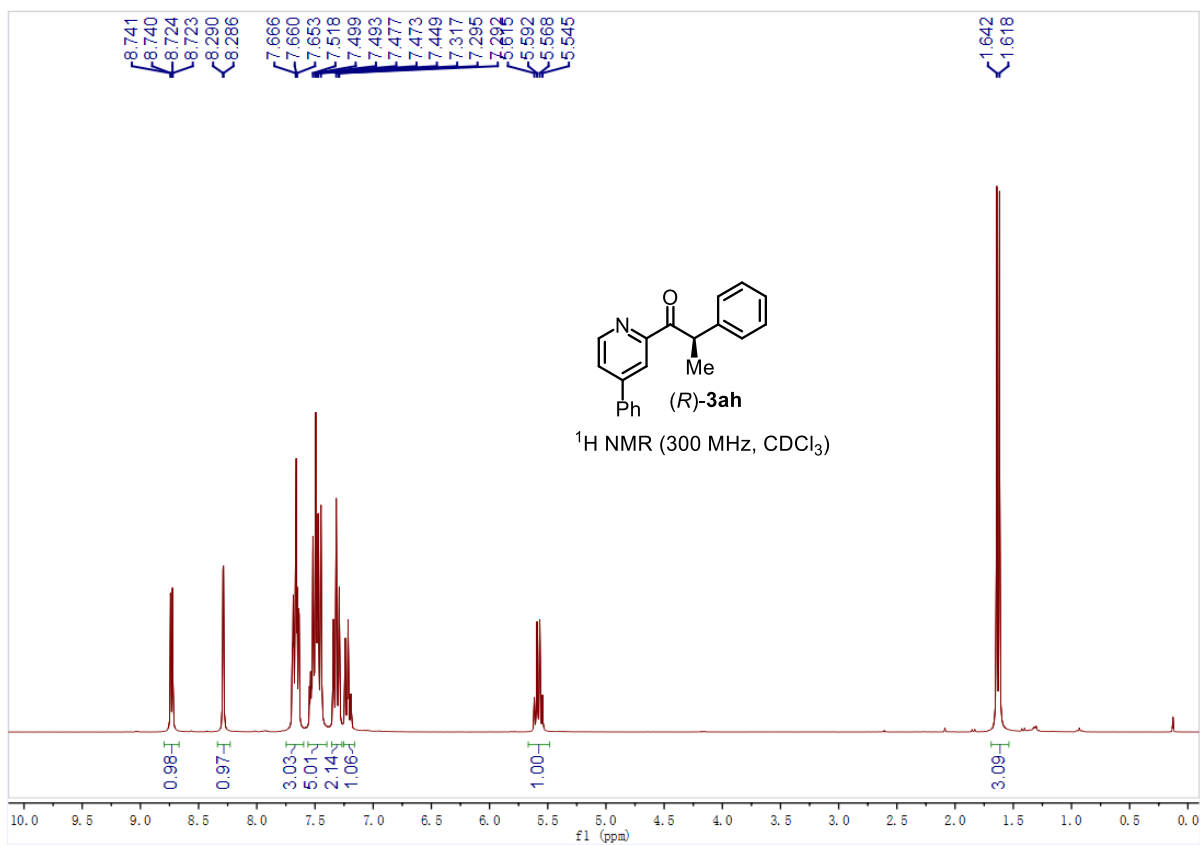


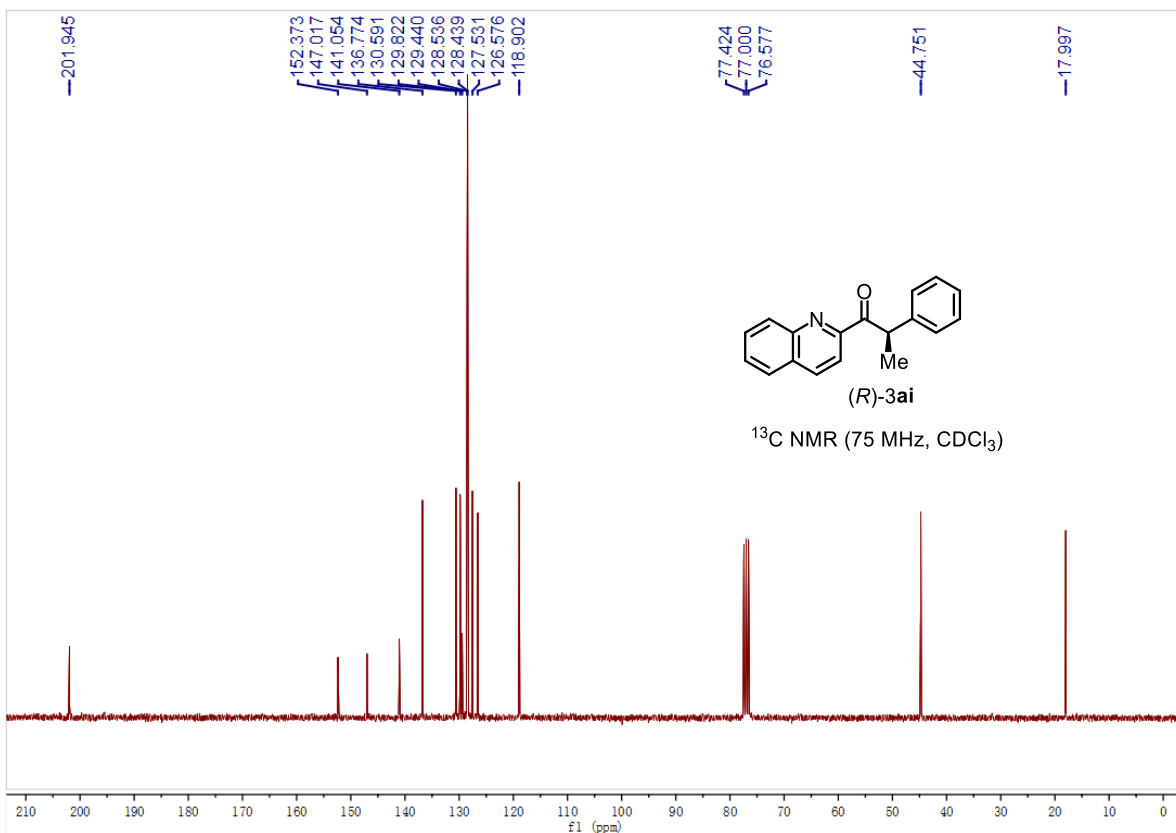
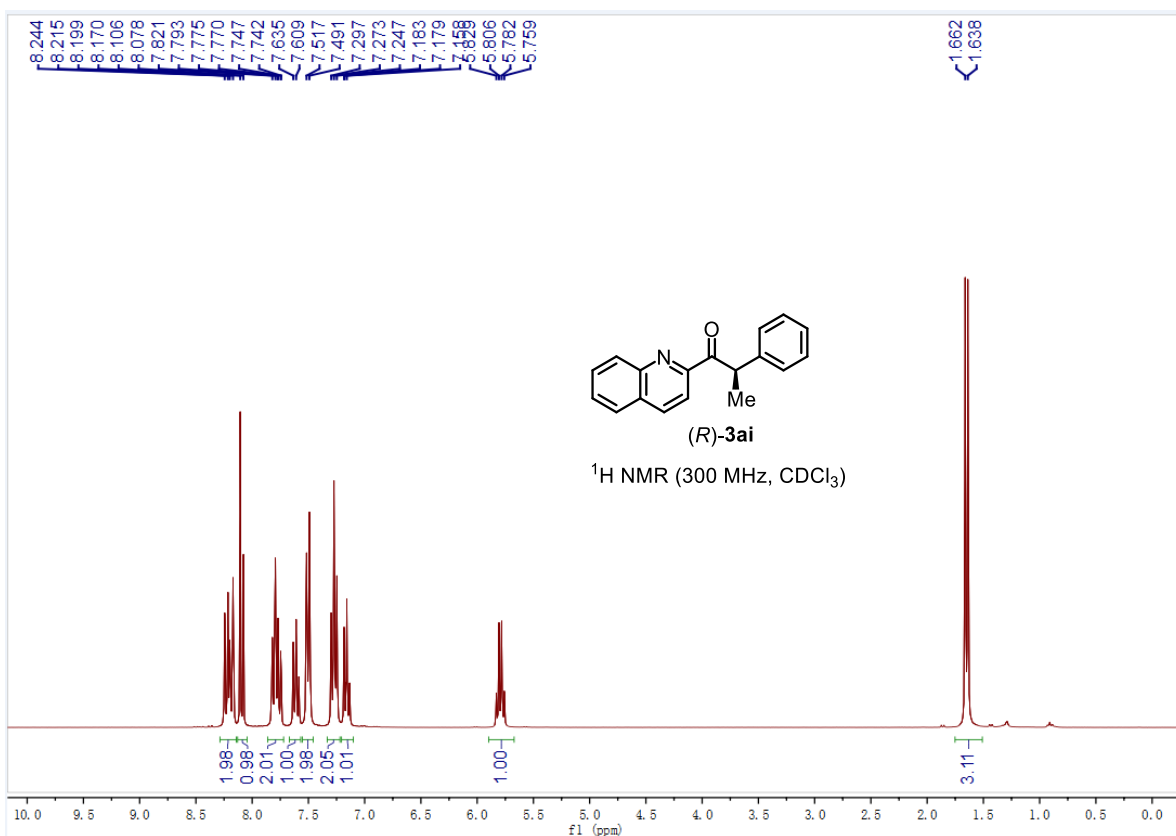


Chapter 5. Appendices

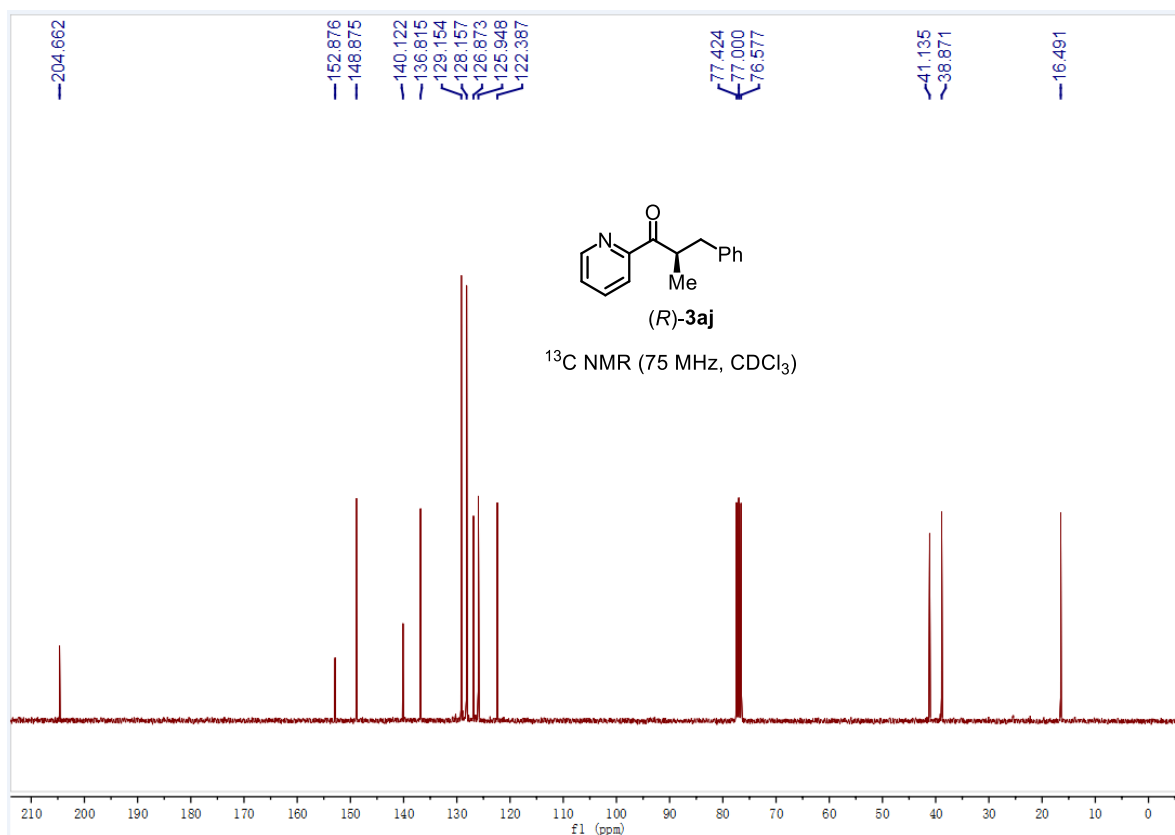
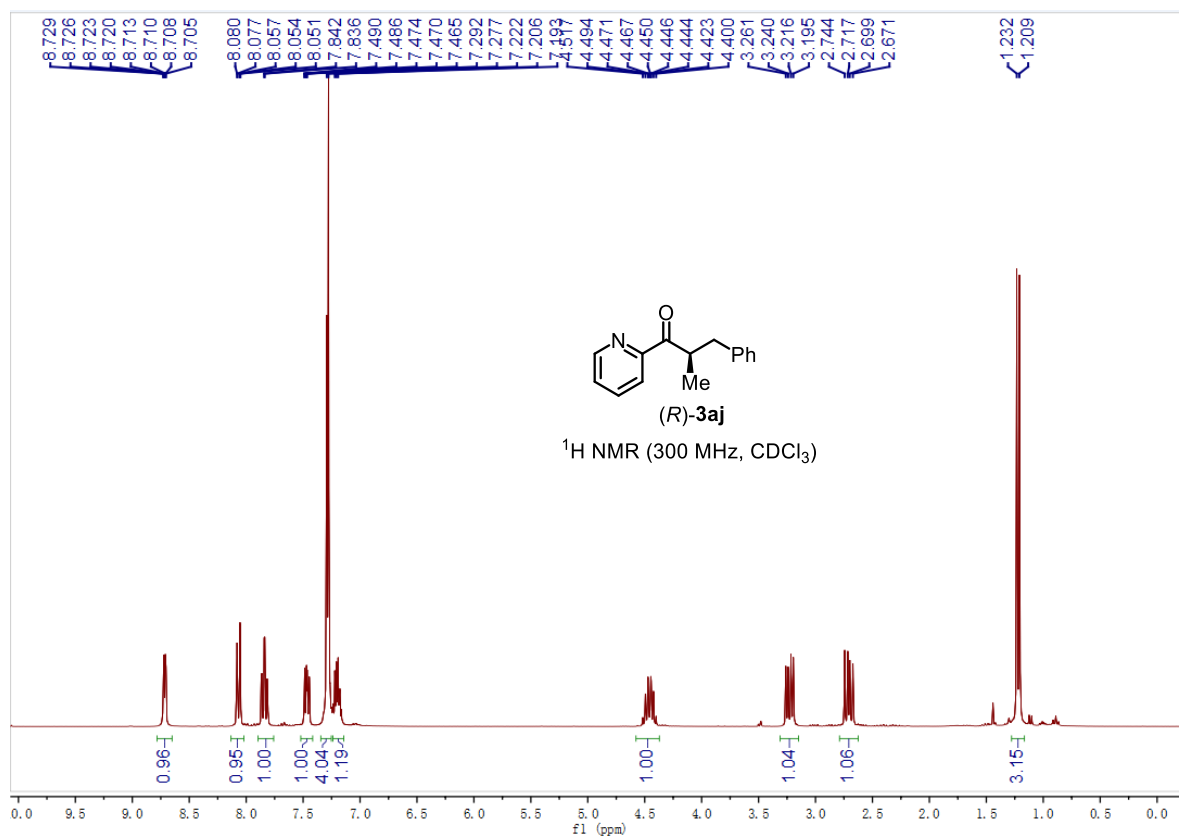


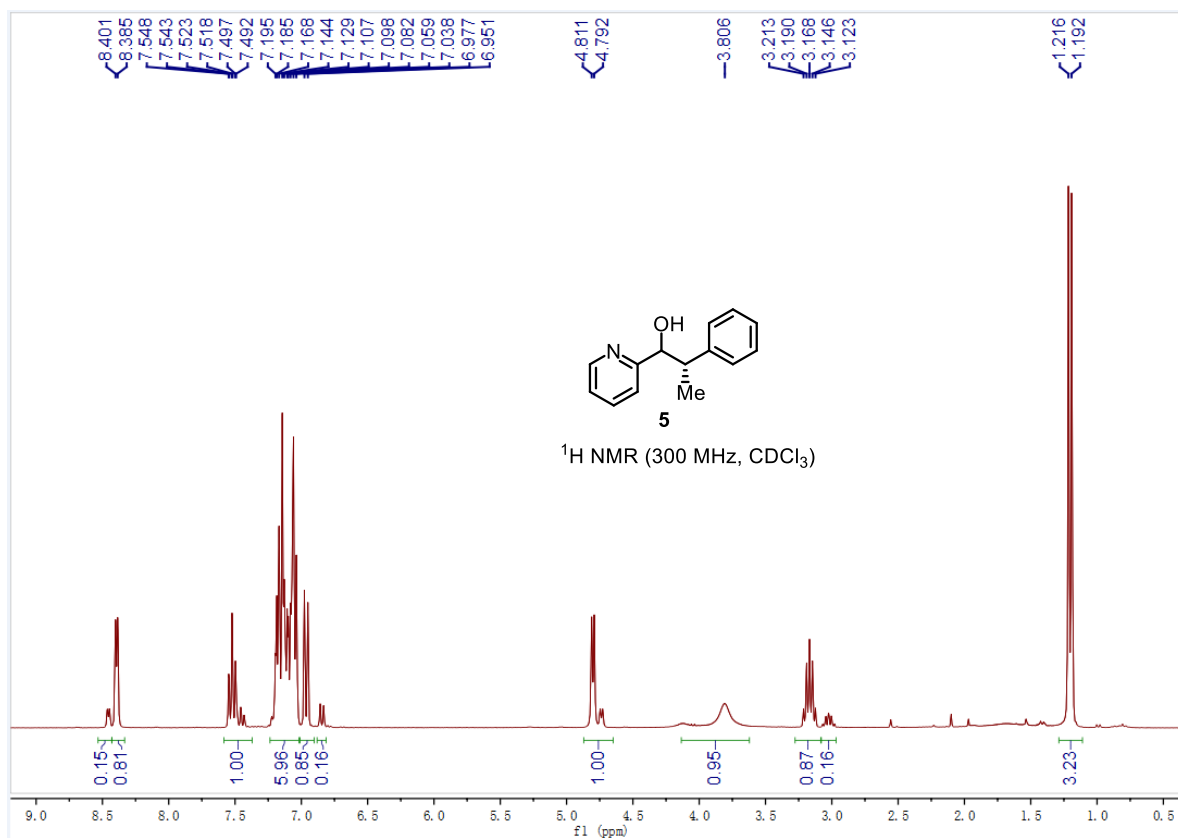
Chapter 5. Appendices

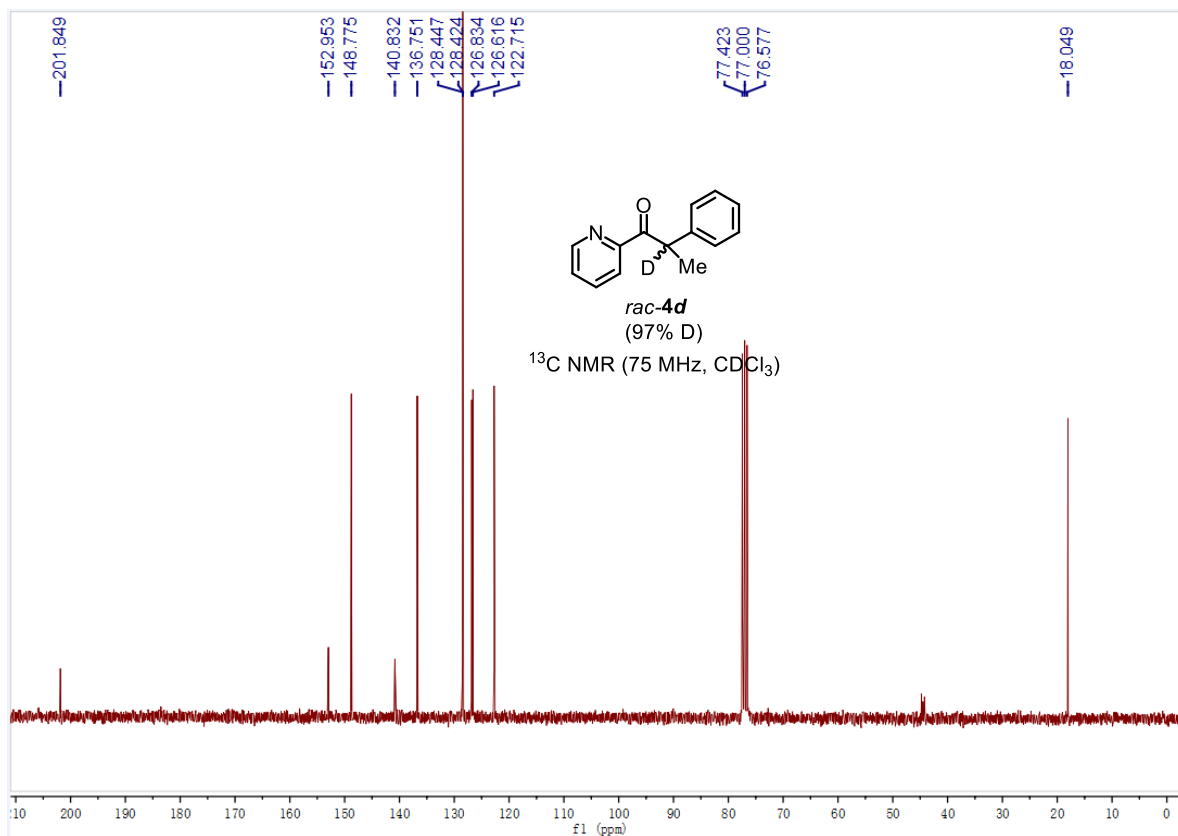
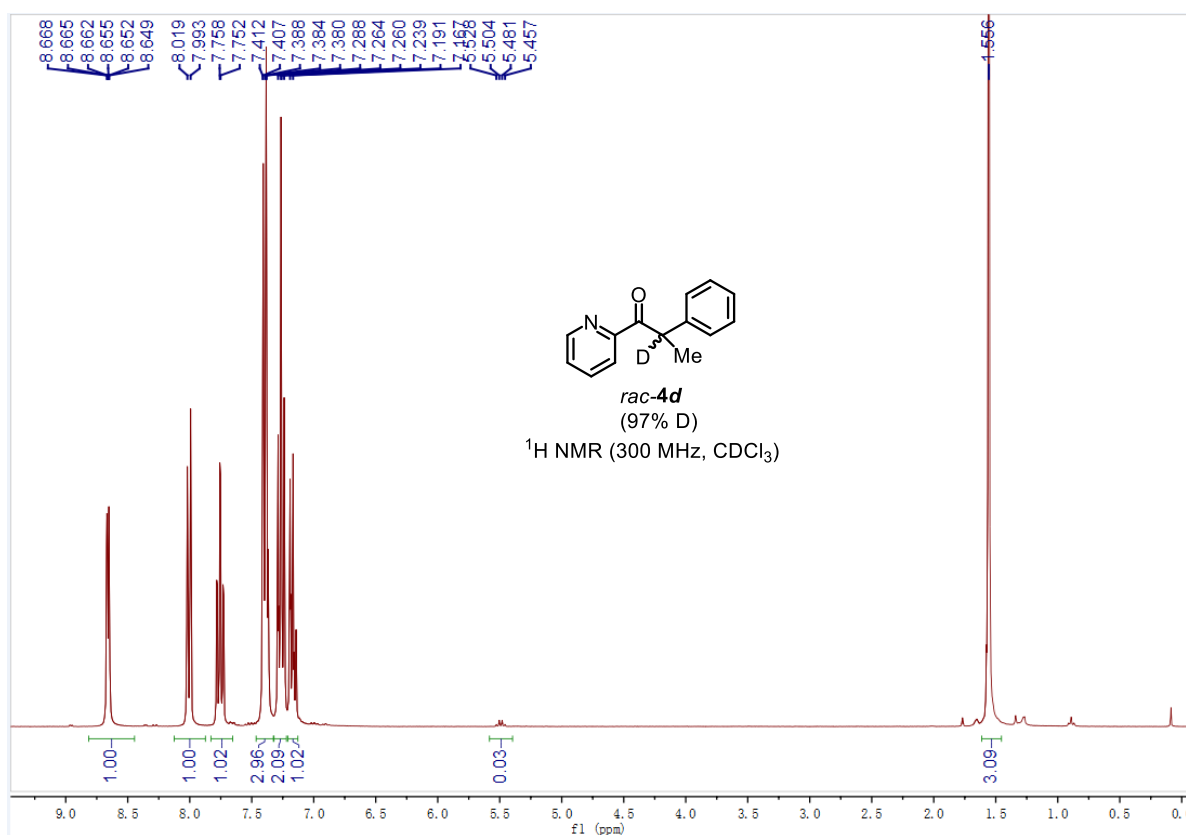


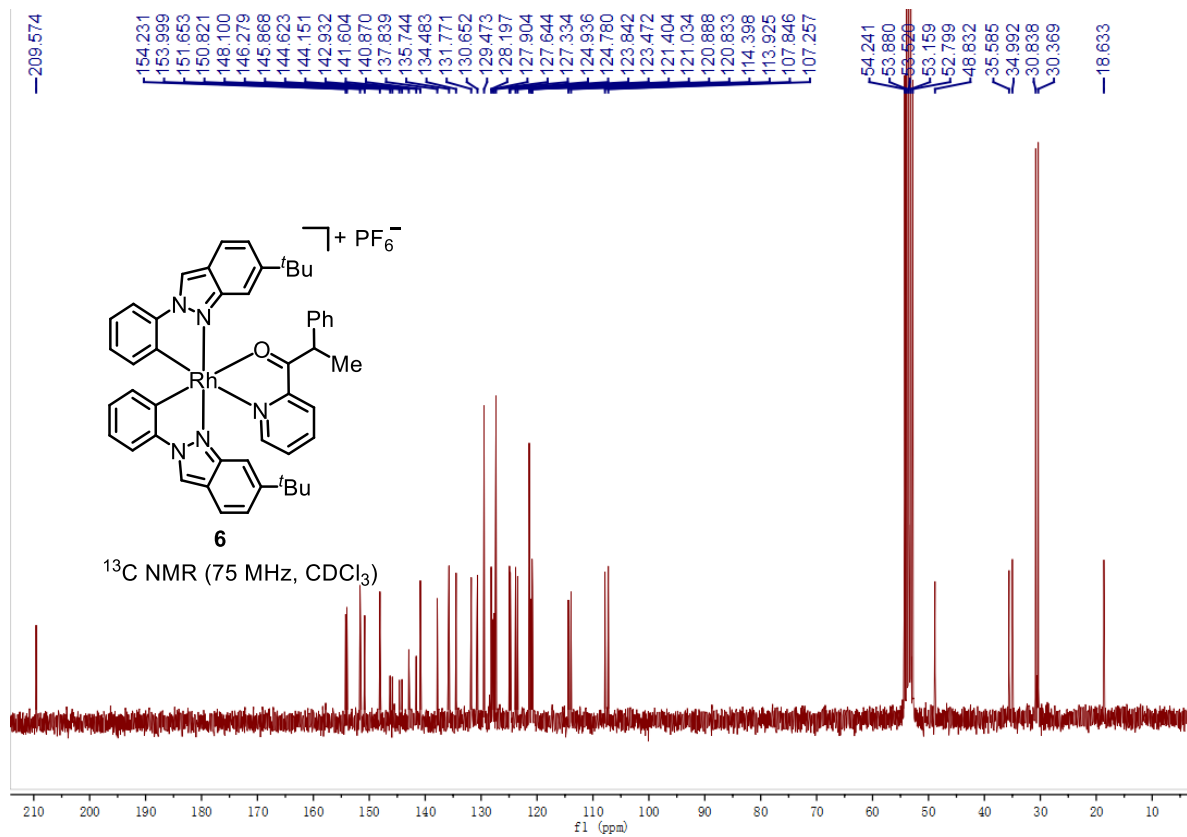
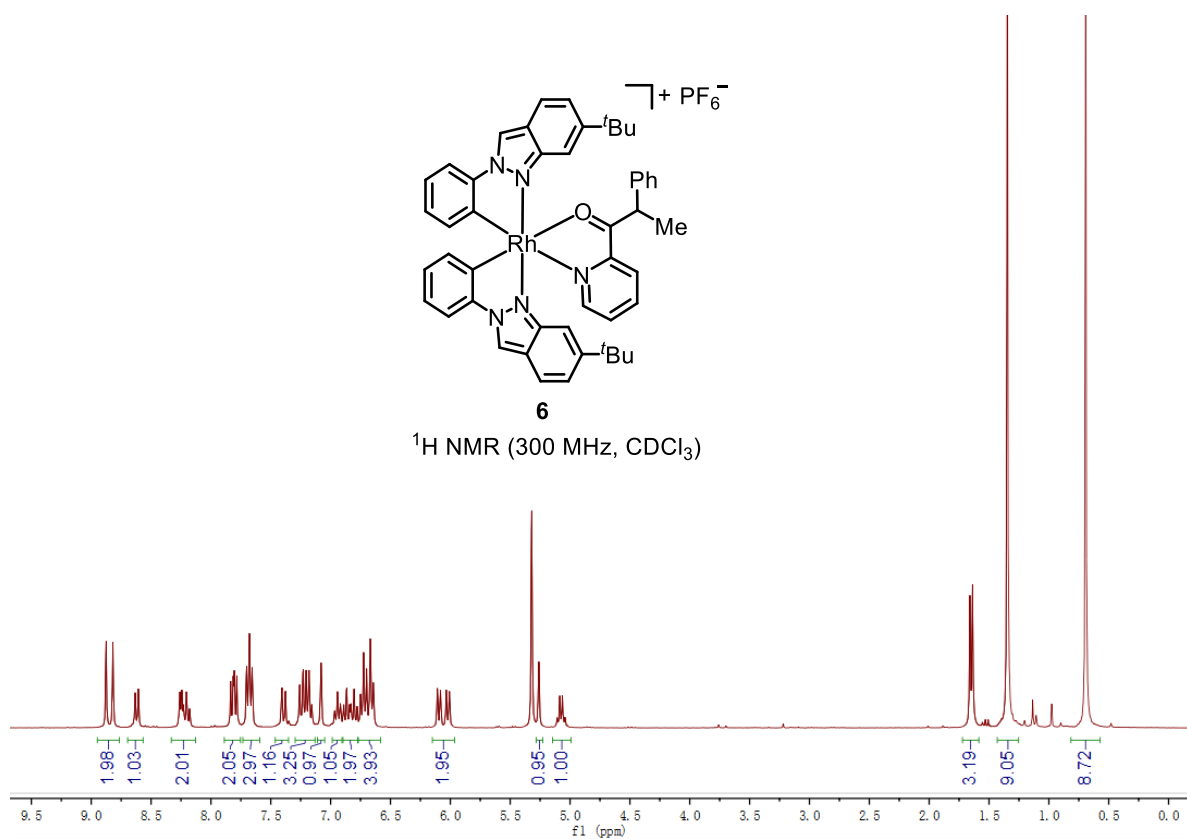


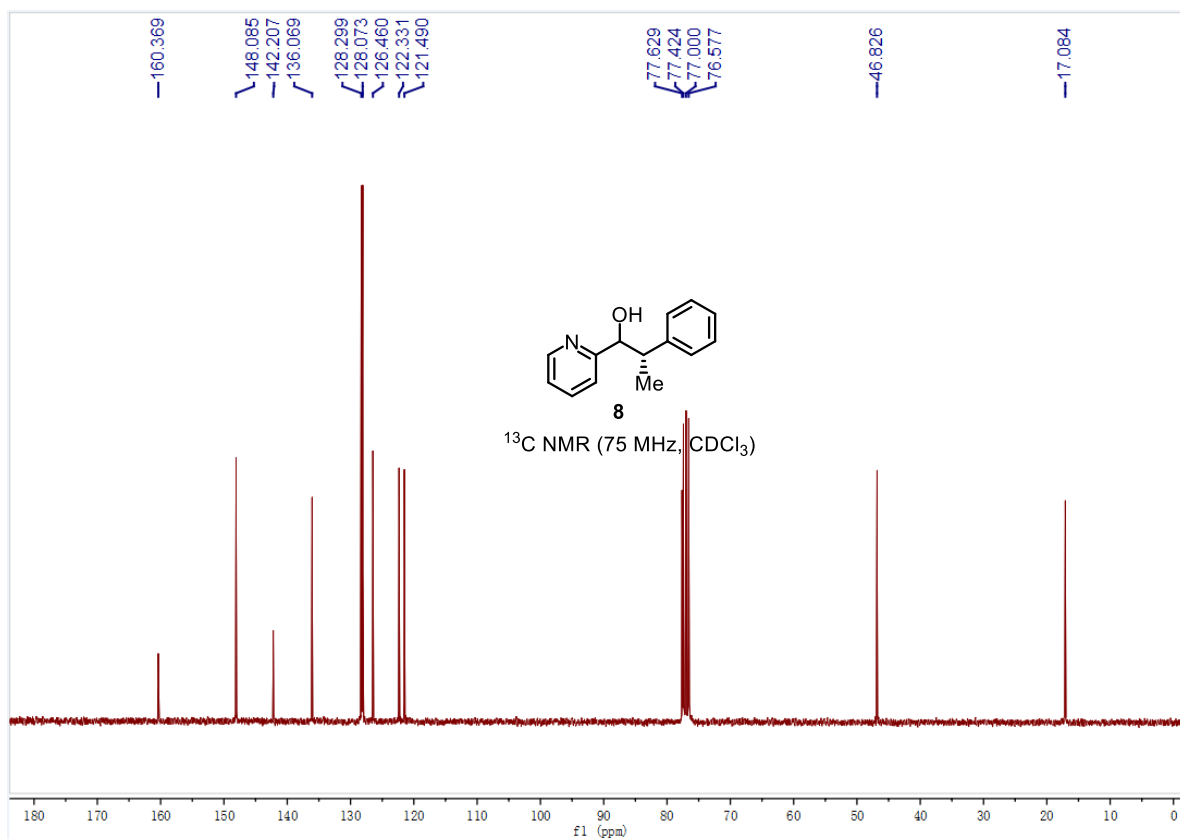
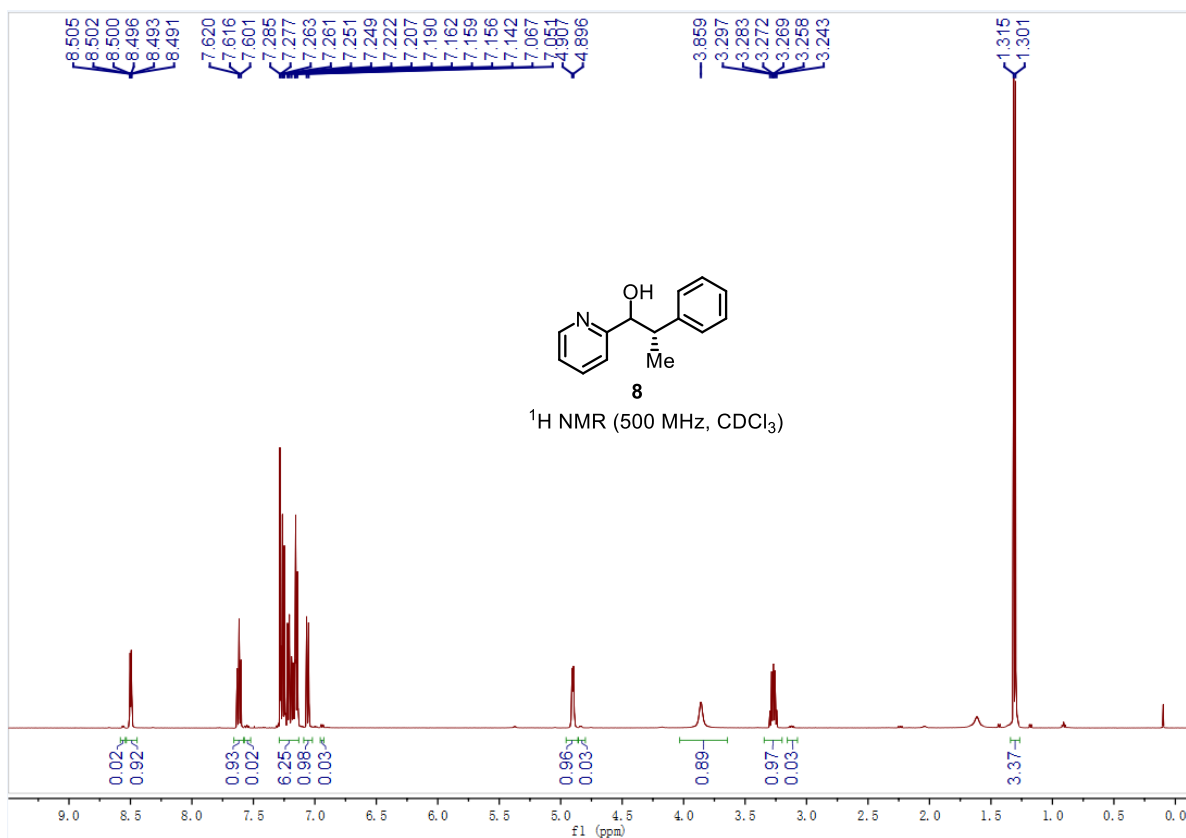
Chapter 5. Appendices

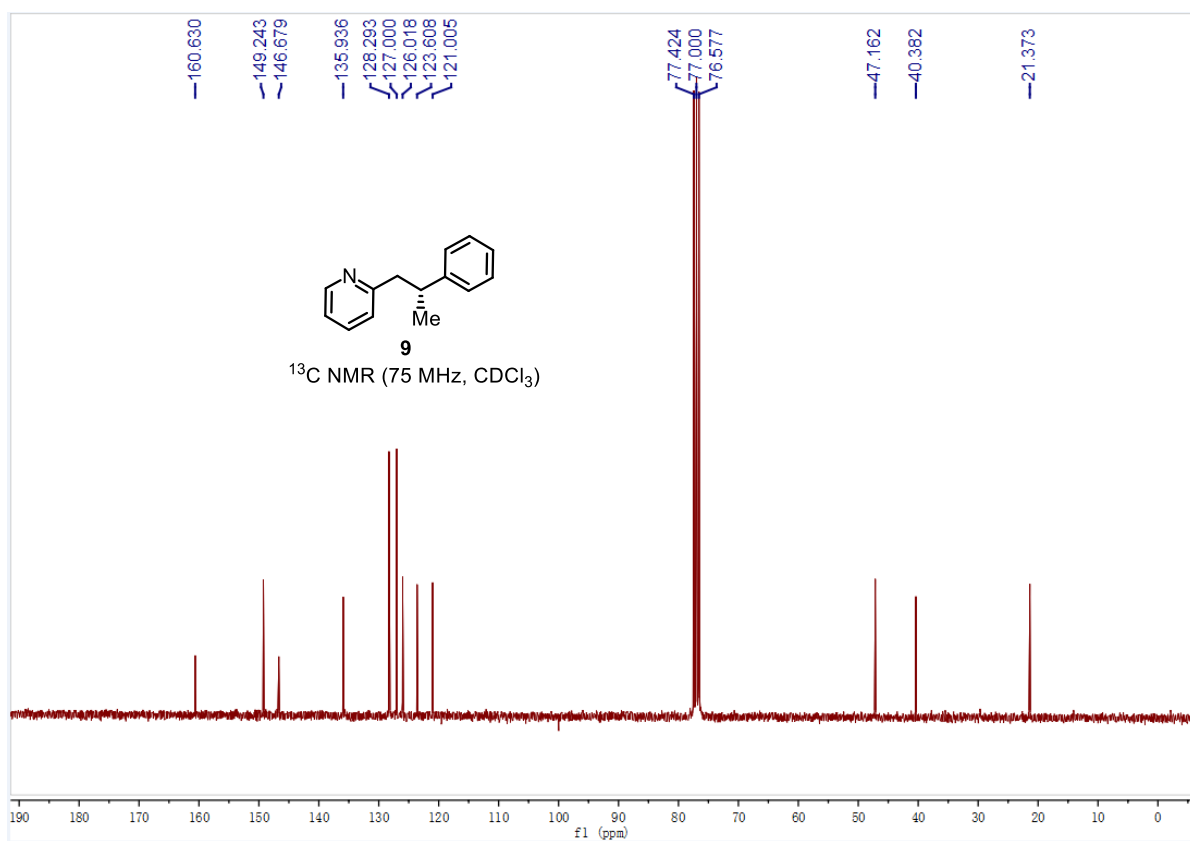
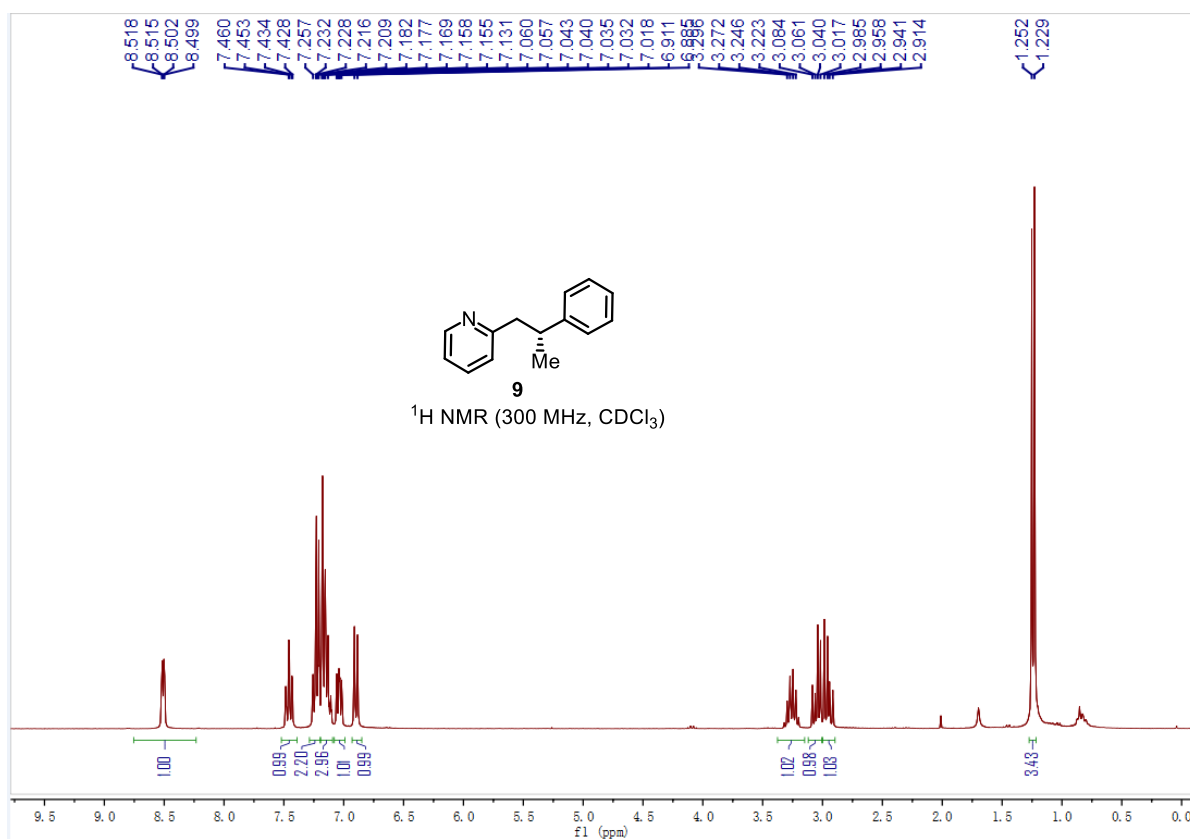




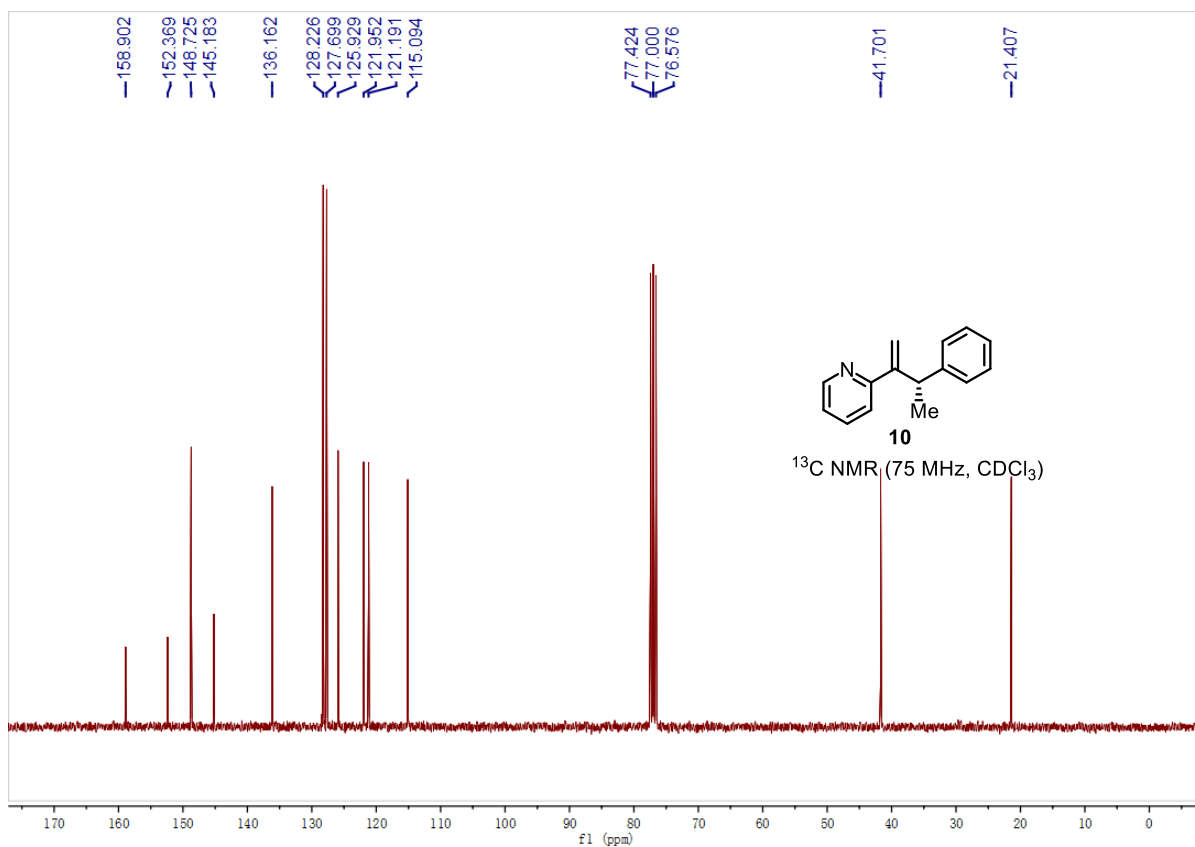
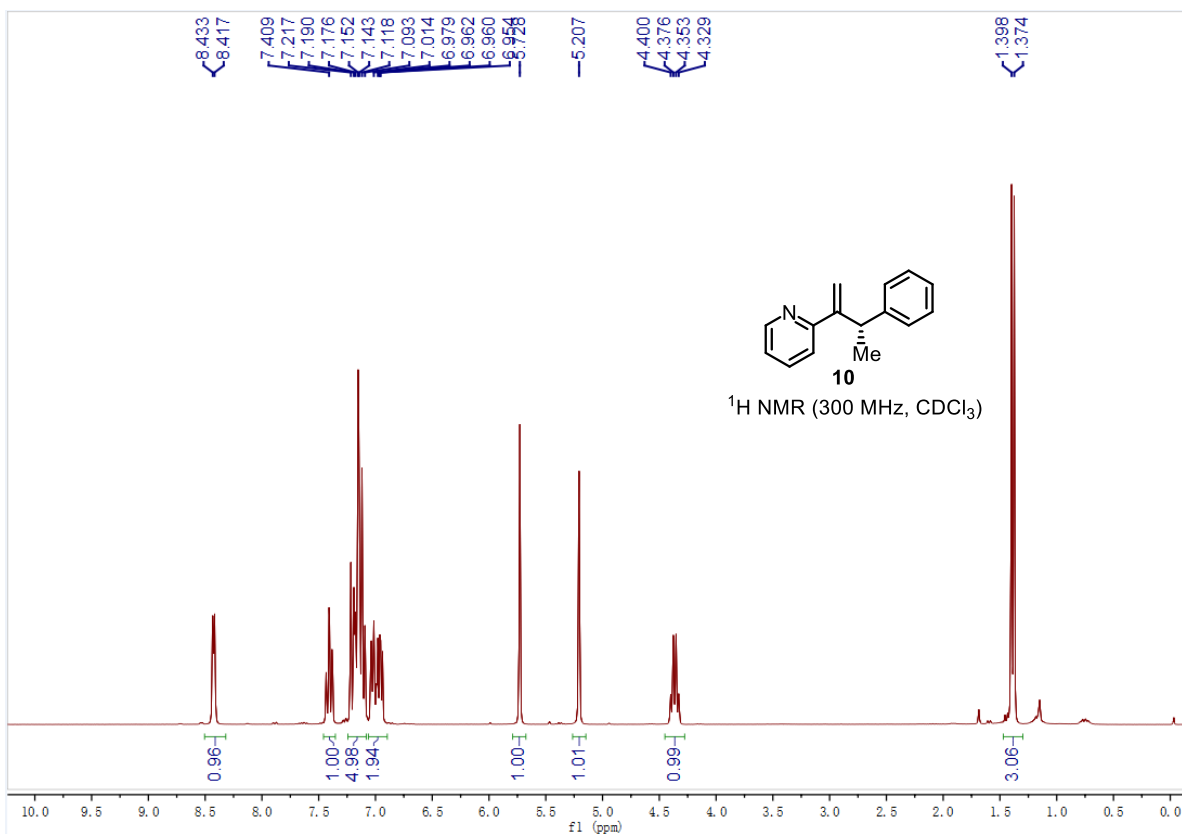




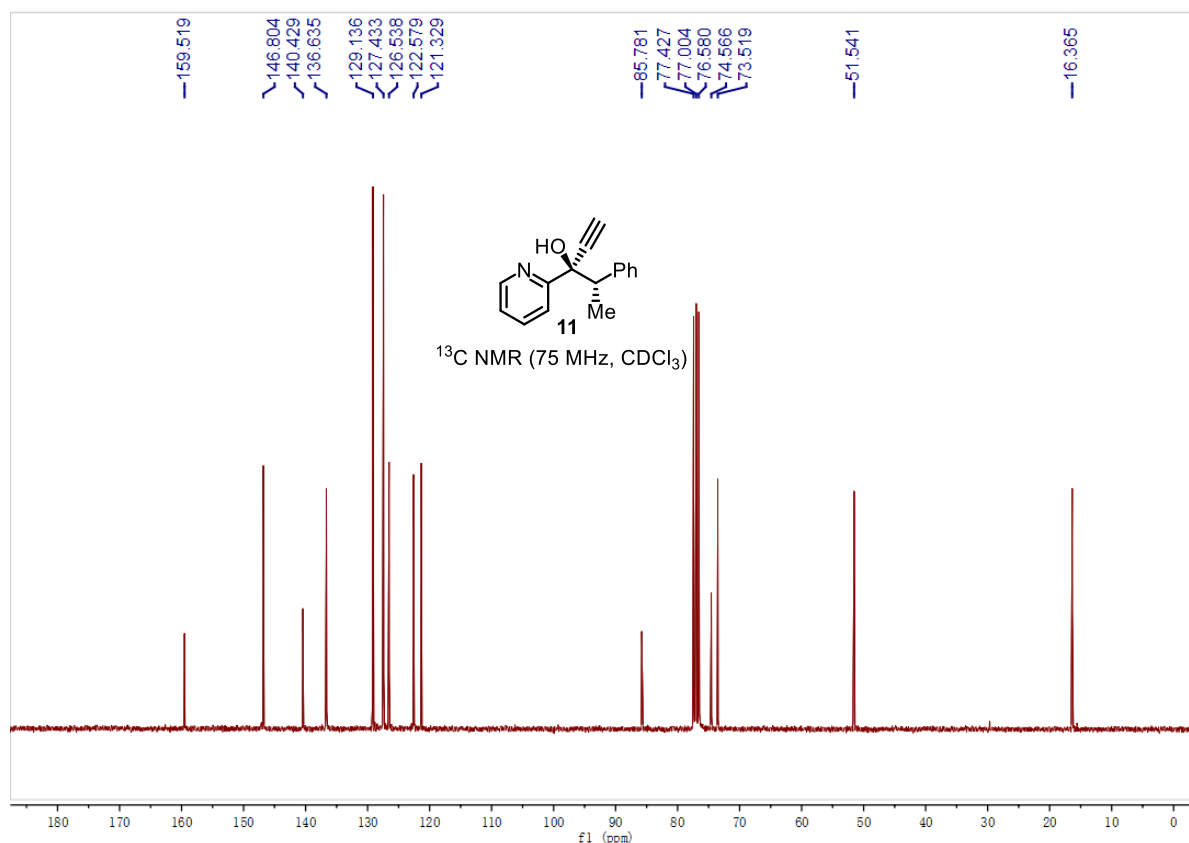
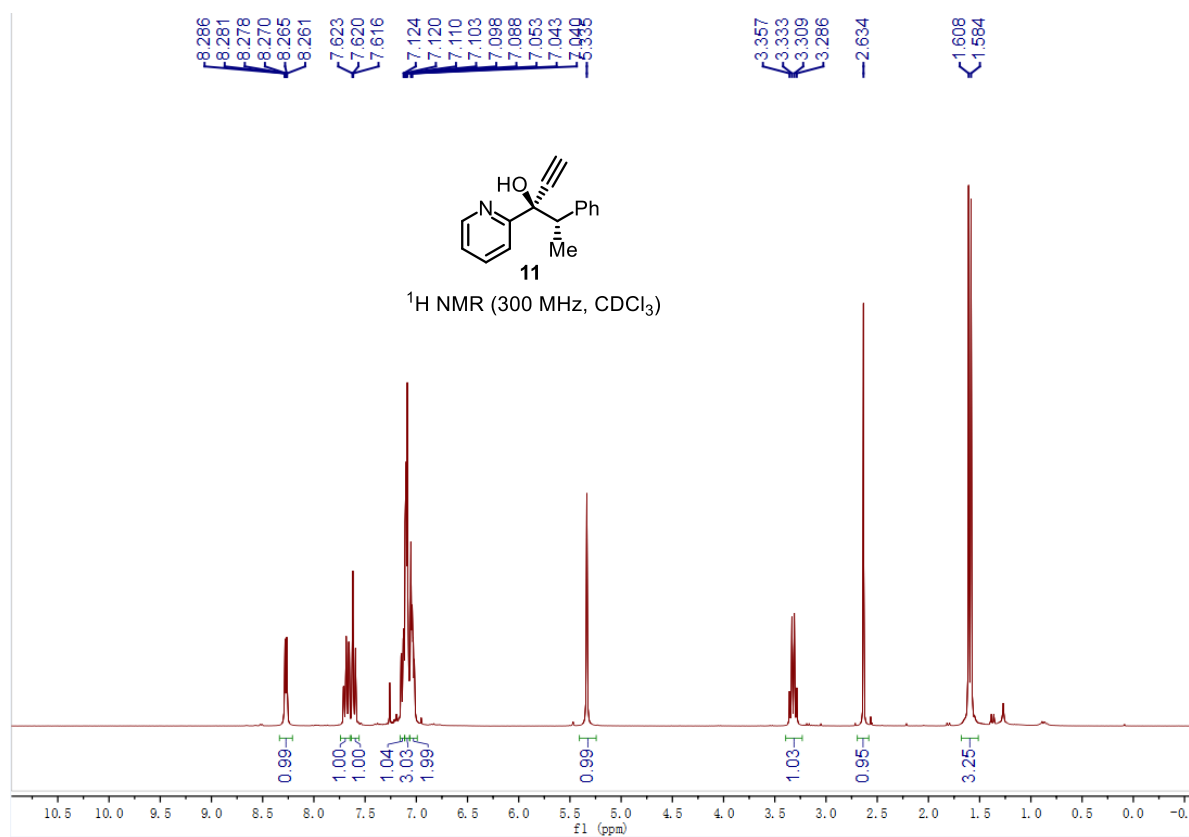


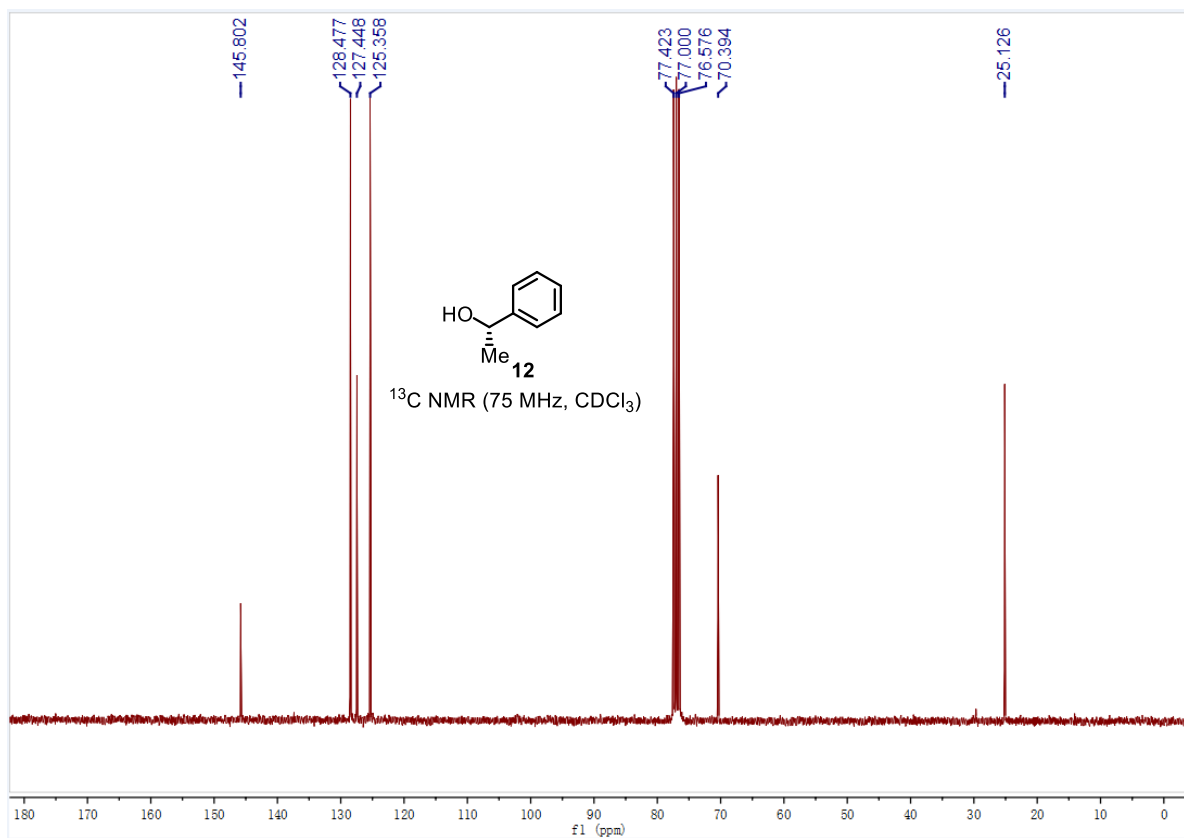
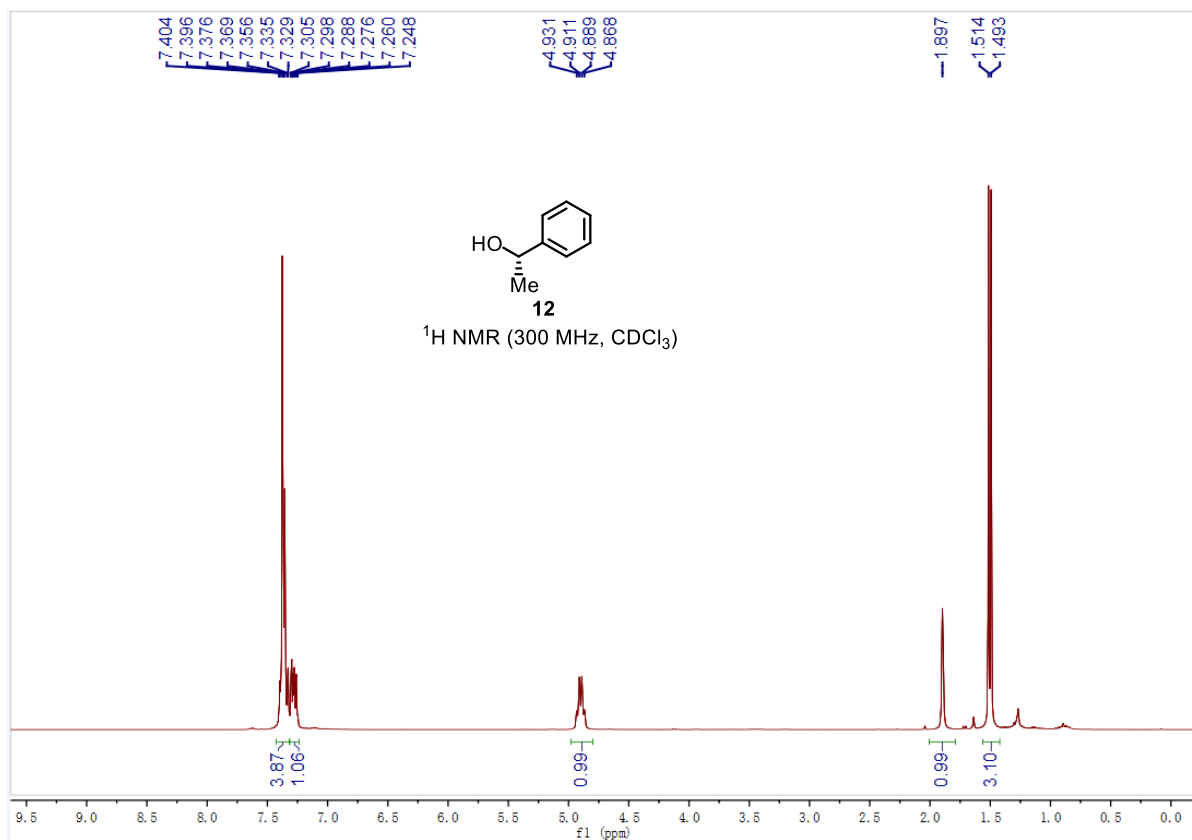


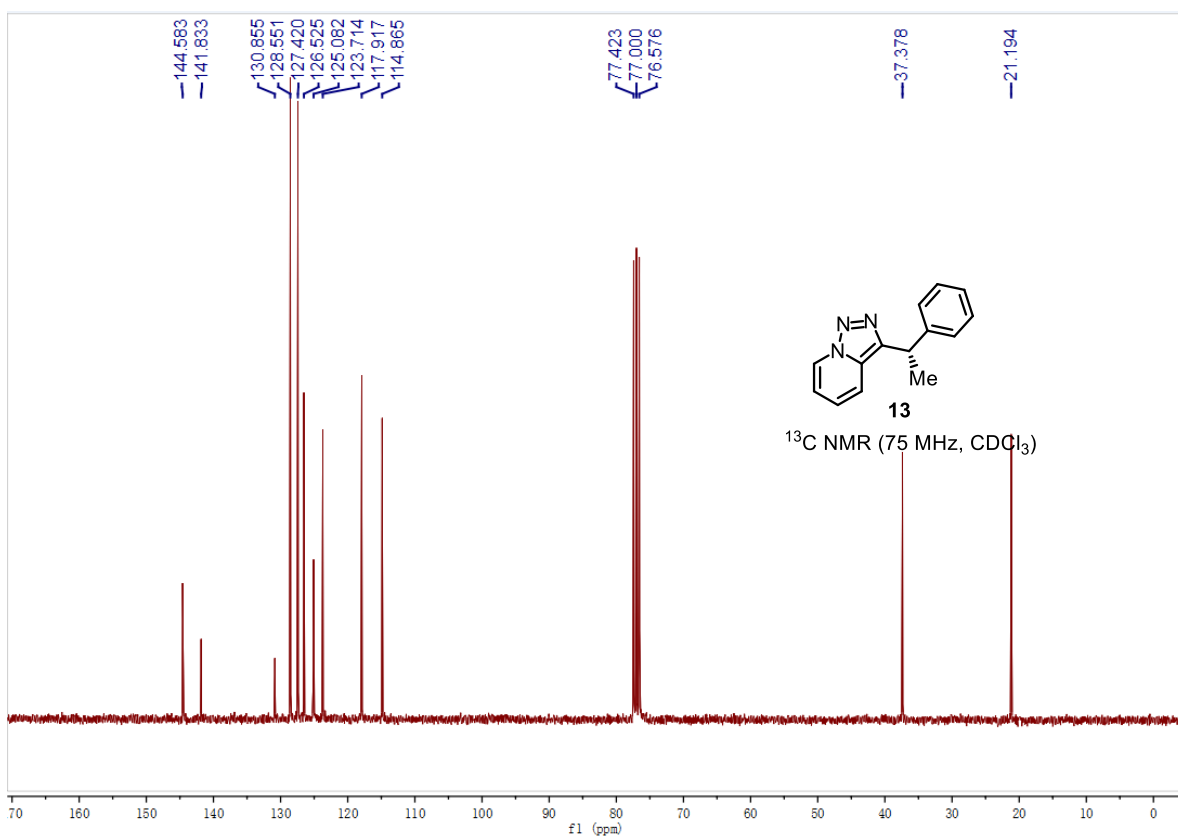
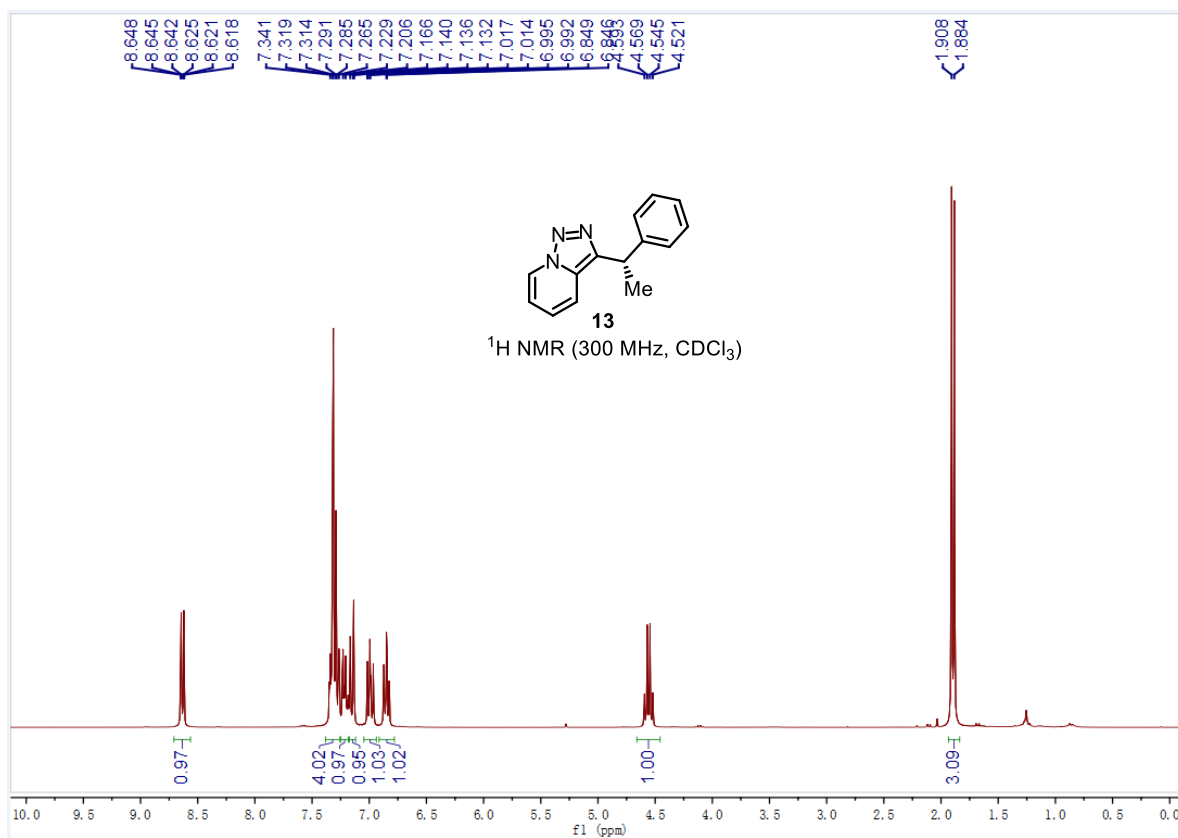
Chapter 5. Appendices

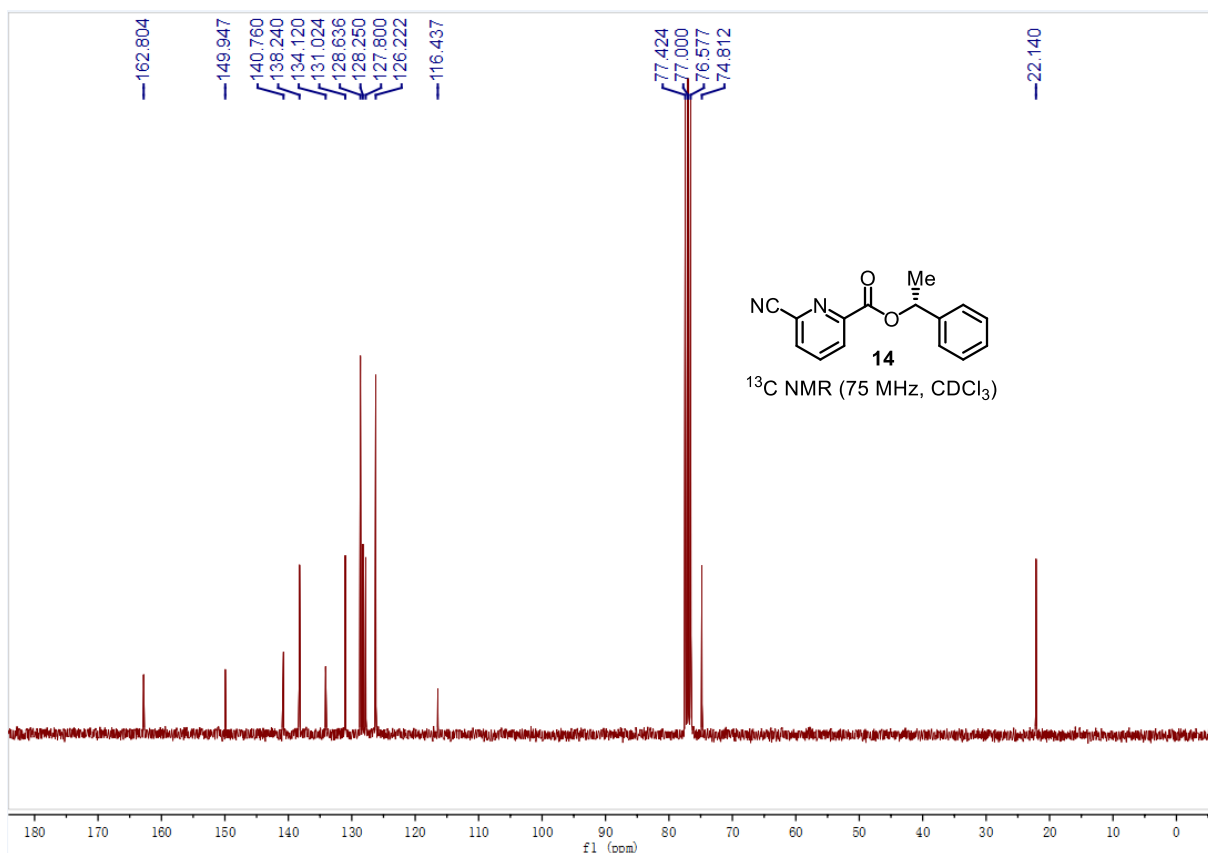
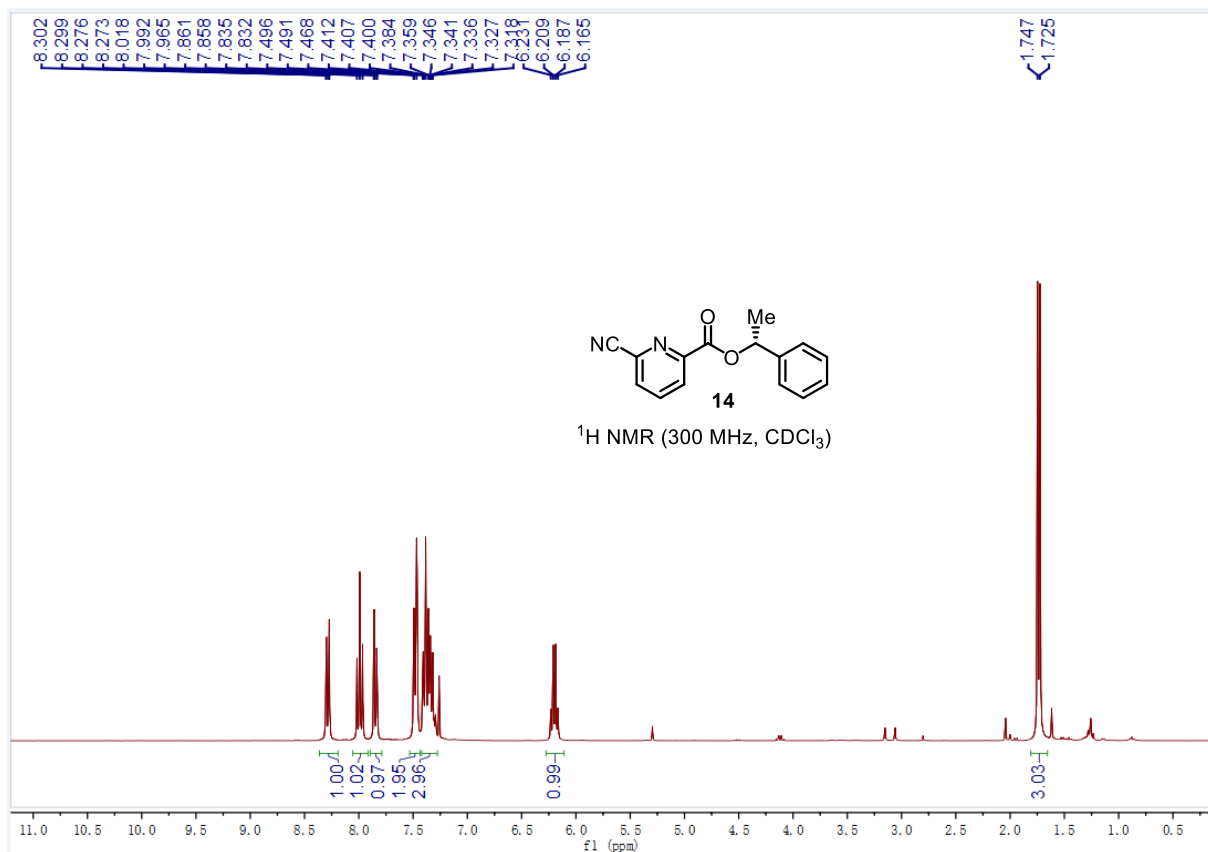


Chapter 5. Appendices









Statement

gemäß § 10, Abs. 1 der Promotionsordnung der mathematisch-naturwissenschaftlichen Fachbereiche und des Medizinischen Fachbereichs für seine mathematisch-naturwissenschaftlichen Fächer der Philipps-Universität Marburg vom 15.07.2009

Ich erkläre, dass eine Promotion noch an keiner anderen Hochschule als der Philipps-Universität Marburg, Fachbereich Chemie, versucht wurde und versichere, dass ich meine vorgelegte Dissertation

Asymmetric Photocatalysis by Hydrogen Atom Transfer with Chiral-at-Rhodium complexes

selbst und ohne fremde Hilfe verfasst, nicht andere als die in ihr angegebenen Quellen oder Hilfsmittel benutzt, alle vollständig oder sinngemäß übernommenen Zitate als solche gekennzeichnet sowie die Dissertation in der vorliegenden oder ähnlichen Form noch bei keiner anderen in- oder ausländischen Hochschule anlässlich eines Promotionsgesuchs oder zu anderen Prüfungszwecken eingereicht habe.

Chenhao Zhang

Marburg, den 30. July.2021

Curriculum Vitae

Chenhao Zhang

Male, born September 1, 1989 in Henan, P. R. China

Email: zchchem@163.com

Education

- 12/2017–present *Ph.D.* Organic Chemistry, University of Marburg, Germany
Advisor: Prof. Eric Meggers
- 09/2013–07/2016 *M.Sc.* Pharmaceutical Chemistry, Henan University, China
Advisor: Prof. Zhiyong Jiang and Prof. Choon-hong Tan
- 09/2009–07/2013 *B.S.* Pharmacy, Henan University of Chinese Medicine, China

Research Experiences

Ph.D. study: Asymmetric Chiral-at-Rhodium Catalysis Driven by Visible Light.

Publications:

1. **C. Zhang**, S. Chen, C-X. Ye, K. Harms, L. Zhang, K. N. Houk, E. Meggers, *Angew. Chem. Int. Ed.* **2019**, *58*, 14462.
2. **C. Zhang**, A. Z. Gao, X. Nie, C-X. Ye, S. Ivlev, S. Chen, E. Meggers (submitted for publication)

M.Sc. study: Photocatalysis and asymmetric catalysis involving DPZ.

Publications:

- 1 **C. Zhang**, S. Li, F. Bureš, R. Lee, X. Ye, Z. Jiang, *ACS Catal.* **2016**, *6*, 6853.
- 2 G. Wei, **C. Zhang**, F. Bureš, X. Ye, C.-H. Tan, Z. Jiang, *ACS Catal.* **2016**, *6*, 3708. (co-first author)
- 3 Y. Zhao, **C. Zhang**, K. F. Chin, O. Pytela, G. Wei, H. Liu, F. Bureš, Z. Jiang, *RSC Adv.* **2014**, *4*, 30062. (co-first author)